Characterisation of *cello*: an ENU-induced mouse model of early-onset hearing loss

A thesis presented for the degree of Doctor of Philosophy (DPhil)

Trinity Term, 2015

Lauren Chessum

Department of Biochemistry, Wolfson College, University of Oxford

Mammalian Genetics Unit, MRC Harwell

Supervisors: Dr Mike Bowl (MRC Harwell)

Professor Steve Brown (MRC Harwell)

Professor Neil Brockdorff (Biochemistry, Oxford)

Word count: 42,674

MRC | Harwell

Mammalian Genetics Unit

Characterisation of *cello*: an ENU-induced mouse model of early-onset hearing loss

Lauren Chessum

Department of Biochemistry, Wolfson College, University of Oxford
Mammalian Genetics Unit, MRC Harwell

A thesis presented for the degree Doctor of Philosophy (DPhil), Trinity Term, 2015

Abstract

cello is a recessive mouse model of early-onset, sensorineural hearing loss that was identified from a large-scale *N*-ethyl-*N*-nitrosourea (ENU) mutagenesis screen undertaken at MRC Harwell. Linkage analysis and whole-genome sequencing identified that *cello* mice have a non-synonymous point mutation in *Ikaros family zinc finger 2* (*Ikzf2*), which encodes a zinc finger transcription factor called helios.

To investigate the role of helios in the auditory system, *cello* mice underwent comprehensive molecular, phenotypic and functional characterisation. The *cello* mutation was found to disrupt a highly conserved, zinc-coordinating residue in the final C-terminal zinc finger domain of helios. *In vitro* analyses demonstrated that mutant helios can still localise to the nucleus, but has an impaired ability to homodimerise – a prerequisite for DNA binding. In both $Ikzf2^{+/+}$ and $Ikzf2^{cello/cello}$ cochleae, helios is expressed in the nuclei of the outer hair cells (OHCs) from the first postnatal week, coinciding with a critical period of OHC functional maturation. Although $Ikzf2^{cello/cello}$ exhibit severely impaired hearing at postnatal day (P) 16, cochlear morphology appears grossly normal up to one month of age, after which the OHCs and inner hair cells begin to progressively degenerate. Transcriptome profiling was subsequently undertaken to identify potential target genes of helios in the auditory system. Results suggested that loss of helios function leads to dysregulation of over 450 genes in $Ikzf2^{cello/cello}$ cochleae at P8. This included the OHC-specific genes *Slc26a5* (which encodes the OHC motor protein, prestin) and *Ocm* (oncomodulin), both of which were significantly decreased in $Ikzf2^{cello/cello}$ mutants compared to $Ikzf2^{+/+}$ controls. Electrophysiological studies demonstrated that $Ikzf2^{cello/cello}$ OHCs fail to acquire full electromotility, a property that is fundamental to their function, but otherwise mature normally. Using luciferase reporter assays, wild-type helios was found to induce transactivation of the *Slc26a5* promoter, whilst this ability was lost in the mutant protein. Additional *in silico* network analyses identified helios as a putative direct regulator of 40 genes that are enriched in the OHCs and upregulated during development, which suggests that helios has a key role in regulating the maturing OHC transcriptome.

Overall, the work presented in this thesis identifies *Ikzf2* as a novel hearing loss-causing gene and establishes that the helios transcription factor is essential for OHC functional maturation in the mammalian auditory system.

Acknowledgements

First and foremost I would like to thank Dr Mike Bowl and Professor Steve Brown, who have been fantastic supervisors during my four years as a DPhil student. This thesis would not have been possible without their invaluable help, guidance and encouragement. Mike's support, both in and outside of the lab, has helped keep me sane during my DPhil (although I still play a better game of beer pong!). I would also like to thank all of the past and present members of the Deafness group who have made the lab such a fun and enjoyable place to work, including Prasshy Shanthakumar, Lea Carrott, Mike Crompton, Tom Purnell, Andy Parker, Phil Mburu, Hilda Tateossian, Carlos Aguilar and Sue Morse. I'm positive that our many coffee breaks and slices of cake helped fuel this thesis!

I am extremely grateful to the staff of the Mary Lyon Centre at MRC Harwell for their excellent care of the *cello* colonies, particularly Sara Wells, Lucie Vizor, Lisa Ireson and Tamzin Osborne. My thanks also go to the core facilities at MRC Harwell, including bioinformatics, proteomics, histology, bioimaging, clinical chemistry and GEMS, who have provided guidance and helped in various aspects of my research. I would also like to thank Jack Prescott for assisting with the cochlear wholemount immunolabelling experiments and George Nicholson for providing statistical advice.

This project would not have been possible without the expertise and support contributed by a number of collaborating researchers: Dr Ronna Hertzano, Sean Daugherty, Dr Beatrice Milon and Maggie Matern at the University of Maryland carried out the RNA-Seq experiment, initial bioinformatics analyses and validations; Dr Rani Elkon at Tel Aviv University assisted with computational regulatory network analyses; and Professor Walter Marcotti and Dr Stuart Johnson at the University of Sheffield performed the electrophysiology experiments.

My thanks also go to the Medical Research Council, the Genetics Society, the Biochemical Society and Action on Hearing Loss for generous funding that has not only enabled me to carry out this research, but also to attend a number of international meetings during the course of my DPhil.

I would also like to thank my beloved Harwell Summer Rounders team, The Nutty Nukes, who have provided a much-needed break from science during summer lunchtimes – now 2011 and 2015 champions!

Finally, a huge thank you to my lovely family: Brenda Chessum, Claire Siddle and Mark Siddle. I could not have done this without their love, support and encouragement. They reassure me when I am stressed (i.e. most of the time) and are always happy to supply me with home-cooked food and a cup of tea.

Statement of Contributions

The *cello* project involved collaboration with a number of colleagues at MRC Harwell and external researchers, all of whom are detailed below.

Within MRC Harwell, Joanne Dorning and Sue Morse in the Deafness group initially identified the *cello* pedigree from the Ageing Screen by clickbox phenotyping at 3 and 6 months of age. The Bioinformatics group carried out the initial analysis of *cello* whole-genome sequencing results, which involved aligning data to the reference genome, filtering out known variants and assigning quality scores. The Genotyping, Expression and Mutation Screens core facility designed and carried out the allelic discrimination genotyping assay for the *cello* pedigree. The Histology team cut and stained paraffin sections with haematoxylin and eosin. The Clinical Chemistry facility ran *cello* samples on the haematological analyser and fluorescence-activated cell sorting system.

Outside of MRC Harwell, Dr Ronna Hertzano, Dr Beatrice Milon and Maggie Matern at the University of Maryland (USA) carried out RNA sequencing of *cello* samples and subsequent validations using quantitative real-time PCR. Sean Daugherty at the University of Maryland performed the initial bioinformatics analysis of *cello* RNA sequencing results, which involved aligning data to the reference genome, normalising sequencing reads and using HTSeq and DESeq software to perform raw read counts and generate a list of differentially expressed genes. Professor Walter Marcotti and Dr Stuart Johnson at The University of Sheffield (UK) investigated the electrophysiological properties of outer hair cells from *cello* mice using single cell patch-clamp analyses.

All other work was undertaken by me. This included preparation of DNA for whole-genome sequencing, validation of whole-genome sequencing results, *in silico* prediction analyses of the *cello* mutation, molecular cloning, *in vitro* analyses of the *cello* protein (including transient transfections, western blotting, subcellular localisation and co-immunoprecipitations), auditory-evoked brainstem response measurements, imaging of histological sections, scanning electron microscopy (including sample preparation, processing, imaging and cell counts), vibratome sectioning, immunolabelling of tissue sections and cochlear wholemounts, confocal microscopy, preparation of RNA for RNA sequencing, analysis of RNA sequencing data using the STRING database, luciferase reporter assays and interpretation of all results (including those from whole genome sequencing, haematological analysis, fluorescence-activated cell sorting, RNA sequencing and electrophysiology recordings).

Publications Arising from DPhil

Carrott L, Bowl MR, Aguilar C, Johnson SL, **Chessum L**, West M, Morse S, Dorning J, Smart E, Hardisty-Hughes R, Ball G, Parker A, Barnard AR, MacLaren RE, Wells S, Marcotti W, Brown SDM (2015). Absence of Neuroplastin-65 affects synaptogenesis in mouse inner hair cells and causes profound hearing loss. ***Journal of Neuroscience**, accepted.*

Mianné J, **Chessum L**, Kumar S, Aguilar C, Codner G, Hutchison M, Parker A, Mallon AM, Wells S, Simon M, Teboul L, Brown SDM, Bowl, MR (2015). Correction of the auditory phenotype in C57BL/6N mice via CRISPR/Cas9-mediated homology directed repair. ***Genome Medicine**, under revision.*

Potter P, Bowl MR, Shanthakumar P, Wisby L, Blease A, Goldsworthy ME, Simon M, Greenaway S, Michel V, Barnard A, Aguilar C, Agnew T, Banks G, Blake A, **Chessum L**, Dorning J, Falcone S, Goosey L, Harris S, Haynes A, Heise I, Hillier R, Hough T, Hoslin A, Hutchison M, King R, Kumar S, Lad H, Law G, MacLaren RE, Morse, S, Nicol T, Parker A, Pickford K, Sethi S, Starbuck B, Stelma F, Cheeseman M, Cross SH, Foster RG, Jackson IJ, Pierson SN, Thakker RV, Vincent T, Scudamore C, Wells S, El-Amraomi A, Petit C, Acevedo-Arozena A, Nolan PM, Cox R, Mallon AM, Brown SDM (2015). Novel gene function revealed by mouse mutagenesis screens for models of age-related disease. ***Nature Communications**, under revision.*

Parker A, **Chessum L**, Mburu P, Sanderson J, Bowl MR (2015). Light and electron microscopic methods for examination of cochlear morphology in mouse models of deafness. ***Current Protocols in Mouse Biology**, submitted.*

Chessum L, Matern M, Johnson SL, Milon B, Prescott J, Dorning J, Morse S, Parker A, Simon M, Daugherty S, Wells S, Elkon R, Hertzano R, Marcotti W, Brown SDM, Bowl MR. Helios is an outer hair cell-expressed transcription factor necessary for prestin-mediated electromotility and hearing. ***Cell**, in preparation.*

Conference Presentations

Podium presentation: The *cello* mouse model of early-onset hearing loss identifies a novel outer hair cell-specific transcription factor expressed during outer hair cell functional maturation. ***The Association for Research in Otolaryngology 38th Annual MidWinter Meeting***, Maryland, USA, 22nd February 2015.

Poster presentation: Identification of novel ENU-induced alleles of known deafness genes. ***The 9th Molecular Biology of Hearing & Deafness Conference***, Stanford School of Medicine, California, USA, 24th June 2013.

Poster presentation: Characterising new ENU-induced mouse models of early-onset hearing loss. ***The Mouse as an Instrument for Ear Research V***, The Jackson Laboratory, Maine, USA, 3rd October 2012.

Table of Contents

Table of Figures

Table of Tables

Abbreviations

3D	Three-dimensional
ABR	Auditory-evoked brainstem response
AMPA	α-amino-3-hydroxy-5-methylisoxazole-4-proprionic acid
ANOVA	Analysis of variance
BL6	C57BL/6J
bp	Base pairs
BSA	Bovine serum albumin
C3H	C3H.pde6b^{+}
C	Cysteine
CD	Cluster of differentiation
cDNA	Complementary deoxyribonucleic acid
chIP	Chromatin immunoprecipitation
Chr	Chromosome
cm	Centimetre
CT	Cycle threshold
CTL	Cytotoxic T-lymphocyte
DAPI	4',6-diamidino-2-phenylindole
dB SPL	Decibel sound pressure level
DC	Dendritic cell
dCT	Delta cycle threshold
ddCT	Delta delta cycle threshold
ddH_2O	Double distilled water
DMEM	Dulbecco's modified eagle medium
DMSO	Dimethyl sulfoxide
DNA	Deoxyribonucleic acid
DPBS	Dulbecco's phosphate-buffered saline
DtC	Deiters' cell
E	Embryonic day
EDTA	Ethylenediaminetetraacetic acid
EGFP	Enhanced green fluorescent protein
EGTA	Ethyleneglycoltetraacetic acid
EMSA	Electrophoretic mobility shift assay
ENU	*N*-ethyl-*N*-nitrosourea
EP	Endocochlear potential
FACS	Fluorescence-activated cell sorting
FBS	Foetal bovine serum
FDR	False detection rate
G1	First generation

G2	Second generation
G3	Third generation
g	Grams
GFP	Green fluorescent protein
GO	Gene ontology
H&E	Haematoxylin and eosin
H	Histidine
HA	Haemagglutinin
HSC	Haematopoietic stem cell
Hz	Hertz
I_{Ca}	Inward calcium current
IHC	Inner hair cell
I_{K}	Classical delayed rectifier potassium current
I_{K1}	Inward rectifier potassium current
$I_{K,f}$	Rapidly-activating large-conductance calcium-activated potassium current
$I_{K,n}$	Negatively-activating delayed rectifier potassium current
$I_{K,neo}$	Outward potassium current
IKZF	Ikaros family zinc finger
Ikzf2	Ikaros family zinc finger 2
IMPC	International Mouse Phenotyping Consortium
I_{Na}	Inward sodium current
IP	Immunoprecipitation
kb	Kilobase pairs
kDa	Kilodaltons
kg	Kilogram
kHz	KiloHertz
LB	Lysogeny broth
LOC	Lateral olivocochlear
M	Molar
Mb	Megabase
MET	Mechanoelectrical transduction
mg	Milligram
ml	Millilitre
mM	Millimolar
MOC	Medial olivocochlear
MPC	*MUTA-PED-C3PDE*
MRC	Medical Research Council
ms	Millisecond
mV	Millivolt
nA	Nanoampere
ng	Nanograms

NK	Natural killer cell
NKT	Natural killer T-cell
nm	Nanometre
ns	Not significant
NuRD	Nucleosome remodelling complex
Ocm	Oncomodulin
OHC	Outer hair cell
P	Postnatal day
pA	Picoampere
PBS	Phosphate-buffered saline
PBST	PBS + 0.1% Tween
PCR	Polymerase chain reaction
pF	Picofarad
PFA	Paraformaldehyde
pmol	Picomolar
Q	Glutamine
qRT-PCR	Quantitative real-time polymerase chain reaction
RNA	Ribonucleic acid
RNA-Seq	Ribonucleic acid sequencing
RPKM	Reads per kilobase per million
rpm	Rotations per minute
RQ	Relative quantitation
RT	Room temperature
s.e.m	Standard error of the mean
SEM	Scanning electron microscopy
SGN	Spiral ganglion neuron
SHIELD	Shared Harvard Inner Ear Laboratory Database
Slc26a5	Solute carrier family 26, member 5
SNP	Single nucleotide polymorphism
STRING	Search tool for the retrieval of interacting genes/proteins
T-reg	Regulatory T-cell
TSS	Transcription start site
µg	Micrograms
µl	Microlitres
µM	Micromolar
V	Volts
V_m	Resting membrane potential
WBC	White blood cell
WGS	Whole-genome sequencing
WT	Wild-type
ZnF	Zinc finger

Chapter 1 : Introduction

1.1 Mammalian Ear Physiology

The ear is the sensory organ which enables the detection of sound and aids balance. The mammalian ear can be divided into three portions: the outer, middle and inner ear (Figure 1.1 A). Together, these form the peripheral auditory system and are responsible for conducting sound signals from the external environment to the brain, where they are processed and interpreted by the central auditory system.

1.1.1. The Outer Ear

The outer ear comprises the pinna and lobule, which are the visible portions of the ear, and the auditory canal. The function of these structures is to collect sound signals from the external environment and funnel them to the tympanic membrane of the middle ear (Carola et al., 1992). The outer ear also has a crude role in sound localisation, as the shape of the pinna means that sounds that are anterior or lateral to the ear are directed to the tympanic membrane more effectively than sounds that are posterior (Heffner et al., 1996, Parsons et al., 1999).

1.1.2. The Middle Ear

The tympanic membrane, also known as the ear drum, is a thin, tense membrane that separates the outer ear from the middle ear. Its primary role is to transduce acoustic energy from one form to another, mechanically converting sound waves in the air-filled outer and middle ear into pressure waves in the fluid-filled inner ear (Merchant et al., 1997). It fulfils this role by causing articulation of the three small bones of the ossicular chain; first the

malleus, which is attached to the tympanic membrane, then the incus and finally the stapes, which contacts the oval window of the cochlea in the inner ear (Stenfelt and Goode, 2005, Stenfelt, 2006, Tortora and Grabowski, 1993). This effectively concentrates acoustic energy from the relatively large surface area of the tympanic membrane to the much smaller footplate of the stapes, increasing the energy that is transmitted to the inner ear (Keele et al., 1982).

1.1.3. The Inner Ear

The inner ear can be further divided into two distinct structures: the cochlea and the vestibular apparatus. The cochlea is the auditory portion of the inner ear, which converts sound-induced pressure waves originating from the middle ear into electrical impulses that travel to the brain for processing (Carola et al., 1992). The three semicircular canals (horizontal, superior, posterior), utricle and saccule are collectively known as the vestibular apparatus and are required for balance and spatial orientation (Emslie-Smith et al., 1988).

1.1.3.1. The Cochlea

The cochlea is comprised of three fluid-fluid compartments, named the scala tympani, scala media and scala vestibuli (Figure 1.1 B) (Tortora and Grabowski, 1993). The scala tympani and scala vestibuli are filled with perilymph fluid that has a high sodium and low potassium content, whereas the scala media is filled with endolymph fluid that, as a result of ion transport from the stria vascularis, has a high potassium and low sodium content (Smith et al., 1954). In terms of exact ion composition, perilymph is comprised of 3.5 mM potassium, 140 mM sodium and 1 mM calcium, whereas endolymph contains 150 mM potassium, 1 mM sodium and 0.02 mM calcium (Petit et al., 2001). This unique composition gives

endolymph fluid a charge of +80 mV known as the endocochlear potential (EP) (von Békésy, 1952).

During sound transduction, sound-induced pressure waves travel through the perilymph and endolymph fluid and stimulate specialised auditory hair cells, which are located in the organ of Corti and are apically bathed in the potassium-rich endolymph of the scala media (Carola et al., 1992).

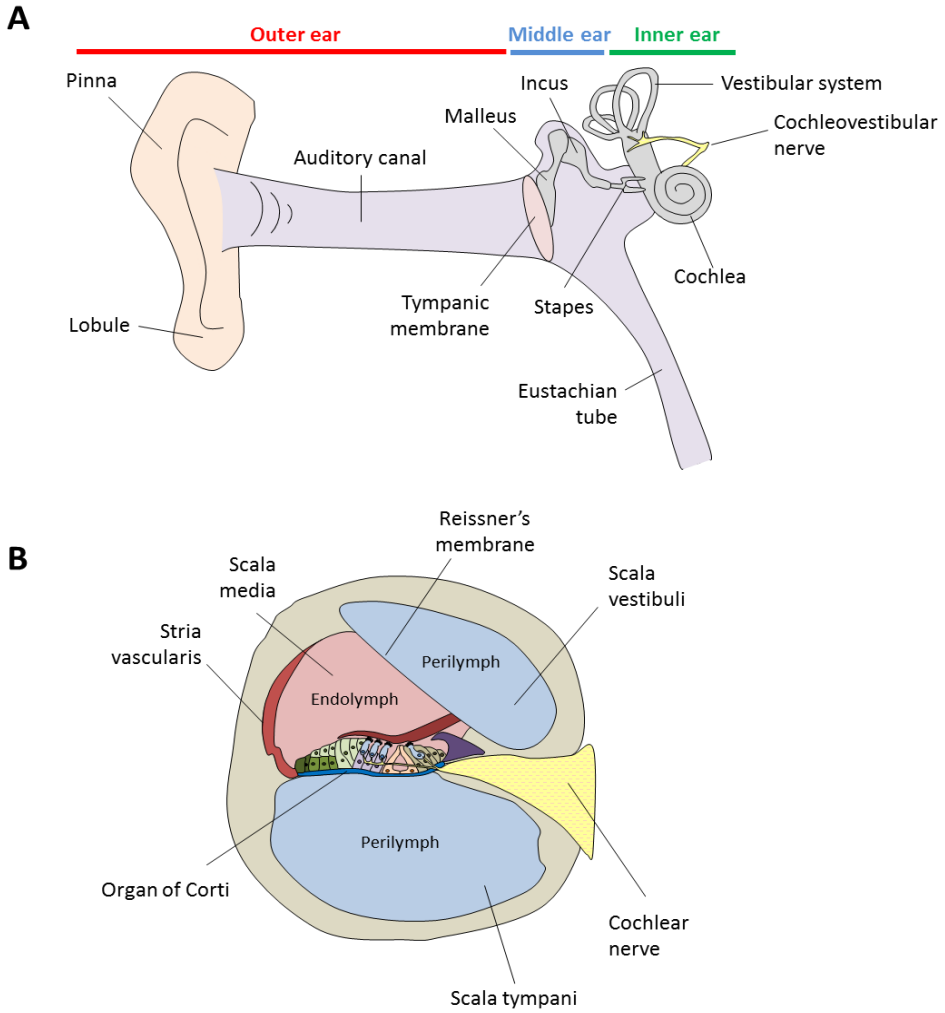

Figure 1.1: Anatomy of the mammalian ear.
(A) The mammalian ear can be divided into three regions: the outer, middle and inner ear, all of which are required for sound detection. Only the inner ear, which contains the vestibular system, is required for balance. **(B)** The cochlea is part of the inner ear and is composed of the scala vestibuli, scala media and scala tympani compartments, which contain perilymph and endolymph extracellular fluid.

1.1.3.2. Auditory Hair Cells

Within the organ of Corti is a single row of inner hair cells (IHCs) and three rows of outer hair cells (OHCs), which sit atop the basilar membrane and are surrounded by epithelial supporting cells (LeMasurier and Gillespie, 2005) (Figure 1.2). There are ~750 IHCs and ~2500 OHCs in the mouse cochlea (Ehret and Frankenreiter, 1977) and ~3500 IHCs and ~11,000 OHCs in the human cochlea (Ashmore, 2008). The increased number of IHCs and OHCs in the human is related to the increased length of the cochlea, which extends for 2½ turns compared to 1¾ turns in the mouse, and enables humans to discriminate sound with greater frequency, temporal and spatial resolution (Vater et al., 2004).

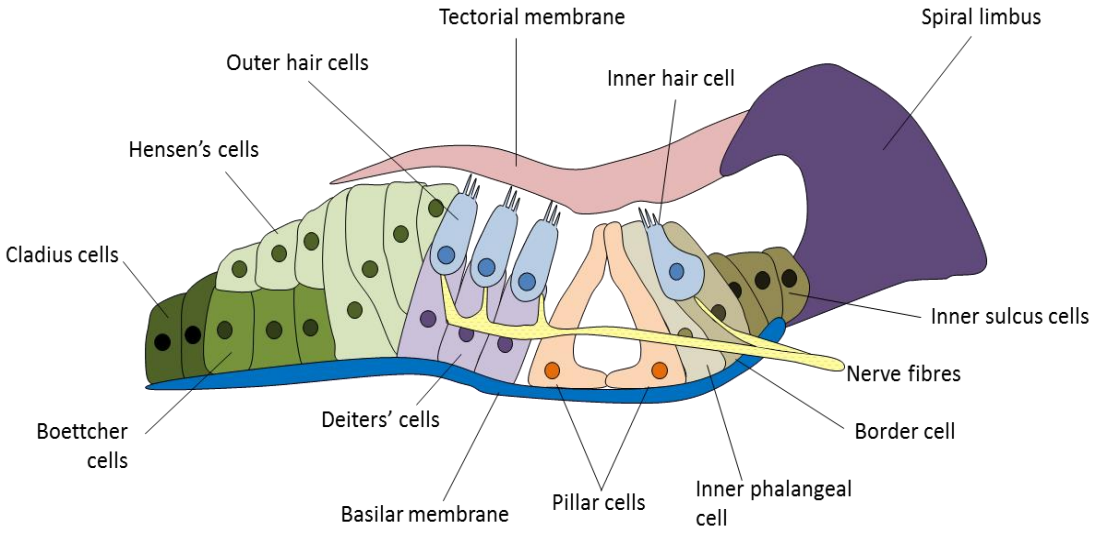

Figure 1.2: The organ of Corti.
The organ of Corti is located in the cochlea and contains one row of IHCs, three rows of OHCs and various supporting cells, all of which sit atop the basilar membrane. The specialised sensory hair cells are vital for detecting and transducing sound pressure waves passing through the cochlea. The Deiters' cells, Hensen's cells, Boettcher cells and Cladius cells neighbour the OHCs, whilst the inner phalangeal cells, border cells and inner sulcus cells support the IHCs. The spiral limbus is located alongside the inner sulcus cells and is involved in the formation of the tectorial membrane and potassium recycling in the cochlea.

On the apical surface of hair cells are bundles of actin-rich protrusions called stereocilia (Flock and Cheung, 1977, Tilney et al., 1980), which develop from microvilli on the cell

surface (Anniko, 1983, Tilney et al., 1992). Mature bundles have a highly organised pattern, with height increments between each of the three rows of stereocilia (Furness et al., 1989), giving a staircase-like appearance. In each developing bundle is a single kinocilium, which originates at the centre of the cell surface and migrates to the periphery during embryonic development. This process polarises the hair bundle and dictates hair bundle orientation (Denman-Johnson and Forge, 1999), resulting in a stepwise increase in stereocilia length towards the kinocilium (Furness et al., 1989, Forge et al., 1997). Although both IHC and OHC stereocilia bundles are graded in height, IHC stereocilia assemble into a linear pattern, whilst OHC stereocilia are organised in a 'W' shape (Lim, 1986). Fine filamentous structures called tip links connect the adjacent rows of stereocilia and play a role in the maintenance of hair bundle structure and sound transduction (see **1.1.3.3.**) (Pickles et al., 1984, Kachar et al., 2000).

IHCs function as the primary sensory receptors of the cochlea. Located at the basal, pre-synaptic 'active zone' of each IHC are electron-dense structures known as ribbons, which tether multiple (100+) vesicles containing the neurotransmitter glutamate (Figure 1.3) (Safieddine et al., 2012). This large 'readily-releasable' pool of vesicles enables rapid multi-vesicular exocytosis of glutamate onto afferent spiral ganglion nerve (SGN) fibres and facilitates fast, graded and sustained neurotransmission from the IHC during sound transduction (Glowatzki and Fuchs, 2002). Previous studies have shown that vesicular glutamate transporter type 3 (VGLUT3) and otoferlin are required for the accumulation of glutamate in synaptic vesicles and its exocytosis at the ribbon synapse (Obholzer et al., 2008, Roux et al., 2006, Ruel et al., 2008, Seal et al., 2008).

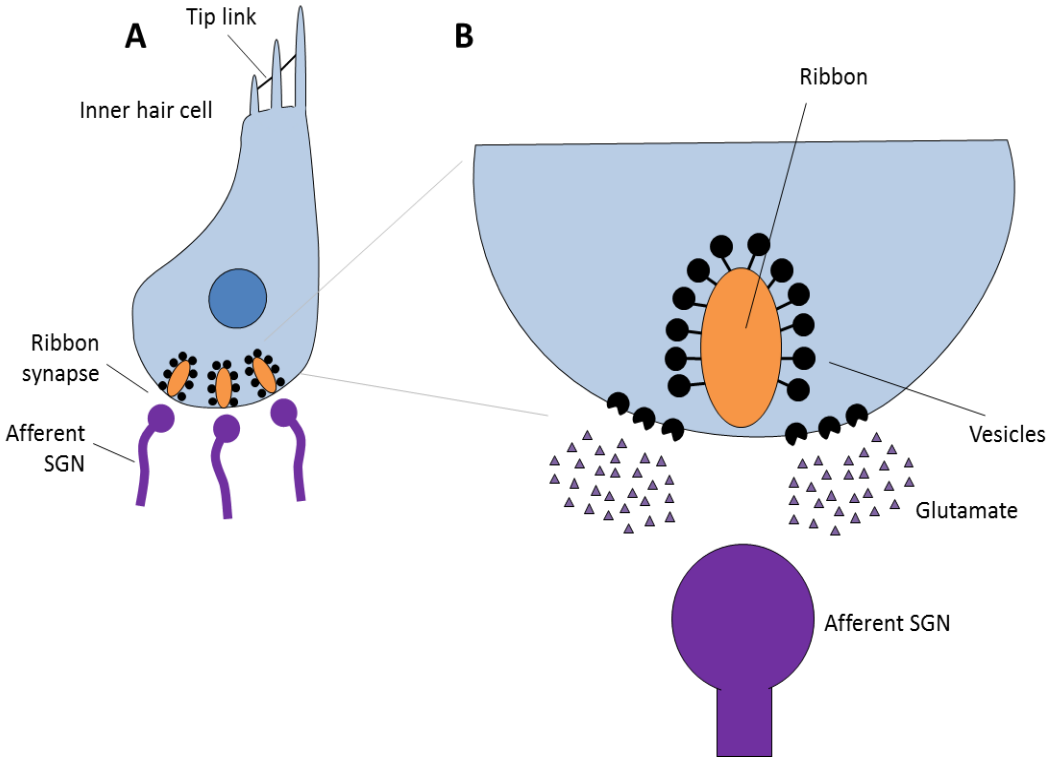

Figure 1.3: The inner hair cell ribbon synapse.
(A) Specialised ribbons are located at the basolateral aspect of IHCs and synapse with afferent SGN fibres. **(B)** Tethered to each ribbon are numerous vesicles containing glutamate neurotransmitter. During sound transduction, vesicles dock at the cell membrane and glutamate is exocytosed into the synaptic cleft. This multi-vesicular release of glutamate enables IHCs respond to stimulation with rapid, graded and sustained neurotransmission. SGN, spiral ganglion neuron.

OHCs boast a unique property which makes them distinct from IHCs, displaying oscillations in cell length during sound transduction. This phenomenon is known as somatic electromotility and is conferred by the intramembrane motor protein prestin (Figure 1.4) (Souter et al., 1995, Zheng et al., 2000a). Prestin is a member of the SLC26 anion transporter family (Mount and Romero, 2004), thought to predominantly function as an electrogenic chloride/bicarbonate exchanger (Mistrik et al., 2012, Muallem and Ashmore, 2006). As a result of allosteric interactions with intracellular chloride, prestin is able to modify its shape in a reversible, voltage-dependent manner (Oliver et al., 2001). Following OHC depolarisation, chloride ions bind prestin and trigger its contraction, whilst

hyperpolarisation is associated with release of chloride ions and elongation of prestin (Song and Santos-Sacchi, 2010). Mutating prestin in mice, either by targeted deletion or more subtle amino acid substitution, results in a loss of OHC electromotility and reduced cochlear sensitivity, corresponding to a hearing loss of 40 – 60 decibels of sound pressure level (dB SPL) (Liberman et al., 2002, Dallos et al., 2008). This has led to OHCs being deemed 'cochlear amplifiers', whose primary role is to amplify sound signals and enhance cochlear sensitivity by increasing movement within the organ of Corti during sound transduction (Ashmore, 1987, Dallos et al., 2006).

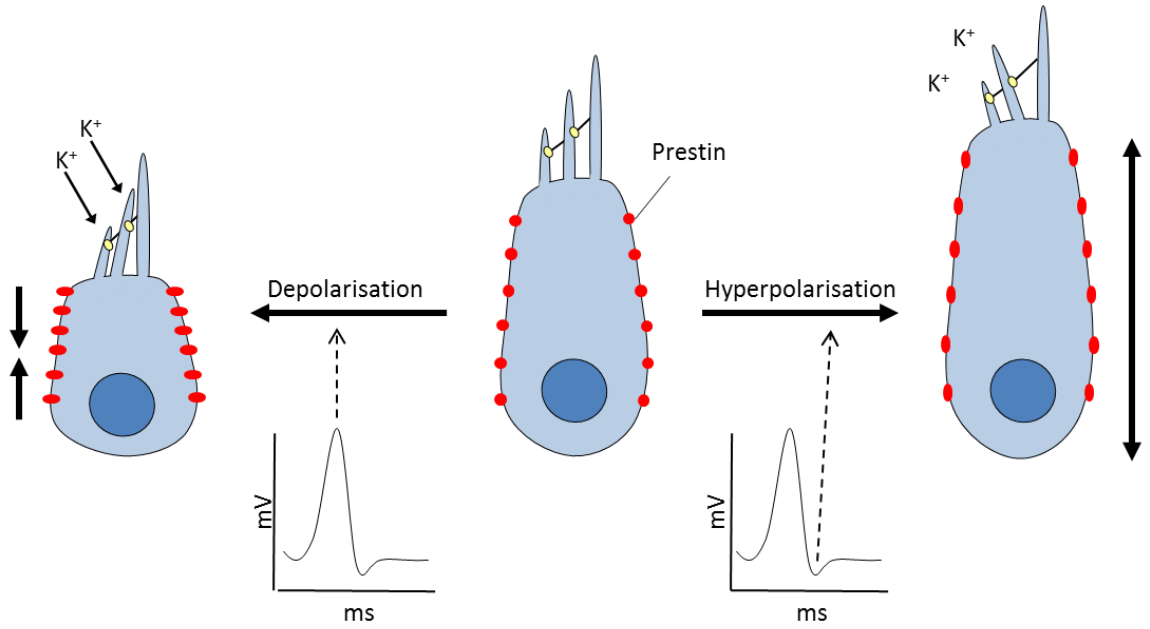

Figure 1.4: Outer hair cell electromotility.
OHCs are capable of oscillating in length during sound transduction, which enables them to function as cochlear amplifiers. This property is known as somatic electromotility and is conferred by the intramembrane protein prestin, which is unique to OHCs and undergoes conformational changes in response to depolarising and hyperpolarising currents. Following stereocilia deflection towards the kinocilium, potassium entry through mechanoelectrical transduction (MET) channels and depolarisation, prestin contracts and causes OHCs to shorten. When stereocilia deflect in the other direction, MET channels close and OHCs are hyperpolarised, causing prestin to elongate and OHCs to lengthen. K^+, potassium; ms, milliseconds; mV, millivolts.

IHCs and OHCs have distinct patterns of afferent and efferent innervation, which reflects their different roles in hearing. Each IHC is densely innervated with multiple afferent type I

SGNs, which comprise ~95% of the total SGN population (Dallos, 1992, Spoendlin, 1969) (Figure 1.5 A). Type I SGNs are large, unbranched, bipolar, myelinated neurons, which are densely packed with ribosomes, endoplasmic reticulum cisternae and Golgi bodies but contain few neurofilaments (Rosenbluth, 1962). Approximately 20 type I SGNs terminate on each IHC (Dallos, 1992, Spoendlin, 1972). As a result of this dense afferent innervation, IHCs rapidly transmit auditory information to the brain during sound transduction. A single lateral olivocochlear (LOC) efferent neuron, descending from the central auditory system, contacts the afferent fibres below the cell and mediates their excitability (Figure 1.5 A) (Groff and Liberman, 2003). LOC neurons are unmyelinated fibres, which originate in the lateral olivary nuclei of the super olivary complex in the brainstem, descend mostly ipsilaterally and are reported to be cholinergic, dopaminergic and γ-aminobutyric acid (GABA)ergic (Eybalin, 1993, Guinan, 1996).

In contrast to the IHCs, a single branching afferent type II SGN (~5% of the SGN population) synapses with numerous OHCs (Figure 1.5 B) (Forge and Wright, 2002). Unlike type I fibres, type II SGNs are unmyelinated and highly filamentous, with smaller cell bodies and fewer organelles (Rosenbluth, 1962). Type II SGNs also have enriched expression of the intermediate filament protein peripherin and the calcium-binding protein calbindin compared to type I fibres, but lower levels of calretinin (Hafidi, 1998, Liu and Davis, 2014). They are extensively branched, with a single type II SGN innervating around ten OHCs in basal regions of the cochlea and up to 50 OHCs in apical regions (Dallos, 1992, Simmons and Liberman, 1988). Both type I and type II SGNs project to the ipsilateral cochlear nucleus in the brainstem, exhibiting frequency-dependent bifurcations; apical, low frequency fibres

innervate ventral regions of the cochlear nuclei, whilst basal, high frequency fibres are distributed more dorsally (Nayagam et al., 2011).

Also in contrast to the IHCs, each OHC is directly innervated by a medial olivocochlear (MOC) efferent neuron (Wilson et al., 1991). These myelinated neurons originate in the medial olivary nuclei of the super olivary complex and descend mostly contralaterally towards the OHCs (Brown, 2014, Guinan, 1996). As a result, OHCs receive efferent feedback from the brain that influences their electromotility (Frolenkov, 2006). This not only enables OHCs to amplify cochlear mechanics (Dallos et al., 1997), but also helps to protect the cochlea from acoustic overstimulation and damage (Maison et al., 2002, Patuzzi and Thompson, 1991).

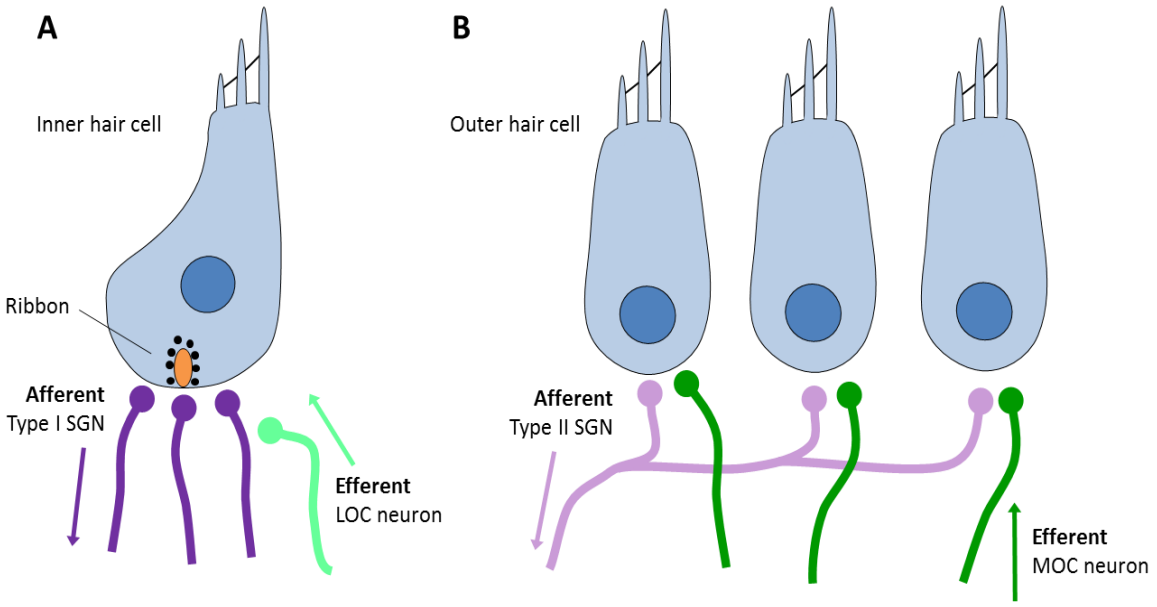

Figure 1.5: Hair cell innervation.
IHCs and OHCs display distinct innervation profiles, which reflect their different roles in auditory transduction. **(A)** Each IHC is directly innervated by multiple afferent type I SGN fibres, enabling rapid signalling to the central auditory system. A single efferent fibre from the LOC system contacts the afferent fibres below the cell. **(B)** Each OHC is innervated by a single afferent type II SGN, which branches within the organ of Corti to synapse with multiple other OHCs. MOC efferent fibres also directly contact each OHC, enabling modulation of OHC electromotility. LOC, lateral olivocochlear; MOC, medial olivocochlear; SGN, spiral ganglion neuron.

1.1.3.3. Non-Sensory Cells

Within the organ of Corti, the IHCs and OHCs are surrounded by a number of non-sensory, supporting cells (Figure 1.2). At the most lateral edge are the Claudius cells, which are in direct contact with the endolymph fluid of the scala media (Galic and Giebel, 1989). They have been shown to express aquaporin channels (Minami et al., 1998, Miyabe et al., 2002, Takumi et al., 1998), as well as the sodium-potassium-chloride co-transporter NKCC (Sakaguchi et al., 1998a), which suggests a role in mediating osmosis and ion homeostasis of the endolymph.

Neighbouring the Claudius cells are the Boettcher cells, which are located on the basilar membrane and are only present in the mid and basal turns of the cochlea (Kimura, 1975). In addition to the sodium-potassium-ATPase pump (Schulte and Steel, 1994), immunogold labelling has demonstrated that the Boettcher cells express high levels of the calcium-binding protein calmodulin (Nakazawa, 2001). As such, these cells have been suggested to mediate ion transport between the endolymph and perilymph fluid, as well as calcium regulation (Nakazawa, 2001).

Similarly to the Claudius cells, the Hensen's cells express aquaporin channels and are likely involved in mediating osmosis and the ionic balance of the endolymph (Minami et al., 1998, Miyabe et al., 2002, Takumi et al., 1998). Both the Hensen's cells and Deiters' cells, the latter of which are arranged in three rows beneath the OHCs, have been shown to express the growth factor heregulin (Zhang et al., 2002). This can bind to receptors on the IHCs, OHCs, pillar cells and SGNs and indicates an important role for these two cell types in supporting cellular proliferation and survival within the organ of Corti (Zhang et al., 2002). A cytoprotective function has also been proposed for the Hensen's cells and Deiters' cells,

owing to their noise-modulated expression of the enzyme cyclooxygenase-2 (COX-2); COX-2 is downregulated following exposure to intense sound stimulation (70 – 90 dB SPL tones at 8 kiloHertz (kHz) for 1 hour), which has been suggested to contribute to diminished cochlear sensitivity, thus providing a protective mechanism against acoustic trauma (Heinrich et al., 2006, Ziegler et al., 2004).

Between the three rows of OHCs and the single row of IHCs are two rows of pillar cells, which are comprised of thousands of parallel microtubules and actin filaments (Slepecky, 1996) and form the tunnel of Corti. By nature of their rigidity, the pillar cells provide mechanical support, coupling movement of the basilar membrane to movement of the entire organ of Corti (Forge and Wright, 2002), which ultimately leads to deflection of the hair cell stereocilia and transduction of sound signals. Pillar cells have also been shown to express nerve growth factor (NGF) and neurotrophin-3 (NT-3), the latter of which is also detected in the single row of inner phalangeal cells which neighbour the IHCs (Sobkowicz et al., 2002). The neuroglial inner phalangeal cells also express brain-derived neurotrophic factor (BDNF) and, together with the pillar cells, have been implicated in synaptogenesis and maintenance of the sensory IHCs (Sobkowicz et al., 2002).

Medial to the inner phalangeal cells are the border cells and the inner sulcus cells, both of which have been postulated to be involved in the endocytic removal of cellular debris that results from acoustic trauma or cell death (Hamernik et al., 1984, Taylor et al., 2012). As with the Claudius cells and Hensen's cells, the inner sulcus cells also express aquaporin channels (Miyabe et al., 2002, Takumi et al., 1998) and likely play a role in osmosis and ion homeostasis of the endolymph fluid.

Collectively, these non-sensory supporting cells also have important roles in potassium recycling (see **1.1.3.6.**), with the Cladius cells, Hensen's cells, Deiters' cells, border cells and inner sulcus cells expressing gap junction proteins connexin 26 and connexin 30 (Taylor et al., 2012).

Whilst not directly responsible for auditory transduction, the supporting cells play vital roles within the auditory system, as demonstrated by findings that mutations within the supporting cells leads to hearing loss. For example, knock-out of the collagen receptor discoidin domain receptor 1 in mice, which is expressed at high levels in the Deiters' cells and pillar cells, leads to detachment of the sensory epithelia from the basilar membrane, IHC degeneration and severe hearing loss (Meyer zum Gottesberge et al., 2008). Furthermore, mutations in connexin 26, which is expressed in a number of the supporting cells, are the most common cause of congenital hearing loss in the human population (Chang et al., 2003, Kemperman et al., 2002).

1.1.3.4. Sound Transduction in the Cochlea

In response to sound-induced pressure waves travelling through the perilymph fluid of the cochlea, the basilar membrane vibrates and subsequently causes movement of the hair cells which sit atop it (Tortora and Grabowski, 1993). This is accompanied by vibration of the tectorial membrane, which overlies the hair cells and is in direct contact with OHC stereocilia (Lim, 1986, Lukashkin et al., 2010). Together, these movements result in back-and-forth deflection of the hair cell stereocilia. Deflection towards the tallest row generates tension in the tip links and causes non-specific cation channels, known as the mechanoelectrical transduction (MET) channels, to open at the lower end of the tip links in the two shorter rows of stereocilia (Figure 1.6 A-B) (Assad et al., 1991, Beurg et al., 2009,

Gillespie, 1995). Although numerous candidates have been proposed as components of the MET channel complex over the past 20 years (Corey, 2006), recent data suggests a key role for the transmembrane channel-like 1 (TMC1) and 2 (TMC2) proteins (Kachar et al., 2015, Kawashima et al., 2011, Pan et al., 2013).

As a result of the large electrochemical gradient between the endolymph fluid (+80 mV) and the hair cells (-60 mV) (Hudspeth, 1989), potassium ions from the endolymph passively enter the hair cells through the open MET channels. This leads to rapid depolarisation of the hair cell, in a process known as mechanoelectrical transduction (Figure 1.6 B) (Shotwell et al., 1981). In the IHCs, depolarisation opens voltage-gated calcium channels and the resulting influx of calcium ions triggers multi-vesicular exocytosis of glutamate from the pre-synaptic ribbon into the synaptic cleft (Figure 1.6 C-D) (Beutner et al., 2001, Brandt et al., 2003, Hackney et al., 1996). Glutamate then binds α-amino-3-hydroxy-5-methylisoxazole-4-proprionic acid (AMPA) receptors at the post-synaptic density of afferent type I SGNs (Matsubara et al., 1996) and generates action potentials that transmit sensory information along the cochlear nerve to the central auditory system of the brain for processing.

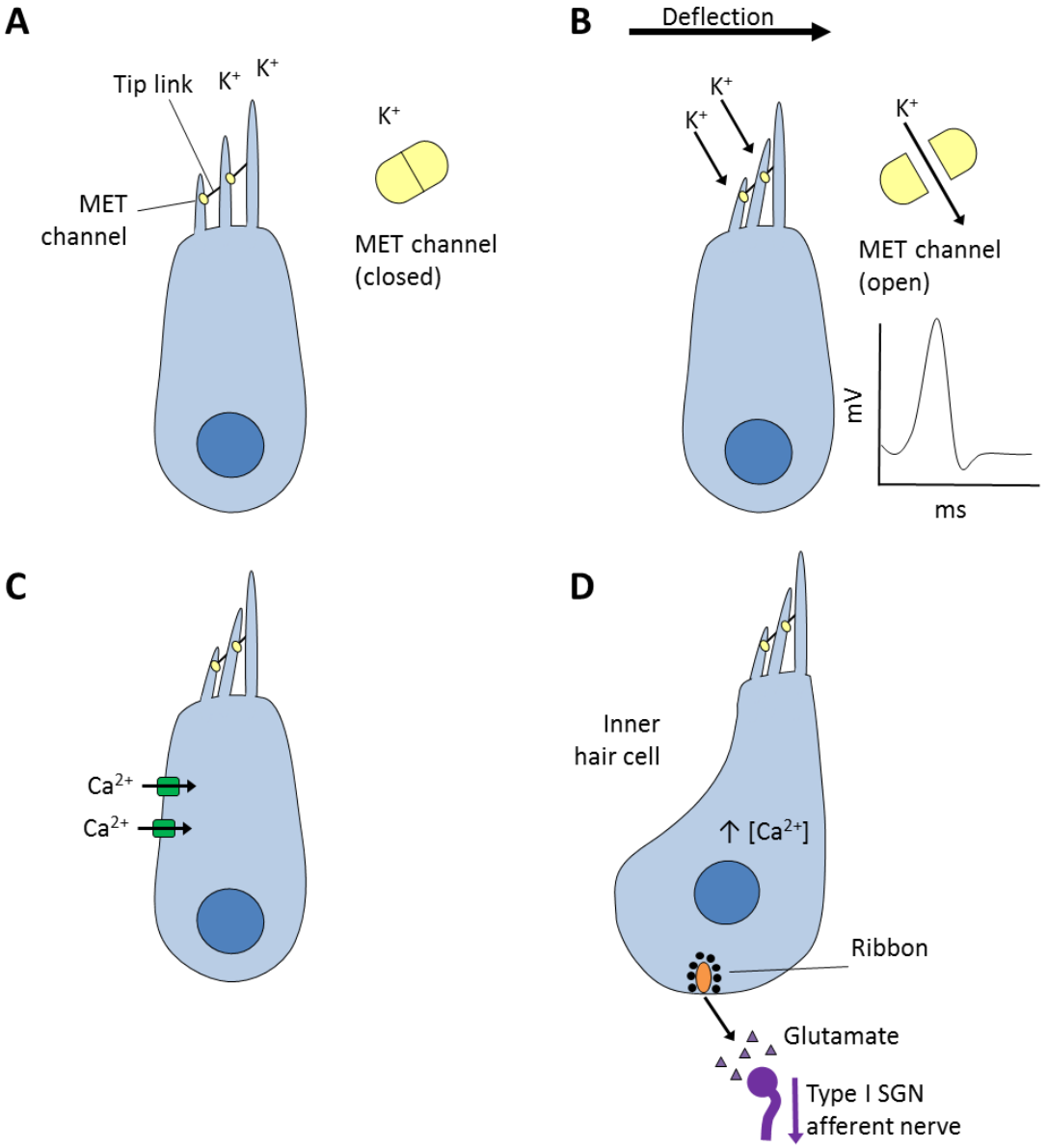

Figure 1.6: Hair cell mechanotransduction.
(A) Atop hair cells sit rows of stereocilia, which are connected by extracellular filaments known as tip links. Under resting conditions, tip links are relaxed and MET channels at the lower end of the tip link on the two shorter rows of stereocilia are closed. **(B)** In response to sound pressure waves passing through the cochlea, stereocilia deflect towards the kinocilium, generating tension in the tip links. This opens the MET channels and enables potassium ions to enter the hair cell from the endolymph, resulting in rapid depolarisation. **(C)** Following depolarisation, voltage-gated calcium channels open, allowing calcium influx into the hair cell. **(D)** In IHCs, this increase in intracellular calcium stimulates multi-vesicular release of glutamate from the ribbon synapse at the base of the cell, exciting afferent type I SGN fibres of the cochlear nerve and signaling to the central auditory system in the brain. Ca^{2+}, calcium; K^{+}, potassium, MET, mechanoelectrical transduction; ms, milliseconds; mV, millivolts; SGN, spiral ganglion neuron.

Previous work studying electrically stimulated LOC fibres has shown they have an important role in mediating the excitability of afferent type I SGNs and are able to enhance or suppress

their action potential firing independently of the OHCs (Groff and Liberman, 2003). This has been proposed to contribute to protection of the cochlear afferents from neural damage during acoustic overstimulation (Darrow et al., 2007), as well as accurate sound localisation, with the LOC system capable of modulating afferent responses from each ear independently in order to maintain binaural accuracy (Groff and Liberman, 2003).

In the OHCs, only a small amount of neurotransmitter is released in response to depolarising currents (Raphael and Altschuler, 2003). The main effect of depolarisation is rapid contraction of prestin, which shortens the cell body (Figure 1.4) (Brownell et al., 1985), thereby amplifying IHC deflection and enhancing IHC neurotransmission. Conversely, deflection of the hair bundle in the other direction, towards the shortest stereocilia, relaxes the tip links and closes the MET channels, preventing potassium influx and hyperpolarising the hair cells (Dabdoub et al., 2005). This lengthens the OHCs and halts neurotransmitter release from IHCs.

During auditory transduction, OHCs receive efferent feedback from the central auditory system that modulates their electromotility by influencing their voltage sensitivity and membrane stiffness (Dallos et al., 1997, Frolenkov et al., 2000, Frolenkov, 2006). The neurotransmitter acetylcholine is released from MOC efferent nerve fibres and binds to calcium-permeable α9α10 nicotinic receptors at the base of the OHC (Elgoyhen et al., 1994, Gomez-Casati et al., 2005) (Figure 1.7). This is followed by a brief influx of calcium into the cell, which causes small conductance calcium-activated potassium (SK) channels to open and rapid efflux of potassium (Figure 1.7) (Evans, 1996). This hyperpolarises the OHC and subsequently induces elongation of prestin, which lengthens the cell body. The acetylcholine-induced calcium increase also leads to phosphorylation of cytoskeletal

proteins, which decreases OHC axial stiffness and enhances electromotile responses (Dallos et al., 1997, Frolenkov et al., 2000, Sziklai et al., 2001). This efferent feedback enables OHCs to generate mechanical forces which amplify sound-induced vibrations within the cochlea in order to enhance cochlear sensitivity and aid in the detection of complex auditory information (Frolenkov, 2006).

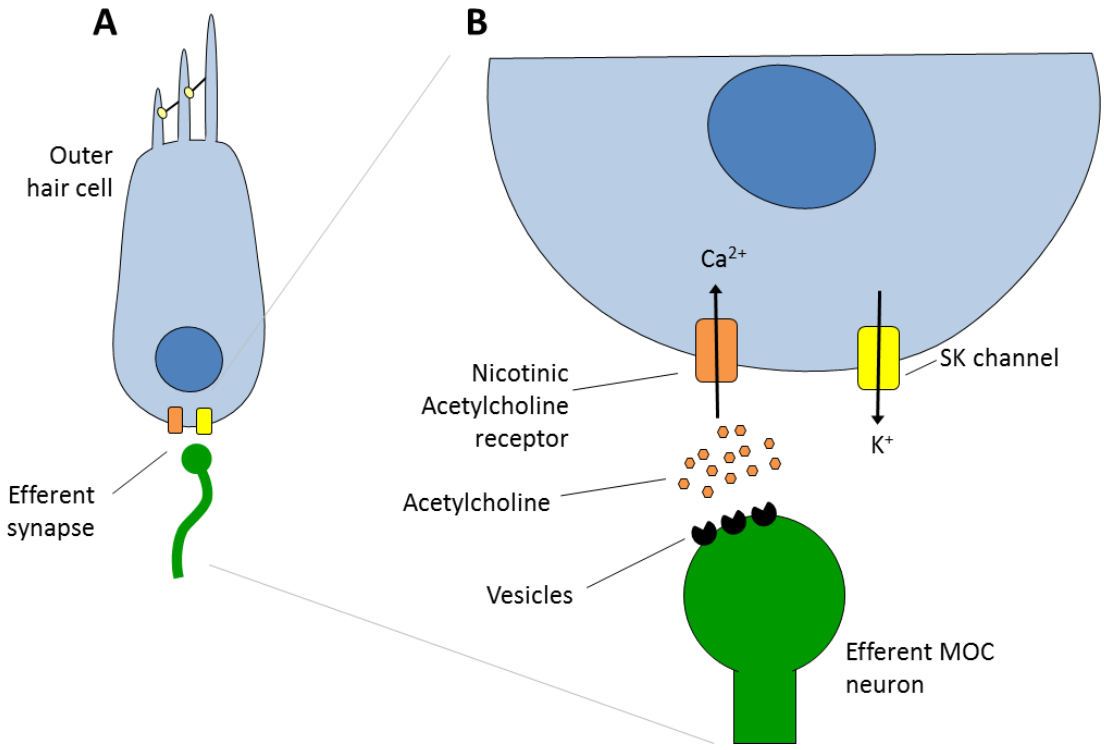

Figure 1.7: Cholinergic efferent feedback in outer hair cells.
(A) OHCs receive direct innervation from efferent neurons that descend from the central nervous system. **(B)** At the efferent synapse, acetylcholine is exocytosed from MOC efferent neurons and binds to calcium-permeable nicotinic α9α10 receptors on the basolateral surface of the OHC. Calcium ions then enter the OHC and activate SK channels, causing an efflux of potassium which hyperpolarises the cell and modulates prestin-driven electromotility. As a result of this cholinergic efferent feedback, OHCs can amplify cochlear mechanics and increase auditory sensitivity. Ca^{2+}, calcium; K^{+}, potassium; MOC, medial olivocochlear; SK, small conductance calcium-activated potassium.

The cochlea is a tonotopic structure, with basal regions responding to high frequency sounds and apical regions to low frequency sounds (von Békésy, 1954, von Békésy, 1955, von Békésy, 1960). In line with this, numerous specialisations have been identified along the

tonotopic axis of the cochlea: the thickness of the tectorial membrane increases from base to apex (Gueta et al., 2007), as does OHC length (Engel et al., 2006) and stereocilia length (Roth and Bruns, 1992, Kaltenbach and Falzarano, 1994); ribbon synapses of IHCs at basal regions are able to sustain greater vesicle release rates compared to those at the apex (Johnson et al., 2008); and the number of ribbon synapses per IHC peaks at the mid-cochlear region, where sensitivity to sound is greatest (Meyer et al., 2009).

1.1.3.5. The Central Auditory System

Following excitation of afferent cochlear nerve fibres, auditory information is transmitted from the cochlea to the cerebral cortex along the ascending pathway. Cochlear nerve fibres project to the cochlear nucleus, which is located in the brainstem and is divided into two regions – the dorsal cochlear nucleus and the ventral cochlear nucleus (Keele et al., 1982). These projections occur in a highly-organised manner, preserving the tonotopic organisation established in the cochlea; nerve fibres that originate from the apical portion of the cochlea and transmit low-frequency sounds primarily innervate ventral regions of the cochlear nuclei, whilst nerve fibres that originate from the basal portion of the cochlea and transmit high-frequency sounds primarily innervate dorsal regions (Fekete et al., 1984, Rouiller, 1997, Simon et al., 2009). Axons from the cochlear nuclei project to the super olivary complex both ipsilaterally and contralaterally via the trapezoid body (Mendoza, 2011). The super olivary complex, comprised of the lateral and medial olivary nuclei, detects and conveys information related to interaural time and intensity differences and is important for sound localisation (Harnischfeger et al., 1985, Moore, 2000). From here, auditory information is transmitted primarily to the lateral lemniscus in the brainstem and the inferior colliculus in the midbrain (Oliver, 2000, Roth et al., 1978) and then on to the medial geniculate body in

the auditory thalamus (Aitkin and Phillips, 1984, Kudo and Niimi, 1978). This, in turn, relays information to the primary auditory cortex in the cerebral cortex, again in a tonotopic manner (Merzenich et al., 1975, Reale and Imig, 1980). Together, these complex structures converge information from the left and right ears and are responsible for detecting and interpreting the fundamental properties of sound, such as frequency, loudness, timing, pitch and rhythm (Emslie-Smith et al., 1988).

In contrast to the ascending pathway, the descending pathway transmits information from the auditory cortex to the cochlear nuclei and is important for modulating the initial processing of acoustic information in the brain (Schofield and Cant, 1999). Previous work has also shown that descending projections of cortical layer V pyramidal neurons to the inferior colliculus are essential for mediating adaptive, learning-induced auditory plasticity (Bajo et al., 2010).

1.1.3.6. Potassium Recycling

Following hair cell depolarisation, the EP must be regenerated in order to bring hair cells back to an excitatory state (Wangemann, 2002). This is achieved by lateral and medial potassium recycling throughout the cochlea (Figure 1.8 A and Figure 1.9) (Kikuchi et al., 2000, Nin et al., 2008). In the lateral recycling pathway, potassium ions which have entered the OHCs from the endolymph diffuse out via the voltage-gated KCNQ4 channel located at the basal membrane of the cell (Kubisch et al., 1999) into the extracellular space of the organ of Corti (Figure 1.8 B). Potassium ions are then taken up by the supporting cells via the potassium-chloride co-transporters KCC3 (Boettger et al., 2003) and KCC4 (Boettger et al., 2002, Zhu and Zhao, 2010) and pass through a network of gap junctions to the fibrocytes of the spiral ligament. Connexin 26 (Kikuchi et al., 1995, Lautermann et al., 1998) and

connexin 31 (Xia et al., 2000) are components of this gap junction system. The transcription factor POU domain class 3 transcription factor 4 (POU3F4) has been found to be vital for maintaining fibrocyte cell-cell contacts (Minowa et al., 1999), thereby enabling potassium recycling. Potassium ions then enter the marginal cells of the stria vascularis via the sodium-potassium-ATPase pump (Iwano et al., 1989, Offner et al., 1987) and sodium-potassium-chloride co-transporter NKCC1 (Crouch et al., 1997), both expressed on the basolateral membrane (Figure 1.8 C). Also present are heteromeric chloride channels, formed by ClC-K and its essential β-subunit Barttin, which enable basolateral efflux of the chloride ions which enter the cell through NKCC1 (Kobayashi et al., 2002, Estevez et al., 2001). The accumulating potassium ions in the marginal cells flow back into the endolymph through a channel at the apical surface formed by KCNQ1 (Neyroud et al., 1997) and KCNE1 (Vetter et al., 1996), completing the cycle.

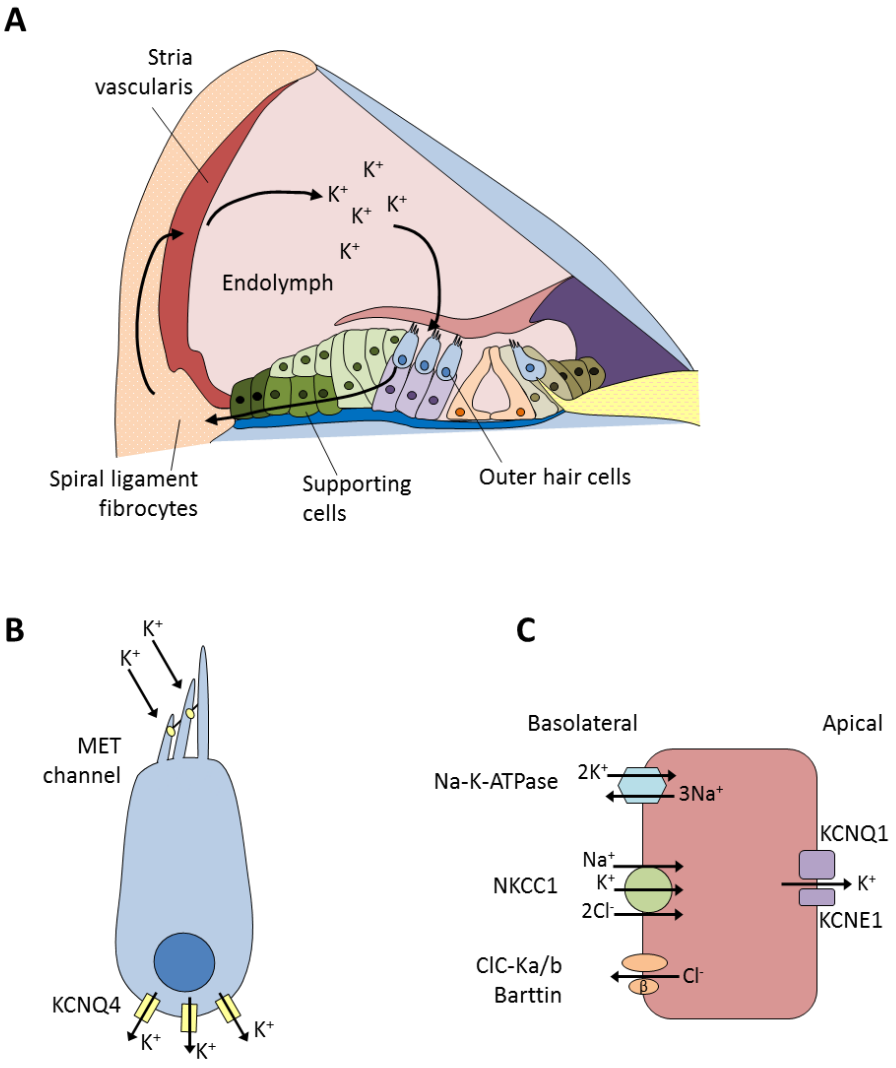

Figure 1.8: Lateral potassium recycling in the cochlea.
(A) In order to maintain the EP of the cochlea, a lateral recycling pathway returns potassium ions from the OHCs back into the endolymph fluid, via the supporting cells, spiral ligament and stria vascularis. **(B)** Following potassium entry through the MET channel and OHC depolarisation, potassium ions exit the OHC at the basal surface through the voltage-gated KCNQ4 channel. **(C)** After being transported through the supporting cells in the organ of Corti and fibrocytes in the spiral ligament, potassium ions enter the marginal cells of the stria vascularis through the Na-K-ATPase pump and NKCC1 co-transporter. Along with the ClC-K/Barttin channel, these enable potassium entry by coupling it with the movement of other ions (sodium and chloride) across the basolateral cell membrane. Finally, potassium ions re-enter the endolymph through a channel formed by KCNQ1 and KCNE1 at the apical surface of the marginal cell. Cl^-, chloride; K^+, potassium; MET, mechanoelectrical transduction; Na^+, sodium.

In the medial recycling pathway, potassium ions from the IHCs diffuse through a network of gap junctions in the neighbouring border cells and inner sulcus cells to the fibrocytes of the spiral limbus (Spicer and Schulte, 1998) (Figure 1.9). Potassium ions then enter the interdental cells of the spiral limbus through a basolateral sodium-potassium-ATPase pump and are returned to the endolymph through apical potassium channels, as in the lateral pathway (Spicer and Schulte, 1998).

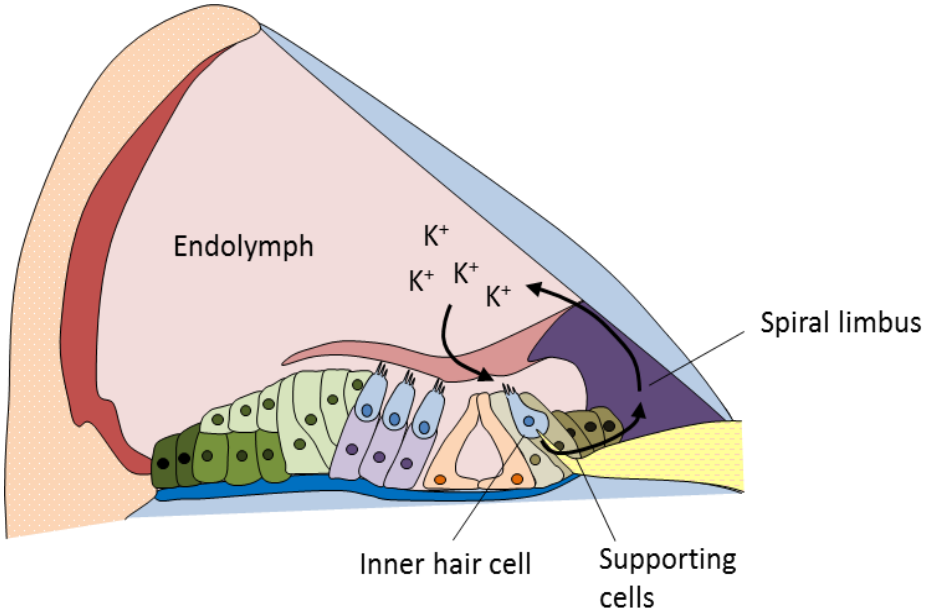

Figure 1.9: Medial potassium recycling in the cochlea.
In order to maintain the EP of the cochlea, a medial recycling pathway returns potassium ions from the IHCs back into the endolymph fluid, via the supporting cells and spiral limbus. Following potassium entry through the MET channel and IHC depolarisation, potassium ions exit the IHC at the basal surface and diffuse through a network of gap junctions in the neighbouring supporting cells and fibrocytes of the spiral limbus. Potassium ions are then transported through interdental cells of the spiral limbus via a basolateral Na-K-ATPase pump and apical potassium channels to re-enter the endolymph. K^+, potassium.

Together, these recycling pathways regenerate the high concentration of potassium ions in the endolymph, re-establishing the EP and bringing hair cells back to an excitatory state. Many of the proteins involved in potassium recycling have been implicated in deafness in both mice and humans, stressing the importance of potassium recycling in hearing:

mutations in connexin 26 are the most common cause of congenital hearing loss in humans (Chang et al., 2003, Kemperman et al., 2002); mutations in KCNQ4 cause DFNA2 in humans, a form of non-syndromic hearing loss (Kubisch et al., 1999); inactivation of NKCC1 through disruption of the *Slc12a2* gene results in decreased endolymph secretion and deafness in mice (Delpire et al., 1999); inner ear-specific deletion of Barttin causes a decrease in EP and profound hearing loss in mice (Rickheit et al., 2008); mutations in ClC-K and Barttin in humans cause sensorineural deafness associated with Bartter syndrome (Birkenhager et al., 2001, Schlingmann et al., 2004); KCNE1 null mice exhibit hair cell degeneration and spiral ganglion cell death, with marginal cells failing to secrete potassium ions (Vetter et al., 1996) and finally mutations in KCNQ1 and KCNE1 in humans cause hearing loss associated with Jervell and Lange-Nielsen syndrome (Neyroud et al., 1997, Tyson et al., 1997).

1.2. Development of the Inner Ear

The inner ear arises during embryonic development from a thickening of ectodermal tissue known as the otic placode (Noramly and Grainger, 2002). A detailed morphological study of mouse inner ear development using paint-fill techniques by Morsli et al. (1998) has revealed numerous morphological changes that occur during embryonic development; at embryonic day (E) 9.5, the otic placode invaginates to form the otocyst, from which the cochlear duct and endolymphatic duct project at E10.5. The cochlear duct then begins to coil at E12 and reaches $1^3/_4$ turns by E15 and the semi-circular canals have formed by E13. Within the developing cochlea, otocyst cells are multi-potent and can develop into pro-sensory, pro-neural or non-sensory lineages (Moody, 2014), ultimately giving rise to the myriad of cell types in the inner ear.

1.2.1. Sensory Cell Fate Specification

Both hair cells and supporting cells are derived from common pro-sensory progenitor cells. A number of molecular markers have been used to identify the positions of developing sensory patches and thus the origins of the inner ear sensory structures (Figure 1.10). One such marker is sex determining region Y-box 2 (SOX2), which is expressed in the otic placode (Uchikawa et al., 1999) and required for development of the pro-sensory domain, hair cells and supporting cells (Kiernan et al., 2005). Also required for the development of sensory cells is fibroblast growth factor receptor 1 (FGFR1). Hypomorphic mutation or deletion of *Fgfr1* results in disruption of the organ of Corti and severe hair cell loss, primarily caused by diminished proliferation of sensory precursor cells (Pirvola et al., 2002). Notch homologue 1 (NOTCH1) and jagged 1 (JAG1) are also considered pro-sensory markers and loss of JAG1 leads to smaller sensory progenitor regions (Pan et al., 2010) and reduced numbers of hair cells (Kiernan et al., 2001). Similarly, lunatic fringe (LFNG), bone morphogenetic protein 4 (BMP4), hairy/enhancer-of-split related with YRPW motif 1 and 2 (HEY1 and HEY2) are markers of developing sensory patches, though are ultimately restricted to supporting cells (Doetzlhofer et al., 2009, Li et al., 2008, Morsli et al., 1998). T-box protein 1 (TBX1) also serves as a pro-sensory marker in the cochlea, required for sensory cell development and suppression of neurogenesis (Raft et al., 2004). These molecules are involved in sensory cell fate specification, directing multi-potent otocyst cells to develop along the pro-sensory lineage path, and analysis of their expression has helped characterise the processes involved in inner ear development.

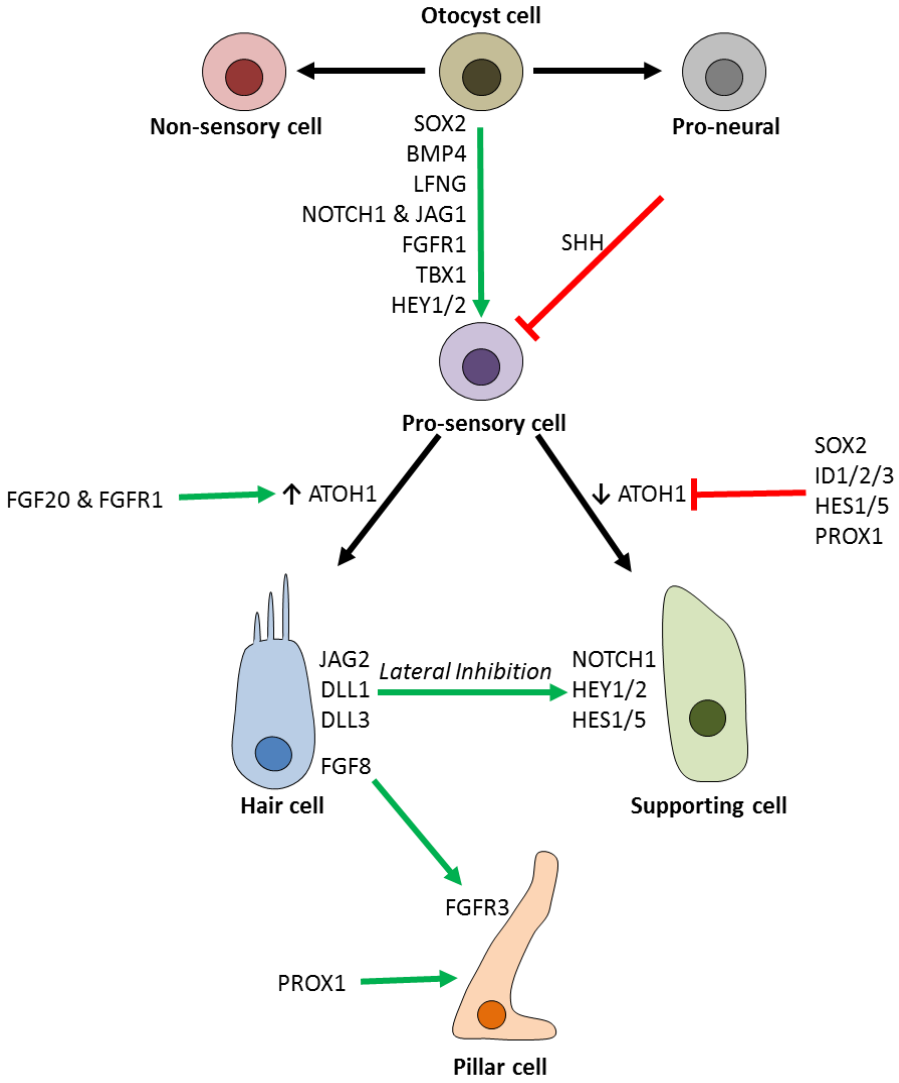

Figure 1.10: Summary of cell fate specification in the developing cochlea.
Green arrows indicate activation, red lines indicate inhibition. Multipotent otocyst cells can give rise to non-sensory, pro-sensory or pro-neural lineages in order to generate the multiple cell types within the cochlea. Numerous factors have been identified that drive otocyst cells towards a pro-sensory fate, including SOX2, NOTCH1, JAG1 and TBX1, whilst SHH is known to inhibit pro-sensory development. Both hair cells and supporting cells of the organ of Corti develop from pro-sensory cells, in a process that is dependent on expression of transcription factor ATOH1. FGF20 and FGFR1 induce ATOH1 expression and drive pro-sensory cells towards a hair cell fate. Developing hair cells then prevent a similar cell fate in neighbouring cells through Notch-mediated lateral inhibition. Briefly, developing hair cells express JAG2, DLL1 and DLL3, which activates NOTCH1, HEY1, HEY2, HES1 and HES5 in surrounding cells. The HES proteins, along with SOX2, ID1, ID2 and ID3 downregulate ATOH1, preventing these cells from committing to a hair cell fate and instead enabling them to differentiate into supporting cells. FGF8 in developing hair cells also activates FGFR3 in a subset of surrounding cells to promote a pillar cell differentiation. Adapted from Driver and Kelley (2009) and Kelley (2007). ATOH1, atonal homologue 1; BMP4, bone morphogenetic protein 4; DLL1, delta-like ligand 1; DLL3, delta-like ligand 3; FGF8, fibroblast growth factor 8; FGF20, fibroblast growth factor 20; FGFR1, fibroblast growth factor receptor 1; FGFR3, fibroblast growth factor receptor 3; HES1/5, hairy and enhancer of split 1 and 5; HEY1/2, hairy/enhancer-of-split related with YRPW motif 1 and 2; ID1/2/3, inhibitors of differentiation proteins 1, 2 and 3; JAG1, jagged 1; JAG2, jagged2; LFNG, lunatic fringe; NOTCH1, notch homologue 1; PROX1, prospero homeobox 1; SHH, sonic hedgehog; SOX2, sex determining region Y-box 2; TBX1, T-box protein 1.

At E13, pro-sensory cells localise to a narrow band that extends the length of the cochlear duct and will eventually become the organ of Corti, the sensory organ of the cochlea (Morsli et al., 1998). Between E12 and E14, over 80% of these progenitor cells exit the cell cycle and become post-mitotic (Ruben, 1967). This forms a zone of non-proliferating cells (ZNPC), which serves to limit the number of cells within the pro-sensory domain and is due to the activity of $p19^{Ink4d}$, $p21^{Cip1}$ and $p27^{Kip1}$. Deletion of these cyclin-dependent kinase inhibitors causes cell cycle re-entry, continued proliferation of pro-sensory cells and supernumerary hair cells and supporting cells (Chen and Segil, 1999, Laine et al., 2007, Lowenheim et al., 1999). The formation of the pro-sensory domain is also regulated by the hedgehog signalling pathway, with the sonic hedgehog (SHH) ligand repressing pro-sensory cell fate (Driver et al., 2008). Post-mitotic differentiation into the various sensory cell types of the organ of Corti then starts at E15 in the mid-basal region of the cochlea, extending bi-directionally (Sher, 1971).

1.2.1.1. Lateral Inhibition

Hair cell and supporting cell fate is specified by a process called lateral inhibition. This is a specialised cell-cell interaction, whereby one cell prevents an identical cell fate in its neighbour during cell division (Lewis, 1998), and is dependent on the helix-loop-helix transcription factor atonal homologue 1 (ATOH1) (Figure 1.11).

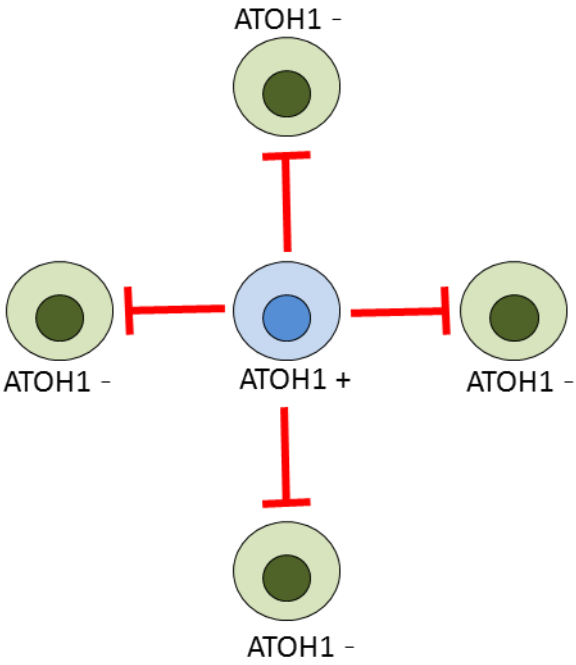

Figure 1.11: Overview of lateral inhibition.
Lateral inhibition is a unique cell-cell interaction, whereby one cell inhibits an identical developmental fate in its neighbour. In the organ of Corti, ATOH1-positive developing hair cells repress ATOH1 expression in adjacent cells, which prevents them from adopting a hair cell fate and enables differentiation into supporting cells. ATOH1, atonal homologue 1.

ATOH1 is expressed in pro-sensory patches of the cochlear duct from E13 (Lanford et al., 2000) in basal-to-apical and medial-to-lateral gradients (Woods et al., 2004) and ultimately becomes restricted to hair cells (Chen et al., 2002, Lumpkin et al., 2003). Genetic manipulation of *Atoh1* has helped characterise its role in the ear; ATOH1-null mice fail to generate hair cells (Bermingham et al., 1999), whilst overexpression of ATOH1 causes supernumerary hair cells (Zheng and Gao, 2000) and forced, ectopic expression outside of the pro-sensory domain induces hair cell fate (Woods et al., 2004). Together, these data indicate that ATOH1 is essential for hair cell development. Furthermore, the intensity and temporal pattern of ATOH1 has been found to contribute to inner and outer hair cell fate specification (Jahan et al., 2013, Pan et al., 2012), as overexpressing ATOH1 transforms OHCs into IHCs (Jahan et al., 2010). Studies into the transcriptional network of ATOH1 have

revealed that it regulates barH-like 1 (*Barhl1*), growth factor independent 1 (*Gfi1*), microRNA 96 (*miR-96*) and POU domain class 4 transcription factor 3 (*Pou4f3*) (Chellappa et al., 2008, Hertzano et al., 2004, Jahan et al., 2012, Masuda et al., 2011). POU4F3 subsequently activates transcription factor LIM homeobox 3 (*Lhx3*) (Hertzano et al., 2007), which is expressed specifically in hair cells during differentiation (Hume et al., 2007). Loss of each of these downstream target genes results in degeneration or arrested development of hair cells (Erkman et al., 1996, Kuhn et al., 2011, Li et al., 2002, Wallis et al., 2003), demonstrating that ATOH1 regulates genes that are crucial for hair cell development and maintenance. ATOH1 itself is induced by fibroblast growth factor 20 (FGF20) and FGFR1 signalling, with ATOH1 expression reduced as a consequence of inhibited FGF signalling (Hayashi et al., 2008b).

Lateral inhibition is mediated by Notch signalling (Figure 1.10); developing hair cells express Notch ligands jagged 2 (JAG2), delta-like ligand 1 (DLL1) and delta-like ligand 3 (DLL3) (Hartman et al., 2007, Lanford et al., 1999, Morrison et al., 1999), which activate NOTCH1 in surrounding progenitor cells (Murata et al., 2006). Downstream targets of NOTCH1, hairy and enhancer of split 1 and 5 (HES1 and HES5), HEY1 and HEY2 become active in these surrounding cells and downregulate ATOH1 (Doetzlhofer et al., 2009, Zheng et al., 2000b, Zine et al., 2001), thus preventing differentiation into hair cells. SOX2 and inhibitors of differentiation proteins ID1, ID2 and ID3 also inhibit ATOH1-induced hair cell differentiation (Dabdoub et al., 2008, Jones et al., 2006). This loss of hair cell commitment enables neighbouring cells to develop as supporting cells. The importance of Notch signalling in sensory cell differentiation in the cochlea is supported by data that show inhibiting Notch

signalling *in vitro* severely reduces the number of differentiated hair cells and supporting cells (Hayashi et al., 2008a).

Prior to cell differentiation, Notch target genes are expressed throughout the cochlea pro-sensory domain. As hair cell differentiation commences, they become restricted to supporting cells so that HES1 and HEY1 define Hensen's cells, HES5 and HEY1 define Deiters' cells and HEY2 defines pillar cells (Doetzlhofer et al., 2009, Li et al., 2008).

Also important in pillar cell specification is prospero homeobox 1 (PROX1) (Bermingham-McDonogh et al., 2006), which represses ATOH1 and GFI1 thus antagonising a hair cell phenotype (Kirjavainen et al., 2008), and FGFR3. FGFR3 is initially expressed at E16 in a region of the cochlea that corresponds to the developing organ of Corti, though is restricted solely to pillar cells by P0 (Mueller et al., 2002). The continuous activation of FGFR3, which is required for pillar cell development, is induced by FGF8 expression from adjacent developing hair cells (Jacques et al., 2007). Deletion of FGFR3 or blocked binding between FGFR3 and FGF8 results in absence of pillar cells, failed tunnel of Corti formation and profound hearing loss (Colvin et al., 1996, Puligilla et al., 2007).

Following terminal differentiation at ~E14.5, NOTCH1 is downregulated in supporting cells (Murata et al., 2006) and quiescence of sensory cells is maintained by the ongoing expression of cyclin-dependent kinase inhibitors, as well as the expression of retinoblastoma protein (Weber et al., 2008) and suppression of cyclin D1 (Laine et al., 2010).

1.2.2. Neural Cell Fate Specification

Cell migration studies in the developing ear have shown that neuroblasts in the otocyst begin to form the cochleovestibular ganglion at E10.5 and by E13.5, developing neurons

have extended dendritic projections that will go on to contact hair cells in the organ of Corti (Carney and Silver, 1983). BDNF and NT-3 are expressed in the otocyst (Staecker et al., 1996) and are involved in this process, supporting the development of afferent innervation of the inner ear (Fritzsch et al., 1999). BDNF has been shown to promote survival of spiral ganglion cells in the developing cochlea (Leake et al., 2011) and addition of BDNF and NT-3 to cochleovestibular ganglion explants induces neurite outgrowth (Pirvola et al., 1992). Furthermore, antagonising BDNF expression in the otocyst impairs neuritogenesis and results in neuronal cell death and a reduced neuronal population of the cochleovestibular ganglion, whilst inhibition of NT-3 leads to random neurite outgrowth (Staecker et al., 1996). BDNF ultimately becomes restricted to sensory cells of the cochlea and NT-3 to sensory cells and supporting cells (Pirvola et al., 1992).

1.2.3. Non-Sensory Cell Fate Specification

Non-sensory cells of the otocyst give rise to the non-sensory structures of the inner ear, including the stria vascularis, Reissner's membrane and spiral ligament. Non-sensory development is partly regulated by LIM homeobox transcription factor 1 alpha (LMX1A), which is restricted to non-sensory epithelia after broad initial expression throughout the otic placode (Nichols et al., 2008) and is required for maintaining sensory and non-sensory domains (Koo et al., 2009). POU3F4 is also vital for the development of mesenchymal tissues in the inner ear, including the spiral limbus, scala tympani and the fibrocytes of the spiral ligament, with mutations in POU3F4 leading to hypoplasia of these structures (Phippard et al., 1999).

1.2.4. Hair Cell Maturation

Both IHCs and OHCs arise from common sensory progenitor cells, which are driven towards a hair cell fate by ATOH1-dependent lateral inhibition and the combined expression of the transcription factors GFI1 and POU4F3 (Bermingham et al., 1999, Costa et al., 2015, Wallis et al., 2003, Xiang et al., 1998). Subsequent hair cell subtype-specific differentiation and maturation occurs between terminal mitosis at E14.5 and the onset of hearing, which occurs at around postnatal day (P) 12 in the mouse (Ehret, 1976). Although IHCs and OHCs are recognisable by their differing hair bundle morphology and location within the organ of Corti as early as E15 (Lim and Anniko, 1985), their biophysical characteristics are essentially indistinguishable during embryonic development (Housley et al., 2006, Marcotti, 2012). After birth (P0), immature hair cells undergo distinct morphological and physiological developmental programmes that ultimately give rise to functionally mature IHCs by ~P12 and OHCs by ~P8 (Marcotti et al., 1999, Marcotti and Kros, 1999). The initial physiological development of IHCs and OHCs at P0 requires *miR-96* (Kuhn et al., 2011), which regulates a number of genes that are essential for proper hair cell maturation and function, including protein tyrosine phosphatase receptor Q and the OHC-specific genes *Slc26a5* (which encodes prestin) and oncomodulin (Goodyear et al., 2003, Lewis et al., 2009, Liberman et al., 2002, Sakaguchi et al., 1998b, Wallis et al., 2003).

1.2.4.1. Stereocilia Development

Stereocilia bundles first appear at E13.5 as unpolarised microvilli on the apical surface of hair cells (Denman-Johnson and Forge, 1999) which, following translocation of the central kinocilium to the periphery of the cell surface, begin to elongate and thicken. This is dependent on several stereociliary proteins that are required for actin polymerization and

the graded elongation of stereocilia, including the actin-binding proteins espin and twinfilin2, epidermal growth factor receptor pathway substrate 8 (EPS8), myosin 7a, myosin 15a and scaffolding protein whirlin (Belyantseva et al., 2003, Kikkawa et al., 2005, Peng et al., 2009, Rzadzinska et al., 2009, Zampini et al., 2011, Zheng et al., 2000c). The actin-binding protein gelsolin and the scaffolding proteins p55 and 4.1R are also involved exclusively in the development of OHC stereocilia (Mburu et al., 2006, Mburu et al., 2010). The activity of these proteins results in the characteristic staircase pattern of stereocilia, with stepwise increases in length towards the kinocilium (Forge et al., 1997). This staircase pattern is evident from P1 and stereocilia development is complete by P7 (Anniko, 1983).

1.2.4.2. Electrophysiological Maturation

The electrophysiological properties and ion channel repertoire of IHCs and OHCs are initially similar throughout embryonic development and only begin to diverge from birth (P0) (Figure 1.12) (Kuhn et al., 2011). Prior to the onset of hearing, immature IHCs express the inward calcium current I_{Ca} (Platzer et al., 2000), sodium current I_{Na} (Marcotti et al., 2003b) and the inward rectifier potassium current I_{K1} (Marcotti et al., 2003a), which causes them to exhibit slow voltage responses and fire spontaneous action potentials (Kros et al., 1998, Marcotti et al., 2003a). Although these slow, spontaneous action potentials are involved in the maturation of synaptic connections (Zhang and Poo, 2001) and exocytosis-induced activation of the auditory pathway (Beutner and Moser, 2001), they are unsuitable for the transduction of high-frequency sounds, which require rapid and graded receptor potentials (Kros et al., 1998). At P12, a rapidly-activating large-conductance calcium-activated potassium current, known as $I_{K,f}$, and the negatively-activating delayed rectifier potassium current $I_{K,n}$, conferred by KCNQ4 (Kharkovets et al., 2000), prevent these action potentials

and reduce the membrane time constant of IHCs (Kros et al., 1998, Marcotti et al., 2003a, Marcotti et al., 2004). Together, these currents enable IHCs to respond to sound with fast, graded voltage responses and so are critical for the maturation of immature IHCs into functional, excitatory sensory receptors (Marcotti et al., 2003a).

Prior to functional maturation, OHCs also express I_{Ca} (Michna et al., 2003), I_{Na} (Oliver et al., 1997) and I_{K1} (Marcotti et al., 1999), as well as the outward potassium current $I_{K,neo}$ (Marcotti and Kros, 1999). At ~P8, functional maturity is reached as OHCs downregulate I_{K1} and $I_{K,neo}$ (Marcotti et al., 1999, Marcotti and Kros, 1999) and express $I_{K,n}$ (Housley and Ashmore, 1992). This coincides with increased expression of prestin, the intramembrane OHC motor protein (Souter et al., 1995, Zheng et al., 2000a) and the resulting onset of electromotility (He et al., 1994).

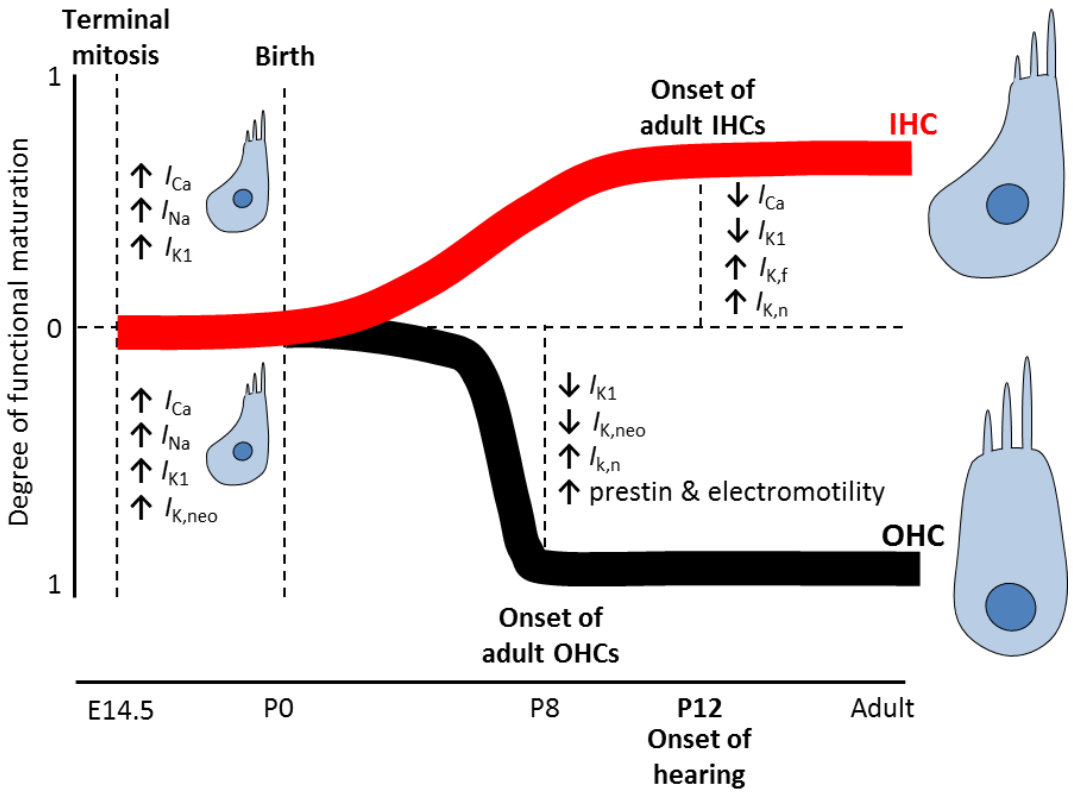

Figure 1.12: Functional maturation of inner hair cells and outer hair cells in the mammalian cochlea.
During embryonic development, immature IHCs and OHCs have a similar repertoire of ion channels and membrane currents, making them electrophysiologically indistinguishable (indicated by '0'). After birth, they begin to diverge in terms of their size, shape and electrophysiological properties in order to become fully differentiated and functionally mature (indicated by '1') prior to the onset of hearing at around P12. This involves the downregulation (↓) and expression (↑) of distinct membrane currents in each hair cell subtype, as well as the expression of prestin and the onset of electromotility in OHCs, and results in functionally mature IHCs by ~P12 and OHCs by ~P8. Adapted from Kuhn et al. (2011). I_{Ca}, inward calcium current; I_{K1}, inward rectifier potassium current; $I_{K,f}$, rapidly-activating large-conductance calcium-activated potassium current; $I_{K,n}$, negatively-activating delayed rectifier potassium current; $I_{K,neo}$, outward potassium current; I_{Na}, inward sodium current; E, embryonic day; IHC, inner hair cell; OHC, outer hair cell; P, postnatal day.

1.2.4.3. Hair Cell Innervation

The innervation patterns of IHCs and OHCs are also largely indistinguishable during embryonic development and begin to diverge after birth, with postnatal reorganisation of afferent and efferent nerve fibres. Between E14.5 and E18.5, following terminal mitosis, immature neurons concentrate around the base of the hair cells and form the first synaptic-like contacts (Sobkowicz, 1992). Initially, afferent type I SGNs project and form ribbon

synapses with both the IHCs and OHCs, before withdrawing from the OHCs between P3 and P6 to become IHC-specific (Echteler, 1992, Huang et al., 2012). Efferent MOC neurons also transiently contact the IHCs, before becoming restricted solely to the OHCs by P10 (Simmons et al., 1996, Simmons, 2002). This differential synaptic pruning gives rise to the distinct innervation patterns of mature IHCs and OHCs and also results in increased efficacy of calcium-induced exocytosis (Beutner and Moser, 2001, Johnson et al., 2005).

Many of these developmental changes occur in gradients along the length of the cochlear duct; stereocilia development occurs in basal-to-apical and medial-to-lateral gradients (Sobin and Anniko, 1984), with maturation of basal OHCs preceding apical OHCs by approximately two days (Waguespack et al., 2007). The onset of OHC electromotility and mechanosensitivity also occurs in basal regions prior to apical regions (He et al., 1994, Lelli et al., 2009).

Although a great deal is known about the signals and molecular mechanisms that are responsible for the initial formation of hair cells at embryonic stages, with ATOH1, Notch signalling and *miR-96* all implicated in early development (Groves et al., 2013), the genetic factors that regulate the postnatal functional maturation of the hair cell subtypes and underlie their unique morphological and functional specialisations are still largely unknown.

1.3. Hearing Loss

Hearing loss is the most common sensory disorder in humans (Acton, 2013) and a significant health burden on the population. At present, more than 10 million people in the UK suffer from some form of hearing loss and current projections indicate that this will increase to

over 14.5 million within the next 20 years (Action-on-Hearing-Loss, 2015). The World Health Organisation (WHO) estimate that approximately 360 million people worldwide suffer from complete or partial hearing loss (WHO, 2015). Understandably, this has a large financial impact on the world economy (Holley, 2005, Ruben, 2000).

Hearing loss impairs quality of life, with hearing-impaired individuals experiencing communication difficulties, social isolation, restricted independence, memory problems, mood disturbances, depression and anxiety (Cox et al., 2005, Tsakiropoulou et al., 2007, McCoy et al., 2005). Congenital and early-onset forms are associated with speech, language and communication difficulties in children (Bess et al., 1998, Culbertson and Gilbert, 1986), which can be hugely detrimental to social and educational development. With an ageing population, late-onset hearing loss, known as presbycusis, is also becoming more prevalent and affects more than 70% of people aged over 70 (Action-on-Hearing-Loss, 2015). Presbycusis is associated with a reduced quality of life (Dalton et al., 2003), cognitive decline and, in some cases, the development of dementia (Lin et al., 2011a), with previous studies in both mice and humans identifying co-morbidity between age-related hearing loss and Alzheimer's disease and Huntington's disease (Ives et al., 1995, Lin et al., 2011b, Uhlmann et al., 1989). It has been suggested that the social isolation, poor verbal communication and reduced stimulatory brain activity associated with hearing loss may contribute to cognitive impairment, although it is not yet clear whether presbycusis is an absolute marker for dementia or a modifiable risk factor (Lin et al., 2011a, Panza et al., 2015).

Hearing loss is a multifactorial disorder and can be caused by environmental factors, such as exposure to loud noises or ototoxic drugs, inherited genetic defects or a combination of

both. Depending on which part of the auditory system is affected, hearing loss can be classed as conductive or sensorineural.

1.3.1. Conductive Hearing Loss

Conductive hearing loss arises from defects in the outer or middle ear, which impair the transduction of sound signals into the inner ear (Keele et al., 1982). Causes of conductive hearing loss include a build-up of cerumen (ear wax), perforation of the tympanic membrane, otosclerosis (calcification of the ossicles) and otitis media (infection, inflammation and fluid build-up in the middle ear), all of which can occur unilaterally or bilaterally (Isaacson and Vora, 2003, Subha and Raman, 2006). Otitis media is the most common cause of hearing impairment and surgery in children in the developed world (Monasta et al., 2012), with approximately 75% of children experiencing at least one episode by the age of three (Faden et al., 1998). Chronic and recurrent forms of otitis media are highly heritable and study of mouse models, such as *Jeff* and *Junbo,* have identified a number of causative genes which increase susceptibility to the condition, including F-box protein 11 (*Fbxo11*), which has also been confirmed in human populations, and ecotropic viral integration site 1 (*Evi1*) (Hardisty-Hughes et al., 2006, Parkinson et al., 2006, Rye et al., 2011, Segade et al., 2006).

Hearing acuity can be assessed using audiometry; this procedure measure hearing thresholds in response to sound stimuli of different frequencies in order to produce an audiogram trace (Figure 1.13 A). Typical audiograms of conductive hearing loss show moderate auditory thresholds (~40 dB SPL) that occur uniformly across all frequencies, known as a 'flat' hearing loss (Figure 1.13 B). Conductive hearing loss can often be successfully treated with either pharmaceutical or surgical intervention; this can include

treatment with cerumenolytics to remove impacted cerumen, a course of antibiotics to treat infection, ossiculoplasty to repair the ossicles or myringotomy to drain fluid and aerate the middle ear (Grevers, 2010, Jabor and Amedee, 1997, Mehta, 1985, Schraff, 2008).

1.3.2. Sensorineural Hearing Loss

Sensorineural hearing loss results from defects in the inner ear, which prevents it from responding to sound signals and transmitting auditory information to the brain for processing. This is most commonly caused by damage to the hair cells, with the OHCs particularly sensitive to damage (Dallos et al., 1972), although can also arise as a result of defects at the hair cell synapses, dysfunction of the supporting cells, atrophy of the stria vascularis, ionic imbalance of the endolymph fluid or trauma to the cochlear nerve. Typical audiograms of sensorineural hearing loss show moderate or severely increased auditory thresholds (between 40 and 100 dB SPL), which can occur across all frequencies or only affect certain frequencies (Figure 1.13 C-D).

Sensorineural hearing loss can vary in terms of onset, depending on the cause and whether damage to the inner ear is caused by inherited genetic defects, environmental factors or a combination of both. For example, whilst mutations in connexin 26 are the most common cause of congenital hearing loss in humans (Denoyelle et al., 1997, Denoyelle et al., 1999, Kemperman et al., 2002, Mueller et al., 1999), mutations in cadherin 23 are associated with a late-onset, age-related hearing loss (Johnson et al., 2000, Noben-Trauth et al., 2003) and environmental factors, such as noise damage or exposure to ototoxic agents, can accelerate the progression of hearing loss and also induce tinnitus (Gates and Mills, 2005). Tinnitus is a phantom ringing in the ears that is detected even in the absence of external sound stimuli (Roberts et al., 2010). In addition to being caused by environmental factors, tinnitus is often

a co-morbidity of age-related hearing loss, with previous work describing an 11% incidence of tinnitus in presbycusis (Podoshin et al., 1997). Although the cause of tinnitus is not fully understood, it has been suggested that hair cell damage could affect the function of associated nerve fibres and result in action potential firing even in the absence of sound stimulation, thus leading to the persistent ringing (Roberts et al., 2010).

Sensorineural hearing loss can present as either an isolated non-syndromic condition or as part of a syndrome with additional co-morbidities. For example, sensorineural hearing loss alongside retinitis pigmentosa is known as Usher syndrome and accounts for approximately 5% of all cases of congenital hearing loss (Marazita et al., 1993). There are three subtypes of Usher syndrome (USH1, USH2 and USH3), which are categorised based on the severity of hearing loss (Smith et al., 1994). Currently, 11 causative genes have been identified in Usher syndrome (Hereditary-Hearing-Loss, 2015), all of which are involved in the development and maintenance of hair cells, including protocadherin 15 (Ahmed et al., 2001) and sans (Weil et al., 2003). Jervell and Lange-Nielsen syndrome is sensorineural hearing loss alongside cardiac arrhythmia and had been attributed to mutations in the potassium channel genes *Kcnq1* and *Kcne1* (Neyroud et al., 1997, Tyson et al., 1997).

Presbycusis is also a type of sensorineural hearing impairment and has been categorised into three main subtypes: sensory presbycusis, which is caused by degeneration of the organ of Corti in basal regions of the cochlea and is associated with high frequency hearing loss (Figure 1.13 D); strial (metabolic) presbycusis, which is characterised by atrophy of the stria vascularis, disruption of the endocochlear potential and a 'flat' hearing loss; and neural presbycusis, which is associated with degeneration of the SGNs and a loss of word discrimination (Schuknecht and Gacek, 1993).

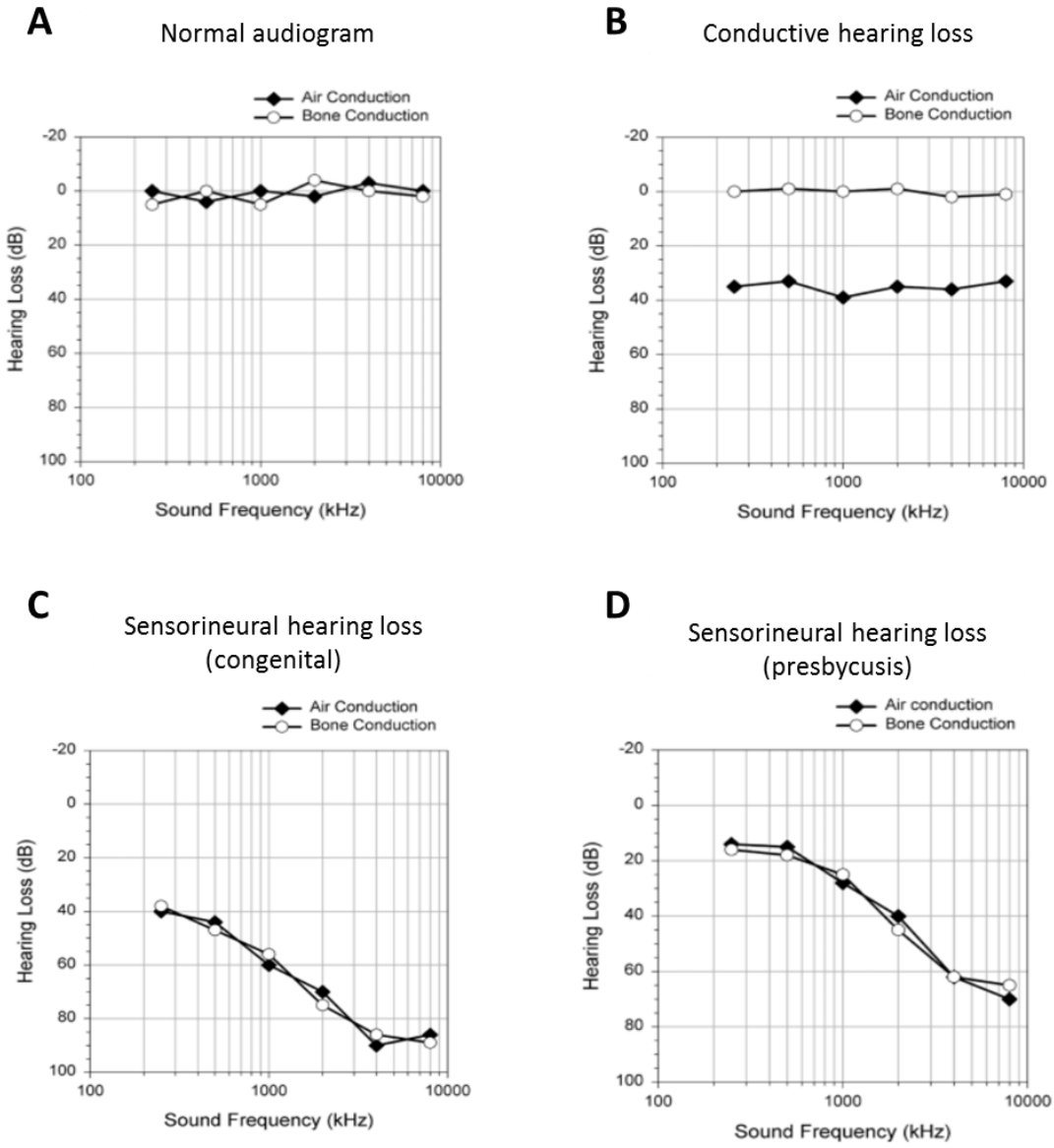

Figure 1.13: Typical audiograms from normal-hearing and hearing-impaired human subjects.
Hearing acuity can be assessed in human subjects by investigating auditory thresholds in response to sound stimuli of different frequencies using an audiometer. In this process, two measurements are collected and plotted to create an audiogram; the first is air conduction thresholds, which are measured in response to a sound that is played into the auditory canal, and the second is bone conduction thresholds, which are measured in response to conduction vibrator placed against the skull. Human audiograms are typically plotted in the reverse orientation to mouse audiograms. **(A)** In a normal-hearing individual, no hearing loss is detected from either the air or bone conduction thresholds. **(B)** An audiogram of a patient with conductive hearing loss typically shows elevated 'flat' air conduction thresholds across all frequencies, but normal bone conduction thresholds. **(C)** In a patient with congenital sensorineural hearing loss, elevated thresholds are detected in both the air and bone conduction measurements. This is detected across all the frequencies tested, although is more severe at the high frequencies in the example shown. **(D)** A typical audiogram of a patient with sensory presbycusis, displaying hearing loss at the high frequencies, but normal hearing at the low frequencies. Audiograms adapted from (Global-Anatomy, 2015). dB, decibel; kHz, kilohertz.

Rodent and human cochleae are known to possess a limited capacity for spontaneous regeneration of hair cells during embryonic and neonatal development (Jan et al., 2013, Kaltenbach and Falzarano, 1994, Mu et al., 1997). At these early stages, uncommitted progenitors and supporting cells can give rise to new hair cells *in vitro* following ototoxic damage or irradiation (Bramhall et al., 2014, Kelley et al., 1995) and *in vivo* following Cre-mediated genetic deletion (Cox et al., 2014). However, this regenerative ability is lost postnatally, owing to the development of thick F-actin bands at the junctions of mature supporting cells, which restrict their ability to move and undergo dynamic changes in shape (Burns and Corwin, 2014). As such, hair cell damage in the mammalian cochlea at this point is irreversible and results in permanent sensorineural hearing loss. This is in contrast with other vertebrates, such as birds, where hair cells can regenerate throughout their lifespan (Cotanche and Corwin, 1991, Lippe et al., 1991).

1.3.3. The Genetics of Hearing Loss

It is estimated that approximately 50% of cases of hearing loss have a genetic basis (Brown et al., 2008). To date, approximately 150 loci have been linked with non-syndromic (isolated) hearing loss in humans (Hereditary-Hearing-Loss, 2015), yet only ~95 causative genes have been identified. This is largely attributed to difficulties in genetic linkage analysis, which are confounded by small family sizes, especially for recessively inherited traits, and the fact that hearing-impaired people often inter-marry (Petit, 2006). Alternative models, such as the mouse, have become an invaluable tool for studying the genetics of hearing loss and providing insights into potential targets for therapeutic intervention.

1.4. Mouse Models of Human Disease

The mouse is frequently used as an animal model to study human disease and biological processes. Comparison of the mouse and human genomes has shown a high degree of genetic similarity, with >90% conserved synteny and >80% of mouse genes known to have a human orthologue (Church et al., 2009, Mouse Genome Sequencing et al., 2002, Pennacchio, 2003). Mouse models can be genetically manipulated in a way that is not ethically possible in human subjects, which enables detailed genetic study; gene expression can be altered using targeted knock-out, knock-in and knock-down approaches as well as through the generation of conditional alleles. Genome editing can also be carried out using clustered regularly interspaced short palindromic repeats (CRISPR) technology, which can generate mutant mice in as little as 3 to 4 months (Jinek et al., 2012, Maddalo et al., 2014, Yin et al., 2014). In addition, random mutations can be introduced into the genome by irradiation or feeding with chemical mutagen, such as *N*-ethyl-*N*-nitrosourea (ENU). Mice are easy to breed in large numbers and have a short generation time, reaching sexual maturity between 5 and 6 weeks of age with a total lifespan of up to two years in laboratory conditions. This assists genetic linkage analysis and enables disease states to be studied throughout the life cycle. Furthermore, space requirements and husbandry costs for maintaining colonies are relatively low.

1.4.1. Mouse Models in Auditory Research

The mouse is an ideal animal model for studying the auditory system and discerning the mechanisms underlying hearing loss. The auditory systems of the mouse and human are morphologically and physiologically similar (Henry and McGinn, 1992) and the mouse ear, unlike the human ear, can be dissected and studied at all stages of development and disease

progression and not just post-mortem. This permits detailed developmental, morphological and electrophysiological examination throughout the time course of auditory impairment and means that insights into audition gained from the mouse can be effectively extrapolated to the human.

It is worth nothing that there are some differences in audition between the mouse and human in terms of optimal hearing ranges; whilst mice can hear between 2 kHz and 85 kHz, with optimal sensitivity between 10 kHz and 20 kHz, the human hearing range is between 20 Hz and 20 kHz, with optimal sensitivity between 2 kHz and 4 kHz (Berlin, 1963, Heffner and Heffner, 2007). Furthermore, due to the small size of the cochlea and the fragility of the temporal bone, it can be difficult to perform surgery on the mouse ear compared to other animal models that are widely-used in auditory research, such as the chinchilla, guinea pig and rat.

Despite this, over the past two decades, both spontaneous and engineered mouse models of hearing loss have revealed novel loci and genes that are required for auditory function, many of which have also been confirmed in human populations (Table 1.1) This highlights the translational potential of mouse auditory research and demonstrates that knowledge gained from the mouse of the genes, pathways and mechanisms involved in hearing loss will help identify therapeutic targets to restore auditory function and improve hearing in human patients.

Table 1.1: Hearing loss-causing genes that were first identified using mouse models and have since been confirmed in human populations.

Gene	Mouse Model	Type of Model	Human Syndrome
Cadherin 23	*Waltzer* (Di Palma et al., 2001)	Spontaneous	DFNB12, USH1D (Bolz et al., 2001, Bork et al., 2001)
Espin	*jerker* (Zheng et al., 2000d)	Spontaneous	DFNB36 (Naz et al., 2004)
Myosin 6	*snell's waltzer* (Avraham et al., 1995)	Spontaneous	DFNA22, DFNB37 (Ahmed et al., 2003a, Melchionda et al., 2001)
Myosin 7a	*shaker-1* (Gibson et al., 1995)	Spontaneous	DFNA11, DFNB2, USH1B (Liu et al., 1997, Weil et al., 1995, Weil et al., 1997)
Myosin 15	*shaker-2* (Probst et al., 1998)	Spontaneous	DFNB3 (Wang et al., 1998a)
Otogelin	*twister* (Simmler et al., 2000b)	Spontaneous	DFNB18 (Schraders et al., 2012)
Protocadherin 15	*Ames waltzer* (Alagramam et al., 2001)	Spontaneous	DFNB23, USH1F (Ahmed et al., 2001, Ahmed et al., 2003b)
Sans	*Jackson shaker* (Kikkawa et al., 2003)	Spontaneous	USH1G (Weil et al., 2003)
Tmhs	*hurry scurry* (Longo-Guess et al., 2005)	Spontaneous	DFNB67 (Shabbir et al., 2006)
Whirlin	*whirler* (Lane, 1963, Mburu et al., 2003)	Spontaneous	DFNB31, USH2D (Ebermann et al., 2007, Mburu et al., 2003)
Loxhd1	*samba* (Grillet et al., 2009)	ENU-induced	DFNB77 (Grillet et al., 2009)
Tmc1	*beethoven* (Vreugde et al., 2002)	ENU-induced	DFNA36, DFNB7, DFNB11 (Hildebrand et al., 2010, Kurima et al., 2002)
Otogelin	-/- (Simmler et al., 2000a)	Knock-out	DFNB18 (Schraders et al., 2012)
Kcne1	-/- (Vetter et al., 1996)	Knock-out	Jervell and Lange-Nielsen syndrome (Schulze-Bahr et al., 1997, Tyson et al., 1997)
Ptprq	-/- (Goodyear et al., 2003)	Knock-out	DFNB84 (Schraders et al., 2010)
Slc26a5	-/- (Liberman et al., 2002)	Knock-out	DFNB61 (Liu et al., 2003)

Using standard nomenclature in the field, autosomal dominant forms of hearing loss are denoted as DFNA; autosomal recessive forms as DFNB; and Usher Syndrome, hearing loss that presents with retinitis pigmentosa, as USH. ENU, *N*-ethyl-*N*-nitrosourea; *Kcne1*, potassium channel, voltage gated subfamily E regulatory beta subunit 1; *Loxhd1,* lipoxygenase homology domains 1; *Ptprq*, Protein tyrosine phosphatase, receptor type Q; *Slc26a5*, Solute carrier family 26, member 5; *Tmc1,* transmembrane cochlear-expressed gene 1; *Tmhs*, Tetraspan membrane protein of hair cell stereocilia.

Indeed, study of rodent models has found that stem cell therapy (Du and Lou, 2014) and gene therapy, such as re-expression of hair cell fate markers (Izumikawa et al., 2005), show promise in regenerating hair cells and improving hearing. For example, mouse embryonic stem cells have been used to generate inner ear progenitor cells, which can then be directed to differentiate into hair cells, supporting cells and neuron-like cells in culture (Koehler and Hashino, 2014, Li et al., 2003). The foremost requirement for a successful therapeutic intervention is, however, the ability to regenerate damaged hair cells postnatally *in vivo.* To this end, recent work has found that pillar cells and Deiters' cells from juvenile mice can be reprogrammed into hair cells *in vivo* by forced expression of *Atoh1* (Liu et al., 2012) and supporting cells from early postnatal mice can be induced to divide and transdifferentiate into hair cells *in vivo* following Cre-loxP-mediated downregulation of Notch signalling (Korrapati et al., 2013, Li et al., 2014). Inner ear progenitor cells derived from mouse embryonic stem cells *in vitro* have also been found to integrate into developing sensory patches and differentiate into hair cells *in vivo* when grafted into otic vesicles (Li et al., 2003).

Cell cycle molecules also represent attractive targets for therapeutic intervention to replace hair cells, given that downregulation of $p27^{Kip1}$ has been associated with post-mitotic supporting cells re-entering the cell cycle, dividing and transdifferentiating into hair cells *in vitro* (White et al., 2006). Furthermore, although hair cell quiescence is initiated at E14.5, expression of the cell cycle progression protein proliferating cell nuclear antigen (PCNA) is still observed in hair cells and supporting cells postnatally (Walters and Zuo, 2013), which suggests these cells retain some ability for cell cycle re-entry. This concept has been explored *in vivo* by hair cell-specific deletion of $p27^{Kip1}$ in neonatal mice, which results in hair

cells re-entering the cell cycle and proliferating postnatally and indicates that hair cells themselves have the potential for autonomous regeneration (Walters et al., 2014).

1.4.2. The Medical Research Council (MRC) Harwell *N*-Ethyl-*N*-Nitrosourea (ENU) Ageing Screen

The Medical Research Council (MRC) Harwell is employing a phenotype-driven ENU mutagenesis screen to identify mouse models of chronic, late-onset or age-related human disease. In this screen, male mice are treated with ENU, an alkylating agent that randomly introduces point mutations in spermatogonial stem cells. ENU mutagenises at a rate of approximately one mutation in 1.01 megabase pairs (Mb), with one in 1.82 Mb potentially functional (Quwailid et al., 2004) and leads to 64% missense, 10% nonsense and 26% splice-site mutations (Justice et al., 1999). The G1 offspring of ENU-treated males typically harbour 30 – 50 potentially functional mutations (Acevedo-Arozena et al., 2008). Due to the random nature of ENU mutagenesis, the Ageing Screen is a powerful tool for identifying novel genes, proteins and molecular pathways involved in disease, as no *a priori* assumptions are made about the underlying genetic cause. Furthermore, ENU mutagenesis can generate various types of genetic mutations, including hypermorph, hypomorph, neomorph and allelic series, which facilitates a forward genetics investigation of gene function.

The Ageing Screen uses a three generation breeding scheme to homozygose ENU-induced mutations and generate large cohorts of G3 mice, which can then be screened for both dominant and recessive phenotypes (Figure 1.14).

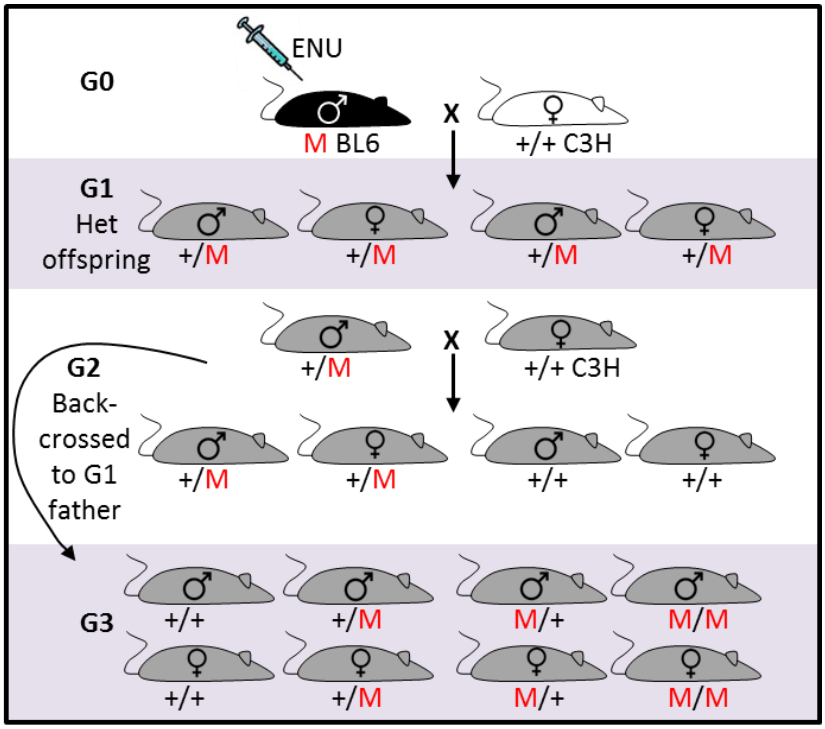

Figure 1.14: Breeding scheme used in the Harwell Ageing Screen.
ENU-mutagenised C57BL/6J males are crossed with wild-type C3H.pde6b^{+} females. G1 males are crossed again with C3H.pde6b^{+} females and the resulting G2 females are then backcrossed to the original G1 male to produce G3 litters that are wild-type (+/+), heterozygous (+/M) and homozygous (M/M) for ENU-induced mutations. G3 mice are then comprehensively phenotyped to identify any phenodeviants. M represents ENU-induced mutations. BL6, C57BL/6J; C3H, C3H.pde6b^{+}; ENU, *N*-ethyl-*N*-nitrosourea.

G3 cohorts are recurrently phenotyped across different disease areas at set time points between three and 18 months of age (Figure 1.15). These disease areas include neuromuscular, neurobehaviour, bone, metabolism, audition, renal function and hepatic function and were chosen for analysis because they relate to ongoing research programmes within MRC Harwell. As phenodeviants of interest are identified, additional cohorts are generated for further investigation. Two distinct inbred strains are used for breeding G3 cohorts (C57BL/6J and C3H.pde6b^{+}), which enables ENU-induced mutations to be mapped using strain-specific single nucleotide polymorphism (SNP) markers across the genome.

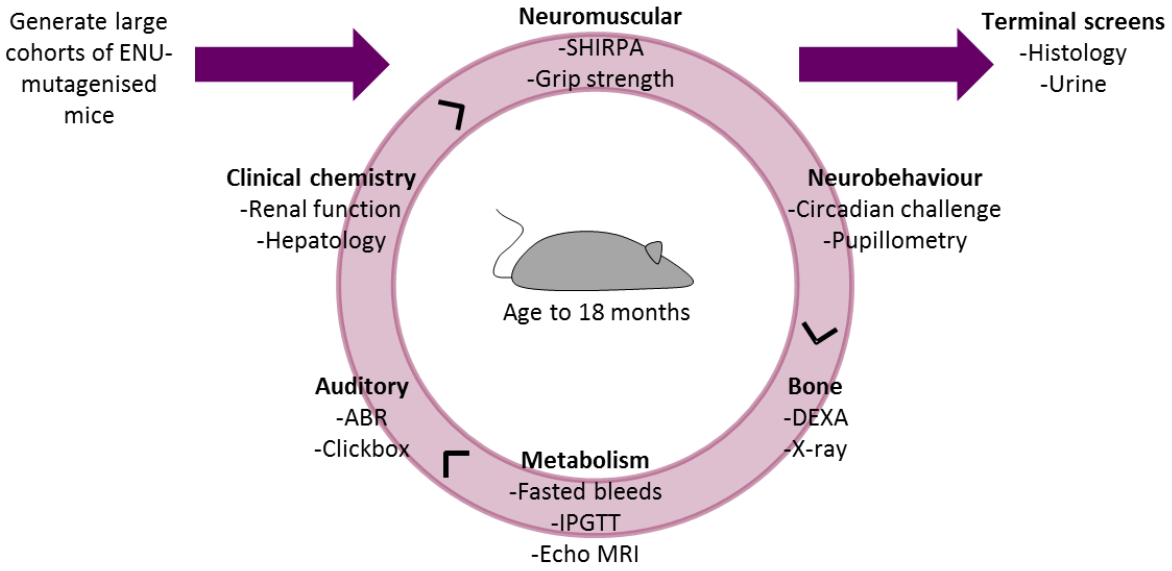

Figure 1.15: Phenotyping pipeline used in the Harwell Ageing Screen.
At three months of age, ENU-mutagenised G3 pedigrees enter a comprehensive phenotyping pipeline, comprising recurrent screening across multiple different disease areas. Each phenotyping test is undertaken at set time points, until cohorts undergo terminal tissue collection at 18 months of age for histological and biochemical analyses. ABR, auditory-evoked brainstem response; DEXA, dual energy X-ray absorption; Echo MRI, echo magnetic resonance imaging; ENU, *N*-ethyl-*N*-nitrosourea; IPGTT, intra-peritoneal glucose tolerance test; SHIRPA, SmithKline Beecham, Harwell, Imperial College, Royal London Hospital phenotype assessment.

Auditory phenotyping uses the clickbox test at three, six, nine and 12 months of age and auditory-evoked brainstem response (ABR) at three and nine months of age to screen for phenodeviants and identify new mouse models of inherited hearing loss. The clickbox is a crude test of hearing, based on response to a brief 20 kHz tone at a sound pressure level (SPL) of 90 dB. Mice with normal hearing display the Preyer reflex, where the ear pinnae flick backwards. ABR measures the electrical activity in the cochlear nerve and brain in response to an auditory stimulus of a specific frequency and SPL to determine auditory threshold (the minimum sound level an individual can hear).

Using these phenotyping tests, the Ageing Screen has the potential to identify mouse models of different types of hearing loss (congenital, early-onset, late-onset, syndromic,

non-syndromic, conductive, sensorineural) and, in doing so, provide valuable insights into the genes required for auditory function and the mechanisms underlying hearing loss.

1.4.3. Identification of *cello* from the Harwell Ageing Screen

Pedigree *MUTA-PED-C3PDE-173* (*MPC-173*) was identified from the Ageing Screen as a potential mouse model of hearing loss at three months of age by Joanne Dorning and Sue Morse at MRC Harwell. Although ABR was not carried out at this time point due to time constraints, 10 mice from the G3 cohort of 60 animals (16.7%) were found to have a reduced or absent clickbox response, indicating impaired hearing function. At six months of age, this had increased to 18 out of 59 mice (30.5%) (Figure 1.16 A), suggesting an early-onset, progressive form of hearing loss. ABR at nine months of age confirmed that all clickbox-affected mice also had severely elevated auditory thresholds (>85 dB SPL) at all frequencies tested compared to unaffected littermates (Figure 1.16 B and Table 9.1 in Appendix). For the hearing-impaired animals, no differences in ABR thresholds were observed between male and female mice, suggesting there is no gender effect. No additional phenodeviants were identified at nine or 12 months of age. The *MPC-173* pedigree was subsequently renamed *cello*.

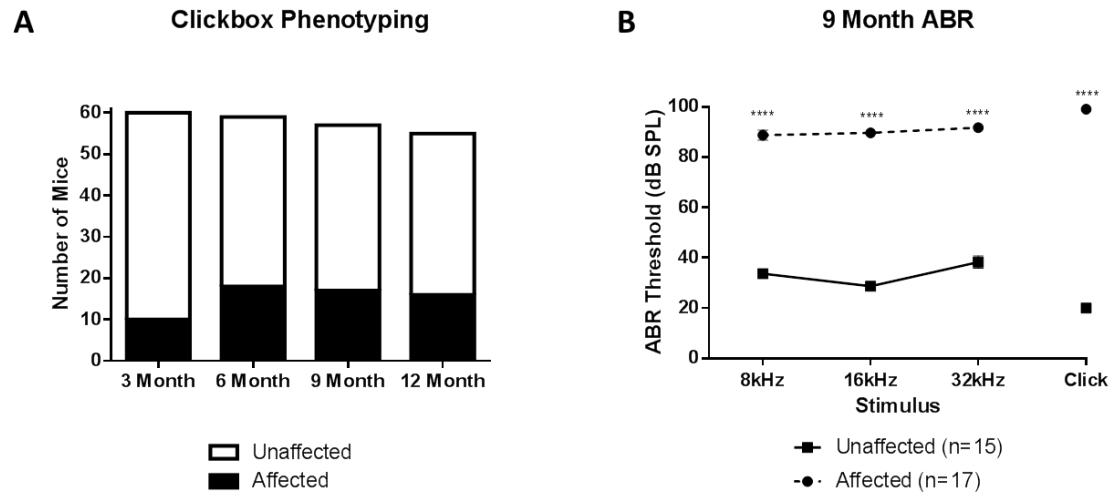

Figure 1.16: *MPC-173* Ageing Screen phenotyping results.
(A) As part of the Ageing Screen, 60 G3 mice from the *MPC-173* pedigree were phenotyped by clickbox at three, six, nine and 12 months of age. At three months of age, 10 mice were found to have reduced or absent clickbox responses. A further 8 affected mice were identified at six months of age. No additional phenodeviants were observed at nine or 12 months of age. **(B)** Of 32 G3 mice assessed by ABR at nine months of age, 17 were found to have severely elevated auditory thresholds (>85 dB SPL) across all frequencies tested. Auditory thresholds were established using the first two peaks (peak I and II) of the corresponding ABR trace. Data are shown as mean ± s.e.m. Statistical analysis: unpaired *t*-test, ****=p≤0.0001. ABR, auditory-evoked brainstem response; dB SPL, decibel sound pressure level; kHz, kiloHertz; *MPC-173, MUTA-PED-C3PDE-173*.

1.5 Aims

This aim of my thesis was to characterise *cello*, an ENU-induced mouse model of hearing loss, in order to provide insights into the genes required for auditory function and elaborate the mechanisms underlying hearing loss.

In order to achieve this aim, I have utilised linkage analysis and whole-genome sequencing to identify the gene responsible for hearing loss in *cello* mice (Chapter 3). I have also undertaken molecular characterisation of the *cello* mutation using *in silico* and *in vitro* approaches in order to predict, model and investigate its effect on protein structure and function (Chapter 3).

I have studied additional phenotypes in *cello* mice, based on the known roles of the *cello* protein reported in the literature. This involved immunological phenotyping using haematological analysis and fluorescence-activated cell sorting, as well as body weight measurements (Chapter 4).

I have also undertaken in-depth auditory phenotyping in order to characterise the *cello* auditory system. This involved ABR measurements to investigate the onset and nature of the hearing impairment in *cello* mice, morphological analysis of the auditory system using histology and scanning electron microscopy, examination of the expression and localisation of the *cello* protein in the ear using immunolabelling and, finally, functional characterisation of *cello* hair cells using transcriptome profiling and electrophysiological analyses (Chapter 5 and Chapter 6).

Chapter 2 : Materials and Methods

2.1. Animal Husbandry

All mice were housed in individually ventilated cages with environmental conditions according to Home Office regulations. All procedures were licensed by the Home Office under the Animals (Scientific Procedures) Act 1986 and Amendment Regulations 2012 (Project Licence numbers 30/2540, 30/2567 and 30/3015) and approved by a local institutional ethical review committee.

2.1.1. Mutagenesis and Generation of G3 Cohorts

10 – 14 week old C57BL/6J male mice underwent intraperitoneal injection with ENU in three doses of 120 mg/kg, 100 mg/kg and 100 mg/kg one week apart. After a period of sterility, mutagenised males (G0) were mated with wild-type 'sighted' C3H.pde6b^{+} females. Inbred C3H mice are carry the recessive *retinal degeneration 1* (*rd1*) allele, which is a mutation in the *Pde6b* gene (*Pde6b*^{rd1}) (Pittler and Baehr, 1991). As such, Harwell uses the C3H.pde6b^{+} substrain, which carry the wild-type *Pde6b* gene derived from BALB/c (Hoelter et al., 2008) and so do not display retinal degeneration. The resulting G1 males, heterozygous for ENU-induced mutations, were crossed with C3H.pde6b^{+} females to produce G2 females, all of which were screened for the hypomorphic *Cdh23*^{ahl} allele that predisposes C57BL/6 mice to age-related hearing loss (Johnson et al., 1997, Noben-Trauth et al., 2003). To generate recessive G3 phenotyping cohorts, only G2 females that were homozygous wild-type for *Cdh23* were backcrossed to their G1 fathers, thereby preventing the production of *Cdh23*$^{ahl/ahl}$ G3 mice. These G3 pedigrees then entered the Ageing Screen longitudinal phenotyping pipeline at three months of age.

2.2. Auditory Phenotyping

2.2.1. Clickbox

Mice were placed in the palm of the hand and a clickbox (Institute of Hearing Research) was held approximately 30 cm away. The button on the clickbox was pressed, emitting a 20 kHz tone at 90 dB. Mice with normal hearing display the Preyer reflex, where ear pinnae flick backwards, along with a startle response. Mice were graded depending on their response: 0 for an absent response, 1 for a reduced response or 2 for a normal response.

2.2.2. Auditory-evoked Brainstem Response (ABR)

Mice were anaesthetised by intraperitoneal injection of ketamine (100 mg/kg) and xylazine (10 mg/kg) then placed on a heated mat in a sound-attenuated chamber. Electrodes were inserted subdermally over the cranial vertex (active), right mastoid (reference) and left mastoid (ground) and a speaker was positioned approximately 1.5 cm away from the right ear, facing directly into the auditory canal. ABR responses were obtained using the TDT System III hardware and software (Tucker Davies Technology), which was calibrated across a range of test frequencies (1 – 32 kHz) using a type 7016 ¼" measuring microphone (ACO-Pacific) and the SigCal software (Tucker Davies Technology). Briefly, the output of the stimulus transducer was used to create a normalisation file to correct the transducer output by boosting or attenuating the frequencies as required, as in Hardisty-Hughes et al. (2010). The normalised output was then checked using the PULSE hardware (a type 4939 ¼" measuring microphone attached to a high frequency 3110 processing module) and software (Brüel and Kjær). Both microphones were calibrated using a type 511e Pistonphone calibrator (ACO-Pacific), which produced a 1 kHz tone at 94 dB SPL and was attached to the PULSE system. For ABR measurements, a 0.1 millisecond (ms) broadband click stimulus and

7 ms tone-burst stimuli at 8, 16 and 32 kHz were played into the ear at decreasing sound pressure levels (from 100 dB SPL to 5 dB SPL in 5 dB SPL steps). Tone-burst stimuli were presented at a rate of 21 per second and repeated 512 times. The collected responses were filtered between 300 Hertz (Hz) and 1.5 kHz, amplified 100,000 times and averaged using TDT System III hardware and software (Tucker Davies Technology), then plotted to produce a trace (Figure 2.1). In a normal hearing mouse, this trace has five peaks (PI – PV), thought to correspond to different regions of the auditory pathway (PI and PII, cochlear nerve; PIII, cochlear nucleus; PIV, super olivary nucleus; PV, inferior colliculus). Auditory thresholds were defined as the lowest sound intensity that produced a recognisable, reproducible trace and were established using peak I and II. Thresholds were verified at least twice. Mice were recovered by subcutaneous injection of 0.1 ml of 20 mg/ml atipamezole.

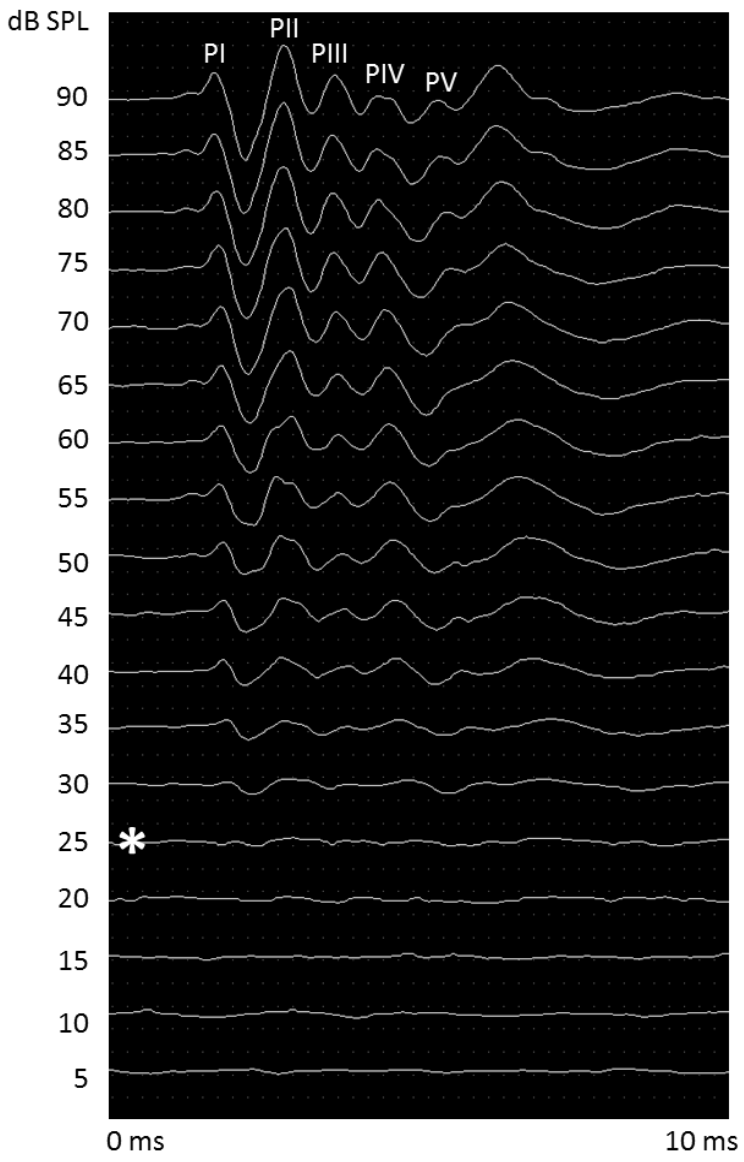

Figure 2.1: Example of an auditory-evoked brainstem response trace collected from a wild-type mouse in response to the click stimulus.

Auditory responses are collected, averaged and plotted in response to stimuli that are played into the auditory canal at decreasing sound pressure levels. ABR traces have five clear peaks, each of which corresponds to a different region along the auditory pathway (PI and PII, cochlear nerve; PIII, cochlear nucleus; PIV, super olivary nucleus; PV, inferior colliculus). The auditory threshold (25 dB, marked with an asterisk) is selected as the lowest sound intensity that produces a recognisable and reproducible trace in response to the stimulus. dB SPL, decibel sound pressure level; ms, milliseconds.

2.3. Genotyping

Tissue was taken and stored at -20°C until ready for genotyping. Ear clips were taken after weaning, at approximately 3 weeks of age. Tail was taken only terminally.

2.3.1. Deoxyribonucleic Acid (DNA) Extraction

For Mapping: Deoxyribonucleic acid (DNA) was extracted from duplicate ear biopsies or tail using the DNeasy Blood and Tissue Kit (Qiagen). In this method, samples were lysed with proteinase K then applied to a silica membrane-based column. DNA selectively binds to the silica membrane and unbound contaminants were removed by a series of wash steps. DNA was eluted from the column using 60 µl of AE buffer (for ear clips) or 200 µl of AE buffer (for tail).

For Whole-Genome Sequencing (WGS): High-quality DNA was extracted from tail using the Illustra™ Nucleon DNA Extraction Kit (GE Healthcare). This method uses proteinase K to lyse samples, sodium perchlorate to deproteinase DNA and chloroform to solubilise lipids and proteins. After adding Nucleon Resin, samples were centrifuged to separate into a lower protein-containing organic phase, a middle Resin phase and an upper DNA-containing aqueous phase. The upper phase was collected and DNA was precipitated with ethanol and resuspended in 100 µl of 10 mM Tris hydrochloride (Tris-HCl) (pH 8.5).

2.3.2. DNA Quantification

DNA was quantified by measuring absorbance at 260 nm using the Epoch Micro-Volume Spectrophotometer System and Take3 Micro-Volume Plate (BioTek). The instrument was first blanked using 2 µl of the appropriate eluent, then 2 µl of DNA solution was loaded for quantification.

2.3.3. Whole-Genome Mapping

DNA was extracted from 13 G3 mice (12 affected and one unaffected control) as in **2.3.1.** For each sample, 30 µl of DNA at 50 ng/µl was sent to Tepnel Life Sciences (Manchester, UK) for SNP-based whole-genome mapping using the Illumina GoldenGate Mouse Medium Density Linkage Panel. This panel contains 1449 SNPs, of which 871 are strain-specific and informative between C57BL/6J and C3H.pde6b^{+}. Results were returned by email.

2.3.4. Whole-Genome Sequencing (WGS)

A total of 5 µg of DNA at 50 ng/µl, extracted from an affected G3 animal as in **2.3.1.**, was taken to the High-Throughput Genomics facility at The Wellcome Trust Centre for Human Genetics (Oxford, UK) for whole-genome sequencing (WGS) using the Illumina HiSeq 2000 system. Results were aligned to *Mus musculus* C57BL/6J mouse reference genome (assembly GRCm38) by the Bioinformatics group at MRC Harwell. Known C57BL/6J and C3H.pde6b^{+} SNPs were filtered out and the remaining variants gained a quality score based on their sequencing read depth. Variants with a quality score of >200 were classed as high confidence.

2.3.5. Polymerase Chain Reaction (PCR)

Polymerase chain reaction (PCR) was used to amplify DNA sequences of interest for fine mapping, validation of ENU-induced lesions and plugging WGS sequencing gaps. Primers were designed using Primer-BLAST (http://www.ncbi.nlm.nih.gov/tools/primer-blast/), synthesised by Eurofins then diluted to 10 µM with double distilled water (ddH_2O). Reactions were set up according to the following protocols, using template DNA at 5 ng/µl:

ReddyMix Master Mix (Thermo Scientific): 20 µl of 1.1x ReddyMix Master Mix was combined with 0.75 µl of each primer (10 µM) and 2.5 µl of DNA (5 ng/µl).

AmpliTaq Gold® DNA Polymerase (Applied Biosystems®): PCR was performed as 25 µl reactions, consisting of 2.5 µl of PCR Gold Buffer (10x), 3 µl of $MgCl_2$ (25 mM) and 0.15 µl of AmpliTaq Gold® (all Applied Biosystems®), 0.5 of µl dNTPs (10 mM) (Invitrogen), 1 µl of each primer (10 µM), 3 µl of DNA (5 ng/µl) and 13.85 µl of ddH_2O. Reactions for Sanger sequencing were scaled up to give a total reaction volume of 50 µl.

HotShot Diamond Master Mix (Idaho Technology Inc): 5 µl of HotShot Diamond Master Mix was combined with 0.2 µl of each primer (10 µM), 2 µl of DNA (5 ng/µl) and ddH_2O up to 10 µl.

PCR reactions were carried out on a Tetrad2 Peltier thermal cycler (Bio-Rad) using the following programme:

1. Initial denaturation: 95°C for 5 minutes
2. 35-40 cycles of:
    a. Denaturation: 95°C for 30 seconds
    b. Annealing: 50-65°C for 30 seconds
    c. Extension: 72°C for 30-90 seconds (60 seconds per kb of amplicon)
3. Final extension: 72°C for 5 minutes

The sequence and specific reaction conditions for each primer pair are listed in Table 2.1.

2.3.6. Restriction Digests

Once ENU-induced mutations had been localised to a chromosomal region by whole-genome mapping, additional strain-specific C57BL/6J and C3H.pde6b$^+$ SNP markers were used to narrow the critical region. SNPs were identified using the Mouse Phenome Database

(http://phenome.jax.org/) then assessed with Webcutter 2.0 (http://rna.lundberg.gu.se/cutter2/) to see if either of the SNP alleles created a unique restriction enzyme site. If so, the SNP and its flanking sequence were amplified by PCR then genotyped using the appropriate restriction enzyme (Table 2.1). 10 µl of PCR product was digested in a reaction that contained 0.5 µl of enzyme, 2 µl of 10x enzyme buffer, 2 µl of 10x BSA (all New England BioLabs) and 5.5 µl of ddH_2O. Digest reactions were incubated at the specified temperature on the Tetrad2 Peltier thermal cycler for 3 – 4 hours then electrophoresed to determine genotype.

2.3.7. Gel Electrophoresis

DNA was analysed by gel electrophoresis using 1 – 2.5% agarose 1x TAE (40 mM Tris acetate and 1 mM ethylenediaminetetraacetic acid (EDTA)) gels containing 0.2 µg/ml of ethidium bromide (Alfa Aesar). When required, samples were first mixed with 1 – 3 µl of Orange G loading dye (Sigma). Samples were run alongside 5 µl of HyperLadder™ 100 base pairs (bp) or 1 kilobase pairs (kb) (Bioline) in order to determine product sizes. Gels were electrophoresed for 20 – 30 minutes at 150 volts (V) then analysed using an ultraviolet gel doc system (Bio-Rad) to visualise DNA.

Table 2.1: Primer pairs and PCR conditions used for *cello* genotyping reactions.

Primer Pairs and PCR Conditions							
Assay	**Forward Primer (5' – 3')**	**Reverse Primer (5' – 3')**	**PCR Kit**	**Tm (°C)**	**Cycles**	**Amplicon (bp)**	**Restriction Enzyme**
Fine Mapping							
rs31425874	AACCAGGGCAGGGAAGTTCGG	CTGTCAGTTCTGGGAGGAGGGGG	ReddyMix + Betaine (0.5M)	59	x40	540	*BspHI*
rs32685810	ACTCATGTGTGGTGTCCTTGAGTCT	TGCTTCTGTACGAGCAGGTGCC	Amplitaq Gold	65	x40	684	*StyI*
rs13475879	CATGGGTGGACGTCTCCTGGT	GGGCCATTCCCTTTGTGTGCG	ReddyMix	65	x40	700	*AflIII*
rs32179751	ACAGCCAAGTGTTCCACTCTAATGC	TGCCTGCTCAGGTTCCAGGACA	ReddyMix	59	x40	620	*BanI*
rs31869113	ATCTCGGTGGGAGATTGCGGG	TCAATGGAAAGAACAGCTTGCTGCC	Amplitaq Gold	65	x40	610	*HphI*
rs30609422	TCCCTATGGATTTGAACAGCAAGCC	TTGTCTGGAACACACGGGTCAGT	ReddyMix	59	x40	436	*HphI*
rs32058458	GGAGGTCTGGAAGTGAATCGCCC	TCTGCAGCCACTTAGATGTGTTTCC	ReddyMix + Betaine (0.5M)	59	x40	669	*BstYI*
rs13475914	GGCACAGCCCCAACAGATGCT	AGGCCCTGTTCCCAGTCAGGT	ReddyMix	59	x40	336	*MwoI*
WGS Validations							
Ikzf2_Val	ACCATTCACATGGGTTGCCA	ATGTATCGTAGCGGCCCTTG	ReddyMix	63	x35	765	-
WGS Gaps							
WGS_Gap1	CATCCTCATCTGACGAGCGG	TCCTGTAGGATCTCCGAGGG	HotShot + DMSO	59.6	x37	276	-
WGS_Gap1Nest	CTACGGGAGCTGCTCTTAAGG	ATCTCCGAGGGCGAACTGGA	HotShot + DMSO	61.8	x37	209	-
WGS_Gap2	TGGTCCTGAAGTCAGGCTACG	CTGCTTTGCACACCGGGG	AmpliTaq Gold + Betaine (1M) + DMSO (10%)	60	x50	700	-
WGS_Gap3	AGAGCAGCTGAAGCACTAGC	AGCGCTTTATTCCTCCAGCA	HotShot + DMSO (10%)	56.7	x42	667	-
WGS_Gap4	TATCTGCCCAGGTGGGACTA	CGGTCCATCAATCCCCTTCC	ReddyMix	50	x40	282	-

DMSO, dimethyl sulfoxide; M, molar.

2.3.8. DNA Purification

PCR amplicons for sequencing were purified using one of the following methods, following the manufacturer's instructions:

QIAquick PCR Purification Kit (Qiagen): This kit uses silica-based spin columns to purify PCR products that are between 100 and 10,000 bp in size. PCR products were mixed with a binding buffer and then applied to a spin column. DNA binds to the silica-based column and contaminants from the PCR reaction (primers, enzyme, unincorporated nucleotides) were washed off. DNA was then eluted in 20 µl of Buffer EB, in two subsequent 10 µl elution steps.

GeneClean II (MP Biomedicals): This kit was used to isolate DNA fragments from a TAE agarose gel, which had been excised using a razor blade over a Chromato-Vue TM20 ultraviolet transilluminator (Ultra-Violet Products Ltd.). Gel slices were melted in a high-salt buffer then mixed with glassmilk, an aqueous suspension of silica matrix to which DNA binds. The glassmilk-DNA complex was pelleted and washed several times to remove contaminants leftover from PCR and gel electrophoresis. The glassmilk-DNA pellet was then resuspended in 25 µl of 1x Tris EDTA (TE) to elute DNA. A final centrifugation step pelleted the glassmilk and enabled the supernatant containing eluted DNA to be collected.

2.3.9. Sanger Sequencing

Purified DNA was sent by courier to Source Bioscience (Oxford, UK) along with gene-specific sequencing primers. Each sequencing reaction required 5 µl of PCR product at a concentration of 1 ng/µl per 100 bp and 5 µl of primer at 3.2 pmol/µl. Results were received by email and analysed using the DNASTAR Lasergene SeqMan programme.

2.3.10. Genotyping

An 5' nuclease allelic discrimination assay was used to genotype *cello* mice for the c.1551C>A mutation by the Genotyping, Expression and Mutation Screens (GEMS) core facility at MRC Harwell. DNA was extracted from ear biopsies using the TaqMan® Sample-to-SNP™ Kit (Applied Biosystems®) and used in duplex real-time PCR reactions with primers that amplified around the *cello* lesion and two 5' fluorophore-labelled TaqMan® probes:

Forward primer: 5'-AAGGCCTAGTGGAATGTGTGCTC-3'

Reverse primer: 5'-AAGCCAGGACCGCTACGAAT-3'

FAM-labelled wild-type TaqMan® probe: 5'-CTCGAACAAT**G**TGTGATGA-3'

TET-labelled mutant TaqMan® probe: 5'-CCTCGAACAAT**T**TGTGATG-3'

Reactions were set up using template DNA at a 1:10 dilution and a pre-made 'assay mix' comprised of 15 µM of each primer and 5 µM of each probe. For each reaction, 5 µl of TaqMan® GTXpress™ Master Mix (Applied Biosystems®) was combined with 2 µl of 'assay mix' (20 µM), 2.5 µl DNA (diluted 1:10) and 0.5 µl of ddH_2O.

This assay relies on the exonuclease activity of *Taq* polymerase, which cleaves each probe following its specific hybridisation to complementary target sequence. This releases a quencher molecule from the 3' end of the probe and results in a fluorescent signal emitted from that probe's distinct fluorophore. A fluorescent signal is only emitted when the amplified target sequence is complementary to the probe, enabling allelic discrimination. In the presence of wild-type target sequence, the FAM-labelled wild-type probe will anneal and undergo cleavage, emitting a FAM signal. In the presence of mutant sequence, the TET-labelled probe will anneal and emit TET fluorescence. In the presence of heterozygous

sequence, a signal will be released from both FAM and TET fluorophores. Assays were run on the 7500 Fast Real-Time PCR system (Applied Biosystems®) using the following protocol:

1. Pre-PCR Read (Holding Stage): 60°C for 1 minute
2. Initial Denaturation: 95°C for 20 seconds
3. 40 cycles of:
    a. Denaturation: 95°C for 3 seconds
    b. Annealing/Extension: 60°C for 30 seconds
4. Post-PCR Read (Holding Stage): 60°C for 1 minute

Results were analysed using the 7500 software v2.0.6 (Applied Biosystems®) to distinguish genotype (Figure 2.2).

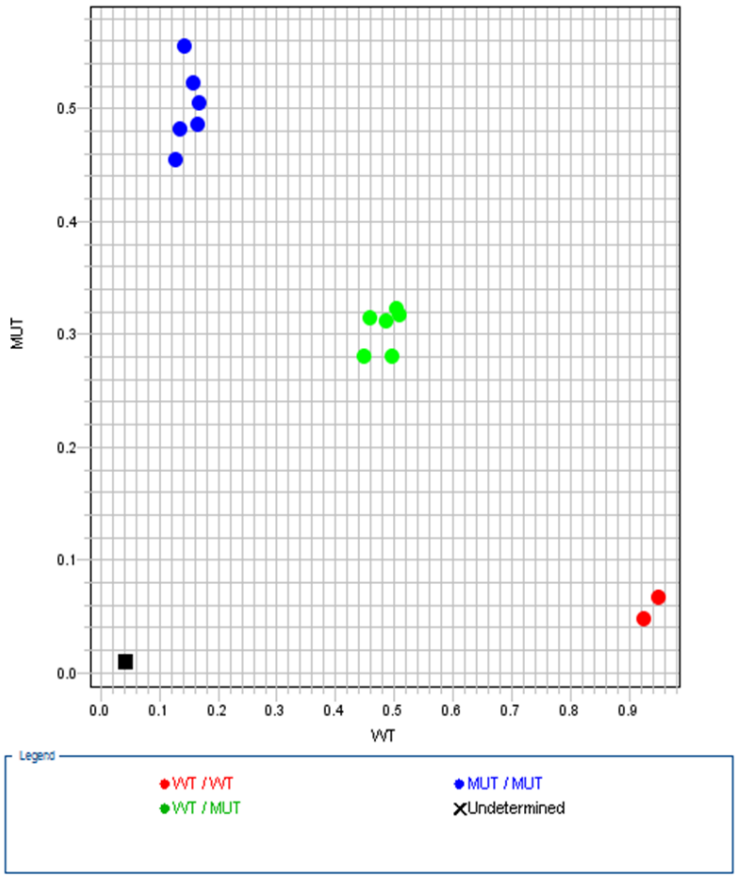

Figure 2.2: Example of an allelic discrimination genotyping plot.
cello mice were genotyped using a 5' nuclease allelic discrimination assay, with a FAM-labelled wild-type TaqMan® probe and a TET-labelled mutant TaqMan® probe. When each probe hybridises to its complementary target sequence, it is cleaved by *Taq* polymerase and a fluorescent signal is emitted from the coupled fluorophore. The relative fluorescence from each fluorophore is then normalised to the fluorescent signal emitted from a passive reference dye (ROX) in order to correct for variations in setting up reactions, pipetting and instrument scanning. Results for each sample are subsequently plotted as the ratio of the respective reporter dye (FAM or TET) to the passive reference dye (ROX) from each well in order to generate an allelic discrimination plot. In the presence of wild-type (*Ikzf2*$^{+/+}$) target sequence, the wild-type probe is cleaved, emitting a FAM fluorescent signal (shown in red). In the presence of homozygous (*Ikzf2*$^{cello/cello}$) target sequence, the mutant probe is cleaved, emitting TET fluorescence (shown in blue). In the presence of heterozygous (*Ikzf2*$^{cello/+}$) target sequence, both FAM and TET fluorescence are emitted (shown in green).

2.4. Tissue Collection and Processing

2.4.1. Histology

For Middle Ear Paraffin Sections: Mice were culled by intraperitoneal injection of Euthatal™ (0.15 ml at 100 mg/ml) and the heads were removed, skinned and bisected sagittally. Samples were fixed in 10% formalin overnight at room temperature (RT) then processed by

the Histology team at MRC Harwell; samples were decalcified for 3 days in Kristenson decalcifying solution (DFB) (Pioneer Research Chemicals Ltd.) then processed using the Shandon Pathcentre™ or Excelsior™ AS Tissue Processor (both Thermo Scientific), which dehydrate samples in increasing concentrations of ethanol, clear samples using xylene and impregnate samples with molten paraffin wax under vacuum. Samples were then embedded in molten paraffin wax and 5 µm transverse sections were cut using the Finesse™ ME+ microtome (Thermo Scientific) and collected onto charged slides. Sections were stained with haematoxylin and eosin (H&E) then scanned using the NanoZoomer Digital Pathology system.

For Inner Ear Paraffin Sections: Mice were culled by cervical dislocation and the heads were removed, skinned and bisected sagittally. Samples were fixed in 10% formalin overnight at room temperature (RT) then dehydrated and embedded by the Histology team at MRC Harwell, as before. 5 µm sagittal sections were cut through the mid-modiolar plane of the cochlea. Sections were collected onto charged slides and stained with H&E then scanned using the NanoZoomer Digital Pathology system.

2.4.2. Scanning Electron Microscopy (SEM)

Mice were culled by cervical dislocation and the inner ears removed and fixed in 2.5% glutaraldehyde in 0.1 M phosphate buffer for 4 hours at 4°C. Following 3x 15 minute washes in 0.1 M phosphate buffer, ears were decalcified in 4.3% EDTA for 48 – 72 hours at 4°C, then washed again and stored in 0.1 M phosphate buffer at 4°C. When ready for processing, decalcified inner ears were fine dissected under a SteREO Discovery.V20 microscope (Zeiss) to remove the cochlear shell and stria vascularis and expose the organ of Corti. Samples underwent osmium tetroxide-thiocarbohydrazide (OTO) processing, consisting of a 1 hour

incubation in 1% osmium tetroxide in 0.1 M sodium cacodylate, a 30 minute incubation in 1% thiocarbohydrazide in ddH_2O, then another 1 hour incubation in 1% osmium tetroxide, all at RT with each step separated by 6x 3 minute ddH_2O washes. This was followed by dehydration in ethanol solutions of increasing strength (25%, 40%, 60%, 80%, 95%, 2x 100%) for 45 minutes at 4°C. Samples were stored in 100% acetone overnight at 4°C then critical-point dried with pressurised liquid carbon dioxide using (Emitech K850, Quorum Technologies). Samples were mounted on 12.5 mm aluminium specimen stubs with carbon adhesive discs and silver paint (all Agar Scientific) and sputter coated using a platinum target (Q150R S, Quorum Technologies). Cochleae were imaged using a JSM-6010LV Scanning Electron Microscope (JEOL).

2.4.2.1. Hair Cell Counts

SEM-processed cochleae were divided into three regions for high resolution imaging and hair cell counts: apical (the first ½ turn of the cochlea), mid (the next ¾ turn) and basal (the remaining ½ turn). Within each region, an area of the organ of Corti containing ten adjacent pillar cells was identified and marked on scanning electron microscopy (SEM) images (Figure 2.3). The number of IHCs and OHCs juxtaposed to these ten pillar cells was then determined by counting IHC and OHC stereocilia bundles. Cells were only counted when at least half of their stereocilia bundle was encompassed within the counting area. Absence of stereocilia bundles was presumed to indicate absence of the associated hair cells.

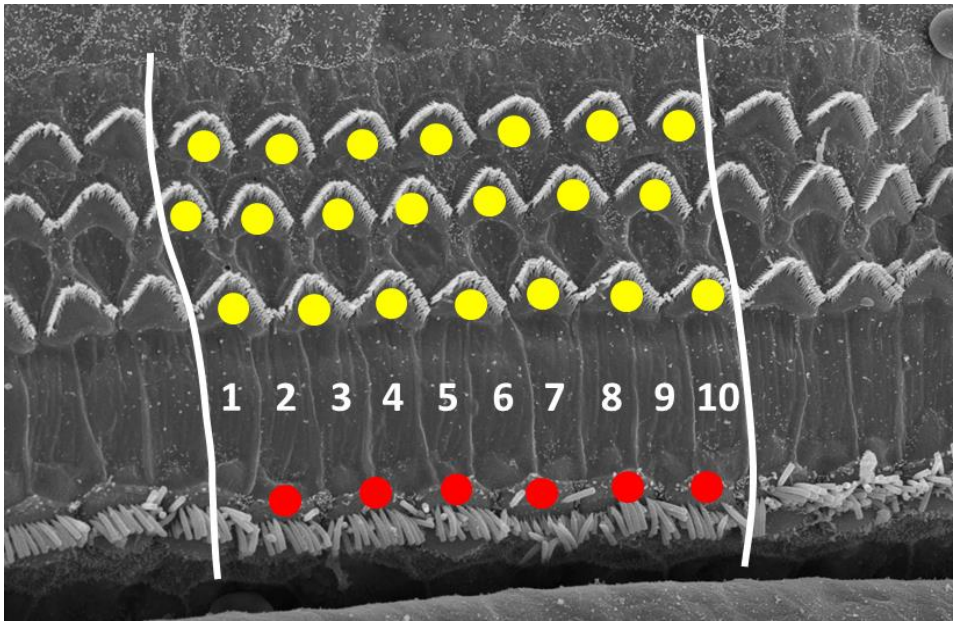

Figure 2.3: Example of hair cell counts using scanning electron micrographs of the organ of Corti.
Scanning electron micrographs were taken of apical, mid and basal cochlear regions to perform hair cell counts. On each image, an area of the organ of Corti containing ten adjacent pillar cells was identified and marked with lines extending along the edges of the first and last pillar cell (white lines). The number of IHC (red circles) and OHC (yellow circles) stereocilia bundles juxtaposed to these ten pillar cells was then counted to quantify each hair cell subtype. In order for cells to be counted, at least half of their stereocilia bundle had to fall within the demarcated counting area.

2.4.3. Cochlear Wholemounts

Mice were culled by cervical dislocation and the inner ears removed and fixed in 2% paraformaldehyde (PFA) for 30 minutes at RT then washed in PBS. Immediately prior to immunolabelling, the cochlear shell, stria vascularis and lateral wall were removed by fine dissection under a Zeiss SteREO Discovery.V20 microscope to expose the sensory epithelia.

2.4.4. Vibratome Sectioning

Mice were culled by cervical dislocation and the inner ears removed and fixed in 4% PFA in PBS overnight at 4°C. After 3x 15 minute PBS washes, inner ears were decalcified in 4% EDTA in PBS for 48 – 72 hours at 4°C, with EDTA replaced every 24 hours. Inner ears were washed for 3x 15 minutes in PBS to remove residual EDTA then blocked in warm 4% low melting temperature agarose (Sigma-Aldrich) in an upturned BEEM® capsule (Agar Scientific). Inner

ears were positioned so that the apex of the cochlea was facing down and the vestibular system was uppermost in the BEEM® capsule. Once set, the agarose block containing the inner ear was removed from the BEEM® capsule and fixed with superglue to the mounting stage of a Leica VT1000S Vibratome. 200 µm sections were cut through the mid-modiolar plane of the inner ear and stored at 4°C in PBS prior to immunolabelling.

2.4.5. Ribonucleic Acid (RNA)

For RNA Sequencing (RNA-Seq): P8 mice were culled by cervical dislocation and the inner ears fine dissected in PBS to detach the cochlear duct from the modiolus bone. Three pairs of cochlear ducts were pooled per genotype, then homogenised in 500µl of TRI-Reagent® (Zymo Research) using a 1 ml needle and 25 gauge syringe. Homogenates were centrifuged at 13,000 rotations per minute (rpm) for 1 minute and the supernatant transferred to RNase-free tubes (Life Technologies) for immediate RNA extraction (see **2.9.1.**).

For quantitative real-time PCR (qRT-PCR): P8 mice were culled by cervical dislocation by Maggie Matern at the University of Maryland (USA) and the inner ears were sub-dissected to detach the cochlear duct from the modiolus bone, as above. Cochlear ducts were flash-frozen on dry ice then stored at -80°C until RNA extraction (see **2.9.1.**).

2.5. Immunolabelling

2.5.1. Cochlear Wholemount Immunolabelling

Fine dissected cochleae were permeablised in 0.2% Triton-X for 10 minutes then blocked with 10% donkey serum (Sigma) in PBST (PBS + 0.1% Tween) for 1 hour at RT. Cochleae were incubated with a polyclonal goat anti-helios primary antibody (1:400, Santa Cruz) overnight at 4°C. Samples were washed for 3x 15 minutes in PBST then incubated for 1 hour at RT with

F-actin marker Alexa Fluor® 488 Phalloidin (1:200, Invitrogen) and donkey anti-goat Alexa Fluor® 568 secondary antibody (1:200, Invitrogen). Following 3x 15 minute washes in PBST, samples were incubated with DAPI at 1 µg/ml for 60 seconds to stain nuclei then washed again. Samples were mounted on charged microscope slides in custom made wells using SlowFade® Gold Antifade Reagent (Life Technologies) and imaged on a Zeiss LSM 710 multiphoton fluorescence confocal microscope. Where necessary, the anti-helios primary antibody was pre-incubated with its supplied immunising peptide (1:40, Santa Cruz) for 30 minutes prior to immunolabelling, in order to pre-block the antibody and confirm its specificity. In addition, when investigating helios expression and localisation in *cello* homozygotes (*Ikzf2*$^{cello/cello}$), wild-type (*Ikzf2*$^{+/+}$) tissues were used as positive controls.

2.5.2. Vibratome Section Immunolabelling

Multiple vibratome cochlear sections were placed in a single well of a 24-well plate for simultaneous immunolabelling. Sections were permeablised and blocked by incubation with 10% donkey serum in 0.3% Triton-X (in PBS) for 30 minutes at RT, then incubated with primary antibodies for 3 hours at RT. Following 3x 15 minute washes in PBST, tissue sections were incubated with fluorophore-conjugated secondary antibodies for 2 hours at RT. Unbound secondary was removed with 3x 15 minute washes in PBST before incubating with DAPI at 1 µg/ml for 5 minutes to stain nuclei. Sections were washed for 3x 15 minute washes in PBST then stored in PBS at 4°C. For visualisation, sections were transferred to a WillCo glass bottom dish (Intracel) and imaged free-floating in PBS using a Zeiss 700 inverted confocal microscope. Primary antibodies: polyclonal goat anti-helios (1:400, Santa Cruz); goat anti-prestin (1:400, Santa Cruz); goat anti-oncomodulin (1:200, Santa Cruz); mouse

anti-β-actin (1:500, Abcam). Secondary antibodies: donkey anti-goat Alexa Fluor® 568 and donkey anti-mouse Alexa Fluor® 488 (Invitrogen, 1:200).

2.6. Cloning

In order to assess the *cello* mutation *in vitro*, N-terminally tagged fusion proteins were generated by cloning wild-type and c.1551C>A *Ikzf2* into c-Myc and Enhanced Green Fluorescent Protein (EGFP) expression vectors.

2.6.1. TA Cloning

An *Ikzf2* complementary DNA (cDNA) clone was obtained from Source BioScience and amplified using primers that added specific restriction enzyme recognition motifs on to the 5' and 3' end of the clone sequence:

EcoRI-Ikzf2_F: 5'-TCGAATTCTGatggaaacagacgcaattgatgg-3'

KpnI-Ikzf2_R: 5'-AAGGTACCctagtggaatgtgtgctcccctcg-3'

The PCR product from this reaction was purified using GeneClean II and ligated into a pGEM®-T vector using the pGEM®-T Vector System I kit (Promega). The pGEM®-T vector is linearised and has 3' T overhangs at both ends. This prevents recircularisation of the vector and improves the efficiency of the ligation reaction. During PCR, *Taq* polymerase adds a single adenosine base to the 3' ends of amplified DNA fragments, in a template-independent manner. The complementary 'T' and 'A' overhangs of the vector and insert anneal and T4 DNA ligase is used to complete ligation of the DNA into the vector, to generate a circular plasmid.

To determine the amount of *Ikzf2* PCR product required for ligation, the following calculation was used, with an insert:vector ratio of 3:1:

$$\frac{\text{25 ng of vector x size of insert (kb)}}{\text{size of vector (3 kb)}} \times \text{insert:vector ratio} = \text{ng of insert required}$$

Each ligation reaction comprised of 1x Rapid Ligation Buffer, 25 ng pGEM®-T vector, 3 Weiss units of T4 DNA ligase (all Promega), the required concentration of *Ikzf2* insert and ddH_2O up to 10 µl. After incubating for 1 hour at RT, ligation reactions were used in transformations.

2.6.2. Transformations

High-efficiency JM109 cells (Promega) were transformed with 2 µl of ligated plasmid DNA by incubating on ice for 30 minutes then heat-shocking in a 42°C waterbath for 45 seconds. Transformations were chilled on ice for a further 2 minutes then mixed with 200 µl of pre-warmed SOC medium (Sigma) and incubated for 1.5 hours in a 37°C shaking incubator at 150 rpm. 150 µl of each transformation was then spread onto a lysogeny broth (LB) agar plate containing 100 µg/ml of ampicillin (Sigma), 0.5 mM of isopropyl β-D-1-thiogalactopyranoside (IPTG) (Promega) and 80 µg/ml of X-Gal (Sigma) and incubated overnight at 37°C. Recombinant plasmids were selected by blue-white screening; the pGEM®-T vector contains a segment of the *LacZ* gene, which encodes the β-galactosidase enzyme. In the presence of IPTG, β-galactosidase is expressed and cleaves X-gal to produce a blue product. In recombinant plasmids, successful ligation of the *Ikzf2* insert into pGEM®-T will interrupt transcription of *LacZ* and produce white colonies. In non-recombinant plasmids, pGEM®-T will self-ligate, enabling transcription of *LacZ* and producing blue

colonies. Single white colonies were picked into LB broth for DNA preparation and Sanger sequencing.

2.6.3. Isolation of Plasmid DNA

By Miniprep: Plasmids were amplified by inoculating 10 ml of LB broth containing ampicillin (100 µg/ml) with single colonies and incubating overnight at 37°C and 200 rpm. Plasmid DNA was recovered using the Wizard® *Plus* SV Miniprep Purification System (Promega). Bacterial cultures were centrifuged at 2000 rpm for 10 minutes to pellet cells and enable culture media to be removed. Cell pellets were then resuspended, lysed and loaded onto a spin column, where plasmid DNA bound to a silica membrane and unbound contaminants (RNA, proteins, metabolites) were removed by a series of wash steps. Plasmid DNA was eluted from the column using 100 µl ddH_2O, yielding a total of 10 – 30 µg.

By Maxiprep: The EndoFree Plasmid Maxi Kit (Qiagen) was used to isolate greater yields of plasmid DNA (500 – 750 µg). 500 µl of bacterial culture, set up as above, was added to 250 ml of LB broth containing ampicillin (50 µg/ml) and incubated overnight at 37°C and 200 rpm. Following centrifugation, cell pellets were resuspended, lysed, filtered and incubated with ER buffer to remove endotoxins, which can interfere with downstream processes such as transfection. Lysates were applied to a Qiagen-tip, which uses anion-exchange chromatography to isolate plasmid DNA from contaminants. DNA was eluted from the tip using a high-salt buffer then concentrated by precipitation with isopropanol and resuspended in 500 µl TE.

Plasmid DNA was sent to Source Bioscience for Sanger sequencing using vector-specific sequencing primers (Table 2.2). Each sequencing reaction required 5 µl of plasmid DNA at 100 ng/µl and 5 µl of primer at 3.2 pmol/µl.

Table 2.2: Vector-specific sequencing primers.

Primer	Vector	Primer Sequence (5' – 3')
T7_F	pGEM®-T	TAATACGACTCACTATAGGG
SP6	pGEM®-T	TATTTAGGTGACACTATAG
pCMV	pCMV-Myc	GATCCGGTACTAGAGGAACTGAAAAAC
BGHR	pCMV-Myc	TAGAAGGCACAGTCGAGG
EGFP	pEGFP-C3	CATGGTCCTGCTGGAGTTCGTG

2.6.4. Site-Directed Mutagenesis

Site-directed mutagenesis with the QuikChange® Lightning Kit (Agilent Technologies) was used to introduce the c.1551C>A mutation into wild-type *Ikzf2* plasmid DNA using the following primers:

173_c1551a: 5'-CGCTACGAATTTTCATCACA**A**ATTGTTCGAGGGGAGCA-3'

173_c1551a_anti: 5'-TGCTCCCCTCGAACAAT**T**TGTGATGAAAATTCGTAGCG-3'

The PCR product was treated with methylation-sensitive enzyme *DpnI* to digest methylated plasmid DNA and leave intact unmethylated, mutagenised *Ikzf2* DNA. Transformation and sequence analysis was carried out as in **2.6.2.** and **2.6.3.** to confirm successful mutagenesis.

2.6.5. Generation of Tagged Constructs

Sequence-verified pGEM®-T DNA preparations were incubated with *EcoRI* and *KpnI* restriction enzymes (see **2.3.6.**) then electrophoresed to digest and separate the 1.5 kb *Ikzf2* insert from the 3 kb pGEM®-T backbone. *Ikzf2* DNA fragments were excised from the gel and purified using Geneclean II (MP Biomedicals). In order to generate N-terminally tagged fusion proteins, wild-type and c.1551C>A *Ikzf2* inserts were ligated in-frame into pCMV-Myc (Clontech) and pEGFP-C3 (Clontech) expression vectors, which had been linearised by restriction digest using *EcoRI* and *KpnI*. Ligation reactions were incubated for 1 hour at RT

and comprised an insert:vector ratio of 2:1, 1 unit of T4 DNA Ligase, 1x Ligase Buffer (both NEB) and ddH_2O up to 10 µl. JM109 cells were transformed with plasmid DNA as in **2.6.2.** and plated onto LB agar plates containing 100 µg/ml of ampicillin (for c-Myc plasmids) or kanamycin (Sigma) (for EGFP plasmids). Plasmid DNA was extracted from single colonies and verified by Sanger sequencing using vector-specific primers (Table 2.2). Sequence-verified plasmid DNA was then used for transfection into mammalian cell lines.

2.7. Tissue Culture

Cos-7 cells (derived from monkey kidney (Gluzman, 1981)) and HEK293T cells (derived from human embryonic kidney (Graham et al., 1977)) were kindly provided by Chris Esapa (MRC Harwell) and cultured using sterile techniques in a BioMAT2 Class 2 Microbiological Safety Cabinet (Contained Air Solutions). Frozen 1 ml cell aliquots were rapidly defrosted in a 37°C waterbath and transferred to 75 cm^2 flasks (Greiner Bio-One) containing 14 ml of pre-warmed high-glucose Dulbecco's Modified Eagle Medium (DMEM) (Invitrogen) with 10% foetal bovine serum (FBS) (Invitrogen) and 1x penicillin/streptomycin (Invitrogen). Cells were grown in a 37°C incubator (Sanyo) with 5% CO_2 until confluent. Prior to carrying out tissue culture procedures, DMEM and Trypsin were pre-warmed in a 37°C waterbath.

2.7.1. Splitting Cells

Once cells had reached 80 – 90% confluency, they were washed in Dulbecco's PBS (DPBS) (Gibco) and detached from the flask by incubating with 2 ml of 0.05% Trypsin-EDTA (Gibco) for 2 – 5 minutes at RT (HEK293T) or 37°C (Cos-7). Trypsin was inactivated by adding 8 ml of DMEM. Depending on the cell density required, 500 µl (1:20 dilution) – 2 ml (1:5 dilution) of

this cell suspension was transferred into a fresh flask containing 14 ml DMEM and incubated at 37°C, 5% CO_2.

2.7.2. Freezing Cells

Cells were washed in DPBS and trypsinised as before. Following inactivation of trypsin with DMEM, cell suspensions were transferred into a 15 ml falcon and centrifuged at 1200 rpm for 5 minutes to pellet the cells. The supernatant was removed and the cell pellet resuspended in 10 ml of freezing media (10% dimethyl sulfoxide (DMSO) in FBS), which was then aliquoted into 1 ml cryotubes and stored at -80°C.

2.7.3. Transfecting Cells

Transient transfections were carried out using JetPEI® (PolyPlus Transfection), a polyethylenimine (PEI)-based transfection reagent. JetPEI® operates by condensing DNA into cationic complexes which bind anionic components of the cell membrane, are internalised by endocytosis then rupture to release DNA. Following manufacturer's instructions, a 'forward transfection' protocol was used on adherent cells which had been plated 24 hours previously. Briefly, confluent cells were trypsinised as before and, prior to centrifugation, counted using a single cell counting chamber (Hawksley) under an Olympus IMT-2 microscope to establish cell density. Cos-7 cells were seeded either directly onto 6-well plates (for Western blotting) or onto 22 x 22 mm^2 sterile coverslips in 6-well plates (for subcellular localisation) at a volume of $1x10^5$ cells per well. HEK293T cells were seeded at a volume of $5x10^5$ cells per well for Western blotting and co-immunoprecipitation (co-IP). Plated cells were incubated for 24 hours at 37°C, 5% CO_2 then transiently transfected with the appropriate helios expression construct. For single transfections, 6 µl of JetPEI® was premixed with 100 µl of 150 mM sodium chloride (NaCl) (PolyPlus Transfection) then added

to 1 µg of plasmid DNA diluted in 100 µl of 150 mM NaCl. For co-IP co-transfections, a total of 2 µg of plasmid DNA was transfected in the following combinations:

- Wild-type: 1 µg c-Myc-tagged wild-type + 1 µg EGFP-tagged wild-type
- Heterozygous: 1 µg c-Myc-tagged wild-type + 1 µg EGFP-tagged H517Q
- Heterozygous: 1 µg c-Myc-tagged H517Q + 1 µg EGFP-tagged wild-type
- Homozygous: 1 µg c-Myc-tagged H517Q + 1 µg EGFP-tagged H517Q

For co-IP experiments, single transfections were also carried out using 1 µg of c-Myc wild-type or 1 µg EGFP wild-type to provide negative controls.

After incubating for 15 – 30 minutes at RT, the transfection complexes were gently pipetted onto plated cells, which were incubated for a further 24 – 48 hours at 37°C, 5% CO_2.

2.8. *In Silico* and *In Vitro* Characterisation

2.8.1 *In Silico* Analyses

The functional impact of the *cello* mutation was assessed *in silico* using the following online prediction tools:

- Sorting Intolerant From Tolerant (SIFT) (http://sift.jcvi.org/)
- Polymorphism Phenotyping version 2 (PolyPhen-2) (http://genetics.bwh.harvard.edu/pph2/)
- Protein Variation Effect Analyser (PROVEAN) (http://provean.jcvi.org/index.php)

RaptorX (http://raptorx.uchicago.edu/) and PyMOL (http://www.pymol.org/) were also used to predict and visualise three-dimensional (3D) molecular structures.

2.8.2. Subcellular Localisation

At 24 hours post-transfection, cells were rinsed twice with cold PBS, fixed in 4% PFA for 10 minutes at RT and permeabilised with 1% Triton-X in PBS for 15 minutes. After blocking in 10% donkey serum in PBST (PBS + 0.1% Tween) for 1 hour at RT, cells were incubated with F-actin marker Texas Red®-X Phalloidin (1:200, Invitrogen) and primary antibodies overnight at 4°C. Cells were rinsed twice in cold PBS then incubated with fluorophore-conjugated secondary antibodies for 1 hour RT. Following two rinses in cold PBS, cells were incubated with DAPI at 1 µg/ml for 60 seconds then rinsed again. Coverslips were mounted onto charged slides with SlowFade® Gold (Life Technologies) and cells were visualised using a Zeiss LSM 710 multiphoton fluorescence confocal microscope.

Primary antibodies: rabbit anti-Myc (1:500, Santa Cruz); goat anti-helios (1:600, Santa Cruz). Secondary antibodies: donkey anti-rabbit Alexa Fluor® 488 and donkey anti-goat Alexa Fluor® 488 (1:500, Invitrogen).

2.8.3. Western Blotting

At 48 hours post-transfection, cells were rinsed twice with cold PBS then lysed in 250 µl of radio-immunoprecipitation assay buffer (150 mM sodium chloride (NaCl), 1% nonidet P-40, 0.5% deoxycholate, 0.1% sodium dodecyl sulphate, 50 mM Tris pH 7.5 in milliQ water) containing 1x Protease Inhibitors (Roche) and scraped into chilled eppendorf tubes. Lysates were sonicated for 10 – 15 seconds to disrupt cell membranes then reduced with NuPAGE® Sample Reducing Agent (Invitrogen) and NuPAGE® LDS Sample Buffer at 70°C for 10 minutes and loaded onto precast NuPAGE® NOVEX® 4 – 12% Bis-Tris gels (Invitrogen) alongside Precision Plus Protein™ Dual Colour Standard (Biorad). Gels were run with 1x NuPAGE® MOPS-sodium dodecyl sulphate running buffer (Invitrogen) for 1 hour at 200 V

then were transferred onto a nitrocellulose membrane using iBlot® Transfer Stacks and the iBlot® machine at 20 V for 7 minutes (both Invitrogen). Membranes were blocked in 5% milk (Sigma) in PBST for 1 hour at RT then incubated with either rabbit anti-Myc primary antibody (1:500, Santa Cruz) or mouse anti-GFP (1:4000, Roche) overnight at 4°C. Mouse 12G10-anti-alpha Tubulin (1:5000, Developmental Studies Hybridoma Bank) was also used as a loading control. After 4x 5 minutes washes in PBST, membranes were incubated with donkey anti-rabbit IRDye 680RD and donkey anti-mouse IRDye 800CW secondary antibodies (1:15,000, LI-COR) for 1 hour at RT. Membranes were washed again in PBST then rinsed in MilliQ ultrapure water and dried for 15 minutes before imaging using the Odyssey® Sa Infared Imaging System (LI-COR).

2.8.4. Co-Immunoprecipitation (Co-IP)

DMEM was removed from cells 24 hours after co-transfection and replaced with fresh media. At 48 hours post-transfection, cells were washed and lysed as in **2.8.3.**, then left on ice for 30 minutes to enable protease inhibitor activity. Lysates were centrifuged at 14,000 rpm for 5 minutes to pellet cell debris and the supernatant was incubated with Protein G beads (Roche) that had been pre-washed in RIPA buffer for 2 hours at 4°C on a rotator. This step pre-cleared the cell lysates in order to prevent non-specific binding during immunoprecipitation. Samples were centrifuged at 1000 rpm for 1 minute to pellet the beads. Immunoprecipitation was then carried out by incubating the supernatant with 1 µg of rabbit anti-Myc (Sigma) or mouse anti-GFP (Roche) antibody overnight at 4°C on a rotator. The following day, pre-washed protein G beads were added to each sample for 1 hour at 4°C on a rotator to capture the immunoprecipitation complex. The beads were pelleted by centrifugation at a slow speed and supernatant was discarded. The bead and

immunoprecipitation complexes were washed with RIPA buffer containing protease inhibitors three times. During the final wash, a similar residual amount of buffer was left in each tube to ensure protein complexes would be at the same approximate concentration between samples. Samples were then reduced at 70°C for 10 minutes using NuPAGE® Sample Reducing Agent and NuPAGE® LDS Sample Buffer (both Invitrogen) to release protein complexes. Samples were loaded onto precast NuPAGE® NOVEX® 4 – 12% Bis-Tris gels (Invitrogen) alongside their corresponding reduced cell lysates and Precision Plus Protein™ Dual Colour Standard (Biorad). Western blotting was carried out as in **2.8.3.** using rabbit anti-Myc primary antibody (1:500, Santa Cruz) and mouse anti-GFP primary antibody (1:4000, Roche) with donkey anti-rabbit IRDye 680RD and donkey anti-mouse IRDye 800CW secondary antibodies (1:15000, LI-COR).

2.9. RNA Methods

2.9.1. RNA Extraction

For RNA-Seq: Three pairs of sub-dissected cochlear ducts from P8 *Ikzf2*$^{+/+}$ and *Ikzf2*$^{cello/cello}$ mice were pooled and homogenised as in **2.4.5.** RNA was extracted using the Direct-zol™ RNA Miniprep Kit (Zymo Research), which uses silica-based spin columns to extract total RNA. An in-column DNaseI digestion step was carried out to ensure complete removal of DNA before RNA was eluted in 30 µl of DNase/RNase-free water and stored at -80°C.

For qRT-PCR Validations: Cochlear ducts were sub-dissected from P8 *Ikzf2*$^{+/+}$, heterozygous (*Ikzf2*$^{cello/+}$) and *Ikzf2*$^{cello/cello}$ mice and flash-frozen as in **2.4.5.** by Maggie Matern at the University of Maryland. Total RNA was extracted from two pairs of cochlear ducts pooled per genotype using the Direct-zol™ RNA Miniprep Kit (Zymo Research), as above.

2.9.2. RNA Quantification and Quality Analysis

RNA concentration and absorbance ratios (260/230 and 260/280) were measured using the Epoch Micro-Volume Spectrophotometer System and Take3 Micro-Volume Plate (BioTek). RNA quality was assessed on a Bioanalyser with the RNA 6000 Nano Kit (Agilent), using 1.5 µl of RNA which had been heat-denatured at 70°C for 2 minutes. This kit provides both quantitative and qualitative data, including RNA concentration, absorbance ratios, RNA Integrity Number (RIN), gel-like images and electropherograms. Only samples with a high RIN (>7) and minimal degradation were used for subsequent RNA-Seq, cDNA synthesis and qRT-PCR.

2.9.3. RNA Sequencing (RNA-Seq)

Frozen cochlear RNA from P8 *Ikzf2*$^{+/+}$ and *Ikzf2*$^{cello/cello}$ mice was sent to Dr Ronna Hertzano at the University of Maryland for sequencing using the HiSeq 2500 system (Illumina). Initial data analysis was performed by Sean Daugherty at the Institute for Genomic Sciences, University of Maryland; sequencing reads were aligned to *Mus musculus* reference genome (assembly GRCm38.74) and normalised for transcript read length and sequencing depth, then analysed using HTSeq software to perform raw read counts and DESeq software to generate a list of differentially expressed genes (Anders and Huber, 2010, Anders et al., 2015). Subsequent analyses, including Gene Ontology (GO) enrichments, were carried out at MRC Harwell using the online Search Tool for the Retrieval of Interacting Genes/Proteins (STRING) database version 10.0 (http://string-db.org/).

2.9.3.1. Computational Regulatory Network Analysis

The transcriptional network of helios was investigated by Dr Ronna Hertzano and Sean Daugherty at The University of Maryland and Dr Rani Elkon at Tel Aviv University (Israel) using the iRegulon package (http://iregulon.aertslab.org/index.html) (Janky et al., 2014).

2.9.4. Parallel Validation of RNA-Seq Results

qRT-PCR was undertaken by Dr Ronna Hertzano, Dr Beatrice Milon and Maggie Matern at the University of Maryland to validate a selection of RNA-Seq results and also investigate the expression of select OHC-enriched, IHC-enriched and hair cell-enriched transcripts (Table 2.3) (Liu et al., 2014). RNA was extracted from two *Ikzf2*$^{+/+}$, *Ikzf2*$^{cello/+}$ and *Ikzf2*$^{cello/cello}$ samples (each a pool of two pairs of cochlear ducts) as in **2.9.1.**, thus providing two biological replicates per genotype group.

2.9.4.1. Complementary DNA (cDNA) Synthesis

Complementary DNA (cDNA) was generated by reverse transcriptase of high-quality cochlear RNA using the Maxima First Strand cDNA Synthesis Kit for qRT-PCR (Thermo Scientific). Reactions were set up according to the manufacturer's instructions, using 80 – 400 ng of RNA in a total reaction volume of 10 µl. cDNA was stored at -20°C.

2.9.4.2. Quantitative Real-Time PCR (qRT-PCR)

cDNA samples were analysed by qRT-PCR using pre-designed 96-well Custom TaqMan® Array Plates (Applied Biosystems®) for the assays listed in Table 2.3. Each assay comprises a primer pair and a TaqMan® probe that has a FAM dye label at the 5' end and a quencher molecule at the 3' end. Upon annealing to complementary target sequence during PCR, each probe is cleaved by the endogenous nuclease activity of *Taq* polymerase. This releases the quencher molecule and emits a florescent signal that is directly proportional to the

amount of DNA template present in the PCR reaction. Accumulated fluorescence is detected in real-time, enabling rapid assaying of gene expression.

Table 2.3: TaqMan® Gene Expression Assays used in Custom TaqMan® Array Plates for validation of RNA-Seq results and investigation of hair-cell enriched transcripts.

Gene	TaqMan® Gene Expression Assay ID	Cochlear Expression Pattern
ATPase, aminophospholipid transporter, class I, type 8A, member 2 (*Atp8a2*)	Mm00443740_m1	OHC-enriched
ATPase, aminophospholipid transporter, class I, type 8b, member 1 (*Atp8b1*)	Mm01257688_m1	OHC-enriched
Dynamin 3 (*Dnm3*)	Mm00554098_m1	OHC-enriched
Elongation of very long chain fatty acids-like 2 (*Elovl2*)	Mm00517086_m1	OHC-enriched
Voltage gated KQT-like subfamily Q, member 4 (*Kcnq4*)	Mm01185500_m1	OHC-enriched
Lim bud and heart development (*Lbh*)	Mm00522506_m1	OHC-enriched
OCIA domain containing 2 (*Ociad2*)	Mm01212031_m1	OHC-enriched
Oncomodulin (*Ocm*)	Mm00712881_m1	OHC-enriched
Phospholipase B domain containing 1 (*Plbd1*)	Mm00482098_m1	OHC-enriched
Solute carrier family 26, member 5 (*Slc26a5*)	Mm00446145_m1	OHC-enriched
Stereocilin (*Strc*)	Mm01328720_m1	OHC-enriched
ATPase, Ca++ transporting, ubiquitous (*Atp2a3*)	Mm00443898_m1	IHC-enriched
Growth factor independent 1 (*Gfi1*)	Mm00515855_m1	IHC and OHC
Myosin 6 (*Myo6*)	Mm00500651_m1	IHC and OHC
Myosin 7a (*Myo7a*)	Mm01274015_m1	IHC and OHC
POU domain class 4 transcription factor 3 (*Pou4f3*)	Mm04213795_s1	IHC and OHC
β-actin	Mm00607939_s1	Endogenous Control
Glyceraldehyde 3-phosphate dehydrogenase (*Gapdh*)	Mm99999915_g1	Endogenous Control

IHC, inner hair cell; OHC, outer hair cell.

First, an unbiased cDNA pre-amplification step was performed using a Custom TaqMan® PreAmp Pool (Applied Biosystems®) with primers for the genes listed in Table 2.3. For each

reaction, 5 µl of cDNA (2 ng/µl) was combined with 5 µl of the Custom Taqman® PreAmp Pool and 10 µl of 2x TaqMan® PreAmp Master Mix. Reactions were run on the following programme: 95°C for 10 minutes, 14 cycles of denaturation at 95°C for 15 seconds and annealing and extension at 60°C for 4 minutes, then hold at 99.9°C for 10 minutes.

qRT-PCR reactions were set up in duplicate in Custom TaqMan® Array Plates using 5 ng of pre-amplified cDNA per well. For each reaction, 0.5 µl of pre-amplified cDNA (10 ng/µl) was combined with 11.5 µl of nuclease-free water and 12 µl of 2x TaqMan® Fast Advanced PCR Master Mix (Applied Biosystems®). 20 µl of this reaction mix was then loaded into the appropriate well of the Custom TaqMan® Array Plate. Two biological replicates were analysed for each genotype group. Reactions were performed on the 7900HT Fast Real-Time PCR System (Applied Biosystems®) using a standard protocol of 95°C for 20 seconds to activate *Taq* polymerase, followed by 40 cycles of denaturation at 95°C for 1 second and annealing and extension at 60°C for 20 seconds.

Results were analysed with the ExpressionSuite software (Life Technologies), using the averaged expression values of β-actin and *Gapdh* as the endogenous controls. Cycle threshold (CT) values were defined as the number of cycles required for the fluorescent signal generated within each reaction to cross the threshold level set by the software. For each biological sample, duplicate CT values for the gene of interest were first averaged then normalised to the expression of β-actin and *Gapdh* using the calculation [mean CT of gene of interest – mean CT of endogenous controls] to give delta CT (dCT) values. dCT values were then averaged for each set of biological replicates to give a single mean dCT value for each genotype group. The comparative CT method was used to assess differences in gene expression between genotype groups; for each assay, the mean dCT value from *Ikzf2*$^{+/+}$ was

set as the calibrator and used in the calculation [mean dCT of genotype – mean dCT of *Ikzf2*$^{+/+}$] to generate delta delta CT (ddCT) values. Relative quantitation (RQ), or fold change, was then calculated for each genotype group by [$2^{\wedge\text{-ddCT}}$]. Statistical significance was assessed using one-way ANOVA performed on the dCT values of each biological replicate.

2.10. Luciferase Reporter Assays

In order to assess gene targets of helios, promoters of interest were cloned into luciferase reporter vectors for co-transfection with c-Myc-tagged wild-type (WT) or H517Q helios constructs. Two potential promoter regions were selected for analysis: a region of DNA encompassing the published *Slc265* (prestin) promoter sequence (Gross et al., 2011a, Gross et al., 2011b) and an intronic region immediately upstream of the oncomodulin ATG start codon (Table 2.4). Both of these regions contain GGGAA motifs, which are known to be core ikaros family zinc finger (IKZF) recognition sites (Bao et al., 2004, Georgopoulos et al., 1994, Molnar and Georgopoulos, 1994, Perdomo et al., 2000). As the strength of these promoter elements was unknown, they were cloned into the pGL3-Enhancer luciferase reporter vector (Promega), which contains a Simian virus 40 (SV40) enhancer.

2.10.1. Cloning into pGL3 Luciferase Reporter Vectors

Prior to cloning into the pGL3-Enhancer vector, promoters of interest were first cloned into the pGEM®-T vector as in **2.6.1.** and **2.6.2.**. Briefly, promoter regions were amplified by PCR primers that added *NheI* and *HindIII* restriction enzyme recognition motifs on to the 5’ and 3’ end (Table 2.4).

Table 2.4: Promoter regions and primers for luciferase assay cloning.

Gene	Cloned Promoter Region	Forward Primer (5' – 3')	Reverse Primer (5' – 3')
Slc26a5 (Prestin)	gtgcagtgatggttttaacttgggactactg ttaaagtcaccaaggacttcctccatggggc tacaagcctcagctctgatcagaatagcaag tgaaactttaagaaaaagggtaaaatacctc acaagacgtgaggtcaatttaaggaccaatc ttaccatctttccttttgtttgccgaatagc tggccagagttcacctgactcacacttcccc ctaatgccgagctattgacagggactgcagg actgtcgttaaacttaccatgaactcttgct gaacacttacacgttacctatttattgctct gaggGGGAAtaaataaggtttatggctttt ttttcatttatttttgctcactatatttgta agtaagcacaactctacacaacaata	TAGCTAGCgtgc agtgatggtttt aacttgg	TAAAGCTTctcg ggaactgcagaa cacatccca
Ocm (Oncomodulin)	gtgagtagctggtgggctcaccagactccga gatcctcttctctgcacgcactgtattagac ttggcacccgggaggattttcacctctgctg catgggctaatcttccacaagggatctgtgg tattgcaatctcgggttgatgcatgacggtg atgttgtgtttatagcatggctaaggtttag ctgcctatgatgattggttaGGGAAggataa tttttgctagaagattggactttaGGGAAaa aaaaccccacttttatttgcttttagaattt taaaagactgggccatgtagctcaggctggt ttggagttcattatgtagtcaaggatgctct tggactctttagcatcctcctcctcctcttt ttcctcctcctccttcttgttcttcttcttg ttcttcctcttcccctttctcttcccccttct ctccctcttcctcctcttcctcctccttctt gttcttcttcctcttcccctttctcctctccc ccttgtcctcctcttccttctcctcctcctc ctcttcttctttctgagtaccaagattgcaa gtgtgcacacgatgaccagcttggtctttct ttgtctttttttttaacttcaattttggag tgaattcaagagcaaccatgtagtcaagagg tggctggagtcttttctgtatctgggtttgg tttagtactctgccccatcacttaacaggtc cttatggccacatcttaaaaaaattctagag atacacggtgtcggtgagtggctgagaatgt gtggtcttcccatttctctgtcaccgtggct cacatcttgtttcctctgttcggccaggtag	TAGCTAGCgtga gtagctggtggg ctcacc	TAAAGCTTctac ctggccgaacag aggaaac

The known ikaros family zinc finger core binding motif (GGGAA) is highlighted in yellow.

Amplicons were purified using GeneClean II then ligated into pGEM®-T and transformed into JM109 competent cells. Plasmid DNA was isolated from single colonies and verified by Sanger sequencing using T7 and SP6 primers. Promoter regions were excised from pGEM®-T by restriction digest using *NheI* and *HindIII* and ligated into linearised pGL3-Enhancer vector (kindly provided by Michael Parsons, MRC Harwell). Ligations were performed using T4 DNA

Ligase as in **2.6.5.**, with insert:vector ratios between 2:1 and 3:1. JM109 cells were transformed with pGL3 ligation reactions then plated onto LB agar plates containing 100 µg/ml of ampicillin. Maxipreps of single colonies were verified by Sanger sequencing then used for luciferase assay co-transfections.

2.10.2. Co-Transfections

Plasmid DNA was co-transfected into HEK293T cells that had been seeded onto 12-well plates 24 hours previously at a volume of $2x10^5$ cells per well. For each co-transfection, 4 µl of JetPEI® (PolyPlus Transfection) was premixed with 50 µl of 150 mM NaCl (PolyPlus Transfection) and was added to 50 µl of 150 mM NaCl containing a total of 3 µg of plasmid DNA:

- 2 µg of pGL3-Enhancer luciferase reporter vector containing the promoter of interest
- 1 µg of c-Myc-tagged wild-type helios, c-Myc-tagged H517Q helios or c-Myc empty vector. To mimic a *cello* heterozygous state, co-transfections were also carried out using 0.5 µg of c-Myc-tagged wild-type helios and 0.5 µg of c-Myc-tagged H517Q helios.
- 2 ng of Promoterless pGL4.70[*hRluc*] *Renilla* luciferase vector (from Michael Parsons, MRC Harwell) to enable normalisation of results

The *Renilla* luciferase vector, derived from sea pansy (Lorenz et al., 1991, Matthews et al., 1977), has constitutive luciferase activity and is used as an internal co-transfection control for experimental firefly luciferase reporter vectors. Using the Dual-Luciferase® Assay Reporter System (Promega), both firefly and *Renilla* luciferase activity can be assayed sequentially from a single sample, which enables firefly luciferase to be normalised to

Renilla luciferase in order to offset any intra- and inter-assay variations in transfection efficiency.

At least two separate experiments were carried out, within which each co-transfection was carried out in triplicate to provide three biological replicates.

2.10.3. Cell Lysis

At 24 hours post-transfection, cells were washed in PBS then incubated with 250 µl 1x Passive Lysis Buffer in ddH_2O (Promega) for 15 minutes at RT. Cell lysates were pipetted up and down to ensure complete disruption then transferred to a luminometer plate (Promega) in 20 µl duplicates to provide two technical replicates. The remaining cell lysates were stored at -20°C.

2.10.4. Luminometer Assay

Cell lysates were analysed using the Dual-Luciferase® Assay Reporter System (Promega) on a Varioskan™ Flash Multimode Reader luminometer (Thermo Scientific) using the SkanIt™ software (Thermo Scientific). Prior to each run, Luciferase Assay Reagent II (LAR II) (Promega) and 1x Stop and Glo® Reagent (Promega) were prepared, according to manufacturer's instructions. These reagents are added to cell lysates sequentially; first, LAR II measures firefly luciferase activity then 1x Stop and Glo® Reagent quenches LAR II and enables *Renilla* luciferase activity to be assayed. The luminometer was set up by washing both injectors with 1500 µl of ddH_2O then priming injector 1 with 800 µl of LAR II and injector 2 with 800 µl 1x Stop and Glo® Reagent. The following programme was carried out:

- Dispense 100 µl LAR II from injector 1 into each well
- Shake plate for 5 seconds at 600 shakes per minute (spm)

- 2 second pre-measurement delay
- Measure firefly luciferase activity for 5000 ms
- Dispense 100 µl 1x Stop & Glo® Reagent from injector 2 into each well
- Shake plate for 5 seconds at 600 spm
- 2 second pre-measurement delay
- Measure renilla luciferase activity for 5000 ms

Prior to statistical analysis, firefly luciferase activity was normalised to *Renilla* luciferase activity and averaged for each set of technical replicates.

2.11. Electrophysiology

Electrophysiological analyses of *Ikzf2*$^{cello/cello}$ and *Ikzf2*$^{cello/+}$ apical-coil OHCs were undertaken at P9, P16 and P18 by Professor Walter Marcotti and Dr Stuart Johnson at the University of Sheffield (UK). Cochleae were dissected in normal extracellular solution (135 mM NaCl, 5.8 mM potassium chloride (KCl), 1.3 mM calcium chloride ($CaCl_2$), 0.9 mM magnesium chloride ($MgCl_2$), 0.7 mM monosodium phosphate (NaH_2PO_4), 10 mM Hepes-sodium hydroxide (NaOH), 5.6 mM D-glucose) containing 2 mM sodium pyruvate, 50x minimum essential medium (MEM) amino acids solution and 100x MEM vitamins solution (Thermo Scientific), with pH adjusted to 7.5. The dissected cochleae were transferred to a microscope chamber, immobilized as previously described (Corns et al., 2014) and continuously perfused with a peristaltic pump using the above extracellular solution. The organs of Corti were viewed using an upright Nikon Eclipse FN1 microscope (x60 objective) with Normarski optics.

2.11.1. Potassium Current Recordings

Patch-clamp recordings of OHCs were performed using an Optopatch Amplifier (Cairn Research Ltd.). Patch pipettes were made from soda glass capillaries (Harvard Apparatus Ltd.) and had a typical resistance in extracellular solution of 2 – 3 MΩ. In order to reduce the electrode capacitance, patch electrodes were coated with surf wax (Mr Zog's Sex Wax®). Potassium current recordings were performed at RT using intracellular solution containing 131 mM KCl, 3 mM $MgCl_2$, 1 mM ethyleneglycoltetraacetic acid (EGTA)-potassium hydroxide (KOH), 5 mM disodium adenosine triphosphate (Na_2ATP), 5 mM Hepes-KOH and 10 mM Na_2-phosphocreatine (pH 7.3). Data acquisition was controlled by pCLAMP software using Digidata® 1440A boards (Molecular Devices). Recordings were low-pass filtered at 2.5 kHz (8-pole Bessel), sampled at 5 kHz and stored on computer for off-line analysis using Origin software (OriginLab Corporation). Membrane potentials in voltage clamp were corrected for the voltage drop across the uncompensated residual series resistance and for a liquid junction potential (-4 millivolts (mV)).

2.11.2. Mechanoelectrical Transducer (MET) Current Recordings

MET currents were elicited by stimulating the hair bundles of OHCs using a fluid jet from a pipette (tip diameter 8 – 10 µm) driven by a piezoelectric disc (Corns et al., 2014). The pipette tip of the fluid jet was positioned near to the bundles to elicit a maximal MET current. Mechanical stimuli were applied as 50 Hz sinusoids (filtered at 0.25 kHz, 8-pole Bessel) with driving voltages of $\pm$ 40 V. MET currents were recorded with a patch pipette solution containing 106 mM cesium-glutamate, 20 mM cesium chloride (CsCl), 3 mM $MgCl_2$, 1 mM EGTA-cesium hydroxide (CsOH), 5 mM Na_2ATP, 0.3 mM disodium guanosine

triphosphate (Na_2GTP), 5 mM Hepes-CsOH and 10 mM sodium phosphocreatine (pH 7.3). Membrane potentials were corrected for the liquid junction potential (–11 mV).

2.11.3. Electromotility Analysis

The presence of electromotile activity in OHCs was estimated by applying a depolarising voltage step from the holding potential of -64 mV to +56 mV. Changes in cell length were viewed and recorded using a Nikon Eclipse FN1 microscope (x75 magnification) with a Flash 4.0 SCCD camera (Hamamatsu). Cell body movement was then tracked using Fiji image processing software. Briefly, lines were drawn across the basal membrane of patched OHCs, perpendicular to the direction of cell motion, and a projected time-based z-stack of the pixels under the line was made (Schindelin et al., 2012). Cell movement was measured with Adobe Photoshop as a pixel shift and then converted to nm (290 pixels = 10 µm).

2.12. Immunological Phenotyping

Owing to the previously reported expression and function of helios in the haematopoietic system (Dovat et al., 2005, Getnet et al., 2010, Kelley et al., 1998, Serre et al., 2011, Nakase et al., 2002, Takatori et al., 2015), *cello* mice were subject to immunological phenotyping using haematological analysis and fluorescence-activated cell sorting (FACS).

2.12.1. Haematological Analysis

Age-matched and sex-matched mice were culled by inhalation of isoflourane. Following cessation of the heartbeat, the retro-orbital sinus was punctured using a glass capillary tube and 200 µl of blood was collected into an EDTA-coated tube. Samples were immediately agitated on a rotary mixer for 30 minutes at RT to prevent clotting then run on an ADVIA®

2120 Haematology System (Siemens) to generate complete blood counts, differential white blood cell counts and platelet counts.

2.12.2. Fluorescence-Activated Cell Sorting (FACS)

Age-matched and sex-matched mice were culled by inhalation of isoflourane. Spleens were collected into 1 ml of Roswell Park Memorial Institute (RPMI)-1640 medium (Sigma) then homogenised in 2.6 ml of RPMI-1640 containing 2% FBS and 400 µl of 7x enzyme cocktail (Table 2.5) using a gentleMACS™ Octo Dissociator (Miltenyi Biotec Ltd.).

Table 2.5: Preparation of 7x Enzyme Cocktail used in homogenisation of samples prior to fluorescence-activated cell sorting analysis.

Reagent	Volume for 7x Enzyme Cocktail
DNase I (1 mg/ml) (Sigma)	500 µl
Collagenase II (70 µg/ml) (Worthington Biochemical)	500 µl
RPMI-1640 containing 2% FBS	4 ml

FBS, foetal bovine serum.

Homogenates were mixed with 300 µl of Stopping Buffer (0.1 M EDTA in PBS) to halt enzymatic digestion, passed through a 70 µm nylon mesh filter to obtain a single-cell suspension then centrifuged at 1300 rpm for 5 minutes at 4°C. Cell pellets were resuspended in 1 ml of FACS Buffer (5 mM EDTA and 0.5% FCS in PBS) and a 1:300 dilution was made for counting using a Moxi™ Z Mini Automated Cell Counter (ORFLO Technologies). Cells were plated into a 96-well plate at a volume of 4 million cells per well, washed with 100 µl of FACS Buffer then resuspended in 100 µl of 1x red blood cell Lysis Buffer (eBioscience) for 1 minute on ice. Cells were pelleted by centrifugation, washed with FACS Buffer then resuspended in 50 µl of Fc Block (1:100, BD Pharmingen) and incubated for 15

minutes on ice to prevent non-specific antibody binding. After pelleting and washing with FACS Buffer, cells were resuspended in 50 µl of the appropriate antibody cocktail (Table 2.6) and incubated for 20 minutes on ice in dark conditions. Cells were again pelleted and washed with FACS Buffer then resuspended in FACS Buffer containing SYTOX® Blue (1:10,000, Life Technologies) to enable discrimination between live and dead cells. Cells were analysed using a BD FACSCanto™ II system (BD Biosciences) equipped with a 405 nm, 488 nm and 633 nm laser, using the parameters and gating strategy listed in Table 2.7.

Table 2.6: Antibody markers used in fluorescence-activated cell sorting analysis.

Panel 1			
Marker	**Dilution**	**Fluorochrome**	**Specificity**
Live/dead	1:10000	SYTOX Blue (Invitrogen)	Live/dead
CD5	1:400	BV421 (BD Pharmingen)	T-cells and Natural killer T-cells
CD4	1:3200	FITC (BD Pharmingen)	T-helper cells
CD8	1:3200	PE-CF594 (Invitrogen)	Cytotoxic T-cells
CD25	1:800	APC (BD Pharmingen)	Regulatory T-cells
CD62L	1:100	APC-Cy7 (BD Pharmingen)	Level of expression distinguishes naïve, effector and memory T-cells
CD44	1:400	PE (BD Pharmingen)	Activated CD4+ and CD8+ T-cells
CD161	1:100	PE-Cy7 (BD Pharmingen)	Natural killer cells and Natural killer T-cells
Panel 2			
Marker	**Dilution**	**Fluorochrome**	**Specificity**
Live/dead	1:10000	SYTOX Blue (Invitrogen)	Live/dead
F4/80	1:50	PE (eBioscience)	Mature macrophages
CD19	1:800	BV510 (BD Horizon)	B-cells
IgD	1:200	APC (BD Pharmingen)	Mature B-cells
Ly6C	1:200	FITC (BD Pharmingen)	Monocytes
Ly6G	1:200	BV421 (BD Pharmingen)	Granulocytes
CD5	1:400	BV421 (BD Pharmingen)	B1 cells
CD11b	1:800	PE-CF594 (BD Pharmingen)	Myeloid cells and dendritic cells
CD11c	1:100	PECy7 (BD Pharmingen)	Dendritic cells
MHCII	1:400	APC-Cy7 (Insight Biotechnology)	Activated dendritic cells

CD, Cluster of Differentiation; IgD, immunoglobulin D; MHCII, Major Histocompatability Complex Class II.

Table 2.7: Gating strategy for fluorescence-activated cell sorting analysis.

Panel 1						
Population	**Subset**	**Parameter 1**	**Parameter 2**	**Parameter 3**	**Parameter 4**	**Parameter 5**
NK Total	Total NK Cells	CD5-	CD161+	CD44+		
NKT Cells	Total NKT Cells	CD5+	CD161+	CD44+		
	Effector NKT Cells	CD5+	CD161+	CD44+	CD62L-	
	Resting NKT Cells	CD5+	CD161+	CD44+	CD62L+	
	Invariant NKT Cells	CD5+	CD161+	CD44+	CD4+	
T-helper Cells	Total CD4+ T-Cells	CD5+	CD4+			
	Effector CD4+ Cells	CD5+	CD4+	CD25-	CD44+	CD62L-
	Resting CD4+ Cells	CD5+	CD4+	CD25-	CD44+	CD62L+
Regulatory T-cells	Total T-regs	CD5+	CD4+	CD25+		
	Effector T-regs	CD5+	CD4+	CD25+	CD44+	CD62L-
	Resting T-regs	CD5+	CD4+	CD25+	CD44+	CD62L+
Cytotoxic T-cells	Total CD8+ T-Cells	CD5+	CD8+			
	Effector CD8+ Cells	CD5+	CD8+	CD44 high	CD62L-	
	Resting CD8+ Cells	CD5+	CD8+	CD44 high	CD62L+	
	Naïve CD8+ Cells	CD5+	CD8+	CD44 low	CD62L+	
T-cells	γδ+ T-Cells	CD5+	CD4- CD8-			
Panel 2						
Population	**Subset**	**Parameter 1**	**Parameter 2**	**Parameter 3**	**Parameter 4**	**Parameter 5**
Myeloid Cells	Neutrophils	CD11b+	Ly6G high			
	Monocytes	CD11b+	Ly6G-	Ly6C high		
	Macrophages	CD11b+	Ly6G-	Ly6C-	F4/80+	MHCII low
	Eosinophils	CD11b+	Ly6G-	Ly6C-	F4/80-	SSC high
B-cells	Total B-cells	CD11b-	CD19+	MHCII+		
	Total B2 Cells	CD11b-	CD19+	MHCII+	CD5-	
	Mature B2 Cells	CD11b-	CD19+	MHCII+	CD5-	IgD+
	Total B1 Cells	CD11b-	CD19+	CD5+	MHCII+	
Dendritic Cells	Total DCs	CD11c+	MHCII+			
	cDC CD8a Type	CD11c+	MHCII+	CD11b-		
	cDC Cd11b Type	Cd11c+	MHCII+	CD11b+		
	Plasmacytoid DCs	CD11c+	MHCII low			

CD, Cluster of Differentiation; DC, Dendritic Cell; Ly6G, Lymphocyte Antigen 6 Complex; MHCII, Major Histocompatability Complex Class II; NK, Natural Killer; NKT, Natural Killer T-cell; T-reg, Regulatory T-cell.

2.13. Statistical Analysis

Results are shown as mean +/- standard error of the mean (s.e.m). Prior to statistical testing, a Levene's test was performed to determine whether experimental groups showed equal variances and assess parametricity. Statistical analyses were then performed with GraphPad Prism, using an unpaired *t*-test with Welch's correction when comparing data from two groups and a one- or two-way analysis of variance (ANOVA) when comparing three groups, with a Tukey post-hoc test to correct for multiple comparisons. In all cases, a threshold of $p<0.05$ was used as the detection limit for significance. Significance levels on graphs are represented as: ns = not significant; * = $p\leq0.05$; ** = $p\leq0.01$; *** = $p\leq0.001$; **** = $p\leq0.0001$. Statistical advice was kindly provided by Dr George Nicholson.

Chapter 3 : Molecular Characterisation of *cello*

3.1. Introduction

The *cello* pedigree, originally known as *MPC-173*, was identified as a mouse model of hearing loss from the Harwell Ageing Screen at three months of age. With this type of phenotype-driven, forward genetics screen, phenodeviants of interest are identified with no knowledge of their underlying genetic lesions. In order to map and identify causative ENU-induced mutations, DNA samples from phenodeviants and their unaffected littermates are used for linkage analysis and DNA sequencing, either using a candidate gene or genome-wide approach. Putative lesions can then be assessed using *in silico* and *in vitro* approaches in order to predict and characterise their functional effects.

As *MPC-173* phenodeviants were identified at an early time point, the original G1 founder male (*MUTA-G1-C3PDE/241.5d*) and G2 females that produced the G3 cohort were still alive and available for further breeding. They were re-mated in order to generate additional G3 litters, which were used for further experimental procedures to identify the genetic basis and functional mechanisms underlying the *cello* hearing impairment.

3.2. Results

3.2.1. Identification of the Causative Gene

Two distinct inbred strains were used to generate G3 colonies for the Ageing Screen: C57BL/6J mice were mutagenised with ENU and wild-type C3H.pde6b^{+} mice were used for subsequent matings. This allows ENU-induced mutations to be mapped using SNP markers that are polymorphic between these two strains. As ENU mutations were induced on a BL6 background, they will be carried on BL6 alleles. For autosomal dominant traits, affected animals would need only a single copy of the mutated BL6 allele (heterozygous), whilst autosomal recessive traits would require two copies (homozygous). According to classic Mendelian ratios, which predict recessive traits to be inherited in a 1:3 proportion, the number of affected *MPC-173* animals (10/60 at three months of age; 18/59 at six months of age) suggests autosomal recessive inheritance. In this case, the causative mutation will be located in region of BL6 homozygosity and phenodeviants will carry two copies of the mutated BL6 allele.

3.2.1.1. Whole-Genome Mapping

An initial linkage study was undertaken to localise the *cello* causative mutation to a candidate chromosomal region. DNA from 13 Ageing Screen G3 mice (12 affected and one unaffected control) was sent to Tepnel Life Sciences (Manchester, UK) for whole-genome mapping using the Illumina Mouse Medium Density Linkage Panel. This panel can distinguish genotype at 1449 SNPs across the genome, with approximately three SNPs per 5 Mb interval, providing a comprehensive genome scan. Of these 1449 SNPs, 871 are strain-specific between C57BL/6J and C3H.pde6b^{+} and thus informative.

Mapping demonstrated linkage to a single 21.57 Mb region of BL6 homozygosity on Chromosome 1, from 51.40 Mb to 72.97 Mb (between SNPs rs13475866 and rs13475919), which was common to all affected mice (genomic coordinates were established using Ensembl assembly GRCm38) (Figure 3.1). The boundaries of this candidate region were defined by the SNP markers where at least one affected animal genotyped as C3H wild-type or heterozygous, rather than BL6 homozygous. The unaffected control animal carried wild-type C3H alleles across this candidate region.

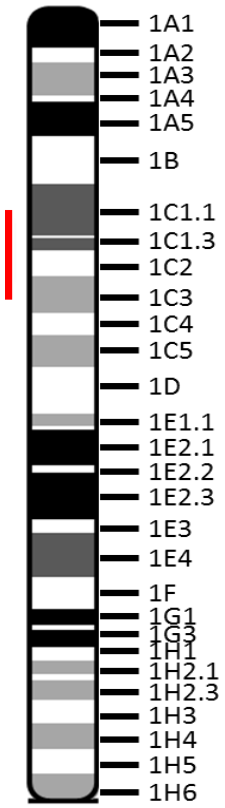

Figure 3.1: Ideogram of the Chromosome 1 candidate region for hearing impairment in *MPC-173/cello.*
Whole-genome mapping identified a 21.57 megabase interval of C57BL/6J homozygosity on Chromosome 1 that was common to all hearing-impaired *MPC-173* animals. The position of this candidate region is indicated by the red line.

3.2.1.2. Fine Mapping

Following localisation of the causative mutation to a 21.57 Mb region on Chromosome 1, *MPC-173* mice (from both the Ageing Screen and additional cohorts) were genotyped in-house using additional SNP markers in order to narrow the candidate interval. Fine mapping using these SNPs refined the region to 8.35 Mb, from 63.28 Mb to 71.63 Mb (between SNPs rs31869113 and rs13475914) (Table 3.1). There were 66 genes within this region, none of which have previously been associated with hearing loss.

Table 3.1: Fine mapping of *MPC-173/cello* mice.

Chromosome 1								
SNP (rs)	31425874	32685810	13475879	32179751	31869113	30609422	32058458	13475914
Location (Mb)	53.22	54.37	57.83	59.08	63.28	68.41	69.00	71.63
MPC-173/2.1b	BL6	BL6	BL6	BL6	BL6	BL6	BL6	Het
MPC-173/2.1d	BL6	BL6	BL6	BL6	BL6	BL6	BL6	Het
MPC-173/2.9a	BL6	BL6	BL6	BL6	BL6	BL6	BL6	BL6
MPC-173/2.13a	BL6	BL6	BL6	BL6	BL6	BL6	BL6	BL6
MPC-173/2.13b	BL6	BL6	BL6	BL6	BL6	BL6	BL6	BL6
MPC-173/2.14h	Het	Het	BL6	BL6	BL6	BL6	BL6	BL6
MPC-173/2.7b	Het	Het	Het	Het	Het	BL6	BL6	BL6
MPC-173/2.14c	Het	Het	Het	Het	Het	Het	Het	Het
MPC-173/2.15b	C3H	C3H	C3H	C3H	C3H	C3H	C3H	C3H
MPC-173/2.15c	C3H	C3H	C3H	C3H	C3H	C3H	C3H	C3H

Affected animals (red text) have a common region of C57BL/6J homozygosity on Chromosome 1. This was narrowed to 8.35 Mb, from 63.2 Mb and 71.63 Mb, as shown by the thick outline in the table. Unaffected animals (black text) are heterozygous or have wild-type C3H.pde6b^{+} alleles in this region, indicating the *cello* mutation is recessive. BL6, C57BL/6J; C3H, C3H.pde6b^{+}; Mb, megabase; *MPC-173, MUTA-PED-C3PDE-173;* rs, reference SNP; SNP, single nucleotide polymorphism.

3.2.1.3. Whole-Genome Sequencing (WGS)

Whilst prioritised gene sequencing can be undertaken, it was deemed more efficient to utilise a WGS approach in order to identify ENU-induced lesions. High-quality DNA from *MPC-173/2.13b*, an affected G3 female, was sequenced by the High-Throughput Genomics

group at The Wellcome Trust Centre for Human Genetics (University of Oxford, UK) using the Illumina HiSeq 2000 system. Briefly, genomic DNA was sheared into multiple short fragments to enable simultaneous parallel sequencing. This produced millions of sequencing reads between 40 and 100 bp in length, which were aligned to the *Mus musculus* C57BL/6J reference genome (assembly GRCm38) by the Bioinformatics group at MRC Harwell (Figure 3.2).

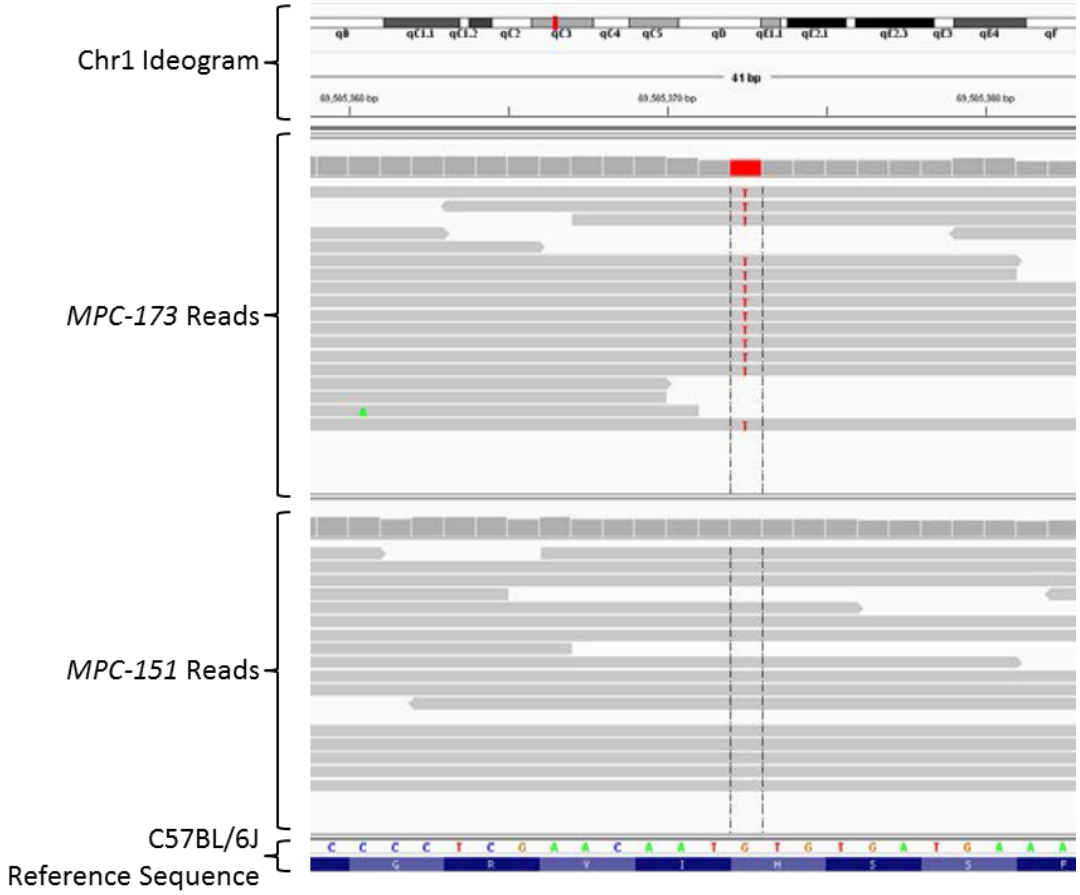

Figure 3.2: Whole-genome sequencing reads across a region of Chromosome 1, aligned to the C57BL/6J reference genome.
WGS was carried out using DNA from an affected *MPC-173* G3 animal. Sequencing reads were aligned to the *Mus musculus* C57BL/6J reference genome (assembly GRCm38) and filtered to remove known single nucleotide polymorphisms between C57BL/6J and C3H.pde6b^{+}. A G>T change was detected at position Chr1:69585372 (red) and is observed within all reads covering this region. Comparison with WGS reads from a second pedigree from the Harwell Ageing Screen (*MPC-151*) confirms that this mutation is not common to the C57BL/6J stock maintained at MRC Harwell and therefore is likely to be an ENU-induced lesion. Chr1, chromosome 1; *MPC-151, MUTA-PED-C3PDE-151; MPC-173, MUTA-PED-C3PDE-173.*

The reliability of sequencing data at each nucleotide was indicated by the 'read depth' - the number of times that nucleotide had been sequenced, with a higher read depth indicating greater coverage. After known C57BL/6J and C3H.pde6b^{+} SNPs were filtered out, the remaining sequencing variants were given a 'quality score' based on the read depth at that position; variants observed in lots of reads gained a high quality score (>200) and were classed as 'high confidence', whereas those seen in only a few reads, usually believed to be a sequencing error, gained a low quality score and were classed as 'low confidence'.

19,915 variants were found across Chromosome 1, of which 19,083 were discounted for being outside of the 8.35 Mb candidate region. Of the 832 variants within the candidate region, 827 were discounted for being non-coding (intergenic, intronic, 3' or 5' untranslated region) and two were discounted for being synonymous. This left three non-synonymous variants (Table 3.2), only one of which was classed as high-confidence: Chr1:69585372G>T, which leads to a C to A transversion at coding nucleotide 1551 of the Ikaros family zinc finger 2 (*Ikzf2*) gene (transcript ENSMUST00000027146, on the reverse strand).

Table 3.2: Non-synonymous coding variants within the Chromosome 1 critical region identified by whole-genome sequencing.

Position	Ensembl ID (ENS)	Gene	Mutation	Read Depth	Quality Score	Confidence
65.15 Mb	MUSG00000044429	Crystallin, gamma A (*Cryga*)	c.152A>C	17	66.48	Low
66.46 Mb	MUSG00000015222	Microtubule-associated protein 2 (*Map2*)	c.2944T>A	5	6.98	Low
69.59 Mb	MUSG00000025997	Ikaros family zinc finger 2 (*Ikzf2*)	c.1551C>A	13	548.41	High

Mb, megabase.

There were 13 sequencing gaps in the 8.35 Mb candidate interval on Chromosome 1, where WGS data failed to align to the reference genome. 11 gaps spanned non-coding sequence and were not pursued. Two gaps spanned coding sequence and were amplified by PCR using DNA from *MPC-173/2.13b* (affected G3) then analysed by Sanger sequencing. No additional variants were identified in either coding gap, demonstrating that the *Ikzf2* c.1551C>A mutation is the only high confidence, non-synonymous, coding lesion within the *cello* critical region.

The c.1551C>A mutation was validated in an affected G3 animal (*MPC-173/2.13b*) compared to an unaffected G3 mouse (*MPC-173/2.12b*) and the *MPC-173* G1 founder male (*MUTA-G1-C3PDE/241.5d*). DNA fragments encompassing the putative lesion were amplified by PCR then Sanger sequenced. Sequence analysis confirmed that the affected G3 animal was homozygous for the c.1551C>A nucleotide transversion, whilst the unaffected G3 animal was wild-type and the G1 animal was heterozygous (Figure 3.3).

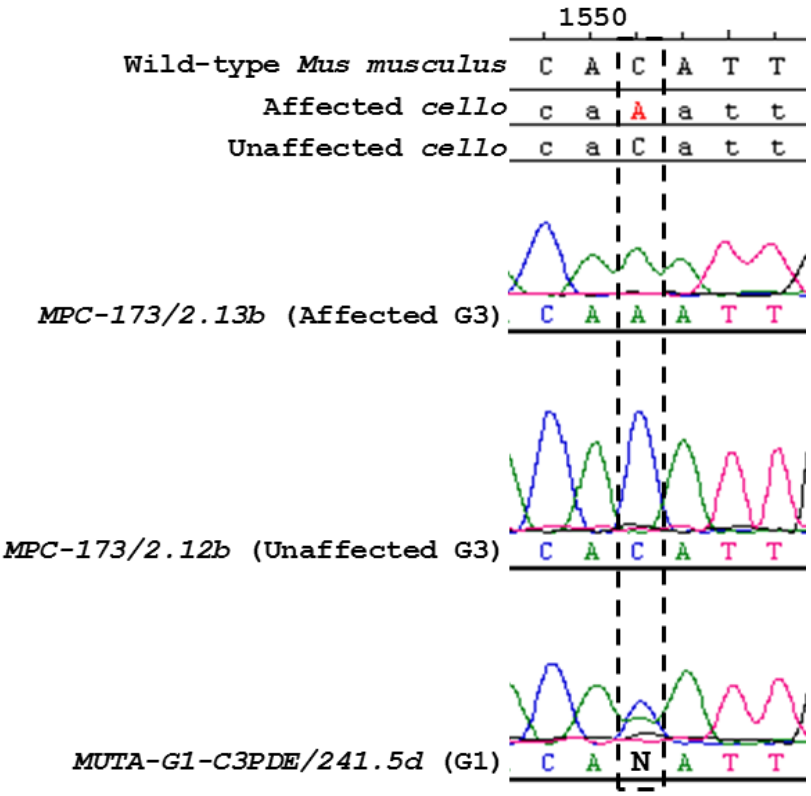

Figure 3.3: Validation of the *Ikzf2* c.1551C>A mutation.
Sanger sequencing was used to validate the putative c.1551C>A lesion. Sequencing chromatograms show that the affected G3 animal was homozygous for the mutant adenine (A) nucleotide at position 1551, whilst the unaffected G3 animal was homozygous for the wild-type cytosine (C) nucleotide. The G1 animal was heterozygous and carried both the mutant adenine and wild-type cystosine (N) nucleotide at position 1551. *MPC-173, MUTA-PED-C3PDE-173.*

The *cello* mutation alters the sequence of codon 517 from wild-type CAC to CA**A**. Once translated, this results in a missense Histidine (His, H) to Glutamine (Gln, Q) substitution at residue 517 of the *Ikzf2* encoded protein, helios (ENSMUSP00000027146.2). Although a helios knock-out has been published (Cai et al., 2009), to date, no auditory phenotyping or hearing impairment have been reported in these mice.

Subsequent genotyping confirmed that all unaffected animals from the Ageing Screen G3 cohort were wild-type (*Ikzf2*$^{+/+}$) or heterozygous (*Ikzf2*$^{cello/+}$), whilst all affected animals were homozygous (*Ikzf2*$^{cello/cello}$), confirming recessive inheritance.

3.2.2. *In Silico* Analyses

3.2.2.1. Predicted Effect of the *cello* Mutation

The functional impact of the p.His517Gln (H517Q) helios mutation was assessed using three separate online homology-based prediction tools: Sorting Intolerant from Tolerant (SIFT), Polymorphism Phenotyping v2 (PolyPhen-2) and Protein Variation Effect Analyser (PROVEAN) (Adzhubei et al., 2010, Choi et al., 2012, Kumar et al., 2009). These tools assess amino acid sequence conservation to predict and score the functional effect of a residue substitution. The H517Q helios mutation was consistently predicted to be deleterious and affect protein function (Table 3.3).

Table 3.3: Predicted effect of the *cello* mutation.

Tool	Prediction	Score
SIFT	Affect protein function	0.00 (damaging)
PolyPhen-2	Probably damaging	1.00 (deleterious)
PROVEAN	Deleterious	-6.899 (severe)

Scoring system: SIFT, 0-1 range, <0.05 damaging, ≥0.05 tolerated; PolyPhen-2, 0-1 range, with values nearer 1 more confidently predicted to be deleterious; PROVEAN, default threshold of -2.5, ≤-2.5 deleterious, >-2.5 neutral.

This is perhaps unsurprising, given that the *cello* mutation causes a radical amino acid substitution and is likely to alter the structural integrity of helios, changing a positively charged Histidine residue with an imidazole ring side chain to a neutral Glutamine residue with an amide side chain (Figure 3.4 A).

The helios protein is a member of the IKZF family of zinc finger transcription factors (Hahm et al., 1998, Kelley et al., 1998). These proteins share a common structure of three to four N-terminal zinc fingers (ZnF1 – ZnF4), which are involved in DNA binding (Hahm et al., 1994, Molnar and Georgopoulos, 1994), and two C-terminal zinc fingers (ZnF5 – 6), which facilitate

homodimerisation and heterodimerisation between family members (Molnar and Georgopoulos, 1994, McCarty et al., 2003, Sun et al., 1996). Each zinc finger is of the classical C_2H_2-type that coordinates a centralised zinc ion using two Cysteine (C_2) and two Histidine (H_2) residues. C_2H_2-type zinc fingers share the core recognition motif X_2-**Cys**-$X_{2,4}$-**Cys**-X_{12}-**His**-$X_{3,4,5}$-**His** (Brown et al., 1985), where the coordinating Cysteine and Histidine residues are separated by a set number of unspecified amino acids (Figure 3.4 B).

The mutagenised Histidine residue in *cello* is at the C-terminus of helios, within the final zinc finger domain (ZnF6) (Figure 3.4 C) that is known to be important for dimerisation. Alignment of the *cello* ZnF6 peptide sequence with its orthologues and paralogues demonstrates that the mutagenised Histidine is highly conserved across species and within the IKZF family (Figure 3.4 D), reinforcing that it is likely important for normal protein function. This alignment also reveals that the mutagenised Histidine is one of the zinc-coordinating residues (Figure 3.4 E). As tetrahedral binding of zinc is critical for folding and stabilisation of C_2H_2 zinc finger domains (Frankel et al., 1987), its substitution is therefore likely to have a detrimental effect on protein structure and may impair the ability of helios to dimerise and function.

A

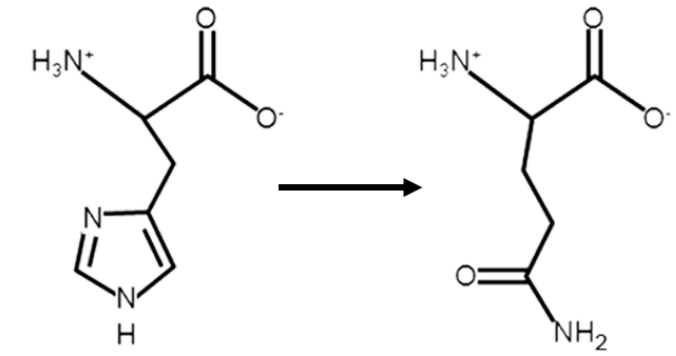

Histidine (+) Glutamine (neutral)

B

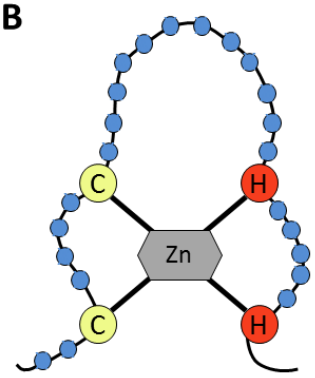

C

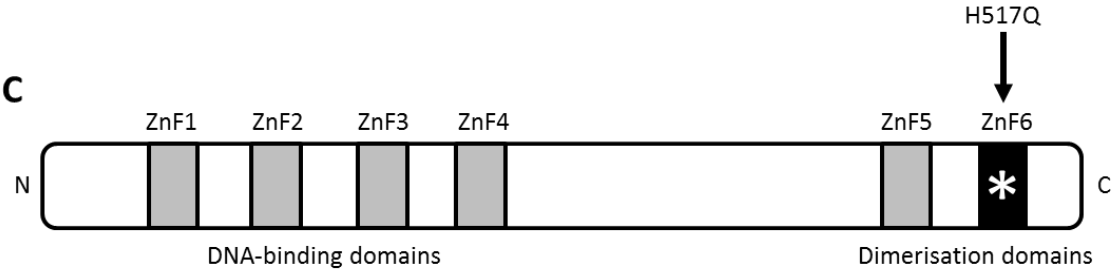

D

	ZnF5	ZnF6
cello	AFKCEHCRVLFLDHVMYTIHMGCHGYRDPLECNICGYRSQDRYEFSSQIVRGEH	
Mus musculus	AFKCEHCRVLFLDHVMYTIHMGCHGYRDPLECNICGYRSQDRYEFSSHIVRGEH	
Homo sapiens	AFKCEHCRVLFLDHVMYTIHMGCHGYRDPLECNICGYRSQDRYEFSSHIVRGEH	
Pan troglodytes	AFKCEHCRVLFLDHVMYTIHMGCHGYRDPLECNICGYRSQDRYEFSSHIVRGEH	
Macaca mulatta	AFKCEHCRVLFLDHVMYTIHMGCHGYRDPLECNICGYRSQDRYEFSSHIVRGEH	
Equus caballus	AFKCEHCRVLFLDHVMYTIHMGCHGYRDPLECNICGYRSQDRYEFSSHIVRGEH	
Bos taurus	AFKCEHCRVLFLDHVMYTIHMGCHGYRDPLECNICGYRSQDRYEFSSHIVRGEH	
Canis lupus familiaris	AFKCEHCRVLFLDHVMYTIHMGCHGYRDPLECNICGYRSQDRYEFSSHIVRGEH	
Gallus gallus	AFKCEHCRVLFLDHVMYTIHMGCHGYRDPLECNICGYRSQDRYEFSSHIVRGEH	
Xenopus tropicalis	AFKCEHCRVLFLDHVMYTIHMGCHGYRDPLECNICGHRSQDRYEFSSHIVRGEH	
Danio rerio	VFQCEHCRVLFLDHVMYTIHMGCHGYRDPLECNICGHCSKDRYEFSSHIVRGEH	
Ikaros *(M. musculus)*	VYKCEHCRVLFLDHVMYTIHMGCHGFRDPFECNMCGYHSQDRYEFSSHITRGEH	
Aiolos *(M. musculus)*	VFRCDHCHVLFLDYVMFTIHMGCHGFRDPFECNMCGYRSHDRYEFSSHIARGEH	
Eos *(M. musculus)*	AFKCEHCRILFLDHVMFTIHMGCHGFRDPFECNICGYHSQDRYEFSSHIVRGEH	
Pegasus *(M. musculus)*	LHHCQHCDVYFADNVLYTVHMGCHGYDSPFQCNVCGCKCKDKYDFACHFARGQH	
Classical C_2H_2 Motif:	--C--C----------H---H	--C--C----------H-----H

E

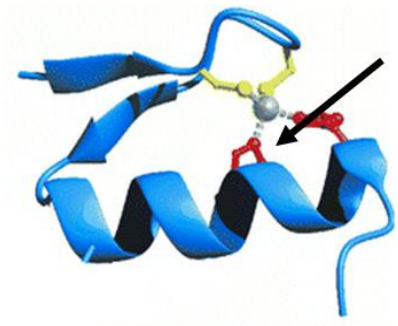

Figure 3.4: *In silico* analysis of the *cello* mutation.
(A) The structural formulae of Histidine and Glutamine indicate that *cello* mutation is a radical substitution, changing a positively charged Histidine with an imidazole ring to a neutral Glutamine with an amide side chain. **(B)** C_2H_2 zinc fingers bind a centralised zinc ion using two cysteine residues (yellow) and two histidine residues (red), with a set number of amino acid residues in between. Image adapted from Miller et al. (1985). **(C)** Helios has six zinc finger domains; ZnF1 – 4 at the N-terminal are for DNA binding and ZnF5 – 6 at the C-terminal for dimerisation. The *cello* H517Q mutation is located in ZnF6 (marked with an asterisk). **(D)** Alignment of the ZnF6 peptide sequence with orthologous and paralogous sequences shows that it is highly conserved, with the mutagenised Histidine residue present in all sequences represented. Comparison with the core C_2H_2 motif also indicates that the mutagenised Histidine is one of the four zinc-coordinating residues (highlighted yellow). **(E)** The tertiary structure of a C_2H_2 zinc finger, which has folded into a beta hairpin and alpha helix configuration around the coordinated zinc ion. The mutagenised Histidine is marked with an arrow. Image adapted from Pabo et al. (2001). C, cysteine; H, histidine; Zn, zinc; ZnF, zinc finger.

3.2.2.2. Three-Dimensional (3D) Mutation Modelling

To model the H517Q mutation, the 3D structures of wild-type and *cello* ZnF6 were predicted with RaptorX (Kallberg et al., 2012), using the corresponding peptide sequence as input, then visualised using pyMOL software. ZnF6 from wild-type helios exhibits the classical C_2H_2 zinc finger structure, with a beta hairpin and alpha helix organised around a centralised zinc ion, which is coordinated by two Cysteine and two Histidine residues (Figure 3.5 A). The mutated Histidine in *cello* is one of the critical zinc-coordinating residues of ZnF6, required to establish the tertiary structure of the protein. Indeed, 3D modelling suggests that *cello* ZnF6 cannot form the tetrahedral geometric shape required to coordinate the zinc ion (Figure 3.5 B). This change in tertiary structure is likely to impair ZnF6 dimerisation and ultimately affect helios protein function.

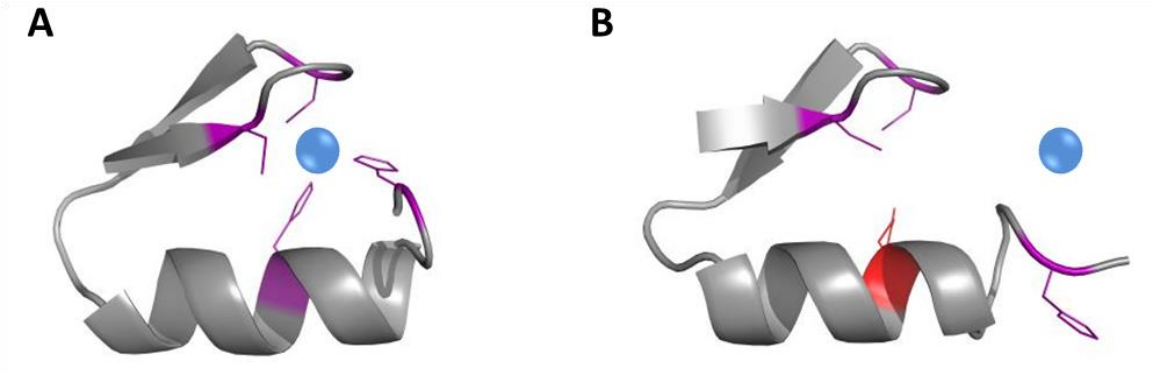

Figure 3.5: *In silico* 3D modelling of the *cello* mutation.
(A) ZnF6 from wild-type helios folds into two beta sheets and an alpha helix around a centralised zinc ion (blue), which is bound by the four coordinating residues (purple). **(B)** In *cello* ZnF6, one of the coordinating Histidine residues is substituted for Glutamine (red). As a result, *cello* ZnF6 cannot form the tetrahedral geometric shape required to coordinate the zinc ion.

3.2.3. *In Vitro* Analyses

Previous work has established that the IKZF family of proteins can homodimerise and heterodimerise through their two conserved C-terminal zinc fingers, ZnF5 and ZnF6 (Honma et al., 1999, McCarty et al., 2003, Molnar and Georgopoulos, 1994, Morgan et al., 1997, Perdomo et al., 2000). Given that the *cello* mutation is located in the dimerisation domain of helios, affecting a zinc-coordinating Histidine in ZnF6, it is likely to impair the ability of helios to dimerise.

In order to assess the *cello* mutation *in vitro*, c-Myc-tagged and EGFP-tagged wild-type (WT) and H517Q mutant helios fusion proteins were generated by molecular cloning. As the dimerisation domain (and the *cello* mutation) is at the C-terminus of helios, N-terminal tags were used in order to minimise interference with the protein-protein interactions. Two mammalian cell lines were used for subsequent *in vitro* analyses; subcellular localisation studies were carried out using Cos-7 cells, due to their adherent nature and ability to

withstand repeated washing, whilst co-immunoprecipitation (co-IP) experiments were performed using HEK293T cells, due to their high transfection efficiency.

3.2.3.1. Western Blotting

To confirm expression of full-length helios, both Cos-7 and HEK293T cells were transiently transfected with tagged WT and H517Q helios expression constructs. At 48 hours post-transfection, protein lysates were prepared and analysed by western blotting.

In Cos-7 cells, c-Myc-tagged WT helios (Myc-WT) and c-Myc-tagged H517Q helios (Myc-H517Q) both migrate at the expected size of ~62 kilodaltons (kDa) (helios, 59.4 kDa; c-Myc, 2.5 kDa), whilst EGFP-tagged WT helios (GFP-WT) and EGFP-tagged H517Q helios (GFP-H517Q) are both detected at the expected size of ~88 kDa (helios, 59.4 kDa; EGFP, 28.3 kDa) (Figure 3.6). The same results were obtained from transfected HEK293T cell lysates, which confirms that full-length helios protein is being expressed from these constructs. No helios is detected in either untransfected (UT) control, indicating that helios is not expressed endogenously by Cos-7 or HEK293T cells.

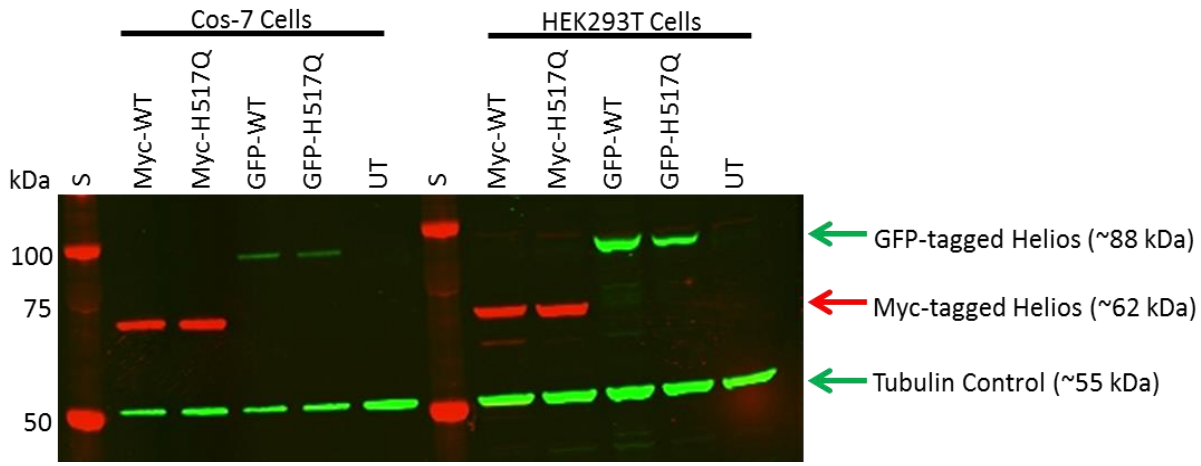

Figure 3.6: Western Blot of c-Myc-tagged and EGFP-tagged wild-type and H517Q helios.
Cos-7 and HEK293T cells were transfected with Myc-WT, Myc-H517Q, GFP-WT or GFP-H517Q helios prior to lysing for western blotting. In both cell lines, Myc-WT and Myc-H517Q helios migrate at a size of ~62 kDa (helios, 59.4 kDa; c-Myc, 2.5 kDa) and GFP-WT and GFP-H517Q helios are detected at ~88 kDa (helios, 59.4 kDa; EGFP, 28.3 kDa), confirming expression of full-length protein. No Helios band is detected in the UT control sample. Western blot was probed using anti-Myc, anti-GFP and anti-alpha tubulin primary antibodies. GFP-H517Q, EGFP-tagged H517Q helios; GFP-WT, EGFP-tagged WT helios; kDa, kilodaltons; Myc-H517Q, c-Myc-tagged H517Q helios; Myc-WT, c-Myc-tagged wild-type helios; S, protein standard; UT, untransfected.

3.2.3.2. Subcellular Localisation

To investigate subcellular localisation of H517Q helios, Cos-7 cells were seeded onto sterile coverslips then transiently transfected with c-Myc-tagged WT and H517Q constructs. Cells were fluorescently labelled with an anti-helios primary antibody, detected using Alexa Fluor® 488 (green), as well as Texas Red®-X Phalloidin to visualise the actin cytoskeleton and DAPI (blue) to visualise the nucleus.

In keeping with its role as a transcription factor, helios is reported to exhibit nuclear localisation in T-cells (Hahm et al., 1998). Indeed, Cos-7 cells transfected with Myc-WT helios demonstrate helios labelling which co-localises with DAPI (Figure 3.7 A-D), confirming that c-Myc-tagged WT helios localises to the nucleus. Cells transfected with Myc-H517Q helios show a similar pattern of staining (Figure 3.7 E-H), which indicates that nuclear localisation is not impaired by the *cello* mutation and confirms that the anti-helios primary antibody can

recognise H517Q helios. As a negative control, untransfected cells were also labelled and show no staining against helios (Figure 3.7 I-L), confirming specificity of the anti-helios primary antibody. Similar results were obtained when repeating this experiment using an anti-Myc primary antibody and when investigating the subcellular localisation of EGFP-tagged wild-type and H517Q constructs (Figure 9.1 and Figure 9.2 in Appendix).

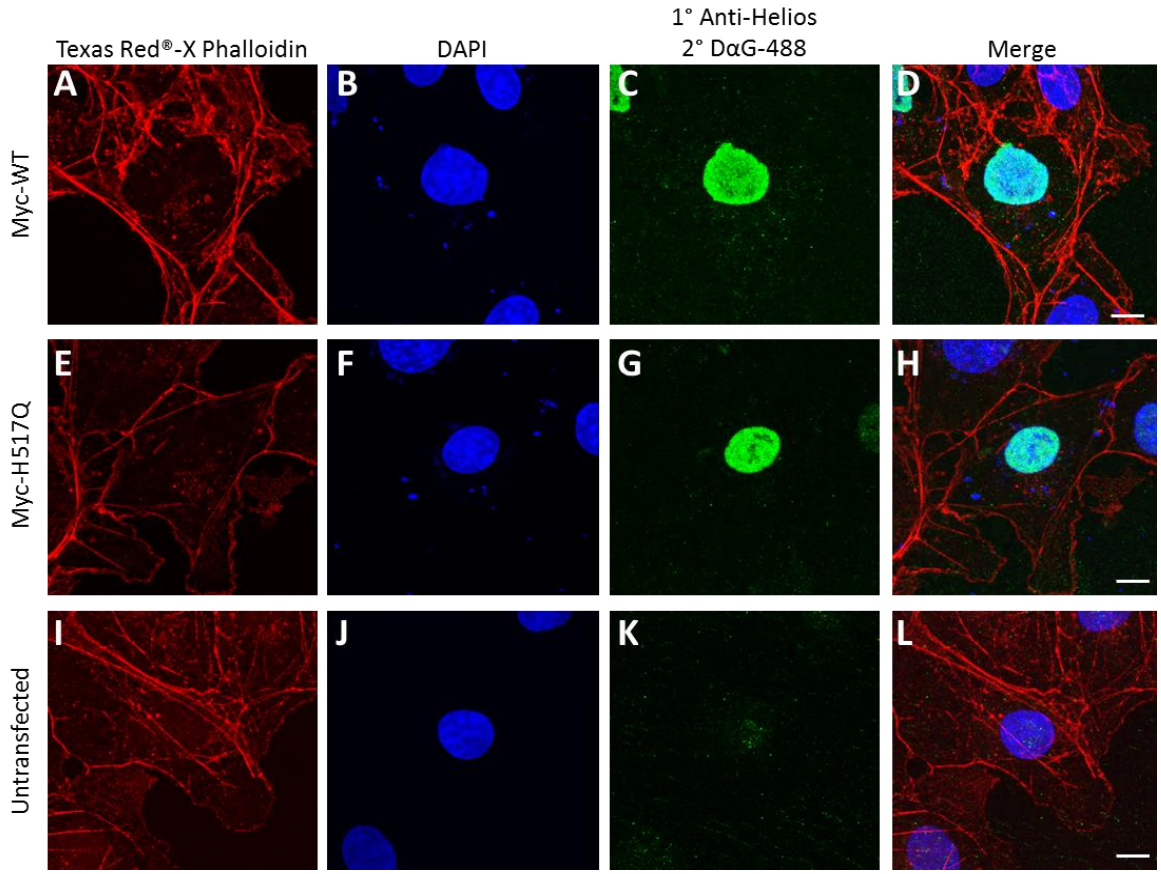

Figure 3.7: *In vitro* subcellular localisation of c-Myc-tagged wild-type and H517Q helios.
Cos-7 cells were transfected with Myc-WT or Myc-H517Q helios then visualised by immunofluorescence. **(A-D)** Myc-WT helios (green) co-localises with DAPI (blue), a nuclear marker, confirming nuclear localisation. **(E-H)** Myc-H517Q helios shows a similar pattern of labelling, indicating that the *cello* mutation does not affect nuclear localisation. **(I-L)** No anti-helios labelling is observed in the untransfected negative control, which confirms binding specificity of the anti-helios primary antibody (x63 magnification, scale bar = 10µm). DαG-488, donkey anti-goat Alexa Fluor® 488.

3.2.3.3. Co-Immunoprecipitation (Co-IP)

Having confirmed that the tagged WT and H517Q helios constructs function as expected, they were subsequently employed to investigate helios dimerisation. Co-IP experiments were carried out after c-Myc-tagged and EGFP-tagged constructs were transiently co-transfected into HEK293T cells in different combinations to mimic a wild-type (Myc-WT + GFP-WT), heterozygous (Myc-WT + GFP-H517Q or Myc-H517Q + GFP-WT) or homozygous (Myc-H517Q + GFP-H517Q) state. An anti-Myc antibody was used to immunoprecipitate c-Myc-tagged helios, which was then captured, along with any interacting partner, using Protein G beads that bind to the IgG domain of the anti-Myc antibody. IP reactions were analysed by western blotting, alongside their corresponding cell lysate (Figure 3.8).

In each lysate, c-Myc-tagged and EGFP-tagged helios are expressed at similar levels, confirming successful co-transfection of the constructs. In the wild-type IP reaction, a band was observed when probing with an anti-Myc antibody, indicating successful immunoprecipitation of c-Myc-tagged helios. In addition, a co-IP band was also detected when probing with an anti-GFP antibody (Figure 3.8, green arrowhead), which shows that Myc-WT helios can pull-down GFP-WT helios. In the heterozygous IP reactions, weaker co-IP bands were detected (Figure 3.8, yellow arrowheads), which indicates that Myc-WT helios can pull-down GFP-H517Q helios and Myc-H517Q helios can pull-down GFP-WT helios, but both at a reduced efficiency compared to the wild-type IP. Finally, in the homozygous IP reaction, Myc-H517Q helios appears not to be able to pull-down GFP-H517Q helios as no co-IP band was visible (Figure 3.8, red arrowhead), indicating that helios dimerisation is severely impaired in the homozygous state. A single transfection with GFP-WT helios was carried out as a negative control for the Myc IP reaction; in this sample, no IP or co-IP band

were observed (Figure 3.8, black arrowhead), which confirmed that EGFP-tagged helios is not binding non-specifically to the Protein G beads.

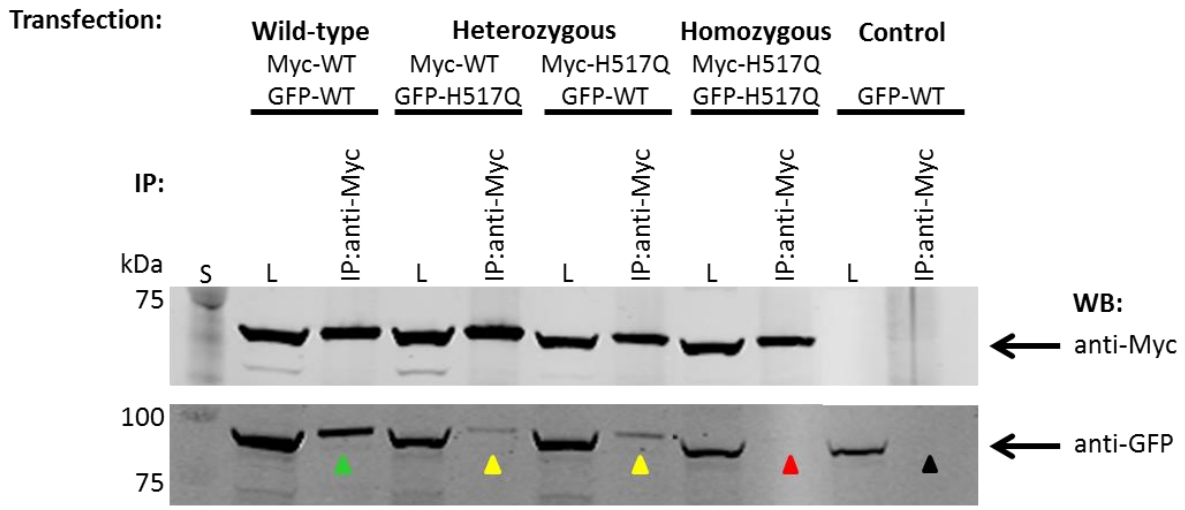

Figure 3.8: Co-immunoprecipitation of c-Myc-tagged and EGFP-tagged helios.
c-Myc-tagged and EGFP-tagged helios fusion proteins were transiently co-transfected into HEK293T cells to mimic a wild-type, heterozygous or homozygous state. IP was carried out with an anti-Myc antibody then IP reactions and their corresponding cell lysate were run on a western blot to investigate helios dimerisation. In each cell lysate, Myc-WT and Myc-H517Q (both ~62 kDa) and GFP-WT and GFP-H517Q (both ~88 kDa) were expressed at similar levels. In wild-type co-transfections, GFP-WT helios was pulled down with Myc-WT helios, as shown by the GFP co-IP band (green arrowhead), confirming homodimerisation. In the heterozygous co-transfections, Myc-WT helios can pull-down GFP-H517Q helios and Myc-H517Q helios call pull-down GFP-WT helios, but at a reduced efficiency, shown by the weaker co-IP bands (yellow arrowheads). In the homozygous co-transfections, no GFP co-IP band was detected (red arrowhead), indicating that Myc-H517Q helios appears not to be able to pull-down GFP-H517Q helios. In the single transfection negative control, no Myc IP or GFP co-IP band was observed (black arrowhead). GFP-H517Q, EGFP-tagged H517Q helios; GFP-WT, EGFP-tagged WT helios; IP, immunoprecipitation; kDa, kilodaltons; L, lysate; Myc-H517Q, c-Myc-tagged H517Q helios; Myc-WT, c-Myc-tagged wild-type helios; S, protein standard; WB, western blot.

Similar results were obtained when repeating this experiment using an anti-GFP antibody for the immunoprecipitation (Figure 9.3 in Appendix). These data demonstrate that the H517Q mutation disrupts helios homodimerisation and is likely a complete or partial loss-of-function allele.

3.3. Discussion

cello mice were identified as a mouse model of hearing loss from the Harwell Ageing Screen and, following linkage analysis and WGS, found to harbour a recessive ENU-induced non-synonymous point mutation (c.1551C>A) in the gene *Ikzf2* (ENSMUST00000027146). This mutation results in a missense Histidine to Glutamine amino acid substitution at position 517 of the encoded protein, helios (ENSMUSP00000027146.2).

Helios is a zinc finger transcription factor, first identified in 1998 as a result of its sequence homology and dimerisation activity with the ikaros protein (encoded by *Ikzf1*) (Hahm et al., 1998, Kelley et al., 1998). Both proteins are members of the IKZF family of zinc finger transcription factors, which also includes aiolos (*Ikzf3*), eos (*Ikzf4*) and pegasus (*Ikzf5*) (Georgopoulos et al., 1992, Honma et al., 1999, Morgan et al., 1997, Perdomo et al., 2000). The IKZF family can function as both transcriptional activators and repressors (Harker et al., 2002, Sabbattini et al., 2001, Trinh et al., 2001). Ikaros, aiolos and helios have been shown to localise to centromeres (Brown et al., 1997, Brown et al., 1999, Hahm et al., 1998) and be involved in chromatin remodelling at target genes through association with the nucleosome remodelling complex, NuRD (Kim et al., 1999, Sridharan and Smale, 2007).

Murine helios shows a high degree of paralogous and orthologous sequence conservation, with 73% similarity to murine ikaros (Kelley et al., 1998) and 97% homology to human helios (Hosokawa et al., 1999). The ikaros proteins are characterised by their presence of up to four N-terminal zinc fingers (depending on the isoform) and two C-terminal zinc fingers. Each zinc finger is of the classical C_2H_2 type, which tetrahedrally coordinates a central zinc ion with two Cysteine and two Histidine residues, in order to stabilise protein structure and binding interactions. These type of zinc fingers were first identified from a study focused on

transcription factor IIIA in *Xenopus laevis* oocytes (Miller et al., 1985) and sequence analysis revealed a core zinc-recognition motif that is common across C_2H_2 zinc finger proteins: X_2-C-$X_{2,4}$-C-X_{12}-H-$X_{3,4,5}$-H (Brown et al., 1985). Studies of the C_2H_2 zinc fingers of the *Saccharomyces* transcription factor alcohol dehydrogenase II synthesis regulator have indicated that residue substitutions and deletions within this motif, even of the non-coordinating residues, impairs tetrahedral zinc binding, causing misfolding of the zinc finger domain and loss of protein activity (Parraga et al., 1990).

Previous work has shown that the IKZF family N-terminal and C-terminal zinc fingers have distinct roles in protein function; Molnar and Georgopoulos (1994) demonstrated that N-terminal zinc fingers are required for DNA binding, finding that glutathione S-transferase (GST)-N-terminal fusion proteins bound to a significant proportion of oligomers containing the core 'GGGAA' ikaros motif, whereas GST-C-terminal fusion proteins did not. Meanwhile, yeast two-hybrid screens and co-immunoprecipitation studies have revealed that each ikaros protein can interact with itself and other family members through their two conserved C-terminal zinc fingers, ZnF5 and ZnF6, deemed the dimerisation domain (Figure 3.9) (Honma et al., 1999, McCarty et al., 2003, Molnar and Georgopoulos, 1994, Morgan et al., 1997, Perdomo et al., 2000, Sun et al., 1996).

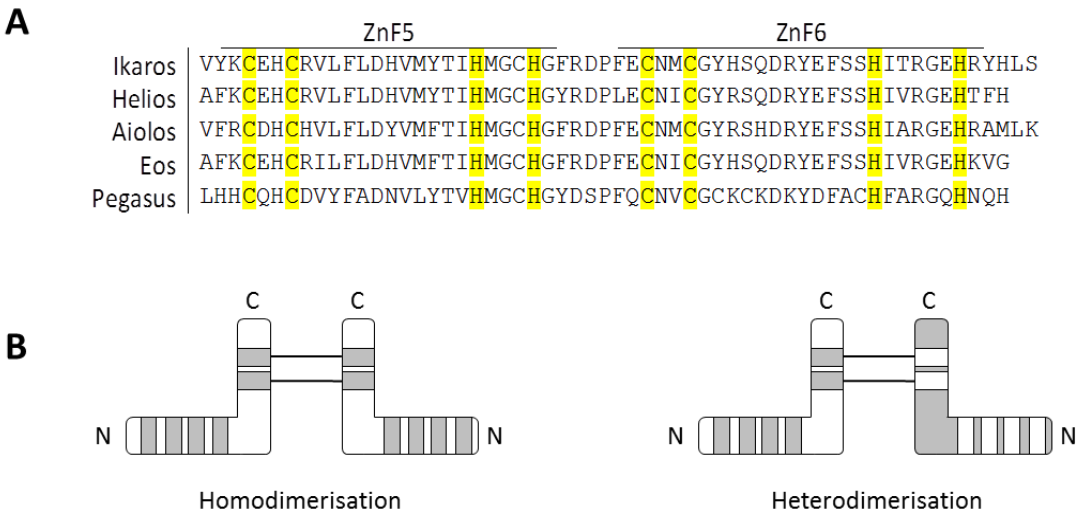

Figure 3.9: Conservation of the C-terminal zinc finger dimerisation domains across the ikaros family zinc finger proteins.
(A) The ikaros family zinc finger proteins share two C-terminal zinc finger domains (ZnF5 and ZnF6), the sequence of which is highly conserved. The coordinating Cysteine and Histidine residues which bind zinc are highlighted in yellow. **(B)** The two C-terminal zinc finger domains are required for dimerisation and their high degree of homology permits heterodimerisation between family members, as well as homodimerisation.

The *cello* mutation is within the C-terminal dimerisation domain, affecting one of the highly-conserved zinc-coordinating residues in ZnF6. As with all C_2H_2 zinc fingers, tetrahedral binding of zinc is associated with conformational changes and stabilisation of secondary and tertiary protein structure (Frankel et al., 1987, Hanas et al., 1983, Parraga et al., 1988). *In silico* analysis using online tools and 3D modelling has predicted that, as a result of impairing this tetrahedral geometry, the *cello* mutation will affect the tertiary structure of ZnF6 and have a deleterious effect on protein function.

Tagged WT and H517Q fusion proteins were generated by molecular cloning for transient transfection into mammalian cell lines in order to functionally characterise the *cello* mutation *in vitro*. Results show that whilst nuclear localisation is not affected by the *cello* mutation, dimerisation is severely impaired; WT helios proteins were confirmed to efficiently dimerise by co-IP, however interaction was found to be weaker between WT and

H517Q proteins and severely impaired in the homozygous state. As the *cello* mutation affects only one of the two C-terminal zinc fingers, leaving ZnF5 intact, it is possible that there may be some residual dimerisation in the homozygous state. Indeed, this is suggested by the GFP immunoprecipitation results (Figure 9.3 in Appendix), where a very weak, rather than absent, co-IP band is observed in the homozygous co-transfections.

Importantly, previous work by Cobb et al. (2000) and Sun et al. (1996) on ikaros has provided evidence that dimerisation is critical for protein function; Cobb et al. (2000) analysed a series of deletion mutants of murine ikaros using subcellular localisation studies and electrophoretic mobility shift assays (EMSAs). Their data showed that ikaros fragments lacking N-terminal ZnF2 or ZnF3 fail to localise to the nucleus or bind DNA probes containing IKZF recognition sites, whilst ikaros fragments lacking both C-terminal ZnF5 and ZnF6 can still localise to the nucleus but no longer exhibit pericentromeric targeting and have impaired DNA binding affinity. Sun et al. (1996) studied murine ikaros following site-directed mutagenesis of the zinc-coordinating Cysteine and Histidine residues in ZnF5 and ZnF6. Their results demonstrated that these C-terminal mutations did not affect the nuclear localisation of ikaros, but prevented homodimerisation, decreased affinity for DNA and perturbed ikaros-mediated transactivation, as shown by co-IP, EMSAs and chloramphenicol acetyltransferase (CAT) transactivation assays. Together, these two studies indicate that although ZnF2 and ZnF3 are required for nuclear localisation, dimerisation is required specifically for pericentromeric targeting and also enhances DNA binding affinity and transcriptional activity. Whilst these experiments were undertaken on ikaros, the same functional properties can likely be inferred about helios, and indeed the other IKZF family members, based on the extensive sequence conservation and homology between these

proteins. As such, the *cello* mutation is likely a complete or partial loss-of-function allele. It is important to note that no hearing loss phenotype is observed in *Ikzf2*$^{cello/+}$ animals, despite co-IP data showing the interaction between WT and H517Q helios proteins is weaker. This could be explained by the fact that in heterozygotes, WT-WT homodimers would still be able to form and efficiently bind DNA to regulate transcription.

Over the past 20 years, the functions of the IKZF transcription factors have been well characterised, with expression data and study of null and knock-down mouse models revealing an important role as regulators of haematopoietic development, differentiation and homeostasis (Georgopoulos et al., 1994, John and Ward, 2011, Nichogiannopoulou et al., 1999, Wang et al., 1996). Helios has been reported to mediate lymphoid cell fate determination and function (Dovat et al., 2005, Getnet et al., 2010, Kelley et al., 1998, Serre et al., 2011, Nakase et al., 2002, Takatori et al., 2015). Although a helios knock-out has been published (Cai et al., 2009), these mice were primarily generated to study the role of helios in the haematopoietic system. As such, it has not yet been ascertained if these mice exhibit hearing loss or any additional auditory phenotypes. Therefore, *Ikzf2*/helios has not previously been implicated in auditory function and so is a novel hearing loss-causing gene/protein.

It is important to bear in mind that two additional non-synonymous mutations were identified in *cello* mice by WGS: c.152A>C in *Cryga* and c.2944T>A in *Map2*. These mutations were classed as low confidence and affected weakly conserved residues of the corresponding encoded proteins and so were not validated or further pursued. Whilst the high confidence c.1551A>C mutation in *Ikzf2* affects a highly conserved residue of helios and was shown by co-IP to impair dimerisation, a property that is fundamental to helios

function, it would be prudent to further investigate the *Cryga* and *Map2* mutations. Initially, this would involve validating both mutations by Sanger sequencing and determining if they co-segregate with the hearing impairment in *cello* mice. Given that *Map2* encodes a microtubule-associated protein, it is reasonable to infer that it may have an important role within the organ of Corti; microtubular kinocilium are known to be important for the polarisation, organisation and development of hair cell stereocilia bundles (Denman-Johnson and Forge, 1999). Furthermore, microtubules are abundant in a number of non-sensory supporting cells, such as the pillar cells and Deiters' cells, where they are thought to provide structural and functional support (Hallworth et al., 2000, Szarama et al., 2012, Tolomeo and Holley, 1997). Although *Ikzf2* appears a strong candidate for the causative mutation in *cello* mice, this should be confirmed using a complementation test, whereby *cello* mice are crossed with helios knock-out mice to create compound heterozygotes ($Ikzf2^{cello/-}$). If the alleles do not complement, resulting in a hearing impairment, this would confirm *Ikzf2* as the causative mutation in *cello*.

In order to further investigate the *cello* phenotype, mice underwent both immunological characterisation (detailed in Chapter 4) and auditory characterisation (detailed in Chapter 5 and Chapter 6).

Chapter 4 : Immunological Characterisation of *cello*

4.1. Introduction

To date, both helios and the other ikaros family transcription factors have primarily been studied in the haematopoietic system. In the mouse, helios is initially expressed in the embryonic liver and thymus, as well as in multipotent adult haematopoietic stem cells (HSCs) before becoming largely restricted to the T-cell lineage (Hahm et al., 1998, Kelley et al., 1998). Helios is abundant in immature thymocytes (Hahm et al., 1998, Thornton et al., 2010) and is also expressed at high levels in the thymus in humans (Hosokawa et al., 1999) indicating a key role in T-cell development.

Several microarray studies have revealed that helios is also expressed in regulatory T-cells (T-regs) (Getnet et al., 2009, Sugimoto et al., 2006), which are a subset of cluster of differentiation (CD) 4+ CD25+ T-cells that have an important role in immune tolerance due to their suppressive abilities (Sakaguchi et al., 1995, Jonuleit et al., 2001). Although initially described as a marker of natural thymic-derived T-regs (Getnet et al., 2010, Haribhai et al., 2009, Sugimoto et al., 2006, Thornton et al., 2010), helios expression has also been shown in peripherally induced T-reg populations (Gottschalk et al., 2012, Zabransky et al., 2012) and is thought to be influenced by the activation status of the cell, rather than its origin (Akimova et al., 2011, Verhagen and Wraith, 2010). Consistent with this, helios has recently been linked with the γδ T-cell subset, where it was found to be upregulated following CD28-mediated cell activation (Peters et al., 2014).

In keeping with this expression pattern, helios has been shown to mediate several lymphopoietic processes, including cell fate determination, T-cell development and T-reg function (Dovat et al., 2005, Getnet et al., 2010, Serre et al., 2011, Takatori et al., 2015). Similarly to ikaros and aiolos, helios also has a key role in tumour suppression, owing to its anti-proliferative function (Antica et al., 2008, Liippo et al., 2001, Nakase et al., 2000, Sun et al., 1999). Previous studies have demonstrated that overexpression of helios decreases CD4+ T-cell proliferation (Zhang et al., 2007), whilst knockdown of helios promotes T-cell growth (Asanuma et al., 2013). Furthermore, non-DNA-binding dominant-negative short isoforms of helios have been associated with lymphoproliferative disorders, including T-cell lymphoma and leukaemia, in both mice and humans (Fujii et al., 2003, Nakase et al., 2002, Tabayashi et al., 2007, Zhang et al., 2007).

In addition to cells of the T-lineage, helios has been reported to play a role in the development of Natural Killer (NK) cells (Kelley et al., 1998, Zhang et al., 2007). *Ikzf2* mRNA has also been detected in Dendritic cells (DCs), although this is at very low levels (Kelley et al., 1998) and does not appear to be translated into helios protein (Cai et al., 2009).

Given the known expression of helios within the haematopoietic system, age- and sex-matched *cello* mice underwent immunological phenotyping in order to assess immune cell populations and to give an overview of immune function. This comprised haematological analysis and flow cytometric analysis using fluorescence-activated cell sorting (FACS).

4.2. Results

4.2.1. Haematological Analysis

Blood samples were collected from nine month old *Ikzf2*$^{+/+}$ and *Ikzf2*$^{cello/cello}$ females for analysis of total and differential blood cell counts. No significant differences were observed in the white blood cell count, red blood cell count, platelet count or haemoglobin concentration of *Ikzf2*$^{cello/cello}$ mice compared to *Ikzf2*$^{+/+}$ controls (Figure 4.1 A-D). Analysis of white blood cell subpopulations also showed no significant differences in the number of lymphocytes, neutrophils, eosinophils or basophils or monocytes in *Ikzf2*$^{cello/cello}$ animals (Figure 4.1 E-I).

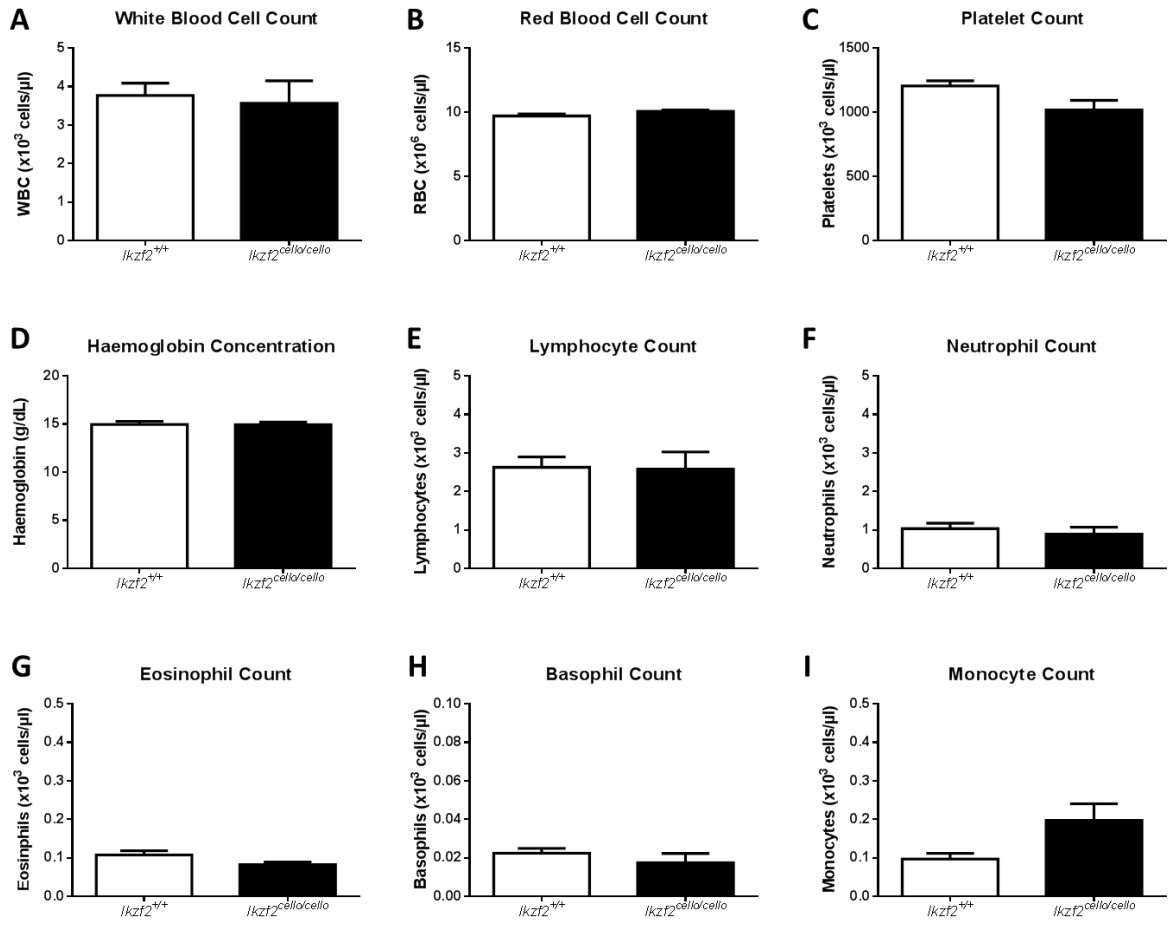

Figure 4.1: Haematological analysis of *Ikzf2*$^{+/+}$ and *Ikzf2*$^{cello/cello}$ females at nine months of age.
Total and differential haematopoietic cell counts were carried out on retro-orbital blood samples collected from *Ikzf2*$^{+/+}$ (n = 4) and *Ikzf2*$^{cello/cello}$ (n = 4) female mice at nine months of age. No significant differences were observed in any of the cell populations investigated. Data are shown as mean ± s.e.m. Statistical analysis: unpaired *t*-test.

4.2.2. Fluorescence-Activated Cell Sorting (FACS)

Splenocytes were collected from nine month old *Ikzf2*$^{+/+}$ and *Ikzf2*$^{cello/cello}$ females and analysed using two comprehensive flow cytometry panels. The first panel assessed the proportion of T-helper cells, T-regs, cytotoxic T-lymphocytes (CTLs), γδ T-cells, NK cells and Natural Killer T-cells (NKTs), whilst the second panel assessed leukocyte cell subtypes, as well as B-cell and DC populations.

T-helper cells are cytokine-producing CD4+ T-cells that help regulate adaptive immune responses by activating CTLs and B-cells, influencing immunoglobulin class switching and augmenting phagocytic responses (Tada et al., 1978). FACS analysis showed no significant differences in the total number of T-helper cells or the proportion of effector and regulatory T-helper cell subtypes in *Ikzf2*$^{cello/cello}$ mice compared to *Ikzf2*$^{+/+}$ controls, although the larger error bars for *Ikzf2*$^{cello/cello}$ data suggest greater variability (Figure 4.2 A-C).

T-regs are non-proliferating CD4+ CD25+ T-cells that have potent suppressive functions and contribute to immune self-tolerance (Sakaguchi et al., 1995, Jonuleit et al., 2001). Although helios is known to be expressed in T-regs, no significant differences were observed in the total, effector or resting T-reg populations of *Ikzf2*$^{cello/cello}$ mice compared to *Ikzf2*$^{+/+}$ controls (Figure 4.2 D-F).

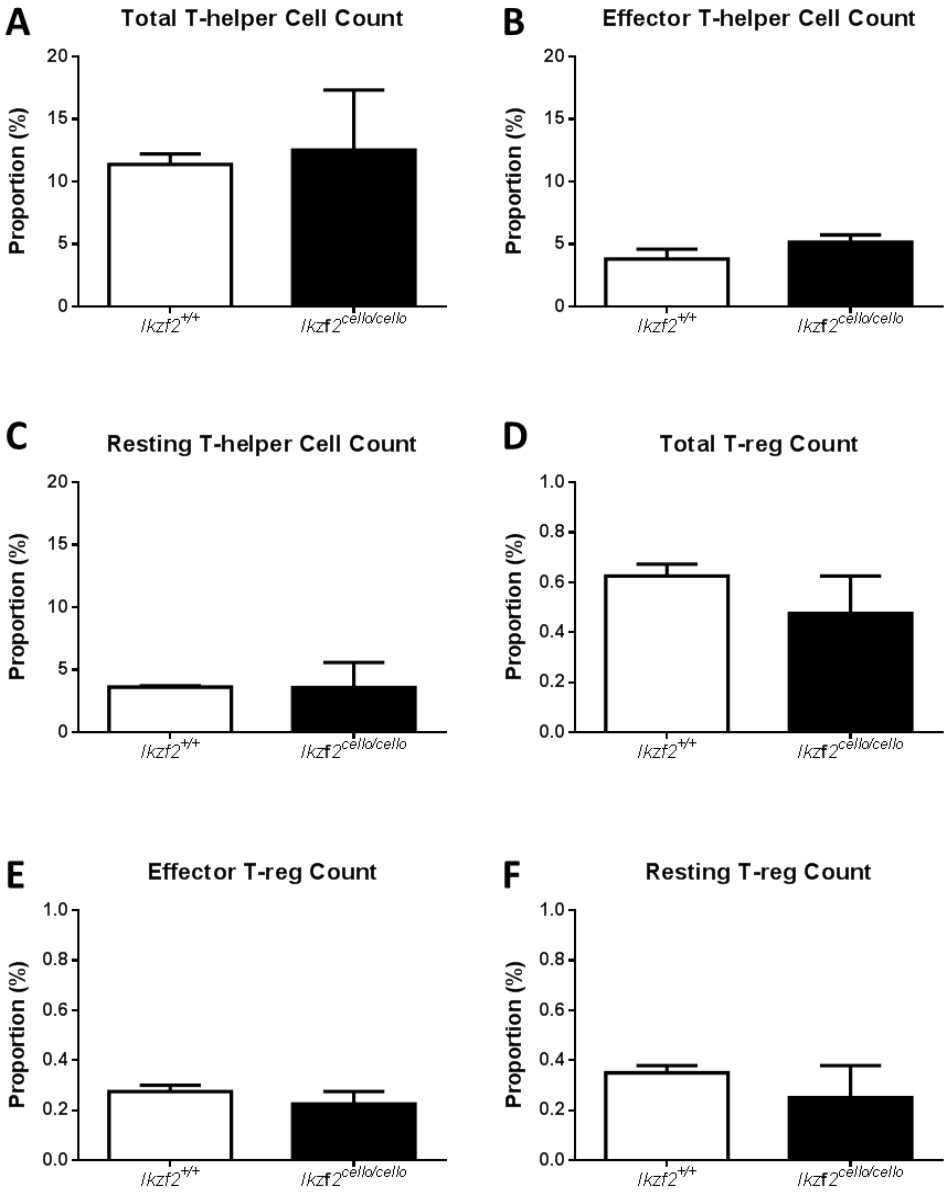

Figure 4.2: Fluorescence-activated cell sorting analysis of CD4+ T-cell populations in *Ikzf2*$^{+/+}$ and *Ikzf2*$^{cello/cello}$ females at nine months of age.

The proportion of CD4+ T-helper cells and T-regs was assessed by FACS analysis of splenocytes collected from *Ikzf2*$^{+/+}$ (n = 4) and *Ikzf2*$^{cello/cello}$ (n = 4) female mice at nine months of age. No significant differences were observed in the proportion of **(A)** total T-helper cells, **(B)** effector T-helper cells or **(C)** resting T-helper cells in *Ikzf2*$^{cello/cello}$ mice compared to *Ikzf2*$^{+/+}$ controls. The proportion of **(D)** total T-regs, **(E)** effector T-regs and **(F)** resting T-regs were also unaffected in *Ikzf2*$^{cello/cello}$ mice. Data are shown as mean ± s.e.m. Statistical analysis: unpaired *t*-test. T-reg, regulatory T-cell.

CTLs are CD8+ T-cells that can induce apoptosis of target cells, particularly those infected with viruses, through the release of cytolytic perforin granules and granzyme proteases (Henkart, 1985). The proportion of total CTLs was similar between *Ikzf2*$^{+/+}$ and *Ikzf2*$^{cello/cello}$ mice (5.4% and 5.7% respectively) (in A). Compared to *Ikzf2*$^{+/+}$ controls, *Ikzf2*$^{cello/cello}$ mice were found to exhibit a small significant increase of 0.4% in the proportion of effector CTLs (0.4% and 0.8% respectively) (Figure 4.3 B). Although no additional significant differences were found in the proportion of resting and naïve CTL subtypes in *Ikzf2*$^{cello/cello}$ mice compared to *Ikzf2*$^{+/+}$ controls, there were again larger error bars for the *Ikzf2*$^{cello/cello}$ data, indicating greater variability (Figure 4.3 C-D).

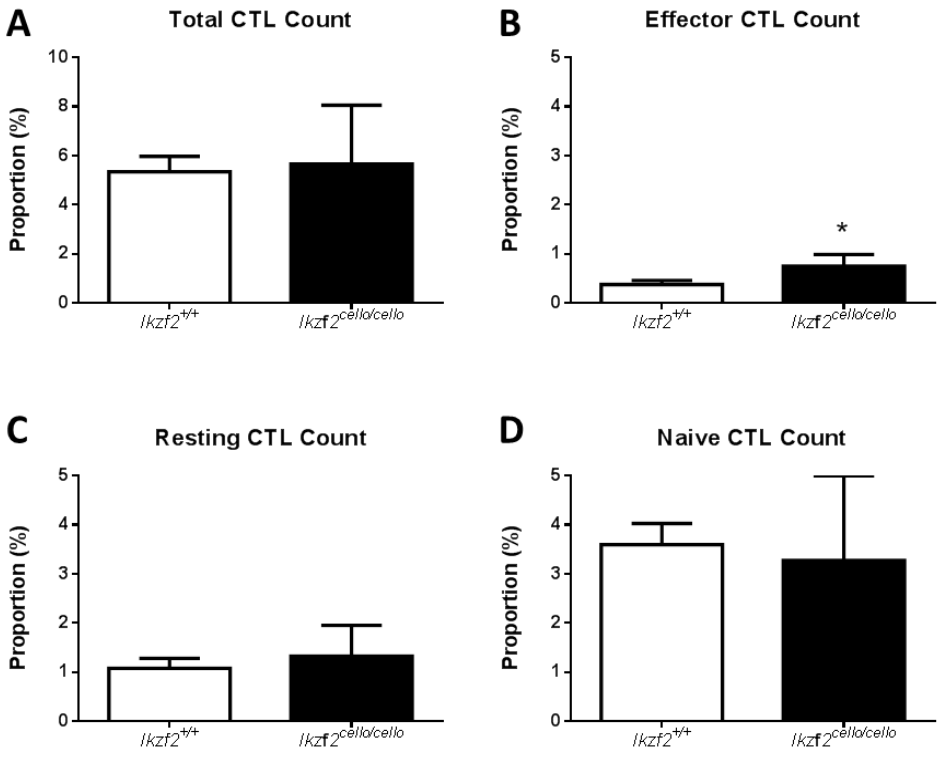

Figure 4.3: Fluorescence-activated cell sorting analysis of CD8+ T-cell populations in *Ikzf2*$^{+/+}$ and *Ikzf2*$^{cello/cello}$ females at nine months of age.

CTL subpopulations were assessed by FACS analysis of splenocytes collected from *Ikzf2*$^{+/+}$ (n = 4) and *Ikzf2*$^{cello/cello}$ (n = 4) female mice at nine months of age. **(A)** No significant differences were observed in the proportion of total CTLs between *Ikzf2*$^{+/+}$ and *Ikzf2*$^{cello/cello}$ animals. **(B)** *Ikzf2*$^{cello/cello}$ mice showed a small significant increase in levels of effector CTLs compared to *Ikzf2*$^{+/+}$ controls. **(C)** The proportion of resting CTLs was similar in both *Ikzf2*$^{+/+}$ and *Ikzf2*$^{cello/cello}$ mice. **(D)** Naïve CTL populations were also unaffected in *Ikzf2*$^{cello/cello}$ animals. Data are shown as mean ± s.e.m. Statistical analysis: unpaired *t*-test, * = $p \leq 0.05$. CTL, CD8+ cytotoxic T-lymphocyte.

The γδ T-cell subset are characterised by a distinct T-cell receptor on their cell surface and are largely abundant in the gut mucosa (Allison and Raulet, 1990). Compared to *Ikzf2*$^{+/+}$ controls, *Ikzf2*$^{cello/cello}$ mice were found to have significantly decreased levels of γδ T-cells (2.7% and 1.9% respectively) (Figure 4.4 A).

NK cells are cytotoxic lymphocytes that are involved in innate immune responses to viral-infected cells (Kiessling et al., 1975). Although the proportion of NK cells was unaffected in *Ikzf2*$^{cello/cello}$ mice there appears to be greater variability in the *Ikzf2*$^{cello/cello}$ data (Figure 4.4 B), as mentioned previously.

NKTs are a unique lymphocyte population that possess both T-cell and NK cell characteristics and play a role in tumour surveillance and immune tolerance (Jerud et al., 2006). No significant differences were observed between *Ikzf2*$^{cello/cello}$ and *Ikzf2*$^{+/+}$ animals in the total proportion of NKTs or within the effector, resting and invariant NKT subpopulations (Figure 4.4 C-F).

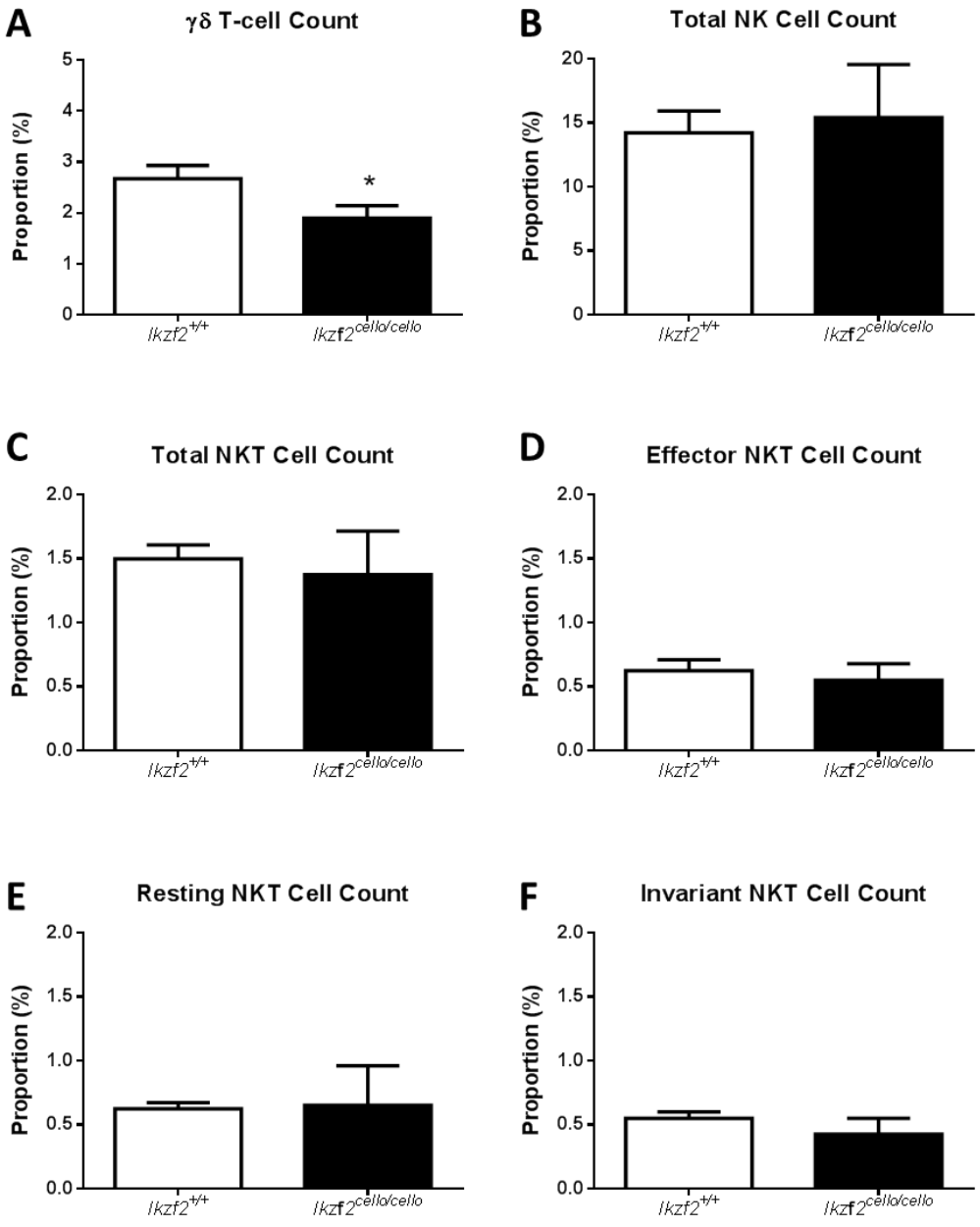

Figure 4.4: Fluorescence-activated cell sorting analysis of δγ T-cells, natural killer cells and natural killer T-cells in *Ikzf2*$^{+/+}$ and *Ikzf2*$^{cello/cello}$ females at nine months of age.

The proportions of δγ T-cells, NK cells and NKT cells were assessed by FACS analysis of splenocytes collected from *Ikzf2*$^{+/+}$ (n = 4) and *Ikzf2*$^{cello/cello}$ (n = 4) female mice at nine months of age. **(A)** A small significant decrease was observed in the proportion of δγ T-cells in *Ikzf2*$^{cello/cello}$ mice compared to *Ikzf2*$^{+/+}$ controls. **(B)** No significant differences were observed in the proportion of NK cells in *Ikzf2*$^{cello/cello}$ mice compared to *Ikzf2*$^{+/+}$ mice. The proportion of **(C)** total NKT cells and **(D)** effector NKT, **(E)** resting NKT and **(F)** invariant NKT subtypes were also unaffected in *Ikzf2*$^{cello/cello}$ animals. Data are shown as mean ± s.e.m. Statistical analysis: unpaired *t*-test, * = p≤0.05. NK, natural killer cell; NKT, natural killer T-cell.

Neutrophils and eosinophils are leukocyte cells of the innate immune system, which fight infection through the release of antimicrobial granules (Hirsch, 1960). Also within the innate leukocyte population are monocytes and their macrophage progeny, which are involved in phagocytosis, antigen presentation and cytokine production (Nathan et al., 1980, Volkman and Gowans, 1965). *Ikzf2*$^{cello/cello}$ mice were found to have normal proportions of neutrophils, eosinophils and monocytes compared to *Ikzf2*$^{+/+}$ mice (Figure 4.5 A-C). A significant reduction of 0.5% was observed in the macrophage population of *Ikzf2*$^{cello/cello}$ mice (0.4%) compared to *Ikzf2*$^{+/+}$ controls (0.9%) (Figure 4.5 D).

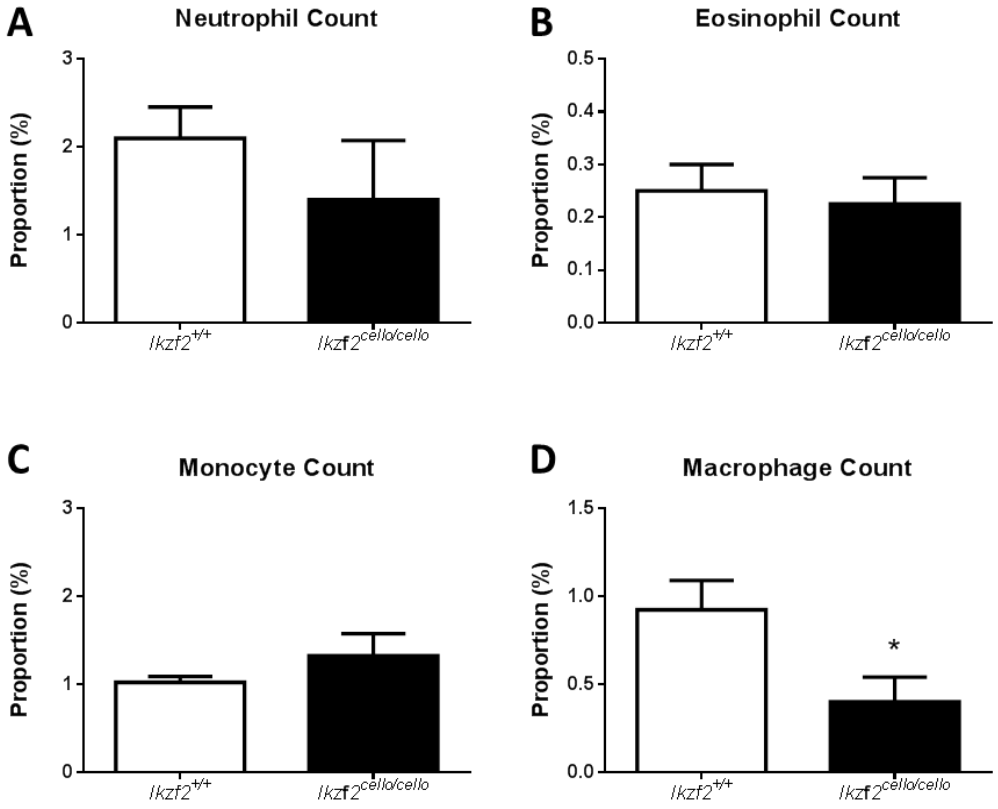

Figure 4.5: Fluorescence-activated cell sorting analysis of leukocyte cell populations in *Ikzf2*$^{+/+}$ and *Ikzf2*$^{cello/cello}$ females at nine months of age.

The proportion of neutrophil, eosinophil, monocyte and macrophage leukocyte cells were assessed by FACS analysis of splenocytes collected from *Ikzf2*$^{+/+}$ (n = 4) and *Ikzf2*$^{cello/cello}$ (n = 4) female mice at nine months of age. **(A)** *Ikzf2*$^{cello/cello}$ mice showed no significant differences in the proportion of neutrophil granulocytes compared to *Ikzf2*$^{+/+}$ controls. **(B)** Eosinophil granulocytes populations were also unaffected in *Ikzf2*$^{cello/cello}$ mice compared to *Ikzf2*$^{+/+}$ mice. **(C)** No significant differences were seen in monocyte cells between *Ikzf2*$^{cello/cello}$ and *Ikzf2*$^{+/+}$ mice. **(D)** A signficant decrease was observed in macrophage cells in *Ikzf2*$^{cello/cello}$ mice compared to *Ikzf2*$^{+/+}$ controls. Data are shown as mean ± s.e.m. Statistical analysis: unpaired *t*-test, * = $p \leq 0.05$.

B-cells produce a diverse repertoire of antibodies and are involved in adaptive immune repsonses (Raff, 1973). FACS analysis showed no significant differences in the total proportion of B-cells or the B2 and B1 B-cell subtypes in *Ikzf2*$^{cello/cello}$ animals compared to *Ikzf2*$^{+/+}$ controls, although again the larger error bars suggest greater variability in the *Ikzf2*$^{cello/cello}$ data (Figure 4.6 A-D).

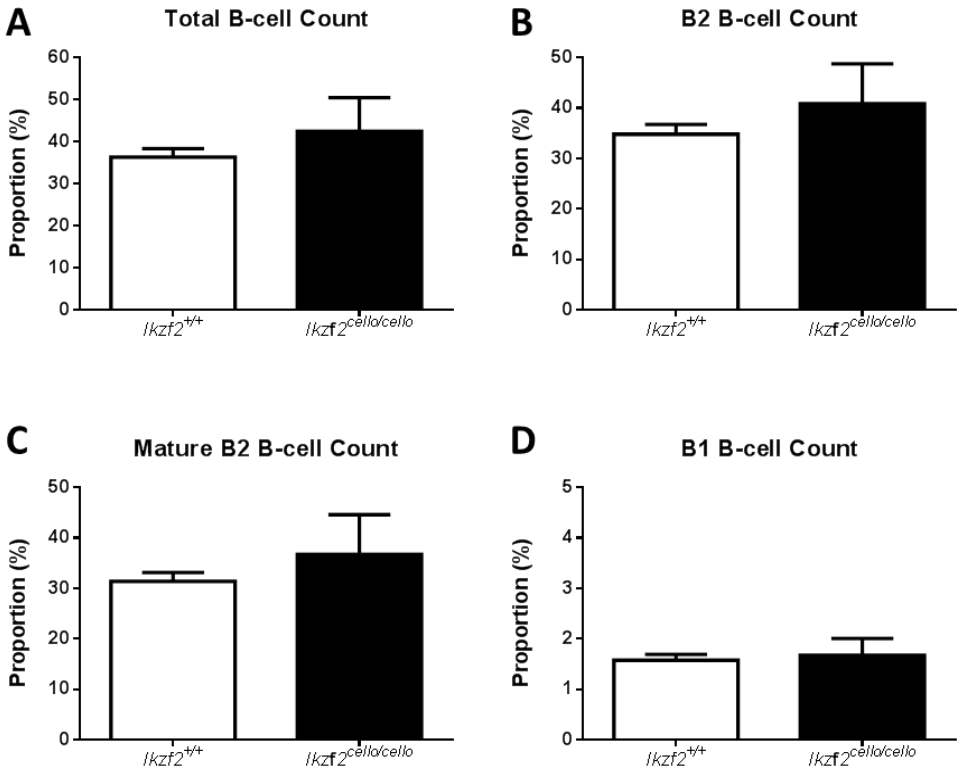

Figure 4.6: Fluorescence-activated cell sorting analysis of B-cell populations in *Ikzf2*$^{+/+}$ and *Ikzf2*$^{cello/cello}$ females at nine months of age.

B-cell populations were assessed by FACS analysis of splenocytes collected from *Ikzf2*$^{+/+}$ (n = 4) and *Ikzf2*$^{cello/cello}$ (n = 4) female mice at nine months of age. No significant differences were observed in the proportion of **(A)** total B-cells or in the **(B)** B2 B-cell, **(C)** mature B2 B-cell or **(D)** B1 B-cell subpopulations in *Ikzf2*$^{cello/cello}$ mice compared to *Ikzf2*$^{+/+}$ controls. Data are shown as mean ± s.e.m. Statistical analysis: unpaired *t*-test.

DCs are antigen-presenting cells that initiate immune responses by secreting cytokines and activating T-cells and B-cells (Banchereau and Steinman, 1998, Steinman and Cohn, 2007). The proportion of total DCs was similar between *Ikzf2*$^{cello/cello}$ and *Ikzf2*$^{+/+}$ mice (Figure 4.7 A). CD8-type, Cd11b-type and plasmacytoid DC subpopulations were also unaffected in *Ikzf2*$^{cello/cello}$ animals (Figure 4.7 B-D). As before, the *Ikzf2*$^{cello/cello}$ data appears to exhibit greater variability.

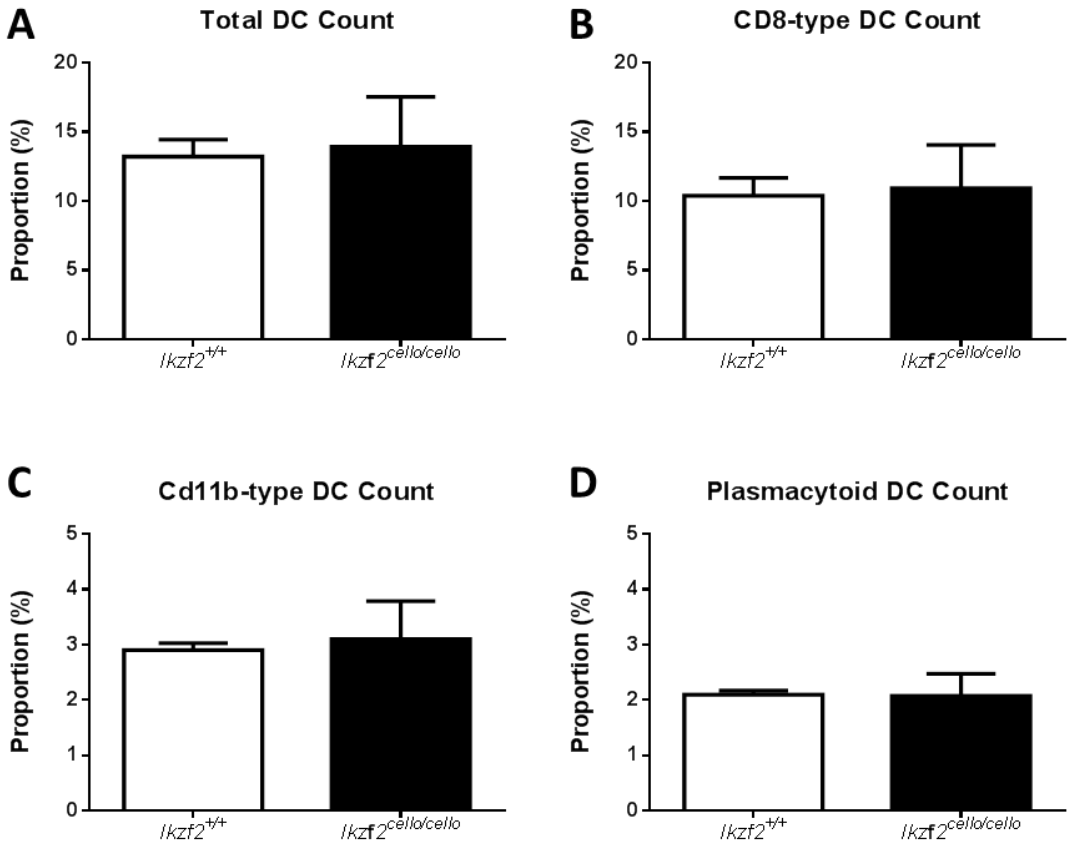

Figure 4.7: Fluorescence-activated cell sorting analysis of dendritic cell populations in *Ikzf2*$^{+/+}$ and *Ikzf2*$^{cello/cello}$ females at nine months of age.

DC subtypes were assessed by FACS analysis of splenocytes collected from *Ikzf2*$^{+/+}$ (n = 4) and *Ikzf2*$^{cello/cello}$ (n = 4) female mice at nine months of age. No significant differences were found in the proportion of **(A)** total DCs or in the **(B)** CD8-type DC, **(C)** Cd11b-type DC and **(D)** plasmacytoid DC subpopulations in *Ikzf2*$^{cello/cello}$ mice compared to *Ikzf2*$^{+/+}$ controls. Data are shown as mean ± s.e.m. Statistical analysis: unpaired *t*-test. DC, dendritic cell.

4.3. Discussion

As detailed in Chapter 3, *cello* mice were found to carry an ENU-induced missense mutation in the transcription factor helios. Previous studies have demonstrated that helios is expressed in haematopoietic lineages and mediates several processes associated with T-cell development and function (Dovat et al., 2005, Getnet et al., 2010, Hahm et al., 1998, Kelley et al., 1998, Serre et al., 2011, Takatori et al., 2015, Zhang et al., 2007).

In order to investigate the effect of the *cello* mutation on immune cell populations and give an overview of immune function, age- and sex-matched *Ikzf2*$^{+/+}$ and *Ikzf2*$^{cello/cello}$ mice were subject to immunological phenotyping using haematological analysis and FACS. Haematological analysis demonstrated no significant differences in total white blood cell, red blood cell and platelet counts or in lymphocyte, neutrophil, eosinophil, basophil and monocyte white blood cell subpopulations between the two genotype groups.

In T-regs, helios has been shown to enhance suppressive function in co-operation with forkhead box P3 (*FoxP3*) (Getnet et al., 2010, Zabransky et al., 2012, Takatori et al., 2015). Interestingly, FACS analysis showed no significant differences in total, effector or resting T-reg populations in *Ikzf2*$^{cello/cello}$ mice compared to *Ikzf2*$^{+/+}$ controls. However, similar findings have been reported in helios null mouse models, where loss of helios, either globally or using a CD4-Cre driver, has no effect T-reg number, maturation or function (Cai et al., 2009, Thornton et al., 2010). This suggests either a non-essential role for helios in T-regs or that there is functional redundancy, with other IKZF proteins compensating for loss of helios function. Indeed, eos has also been shown to be expressed in helios+ FOXP3+ T-regs (Raffin et al., 2013) and can interact with FOXP3 to maintain T-reg suppressive activity (Pan et al., 2009).

FACS also showed that T-helper cell, NK cell, B-cell and DC populations were unaffected in *Ikzf2*$^{cello/cello}$ mice compared to *Ikzf2*$^{+/+}$ controls. In keeping with this, previous work has demonstrated that helios is not essential for T-helper cell differentiation and development (Cai et al., 2009, Serre et al., 2011) and could potentially be compensated by aiolos in these cells (Quintana et al., 2012). In addition, helios expression has not been reported in mature B-cell or DC populations to date (Cai et al., 2009, Dovat et al., 2005, Kelley et al., 1998, Thornton et al., 2010). Although helios is expressed in NK cells (Kelley et al., 1998), normal NK proportions were seen in *Ikzf2*$^{cello/cello}$ animals, which again mirrors the phenotype reported for helios null mice (Cai et al., 2009). This again could be due to redundancy with other IKZF family members, as both aiolos and ikaros are also present in NK cells (Kelley et al., 1998) and have been shown to be essential for their development, maturation and function (Georgopoulos et al., 1994, Holmes et al., 2014, Wang et al., 1996).

A number of significant differences were observed between *Ikzf2*$^{cello/cello}$ mutants and *Ikzf2*$^{+/+}$ controls following FACS analysis. This included a significant increase (of 0.4%) in the proportion of effector CTLs in *Ikzf2*$^{cello/cello}$ mutants, which suggests that loss of helios function may disrupt CTL proliferation. Indeed, helios is known to have an anti-proliferative function in T-cells (Asanuma et al., 2013, Nakase et al., 2002, Zhang et al., 2007) and loss of ikaros has been shown drive hyperproliferation of activated T-cell subsets (Wang et al., 1996). However, it is difficult to know whether an increase of 0.4% would be biologically significant. Furthermore, as the proportion of total, resting and naïve CTL subtypes were unaffected in *Ikzf2*$^{cello/cello}$ animals and no differences were seen in CTL frequencies or function in helios null mice (Cai et al., 2009), it may be that this is a false positive result. This

should be addressed by repeating the FACS experiments with an increased number of biological replicates.

Ikzf2$^{cello/cello}$ animals also exhibited a significant reduction (of 0.8%) in the proportion of γδ T-cells compared to *Ikzf2*$^{+/+}$ controls. This corresponds to previous work demonstrating that forced over-expression of helios increases the frequency of γδ T-cells in the spleen of irradiated mice (Zhang et al., 2007), whilst loss of ikaros decreases the frequency of γδ T-cells in ikaros null mice (Wang et al., 1996). Interestingly, these findings are in contrast to those published by Cai et al. (2009), who did not find any significant differences in the proportion of γδ T-cells in either the thymus or spleen of helios null mice. These inconsistencies may be due to differences in genetic background, with Cai et al. (2009) studying helios null mice on a mixed C57BL/6 and 129/Sv background. However, as before, it is difficult to know if a 0.8% reduction would be biologically significant.

In addition, a significant reduction (of 0.5%) was detected in macrophage populations in *Ikzf2*$^{cello/cello}$ mutants compared to *Ikzf2*$^{+/+}$ controls. Although both macrophage cells and their monocyte precursors have been explicitly shown not to express *Ikzf2* mRNA (Hahm et al., 1998, Kelley et al., 1998, Thornton et al., 2010), it may be that helios is involved in the development of these cells in a secondary manner. Indeed, the differentiation of specific T-helper cell subtypes, a process that helios is known to be involved in (Serre et al., 2011), can influence the production of cytokines and subsequent production and activation of immune effector cells, such as macrophages (Alberts et al., 2002). However, it is again difficult to know if a reduction of 0.5% would be biologically significant.

Interestingly, *Ikzf2*$^{cello/cello}$ mice appeared to exhibit greater variability than *Ikzf2*$^{+/+}$ controls throughout the immunological analyses, as shown by the consistently larger error bars. An

example of this can be seen in Figure 4.2 A, where the larger error bars may be masking a potential trend towards increased T-helper cell counts in *Ikzf2*$^{cello/cello}$ mutants. Although helios has been proposed to have a redundant role in T-helper cell differentiation and development (Cai et al., 2009, Serre et al., 2011), it could be that other IKZF family members are upregulated in *Ikzf2*$^{cello/cello}$ T-helper cells to compensate for loss of helios function, leading to increased T-helper cell differentiation and this such potential trend. Similarly, the larger error bars in Figure 4.3 and Figure 4.6 may be masking potential trends towards increased CTL cell counts and B-cell counts, respectively, in *Ikzf2*$^{cello/cello}$ mutants. As previous work has documented hyperproliferation of activated T-cell and B-cell subtypes in ikaros and aiolos null mice (Kirstetter et al., 2002, Wang et al., 1996, Wang et al., 1998b), it may be that this same phenomenon is occurring in *Ikzf2*$^{cello/cello}$ mice, albeit to a lesser extent. These potential trends should be further explored by repeating the immunological analyses with an increased number of biological replicates. In addition, it is important to note that the current experiments were carried out on unchallenged mice and so are limited in giving only an indication of the resting immune state of *Ikzf2*$^{cello/cello}$ mutants. Future experiments should be undertaken on cohorts of *cello* mice that have been challenged with an immunotoxin, such as lipopolysaccharide (LPS), in order to further study the effect of the *cello* mutation on activated immune responses.

Overall, these data are largely consistent with previous findings that helios is not essential for the development of T-cell and NK cell populations and likely mediates cell fate determination and lymphoid function in a redundant manner (Cai et al., 2009, Thornton et al., 2010, Zhang et al., 2007). Indeed, other ikaros family members are known to be

expressed in T-cells and NK cells and possibly compensate for helios loss-of-function (Cai et al., 2009, Thornton et al., 2010).

Although no haematopoietic phenotypes were reported in the global helios null, homozygotes were found to exhibit high levels of perinatal lethality, reduced size, decreased body weight, abnormal eyelid growth and smaller eye openings (Cai et al., 2009), which suggests that helios has additional important roles outside of the haematopoietic system. Similar phenotypes were also detected in *cello* mice, with *Ikzf2*$^{cello/cello}$ mutants exhibiting decreased body weight compared to *Ikzf2*$^{+/+}$ mice (Figure 9.4 in Appendix), as well as microphthalmia and a 'cloudy eye' phenotype. Although each of these phenotypes requires further analysis to fully elucidate the function of helios, they were not pursued due to time constraints and subsequent work undertaken for this thesis focussed on investigating the role of helios within the mammalian auditory system. To this end, *cello* mice underwent both phenotypic auditory characterisation (detailed in Chapter 5) and functional auditory characterisation (detailed in Chapter 6).

Chapter 5 : Phenotypic Auditory Characterisation of *cello*

5.1. Introduction

Whilst primarily studied in the mammalian immune system, some non-haematopoietic roles have also been reported for the ikaros family of transcription factors; for example, ikaros has been linked with neurogenesis in the developing mouse striatum, cerebral cortex and retina (Agoston et al., 2007, Alsio et al., 2013, Elliott et al., 2008) and eos has been reported to positively regulate post-synaptic density protein-95 (PSD-95) in cochlear afferent neurons (Bao et al., 2004). Outside of the haematopoietic system, helios has been reported to be transiently expressed in several brain structures and epithelial tissues during embryogenesis, including the hippocampus, cerebellum, accessory olfactory bulb, retina and gut lining (Kelley et al., 1998, Martin-Ibanez et al., 2012) and has been shown to promote neurogenesis of a subset of projection neurons in the developing striatum (Martin-Ibanez et al., 2012). However, helios has not previously been implicated in auditory function.

In order to investigate the contribution of helios to hearing and the role of helios within the auditory system, *cello* mice underwent extensive phenotypic characterisation *in vivo* and *ex vivo* at a range of time points from early development (P4 – P16) to juvenile and adult stages (one – nine months of age). This comprised a time course of auditory phenotyping, morphological examination of the ear, ultrastructural examination of the organ of Corti and investigation of the temporospatial expression pattern of helios. By providing insight into the mechanisms underlying the hearing impairment in *cello,* this may help elucidate the normal role and functional importance of helios within the auditory system.

5.2. Results

5.2.1. Auditory Phenotyping Time Course

To establish the onset of the auditory impairment in *cello* mice, ABR analyses of *Ikzf2*$^{+/+}$, *Ikzf2*$^{cello/+}$ and *Ikzf2*$^{cello/cello}$ littermate mice were undertaken at P16, which is just after the onset of hearing at ~P12. ABR measurements were obtained in response to 8 kHz, 16 kHz, 32 kHz and click stimuli then analysed to determine auditory thresholds.

At P16, *Ikzf2*$^{cello/cello}$ mice were found to have significantly elevated thresholds (>65 dB SPL) at all frequencies tested, whilst *Ikzf2*$^{cello/+}$ mice exhibited thresholds comparable to those of *Ikzf2*$^{+/+}$ littermates (<30 dB SPL) (Figure 5.1). This confirms an early-onset, recessive hearing impairment in *cello* mutant mice.

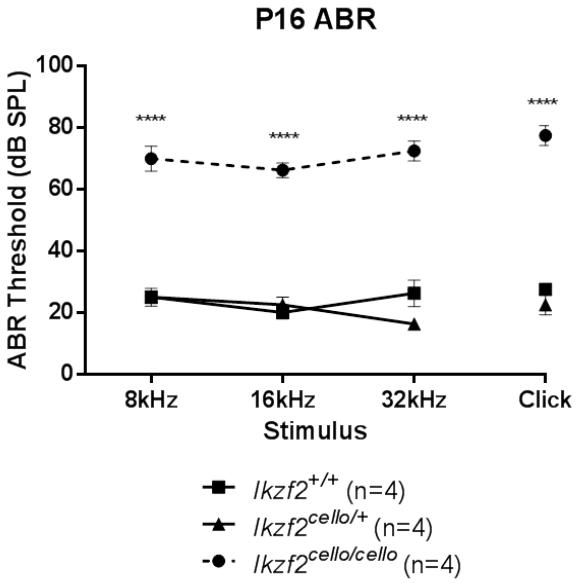

Figure 5.1: Auditory-evoked brainstem response analysis of the cello pedigree at postnatal day 16.
At P16, *Ikzf2*$^{cello/cello}$ mice displayed severely elevated auditory thresholds (>65 dB SPL) at all frequencies tested. Age-matched *Ikzf2*$^{+/+}$ and *Ikzf2*$^{cello/+}$ littermates exhibited thresholds within the normal expected range (<30 dB SPL). Auditory thresholds were established using the first two peaks (peak I and II) of the corresponding ABR trace. Data are shown as mean ± s.e.m. Statistical analysis: one-way ANOVA, **** = $p \leq 0.0001$. ABR, auditory-evoked brainstem response; dB SPL, decibel sound pressure level; kHz, kiloHertz; P16, postnatal day 16.

To determine if the hearing loss in *Ikzf2*$^{cello/cello}$ mice was progressive in nature, additional ABR analyses were carried out at one, three, six and nine months of age, using littermates where possible. At one month of age, *Ikzf2*$^{cello/cello}$ mice displayed severely elevated auditory thresholds (>65 dB SPL) compared to normal hearing *Ikzf2*$^{+/+}$ and *Ikzf2*$^{cello/+}$ controls (< 30dB SPL) (Figure 5.2 A), which is similar to the results observed at P16. At three and six months of age, *Ikzf2*$^{cello/cello}$ thresholds increased slightly (>80dB SPL), whilst *Ikzf2*$^{+/+}$ and *Ikzf2*$^{cello/+}$ thresholds remained in the normal hearing range (<35 dB SPL) (Figure 5.2 B-C). By nine months of age, *Ikzf2*$^{cello/cello}$ thresholds were further elevated (>85 dB SPL) (Figure 5.2 D), which indicates progressive deterioration of hearing function. At all of the time points tested, *Ikzf2*$^{cello/+}$ mice showed auditory thresholds comparable to those of *Ikzf2*$^{+/+}$ littermates, indicating there is no heterozygous progressive or late-onset auditory phenotype.

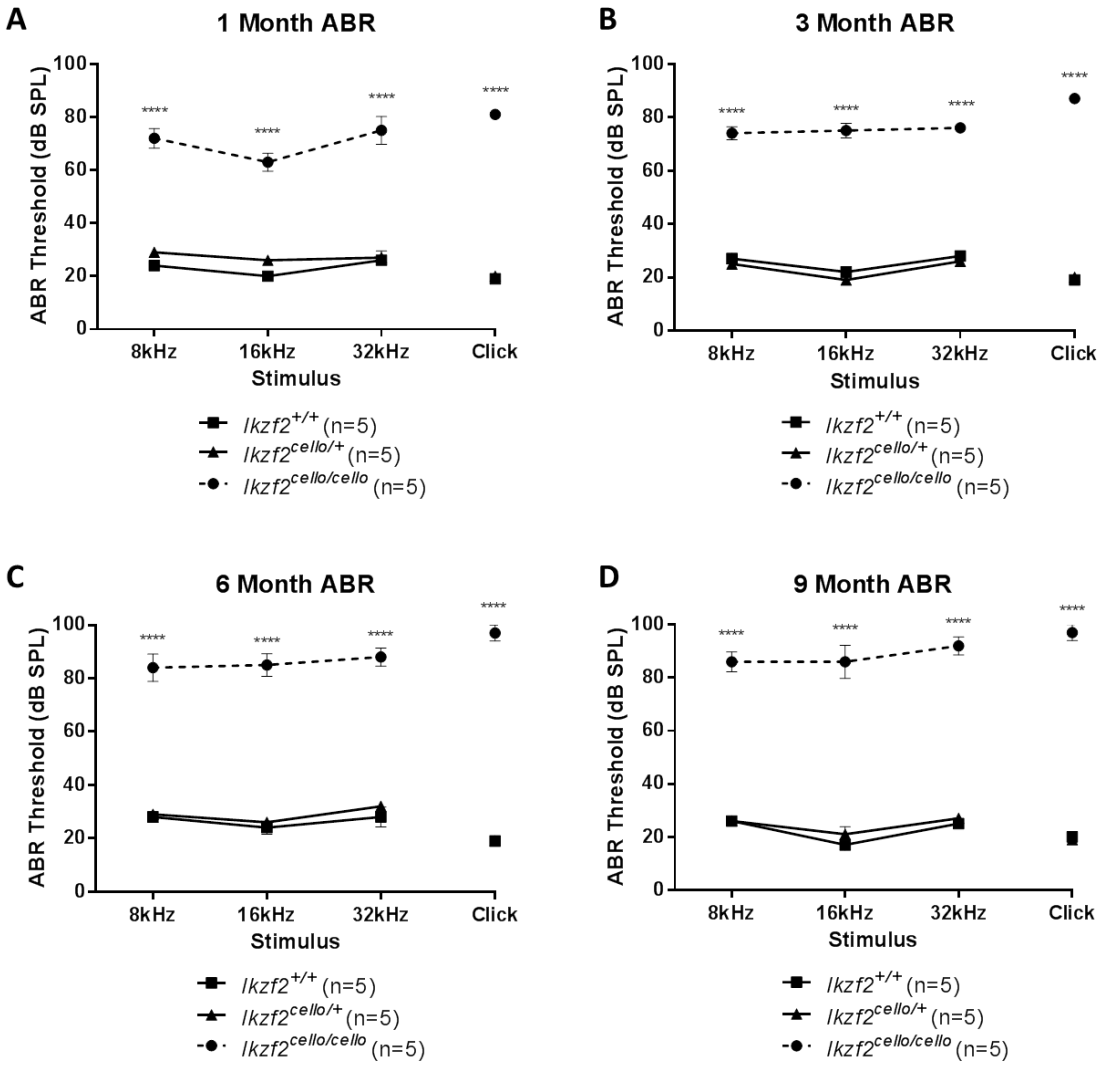

Figure 5.2: Auditory-evoked brainstem response analysis of the *cello* pedigree at one, three, six and nine months of age.

(A) At one month of age, *Ikzf2*$^{cello/cello}$ mice exhibited significantly elevated auditory thresholds (>65 dB SPL) across all frequencies compared to *Ikzf2*$^{+/+}$ and *Ikzf2*$^{cello/+}$ control mice (<30 dB SPL). **(B-C)** ABR analyses at three and six months of age showed a modest increase in *Ikzf2*$^{cello/cello}$ thresholds (>80 dB SPL) compared to controls. **(D)** By nine months of age, ABR thresholds were further elevated in *Ikzf2*$^{cello/cello}$ mice (>85 dB SPL), whilst *Ikzf2*$^{+/+}$ and *Ikzf2*$^{cello/+}$ mice continued to display thresholds within the normal range (<35 dB SPL). Auditory thresholds were established using the first two peaks (peak I and II) of the corresponding ABR trace. Data are shown as mean ± s.e.m. Statistical analysis: one-way ANOVA, **** = p≤0.0001. ABR, auditory-evoked brainstem response; dB SPL, decibel sound pressure level; kHz, kiloHertz.

Comparison of ABR data measured at one and nine months of age indicated that the elevation in *Ikzf2*$^{cello/cello}$ thresholds between these two time points is statistically significant (Figure 5.3).

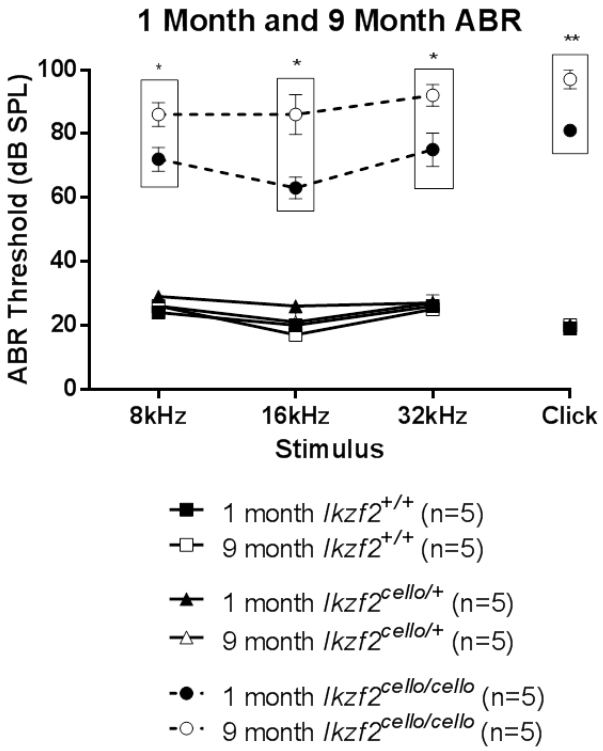

Figure 5.3: Comparison of auditory-evoked brainstem responses of the *cello* pedigree at one and nine months of age.

Comparison of ABR thresholds from one and nine months old animals showed that hearing function does not deteriorate in aged *Ikzf2*$^{+/+}$ and *Ikzf2*$^{cello/+}$ mice. However, there is a statistically significant elevation in *Ikzf2*$^{cello/cello}$ thresholds across all frequencies between one and nine months of age. Auditory thresholds were established using the first two peaks (peak I and II) of the corresponding ABR trace. Data are shown as mean ± s.e.m. Statistical analysis: unpaired *t*-test, * = p≤0.05, ** = p≤0.01. ABR, auditory-evoked brainstem response; dB SPL, decibel sound pressure level; kHz, kiloHertz.

ABR traces typically comprise of five main peaks (PI – PV), each of which corresponds to a different region along the auditory pathway. In addition to determining auditory thresholds, ABR traces can also be assessed for variation in the amplitude or latency of ABR peaks. These measures relate to the number of neurons which fire in response to auditory stimulation and the speed at which auditory signals are transmitted along the auditory pathway (Merzenich et al., 1983).

In click ABR traces from *Ikzf2*$^{+/+}$ mice at one month of age, all five peaks were detected until the 25 dB SPL auditory threshold (Figure 5.4 A). The same was true for *Ikzf2*$^{cello/+}$ click ABR traces, with no obvious defects observed in peak amplitude (Figure 5.4 B). Five ABR peaks were also initially detected in *Ikzf2*$^{cello/cello}$ click ABR traces until the 70 dB SPL auditory threshold, with a slight reduction in amplitude compared to *Ikzf2*$^{+/+}$ and *Ikzf2*$^{cello/+}$ traces (Figure 5.4 C). However, as peak amplitude can be affected by a number of variables including body temperature, electrode placement and physiological noise, it is not considered a reliable indicator of auditory function (Zhou et al., 2006) and so was not pursued further.

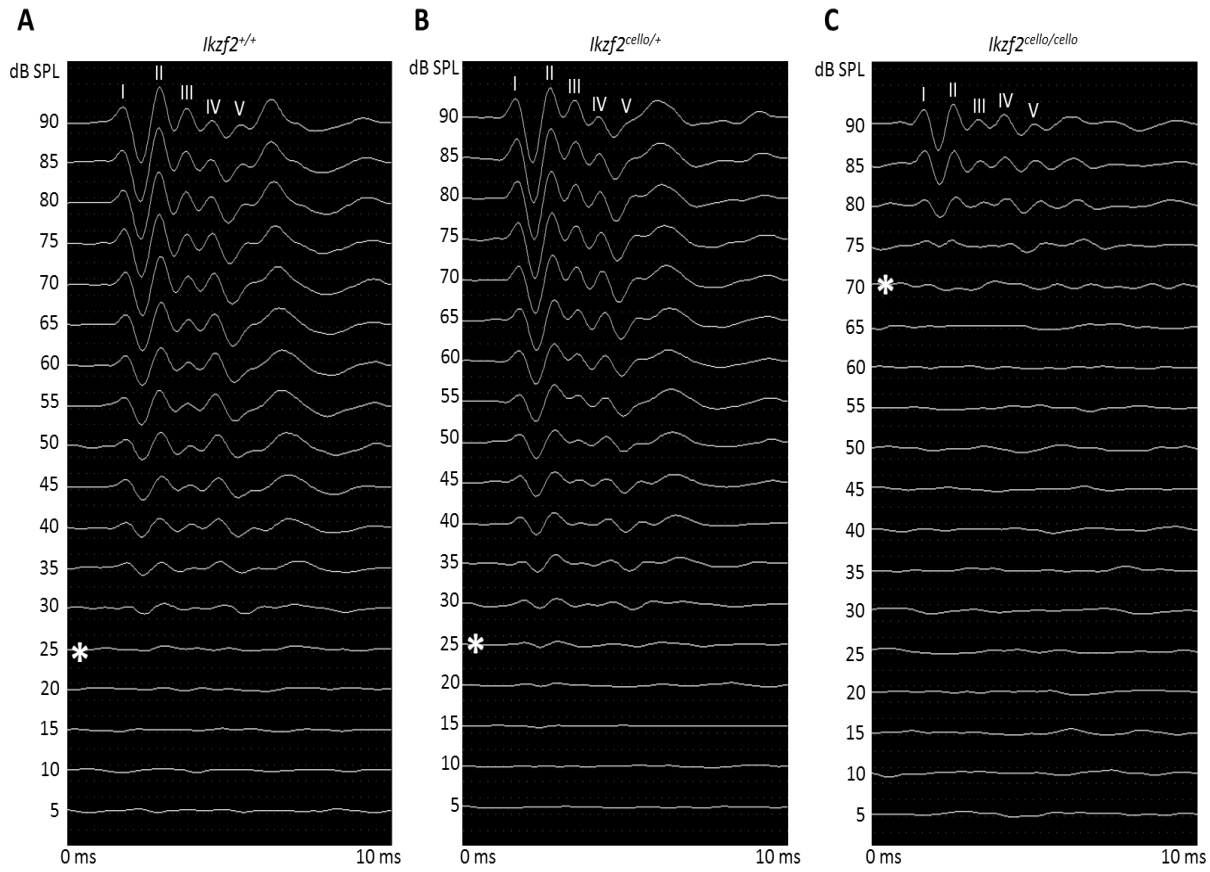

Figure 5.4: Representative click auditory-evoked brainstem response traces from *Ikzf2*$^{+/+}$, *Ikzf2*$^{cello/+}$ and *Ikzf2*$^{cello/cello}$ mice at one month of age.

ABR responses were collected and plotted from *Ikzf2*$^{+/+}$, *Ikzf2*$^{cello/+}$ and *Ikzf2*$^{cello/cello}$ mice at one month of age in response to a broadband click stimulus, played into the auditory canal at decreasing decibel sound pressure levels. ABR traces typically have five clear peaks (PI – PV), which correspond to specific regions along the auditory pathway (PI and PII, cochlear nerve; PIII, cochlear nucleus; PIV, super olivary nucleus; PV, inferior colliculus). In each case, the auditory threshold (marked with an asterisk) is selected as the lowest sound intensity that produces a recognisable and reproducible trace in response to the stimulus. **(A)** In a representative *Ikzf2*$^{+/+}$ click ABR trace, peaks I – V are clearly visible until the auditory threshold (25 dB SPL) is reached. **(B)** In *Ikzf2*$^{cello/+}$ click ABR traces, the five characteristic peaks are also detected until the auditory threshold (25 dB SPL), with grossly similar peak amplitude and interpeak latency compared to *Ikzf2*$^{+/+}$ mice. **(C)** The five main ABR peaks are still observed in *Ikzf2*$^{cello/cello}$ click ABR traces until the auditory threshold (70 dB SPL), with a potential reduction in peak amplitude compared to *Ikzf2*$^{+/+}$ and *Ikzf2*$^{cello/+}$ animals, but no obvious defects in interpeak latency. dB SPL, decibel sound pressure level; ms, milliseconds.

5.2.2. Morphological Analysis of the Inner Ear

The severely elevated auditory thresholds measured in *Ikzf2*$^{cello/cello}$ mice suggest a sensorineural hearing impairment. To assess morphology of the inner ear, three methods were used: examination of histological sections; immunolabelling of cochlear wholemounts and scanning electron microscopy-based ultrastructural analysis of hair cells. Identifying any pathological defects in the ears of *Ikzf2*$^{cello/cello}$ mice may provide insight into the normal role of helios in the ear and the mechanisms underlying the auditory impairment.

5.2.2.1. Haematoxylin and Eosin (H&E) Histology

Mid-modiolar sections through the inner ear were cut from paraffin-embedded *Ikzf2*$^{cello/+}$ (control) and *Ikzf2*$^{cello/cello}$ half heads at four months of age, then stained using haematoxylin and eosin (H&E) to enable morphological examination.

In *Ikzf2*$^{cello/cello}$ sections, gross cochlear morphology resembled that of *Ikzf2*$^{cello/+}$ controls, with the standard mid-modiolar 'clover-leaf' shape visible (Figure 5.5 A-B). Looking at the cochlear duct in more detail, the SGNs, Reissner's membrane and stria vascularis appeared normal in *Ikzf2*$^{cello/cello}$ mice, however, the organ of Corti and the IHCs and OHCs within it were severely disrupted (Figure 5.5 C-D). Whilst *Ikzf2*$^{cello/+}$ controls have one row of IHCs and three rows of OHCs, separated by two pillar cells which form the tunnel of Corti, this neat arrangement was lost in *Ikzf2*$^{cello/cello}$ mice (Figure 5.5 E-F).

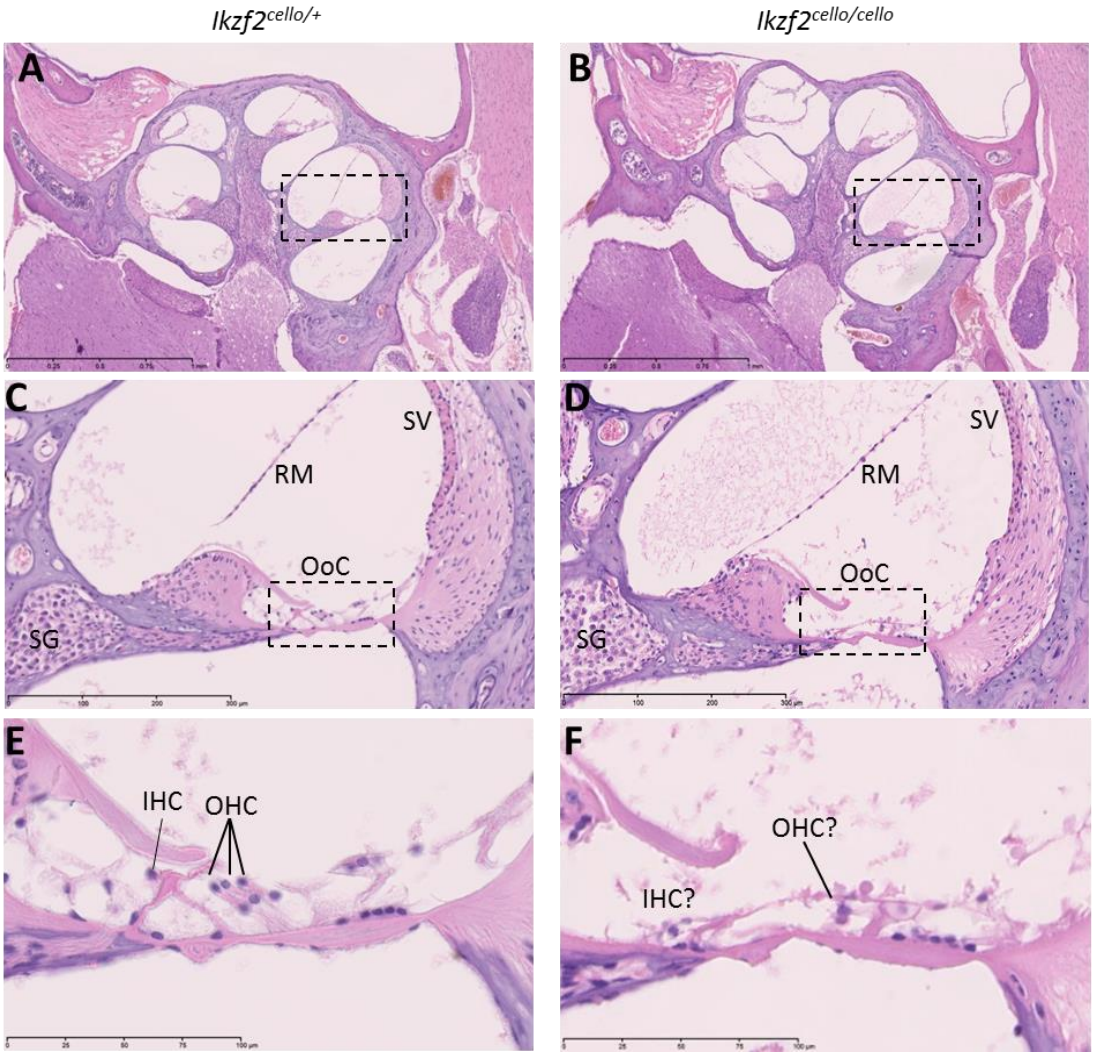

Figure 5.5: Inner ear histology of *Ikzf2*$^{cello/+}$ and *Ikzf2*$^{cello/cello}$ littermates at four months of age.
Mid-modiolar inner ear sections were cut from *Ikzf2*$^{cello/+}$ and *Ikzf2*$^{cello/cello}$ half heads at four months of age and stained with H&E. **(A-B)** The gross morphology of the cochlea was similar between *Ikzf2*$^{cello/+}$ and *Ikzf2*$^{cello/cello}$ sections (x5 magnification, scale bar = 1 mm). **(C-D)** *Ikzf2*$^{cello/cello}$ mice have an intact Reissner's membrane and normal spiral ganglion and stria vascularis, but the organ of Corti was disrupted compared to *Ikzf2*$^{cello/+}$ littermates (x20 magnification, scale bar = 300 µm). **(E-F)** The neat arrangement of hair cells in *Ikzf2*$^{cello/+}$ mice was disrupted in *Ikzf2*$^{cello/cello}$ (x63 magnification, scale bar = 100 µm). Each dashed box is shown as a zoomed-in view in the image directly below. IHC, inner hair cell; OHC, outer hair cell; OoC, organ of Corti; RM, Reissner's membrane; SG, spiral ganglion; SV, stria vascularis.

To establish any pathological changes at later time points, H&E inner ear sections were also examined from nine month old mice. Due to the low number of biological replicates for each genotype (n = 2), only qualitative observations were made. As mentioned previously, the spiral ganglion appeared normal in *Ikzf2*$^{cello/cello}$ mice at four months of age, with cell density approximately equivalent to *Ikzf2*$^{cello/+}$ controls (Figure 5.6 A-B). At nine months of

age, the spiral ganglion appeared less dense in *Ikzf2*$^{cello/cello}$ mice, with a reduced number of neurons compared to *Ikzf2*$^{cello/+}$ controls (Figure 5.6 C-F), although this was not quantified.

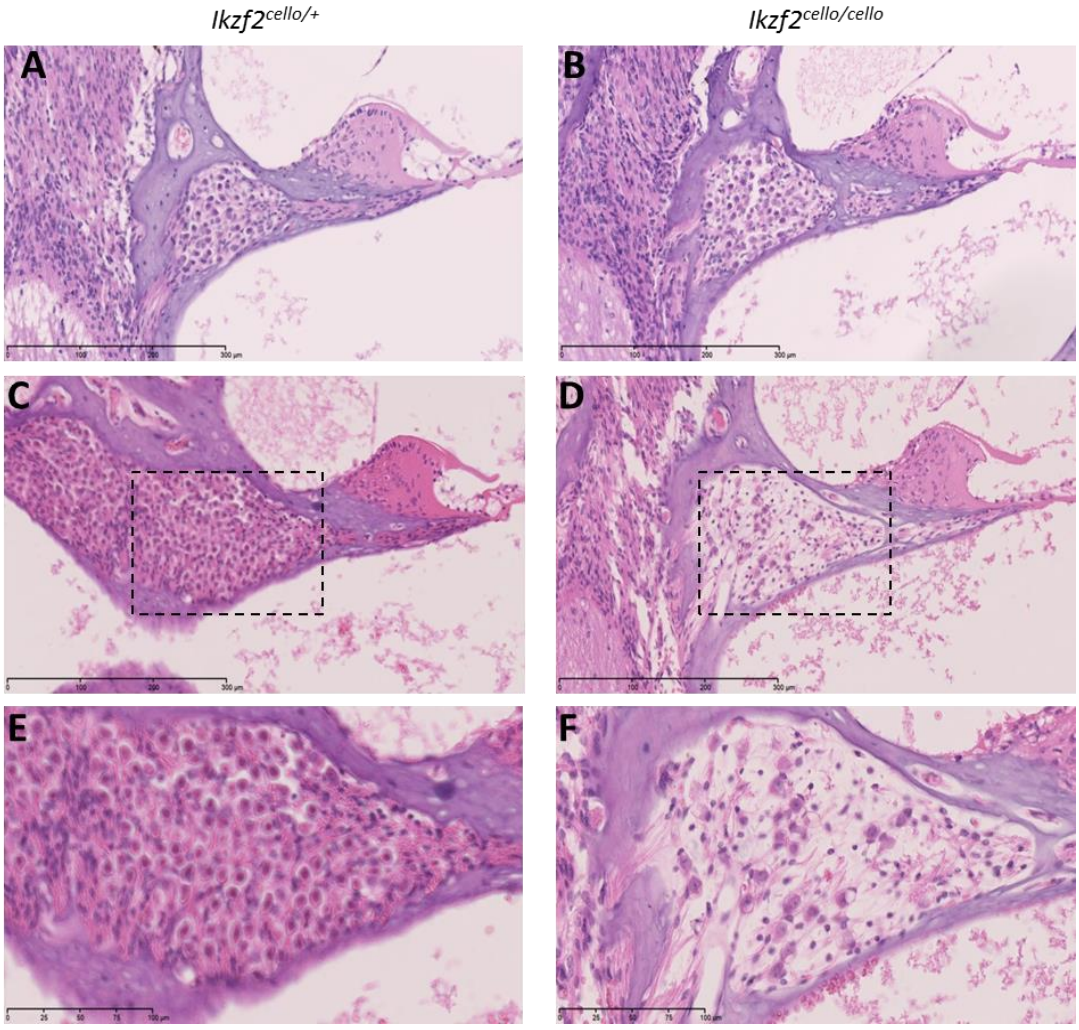

Figure 5.6: Histological sections of the spiral ganglion in *Ikzf2*$^{cello/+}$ and *Ikzf2*$^{cello/cello}$ littermates at four and nine months of age.
(A-B) At four months of age, the spiral ganglion in *Ikzf2*$^{cello/cello}$ mice resembled that of *Ikzf2*$^{cello/+}$ controls (x20 magnification, scale bar = 300 µm). **(C-D)** At nine months of age, the density of the spiral ganglion appeared decreased in *Ikzf2*$^{cello/cello}$ mice compared to *Ikzf2*$^{cello/+}$ littermates (x20 magnification, scale bar = 300 µm). **(E-F)** The number of spiral ganglion neurons was visibly reduced in *Ikzf2*$^{cello/cello}$ at nine months of age (x40 magnification, scale bar = 100 µm). Each dashed box is shown as a zoomed-in view in the image directly below.

Given that this potential degeneration of the spiral ganglion is late-onset and only first detected at nine months of age, it is likely to be a secondary effect of the hearing loss phenotype, rather than the primary cause. Further work is required to fully explore this

phenotype, however I concentrated my studies on the cause of the early-onset hearing impairment in *cello.*

As helios is known to be expressed in lymphoid lineages (Hahm et al., 1998, Kelley et al., 1998, Peters et al., 2014), histological sections of the middle ear were assessed for indicators of otitis media, an inflammatory middle ear disorder that leads to a conductive hearing loss. Typical symptoms include an accumulation of fluid within the middle ear cavity and thickening of the mucosal lining of the middle ear (Hardisty et al., 2003, Kubba et al., 2000, Parkinson et al., 2006). In *Ikzf2*$^{cello/cello}$ mice, the gross morphology of the middle ear resembled that of *Ikzf2*$^{cello/+}$ controls, with no inflammation, fluid accumulation or mucosal thickening detected (Figure 5.7 A-D).

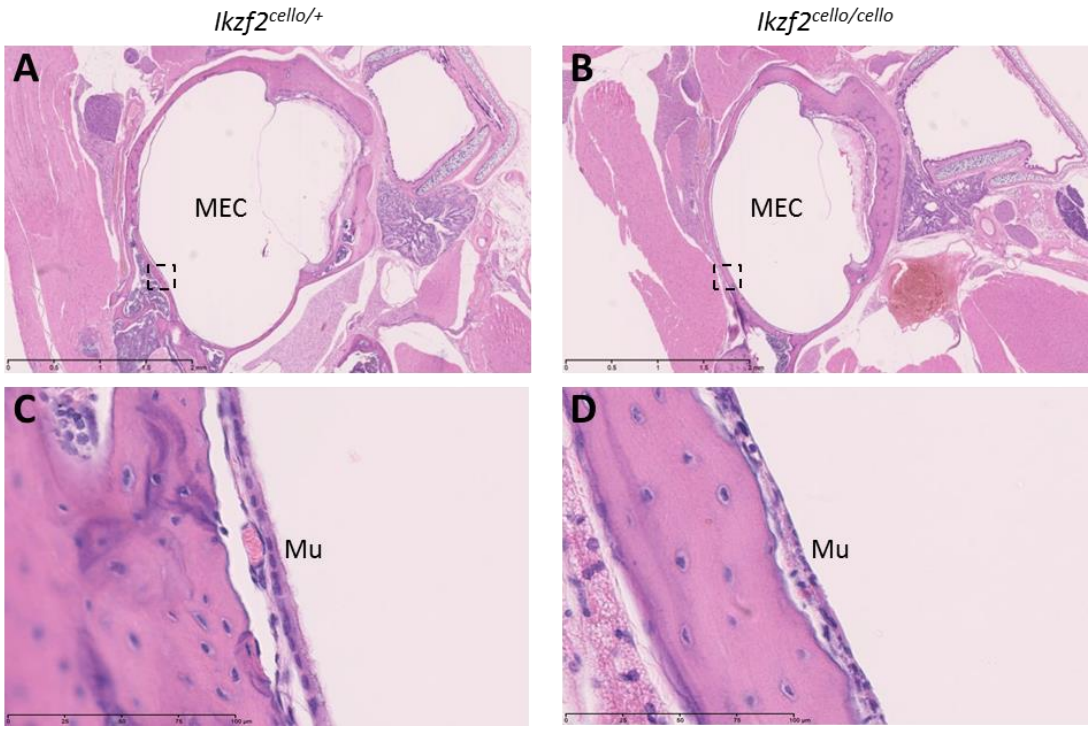

Figure 5.7: Middle ear histology of *Ikzf2*$^{cello/+}$ and *Ikzf2*$^{cello/cello}$ littermates at four months of age.
(A-B) Sections through the middle ear cavity revealed gross morphology in *Ikzf2*$^{cello/cello}$ mice was similar to control littermates, with no typical symptoms of otitis media (inflammation and fluid accumulation) observed (x2.5 magnification, scale bar = 2 mm). **(C-D)** The thickness of the mucosal lining of the middle ear, also associated with otitis media, appeared normal in *Ikzf2*$^{cello/cello}$ mice (x63 magnification, scale bar = 100 µm). Each dashed box is shown as a zoomed-in view in the image directly below. MEC, middle ear cavity; Mu, mucosa.

Overall, histological examination revealed pathological defects in the inner ear of *Ikzf2*$^{cello/cello}$ mice, specifically affecting the hair cells within the organ of Corti, whilst the middle ear appears normal.

5.2.2.2. Actin Immunolabelling of Cochlear Wholemounts

Histological examination of the inner ear revealed that auditory hair cells are disrupted by four months of age in *Ikzf2*$^{cello/cello}$ mice. However, it is unclear whether hair cells fail to develop or are initially present but then degenerate postnatally.

In the mouse, pro-sensory cells begin to terminally differentiate into hair cells from E13, as a result of ATOH1-mediated lateral inhibition (Lanford et al., 2000). Stereocilia develop soon afterwards, first appearing as unpolarised microvilli at E13.5 (Denman-Johnson and Forge, 1999) and then elongating and thickening once bundle polarity is established. This results in the characteristic staircase pattern of stereocilia, which is detectable from P1 (Anniko, 1983).

As a crude investigation of hair cell development and stereocilia morphology, wholemount cochleae were collected from *Ikzf2*$^{+/+}$ and *Ikzf2*$^{cello/cello}$ mice at early postnatal time points (between P4 and P16) and fine dissected to expose the sensory epithelia. Samples were immunolabelled with Alexa Fluor® 488 Phalloidin (green) to stain F-actin in order to visualise hair cells, as well as DAPI (blue) to stain nuclei. At all of the time points investigated, IHCs and OHCs were detected in *Ikzf2*$^{cello/cello}$ cochleae, with the characteristic single row of IHCs, three rows of OHCs and grossly normal stereocilia bundle morphology compared to *Ikzf2*$^{+/+}$ animals (Figure 5.8). This confirms that hair cells do develop in *Ikzf2*$^{cello/cello}$ mutants and appear morphologically normal at early postnatal time points, therefore implying that the

histopathology observed at four months of age is caused by progressive hair cell degeneration.

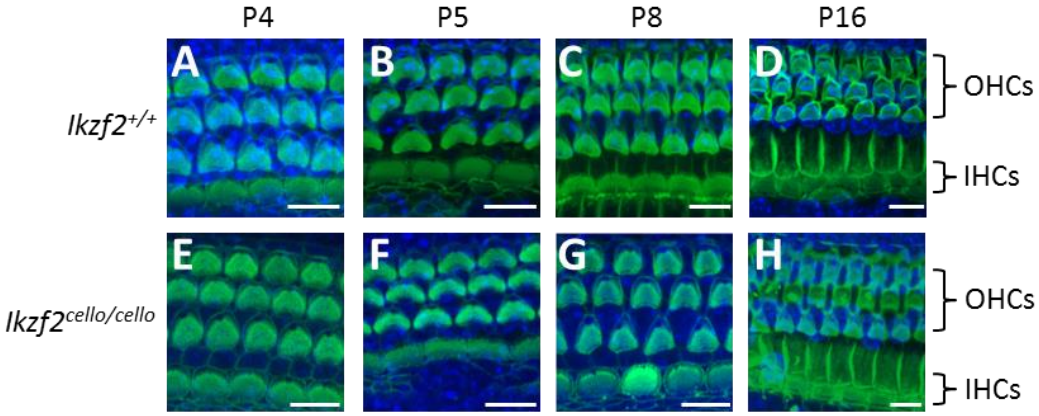

Figure 5.8: Actin immunolabelling of *Ikzf2*$^{+/+}$ and *Ikzf2*$^{cello/cello}$ cochlear wholemounts at early postnatal time points.
(A, B, C, D) *Ikzf2*$^{+/+}$ and **(E, F, G, H)** *Ikzf2*$^{cello/cello}$ hair cells were visualised between P4 and P16 by immunolabelling of wholemount cochleae using Alexa Fluor® 488 Phalloidin (green) to stain F-actin and DAPI to stain nuclei. At all of the time points studied, one row of IHCs and three rows of OHCs were detected in *Ikzf2*$^{cello/cello}$ mice and appeared grossly similar in morphology to those of *Ikzf2*$^{+/+}$ controls (x63 magnification, scale bar = 10 µm). IHCs, inner hair cells; OHCs, outer hair cells; P, postnatal day.

5.2.2.3. Scanning Electron Microscopy (SEM) Ultrastructural Analysis

To investigate potential hair cell degeneration and examine the ultrastructure of the organ of Corti, a time course of SEM was undertaken using inner ears collected from *Ikzf2*$^{+/+}$, *Ikzf2*$^{cello/+}$ and *Ikzf2*$^{cello/cello}$ mice at one, three, six, nine and 18 months of age. Samples were fixed, decalcified and fine dissected to expose the hair cells then treated with osmium tetroxide in order to preserve stereocilia structure and achieve electrical conductivity. Cochleae were arbitrarily divided into three regions – apical, mid and basal – for examination and high resolution imaging. Within each region, hairs cells were analysed qualitatively by visual interrogation and quantitatively by counting the number of IHC and OHC per ten pillar cells. Whilst it is possible that abnormalities in the size and shape of pillar cells in *Ikzf2*$^{cello/cello}$ mutants could bias these measurements, general pillar cell morphology was comparable between each genotype group, with ten pillar cells present per ~33 µm of

tissue. This indicated that pillar cells were a suitable reference cell type for performing the hair cell counts. Micrographs are not shown for *Ikzf2*$^{cello/+}$ mice, as ultrastructure resembled that of *Ikzf2*$^{+/+}$ animals at all time points (Figure 9.5 in Appendix).

At one month of age, *Ikzf2*$^{cello/cello}$ ultrastructure resembled that of *Ikzf2*$^{+/+}$ controls, with the typical organisation of IHC and OHC rows and normal looking stereocilia bundles in all regions along the length of the cochlea (Figure 5.9 A-F). Although occasional OHC loss was observed, cell counts indicated that this was not statistically significant (Figure 5.9 G-H). Furthermore, this mild OHC loss is unlikely to cause the severe auditory thresholds (>65 dB SPL) observed at this time point.

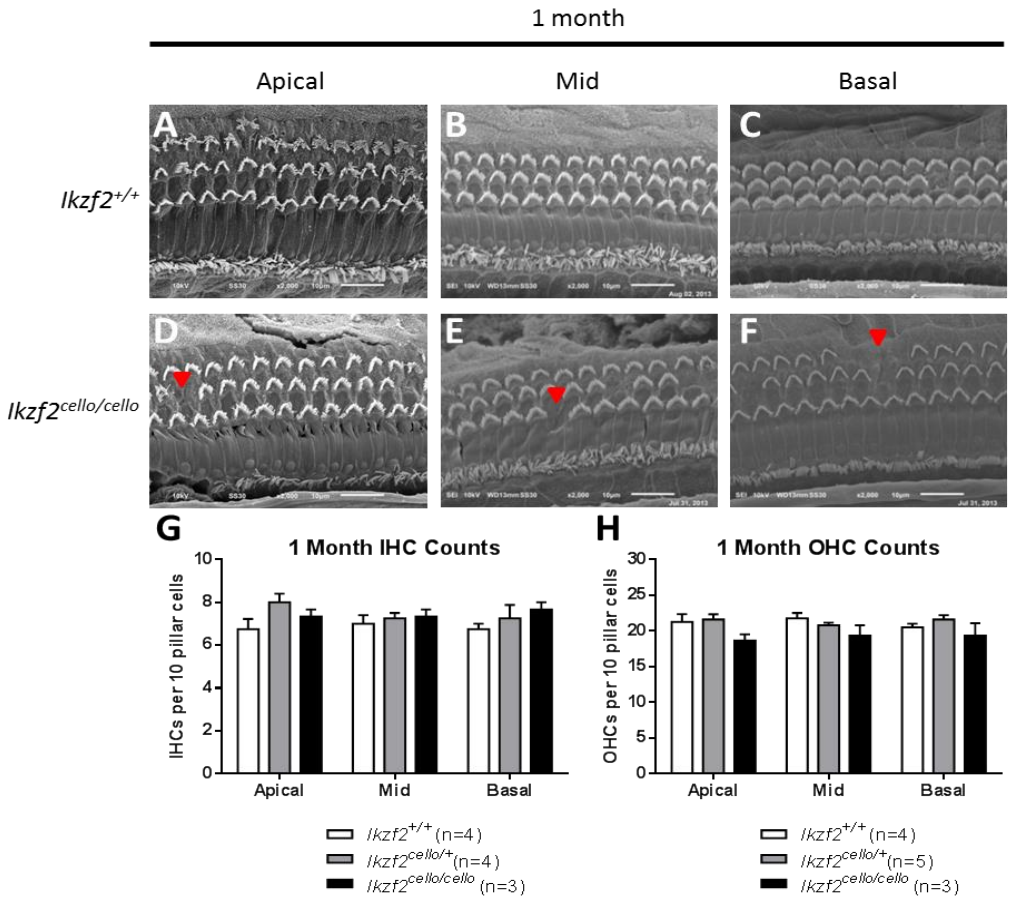

Figure 5.9: Scanning electron micrographs of the organ of Corti of *Ikzf2*$^{+/+}$ and *Ikzf2*$^{cello/cello}$ littermates at one month of age.

Cochleae were collected from *Ikzf2*$^{+/+}$ and *Ikzf2*$^{cello/cello}$ mice at one month of age, then fine dissected to expose hair cells and processed for scanning electron microscopy. At one month of age, the gross ultrastructure of the organ of Corti was comparable between **(A-C)** *Ikzf2*$^{+/+}$ and **(D-F)** *Ikzf2*$^{cello/cello}$ mice, although occasional OHC loss was observed in *Ikzf2*$^{cello/cello}$ animals (red arrowheads) (x2000 magnification, scale bar = 10 µm). **(G-H)** Counts of the number of hair cells per 10 pillar cells showed no significant differences in IHC or OHC number between *Ikzf2*$^{+/+}$, *Ikzf2*$^{cello/+}$ and *Ikzf2*$^{cello/cello}$ animals. Data are shown as mean ± s.e.m. Statistical analysis: one-way ANOVA. IHC, inner hair cell; OHC, outer hair cell.

At three months of age, OHC loss was more pronounced in *Ikzf2*$^{cello/cello}$ mutants (Figure 5.10 A-F) and some of the remaining OHCs displayed fused stereocilia (Figure 5.10 G-H), which is indicative of hair cell damage and often precedes cell death. Whilst IHCs were unaffected, cell counts showed that the OHC loss was statistically significant across all regions of the cochlea compared to *Ikzf2*$^{+/+}$ and *Ikzf2*$^{cello/+}$ controls (Figure 5.10 I-J).

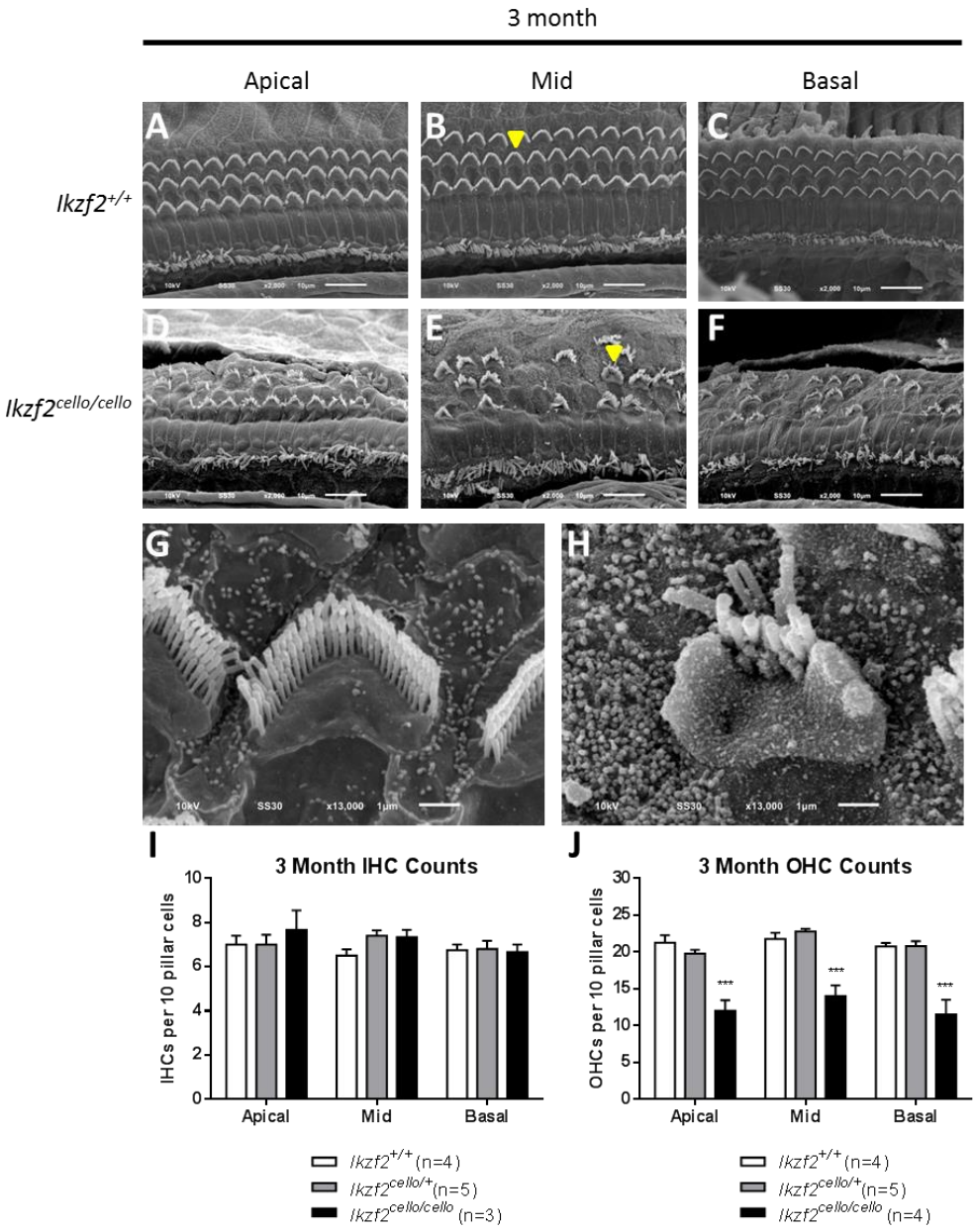

Figure 5.10: Scanning electron micrographs of the organ of Corti of *Ikzf2*$^{+/+}$ and *Ikzf2*$^{cello/cello}$ littermates at three months of age.

At three months of age, **(A-C)** *Ikzf2*$^{+/+}$ cochleae displayed the typical organisation of one row of IHCs and three rows of OHCs, whilst **(D-F)** *Ikzf2*$^{cello/cello}$ mice showed pronounced OHC loss across all regions of the cochlea (x2000 magnification, scale bar = 10 µm). Each OHC marked with a yellow arrowhead is shown in more detail in the micrograph below. **(G)** On the apical surface of *Ikzf2*$^{+/+}$ OHCs, hair bundles form a 'W' shape and consist of three neatly organised rows of stereocilia, with stepwise increases in length between each row (x13000 magnification, scale bar = 1 µm). **(H)** This arrangement was perturbed in some of the remaining *Ikzf2*$^{cello/cello}$ OHCs, with fusion between adjacent stereocilia evident (x13000 magnification, scale bar = 1 µm). **(I-J)** Cell counts indicated that IHC number was unaffected in *Ikzf2*$^{cello/cello}$ mice, but the number of OHCs was significantly lower across all regions of the cochlea compared to *Ikzf2*$^{+/+}$ and *Ikzf2*$^{cello/+}$ controls. Data are shown as mean ± s.e.m. Statistical analysis: one-way ANOVA, *** = p≤0.001. IHC, inner hair cell; OHC, outer hair cell.

At six months of age, IHCs remained grossly normal in *Ikzf2*$^{cello/cello}$ mice but severe OHC loss was observed throughout the cochlea (Figure 5.11 A-F). Cell counts confirmed that the number of IHCs in *Ikzf2*$^{cello/cello}$ animals was similar compared to *Ikzf2*$^{+/+}$ and *Ikzf2*$^{cello/+}$ controls, whilst the number of OHCs was significantly reduced (Figure 5.11 G-H).

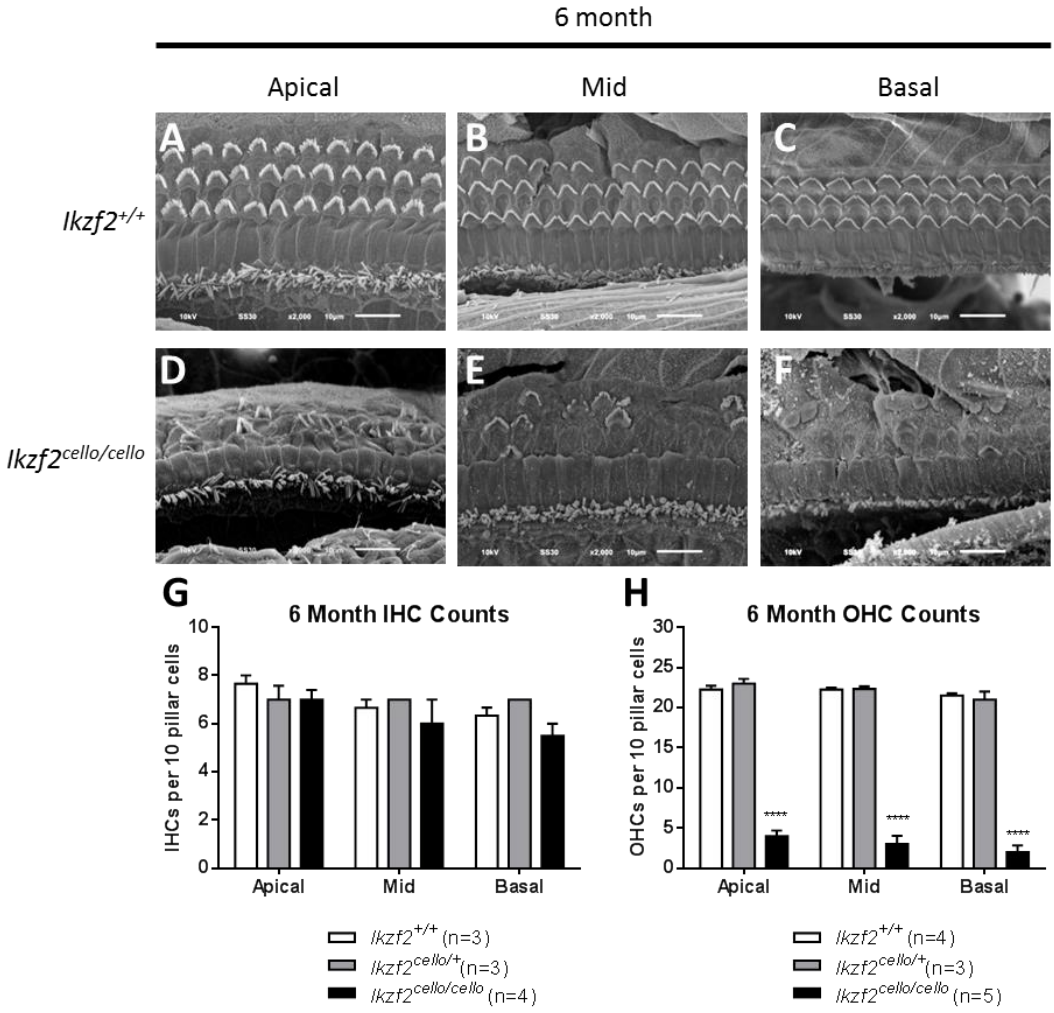

Figure 5.11: Scanning electron micrographs of the organ of Corti of *Ikzf2*$^{+/+}$ and *Ikzf2*$^{cello/cello}$ littermates at six months of age.

(A-C) At six months of age, the characteristic pattern of hair cells was observed in *Ikzf2*$^{+/+}$ cochleae, with one row of IHCs and three rows of OHCs (x2000 magnification, scale bar = 10 µm). **(D-F)** IHCs were unaffected in *Ikzf2*$^{cello/cello}$ mice, but severe OHC loss was seen throughout the cochlea (x2000 magnification, scale bar = 10 µm). **(G-H)** Cell counts confirmed that the number of IHCs in *Ikzf2*$^{cello/cello}$ animals was similar to *Ikzf2*$^{+/+}$ and *Ikzf2*$^{cello/+}$ controls, whilst the number of OHCs was significantly lower across all regions of the cochlea. Data are shown as mean ± s.e.m. Statistical analysis: one-way ANOVA, **** = p≤0.0001. IHC, inner hair cell; OHC, outer hair cell.

At nine months of age, only a small number of OHCs remained in *Ikzf2*$^{cello/cello}$ cochleae (Figure 5.12 A-F). Some IHC loss was also observed in basal regions, which was found to be statistically significant compared to *Ikzf2*$^{+/+}$ and *Ikzf2*$^{cello/+}$ controls (Figure 5.12 G-H).

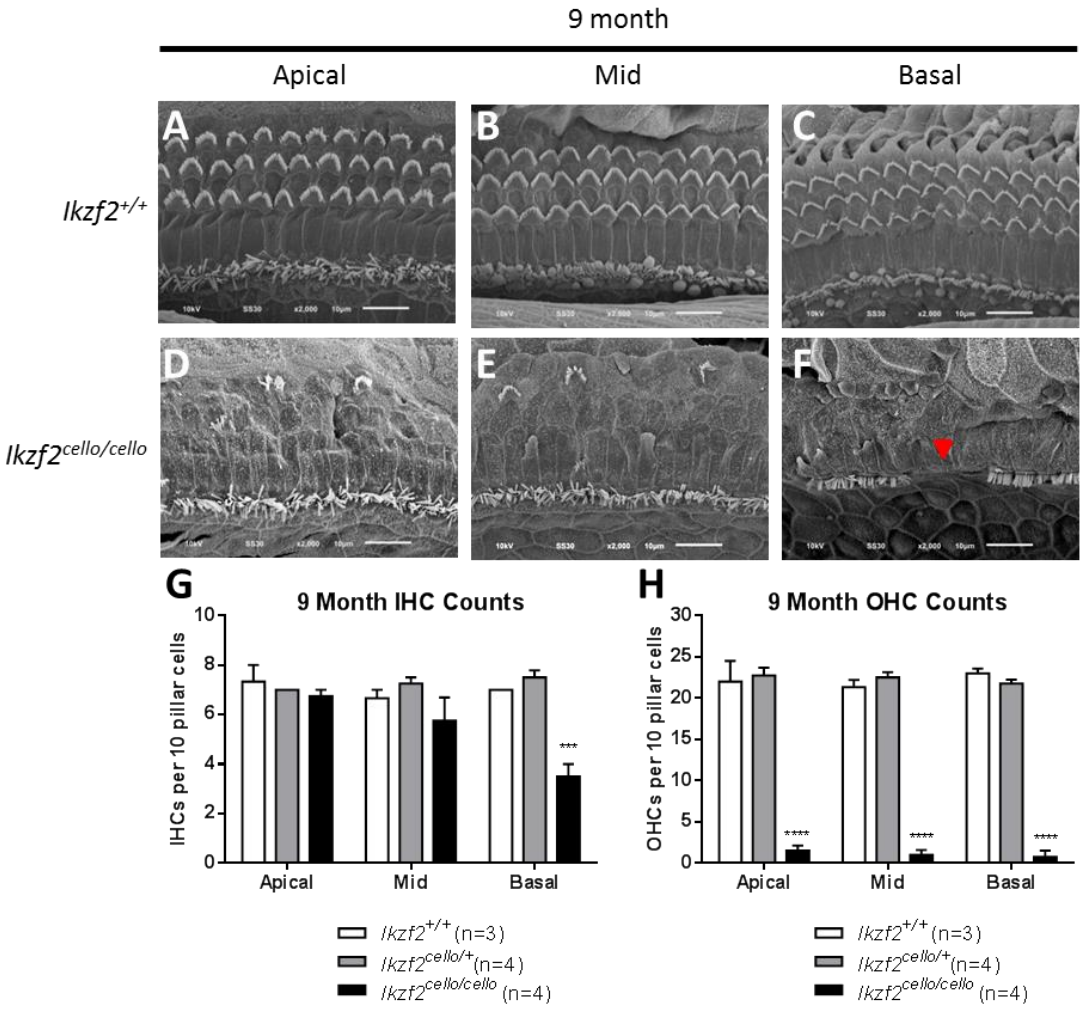

Figure 5.12: Scanning electron micrographs of the organ of Corti of *Ikzf2*$^{+/+}$ and *Ikzf2*$^{cello/cello}$ littermates at nine months of age.

At nine months of age, **(A-C)** *Ikzf2*$^{+/+}$ cochleae displayed the typical arrangement of IHCs and OHCs, whilst **(D-F)** *Ikzf2*$^{cello/cello}$ cochleae showed severe OHC loss across all regions, as well as some basal IHC loss (red arrowhead) (x2000 magnification, scale bar = 10 µm). **(G-H)** Cell counts showed that this basal IHC loss and the widespread OHC loss was statistically significant compared to *Ikzf2*$^{+/+}$ and *Ikzf2*$^{cello/+}$ controls. Data are shown as mean ± s.e.m. Statistical analysis: one-way ANOVA, *** = p≤0.001, **** = p≤0.0001. IHC, inner hair cell; OHC, outer hair cell.

By 18 months of age, OHCs were virtually absent in *Ikzf2*$^{cello/cello}$ cochleae and a significant reduction in the number of IHCs was detected in mid and basal regions compared to *Ikzf2*$^{+/+}$ and *Ikzf2*$^{cello/+}$ controls (Figure 5.13).

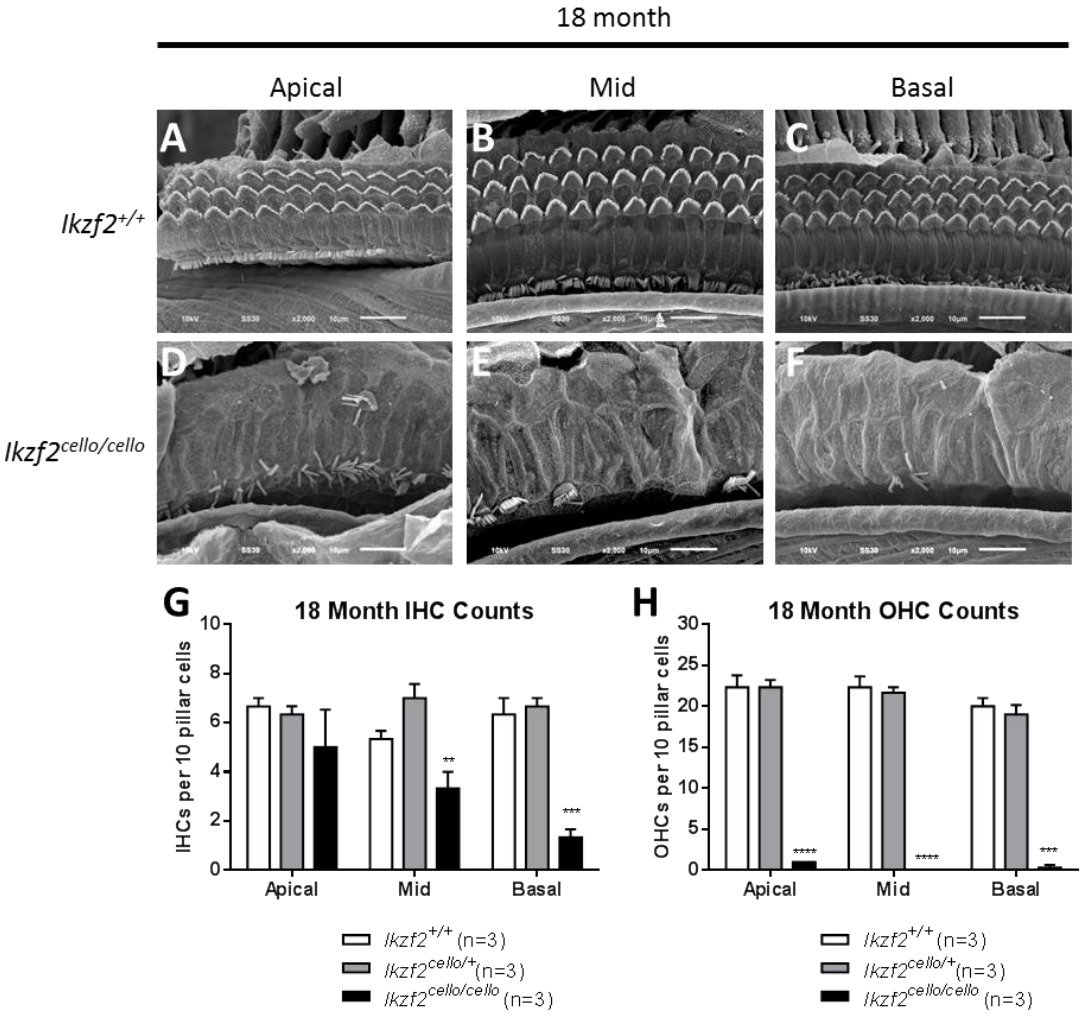

Figure 5.13: Scanning electron micrographs of the organ of Corti of *Ikzf2*$^{+/+}$ and *Ikzf2*$^{cello/cello}$ littermates at 18 months of age.

(A-F) At 18 months of age, very few OHCs remained in *Ikzf2*$^{cello/cello}$ cochleae compared to *Ikzf2*$^{+/+}$ controls and some IHC degeneration was also evident in mid and basal regions (x2000 magnification, scale bar = 10 µm). **(G-H)** Cell counts confirmed a significant reduction in the number of IHCs in mid and basal regions in *Ikzf2*$^{cello/cello}$ animals compared to *Ikzf2*$^{+/+}$ and *Ikzf2*$^{cello/+}$ controls. OHC number was also significantly reduced in all regions of the cochlea. Data are shown as mean ± s.e.m. Statistical analysis: one-way ANOVA, ** = p≤0.01, *** = p≤0.001, **** = p≤0.0001. IHC, inner hair cell; OHC, outer hair cell.

Taken together, these results show that *Ikzf2*$^{cello/cello}$ mice have widespread OHC loss, which first becomes statistically significant compared to *Ikzf2*$^{+/+}$ controls by three months of age and appears to increase in severity with time. Some IHC loss is also observed, although this is only evident at later time points in the mid and basal regions of the cochlea.

To assess this hair cell degeneration in more detail, the number of OHCs and IHCs were compared across time points within each individual genotype group. In *Ikzf2*$^{+/+}$ controls, the number of OHCs in apical, mid and basal regions of the cochlea did not significantly change over time (Figure 5.14 A and Table 9.2 in Appendix). The same was true for *Ikzf2*$^{cello/+}$ mice (Figure 5.14 B and Table 9.2). Conversely, *Ikzf2*$^{cello/cello}$ mutants showed progressive OHC loss (Figure 5.14 C), with a significant reduction in OHC number detected in each region of the cochlea between one and three months of age and also between three and six months of age (Figure 5.14 D). No further significant degeneration was observed between six, nine and 18 months of age, although the final number of OHCs remaining in each region at 18 months of age was significantly less than at one month of age (Figure 5.14 D).

Similarly, in *Ikzf2*$^{+/+}$ and *Ikzf2*$^{cello/+}$ controls, the number of IHCs in each region of the cochlea remained unchanged over time (Figure 5.14 E-F and Table 9.3 in Appendix). In *Ikzf2*$^{cello/cello}$ mice, whilst the number of IHCs in apical regions did not significantly change over time, a gradual decline in IHC number was observed in mid and basal regions (Figure 5.14 G). In the mid region, this IHC degeneration was only significant when comparing final IHC counts at 18 months of age to those at one and three months of age and not between subsequent time points (Figure 5.14 H). In basal regions, the decline in IHC number was also significant between six and nine months of age and also nine and 18 months of age a (Figure 5.14 H).

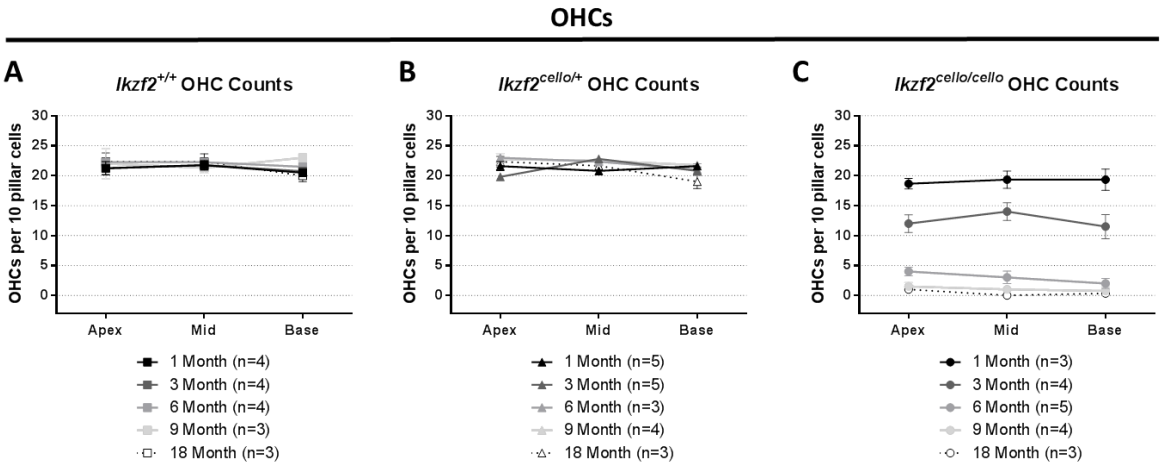

D

	Ikzf2$^{cello/cello}$ OHC Counts at Apex				*Ikzf2*$^{cello/cello}$ OHC Counts at Mid				*Ikzf2*$^{cello/cello}$ OHC Counts at Base			
	1 m	3 m	6 m	9 m	1 m	3 m	6 m	9 m	1 m	3 m	6 m	9 m
1 m	-	-	-	-	-	-	-	-	-	-	-	-
3 m	0.0021	-	-	-	0.0392	-	-	-	0.0086	-	-	-
6 m	<0.0001	<0.0001	-	-	<0.0001	<0.0001	-	-	<0.0001	0.0005	-	-
9 m	<0.0001	<0.0001	>0.05	-	<0.0001	<0.0001	>0.05	-	<0.0001	0.0003	>0.05	-
18 m	<0.0001	<0.0001	>0.05	>0.05	<0.0001	<0.0001	>0.05	>0.05	<0.0001	0.0004	>0.05	>0.05

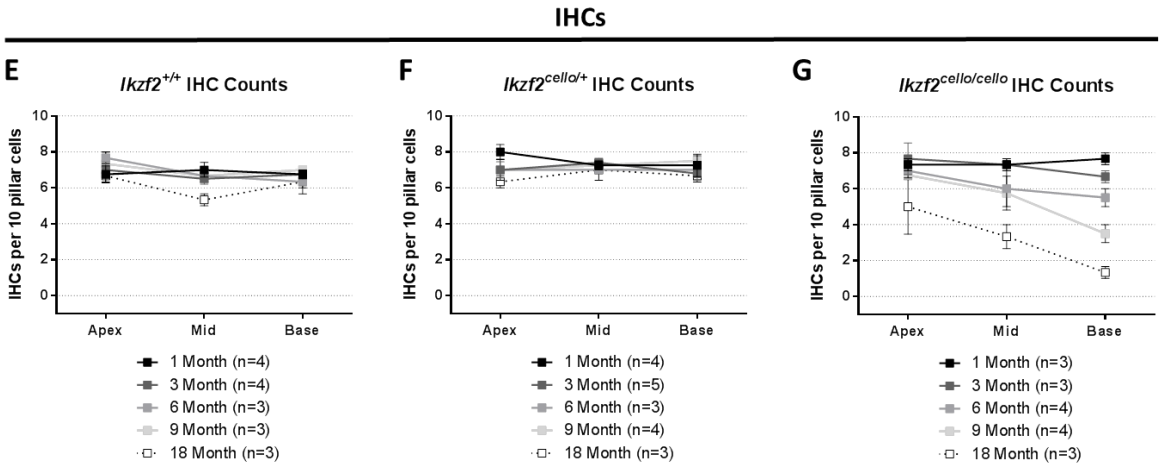

H

	Ikzf2$^{cello/cello}$ IHC Counts at Apex				*Ikzf2*$^{cello/cello}$ IHC Counts at Mid				*Ikzf2*$^{cello/cello}$ IHC Counts at Base			
	1 m	3 m	6 m	9 m	1 m	3 m	6 m	9 m	1 m	3 m	6 m	9 m
1 m	-	-	-	-	-	-	-	-	-	-	-	-
3 m	>0.05	-	-	-	>0.05	-	-	-	>0.05	-	-	-
6 m	>0.05	>0.05	-	-	>0.05	>0.05	-	-	0.0306	>0.05	-	-
9 m	>0.05	>0.05	>0.05	-	>0.05	>0.05	>0.05	-	0.0002	0.0021	0.0312	-
18 m	>0.05	>0.05	>0.05	>0.05	0.0426	0.0426	>0.05	>0.05	<0.0001	<0.0001	0.0002	0.0306

Figure 5.14: Summary of outer hair cell and inner hair cell counts for *Ikzf2*$^{+/+}$, *Ikzf2*$^{cello/+}$ and *Ikzf2*$^{cello/cello}$ littermates at one, three, six, nine and 18 months of age.

In both **(A)** *Ikzf2*$^{+/+}$ and **(B)** *Ikzf2*$^{cello/+}$ animals, the number of OHCs in the apical, mid and basal regions of the cochlea did not change between one, three, six, nine and 18 months. **(C)** In *Ikzf2*$^{cello/cello}$ cochleae, the number of OHCs progressively decreased over time across all regions of the cochlea. **(D)** Statistical analysis of OHC counts for *Ikzf2*$^{cello/cello}$ mice in each region of the cochlear spiral. In both **(E)** *Ikzf2*$^{+/+}$ and **(F)** *Ikzf2*$^{cello/+}$ cochleae, the number of IHCs in each region remained unchanged over time. **(G)** In *Ikzf2*$^{cello/cello}$ cochleae, apical IHCs did not show any significant degeneration but a reduction in IHC number was observed in mid and basal regions at the later time points. **(H)** Statistical analysis of IHC counts for *Ikzf2*$^{cello/cello}$ mice in each region of the cochlear spiral. Data are shown as mean ± s.e.m. Statistical analysis: one-way ANOVA. Statistically significant results are highlighted in purple. IHC, inner hair cell; m, month; OHC, outer hair cell.

Overall, these data show that *Ikzf2*$^{cello/cello}$ hair cells are initially similar in number and gross morphological appearance to those of *Ikzf2*$^{+/+}$ and *Ikzf2*$^{cello/+}$ littermates. Progressive loss of OHCs was evident in *Ikzf2*$^{cello/cello}$ animals from three months of age onwards. Although this could account for the decline in hearing function in aged mice, it suggests another factor is primarily responsible for the initial hearing impairment observed at P16 and that OHC loss subsequently occurs as a likely secondary effect. Furthermore, the late-onset IHC degeneration observed at nine months is likely to be secondary to the OHC phenotype.

5.2.3. Expression and Localisation of Helios

Although helios has not previously been implicated in auditory development or function, the hearing loss phenotype and cochlear pathology observed in *Ikzf2*$^{cello/cello}$ mutants suggest a role for helios in the inner ear.

During the course of this thesis, an RNA-Seq study was published investigating cell-type specific gene expression within the inner ear during early development (Scheffer et al., 2015). Scheffer et al. (2015) collected cochleae and utricles from transgenic mice which expressed GFP under the control of the hair cell-specific *Pou4f3* promoter (Erkman et al., 1996). Tissue was collected at four developmental stages (E16, P0, P4 and P7) then separately processed to dissociate and sort cells into four distinct populations for RNA extraction and sequencing: cochlear GFP+ cells (sensory IHCs and OHCs); cochlear GFP- cells (surrounding non-sensory cells); utricle GFP+ cells (sensory vestibular hair cells); and utricle GFP- cells (surrounding non-sensory cells) (Figure 5.15 A). Results from this dataset were made publicly available to download from the Shared Harvard Inner Ear Laboratory Database (SHIELD) (https://shield.hms.harvard.edu/), thus providing an excellent resource for quickly examining the expression of genes of interest in the inner ear.

In order to help guide the time points used to investigate helios expression, the expression of *Ikzf2* was examined within this dataset. Results indicated that *Ikzf2* is strongly upregulated in cochlear GFP+ hair cells during postnatal development, but is expressed at lower, stable levels in cochlear GFP- non-sensory cells and in the utricle (Figure 5.15 B); a total of 1328 *Ikzf2* read counts were initially detected in cochlear GFP+ hair cells at E16, which decreased to 497 read counts at P0, before markedly increasing to 4248 read counts by P4 and 15,194 by read counts P7.

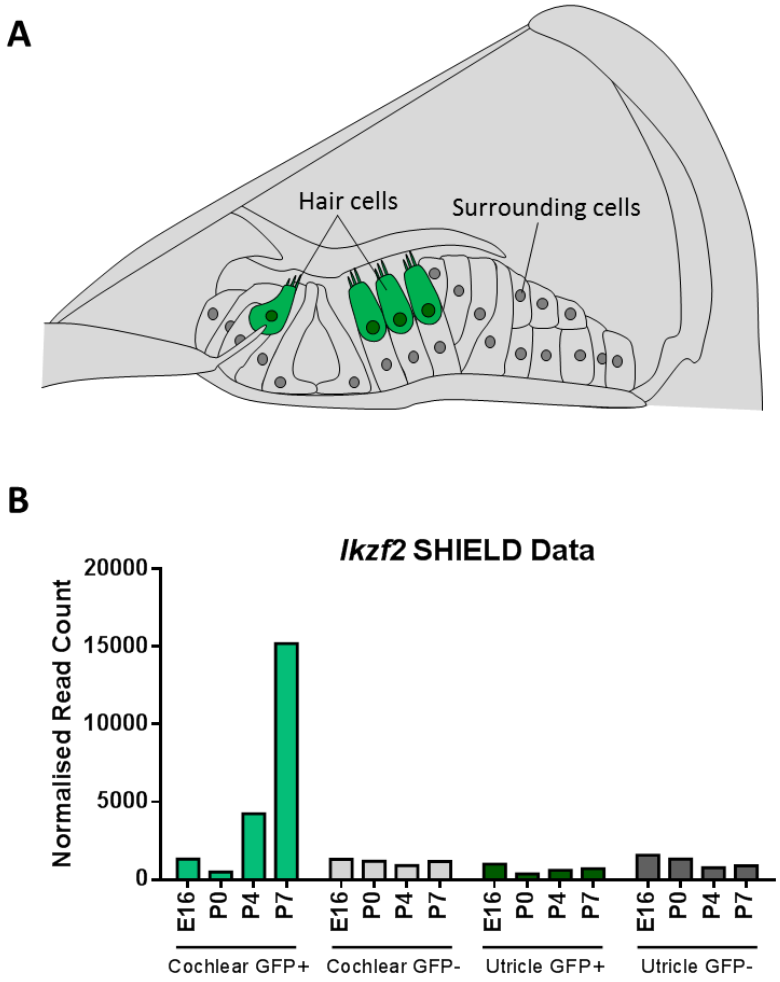

Figure 5.15: Expression of *Ikzf2* in sorted cell populations from the mouse inner ear during development. The gene expression profile of *Ikzf2* in the inner ear was obtained from the SHIELD website (https://shield.hms.harvard.edu/datasets.html). In this dataset, Scheffer et al. (2015) collected cochleae and utricles from transgenic mice expressing GFP driven by the *Pou4f3* promoter at four developmental stages: E16, P0, P4 and P7. Samples were separated into four distinct cell populations (cochlear GFP+ hair cells, cochlear GFP- surrounding non-sensory cells, utricle GFP+ hair cells and utricle GFP- surrounding non-sensory cells) by fluorescence-activated cell sorting (FACS) prior to RNA-Seq. **(A)** Schematic of the cell populations obtained from the cochlea through FACS of *Pou4f3*-GFP transgenic mice. **(B)** SHIELD results indicate that *Ikzf2* is developmentally upregulated in cochlear GFP+ hair cells, but is expressed at lower and stable levels in the other cell populations of the inner ear. E, embryonic day; GFP, green fluorescent protein; P, postnatal day; SHIELD, Shared Harvard Inner Ear Laboratory Database.

Based on the SHIELD results, helios expression in the cochlea was initially examined during early postnatal development. Two methods were employed to investigate the temporospatial expression of helios: immunolabelling of cochlear vibratome sections and immunolabelling of cochlear wholemounts.

5.2.3.1. Vibratome Immunolabelling

To investigate helios localisation, fixed and decalcified inner ears from P8 *Ikzf2*$^{+/+}$ and *Ikzf2*$^{cello/cello}$ mice were embedded in agarose for vibratome sectioning through the mid-modiolar plane of the cochlea. Sections were immunolabelled with an anti-helios primary antibody (red), as well as an anti-β-actin primary antibody (green) and DAPI (blue) to stain nuclei, then visualised by confocal imaging.

In *Ikzf2*$^{+/+}$ cochleae, helios labelling was detected solely within the organ of Corti and not in any other cochlear structures, such as the spiral ganglion, stria vascularis or spiral ligament (Figure 5.16 A). Helios was found to be localised specifically to the nuclei of the three rows of OHCs, with no labelling observed in the nuclei of the IHCs (Figure 5.16 B-D). Labelling of *Ikzf2*$^{cello/cello}$ cochleae demonstrated a similar pattern of expression, with mutant helios co-localised with DAPI staining of the OHC nuclei (Figure 5.16 E-G).

Additional *Ikzf2*$^{+/+}$ sections were labelled with anti-helios primary antibody which had been pre-incubated with the immunising peptide. No immunolabelling was observed in these sections (Figure 5.16 H-J), confirming the specificity of the anti-helios primary antibody.

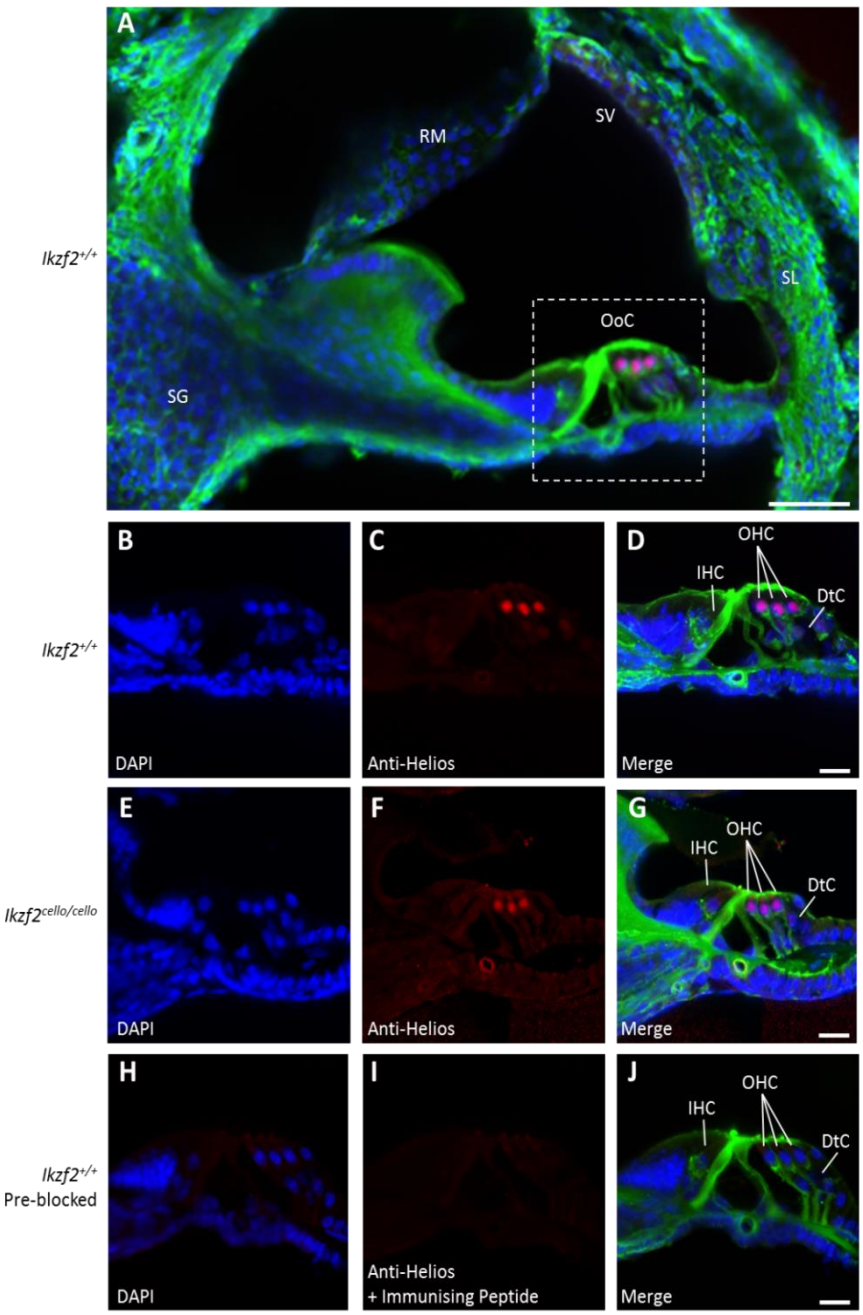

Figure 5.16: Immunolabelling of *Ikzf2*$^{+/+}$ and *Ikzf2*$^{cello/cello}$ vibratome cochlear sections at postnatal day 8. Helios localisation was assessed in mid-modiolar vibratome sections from postnatal day 8 *Ikzf2*$^{+/+}$ and *Ikzf2*$^{cello/cello}$ cochleae. Samples were labelled with DAPI (blue) to stain nuclei, anti-β-actin with an Alexa Fluor® 488 secondary antibody (green) and anti-helios with an Alexa Fluor® 568 secondary antibody (red). **(A)** In *Ikzf2*$^{+/+}$, helios labelling was detected only within the organ of Corti and was not observed in any other structures of the cochlear duct, such as the spiral ganglion, stria vascularis or spiral ligament (x10 magnification, scale bar = 50 µm). The organ of Corti, marked with a dashed box, was further assessed in *Ikzf2*$^{+/+}$ and *Ikzf2*$^{cello/cello}$ mice and is shown in the images below. **(B-D)** Helios labelling was found to co-localise with DAPI staining of the three rows of OHC nuclei (x40 magnification, scale bar = 20 µm). **(E-G)** In *Ikzf2*$^{cello/cello}$ cochleae, helios labelling also localised to the nuclei of the three rows of OHCs (x40 magnification, scale bar = 20 µm). **(H-J)** Pre-incubation of the anti-helios primary antibody with its immunising peptide prevented helios labelling of the OHCs, indicating that the anti-helios antibody binds specifically (x40 magnification, scale bar = 20 µm). DtC, Deiters' cell; IHC, inner hair cell; OHC, outer hair cell; OoC, organ of Corti; RM, Reissner's membrane; SG, spiral ganglion; SL, spiral ligament; SV, stria vascularis.

To investigate the expression of helios in adult-stage mice, vibratome sections from *Ikzf2*$^{+/+}$ animals at one month of age were also immunolabelled. Helios labelling was still observed in OHC nuclei at this time point (Figure 5.17 A-D), indicating that helios is maintained in the adult cochlea. Although a signal was observed in a region corresponding to the inner pillar cell body (Figure 5.17 C), this did not co-localise with the nucleus nor was it consistently seen.

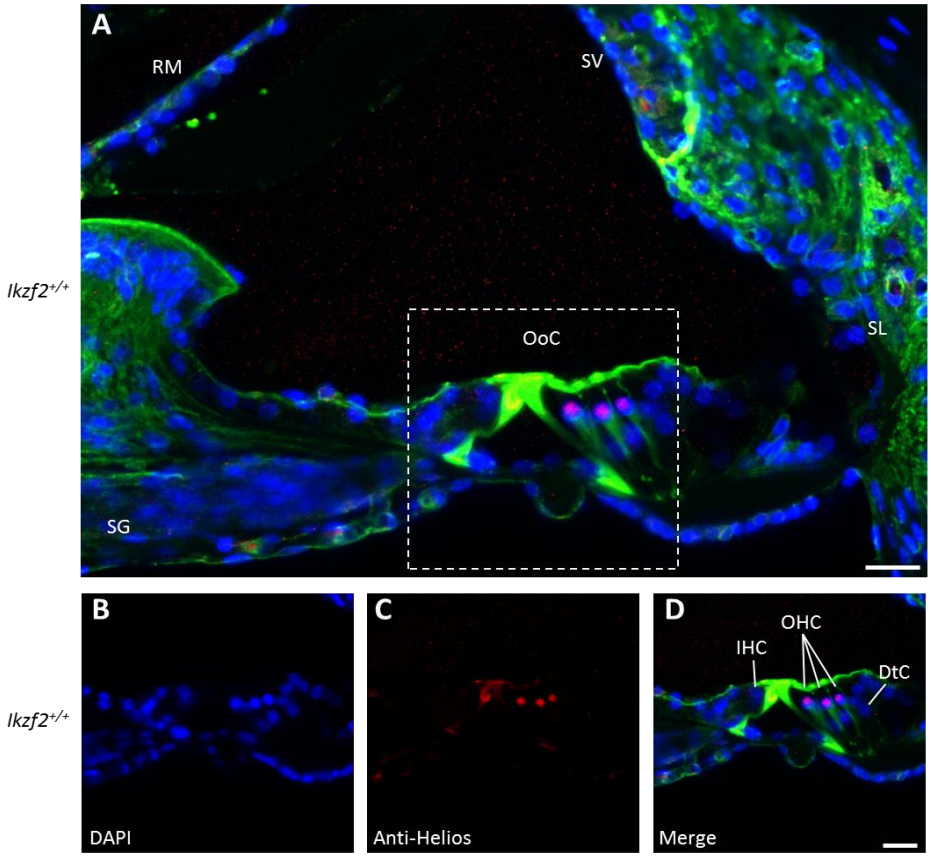

Figure 5.17: Immunolabelling of *Ikzf2*$^{+/+}$ vibratome cochlear sections at one month of age.
Helios localisation was assessed in mid-modiolar vibratome sections from one month old *Ikzf2*$^{+/+}$ cochleae. Samples were labelled with DAPI (blue) to stain nuclei, anti-β-actin with an Alexa Fluor® 488 secondary antibody (green) and anti-helios with an Alexa Fluor® 568 secondary antibody (red). **(A)** Helios labelling was observed only within the organ of Corti and not in any other structures of the cochlear duct (x20 magnification, scale bar = 20 µm). The organ of Corti, marked with a dashed box, was further assessed in *Ikzf2*$^{+/+}$ mice and is shown in the images below. **(B-D)** Helios labelling was co-localised with DAPI staining of the three rows of OHC nuclei (x40 magnification, scale bar = 20 µm). DtC, Deiters' cell; IHC, inner hair cell; OHC, outer hair cell; OoC, organ of Corti; RM, Reissner's membrane; SG, spiral ganglion; SL, spiral ligament; SV, stria vascularis.

5.2.3.2. Wholemount Immunolabelling

The cochlea exhibits various gradients along its length which help to confer auditory tonotopy. This includes morphological and physiological gradients, such as increased OHC length, stereocilia length and tectorial membrane thickness from base to apex (Engel et al., 2006, Gueta et al., 2007, Kaltenbach and Falzarano, 1994, Roth and Bruns, 1992), as well as well as gradients in gene and protein expression. For example, expression of *Tectb* (β-tectorin) and *Slc26a5* (prestin) increases from base to apex (Judice et al., 2002, Son et al., 2012), whilst ATOH1 is initially higher in basal regions (Cai et al., 2013).

To investigate for gradients in helios expression, P8 *Ikzf2*$^{+/+}$ cochleae were fine dissected to expose the sensory epithelia then immunolabelled using a helios-specific primary antibody (red), anti-Phalloidin (green) and DAPI (blue). Helios was detected along the length of the cochlea (Figure 5.18 A-D) and was consistently expressed in all three rows of OHC nuclei at comparable levels (Figure 5.18 E-G), with no longitudinal or radial gradients observed.

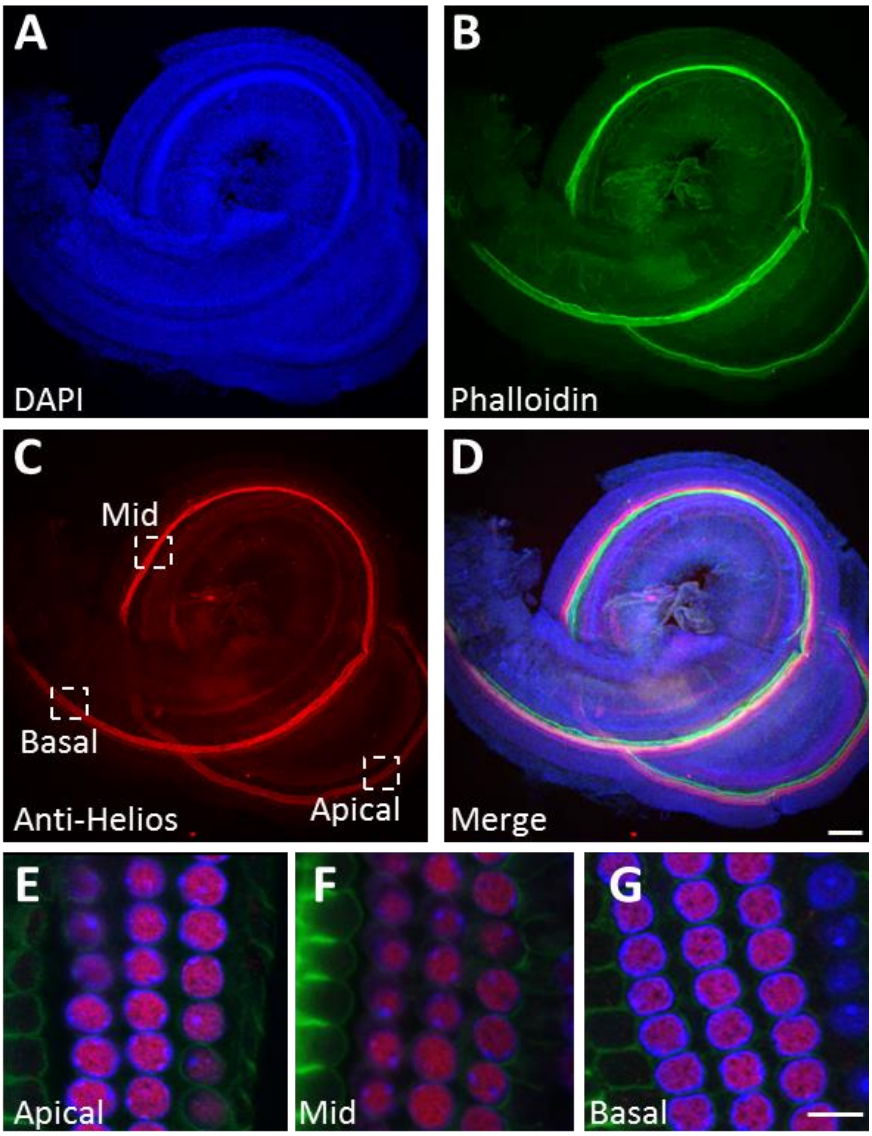

Figure 5.18: Helios immunolabelling of *Ikzf2*$^{+/+}$ cochlear wholemounts at postnatal day 8.
Cochleae from *Ikzf2*$^{+/+}$ mice at postnatal day 8 were assessed for gradients of helios expression by wholemount immunolabelling. Samples were labelled with **(A)** DAPI (blue) to stain nuclei, **(B)** Alexa Fluor® 488 Phalloidin (green) to stain F-actin and **(C)** anti-helios with an Alexa Fluor® 568 secondary antibody (red). **(A-D)** Helios was detected along the length of the cochlea, with no differential expression observed along the longitudinal axis (x10 magnification, scale bar = 100 µm). The regions marked with dashed boxes were assessed at higher magnification and are shown in the images below. At **(E)** apical, **(F)** mid and **(G)** basal regions of the cochlea, all three rows of OHCs were found to express helios, with no radial gradients observed (x63 magnification, scale bar = 10 µm).

Vibratome and wholemount immunolabelling demonstrated that helios is expressed in OHC nuclei along the length of the cochlea at P8 and is maintained at adult stages. In order to investigate the onset and temporal expression pattern of helios in more detail, a time course of wholemount immunolabelling was undertaken using cochleae from *Ikzf2*$^{+/+}$ mice between P3 and P16.

Interestingly, helios labelling was not observed in the OHCs or any of the neighbouring supporting cells of the organ of Corti at P3 (Figure 5.19 A-D), despite SHIELD data detecting the *Ikzf2* transcript at E16 and P0. It may be that the helios protein is below the level of detection of the anti-helios primary antibody at this time point. Alternatively, a lag between detection of the *Ikzf2* transcript and the helios protein could indicate that *Ikzf2* is subject to post-transcriptional regulation or modification.

Helios was first observed at P4 in the three rows of OHC nuclei (Figure 5.19 E-F) and was maintained throughout the time course (Figure 5.19 G-N). Helios was not detected in the IHCs at any of the time points tested, although some potential weak labelling was observed in the nuclei of the Deiters' cells which surround the OHCs at P12 and P16 (Figure 5.19 K-N). Antibody binding specificity was confirmed by labelling cochleae with anti-helios primary antibody that had been pre-incubated with its immunising peptide (Figure 5.19 O-P).

Together, these data indicate that helios is expressed in OHC nuclei from P4 and is maintained throughout postnatal development. Interestingly, this expression is coincident with the postnatal functional maturation of OHCs in the mouse, which occurs between birth at P0 and the onset of hearing at ~P12.

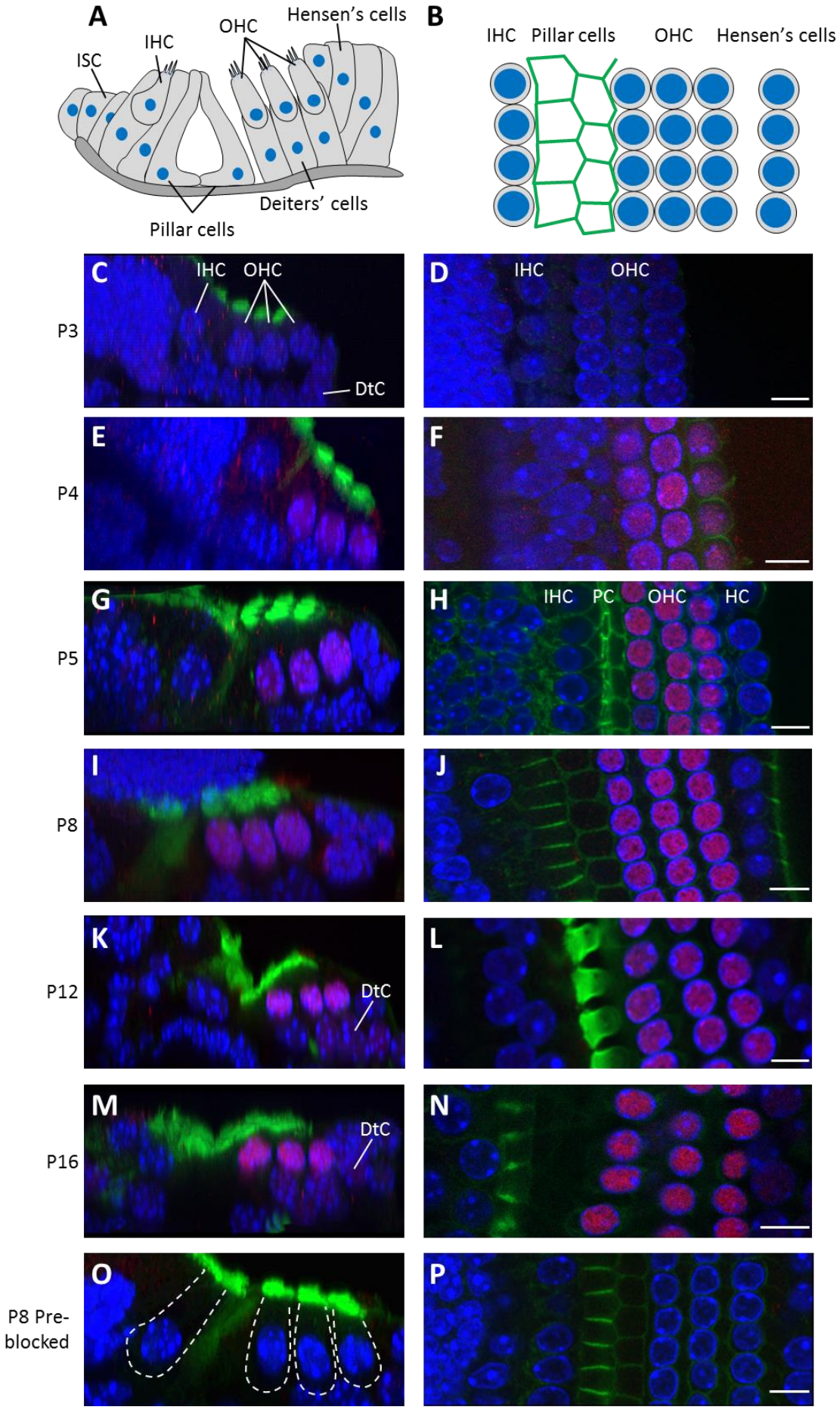
A
ISC
IHC
OHC
Hensen's cells
Deiters' cells
Pillar cells
B
IHC
Pillar cells
OHC
Hensen's cells
C
IHC
OHC
DtC
D
IHC
OHC
P3
E
F
P4
G
H
IHC
PC
OHC
HC
P5
I
J
P8
K
DtC
L
P12
M
DtC
N
P16
O
P
P8 Pre-blocked

Figure 5.19: Helios immunolabelling of *Ikzf2*$^{+/+}$ cochlear wholemounts at early postnatal time points.
To assess the onset and temporal expression pattern of helios, *Ikzf2*$^{+/+}$ cochleae were collected at time points between postnatal day (P) 3 and P16 and immunolabelled with DAPI (blue), Alexa Fluor® 488 Phalloidin (green) and anti-helios with an Alexa Fluor® 568 secondary antibody (red). Schematics of the **(A)** cross-sectional and **(B)** dorsal view through the organ of Corti show the relative position of each cell type. **(C-D)** At P3, helios labelling is not observed in any of the cells of the organ of Corti. **(E-F)** At P4, helios is detected solely in the nuclei of the three rows of OHCs. At **(G-H)** P5 and **(I-J)** P8, helios expression is maintained in the OHC nuclei. At **(K-L)** P12 and **(M-N)** P16, some potential weak helios labelling is also observed in the supporting Deiters' cells which neighbour the OHCs. **(O-P)** No helios labelling is detected in P8 cochleae labelled with pre-blocked helios antibody, which confirms antibody binding specificity. The position of the hair cells is indicated by a dashed line. x63 magnification, scale bar = 10 µm. DtC, Deiters' cell; HC, Hensen's cell; IHC, inner hair cell; ISC, inner sulcus cell; OHC, outer hair cell; P, postnatal day; PC, pillar cell.

5.3. Discussion

The *cello* pedigree was identified as a mouse model of hearing loss from the Harwell Ageing Screen and found to harbour an ENU-induced missense mutation in the zinc finger transcription factor helios. Helios has only previously been reported to mediate lymphopoietic processes (Getnet et al., 2010, Nakase et al., 2002, Serre et al., 2011) and neurogenesis of striatal neurons (Martin-Ibanez et al., 2012), therefore my data suggest a novel role for helios in the mammalian auditory system.

To further elaborate upon the requirement of helios in the auditory system, *cello* mice were characterised using a collection of *in vivo* and *ex vivo* auditory phenotyping techniques at a range of postnatal time points. This included a time course of ABR measurements, histopathological examination of the inner and middle ear, ultrastructural analysis of the organ of Corti by SEM and investigation of the temporospatial expression pattern of *Ikzf2* and helios.

ABR data from the original *cello* (née *MPC-173*) Ageing Screen cohort was only generated at nine months of age and demonstrated that affected mice had significantly increased (+60 dB SPL) auditory thresholds compared to unaffected littermates at this time point. Although clickbox data suggested that the hearing function was impaired at three months of age, with 16.7% of the G3 cohort showing reduced or absent clickbox responses, the onset and nature of the hearing impairment was unknown. To this end, a time course of ABR phenotyping was performed on $Ikzf2^{+/+}$, $Ikzf2^{cello/+}$and $Ikzf2^{cello/cello}$ littermates to assess hearing capacity at a range of time points between P16 (just after the onset of audition in normal-hearing mice) and nine months of age. $Ikzf2^{cello/cello}$ mutants were found to have significantly elevated (+45 dB SPL) auditory thresholds across all frequencies tested at P16 compared to

Ikzf2$^{+/+}$ and *Ikzf2*$^{cello/+}$ mice. *Ikzf2*$^{cello/cello}$ auditory thresholds remained similar between P16 and one month of age (+45 dB SPL), but showed a further, significant increase to +60 dB SPL by nine months of age. Together, these data indicate an early-onset hearing impairment that is progressive in nature. At all of the time points investigated, *Ikzf2*$^{cello/+}$ auditory thresholds resembled those of *Ikzf2*$^{+/+}$ controls, which confirms the recessive nature of the *cello* mutation. Co-IP data demonstrated reduced levels of dimerisation between WT and H517Q helios proteins in the heterozygous state (Figure 3.8). Although it is unclear whether these WT-H517Q dimers are functional, WT-WT dimers will also be able to form in *Ikzf2*$^{cello/+}$ mice, which would be functional and able to elicit transcription from helios target genes (Figure 5.20), thus likely accounting for the normal auditory phenotype in *Ikzf2*$^{cello/+}$ mice.

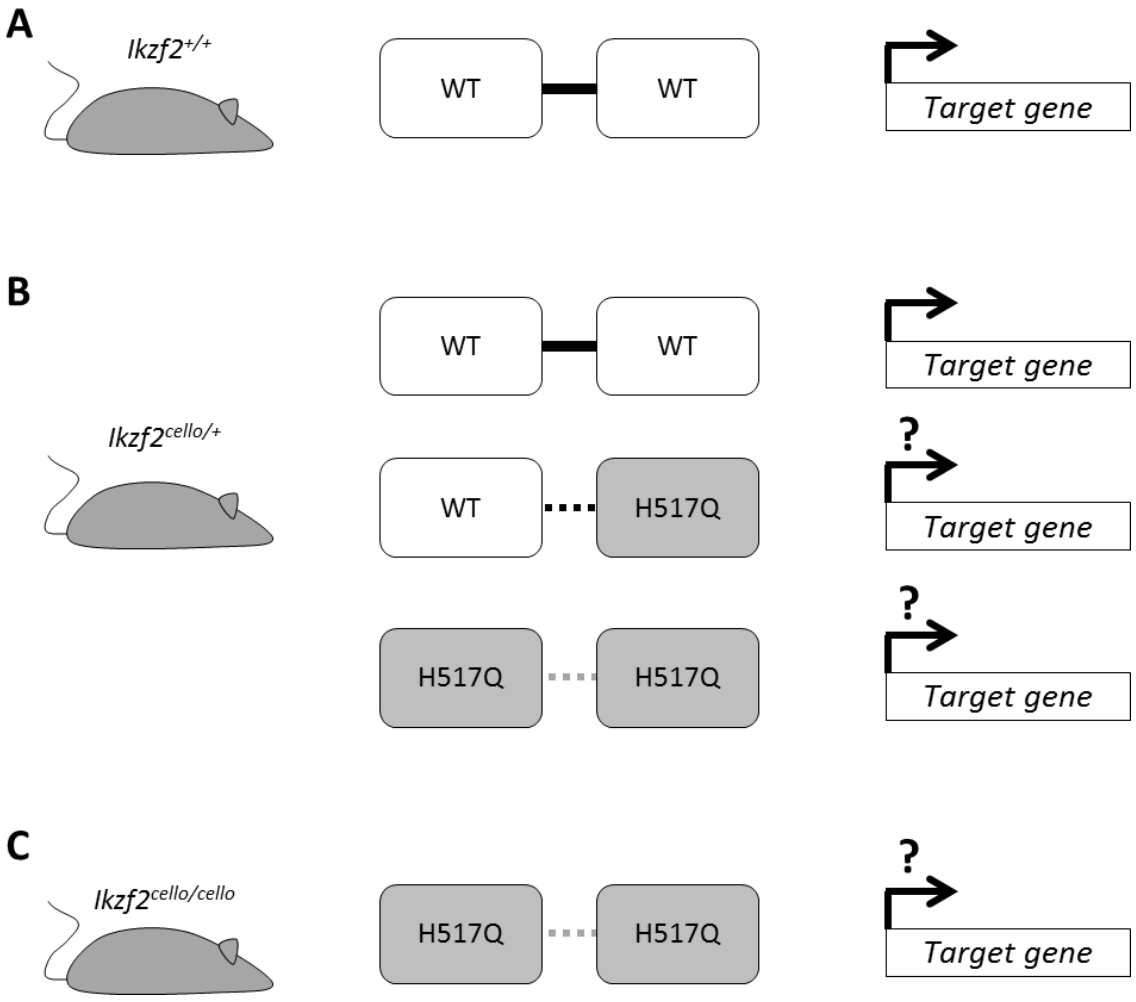

Figure 5.20: The formation of functional helios homodimers in the *cello* pedigree.
(A) In *Ikzf2*$^{+/+}$ mice, WT helios proteins homodimerise and subsequently bind DNA, causing transcription of target genes. **(B)** In *Ikzf2*$^{cello/+}$ mice, dimerisation is reduced between WT and H517Q helios proteins and severely impaired between H517Q helios proteins, which may impair transcription of target genes. However, functional WT-WT dimers will still form and be able to bind DNA and regulate helios targets. **(C)** In *Ikzf2*$^{cello/cello}$ mice, dimerisation is severely impaired between H517Q helios proteins, which is likely to disrupt DNA binding and transcription of target genes, leading to the *cello* mutant auditory phenotype. WT, wild-type.

Whilst the time course of ABR provided an indication of auditory acuity in *Ikzf2*$^{cello/cello}$ mutants, traces were only analysed for hearing thresholds. Quantitative measures of peak amplitude and interpeak latency were not carried out, meaning that the current analyses are unable to provide information about potential defects in central auditory processing. Given that helios, and the other IKZF proteins, have been implicated in neurogenesis in the developing brain (Agoston et al., 2007, Alsio et al., 2013, Martin-Ibanez et al., 2010, Martin-

Ibanez et al., 2012), it is possible that loss of helios function in *Ikzf2*$^{cello/cello}$ mice may also result in abnormalities in the central auditory system. As such, auditory processing should be further investigated by conducting peak amplitude and interpeak latency measurements. The ability of *Ikzf2*$^{cello/cello}$ mutants to localise sound signals and adapt to altered spatial cues could also be assessed, although this would have to be undertaken at young ages (~P14) due to their early-onset progressive hearing loss. In addition, immunolabelling of brain sections and injection of neural tracers could be used to investigate the effect of the *cello* mutation on the morphology of the different areas of the central auditory system and the neuronal projections between them. As helios is reported to promote neurogenesis during embryonic development (Martin-Ibanez et al., 2012), this should be carried out at embryonic and early postnatal time points, along with immunolabelling to investigate helios expression in the central auditory system.

To further understand the role of helios in the auditory system and the potential mechanisms underlying hearing loss in *cello* mutants, the inner and middle ears of *Ikzf2*$^{cello/cello}$ mice were assessed for pathological defects. Interestingly, although *Ikzf2*$^{cello/cello}$ animals have severely elevated ABR thresholds from P16, their cochlear morphology was found to initially resemble that of *Ikzf2*$^{+/+}$ and *Ikzf2*$^{cello/+}$ controls; actin immunolabelling and SEM demonstrated that hair cells were present in *Ikzf2*$^{cello/cello}$ mutants at both P16 and one month of age, with no defects in the morphology of stereocilia bundles, the organisation of hair cell rows or the number of IHCs and OHCs along the length of the cochlea. Morphological abnormalities were first observed at three months of age, when *Ikzf2*$^{cello/cello}$ mice exhibited a significant reduction in OHC number across all regions of the cochlea compared to controls. This OHC loss progressed over subsequent time points, so that very

few OHCs remained by nine months of age. From nine months of age, degeneration of mid and basal IHCs and potential loss of SGNs was also observed in *Ikzf2*$^{cello/cello}$ mice. However, the late-onset nature of these phenotypes suggests that they likely result from the earlier OHC loss. Importantly, as the widespread OHC degeneration in *Ikzf2*$^{cello/cello}$ mice occurs after the onset of hearing loss, it is most likely a secondary effect rather than the primary cause and implies that another mechanism is instead underlying the hearing impairment. This could be defective hair cell maturation, function or innervation, all of which have previously been shown to result in the deterioration and eventual death of hair cells (Hequembourg and Liberman, 2001, Jacobson et al., 2003, Kim et al., 2002, Spiden et al., 2008, Stamataki et al., 2006). Whilst the electrophysiological and functional properties of *Ikzf2*$^{cello/cello}$ OHCs are assessed in more detail in Chapter 6, further work is required to study hair cell innervation. This should involve immunolabelling of cochlear wholemounts using known neural and synaptic markers, undertaking additional electrophysiological analyses to measure exocytosis and action potential firing and carrying out distortion product otoacoustic emissions (DPOAEs) to assess efferent function, as in Varghese et al. (2005).

Given the known immunological function of helios, *Ikzf2*$^{cello/cello}$ mice were also assessed for indicators of otitis media, an inflammatory disorder of the middle ear. Histological examination revealed grossly normal middle ear morphology in *Ikzf2*$^{cello/cello}$ animals, with no typical symptoms of otitis media (inflammation, infiltration of immune cells, mucosal thickening) observed.

Together, the morphological characterisation data indicate that the hearing impairment in *Ikzf2*$^{cello/cello}$ mutants can be classified as sensorineural, as it originates from pathological defects affecting the hair cells within the inner ear. This correlates with the severe auditory

thresholds (+45 – 60 dB SPL) observed in *Ikzf2*$^{cello/cello}$ mice and suggests a role for helios specifically within the inner ear. Indeed, data from the recently published SHIELD study demonstrated that *Ikzf2* is expressed in the cochlea and is developmentally upregulated specifically in hair cells (Scheffer et al., 2015). The corresponding helios protein was detected in *Ikzf2*$^{+/+}$ cochleae from P4 and is maintained at adult stages, where it was found to localise to the nuclei of the three rows of OHCs along the length of the cochlea. Helios was not detected in the IHCs at any of the time points studied, although some potential weak labelling was observed in the nuclei of the Deiters' cells that surround the OHCs at P12 and P16. Although SHIELD data indicates that the *Ikzf2* transcript is detected as early as E16, it may be that the helios protein is below the level of detection of the anti-helios primary antibody prior to P4. Alternatively, the delay between the detection of *Ikzf2* and helios may indicate that *Ikzf2* mRNA is subject to post-transcriptional regulation.

Immunolabelling also demonstrated that helios was still expressed and localised to OHC nuclei in *Ikzf2*$^{cello/cello}$ cochleae, which is consistent with the *in vitro* subcellular localisation analysis of c-Myc-tagged H517Q helios (Figure 3.7). This is not unexpected, given that the *cello* mutation is a missense allele and, as such, a full-length mutant protein is likely produced. This is also consistent with previous work on ikaros, which has shown that nuclear localisation relies on N-terminal ZnF2 and ZnF3 (Cobb et al., 2000) and is not affected by mutations that disrupt the C-terminal zinc fingers and dimerisation (Sun et al., 1996).

Interestingly, the onset of helios expression in the OHCs occurs at a time when the IHCs and OHCs are undergoing subtype-specific postnatal maturation. In OHCs, this involves the upregulation of $I_{K,n}$ and downregulation of I_{K1} and $I_{K,neo}$ currents (Housley and Ashmore,

1992, Marcotti et al., 1999, Marcotti and Kros, 1999), as well as increased expression of prestin and the associated onset of electromotility (He et al., 1994, Souter et al., 1995), resulting in fully differentiated, functionally mature OHCs by ~P8.

Whilst a hearing impairment is only detected in *Ikzf2*$^{cello/cello}$ homozygotes and the localisation of helios to the OHCs fits with the OHC pathology observed by SEM, a complementation test is still required in order to definitively prove that helios is the causative mutation in *cello* mice. As the two additional mutations mentioned in Chapter 3 (c.152A>C in *Cryga* and c.2944T>A in *Map2*) currently remain unvalidated, it is possible that they may also co-segregate with the hearing impairment in *cello* mice. If this is found to be so following additional Sanger sequencing, *in silico* and *in vitro* characterisation should be undertaken, as for *Ikzf2*, to determine if the mutation(s) are likely to be detrimental to protein structure and function. Immunolabelling should also be carried out to investigate the expression of the respective encoded proteins (CRYGA and MAP2) in the inner ear and determine if *cello* mutants show any defects in protein expression or localisation that could be linked to their hearing impairment.

Overall, my study of *cello* mice suggests that the helios transcription factor is required for auditory function and demonstrates that helios is expressed in the OHCs from P4. Together, this suggests that helios may play a critical role in the postnatal functional maturation of the OHCs. Furthermore, whilst other ikaros family members can likely compensate for helios loss-of-function in T-cells and NK cells (Cai et al., 2009, Thornton et al., 2010), this may not be possible in the OHCs as, to date, no other IKZF proteins have been reported in these cells.

Chapter 6 : Functional Auditory Characterisation of *cello*

6.1. Introduction

The ikaros family have been shown to function as both transcriptional activators and repressors, regulating the expression of a broad range of haematopoietic target genes (Ferreiros-Vidal et al., 2013, Harker et al., 2002, Sabbattini et al., 2001, Trinh et al., 2001, Yoshida and Georgopoulos, 2014). Critical to their function as transcription factors is the ability of the IKZF proteins to dimerise, with previous work demonstrating that homodimerisation of ikaros increases its affinity for target DNA sequences and subsequent transcriptional activity (Cobb et al., 2000, Sun et al., 1996). Given that the *cello* mutation impairs helios homodimerisation, it is therefore likely to reduce the transcriptional activity of helios in *cello* mice, leading to dysregulation of target genes. Although helios has been shown to directly regulate interleukin-2 *(Il-2)* and is associated with increased expression of *CD103,* glucocorticoid-induced tumour necrosis factor receptor (*GITR*), glycoprotein A repetitions predominant (*GARP*) and folate receptor 4 (*FR4*) in T-regs (Baine et al., 2013, Takatori et al., 2015, Zabransky et al., 2012), its targets within the ear are currently unknown.

In order to identify potential helios target genes, cochlear RNA extracted from *cello* mice underwent transcriptome profiling using RNA-Seq. A selection of differentially expressed genes were validated by qRT-PCR then further analysed using luciferase reporter assays to characterise their relationship with helios. This was carried out alongside investigation of the electrophysiological properties of *cello* OHCs. Together, this will provide insight into the

effect of the *cello* mutation on OHC function and the mechanisms underlying the hearing impairment in *cello*. Furthermore, as helios is unique to the OHCs and not expressed in the IHCs, these data may help elaborate upon the genetic regulation of OHC-specific morphological and functional specialisations.

6.2. Results

6.2.1. RNA Sequencing (RNA-Seq)

To gain insight into the potential target genes and regulatory networks influenced by helios, RNA-Seq was undertaken by Dr Ronna Hertzano at the University of Maryland (USA) using cochlear RNA extracted from P8 *Ikzf2*$^{+/+}$ and *Ikzf2*$^{cello/cello}$ mice. This time point was chosen for analysis as the OHCs normally begin to exhibit adult-like characteristics at ~P8 (Abe et al., 2007, He et al., 1994, Marcotti and Kros, 1999). Two *Ikzf2*$^{+/+}$ and two *Ikzf2*$^{cello/cello}$ RNA samples, each a pool of three pairs of sub-dissected cochlear ducts, were prepared at MRC Harwell then shipped to the USA for sequencing. Reads from the RNA-Seq data were aligned to *Mus musculus* reference genome (assembly GRCm38.74) then analysed using HTSeq and DESeq software (Anders and Huber, 2010, Anders et al., 2015) by Sean Daugherty at the University of Maryland to perform raw read counts, normalise data and generate a list of differentially expressed genes. Alignment statistics indicated that the total number of sequencing reads and the proportion of mapped reads were similar for each sample (Table 6.1).

Table 6.1: Alignment statistics for raw RNA-Seq data of *Ikzf2*$^{+/+}$ and *Ikzf2*$^{cello/cello}$ cochleae at postnatal day 8.

Sample ID	Total Reads	Total Mapped Reads	Percentage Mapped Reads
Ikzf2$^{+/+}$ #1	98,882,398	85,079,808	86.04%
Ikzf2$^{+/+}$ #2	83,834,716	71,896,892	85.76%
Ikzf2$^{cello/cello}$ #1	85,124,656	73,070,872	85.84%
Ikzf2$^{cello/cello}$ #2	93,977,172	80,970,876	86.04%

Prior to analysis, sequencing data for each sample were normalised for transcript read length and sequencing depth using DESeq to remove any technical bias (Mortazavi et al., 2008). Each RNA-Seq dataset showed a similar distribution of reads per kilobase per million (RPKM) mapped reads (Figure 6.1 A), which indicates they can be used for comparative

analysis of gene expression. The four RNA-Seq datasets were also assessed for hierarchical clustering; the *Ikzf2*$^{+/+}$ and *Ikzf2*$^{cello/cello}$ samples were found to form two distinct clusters, with sequencing results from *Ikzf2*$^{+/+}$ #1 most similar to *Ikzf2*$^{+/+}$ #2 and results from *Ikzf2*$^{cello/cello}$ #1 most similar to *Ikzf2*$^{cello/cello}$ #2 (Figure 6.1 B). This indicates that sequencing data was replicable within each genotype group (biological replicate), but different between *Ikzf2*$^{+/+}$ and *Ikzf2*$^{cello/cello}$ animals.

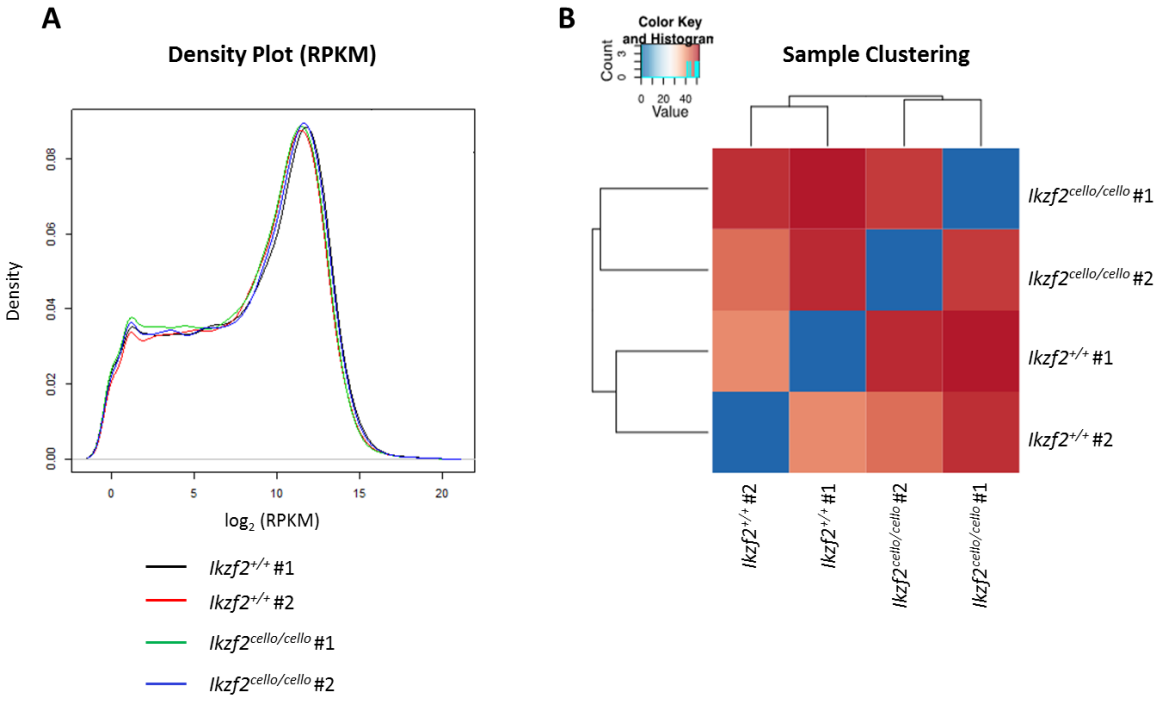

Figure 6.1: Normalisation and hierarchical cluster analysis of RNA-Seq datasets from *Ikzf2*$^{+/+}$ and *Ikzf2*$^{cello/cello}$ cochleae at postnatal day 8.
(A) Following normalisation for total read length and number of sequencing reads, the four RNA-Seq datasets were found to have a similar distribution of RPKM mapped reads. **(B)** A hierarchical cluster matrix was generated for the four RNA-Seq datasets, based on the expression of all detected genes in that sample. The matrix shows that both of the *Ikzf2*$^{+/+}$ samples (*Ikzf2*$^{+/+}$ #1 and *Ikzf2*$^{+/+}$ #2) cluster together, as do both of the *Ikzf2*$^{cello/cello}$ samples (*Ikzf2*$^{cello/cello}$ #1 and *Ikzf2*$^{cello/cello}$ #2), with each genotype cluster distinct from the other. Graphs prepared by Dr Ronna Hertzano and Sean Daugherty at the University of Maryland. RPKM; reads per kilobase per million.

Ikzf2$^{+/+}$ and *Ikzf2*$^{cello/cello}$ sequencing data were analysed for differential gene expression with DESeq software using the negative binomial distribution and a false detection rate (FDR) threshold of 0.05 and then visualised using an MA plot (M, log ratio; A, average) (Figure 6.2). This highlights an important general property of RNA-Seq data; weakly expressed genes with a lower normalised read count require a greater log fold change to yield a significant call. Conversely, as the normalised read count increases, the log fold change needed for a gene to reach significance becomes smaller.

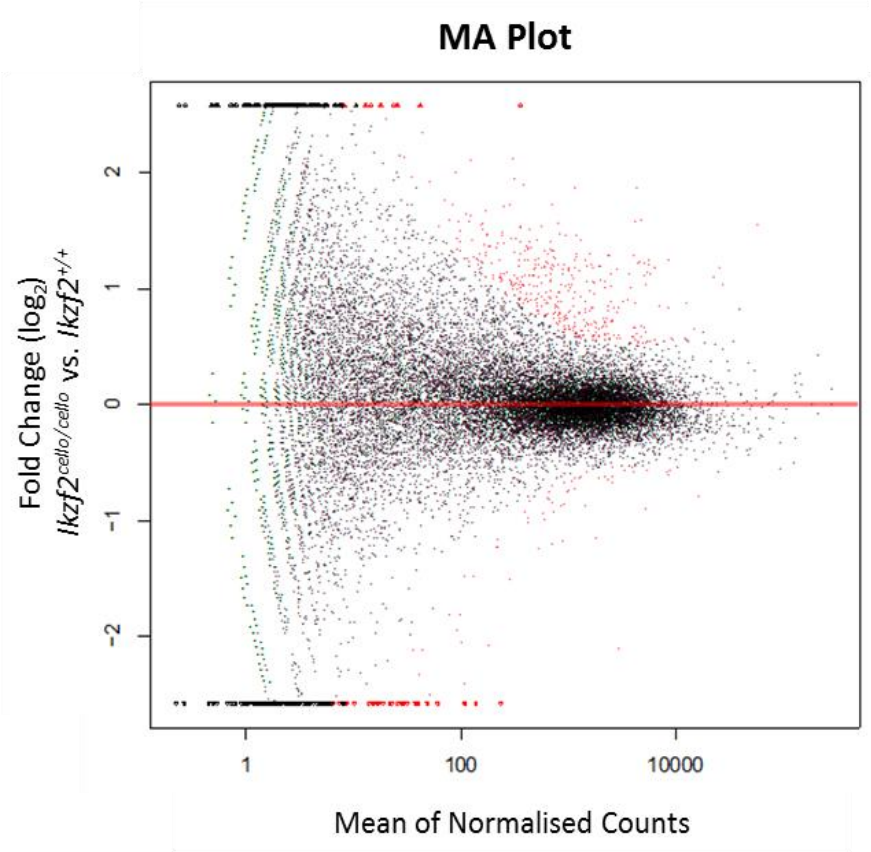

Figure 6.2: MA plot providing an overview of differentially expressed genes identified by RNA-Seq between *Ikzf2*$^{+/+}$ and *Ikzf2*$^{cello/cello}$ cochleae at postnatal day 8.
An MA plot (M, log ratio; A, average) was generated to visualise differentially expressed genes between *Ikzf2*$^{+/+}$ and *Ikzf2*$^{cello/cello}$ RNA-Seq datasets. An FDR cut-off of 0.05 was used to determine statistical significance. Each gene is represented by a single dot; genes that are not significantly differentially expressed between the two genotype groups (FDR>0.05) are shown in black, whilst genes that are significantly differentially expressed (FDR≤0.05) are marked in red. The red line at 0 on the *y* axis represents no fold change. This demonstrates that genes with a larger normalised read count require a smaller log fold change to reach significance and vice versa. Graph prepared by Dr Ronna Hertzano and Sean Daugherty at the University of Maryland.

The expression of 467 genes was found to be significantly different in *Ikzf2*$^{cello/cello}$ cochleae compared to *Ikzf2*$^{+/+}$ controls at P8; 89 of these were downregulated and 378 were upregulated (Table 9.4 in Appendix). Due to the high false positive rate associated with analysing differential gene expression using RNA-Seq (Rocke et al., 2015, Tarazona et al., 2011), a fold change cut-off of +/-2 was used for subsequent analyses; as such, only downregulated genes with a fold change of ≥ -2 (i.e. expression reduced by at least 50%) and upregulated genes with a fold change of ≥ +2 (i.e. expression increased by at least 100%) were further examined. Using these cut-off criteria, 57 genes were found to be significantly downregulated with a fold change ≥ -2 (Table 6.2).

Table 6.2: The 57 genes identified by RNA-Seq to be significantly downregulated with a fold change ≥ -2 in *Ikzf2*$^{cello/cello}$ cochleae compared to *Ikzf2*$^{+/+}$ at postnatal day 8.

Ensembl ID (ENS)	Read Count *Ikzf2*$^{+/+}$	Read Count *Ikzf2*$^{cello/cello}$	Fold Change	p Value	FDR	Gene Symbol
MUSG00000039714	16.95	0.00	N/A	1.01E-05	1.23E-03	*Cplx3*
MUSG00000073658	12.18	0.00	N/A	1.44E-04	1.13E-02	*Crygb*
MUSG00000034384	11.57	0.00	N/A	1.99E-04	1.45E-02	*Barhl2*
MUSG00000020428	11.12	0.00	N/A	2.72E-04	1.85E-02	*Gabra6*
MUSG00000059632	10.96	0.00	N/A	2.76E-04	1.87E-02	*Krtap8-1*
MUSG00000029595	10.06	0.00	N/A	5.22E-04	3.12E-02	*Lhx5*
MUSG00000029546	9.53	0.00	N/A	7.29E-04	4.04E-02	*Uncx*
MUSG00000031354	466.54	2.10	-221.88	1.67E-49	4.37E-45	*Amelx*
MUSG00000029286	61.89	1.02	-60.76	5.85E-11	2.64E-08	*Enam*
MUSG00000030399	32.15	0.54	-59.30	1.24E-07	2.35E-05	*Ckm*
MUSG00000040046	94.20	2.45	-38.48	5.88E-13	4.27E-10	*Tph1*
MUSG00000024992	16.87	0.48	-35.40	7.45E-05	6.63E-03	*Pde6c*
MUSG00000029288	266.29	7.93	-33.56	5.87E-25	3.07E-21	*Ambn*
MUSG00000037771	14.30	0.48	-30.01	2.84E-04	1.91E-02	*Slc32a1*
MUSG00000038255	44.09	1.56	-28.25	5.09E-08	1.09E-05	*Neurod2*
MUSG00000048015	29.05	1.08	-26.80	2.08E-06	3.00E-04	*Neurod4*
MUSG00000043301	12.47	0.48	-26.17	6.76E-04	3.80E-02	*Kcnj6*
MUSG00000031972	207.60	10.33	-20.09	1.04E-17	3.01E-14	*Acta1*
MUSG00000026468	15.12	1.02	-14.84	6.39E-04	3.65E-02	*Lhx4*
MUSG00000061816	113.70	7.67	-14.82	2.59E-11	1.33E-08	*Myl1*
MUSG00000034701	112.17	7.61	-14.75	7.73E-11	3.37E-08	*Neurod1*
MUSG00000041578	28.60	2.04	-14.04	2.74E-05	2.89E-03	*Crx*

Ensembl ID (ENS)	Read Count *Ikzf2*$^{+/+}$	Read Count *Ikzf2*$^{cello/cello}$	Fold Change	p Value	FDR	Gene Symbol
MUSG00000049583	18.74	1.43	-13.11	3.68E-04	2.35E-02	*Grm5*
MUSG00000002100	25.79	1.97	-13.08	6.99E-05	6.35E-03	*Mybpc3*
MUSG00000041534	41.76	3.40	-12.28	6.47E-06	8.37E-04	*Rbp3*
MUSG00000068154	51.95	4.49	-11.58	1.39E-06	2.08E-04	*Insm1*
MUSG00000027168	46.78	4.55	-10.28	5.97E-06	7.85E-04	*Pax6*
MUSG00000025386	39.36	4.07	-9.66	2.18E-05	2.36E-03	*Pde6g*
MUSG00000031097	71.55	8.48	-8.44	8.95E-07	1.50E-04	*Tnni2*
MUSG00000024041	33.33	4.01	-8.31	1.28E-04	1.03E-02	*Cryaa*
MUSG00000055775	85.28	11.42	-7.47	1.35E-06	2.05E-04	*Myh8*
MUSG00000028602	50.75	7.39	-6.86	2.27E-05	2.45E-03	*Tnfrsf8*
MUSG00000086938	29.47	4.62	-6.38	4.03E-04	2.53E-02	*4930481A15Rik*
MUSG00000027073	186.50	30.46	-6.12	2.51E-09	8.01E-07	*Prg2*
MUSG00000023439	64.21	10.60	-6.06	4.49E-05	4.37E-03	*Gnb3*
MUSG00000026535	88.01	15.62	-5.63	5.27E-06	7.13E-04	*Ifi202b*
MUSG00000030672	188.78	35.40	-5.33	4.42E-08	9.63E-06	*Mylpf*
MUSG00000052234	69.56	13.90	-5.01	5.73E-05	5.31E-03	*Epx*
MUSG00000057003	59.37	13.63	-4.35	4.68E-04	2.86E-02	*Myh4*
MUSG00000036972	72.49	16.69	-4.34	2.09E-04	1.50E-02	*Zic4*
MUSG00000029618	4953.53	1150.91	-4.30	4.43E-37	5.79E-33	*Ocm*
MUSG00000032368	303.21	71.56	-4.24	8.59E-09	2.32E-06	*Zic1*
MUSG00000032517	166.05	40.13	-4.14	2.05E-06	2.98E-04	*Mobp*
MUSG00000049598	150.94	39.36	-3.83	6.50E-06	8.37E-04	*Vsig8*
MUSG00000095526	159.09	45.38	-3.51	1.19E-05	1.43E-03	*Gm10243*
MUSG00000044254	123.79	35.40	-3.50	1.18E-04	9.71E-03	*Pcsk9*
MUSG00000002930	434.32	153.18	-2.84	4.14E-07	7.22E-05	*Ppp1r17*
MUSG00000031654	161.14	57.61	-2.80	3.45E-04	2.25E-02	*Cbln1*
MUSG00000039783	199.70	71.48	-2.79	7.43E-05	6.63E-03	*Kmo*
MUSG00000033498	768.83	325.84	-2.36	1.29E-07	2.43E-05	*Strc*
MUSG00000020932	301.60	128.54	-2.35	3.78E-04	2.40E-02	*Gfap*
MUSG00000027863	312.62	133.62	-2.34	1.58E-04	1.22E-02	*Cd2*
MUSG00000029015	1016.59	440.68	-2.31	1.66E-08	4.13E-06	*Slc26a5*
MUSG00000044086	1270.23	564.31	-2.25	3.83E-09	1.18E-06	*Lmod3*
MUSG00000003411	312.65	139.04	-2.25	2.51E-04	1.75E-02	*Rab3b*
MUSG00000073643	2547.71	1152.72	-2.21	3.55E-11	1.69E-08	*Wdfy1*
MUSG00000031883	571.81	281.63	-2.03	6.06E-05	5.56E-03	*Car7*

FDR, false detection rate; N/A, not applicable.

A total of 219 genes were found to be significantly upregulated with a fold change ≥ +2 in *Ikzf2*$^{cello/cello}$ cochleae compared to *Ikzf2*$^{+/+}$ controls at P8 (Table 6.3).

Table 6.3: The 219 genes identified by RNA-Seq to be significantly upregulated with a fold change ≥ +2 in *Ikzf2*$^{cello/cello}$ cochleae compared to *Ikzf2*$^{+/+}$ at postnatal day 8.

Ensembl ID (ENS)	Read Count *Ikzf2*$^{+/+}$	Read Count *Ikzf2*$^{cello/cello}$	Fold Change	p Value	FDR	Gene Symbol
MUSG00000098050	0.00	50.95	∞	4.14E-12	2.51E-09	*Gm5345*
MUSG00000074252	0.00	25.87	∞	5.32E-08	1.12E-05	*Gm10654*
MUSG00000085926	0.00	16.36	∞	6.13E-06	8.01E-04	*Gm12299*
MUSG00000076038	0.00	9.53	∞	2.71E-04	1.85E-02	*Gm22774*
MUSG00000093843	0.00	8.82	∞	7.17E-04	3.99E-02	*Gm25939*
MUSG00000073491	0.98	27.85	28.46	1.11E-06	1.78E-04	*Pydc4*
MUSG00000038257	0.98	24.67	25.22	6.74E-06	8.59E-04	*Glra3*
MUSG00000005681	0.53	12.70	23.98	3.29E-04	2.16E-02	*Apoa2*
MUSG00000028081	65.19	648.90	9.95	2.12E-26	1.39E-22	*Rps3a1*
MUSG00000060087	10.07	73.17	7.27	1.62E-06	2.40E-04	*Gm10074*
MUSG00000073902	5.95	41.18	6.92	7.46E-05	6.63E-03	*Gm1966*
MUSG00000047495	4.81	30.85	6.41	3.09E-04	2.06E-02	*Dlgap2*
MUSG00000097503	6.32	34.78	5.50	4.85E-04	2.94E-02	*3110045C21Rik*
MUSG00000090222	14.51	73.87	5.09	5.18E-05	4.92E-03	*Gm16340*
MUSG00000060441	11.13	49.03	4.41	9.08E-04	4.82E-02	*Trim5*
MUSG00000001494	117.32	509.24	4.34	7.08E-12	4.21E-09	*Sost*
MUSG00000075014	47.86	206.77	4.32	2.54E-07	4.55E-05	*Gm10800*
MUSG00000085698	36.07	144.46	4.00	4.81E-06	6.58E-04	*Gm16022*
MUSG00000078921	14.84	57.62	3.88	6.75E-04	3.80E-02	*Tgtp2*
MUSG00000027955	133.29	513.50	3.85	4.48E-11	2.09E-08	*Fam198b*
MUSG00000005994	21.97	83.35	3.79	1.30E-04	1.04E-02	*Tyrp1*
MUSG00000068794	165.79	619.26	3.74	8.96E-13	5.85E-10	*Col28a1*
MUSG00000023034	505.10	1838.41	3.64	4.37E-22	1.43E-18	*Nr4a1*
MUSG00000044349	1904.66	6926.18	3.64	2.10E-30	1.83E-26	*Snhg11*
MUSG00000042817	32.85	110.99	3.38	1.76E-04	1.33E-02	*Flt3*
MUSG00000052861	40.27	132.72	3.30	5.83E-05	5.39E-03	*Dnah6*
MUSG00000074652	135.35	445.40	3.29	4.32E-09	1.31E-06	*Myh7b*
MUSG00000063253	341.79	1123.25	3.29	3.55E-16	7.46E-13	*Scoc*
MUSG00000086844	121.92	399.34	3.28	2.99E-08	7.11E-06	*B230206H07Rik*
MUSG00000025370	82.41	261.83	3.18	9.59E-07	1.59E-04	*Cdh9*
MUSG00000039488	55.39	172.65	3.12	2.62E-05	2.78E-03	*Cntn5*
MUSG00000038756	61.17	188.89	3.09	1.95E-05	2.17E-03	*Ttll6*
MUSG00000047976	2403.59	7210.20	3.00	3.98E-24	1.49E-20	*Kcna1*
MUSG00000025189	40.14	120.37	3.00	3.12E-04	2.07E-02	*Cnnm1*

Ensembl ID (ENS)	Read Count *Ikzf2*$^{+/+}$	Read Count *Ikzf2*$^{cello/cello}$	Fold Change	p Value	FDR	Gene Symbol
MUSG00000054162	2163.48	6473.00	2.99	1.84E-24	8.03E-21	*Spock3*
MUSG00000022651	48.14	143.68	2.98	3.67E-04	2.35E-02	*Retnlg*
MUSG00000066258	60.25	179.67	2.98	1.26E-04	1.02E-02	*Trim12a*
MUSG00000067261	82.85	245.40	2.96	4.08E-06	5.68E-04	*Foxd3*
MUSG00000016346	421.88	1242.66	2.95	3.29E-15	3.90E-12	*Kcnq2*
MUSG00000074796	81.36	239.49	2.94	2.87E-05	3.00E-03	*Slc4a11*
MUSG00000056569	30329.58	88599.24	2.92	1.10E-08	2.92E-06	*Mpz*
MUSG00000040724	290.58	846.92	2.91	1.18E-11	6.70E-09	*Kcna2*
MUSG00000028176	33.13	96.46	2.91	6.79E-04	3.81E-02	*Lrrc7*
MUSG00000034683	186.32	539.30	2.89	4.97E-09	1.49E-06	*Ppp1r1c*
MUSG00000030283	189.64	543.33	2.86	1.31E-08	3.32E-06	*St8sia1*
MUSG00000026826	227.94	648.35	2.84	6.57E-09	1.87E-06	*Nr4a2*
MUSG00000021268	84.25	239.58	2.84	2.03E-05	2.25E-03	*Meg3*
MUSG00000031688	52.04	147.66	2.84	1.97E-04	1.45E-02	*Pou4f2*
MUSG00000033849	129.08	361.73	2.80	1.07E-06	1.73E-04	*B3galt2*
MUSG00000091712	94.52	262.69	2.78	1.65E-05	1.88E-03	*Sec14l5*
MUSG00000064329	452.18	1254.18	2.77	3.04E-14	2.94E-11	*Scn1a*
MUSG00000027978	97.12	267.70	2.76	1.28E-05	1.52E-03	*Prss12*
MUSG00000038128	655.47	1803.43	2.75	8.93E-17	2.12E-13	*Camk4*
MUSG00000040797	520.61	1430.39	2.75	1.11E-14	1.20E-11	*Iqsec3*
MUSG00000029544	134.25	368.00	2.74	1.37E-06	2.07E-04	*Cabp1*
MUSG00000007594	163.08	440.54	2.70	4.66E-07	8.07E-05	*Hapln4*
MUSG00000051596	50.54	136.45	2.70	8.92E-04	4.75E-02	*Otop1*
MUSG00000070866	182.28	491.06	2.69	8.07E-08	1.62E-05	*Zfp804a*
MUSG00000079597	70.79	190.04	2.68	3.10E-04	2.06E-02	*Gm5483*
MUSG00000041828	285.45	764.47	2.68	6.89E-10	2.47E-07	*Abca8a*
MUSG00000028546	729.72	1944.68	2.66	3.99E-16	7.46E-13	*Elavl4*
MUSG00000037872	55.26	146.67	2.65	4.09E-04	2.55E-02	*Darc*
MUSG00000058975	385.07	1021.60	2.65	1.29E-11	7.01E-09	*Kcnc1*
MUSG00000059213	203.05	537.69	2.65	1.31E-07	2.45E-05	*Ddn*
MUSG00000047746	244.55	646.16	2.64	1.13E-08	2.96E-06	*Fbxo40*
MUSG00000058740	126.26	332.24	2.63	5.29E-06	7.13E-04	*Kcnt1*
MUSG00000033061	142.10	372.15	2.62	1.70E-06	2.50E-04	*Resp18*
MUSG00000036123	94.75	246.73	2.60	3.44E-05	3.44E-03	*Slc9a3*
MUSG00000052468	234.79	606.33	2.58	4.01E-08	8.97E-06	*Pmp2*
MUSG00000042846	107.62	277.70	2.58	1.75E-05	1.98E-03	*Lrrtm3*
MUSG00000025221	102.41	263.97	2.58	3.38E-05	3.41E-03	*Kcnip2*
MUSG00000097545	122.95	314.53	2.56	1.48E-05	1.72E-03	*A930011O12Rik*
MUSG00000036062	240.57	613.97	2.55	3.33E-08	7.72E-06	*N28178*
MUSG00000020836	259.18	661.23	2.55	5.63E-08	1.17E-05	*Coro6*
MUSG00000090125	242.32	614.68	2.54	3.26E-08	7.62E-06	*Pou3f1*

Ensembl ID (ENS)	Read Count *Ikzf2*$^{+/+}$	Read Count *Ikzf2*$^{cello/cello}$	Fold Change	p Value	FDR	Gene Symbol
MUSG00000087620	53.06	134.49	2.53	7.53E-04	4.16E-02	*5330434G04Rik*
MUSG00000038276	400.61	1010.16	2.52	1.58E-10	6.15E-08	*Asic3*
MUSG00000046844	409.96	1031.33	2.52	3.38E-11	1.63E-08	*Vat1l*
MUSG00000086096	57.87	145.36	2.51	9.31E-04	4.91E-02	*Gm12688*
MUSG00000063531	427.98	1074.74	2.51	6.30E-11	2.79E-08	*Sema3e*
MUSG00000053863	350.53	875.92	2.50	5.63E-08	1.17E-05	*Mepe*
MUSG00000021301	232.41	580.48	2.50	1.15E-07	2.23E-05	*Hecw1*
MUSG00000031376	185.22	460.31	2.49	1.29E-06	2.00E-04	*Atp2b3*
MUSG00000060924	101.03	250.29	2.48	8.34E-05	7.36E-03	*Csmd1*
MUSG00000028931	706.97	1745.42	2.47	8.17E-13	5.76E-10	*Kcnab2*
MUSG00000033316	87.42	215.71	2.47	1.80E-04	1.35E-02	*Galnt9*
MUSG00000040428	944.87	2323.83	2.46	2.73E-14	2.86E-11	*Plekha4*
MUSG00000032796	215.18	527.85	2.45	5.71E-07	9.76E-05	*Lama1*
MUSG00000022523	382.30	937.65	2.45	7.52E-10	2.66E-07	*Fgf12*
MUSG00000027833	101.27	247.74	2.45	1.10E-04	9.20E-03	*Shox2*
MUSG00000027273	2410.71	5895.21	2.45	6.02E-17	1.57E-13	*Snap25*
MUSG00000074802	1381.04	3364.42	2.44	1.95E-15	2.43E-12	*Gas2l3*
MUSG00000066058	1457.55	3543.15	2.43	3.87E-16	7.46E-13	*Cldn19*
MUSG00000021613	440.69	1068.80	2.43	1.52E-10	6.15E-08	*Hapln1*
MUSG00000026452	708.73	1717.65	2.42	5.30E-13	4.07E-10	*Syt2*
MUSG00000060212	77.43	187.42	2.42	3.70E-04	2.36E-02	*Pcnxl2*
MUSG00000061911	83.25	199.50	2.40	2.72E-04	1.85E-02	*Myt1l*
MUSG00000075316	70.38	168.47	2.39	5.29E-04	3.14E-02	*Scn9a*
MUSG00000023064	318.66	760.75	2.39	1.62E-08	4.07E-06	*Sncg*
MUSG00000055567	451.03	1075.00	2.38	1.38E-09	4.69E-07	*Unc80*
MUSG00000053198	5134.22	12230.65	2.38	1.87E-15	2.43E-12	*Prx*
MUSG00000021730	137.58	327.21	2.38	3.43E-05	3.44E-03	*Hcn1*
MUSG00000039838	89.08	211.31	2.37	2.73E-04	1.85E-02	*Slc45a1*
MUSG00000060240	883.13	2092.43	2.37	1.06E-13	9.86E-11	*Cend1*
MUSG00000022212	210.11	497.65	2.37	1.33E-06	2.04E-04	*Cpne6*
MUSG00000020396	3447.29	8160.12	2.37	4.72E-16	8.23E-13	*Nefh*
MUSG00000045994	296.78	702.27	2.37	1.19E-07	2.28E-05	*B3gat1*
MUSG00000055430	697.53	1649.91	2.37	2.27E-12	1.41E-09	*Nap1l5*
MUSG00000055561	254.53	601.16	2.36	3.05E-06	4.34E-04	*Spink5*
MUSG00000033981	243.52	575.05	2.36	9.79E-07	1.59E-04	*Gria2*
MUSG00000027584	73.15	172.47	2.36	8.32E-04	4.51E-02	*Oprl1*
MUSG00000022449	383.98	899.17	2.34	1.19E-08	3.07E-06	*Adamts20*
MUSG00000043557	2828.80	6623.66	2.34	9.80E-16	1.42E-12	*Mdga1*
MUSG00000033579	392.45	916.23	2.33	8.19E-09	2.28E-06	*Fa2h*
MUSG00000022055	2741.14	6398.86	2.33	7.32E-16	1.20E-12	*Nefl*
MUSG00000049252	117.79	274.83	2.33	1.79E-04	1.34E-02	*Lrp1b*

Ensembl ID (ENS)	Read Count *Ikzf2*$^{+/+}$	Read Count *Ikzf2*$^{cello/cello}$	Fold Change	p Value	FDR	Gene Symbol
MUSG00000046613	98.76	230.16	2.33	3.84E-04	2.43E-02	*Vwa5b2*
MUSG00000033615	3150.91	7332.00	2.33	9.25E-16	1.42E-12	*Cplx1*
MUSG00000022054	3419.12	7923.86	2.32	1.62E-15	2.23E-12	*Nefm*
MUSG00000053519	89.29	206.77	2.32	5.67E-04	3.35E-02	*Kcnip1*
MUSG00000008874	301.58	698.16	2.31	1.09E-06	1.75E-04	*Clec3a*
MUSG00000039114	330.70	764.73	2.31	6.67E-08	1.37E-05	*Nrn1*
MUSG00000054423	493.58	1140.14	2.31	3.81E-10	1.44E-07	*Cadps*
MUSG00000054459	1009.97	2332.24	2.31	4.34E-13	3.44E-10	*Vsnl1*
MUSG00000046709	567.01	1305.34	2.30	1.56E-10	6.15E-08	*Mapk10*
MUSG00000017400	441.24	1015.64	2.30	1.34E-09	4.60E-07	*Stac2*
MUSG00000015134	1220.43	2802.27	2.30	1.11E-13	1.00E-10	*Aldh1a3*
MUSG00000027350	930.30	2132.24	2.29	8.37E-13	5.76E-10	*Chgb*
MUSG00000024042	1193.42	2729.74	2.29	8.10E-12	4.71E-09	*Sik1*
MUSG00000037868	450.85	1029.23	2.28	6.43E-09	1.85E-06	*Egr2*
MUSG00000060568	213.68	487.75	2.28	2.56E-05	2.72E-03	*Fam78b*
MUSG00000020264	373.37	852.02	2.28	1.91E-07	3.46E-05	*Slc36a2*
MUSG00000040907	4005.25	9115.24	2.28	9.58E-15	1.09E-11	*Atp1a3*
MUSG00000062785	725.58	1650.45	2.27	1.11E-10	4.69E-08	*Kcnc3*
MUSG00000018217	16228.21	36859.87	2.27	2.02E-09	6.60E-07	*Pmp22*
MUSG00000028370	381.35	866.03	2.27	4.34E-08	9.57E-06	*Pappa*
MUSG00000003657	4036.87	9155.44	2.27	2.87E-14	2.88E-11	*Calb2*
MUSG00000031543	629.15	1425.33	2.27	1.54E-10	6.15E-08	*Ank1*
MUSG00000082229	312.50	707.52	2.26	2.64E-07	4.69E-05	*Nap1l2*
MUSG00000050578	426.13	963.20	2.26	8.71E-08	1.72E-05	*Mmp13*
MUSG00000070570	1061.48	2396.21	2.26	8.68E-13	5.82E-10	*Slc17a7*
MUSG00000021700	349.68	788.49	2.25	1.10E-07	2.14E-05	*Rab3c*
MUSG00000056755	93.54	210.83	2.25	8.60E-04	4.62E-02	*Grm7*
MUSG00000026904	643.17	1448.87	2.25	2.78E-09	8.76E-07	*Slc4a10*
MUSG00000000223	1761.77	3961.03	2.25	9.25E-13	5.90E-10	*Drp2*
MUSG00000034891	451.29	1011.09	2.24	5.96E-09	1.73E-06	*Sncb*
MUSG00000043670	300.05	672.09	2.24	5.23E-07	8.99E-05	*Diras1*
MUSG00000005338	559.80	1252.93	2.24	5.30E-10	1.93E-07	*Cadm3*
MUSG00000037996	810.54	1805.69	2.23	1.75E-11	9.34E-09	*Slc24a2*
MUSG00000024743	644.61	1435.98	2.23	1.96E-10	7.55E-08	*Syt7*
MUSG00000032355	169.21	372.24	2.20	4.69E-05	4.53E-03	*Mlip*
MUSG00000027254	3502.79	7699.18	2.20	1.75E-13	1.48E-10	*Map1a*
MUSG00000036564	3742.38	8209.62	2.19	1.34E-13	1.16E-10	*Ndrg4*
MUSG00000025154	2352.69	5160.21	2.19	3.02E-13	2.47E-10	*Arhgap19*
MUSG00000026424	440.57	962.74	2.19	6.96E-08	1.42E-05	*Gpr37l1*
MUSG00000035226	150.41	328.20	2.18	1.19E-04	9.79E-03	*Rims4*
MUSG00000036634	568.30	1239.04	2.18	2.23E-09	7.21E-07	*Mag*

Ensembl ID (ENS)	Read Count *Ikzf2*$^{+/+}$	Read Count *Ikzf2*$^{cello/cello}$	Fold Change	p Value	FDR	Gene Symbol
MUSG00000032854	1624.54	3537.96	2.18	5.68E-13	4.24E-10	*Ugt8a*
MUSG00000000792	163.25	355.42	2.18	1.55E-04	1.19E-02	*Slc5a5*
MUSG00000029307	3235.45	7028.21	2.17	2.65E-11	1.33E-08	*Dmp1*
MUSG00000026344	276.36	600.24	2.17	1.67E-05	1.90E-03	*Lypd1*
MUSG00000042453	298.21	647.41	2.17	1.90E-06	2.78E-04	*Reln*
MUSG00000027834	688.43	1494.47	2.17	1.42E-10	5.90E-08	*Serpini1*
MUSG00000027071	256.17	555.67	2.17	3.22E-06	4.54E-04	*P2rx3*
MUSG00000031465	128.64	278.26	2.16	5.02E-04	3.01E-02	*Angpt2*
MUSG00000095139	313.97	678.93	2.16	1.17E-06	1.84E-04	*Pou3f2*
MUSG00000065037	278.70	602.59	2.16	1.53E-05	1.77E-03	*Rn7sk*
MUSG00000031762	201.83	436.38	2.16	5.01E-05	4.78E-03	*Mt2*
MUSG00000048385	404.89	875.29	2.16	9.07E-08	1.78E-05	*Scrt1*
MUSG00000049176	305.60	659.00	2.16	2.22E-06	3.19E-04	*Frmpd4*
MUSG00000043298	109.56	235.92	2.15	8.73E-04	4.66E-02	*Smco3*
MUSG00000026204	111.78	240.21	2.15	5.78E-04	3.38E-02	*Ptprn*
MUSG00000020953	14590.11	31286.40	2.14	1.45E-07	2.69E-05	*Coch*
MUSG00000068615	155.01	331.52	2.14	1.27E-04	1.03E-02	*Gjd2*
MUSG00000031391	346.51	740.70	2.14	7.47E-07	1.26E-04	*L1cam*
MUSG00000056054	244.90	523.33	2.14	7.12E-05	6.42E-03	*S100a8*
MUSG00000002190	148.74	317.68	2.14	2.22E-04	1.58E-02	*Clgn*
MUSG00000026959	217.33	462.87	2.13	3.12E-05	3.21E-03	*Grin1*
MUSG00000034958	219.86	467.32	2.13	2.30E-05	2.48E-03	*Atcay*
MUSG00000037224	154.25	327.70	2.12	2.49E-04	1.75E-02	*Zfyve28*
MUSG00000034842	730.74	1551.60	2.12	2.01E-09	6.60E-07	*Art3*
MUSG00000007944	131.18	278.12	2.12	3.65E-04	2.35E-02	*Ttc9b*
MUSG00000051243	452.33	956.00	2.11	3.69E-08	8.44E-06	*Islr2*
MUSG00000008658	186.41	392.79	2.11	1.08E-04	9.15E-03	*Rbfox1*
MUSG00000048148	159.58	334.97	2.10	3.66E-04	2.35E-02	*Nwd1*
MUSG00000097767	1319.94	2766.47	2.10	4.21E-10	1.57E-07	*Miat*
MUSG00000032549	1134.89	2377.60	2.10	5.48E-11	2.51E-08	*Rab6b*
MUSG00000042115	198.31	415.17	2.09	8.82E-05	7.76E-03	*Klhdc8a*
MUSG00000029361	445.87	933.23	2.09	3.34E-07	5.89E-05	*Nos1*
MUSG00000007021	155.59	325.22	2.09	2.11E-04	1.51E-02	*Syngr3*
MUSG00000016349	1441.14	3009.00	2.09	1.23E-11	6.87E-09	*Eef1a2*
MUSG00000043924	988.99	2059.82	2.08	5.20E-10	1.92E-07	*Ncmap*
MUSG00000056306	238.78	496.41	2.08	3.68E-05	3.66E-03	*Sertm1*
MUSG00000037217	369.37	766.40	2.07	1.16E-06	1.83E-04	*Syn1*
MUSG00000019775	218.29	452.03	2.07	6.46E-05	5.90E-03	*Rgs17*
MUSG00000027500	1181.72	2441.73	2.07	3.01E-11	1.48E-08	*Stmn2*
MUSG00000039278	194.70	401.19	2.06	9.83E-05	8.43E-03	*Pcsk1n*
MUSG00000035849	233.90	481.14	2.06	5.36E-05	5.03E-03	*Krt222*

Ensembl ID (ENS)	Read Count *Ikzf2*$^{+/+}$	Read Count *Ikzf2*$^{cello/cello}$	Fold Change	p Value	FDR	Gene Symbol
MUSG00000032011	668.66	1374.73	2.06	7.95E-09	2.24E-06	*Thy1*
MUSG00000025375	3470.91	7127.15	2.05	2.64E-11	1.33E-08	*Aatk*
MUSG00000015467	293.45	602.48	2.05	1.43E-05	1.68E-03	*Egfl8*
MUSG00000011751	195.25	400.78	2.05	1.91E-04	1.41E-02	*Sptbn4*
MUSG00000041607	18596.26	38127.81	2.05	1.92E-07	3.46E-05	*Mbp*
MUSG00000027438	731.95	1497.58	2.05	9.29E-09	2.48E-06	*Napb*
MUSG00000039252	257.62	526.69	2.04	4.12E-05	4.06E-03	*Lgi2*
MUSG00000032564	213.23	435.67	2.04	9.22E-05	8.03E-03	*Cpne4*
MUSG00000039057	251.28	512.93	2.04	3.04E-05	3.14E-03	*Myo16*
MUSG00000021194	586.13	1196.31	2.04	3.81E-08	8.58E-06	*Chga*
MUSG00000029861	129.02	263.07	2.04	6.64E-04	3.76E-02	*Fam131b*
MUSG00000017737	1676.93	3419.29	2.04	3.39E-09	1.06E-06	*Mmp9*
MUSG00000030500	344.90	702.75	2.04	4.27E-06	5.91E-04	*Slc17a6*
MUSG00000018865	631.34	1284.36	2.03	2.40E-08	5.87E-06	*Sult4a1*
MUSG00000030683	203.18	413.05	2.03	1.33E-04	1.06E-02	*Sez6l2*
MUSG00000061451	262.44	532.21	2.03	3.37E-05	3.41E-03	*Tmem151a*
MUSG00000008489	327.62	662.82	2.02	6.59E-06	8.44E-04	*Elavl2*
MUSG00000053332	1495.41	3014.77	2.02	1.25E-09	4.37E-07	*Gas5*
MUSG00000030337	2613.45	5263.62	2.01	1.06E-10	4.55E-08	*Vamp1*
MUSG00000070695	245.74	494.31	2.01	5.37E-05	5.03E-03	*Cntnap5a*
MUSG00000000120	720.79	1447.21	2.01	8.46E-09	2.32E-06	*Ngfr*

FDR, false detection rate.

Of the 57 downregulated and 219 upregulated genes in *Ikzf2*$^{cello/cello}$ mutants at P8, 41 have been shown to be either expressed in the ear or mutated in mouse models or human forms of hearing loss (Table 6.4). Furthermore, three of the significantly downregulated genes are OHC-specific, reflecting the expression pattern of helios itself. This includes *Slc26a5* (prestin), which encodes the OHC motor protein and is required for electromotility (Liberman et al., 2002); *Ocm* (oncomodulin), which encodes an eponymous calcium-binding protein proposed to play a role in efferent cholinergic modulation of electromotility (Sakaguchi et al., 1998b, Simmons et al., 2010); and *Strc* (stereocilin), which is essential for the formation of inter-stereocilia links and tectorial membrane attachment crowns in OHCs (Verpy et al., 2008, Verpy et al., 2011).

Interestingly, the majority of dysregulated genes in *Ikzf2*$^{cello/cello}$ mice are not restricted to the OHCs or are expressed in other cell types of the organ of Corti. This includes *Neurod1*, which is required for neurogenesis of the cochleovestibular ganglion (Liu et al., 2000); *Snap25*, which triggers neurotransmitter release from hair cells (Safieddine and Wenthold, 1999); and *Kcnq2* and *Kcna2*, which are expressed in SGNs and proposed to regulate neuronal excitability and coding (Jin et al., 2009, Wang et al., 2013). This may indicate that loss of helios function in the OHCs has effects outside of just OHC biology.

Table 6.4: Significantly dysregulated genes identified by RNA-Seq in *Ikzf2*$^{cello/cello}$ cochleae compared to *Ikzf2*$^{+/+}$ at postnatal day 8 that are known to be expressed within the ear or required for hearing in the human or mouse.

Ensembl ID (ENS)	Read Count *Ikzf2*$^{+/+}$	Read Count *Ikxf2*$^{cello/cello}$	Fold Change	p Value	FDR	Gene Symbol	Gene Name	Auditory Association
MUSG00000034701	112.17	7.61	-14.75	7.73E-11	3.37E-08	*Neurod1*	Neurogenic differentiation 1	Sensorineural hearing loss (Liu et al., 2000)
MUSG00000027168	46.78	4.55	-10.28	5.97E-06	7.85E-04	*Pax6*	Paired box gene 6	Syndromic hearing loss – congenital aniridia (Bamiou et al., 2007)
MUSG00000029618	4953.53	1150.91	-4.30	4.43E-37	5.79E-33	*Ocm*	Oncomodulin	OHC-specific Progressive hearing loss (Sakaguchi et al., 1998b, Simmons et al., 2015)
MUSG00000032368	303.21	71.56	-4.24	8.59E-09	2.32E-06	*Zic1*	Zinc finger protein of the cerebellum 1	Expressed in developing inner ear (Warner et al., 2003)
MUSG00000033498	768.83	325.84	-2.36	1.29E-07	2.43E-05	*Strc*	Stereocilin	OHC-specific DFNB16 (Verpy et al., 2001, Verpy et al., 2011)
MUSG00000020932	301.60	128.54	-2.35	3.78E-04	2.40E-02	*Gfap*	Glial fibrillary acidic protein	Syndromic hearing loss – Alexander disease (Masuda et al., 2008)
MUSG00000029015	1016.59	440.68	-2.31	1.66E-08	4.13E-06	*Slc26a5*	Solute carrier family 26, member 5	OHC-specific DFNB61 (Liu et al., 2003, Souter et al., 1995)
MUSG00000001494	117.32	509.24	4.34	7.08E-12	4.21E-09	*Sost*	Sclerostin	Syndromic hearing loss – craniodiaphyseal dysplasia (Kim et al., 2011)
MUSG00000023034	505.10	1838.41	3.64	4.37E-22	1.43E-18	*Nr4a1*	Nuclear receptor subfamily 4, group A, member 1	Noise-induced hearing loss (Cho et al., 2004)
MUSG00000074652	135.35	445.40	3.29	4.32E-09	1.31E-06	*Myh7b*	Myosin, heavy chain 7B, cardiac muscle, beta	Sensorineural hearing loss (Haraksingh et al., 2014)

Ensembl ID (ENS)	Read Count *Ikzf2*$^{+/+}$	Read Count *Ikxf2*$^{cello/cello}$	Fold Change	p Value	FDR	Gene Symbol	Gene Name	Auditory Association
MUSG00000047976	2403.59	7210.20	3.00	3.98E-24	1.49E-20	*Kcna1*	Potassium voltage-gated channel, shaker-related subfamily, member 1	Syndromic hearing loss – episodic ataxia type 1 (Tomlinson et al., 2013)
MUSG00000016346	421.88	1242.66	2.95	3.29E-15	3.90E-12	*Kcnq2*	Potassium voltage-gated channel, subfamily Q, member 2	Expressed in SGNs (Jin et al., 2009)
MUSG00000074796	81.36	239.49	2.94	2.87E-05	3.00E-03	*Slc4a11*	Solute carrier family 4, sodium bicarbonate transporter-like, member 11	Strial hearing loss (Groger et al., 2010)
MUSG00000056569	30329.58	88599.24	2.92	1.10E-08	2.92E-06	*Mpz*	Myelin protein zero	Syndromic hearing loss – Charcot-Marie-Tooth disease (De Jonghe et al., 1999)
MUSG00000040724	290.58	846.92	2.91	1.18E-11	6.70E-09	*Kcna2*	Potassium voltage-gated channel, shaker-related subfamily, member 2	Expressed in SGNs (Wang et al., 2013)
MUSG00000031688	52.04	147.66	2.84	1.97E-04	1.45E-02	*Pou4f2*	POU domain, class 4, transcription factor 2	Expressed in SGNs (Deng et al., 2014)
MUSG00000058975	385.07	1021.60	2.65	1.29E-11	7.01E-09	*Kcnc1*	Potassium voltage gated channel, Shaw-related subfamily, member 1	Age-related hearing loss (von Hehn et al., 2004)
MUSG00000063531	427.98	1074.74	2.51	6.30E-11	2.79E-08	*Sema3e*	Sema domain, immunoglobulin domain (Ig), short basic domain, secreted, (semaphorin) 3E	Syndromic hearing loss – CHARGE syndrome (Lalani et al., 2004)
MUSG00000060924	101.03	250.29	2.48	8.34E-05	7.36E-03	*Csmd1*	CUB and Sushi multiple domains 1	Hearing loss (Girotto et al., 2014)
MUSG00000028931	706.97	1745.42	2.47	8.17E-13	5.76E-10	*Kcnab2*	Potassium voltage-gated channel, shaker-related subfamily, beta member 2	Syndromic hearing loss - 1p36 deletion syndrome (Nabatame et al., 2007)

Ensembl ID (ENS)	Read Count *Ikzf2*$^{+/+}$	Read Count *Ikxf2*$^{cello/cello}$	Fold Change	p Value	FDR	Gene Symbol	Gene Name	Auditory Association
MUSG00000027273	2410.71	5895.21	2.45	6.02E-17	1.57E-13	*Snap25*	Synaptosomal-associated protein 25	Expressed in hair cells and SGNs (Safieddine and Wenthold, 1999)
MUSG00000053198	5134.22	12230.65	2.38	1.87E-15	2.43E-12	*Prx*	Periaxin	Expressed in hair cells (Choi et al., 2008)
MUSG00000021730	137.58	327.21	2.38	3.43E-05	3.44E-03	*Hcn1*	Hyperpolarization-activated, cyclic nucleotide-gated K+ 1	Expressed in hair cells (Ramakrishnan et al., 2012)
MUSG00000020396	3447.29	8160.12	2.37	4.72E-16	8.23E-13	*Nefh*	Neurofilament, heavy polypeptide	Expressed in SGNs (Dau and Wenthold, 1989)
MUSG00000054459	1009.97	2332.24	2.31	4.34E-13	3.44E-10	*Vsnl1*	Visinin-like 1	Expressed in developing cochlea (Ola et al., 2012)
MUSG00000015134	1220.43	2802.27	2.30	1.11E-13	1.00E-10	*Aldh1a3*	Aldehyde dehydrogenase family 1, subfamily A3	Expressed in otic vesicle (Mic et al., 2000)
MUSG00000024042	1193.42	2729.74	2.29	8.10E-12	4.71E-09	*Sik1*	Salt inducible kinase 1	Expressed in vestibular system (Degerman et al., 2011)
MUSG00000040907	4005.25	9115.24	2.28	9.58E-15	1.09E-11	*Atp1a3*	ATPase, Na+/K+ transporting, alpha 3 polypeptide	Expressed in SGNs (McLean et al., 2009)
MUSG00000062785	725.58	1650.45	2.27	1.11E-10	4.69E-08	*Kcnc3*	Potassium voltage gated channel, Shaw-related subfamily, member 3	Expressed in SGNs (Chen and Davis, 2006)
MUSG00000003657	4036.87	9155.44	2.27	2.87E-14	2.88E-11	*Calb2*	Calbindin 2	Expressed in the posterior ventral cochlear nucleus (Friedland et al., 2006)
MUSG00000056755	93.54	210.83	2.25	8.60E-04	4.62E-02	*Grm7*	Glutamate receptor, metabotropic 7	Age-related hearing loss (Friedman et al., 2009)
MUSG00000024743	644.61	1435.98	2.23	1.96E-10	7.55E-08	*Syt7*	Synaptotagmin VII	Expressed in IHCs (Beurg et al., 2010)
MUSG00000027254	3502.79	7699.18	2.20	1.75E-13	1.48E-10	*Map1a*	Microtubule-associated protein 1 A	Expressed in SGNs (Oshima et al., 1992)

Ensembl ID (ENS)	Read Count *Ikzf2*$^{+/+}$	Read Count *Ikxf2*$^{cello/cello}$	Fold Change	p Value	FDR	Gene Symbol	Gene Name	Auditory Association
MUSG00000029307	3235.45	7028.21	2.17	2.65E-11	1.33E-08	*Dmp1*	Dentin matrix protein 1	Expressed in osteocytes of vestibular system (Lv et al., 2010)
MUSG00000042453	298.21	647.41	2.17	1.90E-06	2.78E-04	*Reln*	Reelin	Otosclerosis (Schrauwen et al., 2009)
MUSG00000027071	256.17	555.67	2.17	3.22E-06	4.54E-04	*P2rx3*	Purinergic receptor P2X, ligand-gated ion channel, 3	Expressed in SGNs (Huang et al., 2005)
MUSG00000020953	14590.11	31286.40	2.14	1.45E-07	2.69E-05	*Coch*	Coagulation factor C homolog	DFNA9 (Robertson et al., 1998)
MUSG00000031391	346.51	740.70	2.14	7.47E-07	1.26E-04	*L1cam*	L1 cell adhesion molecule	Expressed in SGNs (Hrynkow et al., 1998)
MUSG00000029361	445.87	933.23	2.09	3.34E-07	5.89E-05	*Nos1*	Nitric oxide synthase 1, neuronal	Expressed in hair cells, SGNs and super olivary complex (Hess et al., 1998, Reuss, 1998)
MUSG00000041607	18596.26	38127.81	2.05	1.92E-07	3.46E-05	*Mbp*	Myelin basic protein	Expressed in cochlear nerve (Knipper et al., 1998)
MUSG00000030337	2613.45	5263.62	2.01	1.06E-10	4.55E-08	*Vamp1*	Vesicle-associated membrane protein 1	Expressed in hair cells (Safieddine and Wenthold, 1999)

Using standard nomenclature in the field, autosomal dominant forms of human hearing loss are denoted as DFNA and autosomal recessive forms as DFNB. OHC-specific genes are highlighted in purple. FDR, false detection rate; OHC, outer hair cell; SGN, spiral ganglion neuron.

To gain insight to the biological processes and functional pathways that may be regulated by helios, the dysregulated genes were analysed for Gene Ontology (GO) enrichments using the Search Tool for the Retrieval of Interacting Genes/Proteins (STRING) database version 10.0 (Franceschini et al., 2013, Jensen et al., 2009). GO analysis demonstrated significant enrichment of 13 biological processes within the 57 downregulated genes in *Ikzf2*$^{cello/cello}$ mutants at P8 (Table 6.5 and Table 9.5 in Appendix). Interestingly, this included a number of GO terms related to developmental and neuronal processes, including:

- Neuron differentiation
- Neurogenesis
- Organ morphogenesis
- Organ development
- System development
- Cell differentiation

Table 6.5: Gene ontology enrichment of biological processes within the 57 significantly downregulated genes identified by RNA-Seq analysis of *Ikzf2*$^{cello/cello}$ cochleae at postnatal day 8.

GO ID	GO Term	Number of Genes	p Value Bonferroni-Corrected
GO:0030182	neuron differentiation	14	7.56E-05
GO:0048699	generation of neurons	15	2.47E-03
GO:0003310	pancreatic A cell differentiation	3	3.82E-03
GO:0022008	neurogenesis	15	5.45E-03
GO:0044707	single-multicellular organism process	31	1.02E-02
GO:0009887	organ morphogenesis	12	1.09E-02
GO:0048513	organ development	20	1.17E-02
GO:0006936	muscle contraction	6	1.36E-02
GO:0048731	system development	23	1.38E-02
GO:0032501	multicellular organismal process	31	1.85E-02
GO:0009888	tissue development	15	1.89E-02
GO:0021510	spinal cord development	5	2.15E-02
GO:0030154	cell differentiation	21	4.14E-02

GO, gene ontology.

Within the 219 significantly upregulated genes in *Ikzf2*$^{cello/cello}$ mice at P8, GO analysis demonstrated significant enrichment of 15 biological processes (Table 6.6 and Table 9.6 in Appendix). Interestingly, all of these were related to ion transport, such as:

- Voltage-gated potassium channel activity
- Ion channel activity
- Gated channel activity

Table 6.6: Gene ontology enrichment of biological processes within the 219 significantly upregulated genes identified by RNA-Seq analysis of *Ikzf2*$^{cello/cello}$ cochleae at postnatal day 8.

GO ID	GO Term	Number of Genes	p Value Bonferroni-Corrected
GO:0022843	voltage-gated cation channel activity	8	1.30E-04
GO:0005261	cation channel activity	10	1.64E-04
GO:0046873	metal ion transmembrane transporter activity	11	2.76E-04
GO:0015077	monovalent inorganic cation transmembrane transporter activity	10	5.19E-04
GO:0005249	voltage-gated potassium channel activity	6	9.54E-04
GO:0022890	inorganic cation transmembrane transporter activity	11	2.69E-03
GO:0008324	cation transmembrane transporter activity	12	2.78E-03
GO:0005267	potassium channel activity	6	5.32E-03
GO:0015079	potassium ion transmembrane transporter activity	6	1.58E-02
GO:0005251	delayed rectifier potassium channel activity	4	3.58E-02
GO:0005216	ion channel activity	7	1.93E-01
GO:0005244	voltage-gated ion channel activity	5	2.38E-01
GO:0015267	channel activity	7	3.67E-01
GO:0022836	gated channel activity	6	8.51E-01
GO:0005272	sodium channel activity	3	8.73E-01

GO, gene ontology.

Together, this suggests that helios plays a key role in regulating development and auditory transduction within the cochlea. Although many interesting dysregulated genes were identified by RNA-Seq of *Ikzf2*$^{cello/cello}$ cochleae, due to time constraints, two genes were

selected for further investigation: *Slc26a5* and *Ocm.* As both of these are OHC-specific and therefore expressed within the same cell type as helios itself, they were considered most likely to be direct downstream targets of helios.

6.2.1.1. Parallel Validation of RNA-Seq Results

To validate the reduction in *Slc26a5* and *Ocm* expression in *Ikzf2*$^{cello/cello}$ mutants, qRT-PCR was carried out by Dr Ronna Hertzano, Dr Beatrice Milon and Maggie Matern at the University of Maryland using two cochlear RNA samples from P8 *Ikzf2*$^{+/+}$, *Ikzf2*$^{cello/+}$ and *Ikzf2*$^{cello/cello}$ mice. Each sample comprised a pool of two pairs sub-dissected cochlear ducts, which were collected from mice independent of those used for the RNA-Seq experiment.

Alongside this, the expression of a number OHC-enriched, IHC-enriched and hair cell-expressed transcripts was also investigated to further search for potential target genes of helios and determine if the *cello* mutation causes a global disruption of the OHCs. These transcripts were selected based on data from a recently published hair cell subtype-specific study (Liu et al., 2014), which generated gene expression profiles for 2000 individually collected IHCs and OHCs from adult (P25 – P30) mouse cochleae using microarray. A total of 16 genes were examined by qRT-PCR; this included *Atp8a2, Atp8b1, Dnm3, Elovl2, Kcnq4, Lbh, Ociad2, Ocm, Plbd1, Slc26a5* and *Strc* as genes enriched in the OHCs (by at least 2-fold); *Atp2a3* as a gene enriched in the IHCs (by at least 2-fold); and *Gfi1*, *Myo6, Myo7a* and *Pou4f3* as genes expressed in both the IHCs and OHCs.

Results demonstrated that two of the OHC-enriched genes, *Elovl2* and *Slc26a5,* were significantly dysregulated in *Ikzf2*$^{cello/cello}$ mutants at P8 (Figure 6.3 A). Although not identified in the original RNA-Seq dataset, *Elovl2* showed a significant 192% increase in *Ikzf2*$^{cello/cello}$ mutants compared to *Ikzf2*$^{+/+}$ controls. Interestingly, a 89% increase in *Elovl2*

expression was also detected in *Ikzf2*$^{cello/+}$ animals compared to *Ikzf2*$^{+/+}$ controls, although this was not statistically significant. Conversely, *Slc26a5* was significantly decreased by 47% in *Ikzf2*$^{cello/cello}$ mutants compared to *Ikzf2*$^{+/+}$ controls, which is consistent with the -2.31-fold change (57% decrease) identified by RNA-Seq. *Ikzf2*$^{cello/+}$ animals also exhibited a milder, non-significant 24% decrease in *Slc26a5* expression compared to *Ikzf2*$^{+/+}$ controls.

A reduction in *Ocm* expression was also detected in *Ikzf2*$^{cello/cello}$ mutants, decreased by 63% compared to *Ikzf2*$^{+/+}$ controls. This was not statistically significant, which suggests that the initial RNA-Seq result for *Ocm* may be a false positive. However, given this 63% reduction is consistent with the -4.30-fold change (77% decrease) identified by RNA-Seq, this could also suggest that the current qRT-PCR study is underpowered due to the low number of biological replicates (n = 2).

The remaining OHC-enriched transcripts (*Atp8a2, Atp8b1, Dnm3, Kcnq4, Lbh, Ociad2, Plbd1* and *Strc*) were found to be expressed at similar levels in all genotypes (Figure 6.3 A). Furthermore, no significant changes in transcript levels were detected for the IHC-enriched gene (*Atp2a3*) or the IHC/OHC-expressed genes (*Gfi1, Myo6*, *Myo7a* and *Pou4f3*) (Figure 6.3 B). Interestingly, the RNA-Seq results demonstrating a -2.36-fold change (58% decrease) in *Strc* and a -1.81-fold change (45% decrease) in *Pou4f3* were not validated by qRT-PCR, again suggesting they may be false positives.

To more conclusively investigate the expression of these 16 transcripts in *cello* mice, this qRT-PCR experiment should be expanded to include at least six biological replicates per genotype group.

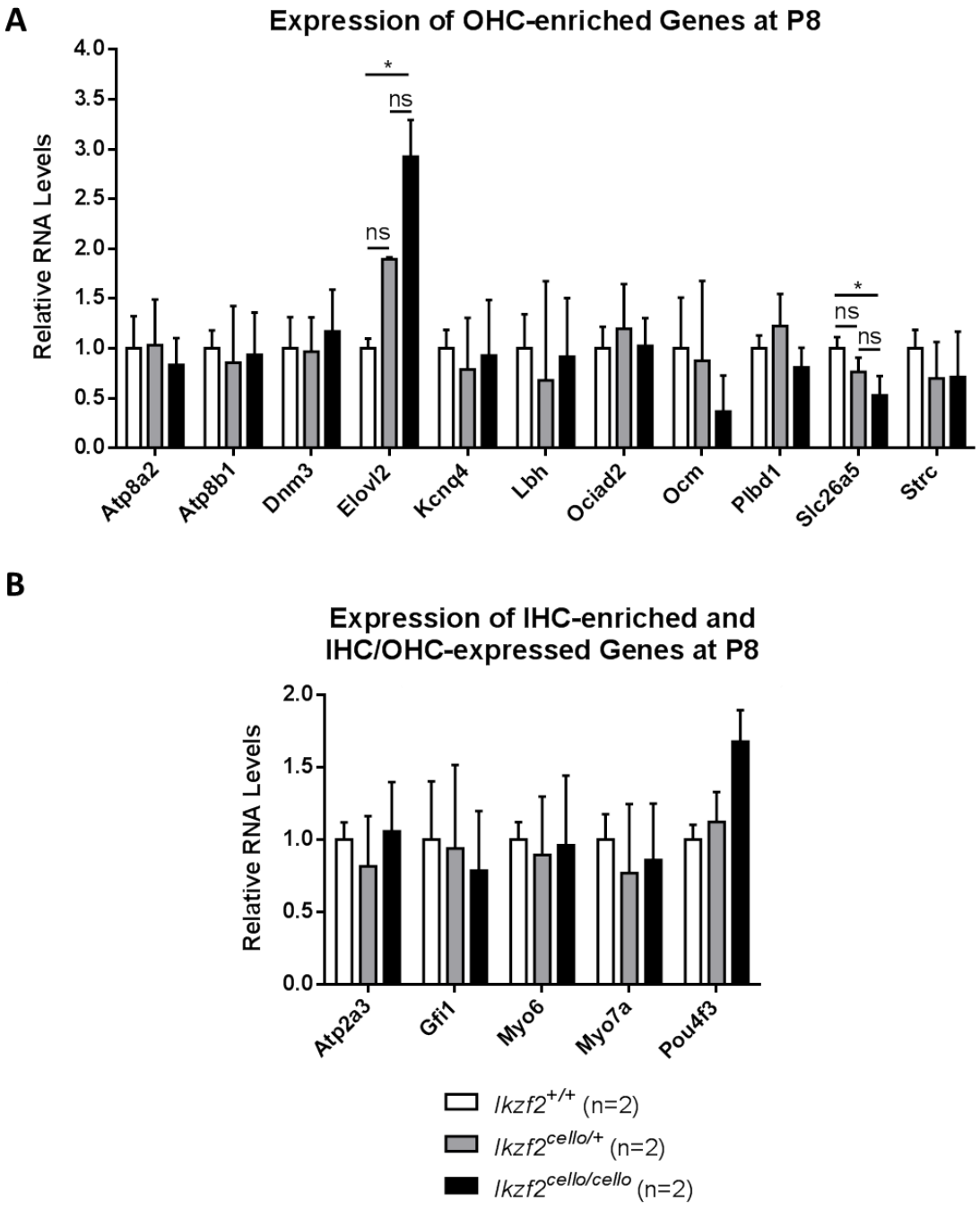

Figure 6.3: Expression levels of select outer hair cell-enriched, inner hair cell-enriched and hair cell-expressed genes in *Ikzf2*$^{+/+}$, *Ikzf2*$^{cello/+}$ and *Ikzf2*$^{cello/cello}$ cochleae at postnatal day 8.

To validate RNA-Seq results and identify additional potential targets of helios, the expression of select OHC-enriched, IHC-enriched and hair cell-expressed transcripts was investigated in *Ikzf2*$^{+/+}$, *Ikzf2*$^{cello/+}$ and *Ikzf2*$^{cello/cello}$ cochlear duct total RNA at P8. **(A)** Two of the OHC-enriched genes were found to be significantly dysregulated in *Ikzf2*$^{cello/cello}$ mutants: *Elovl2* was increased by 192%, whilst *Slc26a5* was decreased by 47% in *Ikzf2*$^{cello/cello}$ cochleae compared to *Ikzf2*$^{+/+}$ controls. Although not statistically significant, *Ocm* was reduced by 63% in *Ikzf2*$^{cello/cello}$ mutants compared to *Ikzf2*$^{+/+}$ controls. The reduction in *Slc26a5* and *Ocm* expression in *Ikzf2*$^{cello/cello}$ mice reflects the results obtained from the *cello* RNA-Seq study. **(B)** The IHC-enriched gene (*Atp2a3*) and the IHC/OHC-expressed genes (*Gfi1, Myo6, Myo7a, Pou4f3*) were expressed at similar levels across all genotype groups. Data are shown as mean ± s.e.m. Statistical analysis: one-way ANOVA, * = $p \leq 0.05$. IHC, inner hair cell; OHC, outer hair cell; P, postnatal day.

6.2.1.2. Orthogonal Validation of RNA-Seq Results

To further investigate the reduction in *Slc26a5* and *Ocm* transcripts, the expression of the corresponding encoded proteins, prestin and oncomodulin, was qualitatively assessed by immunolabelling of P8 cochlear vibratome sections. Unfortunately, due to availability of animals, *Ikzf2*$^{+/+}$ tissue was not available and so *Ikzf2*$^{cello/+}$ cochleae were used as the experimental control.

In *Ikzf2*$^{cello/+}$ cochleae, prestin labelling was localised specifically to the OHCs and was not observed in the IHCs (Figure 6.4 A). Prestin was also detected in the OHCs of *Ikzf2*$^{cello/cello}$ mice, with a potential slight reduction in labelling intensity compared to *Ikzf2*$^{cello/+}$ mice (Figure 6.4 B). As mentioned above, relative fluorescence was not quantified and this was only a qualitative observation. It important to bear in mind that, in addition to the significant 47% reduction in *Slc26a5* expression in *Ikzf2*$^{cello/cello}$ mutants, qRT-PCR data also showed a 24% reduction in *Slc26a5* in *Ikzf2*$^{cello/+}$ animals compared to *Ikzf2*$^{+/+}$ controls, although this was not statistically significant. As such, it may be that the corresponding ~30% reduction in prestin protein levels in *Ikzf2*$^{cello/cello}$ mice compared to *Ikzf2*$^{cello/+}$ mice is not easily detectable using a qualitative immunolabelling technique.

Oncomodulin labelling was observed in the OHCs of both *Ikzf2*$^{cello/+}$ and *Ikzf2*$^{cello/cello}$ mice using equivalent imaging parameters, although at a reduced intensity in *Ikzf2*$^{cello/cello}$ mice (Figure 6.4 C-D). Although this was not quantified, this is consistent with RNA-Seq and qRT-PCR results, which suggests that *Ocm* expression may be decreased in *Ikzf2*$^{cello/cello}$ animals compared to both *Ikzf2*$^{+/+}$ and *Ikzf2*$^{cello/+}$ mice.

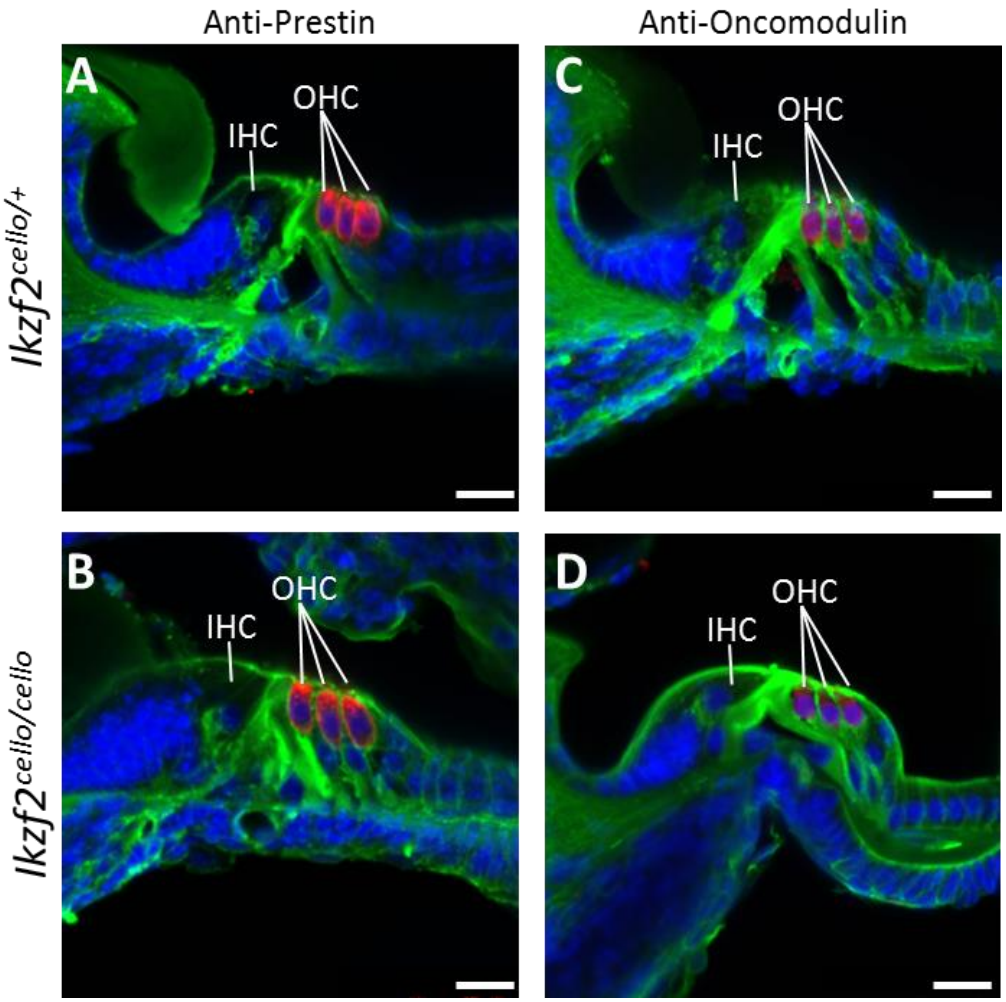

Figure 6.4: Prestin and oncomodulin immunolabelling of *Ikzf2*$^{cello/+}$ and *Ikzf2*$^{cello/cello}$ vibratome cochlear sections at postnatal day 8.

Prestin and oncomodulin expression was assessed in mid-modiolar vibratome sections from postnatal day 8 *Ikzf2*$^{cello/+}$ (n = 3) and *Ikzf2*$^{cello/cello}$ (n = 3) cochleae. Samples were labelled with DAPI (blue) to stain nuclei, anti-β-actin with an Alexa Fluor® 488 secondary antibody (green) and either anti-prestin or anti-oncomodulin with an Alexa Fluor® 568 secondary antibody (red). Representative images are shown. **(A)** In *Ikzf2*$^{cello/+}$ cochleae, prestin labelling localised to the three rows of OHCs and was not detected in the IHCs. **(B)** Prestin labelling was also observed in *Ikzf2*$^{cello/cello}$ OHCs, with no obvious difference in intensity compared to littermate *Ikzf2*$^{cello/+}$ controls. **(C)** In *Ikzf2*$^{cello/+}$ cochleae, oncomodulin labelling localised specifically to the three rows of OHCs. **(D)** Oncomodulin labelling was also detected in *Ikzf2*$^{cello/cello}$ cochleae, at a reduced intensity compared to *Ikzf2*$^{cello/+}$ controls (x40 magnification, scale bar = 20 µm). IHC, inner hair cell; OHC, outer hair cell.

6.2.2. Electrophysiological Analysis

RNA-Seq results demonstrated significant dysregulation of a plethora of genes in *Ikzf2*$^{cello/cello}$ cochleae at P8. Whilst phenotypic characterisation of the *cello* pedigree revealed that *Ikzf2*$^{cello/cello}$ mice have severely elevated auditory thresholds at P16 (Figure 5.1), their hair cells are initially similar in number and morphological appearance to those of *Ikzf2*$^{+/+}$ and *Ikzf2*$^{cello/+}$ littermates (Figure 5.9). A significant reduction in OHC number was not observed in *Ikzf2*$^{cello/cello}$ animals until three months of age (Figure 5.10). This indicates that something other than OHC loss underlies the hearing impairment in *cello* mutants, which is likely dysregulation of helios target genes leading to OHC dysfunction.

To investigate the effect of the *cello* mutation on OHC development and function, electrophysiological analyses were undertaken by Professor Walter Marcotti and Dr Stuart Johnson at the University of Sheffield (UK). Due to experimental design and the breeding scheme employed, OHCs from *Ikzf2*$^{cello/+}$ mice rather than *Ikzf2*$^{+/+}$ mice were used as controls. Importantly, the auditory thresholds, hair cell morphology and hair cell counts of *Ikzf2*$^{cello/+}$ mice are comparable to those of *Ikzf2*$^{+/+}$ animals (Figure 5.1, Figure 5.2, Figure 5.14 and Figure 9.5 in Appendix).

Electrophysiological analyses comprised patch-clamp recordings of potassium currents, MET currents and electromotile activity from single apical-coil OHCs from *Ikzf2*$^{cello/+}$ (control) and *Ikzf2*$^{cello/cello}$ littermates.

6.2.2.1. Potassium Current Recordings

In mouse OHCs, the onset of adult-like characteristics occurs at around P8 (Marcotti and Kros, 1999) and is associated with the expression of the negatively-activating potassium current $I_{K,n}$, which is carried by the KCNQ4 channel (Kubisch et al., 1999). To gain insight into

the maturation state of the OHCs, potassium currents were elicited by applying a series of voltage steps in 10 mV increments from the holding potential of -64 mV.

Interestingly, during these patch-clamp experiments, membrane capacitance was found to be significantly reduced in OHCs from P16 – P18 *Ikzf2*$^{cello/cello}$ mice compared to *Ikzf2*$^{cello/+}$ controls (Figure 6.5). This indicates reduced OHC surface area in *Ikzf2*$^{cello/cello}$ mutants.

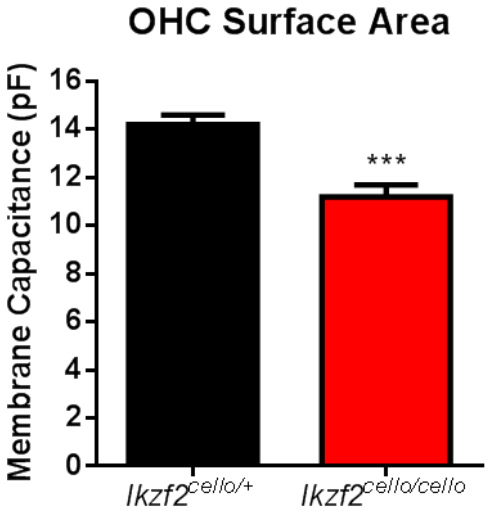

Figure 6.5: Surface area of adult outer hair cells from *Ikzf2*$^{cello/+}$ and *Ikzf2*$^{cello/cello}$ littermates.
Apical-coil OHCs from P16 – P18 *Ikzf2*$^{cello/+}$ (n = 9) and *Ikzf2*$^{cello/cello}$ (n = 7) littermates were analysed using single cell patch-clamp. *Ikzf2*$^{cello/cello}$ OHCs had a significantly reduced membrane capacitance compared to *Ikzf2*$^{cello/+}$ OHCs, which indicates reduced cell surface area. Data are shown as mean ± s.e.m. Statistical analysis: unpaired *t*-test, *** = p≤0.001. OHC, outer hair cell; pF, picofadar.

Adult *Ikzf2*$^{cello/cello}$ OHCs were found to express the same complement of potassium currents as *Ikzf2*$^{cello/+}$ littermate controls (Figure 6.6 A-C). Although the size of the $I_{K,n}$ current and the total outward potassium current, which includes both $I_{K,n}$ and the classical delayed rectifier potassium current I_K (Marcotti and Kros, 1999), were smaller in *Ikzf2*$^{cello/cello}$ OHCs compared to *Ikzf2*$^{cello/+}$ OHCs (Figure 6.6 A-B), this was not significant once normalised to the reduced surface area of *Ikzf2*$^{cello/cello}$ OHCs (Figure 6.6 D-E). The resting membrane potential (V_m) of OHCs, measured as zero-current potential, was also similar between the two genotypes

(Figure 6.6 C). Together, these data indicate that the *cello* mutation does not affect the normal expression of ion channels in developing OHCs.

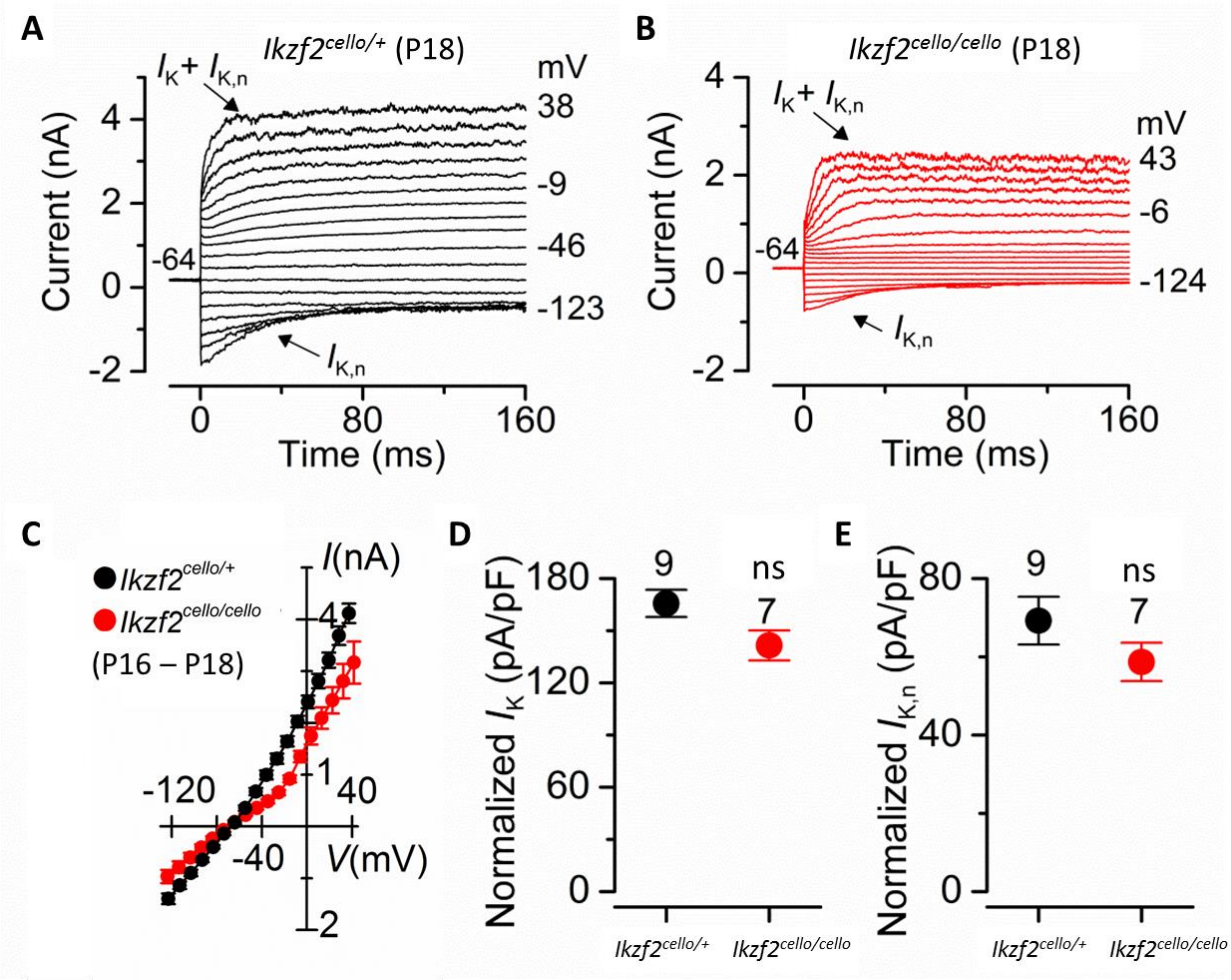

Figure 6.6: Potassium current responses in mature outer hair cells from *Ikzf2*$^{cello/+}$ and *Ikzf2*$^{cello/cello}$ littermates.

Apical-coil OHCs from P16 – P18 *Ikzf2*$^{cello/+}$ (n = 9) and *Ikzf2*$^{cello/cello}$ (n = 7) littermates were analysed using single cell patch-clamp. Potassium currents were elicited from **(A)** *Ikzf2*$^{cello/+}$ and **(B)** *Ikzf2*$^{cello/cello}$ OHCs by applying depolarising voltage steps from -124 mV and the holding potential of -64 mV in 10 mV increments. *Ikzf2*$^{cello/cello}$ OHCs had a significantly reduced total outward potassium current at 0 mV, which includes both I_K and $I_{K,n}$ (*Ikzf2*$^{cello/+}$: 2342 ± 89 pA; *Ikzf2*$^{cello/cello}$: 1593 ± 151 pA; p = <0.001). The isolated $I_{K,n}$ current, measured between the -64 mV holding potential and -124 mV, was also significantly reduced in *Ikzf2*$^{cello/cello}$ OHCs compared to *Ikzf2*$^{cello/+}$ (*Ikzf2*$^{cello/+}$: 972 ± 73 pA; *Ikzf2*$^{cello/cello}$: 663 ± 77 pA; p = <0.05). **(C)** Average peak current-voltage relationship for the total potassium current recorded from *Ikzf2*$^{cello/+}$ and *Ikzf2*$^{cello/cello}$ OHCs. After normalisation to OHC membrane capacitance, the **(D)** total I_K current and **(E)** isolated $I_{K,n}$ current were not significantly different in *Ikzf2*$^{cello/cello}$ OHCs compared to *Ikzf2*$^{cello/+}$ OHCs. Data are shown as mean ± s.e.m. Statistical analysis: unpaired *t*-test, ns = not significant. Graphs prepared by Professor Walter Marcotti and Dr Stuart Johnson at the University of Sheffield. I_K, classical delayed rectifier potassium current; $I_{K,n}$, negatively-activating delayed rectifier potassium current; nA, nanoampere; ms, millisecond; mV, millivolt; P, postnatal day; pA, picoampere; pF, picofadar; V_m, resting membrane potential.

6.2.2.2. Mechanoelectrical Transducer (MET) Current Recordings

MET currents were recorded from P9 OHCs by displacing their hair bundles in excitatory and inhibitory directions using a piezo-driven fluid-jet (Corns et al., 2014). At hyperpolarised membrane potentials (-121 mV), the displacement of the hair bundle in the excitatory direction (towards the tallest stereocilia) elicited a large inward MET current from both *Ikzf2*$^{cello/+}$ and *Ikzf2*$^{cello/cello}$ OHCs (Figure 6.7 A-B, arrowheads). Conversely, displacement of the hair bundle in the inhibitory direction (away from the tallest stereocilia) reduced the resting current in *Ikzf2*$^{cello/+}$ and *Ikzf2*$^{cello/cello}$ OHCs, indicating closure of the MET channels (Figure 6.7 A-B, arrows). The maximal MET current in *Ikzf2*$^{cello/cello}$ OHCs was not found to be significantly different to that in *Ikzf2*$^{cello/+}$ OHCs (Figure 6.7 C). Because the MET current reverses near 0 mV, it became outward when excitatory bundle stimulation was applied during voltage steps positive to its reversal potential (Figure 6.7 D). Subsequently, at positive membrane potentials (+99 mV), excitatory bundle stimulation elicited an outward MET current from both *Ikzf2*$^{cello/+}$ and *Ikzf2*$^{cello/cello}$ OHCs with larger resting amplitudes, which are due to an increased open probability of the MET channel (Figure 6.7 A-B, asterisks). Overall, these results indicate that there are no differences in MET channel currents or function in *Ikzf2*$^{cello/cello}$ OHCs compared to *Ikzf2*$^{cello/+}$ OHCs.

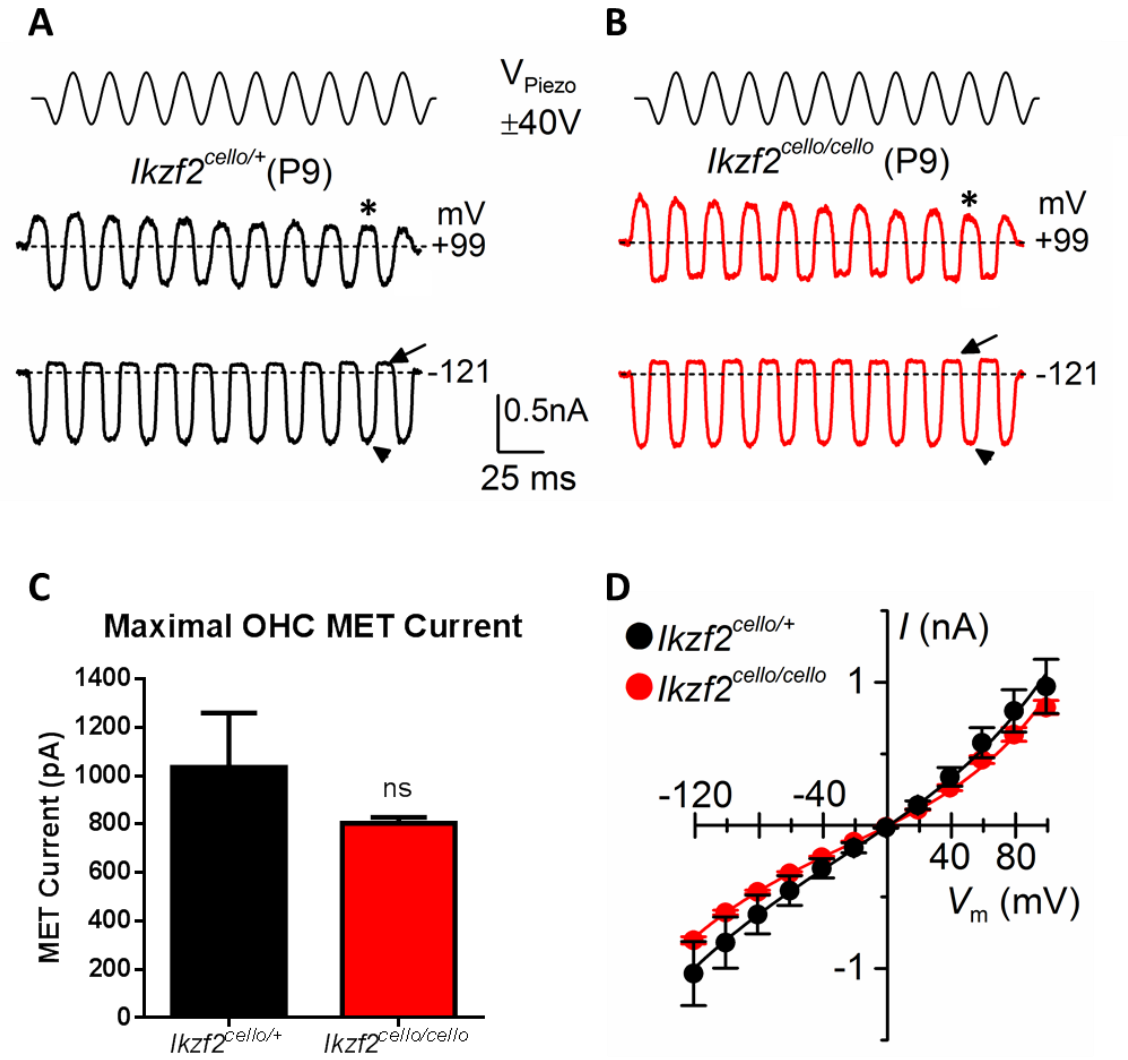

Figure 6.7: Mechanoelectrical transducer currents in mature outer hair cells from *Ikzf2*$^{cello/+}$ and *Ikzf2*$^{cello/cello}$ littermates.

Apical-coil OHCs from P9 *Ikzf2*$^{cello/+}$ (n = 4) and *Ikzf2*$^{cello/cello}$ (n = 3) littermates were analysed using single cell patch-clamp. Saturating MET currents were recorded from **(A)** *Ikzf2*$^{cello/+}$ and **(B)** *Ikzf2*$^{cello/cello}$ OHCs by applying a series of voltage steps from -121 mV to +99 mV in 20 mV increments and displacing hair bundles using a 50 Hz sinusoidal force stimuli (the driver voltage to the fluid jet is shown above the traces). For clarity, MET current traces are only shown for two voltage steps. Dashed lines indicate the holding current at the holding potential of -81 mV. At hyperpolarised membrane potentials (-121 mV), excitatory bundle stimulation elicited a large inward MET current in both *Ikzf2*$^{cello/+}$ and *Ikzf2*$^{cello/cello}$ OHCs (arrowheads), whilst inhibitory bundle stimulation closed the MET channels and reduced the resting current (arrows). At positive membrane potentials (+99 mV), excitatory bundle stimulation elicited an outward MET current in both *Ikzf2*$^{cello/+}$ and *Ikzf2*$^{cello/cello}$ OHCs with larger resting amplitudes (asterisks). **(C)** At -121 mV, the maximal MET current elicited from *Ikzf2*$^{cello/cello}$ OHCs was not significantly different to that in *Ikzf2*$^{cello/+}$ OHCs. **(D)** Peak-to-peak current-voltage curves do not show any significant differences between *Ikzf2*$^{cello/+}$ OHCs (n = 10) and *Ikzf2*$^{cello/cello}$ OHCs (n = 8). Data are shown as mean ± s.e.m. Statistical analysis: unpaired *t*-test, ns = not significant. Graphs **A, B** and **D** prepared by Professor Walter Marcotti and Dr Stuart Johnson at the University of Sheffield. nA, nanoampere; MET, mechanoelectrical transduction; mV, millivolt; OHC, outer hair cell; P, postnatal day; pA, picoampere; V, volt; V_m, resting membrane potential.

6.2.2.3. Electromotility Analysis

In the mouse, the onset of prestin-mediated electromotile activity occurs at ~P8 and is characteristic of mature OHCs (Ashmore, 1987, Brownell et al., 1985). In response to depolarising currents, prestin contracts and OHCs shorten, while hyperpolarisation induces elongation of prestin and lengthening of OHCs (Song and Santos-Sacchi, 2010). As a result of these oscillations in length, OHCs amplify sound signals during sound transduction and enhance cochlear sensitivity.

RNASeq and qRT-PCR data showed a significant reduction in *Slc26a5* expression in *Ikzf2*$^{cello/cello}$ cochleae. To investigate the effect of the *cello* mutation on electromotility, adult OHCs from P16 – P18 *Ikzf2*$^{cello/+}$ and *Ikzf2*$^{cello/cello}$ littermates were patch-clamped and measured following a depolarising voltage step by imaging the membrane at the base of the cells. Stepping the membrane potential from the -64 mV holding potential to +56 mV caused OHCs from both *Ikzf2*$^{cello/+}$ and *Ikzf2*$^{cello/cello}$ mice to shorten, as previously described (Ashmore, 1987, Brownell et al., 1985, Marcotti and Kros, 1999) (Figure 6.8 A-D). However, *Ikzf2*$^{cello/+}$ OHCs moved 548 nm on average whilst *Ikzf2*$^{cello/cello}$ OHCs moved only 138 nm, a ~75% reduction (Figure 6.8 E). This decrease in electromotility remained highly significant even after normalisation to the reduced cell size (Figure 6.8 F).

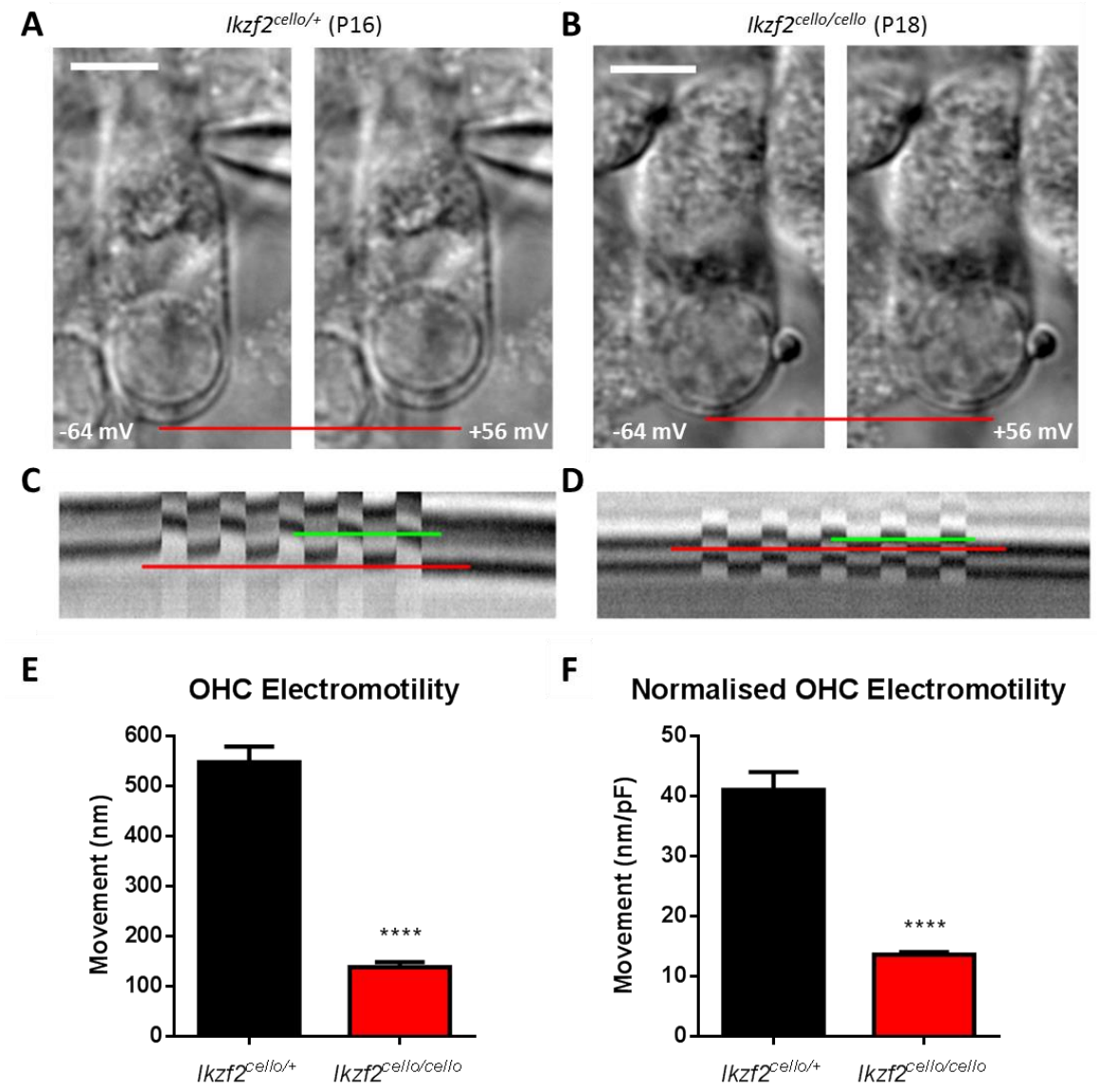

Figure 6.8: Electromotile activity in mature outer hair cells from *Ikzf2*$^{cello/+}$ and *Ikzf2*$^{cello/cello}$ littermates.
Apical-coil OHCs from P16 – P18 *Ikzf2*$^{cello/+}$ (n = 10) and *Ikzf2*$^{cello/cello}$ (n = 21) littermates were analysed using single cell patch-clamp. Voltage-dependent motility was measured by imaging the membrane at the base of **(A)** *Ikzf2*$^{cello/+}$ and **(B)** *Ikzf2*$^{cello/cello}$ OHCs in response to a depolarising voltage step from the holding potential of -64 mV to +56 mV. OHCs from both *Ikzf2*$^{cello/+}$ and *Ikzf2*$^{cello/cello}$ were found to shorten, as shown by the red lines which indicate the position of the basal membrane before (left) and during (right) the voltage step (scale bar = 5 µm). Fiji software was used create time-based z-stack projections of movement in a **(C)** *Ikzf2*$^{cello/+}$ and a **(D)** *Ikzf2*$^{cello/cello}$ OHC. The red lines indicate the resting position of the OHC basal membrane and the green lines indicate the movement of the OHC in response to the depolarising voltage step. Quantification of this distance revealed that the *Ikzf2*$^{cello/+}$ OHC moved 690 nm, whilst the *Ikzf2*$^{cello/cello}$ OHC moved 207 nm. **(E)** The average movement of OHCs in response to the depolarising voltage step was significantly reduced in *Ikzf2*$^{cello/cello}$ mutants compared to *Ikzf2*$^{cello/+}$ mice. **(F)** Even after normalisation to membrane capacitance, the reduction in electromotility of *Ikzf2*$^{cello/cello}$ OHCs remained highly significant compared to *Ikzf2*$^{cello/+}$ OHCs. Data are shown as mean ± s.e.m. Statistical analysis: unpaired *t*-test, **** = p≤0.0001. Images prepared by Professor Walter Marcotti and Dr Stuart Johnson at the University of Sheffield. mV, millivolt; nm, nanometer; OHC, outer hair cell; P, postnatal day; pF, picofadar.

6.2.3. Luciferase Reporter Assays

RNASeq, qRT-PCR and electrophysiology data showed a reduction in *Slc26a5* and *Ocm* levels, as well as decreased OHC electromotility in *Ikzf2*$^{cello/cello}$ cochleae. Together, this data suggests that helios may be regulating *Slc26a5* and *Ocm*. A series of luciferase reporter assays were undertaken to establish whether helios interacts with the *Slc26a5* and *Ocm* promoters and to quantify the transcriptional capacity of WT helios compared to the H517Q mutant.

The promoter region of *Slc26a5* (Gross et al., 2011a, Gross et al., 2011b) was amplified and cloned upstream of firefly luciferase (Figure 6.9 A), then co-transfected into mammalian cells with c-Myc-tagged WT and/or c-Myc-tagged H517Q helios constructs to mimic wild-type, heterozygous and homozygous states. Prior to analysis, firefly luciferase activity was normalised to that of an internal *Renilla* luciferase control. Co-expression of the *Slc26a5* promoter with WT helios alone resulted in a significant 2.08-fold increase in luciferase activity relative to that observed in transfections with the c-Myc empty vector (Empty) (Figure 6.9 B). A significant 1.74-fold increase in relative luciferase activity was also recorded following co-transfection with both WT and H517Q helios, mimicking the heterozygous state (Figure 6.9 B). Interestingly, this level of transactivation is slightly reduced compared to transfections with just WT helios. Transactivation of the *Slc26a5* promoter with H517Q helios alone did not have a significant effect on luciferase activity, resulting in only a 1.17-fold increase in transcriptional activity relative to Empty (Figure 6.9 B). Together, these data suggest that *Slc26a5* is a primary target of helios and transactivation of the *Slc26a5* promoter by helios is impaired by the *cello* mutation.

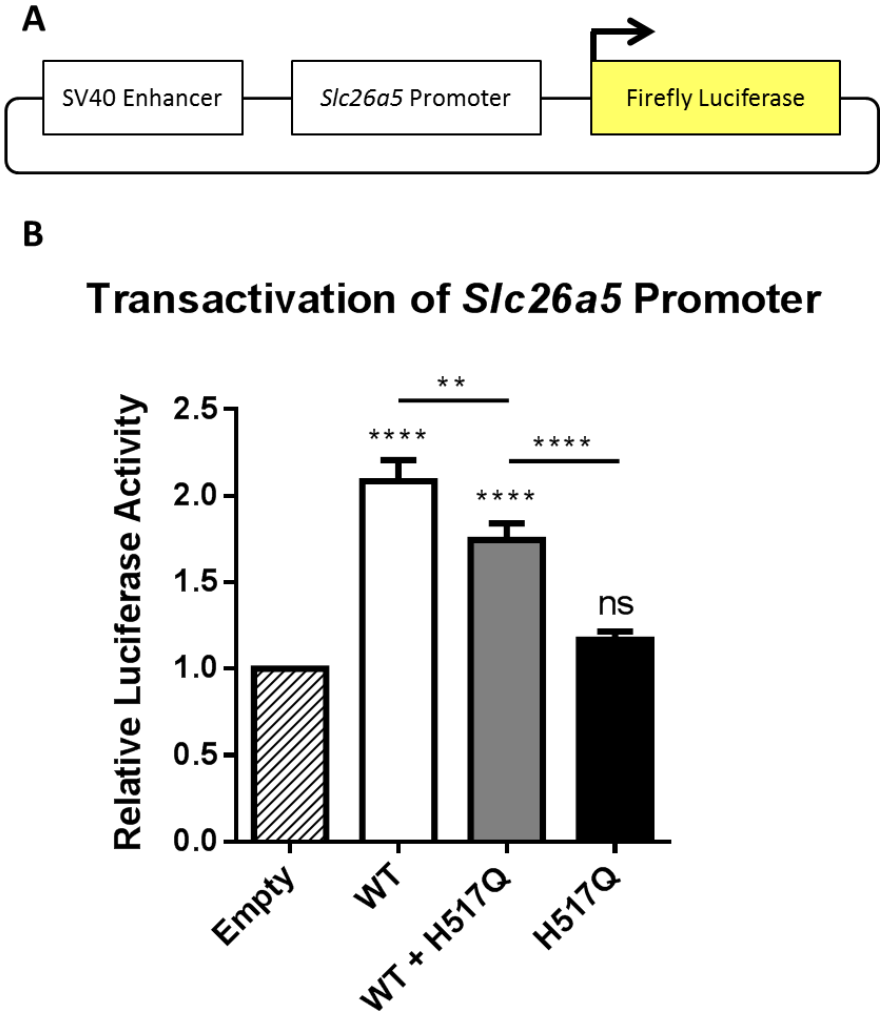

Figure 6.9: Luciferase reporter assays to assess activity of helios on the *Slc26a5* promoter.
(A) The promoter region of *Slc26a5* was cloned into the pGL3-Enhancer luciferase reporter vector, where it was positioned downstream of the SV40 enhancer element and upstream of the firefly luciferase gene. **(B)** The pGL3-Enhancer vector containing the *Slc26a5* promoter was co-transfected with the *Renilla* luciferase plasmid into HEK293T cells, along with c-Myc-tagged WT helios, c-Myc-tagged H517Q helios or c-Myc empty vector. A total of nine co-transfections were performed for each group, over three separate experiments. Luminescence was assayed 24 hours post-transfection using the Dual-Luciferase® Assay Reporter System (Promega). For each sample, firefly luciferase activity was normalised to that of the *Renilla* plasmid in order to control for transfection efficiency. Co-expression of WT helios and the *Slc26a5* promoter resulted in a significant increase in relative luciferase activity, 2.08-fold above that observed in transfections with Empty. To mimic a heterozygous state, both WT and H517Q helios were expressed in combination with the *Slc26a5* promoter. This caused a significant 1.74-fold increase in luciferase activity relative to Empty, but weaker transactivation than that detected when using WT helios alone. Transfection of H517Q helios alone with the *Slc26a5* promoter did not significantly increase luciferase activity relative to Empty. Data are shown as mean ± s.e.m. Statistical analysis: two-way ANOVA, ns = not significant, ** = $p \leq 0.01$, **** = $p \leq 0.0001$. Empty, c-Myc empty vector; H517Q, c-Myc-tagged H517Q helios; WT, c-Myc-tagged WT helios.

As no reports of the *Ocm* promoter sequence were found in the literature, a region immediately upstream of the ATG start codon that contained a 'GGGAA' core IKZF binding motif (Bao et al., 2004, Georgopoulos et al., 1994, Molnar and Georgopoulos, 1994, Perdomo et al., 2000) was selected for analysis. This proposed promoter sequence was amplified and cloned upstream of firefly luciferase (Figure 6.10 A), then used for luciferase reporter assays as before. Co-expression of the proposed *Ocm* promoter sequence with helios in either the wild-type, heterozygous or homozygous state did not have a significant effect on luciferase activity relative to that observed in transfections with Empty (Figure 6.10 B).

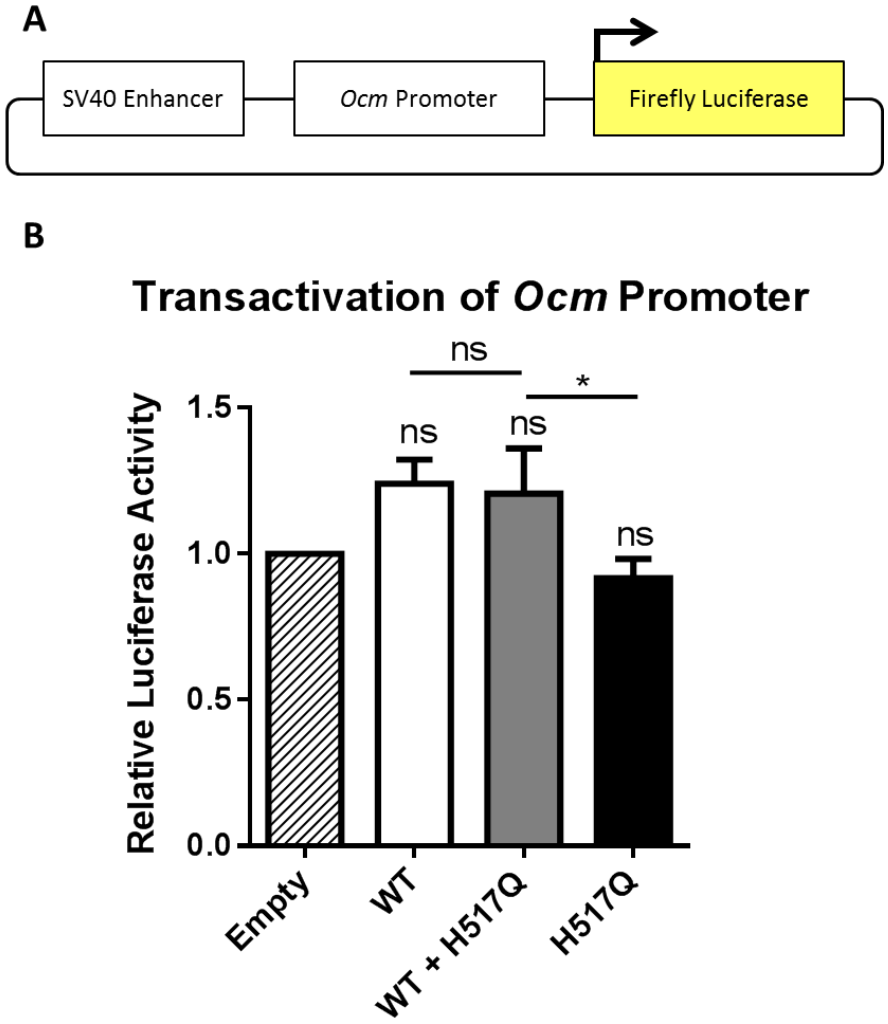

Figure 6.10: Luciferase reporter assays to assess activity of helios on a potential promoter of *Ocm*.
(A) A region of DNA proposed as the promoter sequence of *Ocm* was cloned into the pGL3-Enhancer luciferase reporter vector, where it was positioned downstream of the SV40 enhancer element and upstream of the firefly luciferase gene. **(B)** The pGL3-Enhancer vector containing the proposed *Ocm* promoter was co-transfected with the *Renilla* luciferase plasmid into HEK293T cells, along with c-Myc-tagged WT helios, c-Myc-tagged H517Q helios or c-Myc empty vector. A total of six co-transfections were performed for each group, over two separate experiments. Luminescence was assayed 24 hours post-transfection using the Dual-Luciferase® Assay Reporter System (Promega). For each sample, firefly luciferase activity was normalised to that of the *Renilla* plasmid in order to control for transfection efficiency. Co-expression of WT helios and the proposed *Ocm* promoter sequence did not have a significant effect on luciferase activity relative to transfections with Empty. To mimic a heterozygous state, both WT and H517Q helios were expressed in combination with the proposed *Ocm* promoter sequence. Similarly to WT transfections, this did not significantly alter relative luciferase activity. Transfection of H517Q helios alone with the proposed *Ocm* promoter also had no effect on luciferase activity relative to Empty. Data are shown as mean ± s.e.m. Statistical analysis: two-way ANOVA, ns = not significant, * = $p \leq 0.05$. Empty, c-Myc empty vector; H517Q, c-Myc-tagged H517Q helios; WT, c-Myc-tagged WT helios.

6.3. Discussion

As previously detailed, *cello* mice have a loss-of-function mutation in helios that impairs homodimerisation and was hypothesised to disrupt the expression of helios target genes. In order to identify potential target genes of helios in the auditory system, transcriptome profiling of cochlear duct total RNA was carried out using RNA-Seq. A total of 467 genes showed significant differential expression in P8 *Ikzf2*$^{cello/cello}$ cochleae compared to *Ikzf2*$^{+/+}$ controls, however, only those with at least a 2-fold change in expression were further examined in this thesis. This comprised 57 downregulated genes and 219 upregulated genes, 41 of which have been previously shown to be expressed in the ear or mutated in mouse models or human forms of hearing loss. This included three OHC-specific genes, all of which were significantly downregulated in *Ikzf2*$^{cello/cello}$ cochleae: *Slc26a5* (prestin), which encodes the OHC motor protein; *Ocm* (oncomodulin), which is involved in calcium buffering; and *Strc* (stereocilin), which is required for stereocilia links. The remainder of these genes are either not restricted solely to the OHCs or are expressed in other cell types, including the IHCs and SGNs. This may suggest that helios is functioning outside of the OHC (although anti-helios immunolabelling has only been detected in the OHCs in this study) or that the dysregulation of OHC function causes effects on neighbouring non-sensory supporting cells.

Interestingly, a number of GO terms related to developmental and neuronal processes were significantly enriched within the 57 downregulated genes, including organ morphogenesis, cell differentiation and neuron differentiation, the latter of which is consistent with previous data showing that helios promotes neurogenesis in the developing striatum (Martin-Ibanez et al., 2012). Indeed, it may be that helios has a similar role in the developing cochlea, as well as potentially within the developing central auditory system. If this is so, defective

neural development and innervation may contribute directly to the early-onset hearing impairment observed in *Ikzf2*$^{cello/cello}$ mice at P16. As mentioned in Chapter 3, additional work should be undertaken to address this. Initially, this should involve immunolabelling of embryonic and neonatal cochlear wholemounts and brain sections using known neural and synaptic markers, as well as carrying out additional electrophysiological analyses and DPOAEs. Together, these experiments would provide insight into the effect of the *cello* mutation on neural development, morphology and function in *Ikzf2*$^{cello/cello}$ mice.

Although RNA-Seq highlighted numerous potential target genes and functional pathways that helios may be regulating, time constraints necessitated that further analysis focused on two differentially expressed genes: *Slc26a5* and *Ocm*. As both of these are expressed exclusively in OHCs, reflecting the expression pattern of helios itself, they were considered most likely to be direct targets of helios. *Slc26a5* and its encoded protein prestin are essential for OHC electromotility. In rodent OHCs, prestin is expressed at low levels from birth (Belyantseva et al., 2000, Souter et al., 1995, Zheng et al., 2000a) then progressively increases during the first postnatal week to reach adult levels by ~P9 – P10 (Abe et al., 2007, Belyantseva et al., 2000). Coincident with this, OHCs begin to acquire electromotile properties at ~P8 (He et al., 1994, Marcotti and Kros, 1999), which is vital for their development into functionally mature cochlear amplifiers (Ashmore, 1987, Brownell et al., 1985). During auditory transduction, mature OHCs undergo voltage-dependent changes in size (Kachar et al., 1986), providing electromechanical amplification that vastly improves sound detection by enhancing acoustic sensitivity and frequency selectivity (Dallos, 2008, Liberman et al., 2002). Importantly, electromotile responses are known to be enhanced by cholinergic efferent feedback, which alters OHC voltage sensitivity and membrane stiffness through calcium-dependent mechanisms (Dallos et al., 1997, Frolenkov et al., 2000,

Frolenkov, 2006, Sziklai et al., 2001). Oncomodulin is a calcium-binding protein, thought to be involved in cytosolic calcium buffering and sensing in the OHC (Sakaguchi et al., 1998b, Simmons et al., 2010). Although its function is not yet fully understood, previous studies have suggested a role in calcium-sensitive processes within the OHC, including the efferent modulation of electromotility (Sakaguchi et al., 1998b, Simmons et al., 2010, Yang et al., 2004).

Both *Slc26a5* and *Ocm* have previously been reported as deafness-causing genes. In prestin knock-out (*Slc26a5*$^{-/-}$) mice, OHCs are significantly shorter and OHC electromotility is completely abolished compared to *Slc26a5*$^{+/+}$ controls, which causes significantly elevated auditory thresholds at all frequencies from P14 (45 – 65 dB SPL higher than *Slc26a5*$^{+/+}$ mice) and progressive hair cell loss (Liberman et al., 2002, Wu et al., 2004). An intermediate OHC length and electromotility phenotype is observed in *Slc26a5*$^{+/-}$ heterozygotes and auditory thresholds are only moderately increased at the higher frequencies in these mice (~20 dB SPL higher than *Slc26a5*$^{+/+}$ controls at frequencies >30 dB SPL) (Liberman et al., 2002). In addition, deletion of oncomodulin in the mouse has recently been shown to cause progressive hearing loss (Simmons et al., 2015).

The expression of these two genes in *Ikzf2*$^{cello/cello}$ mutants was further investigated using qRT-PCR. This confirmed a significant 47% reduction in *Slc26a5* expression in *Ikzf2*$^{cello/cello}$ mice compared to *Ikzf2*$^{+/+}$ controls, validating the result obtained by RNA-Seq. A 63% reduction in *Ocm* expression was also detected in *Ikzf2*$^{cello/cello}$ mutants, although this was not statistically significant compared to *Ikzf2*$^{+/+}$ controls. It may be that the initial RNA-Seq result for *Ocm* was a false positive, particularly as analysis of differential gene expression using RNA-Seq is known to have a large false discovery rate (Rocke et al., 2015, Tarazona et

al., 2011). However, as this 63% reduction is largely consistent with the 77% decrease detected by RNA-Seq, this result may also be due to the low power of the current qRT-PCR experiment or even probe bias, whereby qRT-PCR may detect only certain transcript variants, whilst RNA-Seq can provide expression data for all gene isoforms (Wang et al., 2014). As such, *Ocm* expression should be further investigated, along with other unvalidated genes *Strc* and *Pou4f3*, by expanding the qRT-PCR study to incorporate additional biological replicates.

Dysregulation of *Slc26a5* and *Ocm* was also investigated at the protein level using immunolabelling of cochlear vibratome sections. A potential reduction was observed in prestin and oncomodulin labelling between *Ikzf2*$^{cello/+}$ and *Ikzf2*$^{cello/cello}$ mice, however, these observations were only qualitative and not quantitative. In addition, it is important to bear in mind that electrophysiology data showed that OHCs from *Ikzf2*$^{cello/cello}$ mice have a significantly decreased surface area compared to those from *Ikzf2*$^{cello/+}$ animals. As such, whilst *Ikzf2*$^{cello/cello}$ OHCs may express reduced levels of prestin and oncomodulin, these proteins are likely to be condensed into a smaller area than in *Ikzf2*$^{cello/+}$ control OHCs, which may result in an immunolabelling signal that appears similar in intensity and so is difficult to assess qualitatively. Ideally, this experiment should be repeated to include *Ikzf2*$^{+/+}$ controls, which would enable quantification of the relative fluorescence of immunolabelled tissue between all three genotypes.

qRT-PCR was also used to examine the expression of select OHC-enriched, IHC-enriched and IHC/OHC-expressed transcripts, which were identified from a recent dataset of adult (P25 – P30) IHC- and OHC-specific gene expression (Liu et al., 2014). One additional OHC-enriched gene was found to be signficantly disrupted in *cello* mice: a 192% increase in *Elovl2*

expression was detected in *Ikzf2*$^{cello/cello}$ mutants compared to *Ikzf2*$^{+/+}$ controls, as well as a milder, non-significant 89% increase in *Ikzf2*$^{cello/+}$ animals. *Elovl2* encodes the elongation of very long chain fatty acids-like 2 enzyme, which has been shown to play a role in lipid metabolism and homeostasis by catalysing the synthesis of very long chain fatty acids and triglycerides (Kobayashi et al., 2007, Pauter et al., 2014). Although *Elovl2* was identified as a top OHC-enriched gene in the Liu et al. (2014) dataset, to date, it has not been characterised in the auditory system or implicated in hearing loss. Examination of *Elovl2* expression using the SHIELD dataset indicates that it is initially expressed at high levels in cochlear GFP+ hair cells at E16 (420 read counts) before being downregulated during postnatal development (90 read counts at P0; 115 read counts at P4; 76 read counts at P7) (Figure 6.11). Interestingly, this decrease in *Elovl2* transcript levels in cochlear sensory hair cells occurs at around the onset of helios expression in the OHCs. Combined with the finding that *Elovl2* is expressed at higher levels in *Ikzf2*$^{cello/cello}$ mutants than *Ikzf2*$^{+/+}$ controls, this suggests that *Elovl2* may, in part, be transcriptionally repressed by helios. In the future, *Elovl2* mouse models could be employed to the further investigate the role of this gene in the mammalian auditory system and its requirement for auditory function. Given the increase in *Elovl2* observed in *Ikzf2*$^{cello/cello}$ mutants, an OHC over-expression model would be ideal. However, as it can be technically difficult to generate knock-in over-expression mouse models, ELOVL2 knock-out mice could initially be requested through the International Mouse Phenotyping Consortium (IMPC) for auditory phenotyping.

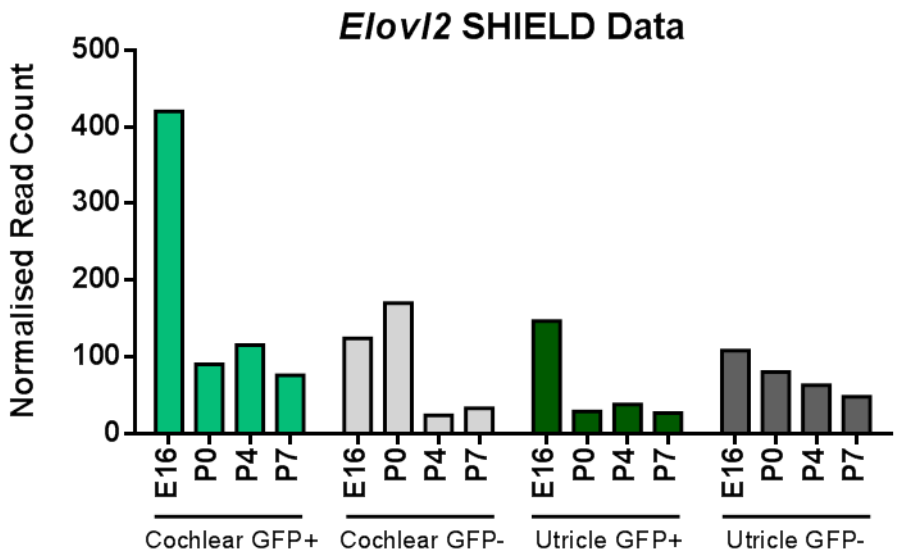

Figure 6.11: Expression of *Elovl2* in sorted cell populations from the mouse inner ear during development. The gene expression profile of *Elovl2* in the inner ear was obtained from the SHIELD website (https://shield.hms.harvard.edu/datasets.html). In this dataset, Scheffer et al. (2015) collected cochleae and utricles from transgenic mice expressing GFP driven by the *Pou4f3* promoter at four developmental stages: E16, P0, P4 and P7. Samples were then sorted into four distinct cell populations (cochlear GFP+ hair cells, cochlear GFP- surrounding non-sensory cells, utricle GFP+ hair cells and utricle GFP- surrounding non-sensory cells) prior to RNA-Seq. Results indicate that *Elovl2* is initially expressed at high levels in cochlear GFP+ hair cells at E16, but is then downregulated at subsequent postnatal time points. E, embryonic day; GFP, green fluorescent protein; P, postnatal day; SHIELD, Shared Harvard Inner Ear Laboratory Database.

To investigate the effect of the *cello* mutation on OHC development and function, electrophysiological analyses were carried out on OHCs from *Ikzf2*$^{cello/+}$ control and *Ikzf2*$^{cello/cello}$ littermates at early postnatal time points. During patch-clamp recordings, OHCs from P16 – P18 *Ikzf2*$^{cello/cello}$ mutants were found to have a significantly reduced surface area compared to OHCs from *Ikzf2*$^{cello/+}$ control littermates. Similar results have also been reported in prestin knock-out (*Slc26a5*$^{-/-}$) mice (Cheatham et al., 2007, Liberman et al., 2002, Wu et al., 2004), which is consistent with prestin being abundantly expressed in the OHC membrane (Belyantseva et al., 2000, Zheng et al., 2000a). Whilst these studies reported a ~40% reduction in OHC size, a milder ~20% reduction was observed in *Ikzf2*$^{cello/cello}$ OHCs,

which correlates with *Ikzf2*$^{cello/cello}$ mutants having only a 47% reduction in *Slc26a5* transcript levels, whereas prestin knock-out mice have a complete absence.

At P16 – P18, *Ikzf2*$^{cello/cello}$ OHCs were also found to have a smaller total outward potassium current than *Ikzf2*$^{cello/+}$ controls. However this was not significant following normalisation to OHC size, with I_K and $I_{K,n}$ currents resembling those of *Ikzf2*$^{cello/+}$ control OHCs, which indicates that *Ikzf2*$^{cello/cello}$ and *Ikzf2*$^{cello/+}$ OHCs express the same complement of potassium channels. Electrophysiological analyses also showed that MET function was normal in P9 *Ikzf2*$^{cello/cello}$ OHCs, with no significant differences detected in the inward, outward or maximal MET currents following displacement of stereocilia bundles.

OHCs from P16 – P18 *Ikzf2*$^{cello/cello}$ mice and *Ikzf2*$^{cello/+}$ controls were also assessed for electromotile activity. By this age, electromotility is fully developed in the mouse and the postnatal maturation of OHCs into fully functional mechanosensory cells is complete (Abe et al., 2007, Marcotti and Kros, 1999). Following a depolarising voltage step, *Ikzf2*$^{cello/cello}$ OHCs showed significantly reduced motility compared to *Ikzf2*$^{cello/+}$ OHCs, even after normalization to OHC size. Importantly, the finding that *Ikzf2*$^{cello/cello}$ mice have normal potassium currents but disrupted electromotility is consistent with qRT-PCR data showing normal expression of *Kcnq4* and a significant reduction of *Slc26a5* in *Ikzf2*$^{cello/cello}$ mutants compared to *Ikzf2*$^{+/+}$ controls. Furthermore, taken together, the qRT-PCR and electrophysiology results suggest that helios is likely regulating specific downstream pathways and that loss of helios function does not cause a global maturation arrest of the OHCs in *Ikzf2*$^{cello/cello}$ mutants, but rather a specific effect whereby the normal acquisition of OHC electromotile function is disrupted.

The electromotility data for *cello* resembles previous results reported for prestin knock-out mice, whereby even a 50% reduction in prestin in *Slc26a5*$^{+/-}$ heterozygotes caused a

significant decrease in electromotility (Liberman et al., 2002). Interestingly, although prestin-mediated electromotility is required for cochlear amplification (Dallos et al., 2008), *Slc26a5*$^{+/-}$ mice have only a mild, high-frequency hearing impairment (Liberman et al., 2002). Therefore, the severe, broad-frequency hearing loss observed in *Ikzf2*$^{cello/cello}$ mice (Figure 5.1 and Figure 5.2) is almost certainly not just due to the 47% reduction in *Slc26a5* and resultant impaired electromotility, but is most likely caused by the reduction in *Slc26a5* coupled with effects arising from additional dysregulated genes and their functional processes. Indeed, this is suggested by the GO analyses, which indicate that loss of helios function causes dysregulation of genes involved in a broad range of biological processes required for auditory transduction and hearing, such as neurogenesis and ion transport. As such, a limitation of this current work is that, due to time constraints, only three OHC functional properties (potassium currents, MET function and electromotility) were explored in *Ikzf2*$^{cello/cello}$ mutants. Future work should address this by investigating the morphology, innervation and function of both the hair cells and central auditory system in more detail, as mentioned previously, in order to more fully characterise the role of helios in audition.

Although multiple dysregulated genes likely contribute to the hearing impairment in *Ikzf2*$^{cello/cello}$ mutants, downstream work focused on further characterising the relationship of helios with *Slc26a5* and *Ocm* using luciferase reporter assays. Results showed that WT helios induced a significant 2.08-fold increase in transcription from the *Slc26a5* promoter. In the heterozygous state, helios retained the ability to transactivate the *Slc26a5* promoter, although at a slightly reduced level than in the wild-type state, causing a 1.74-fold increase in transcription. This is consistent with the reduced dimerisation observed between WT and H517Q helios by co-IP (Figure 3.8) and also the intermediate *Slc26a5* transcript levels in *Ikzf2*$^{cello/+}$ mice shown by qRT-PCR. However, this level of transactivation and *Slc26a5*

expression is likely sufficient for normal OHC function, given that the *cello* mutation is recessively inherited and *Ikzf2*$^{cello/+}$ mice have auditory thresholds comparable to *Ikzf2*$^{+/+}$ controls (Figure 5.1 and Figure 5.2). In the homozygous state, helios did not significantly transactivate the *Slc26a5* promoter, demonstrating that the *cello* mutation perturbs the transcriptional activity of helios. Again, this is consistent with co-IP findings that homodimerisation is severely impaired between H517Q helios proteins (Figure 3.8) and qRT-PCR data showing that *Slc26a5* expression is significantly decreased in *Ikzf2*$^{cello/cello}$ mutants.

Conversely, WT helios was not found to induce any significant change in relative luciferase activity from the *Ocm* promoter sequence tested in this study. This suggests that either: *Ocm* is not a true target of helios, as suggested by the unvalidated qRT-PCR result; that *Ocm* is a true target of helios, but the binding motif is present outside of the proximal promoter sequence tested; or that *Ocm* is a secondary target, which is instead regulated through an intermediate factor.

Alongside the work carried out for this thesis, collaborating researchers Dr Ronna Hertzano and Sean Daugherty from the University of Maryland and Dr Rani Elkon at Tel Aviv University (Israel) performed *in silico* analyses to further investigate the transcriptional network of helios and examine whether it may have a role in regulating the OHC transcriptome. To this end, they analysed a recently published inner ear cell type-specific gene expression dataset (Scheffer et al., 2015), where gene expression was recorded from isolated GFP+ hair cells and all other GFP- cells of the developing cochlea and utricle between E16 and P7 and made publicly available to download from the SHIELD (https://shield.hms.harvard.edu/). Consistent with my cochlear wholemount anti-helios immunolabelling (Figure 5.19), this dataset indicated that *Ikzf2* was specifically and strongly

induced in cochlear hair cells during early development, while showing no significant change in expression in other cell types (Figure 6.12 A). To seek targets of *Ikzf2* in the inner ear, Dr Ronna Hertzano and colleagues then searched this dataset for genes whose expression pattern was highly correlated (r>0.9) with that of *Ikzf2*, reasoning that target genes of a developmental transcriptional regulator should follow a kinetic pattern closely related to the one exhibited by the regulator itself. This detected a cluster of 96 such genes showing upregulation in cochlear hair cells between E16 and P7 (Figure 6.12 B), which included *Slc26a5* and *Ocm* (Table 9.7 in Appendix).

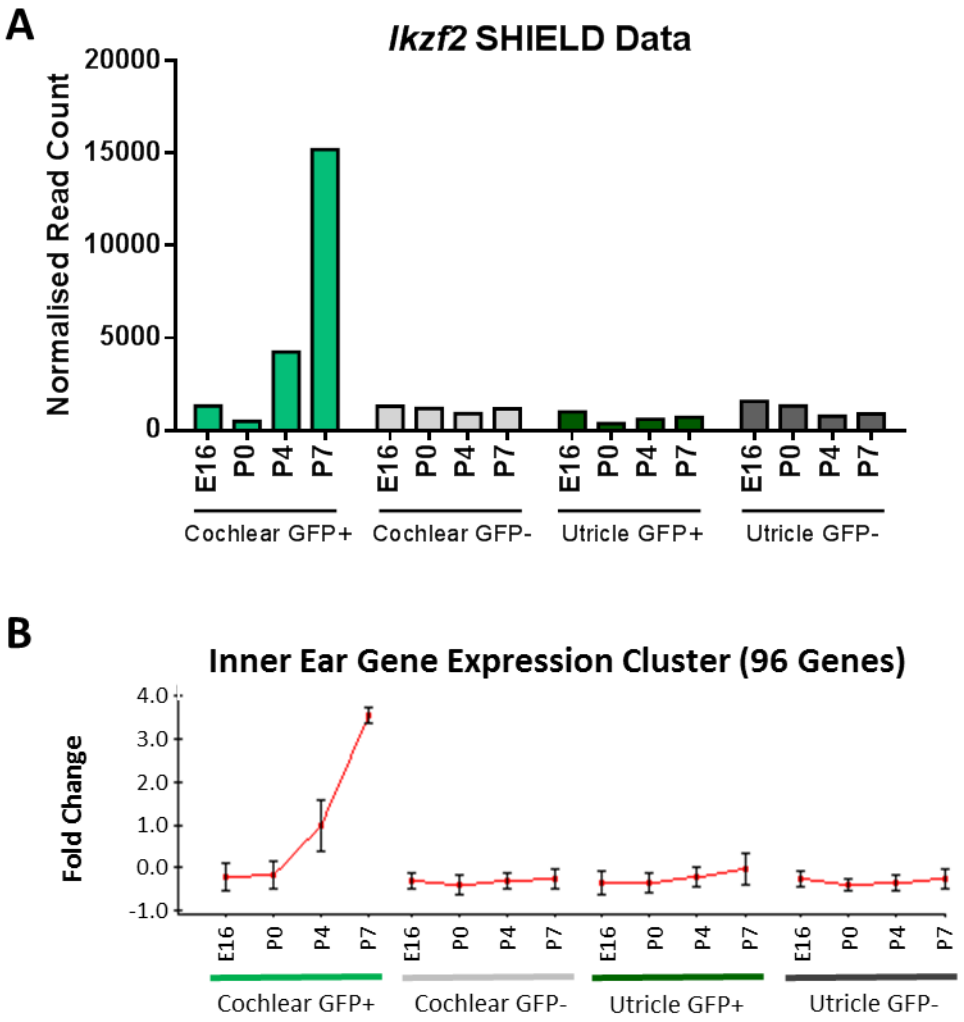

Figure 6.12: Perinatal expression of *Ikzf2* and genes showing a similar profile.

(A) The gene expression profile of *Ikzf2* in the inner ear was obtained from the SHIELD website (https://shield.hms.harvard.edu/datasets.html). In this study, Scheffer et al. (2015) used transgenic mice expressing GFP driven by the hair cell-specific *Pou4f3* promoter. Cochleae and utricles were collected from these mice at four developmental stages (E16, P0, P4 and P7) then separated into four distinct cell populations by fluorescence-activated cell sorting prior to RNA-Seq: cochlear GFP+ hair cells, cochlear GFP- surrounding non-sensory cells, utricle GFP+ hair cells and utricle GFP- surrounding non-sensory cells. Results demonstrate that *Ikzf2* is developmentally upregulated in cochlear GFP+ hair cells, but is expressed at lower and stable levels in the other cell populations of the inner ear. **(B)** Analysis of the SHIELD dataset identified a cluster of 96 genes with a temporospatial expression pattern highly correlated to that of *Ikzf2*. These genes specifically increase in hair cells during early postnatal development, while remaining unchanging in all other cell types of the inner ear. Data are shown as mean of all genes in the cluster ± standard deviation (for visualisation purposes, expression levels of each gene were standardised (mean = 0, standard deviation = 1) to use a common scale). Graph **(B)** prepared by Dr Ronna Hertzano and Sean Daugherty at the University of Maryland and Dr Rani Elkon at Tel Aviv University. E, embryonic day; GFP, green fluorescent protein; P, postnatal day; SHIELD, Shared Harvard Inner Ear Laboratory Database.

To further define a set of putative direct targets of helios amongst these 96 genes, Dr Hertzano and colleagues undertook a computational analysis of *cis*-regulatory DNA elements of this cluster using iRegulon (Janky et al., 2014). This tool searches for DNA motifs that are statistically enriched in the 20 kb region surrounding the transcription start site (TSS) of a set of co-expressed genes in order to reverse-engineer regulatory networks. iRegulon analysis identified the helios binding motif as highly over-represented within this cluster (normalised enrichment score = 4.34), specifically identified near the TSS of 40 of the 96 genes (Figure 6.13). This suggests that expression of these 40 genes in cochlear OHCs is directly regulated by helios. Notably, this set of putative direct targets contains: *Ikzf2* itself, which implies that helios regulates its own expression, as reported for ikaros (Perotti et al., 2015, Yoshida et al., 2013); *Slc26a5*, which confirms the luciferase data; but not *Ocm.*

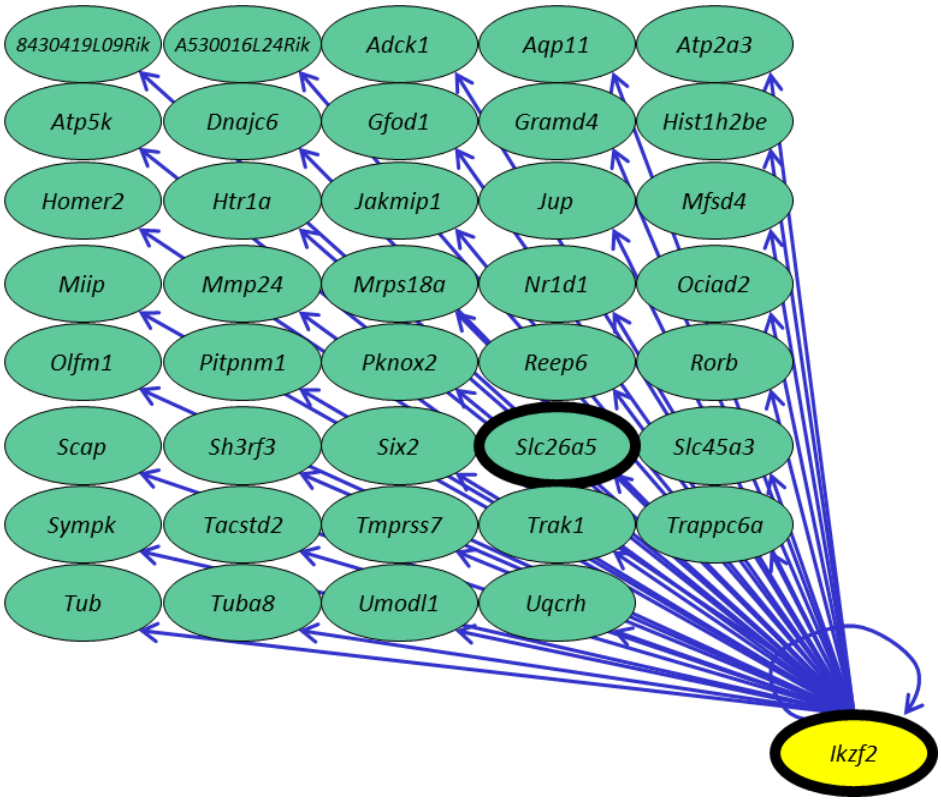

Figure 6.13: Putative direct target genes of helios identified by iRegulon analysis.
iRegulon analysis of a cluster of 96 genes that are developmentally upregulated in mouse cochlear hair cells identified 40 putative direct targets of helios, including *Slc26a5* and *Ikzf2* itself (thick black outlines).

The helios DNA-binding motif identified by iRegulon contains two potential core IKZF 'GGGAA' recognition sites; the first at position 5 – 9 and the second between position 10 – 18 (Figure 6.14 A). Notably, the *Slc26a5* promoter sequence used for the luciferase reporter assays was found to contain a motif that closely resembled the predicted iRegulon helios motif (Figure 6.14 B). Although this motif does not include a core 'GGGAA' site or encompass the 'GGGAA' sequence present towards the end of the *Slc26a5* promoter, taken together, these data support the hypothesis that *Slc26a5* is a direct target gene of helios.

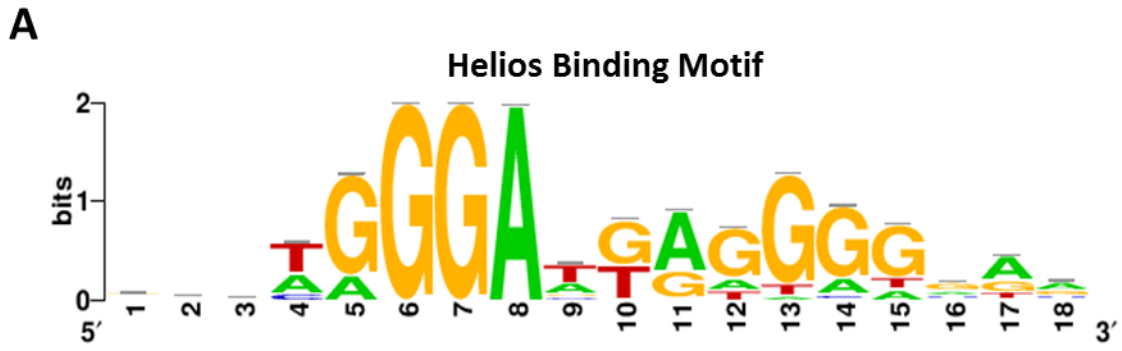

B

***Slc26a5* Promoter Sequence**

5′- gtgcagtgatggttttaacttgggactactgttaaagtcaccaagga
cttcctccatggggctacaagcctcagctctgatcagaatagcaagtgaaa
ctttaagaaaaagggtaaaatacctcacaagacgtgaggtcaatttaagga
ccaatcttaccatctttccttttgtttgccgaatagctggccagagttcac
ctgactcacacttccccctaatgccgagctattGACAGGGACTGCAGGACT
gtcgttaaacttaccatgaactcttgctgaacacttacacgttacctattt
attgctctgagggggaataaataaggtttatggctttttttttcatttatt
tttgctcactatatttgtaagtaagcacaactctacacaacaata – 3′

Figure 6.14: Analysis of the helios DNA-binding motif.
(A) The DNA-binding motif of helios identified from iRegulon analysis. **(B)** Investigation of the *Slc26a5* promoter sequence that was cloned for luciferase reporter assays showed that it contained a variation of this motif (highlighted in grey, with bold text indicating sequence identity with the predicted iRegulon motif). However, this does not include a core ikaros family 'GGGAA' motif or encompass the 'GGGAA' sequence that is present towards the 3' end of the *Slc26a5* promoter sequence (highlighted in yellow). Figure **(A)** prepared by Dr Ronna Hertzano and Sean Daugherty at the University of Maryland and Dr Rani Elkon at Tel Aviv University.

Conversely, the luciferase data and iRegulon results together suggest that *Ocm* is unlikely to be a direct target gene of helios, if a true target at all. However, it is possible that helios binds distal *cis*-regulatory elements of *Ocm*, the sequence of which was not cloned for the *Ocm* luciferase reporter assays or detected by iRegulon. As such, if a significant decrease in *Ocm* expression is found in *Ikzf2*$^{cello/cello}$ mutants following the expanded qRT-PCR study, further work should be undertaken to identify the promoter region of *Ocm* and investigate potential transactivation by helios using additional luciferase reporter assays.

To date, just three of the 40 putative target genes identified by iRegulon – *Homer2, Slc26a5* and *Tub* – have been reported as deafness-causing genes in the mouse (Azaiez et al., 2015, Liberman et al., 2002, Ohlemiller et al., 1997, Wu et al., 2004) which indicates that further investigation of helios targets may help to uncover novel candidate genes that are required for auditory function. Interestingly, within the *cello* RNA-Seq dataset, only two of these 40 genes were found to be significantly dysregulated in *Ikzf2*$^{cello/cello}$ cochlear duct total RNA compared to *Ikzf2*$^{+/+}$ controls at P8 (Table 9.8 in Appendix): *Slc26a5* was decreased by 57% and *Umodl1* was decreased by 46%. It may be that the remaining 38 genes are not true targets of helios, such as *Atp2a3* and *Ociad2,* both of which were found to be expressed at comparable levels in *Ikzf2*$^{cello/cello}$ and *Ikzf2*$^{+/+}$ cochleae by qRT-PCR (Figure 6.3). Indeed, whilst iRegulon can be a useful tool to predict regulatory networks *in silico*, any potential interactions must be confirmed or disproved with robust experimental work. It is also important to note that the RNA-Seq and qRT-PCR data provide only a snapshot of gene expression in *Ikzf2*$^{cello/cello}$ mice at a single time point (P8) and it may be that the majority of these putative target genes are dynamically regulated by helios. In addition, whilst these 40 genes may be direct targets of helios, other transcription factors are also likely to be contributing to their regulation and may compensate for loss of helios function. Together,

this may explain why the majority of these genes were not significantly different in *Ikzf2*$^{cello/cello}$ mice compared to *Ikzf2*$^{+/+}$ mice at P8.

To further substantiate a role for helios in the regulation of these 40 putative target genes, their expression was investigated in the *cello* RNA-Seq dataset by Dr Ronna Hertzano and colleagues. Their results demonstrated that, although the effect of mutant helios on the expression of each of these 40 putative targets individually was mild (Table 9.8 in Appendix), their expression level as a whole was significantly decreased in *Ikzf2*$^{cello/cello}$ cochleae compared to *Ikzf2*$^{+/+}$ controls at P8 (Figure 6.15 A). Furthermore, comparison with results from a recently published IHC- and OHC-specific gene expression study (Liu et al., 2014) indicated that these 40 putative target genes are enriched in the OHCs compared to the IHCs (Figure 6.15 B). Reciprocally, the expression of the top 200 OHC-enriched and IHC-enriched genes from the Liu et al. (2014) study was then examined in the *cello* RNA-Seq dataset by Dr Ronna Hertzano and colleagues. Interestingly, while no significant effect was observed on the expression of the top 200 IHC-enriched transcripts from the Liu et al. (2014) dataset, the expression of the top 200 OHC-enriched transcripts was significantly attenuated in *Ikzf2*$^{cello/cello}$ mutants compared to *Ikzf2*$^{+/+}$ mice at P8 (Figure 6.15 C), supporting a role for helios as an OHC-specific regulator.

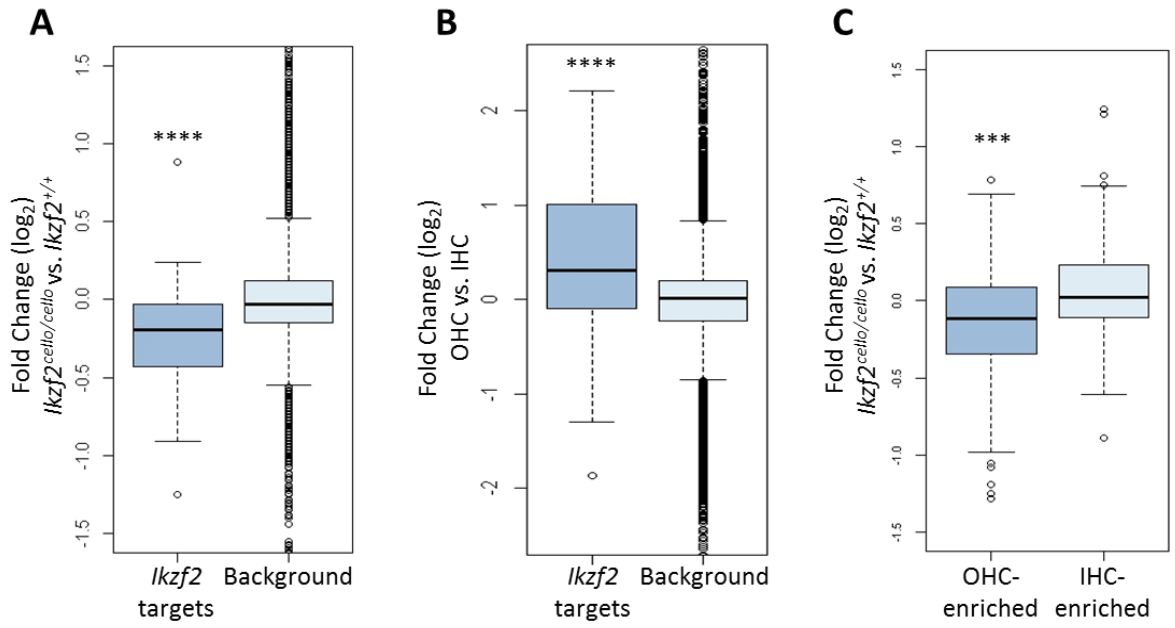

Figure 6.15: Analysis of helios as an outer hair cell-specific transcriptional regulator.
(A) The expression of the 40 putative direct target genes of helios were examined in the *cello* RNA-Seq dataset. Results showed that the expression level of this set of 40 putative targets, as a whole, was significantly decreased in *Ikzf2*$^{cello/cello}$ cochleae compared to *Ikzf2*$^{+/+}$ controls. **(B)** Using hair cell subtype-specific gene expression data published by Liu et al. (2014), the 40 putative target genes of helios were found to be significantly elevated in the OHCs compared to the IHCs. **(C)** The top 200 OHC-enriched genes from the Liu et al. (2014) study showed significantly decreased expression in the *cello* RNA-Seq dataset, whilst the top 200 IHC-enriched genes were unaffected. Data are shown as mean ± s.e.m. Statistical analysis: unpaired *t*-test, *** = p≤0.001, **** = p≤0.0001. Graphs prepared by Dr Ronna Hertzano and Sean Daugherty at the University of Maryland and Dr Rani Elkon at Tel Aviv University. IHC, inner hair cell; OHC, outer hair cell.

It is important to bear in mind that the iRegulon analysis is somewhat limited as it only examines DNA sequences that are within 20 kb of the gene TSS and not distal regulatory elements, such as enhancers. In addition, the cluster of 96 genes analysed by iRegulon included only those that are developmentally upregulated in cochlear hair cells and not those that are developmentally downregulated, such as *Elovl2*. As such, the current iRegulon analysis only has the power to identify putative targets that are transcriptionally activated by helios and not those genes that are repressed. To address this, a reciprocal iRegulon analysis should be undertaken; this would involve first searching SHIELD for genes with an inverse expression pattern to that of *Ikzf2* in cochlear hair cells and then examining

them using iRegulon to determine if the helios binding motif is enriched in their proximal promoter regions. A STRING analysis should also be undertaken on the combined gene dataset (upregulated and downregulated clusters) in order to identify potential hubs, pathways or networks regulated by helios. The RNA-Seq dataset should be similarly examined using iRegulon to gain further insight into which dysregulated genes are likely direct targets of helios.

Overall, the data presented in this chapter suggests that loss of helios function results in significant dysregulation of a number of genes in P8 *Ikzf2*$^{cello/cello}$ cochleae, many of which are associated with aspects of neurosensory development and auditory transduction. Much work will be required to validate which of these dysregulated genes are real and to determine how their dysregulation has contributed to the hearing loss phenotype exhibited by *Ikzf2*$^{cello/cello}$ mice. In this thesis, only the relationship between helios and *Slc26a5* was characterised in detail; the luciferase data provides evidence that the *cello* mutation perturbs transactivation of the *Slc26a5* promoter *in vitro* and is therefore likely responsible for the decrease in *Slc26a5* expression and reduced OHC electromotility observed in *Ikzf2*$^{cello/cello}$ mutants. An interaction between WT helios and *Slc26a5* should be now be confirmed *in vivo* using a targeted chromatin IP (chIP). Although a complementation test should be undertaken to definitively prove helios is the causative mutation, the data presented in this thesis strongly suggest that helios directly regulates *Slc26a5* and is required for the timely expression of prestin and the subsequent acquisition of adult-like electromotile properties during OHC postnatal development. Together with the iRegulon analysis, this suggests a key role for helios in regulating the transcriptome and functional maturation of the OHCs.

Chapter 7 : Discussion

7.1. Introduction

The aim of my thesis was to characterise *cello*, an ENU-induced mouse model of early-onset hearing loss, in order to increase our understanding of the genes and pathways that are required for auditory function. This involved identification of the causative mutation in *cello*, *in silico* and *in vitro* analyses of the mutation, in-depth auditory phenotyping and functional characterisation of *cello* hair cells.

The *cello* pedigree was originally identified from the MRC Harwell ENU Ageing Screen. The major benefit of this phenotype-driven approach is that no *a priori* assumptions are made about the genetic basis of disease, making it a powerful discovery tool for identifying novel associated genes and pathways. Indeed, linkage analysis and WGS revealed that *cello* mice harbour a non-synonymous point mutation (c.1551C>A) in the novel hearing loss-causing gene *Ikzf2*, which results in a missense substitution (p.H517Q) in the encoded protein, helios.

7.1.1. The Ikaros Family

Helios is a zinc finger protein which belongs to the ikaros family of transcription factors (Hahm et al., 1998, Kelley et al., 1998). The five family members – ikaros, helios, aiolos, eos and pegasus – are characterised by their extensive homology and common domain structure, which comprises three to four N-terminal zinc fingers (ZnF1 – 4) that are required for DNA binding and two C-terminal zinc fingers (ZnF5 – 6) that mediate homodimerisation and heterodimerisation between family members (Honma et al., 1999, McCarty et al., 2003, Molnar and Georgopoulos, 1994, Morgan et al., 1997, Perdomo et al., 2000, Sun et al.,

1996). Each of these zinc fingers is of the classical C_2H_2-type, which coordinate a centralised zinc ion using two Cysteine and two Histidine residues in order to stabilise protein structure and binding interactions (Brown et al., 1985, Frankel et al., 1987, Parraga et al., 1988, Parraga et al., 1990). The ikaros family have been reported to function as both transcriptional activators and repressors (Harker et al., 2002, Sabbattini et al., 2001, Trinh et al., 2001) and be involved in chromatin remodelling at target genes through association with the nucleosome remodelling complex, NuRD (Kim et al., 1999, Sridharan and Smale, 2007). Critically, dimerisation of the IKZF proteins is required for pericentromeric targeting and has been shown to enhance their DNA binding affinity and transcriptional activity (Cobb et al., 2000, Sun et al., 1996).

The IKZF proteins have primarily been studied in the mammalian haematopoietic system, where they are key regulators of haematopoietic differentiation and tumour suppression (Table 7.1) (Georgopoulos et al., 1994, John and Ward, 2011, Fujii et al., 2003, Nakase et al., 2002). During embryogenesis, helios is abundantly expressed in the liver and thymus before becoming largely restricted postnatally to adult HSCs and T-cells (Kelley et al., 1998, Hahm et al., 1998, Thornton et al., 2010). Helios has been shown to mediate lymphoid cell fate determination and T-reg function (Dovat et al., 2005, Getnet et al., 2010, Takatori et al., 2015), although likely functions in a redundant manner given that helios knockout mice exhibit normal T-cell phenotypes (Cai et al., 2009, Thornton et al., 2010).

Several IKZF proteins are also expressed in non-haematopoietic tissues, where they have a similar role in regulating cell differentiation and maturation (Ezzat and Asa, 2008, Kiehl et al., 2008, Martin-Ibanez et al., 2012) (Table 7.1). For example, ikaros is transiently expressed in developing striatal neurons (Agoston et al., 2007, Kiehl et al., 2008) and has been

implicated in neurogenesis in the forebrain and retina (Alsio et al., 2013, Elliott et al., 2008, Martin-Ibanez et al., 2010), whilst eos is found throughout the developing nervous system (Honma et al., 1999). Interestingly, eos has also been reported in afferent spiral ganglion neurons of the cochlea, where it regulates the expression of PSD-95 (Bao et al., 2004). Outside of the haematopoietic system, helios is expressed in several epithelial tissues and brain structures during embryogenesis, including the gut lining, olfactory epithelium, striatum and hippocampus, and promotes the neurogenesis of spiny projection neurons (Kelley et al., 1998, Martin-Ibanez et al., 2012).

Table 7.1: Expression patterns and functions reported in the literature for the ikaros family proteins.

Protein (Gene)	Within Haematopoietic System	Outside Haematopoietic System
Ikaros (*Ikzf1*)	**Expression Pattern:** • **Embryo:** thymus • **Adult:** haematopoietic stem cells; immature thymocytes; mature T-cells; mature B-cells. **Roles:** • **Promotes:** differentiation and function of all lymphoid lineages; negative selection in T-cells; immunoglobulin gene rearrangement and class switching in B-cells; tumour suppression. • **Represses:** development of erythroid and myeloid lineages. (Allman et al., 2006, Boggs et al., 1998, Georgopoulos et al., 1992, Georgopoulos et al., 1994, Kirstetter et al., 2002, Molnar and Georgopoulos, 1994, Nichogiannopoulou et al., 1999, Reynaud et al., 2008, Sellars et al., 2009, Urban and Winandy, 2004, Wang et al., 1996, Winandy et al., 1995).	**Expression Pattern:** • **Embryo:** brain; liver; cerebral cortex; retinal progenitor cells; striatal neurons, hypothalamic neurons; anterior pituitary gland. **Roles:** **Promotes:** differentiation of striatal, cortical and retinal neurons; differentiation, growth and survival of neuroendocrine cells in the anterior pituitary and hypothalamus; expression of hormones (growth hormone, prolactin, proopiomelanocortin) in the anterior pituitary gland and hypothalamus. (Agoston et al., 2007, Alsio et al., 2013, Elliott et al., 2008, Ezzat et al., 2005a, Ezzat et al., 2005b, Ezzat et al., 2006, Ezzat and Asa, 2008, Georgopoulos et al., 1992, Kiehl et al., 2008, Martin-Ibanez et al., 2010, Molnar and Georgopoulos, 1994).
Helios (*Ikzf2*)	**Expression Pattern:** • **Embryo:** yolk sac; liver; thymus. • **Adult:** thymus; bone marrow; adult haematopoietic stem cells; immature T-cells; T-regs; T-helper cells; γδ T-cells; NK cells; dendritic cells. **Roles:** • **Promotes:** T-cell development; T-helper	**Expression Pattern:** • **Embryo:** brain (cerebrellar neurons, lateral ganglionic eminence, striatum, hippocampus, accessory olfactory bulb); kidney; epithelial tissues (retina, tongue, palate, salivary glands, kidney tubules, lining of the gut, lining of the respiratory tract).

Protein (Gene)	Within Haematopoietic System	Outside Haematopoietic System
	cell differentiation; T-reg function; tumour suppression. (Getnet et al., 2009, Getnet et al., 2010, Hahm et al., 1998, Hosokawa et al., 1999, Kelley et al., 1998, Nakase et al., 2002, Peters et al., 2014, Serre et al., 2011, Sugimoto et al., 2006, Sugita et al., 2015, Takatori et al., 2015, Thornton et al., 2010, Zabransky et al., 2012, Zhang et al., 2007).	• **Adult:** at low levels in the brain and skeletal muscle. **Roles:** • **Promotes**: neurogenesis in developing striatum. (Hahm et al., 1998, Hosokawa et al., 1999, Kelley et al., 1998, Martin-Ibanez et al., 2012).
Aiolos (*Ikzf3*)	**Expression Pattern:** • **Embryo:** thymus. • **Adult:** thymus; spleen; bone marrow, mature T-cells; mature B-cells. **Roles:** • **Promotes:** differentiation of T-regs and T-helper 17 cells; activation and maturation of effector B-cells; maturation of peripheral NK cells; tumour suppression (Cariappa et al., 2001, Cortes and Georgopoulos, 2004, Gandhi et al., 2010, Holmes et al., 2014, Liippo et al., 2001, Morgan et al., 1997, Quintana et al., 2012, Rebollo and Schmitt, 2003, Wang et al., 1998b).	**Expression Pattern:** • None reported. **Roles:** • None reported.
Eos (*Ikzf4*)	**Expression Pattern:** • **Adult:** thymus; spleen; liver; activated T-regs; T-cells; B-cells; several myeloid, erythroid and megakaryocytic cells lines. **Roles:** • **Promotes:** T-reg function. (Pan et al., 2009, Perdomo et al., 2000, Sharma et al., 2013).	**Expression Pattern:** • **Embryo:** brain; central and peripheral nervous system. • **Adult:** cochlear SGNs; skeletal muscle. Also at low levels in pyramidal neurons and granule neurons of the hippocampus; heart; kidney. **Roles:** • **Promotes:** PSD-95 expression in cochlear afferent SGNs. (Bao et al., 2004, Honma et al., 1999, Perdomo et al., 2000).
Pegasus (*Ikzf5*)	**Expression Pattern:** • **Adult:** liver; various haematopoietic cell lines. **Roles:** • **Promotes:** globin switching during erythroid differentiation. (Perdomo et al., 2000, Yu et al., 2011).	**Expression Pattern:** • **Adult:** skeletal muscle; brain; heart; kidney. **Roles:** • None reported. (Perdomo et al., 2000).

NK, natural killer cell; PSD-95, post-synaptic density protein-95; SGN, spiral ganglion neurons; T-reg, regulatory T-cell.

During the course of this thesis, two transcriptomic studies of cell-type specific gene expression within the inner ear were published (Liu et al., 2014, Scheffer et al., 2015) and made publicly available to download from the SHIELD website (https://shield.hms.harvard.edu). These datasets provide an excellent resource for quickly examining the expression of genes of interest, such as the ikaros family, in the inner ear.

Employing transgenic mice expressing GFP under the control of the hair cell-specific *Pou4f3* promoter, Scheffer et al. (2015) were able to selectively sort cells to enable gene expression to be measured specifically from GFP+ cells (sensory hair cells) and GFP- cells (surrounding non-sensory cells) of the developing cochlea and utricle between E16 and P7 (Figure 7.1 A). Results from this dataset indicated that *Ikzf1* (ikaros) is expressed at low levels in the cochlea and vestibular GFP+ hair cells, but is developmentally upregulated in vestibular GFP- non-sensory cells (Figure 7.1 B). *Ikzf2* (helios) was found to be developmentally upregulated in cochlear GFP+ hair cells, but is expressed at lower, stable levels in the other cell populations of the inner ear (Figure 7.1 C), which supports the immunolabelling data presented in this thesis. *Ikzf3* (aiolos) is expressed at negligible levels in all cell types of the inner ear during development (Figure 7.1 D), whilst *Ikzf4* (eos) is transiently expressed, at the highest levels in cochlear GFP- non-sensory cells at P0 and vestibular GFP+ hair cells at E16 and P0 (Figure 7.1 E). Finally, *Ikzf5* (pegasus) is detected in all cell populations of the inner ear, with expression appearing to decrease as the ear matures (Figure 7.1 F).

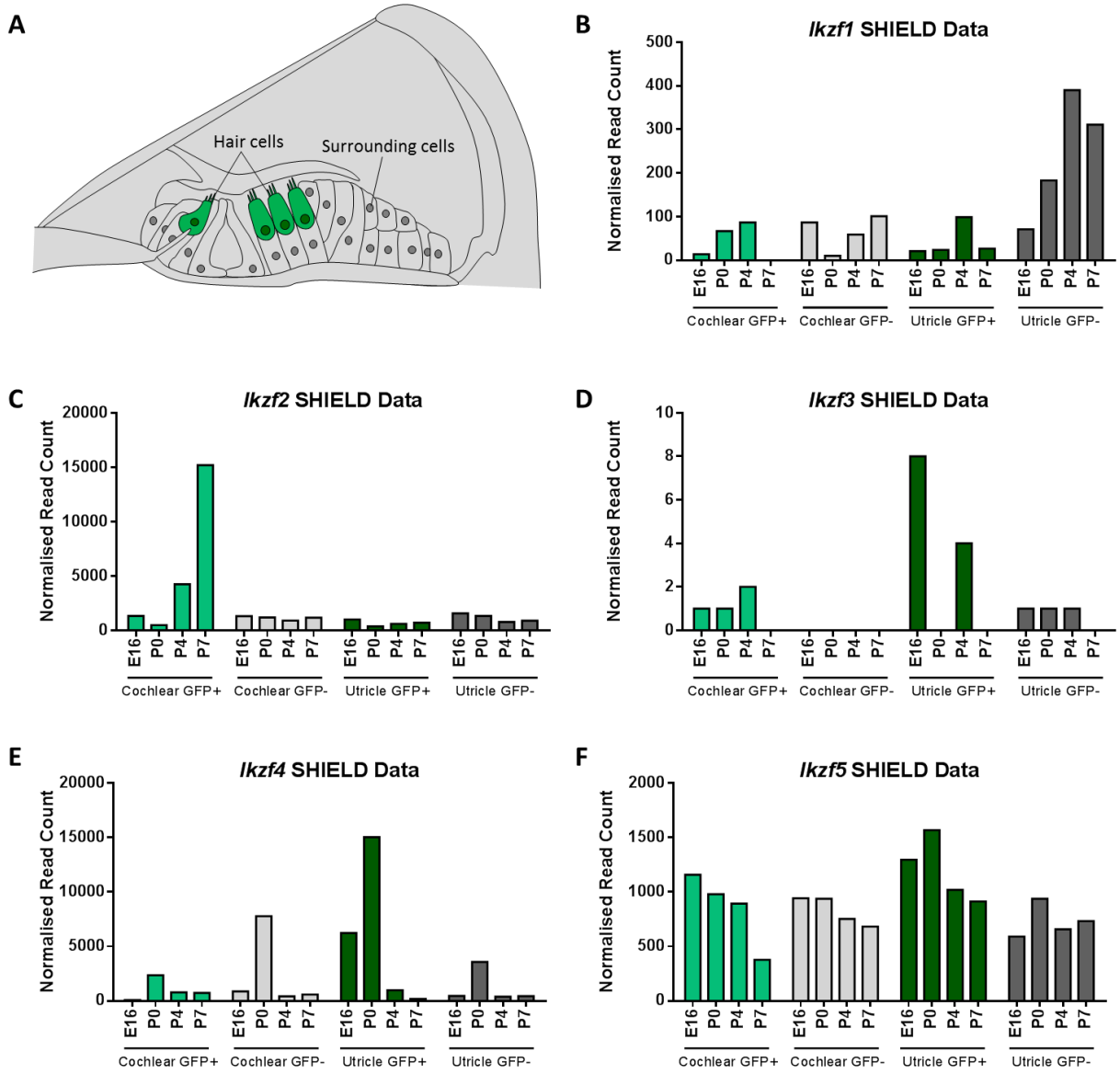

Figure 7.1: Gene expression of the ikaros family in sorted cell populations from the mouse inner ear during development.

Gene expression profiles were obtained for the five members of the ikaros family by RNA-Seq of inner ear cell populations from *Pou4f3*-GFP transgenic mice. Cochleae and utricles were collected at four stages during development (E16, P0, P4 and P7) then separated into four distinct cell populations prior to RNA-Seq: cochlear GFP+ hair cells; cochlear GFP- surrounding non-sensory cells; utricle GFP+ hair cells and utricle GFP- surrounding non-sensory cells. **(A)** Schematic of the cell populations obtained from the cochlea of *Pou4f3*-GFP transgenic mice. **(B)** *Ikzf1* is expressed at low levels in the cochlea and in vestibular GFP+ hair cells, but is developmentally upregulated in vestibular GFP- non-sensory cells. **(C)** *Ikzf2* is developmentally upregulated in cochlear GFP+ hair cells, but is expressed at lower, stable levels in the other cell populations of the inner ear. **(D)** *Ikzf3* is expressed at negligible levels in all cell types of the inner ear during development. **(E)** *Ikzf4* is transiently expressed in the inner ear, at the highest levels in cochlear GFP- non-sensory cells at P0 and vestibular GFP+ hair cells at E16 and P0. **(F)** *Ikzf5* is detected in all cell populations of the inner ear, with expression decreasing as the ear matures. Graphs prepared using gene expression data downloaded from the SHIELD website (https://shield.hms.harvard.edu/datasets.html) and published by Scheffer et al. (2015). Data are shown as normalised read counts. E, embryonic day; GFP, green fluorescent protein; P, postnatal day; SHIELD, Shared Harvard Inner Ear Laboratory Database.

Liu et al. (2014) undertook transcriptome profiling of 2000 individually collected IHCs and OHCs from adult (P25 – P30) mouse cochleae using microarray. Results from this dataset indicated that *Ikzf1*, *Ikzf3* and *Ikzf4* are expressed at negligible levels in mature IHCs and OHCs, whilst *Ikzf2* is expressed largely in the OHCs and *Ikzf5* is in both IHCs and OHCs (Figure 7.2). This data also demonstrates significant differential expression of *Ikzf2* and *Ikzf5* between the two hair cell subtypes; *Ikzf2* is approximately 4-fold higher in the OHCs than the IHCs, whereas *Ikzf5* is approximately 1.5-fold higher in the IHCs. Although this array detected low levels of *Ikzf2* in the IHCs, anti-helios immunolabelling was not observed in the IHCs at any of the time points studied in this thesis. This suggests that the *Ikzf2* transcript may be degraded and not translated into protein in the IHCs. Alternatively, it may be that helios is present in the IHCs, but at such levels to be undetectable by immunolabelling. Furthermore, it is important to bear in mind that the dissociation of IHCs and OHCs, as performed by Liu et al. (2014) in this study, may affect their respective transcriptomes. As such, expression of the ikaros family members should be further investigated using qRT-PCR and immunolabelling of whole cochleae.

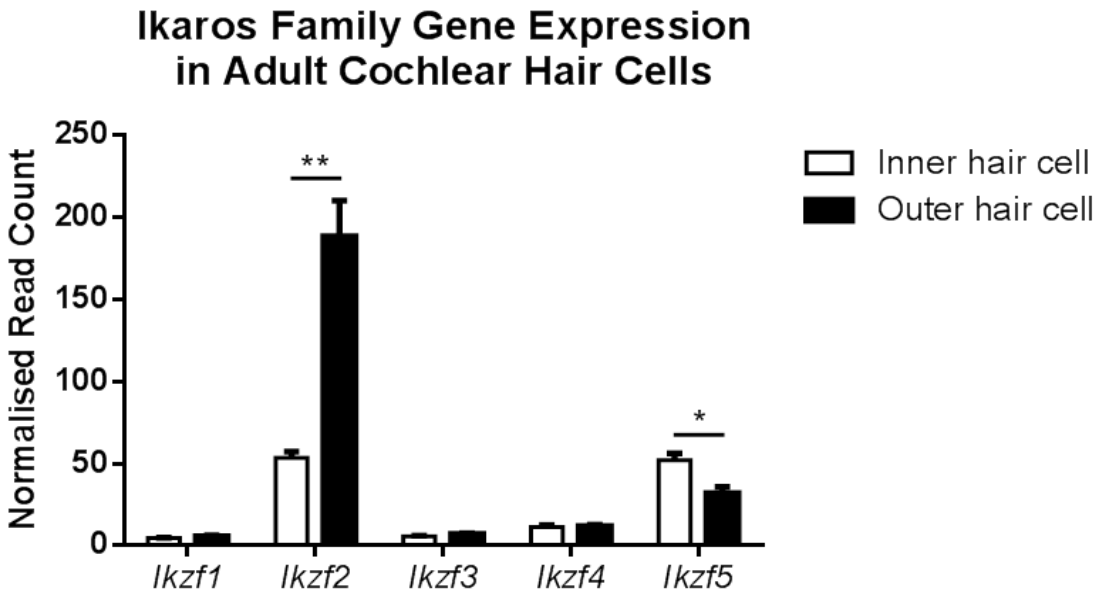

Figure 7.2: Gene expression levels of the ikaros family in inner and outer hair cells collected from adult mouse cochleae.
Gene expression profiles were obtained for the five members of the ikaros family using GeneChip® Mouse Gene 2.0 ST Arrays of RNA prepared from 2000 individually collected IHCs and OHCs from adult (P25 – P30) CBA/j mice. *Ikzf1*, *Ikzf3* and *Ikzf4* transcripts were detected at negligible levels in the two hair cell subtypes, whilst *Ikzf2* was detected in the OHCs at significantly higher levels than in the IHCs. *Ikzf5* was found to be expressed in both hair cell subtypes, though is significantly higher in the IHCs. Graph prepared using gene expression data downloaded from the SHIELD website (https://shield.hms.harvard.edu/datasets.html) and published by Liu et al. (2014). Data are shown as mean ± s.e.m. Statistical analysis: unpaired *t*-test, * = $p \leq 0.05$, ** = $p \leq 0.01$.

Despite this expression data and the identification of eos in cochlear spiral ganglion neurons (Bao et al., 2004), to date, none of the ikaros family members have been reported to be required for auditory function. To further explore this, IKZF-related phenotypes were investigated by searching the IMPC web portal (http://www.mousephenotype.org/). The IMPC is a large-scale, internationally collaborative project which aims to generate and comprehensively phenotype knock-out mouse models of every protein-coding gene in the genome, in order to increase our understanding of mammalian gene function (Figure 7.3) (Brown and Moore, 2012, Skarnes et al., 2011).

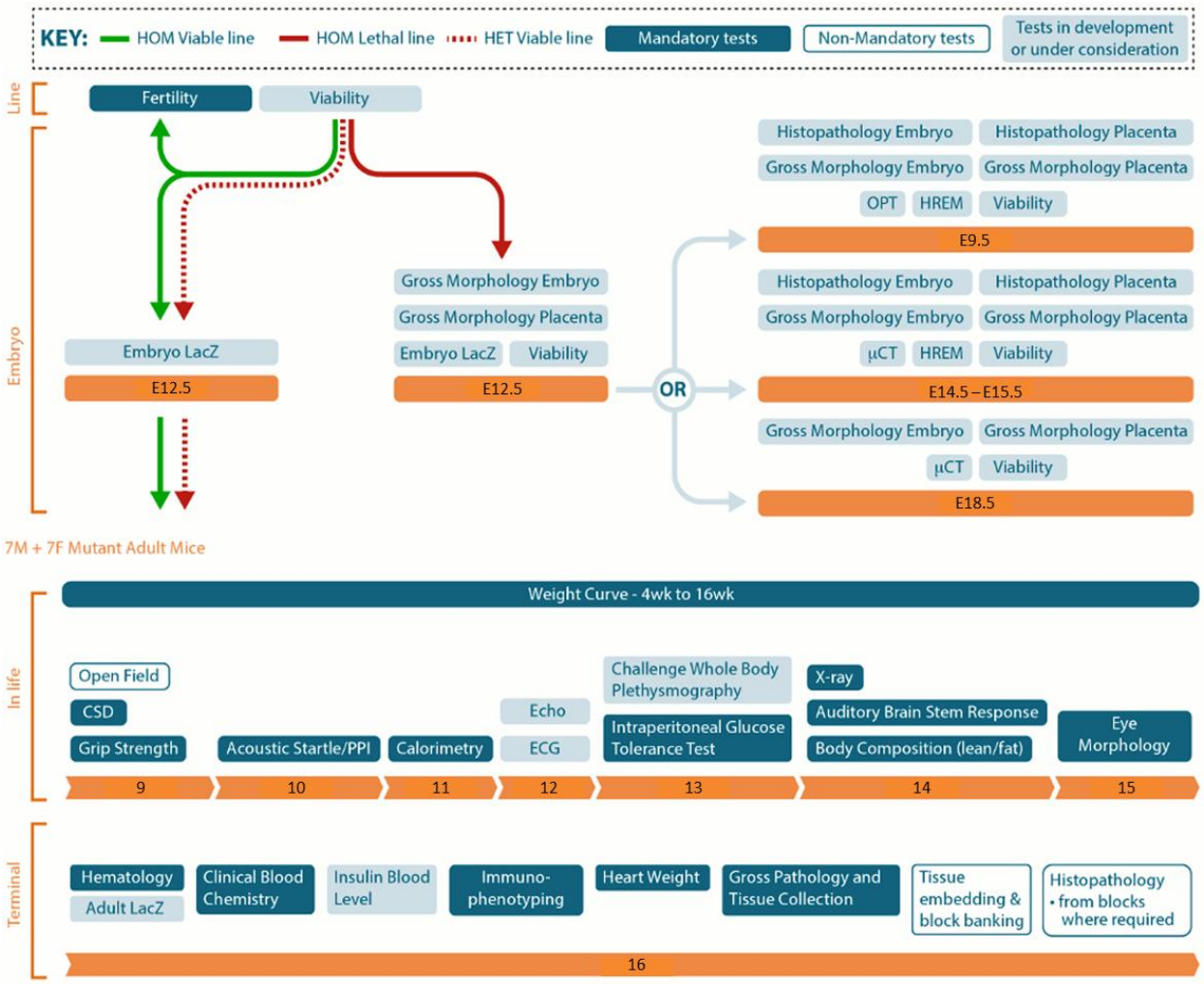

Figure 7.3: The phenotyping pipeline employed by the International Mouse Phenotyping Consortium.
The IMPC aims to generate knock-out mice for every protein-coding gene in the genome. Each knock-out pedigree is assessed for fertility and viability; those that are homozygous (HOM) lethal are assessed at embryonic stages using a number of morphological imaging techniques, whilst those that are homozygous or heterozygous (HET) viable are bred to produce experimental cohorts (ideally 7 male and 7 female mutants) which enter a postnatal phenotyping pipeline at 9 weeks of age. Mandatory tests are performed on all pedigrees, non-mandatory tests can be requested if interest is registered in a particular pedigree or phenotype. Image downloaded from the International Mouse Phenotyping Resource of Standardised Screens (http://www.mousephenotype.org/impress). CSD, combined SmithKline Beecham, Harwell, Imperial college, Royal London hospital phenotype assessment and dysmorphology; E, embryonic day; ECG, electrocardiogram; Echo, echo magnetic resonance imaging; HREM, high resolution electron microscopy; OPT, optical projection tomography; PPI, pre-pulse inhibition; µCT, micro computed tomography.

At this stage, phenotyping data are only available for aiolos and pegasus knock-out mice, as ikaros, helios and eos mice have not yet been generated. Both the aiolos (*Ikzf3*$^{tm1(KOMP)Vlgc}$) and pegasus (*Ikzf5*$^{tm1(KOMP)Wtsi}$) mice carry tm1 alleles, which are LacZ reporter-tagged

deletion alleles (Figure 7.4 A). The *Ikzf3*$^{tm1(KOMP)Vlgc/tm1(KOMP)Vlgc}$ homozygote mice have various haematopoietic phenotypes, including decreased numbers of lymphocytes, leukocytes, basophils, platelets and eosinophils, as well as abnormal grip strength and abnormal optic disc morphology, although no auditory phenotypes were detected (see https://www.mousephenotype.org/data/genes/MGI:1342542 for more information). The *Ikzf5*$^{tm1(KOMP)Wtsi/tm1(KOMP)Wtsi}$ homozygote mice have a range of phenotypes, including decreased numbers of NK cell subsets, decreased bone mineral content, abnormal joint morphology and impaired heart function, as well as significantly elevated auditory thresholds at 24 and 30 kHz (Figure 7.4 B) (see https://www.mousephenotype.org/data/genes/MGI:1914393 for more information). These phenotyping data are consistent with the SHIELD data (Liu et al., 2014, Scheffer et al., 2015) showing minimal expression of *Ikzf3* in the ear, but reasonable expression of *Ikzf5* in all cell populations.

Together with the data presented in this thesis on *cello*, this provides the first evidence that members of the ikaros family are required for auditory function, specifically identifying *Ikzf2* (helios) and *Ikzf5* (pegasus) as novel hearing loss-causing genes. Interestingly, the audiograms of *Ikzf2*$^{cello/cello}$ and *Ikzf5*$^{tm1(KOMP)Wtsi/tm1(KOMP)Wtsi}$ mutant mice suggest distinct auditory phenotypes, with the former exhibiting a broad hearing loss across all frequencies and the latter exhibiting a high frequency hearing loss. This could be due to differential expression patterns of the respective IKZF proteins within the auditory system; for example, whilst wholemount immunolabelling has shown that helios is expressed throughout the cochlear spiral, it may be that pegasus expression occurs in a gradient and is greater in basal regions of the cochlea, resulting in a high frequency hearing impairment in the knock-out.

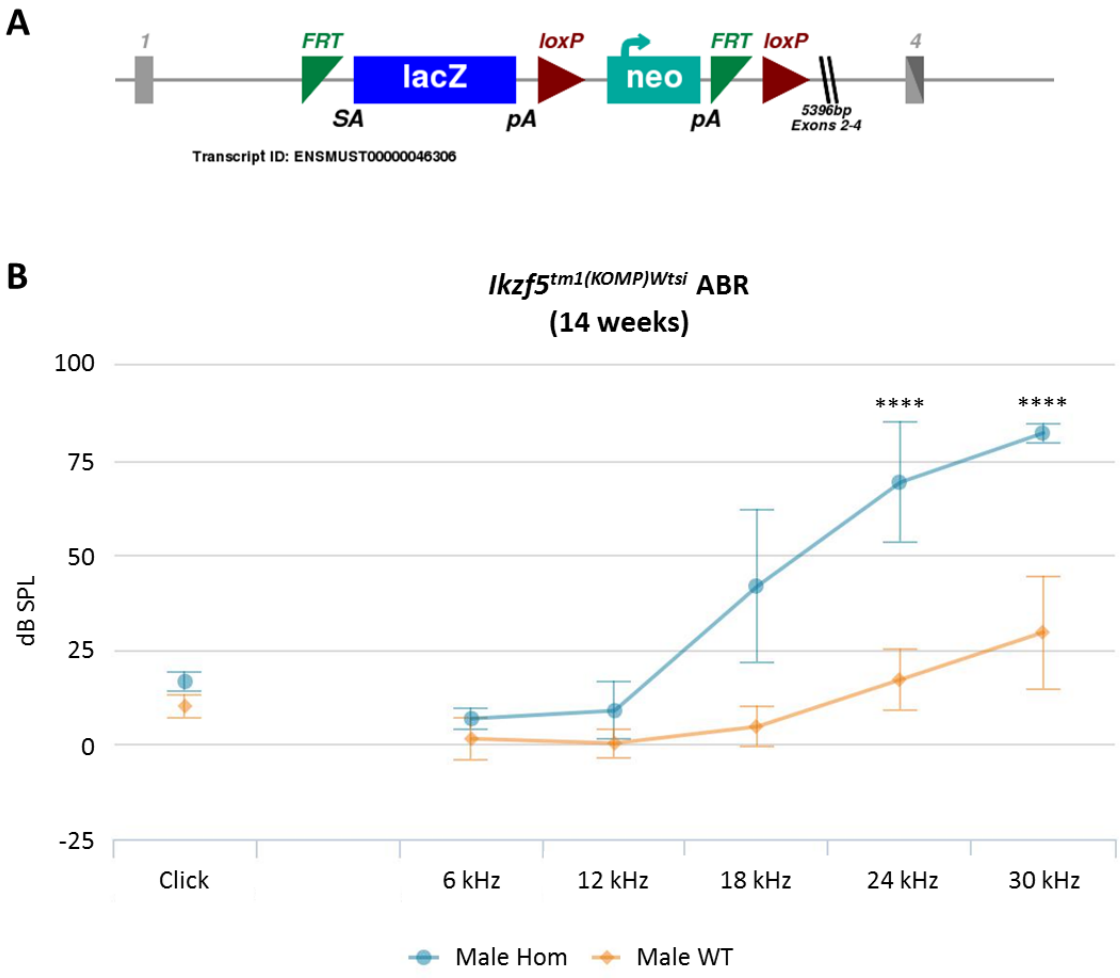

Figure 7.4: Allele map and auditory-evoked brainstem response data for pegasus knock-out (*Ikzf5*$^{tm1(KOMP)Wtsi/tm1(KOMP)Wtsi}$) mice from the International Mouse Phenotyping Consortium.

(A) Pegasus knock-out mice were generated by the IMPC using a tm1 LacZ reporter-tagged deletion allele which deletes critical exons 2 and 3 and half of exon 4. **(B)** ABR analysis was carried out on male pegasus knock-out mice at 14 weeks of age (Hom, *Ikzf5*$^{tm1(KOMP)Wts/\ tm1(KOMP)Wtsi}$, n = 4) and thresholds were compared to the running mean of B6NTac and baseline controls (WT, n = 126 – 129). Results indicated that *Ikzf5*$^{tm1(KOMP)Wtsi/\ tm1(KOMP)Wtsi}$ knock-out mice had significantly elevated auditory thresholds at 24 and 30 kHz. Graph and accompanying statistics downloaded from the IMPC web portal (https://www.mousephenotype.org/data/genes/MGI:1914393). Statistical analysis: mixed model framework, **** = p≤0.0001. ABR, auditory-evoked brainstem response; dB SPL, decibel sound pressure level; kHz, kiloHertz.

7.2. Summary of Results and Future Work

Taken together, the data presented in this thesis show that *cello* mice exhibit early-onset hearing loss that results, at least in part, from impaired OHC electromotility. Linkage analysis and WGS demonstrated that all hearing-impaired mice harbour a missense mutation in the novel OHC transcription factor helios. This mutation was found to impair the ability of helios to homodimerise – a property that, based on previous functional analyses of the ikaros protein, is likely critical for efficient DNA binding and transcriptional activity (Cobb et al., 2000, Sun et al., 1996). In keeping with this hypothesis, a number of cochlear genes were found to be dysregulated in *Ikzf2*$^{cello/cello}$ mutants at P8 using RNA-Seq, including *Slc26a5*. Subsequent luciferase reporter assays indicated that WT helios can transactivate the *Slc26a5* promoter, whilst the *cello* mutation perturbed this transactivation, thus supporting a role for helios as a regulator of this OHC-specific gene and the acquisition of OHC electromotility.

Although these data strongly implicate a role for helios in the auditory system, it is important to bear in mind that the mutations in *Cryga* and *Map2* have not yet been assessed in *Ikzf2*$^{cello/cello}$ mice and so cannot be conclusively discounted. Indeed, it is possible that *Ikzf2*$^{cello/cello}$ animals may carry one or both of these mutations in addition to the *Ikzf2* mutation, with each having a distinct effect on the auditory function of *cello* mutant mice. For example, although there is strong experimental evidence that the *Ikzf2* mutation impairs OHC electromotility, a mutation in *Cryga* or *Map2*, if present, could be responsible for other pathologies contributing to the hearing impairment. To further investigate this, and gain a fuller understanding of the contribution of helios to auditory function, the *Cryga* and *Map2* mutations should be validated by Sanger sequencing; if they are not present in all affected

mice, they can be irrefutably discounted. However, if present, the different mutations in *cello* animals should be segregated by breeding so their phenotypic and functional effects can be characterised individually in order to define the role of each gene in the auditory system.

Previous work has largely focused on studying helios in the haematopoietic system (Dovat et al., 2005, Getnet et al., 2010, Kelley et al., 1998, Serre et al., 2011, Nakase et al., 2002, Takatori et al., 2015). Following FACS, *Ikzf2*$^{cello/cello}$ mutants were found to exhibit a small but significant increase in the proportion of CTLs and decrease in the proportion of γδ T-cells and macrophages. The biological significance of these results is currently unclear and needs to be further investigated by repeating the immunological phenotyping on a larger cohort of immunotoxin-challenged mice. No additional defects in lymphoid or myeloid subpopulations were identified, although *Ikzf2*$^{cello/cello}$ animals were found to exhibit decreased body weight and microphthalmia, which resembles the phenotypes reported for helios null mice (Cai et al., 2009) and supports *Ikzf2* as the causative mutation in *cello*. The largely normal immune phenotype in *Ikzf2*$^{cello/cello}$ and helios null mice is most likely due to redundancy of helios with the other IKZF transcription factors, as ikaros, aiolos and eos are also expressed in lymphoid cells (Kelley et al., 1998, Raffin et al., 2013, Quintana et al., 2012). However, this compensation may not be possible in the OHCs, depending on whether any ikaros proteins other than helios are expressed in these cells. Alternatively, it may be that helios regulates target genes in the OHCs via a distinct binding motif that is not recognised by other family members.

A limitation of the current study is that only a small number of dysregulated genes identified from the RNA-Seq were further investigated by qRT-PCR. As RNA-Seq is associated with a

high false discovery rate, it is imperative to individually validate each gene to determine those that are truly dysregulated from those that are false positives. In addition, given the low power of the current qRT-PCR study, the validation results presented in this thesis may not be experimentally robust. As such, the qRT-PCR experiment needs to be expanded to include not only additional targets for validation (from both the RNA-Seq study and the iRegulon analysis), but also additional biological replicates to increase power.

It is also important to bear in mind that this RNA-Seq study was undertaken at a single time point (P8) using RNA extracted from whole cochlear ducts and thus provides just a crude snapshot of differential gene expression between *Ikzf2*$^{cello/cello}$ and *Ikzf2*$^{+/+}$ mice. Furthermore, as the OHCs would only account for a small proportion of the total cells analysed, any small changes in gene expression might be masked. To address this, the current RNA-Seq study should be followed with a time course of OHC-specific RNA-Seq, undertaken at both earlier and later stages during hair cell development. To this end, ideally I would cross the *cello* pedigree with the *RiboTag* strain from the Jackson Laboratory, USA (*B6N.129-Rpl22*$^{tm1.1Psam}$) and a *Slc26a5-Cre* recombinase line (Figure 7.5). The *RiboTag* mouse was developed at the University of Washington and enables simple and efficient isolation of ribosomal RNA from specific cell types of interest in complex tissues (Sanz et al., 2009, Sanz et al., 2013) – in this case, cochlear OHCs.

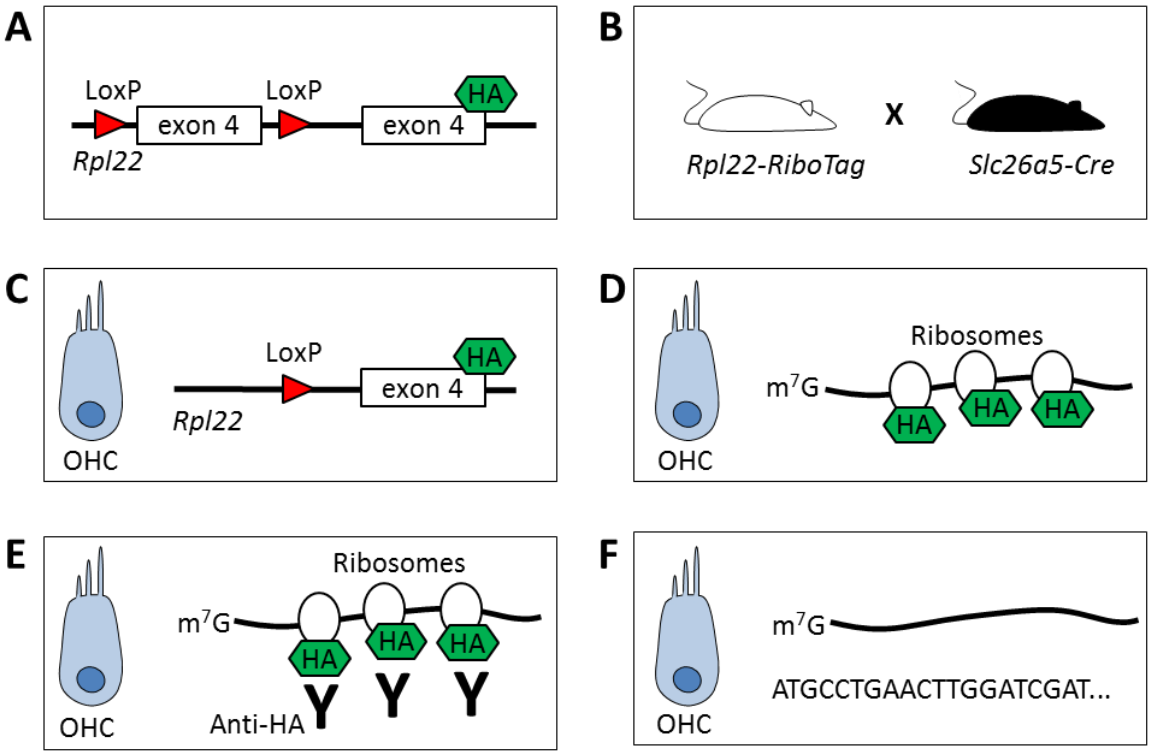

Figure 7.5: Overview of isolation of outer hair cell-specific RNA using the *RiboTag* mouse strain.
(A) The *RiboTag* mouse carries a modified *Rpl22* allele, whereby the final coding exon 4 is flanked with LoxP recombination sites and is followed by an identical HA-tagged exon. **(B)** In order to isolate OHC RNA, the *RiboTag* mouse would be crossed with an OHC-specific Cre recombinase driver line, *Slc26a5-Cre*. **(C)** This will delete the floxed exon 4 of *Rpl22* specifically in the OHCs and leave only the HA-tagged exon. **(D)** As a result, these mice would now express RPL22 HA-tagged ribosomes in the OHCs. **(E)** In order to capture ribosome-associated RNA transcripts from the OHCs, an immunoprecipitation reaction would be performed on homogenised cochleae using an anti-HA antibody. **(F)** RNA-Seq would then be carried out on the captured transcripts to generate OHC-specific transcriptomes. Modified from (Sanz et al., 2009). HA, haemagglutinin; m^7G, 7-methylguanosine 5' RNA cap; OHC, outer hair cell; *Rpl22,* Ribosomal protein 22.

Following the production of *Ikzf2*$^{cello/cello}$; *B6N.129-Rpl22*$^{tm1.1Psam/+}$; *Slc26a5*$^{Cre/+}$ mutants and *Ikzf2*$^{+/+}$; *B6N.129-Rpl22*$^{tm1.1Psam/+}$; *Slc26a5*$^{Cre/+}$ controls, I would aim to generate OHC-specific transcriptomes for *Ikzf2*$^{cello/cello}$ and *Ikzf2*$^{+/+}$ animals at a range of time points during postnatal development (eg. P0, P4, P8, P12, P16) to assess dynamic changes in gene expression that are potentially regulated by helios. This will not only help to validate if any of the putative iRegulon target genes exhibit perturbed expression during development, but also increase our understanding of the transcriptional network of helios and its overall role in regulating the maturing OHC transcriptome.

Together, the luciferase reporter assays and iRegulon network analysis suggest that *Slc26a5* is a primary target of helios. Although the luciferase data indicate that WT helios is capable of transactivating the *Slc26a5* promoter, there is the possibility that this artificial *in vitro* over-expression system may produce false positive results; for example, helios may be acting upon an intermediary factor, endogenous to the cell line, which in turn regulates *Slc26a5* transactivation. In order to address this and establish a direct interaction between helios and *Slc26a5*, site-directed mutagenesis should be undertaken to disrupt key nucleotides of the helios binding motif in the *Slc26a5* promoter pGL3 construct (Figure 7.6). If *Slc26a5* is a true primary target of helios, this is expected to abolish any helios-induced transactivation.

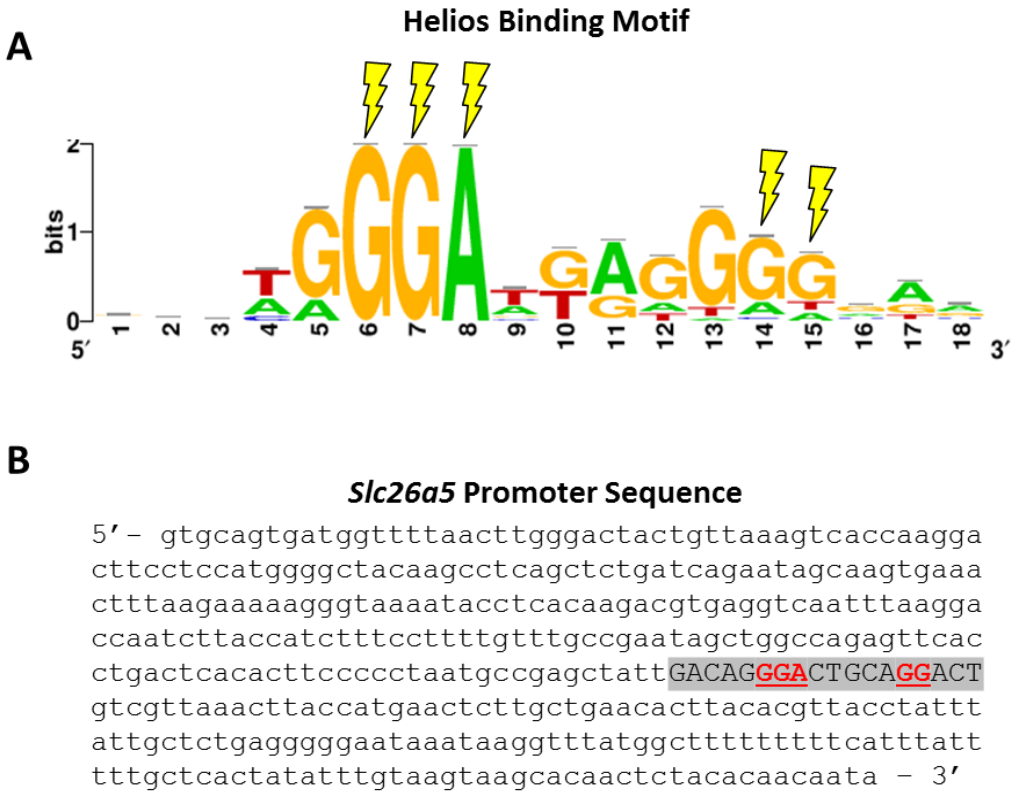

Figure 7.6: Site-directed mutagenesis of the *Slc26a5* promoter for luciferase reporter assays.
(A) To confirm that *Slc26a5* is a direct target of helios, site-directed mutagenesis should be undertaken to disrupt a number of key nucleotides of the helios DNA-binding motif (marked with lightning bolts) within the *Slc26a5* promoter prior to carrying out luciferase reporter assays. **(B)** The location of this DNA-binding motif in the *Slc26a5* promoter sequence is highlighted in grey, with the residues that will be targeted for mutagenesis underlined and coloured red.

This could also be supported with a targeted chIP study to further investigate the interaction of both WT and H517Q helios with *Slc26a5.* Whilst an *in vivo* endogenous chIP would be ideal, the relatively low abundance of OHCs (~2500 in the mouse cochlea) (Ehret and Frankenreiter, 1977) means that a large amount of starting tissue would be required (between 400 – 4000 cochleae to achieve the typical chIP requirement of $10^6 – 10^7$ cells). As such, this approach is not only impractical but also unethical in accordance with the National Centre for the Replacement, Refinement and Reduction of Animals in Research guidelines (NC3Rs, 2015). Instead, a 'micro-chIP' protocol could carried out (Dahl and Collas, 2008, 2009), which is suitable for small cell numbers in the range of 100 – 100,000 and has been recently adapted for use in hair cells (Cai et al., 2015). Alternatively, if a stable OHC line was established, an *in vitro* artificial method could also be used (Masuda et al., 2011), whereby chIP would be performed on cultured OHCs that have been co-transfected with either Myc-WT or Myc-H517Q helios. To further investigate protein-DNA interactions, chIP studies should also be followed by EMSAs. Similarly, this approach should be repeated for other putative RNA-Seq and iRegulon target genes, such as *Ocm* and *Elovl2*, following validation of their dysregulated expression by additional qRT-PCR. For example, if a significant decrease in *Ocm* expression was confirmed in *Ikzf2*$^{cello/cello}$ mutants, the ability of helios to bind and transactivate the regulatory elements of *Ocm* could be investigated using the chIP protocols detailed above, as well as EMSAs and luciferase reporter assays once a binding motif is determined.

In addition to identifying downstream genes that are regulated by helios, it would also be interesting to investigate what is upstream of helios, controlling its expression. To this end, *in vitro* promoter deletion analyses ('promoter bashing') should be undertaken (Matsukura et al., 1999, Xu et al., 2013), although this would again require a stable OHC line. This

technique would involve cloning the promoter and/or regulatory regions of *Ikzf2* and mutagenising distinct binding sites prior to ligation to a reporter gene, such as *luciferase*. Transcription from the mutagenised *Ikzf2* sequences could then be assayed in cultured OHCs in order to determine which binding sites are required for transcription. This could be followed by a 'reverse chIP' experiment (Dejardin and Kingston, 2009), whereby biotinylated DNA probes against the required *Ikzf2* binding sites would be used to pull-down associated proteins, which are then identified by mass spectrometry. Once putative regulators have been identified, their relationship with *Ikzf2* could be confirmed using classical chIP experiments and EMSAs, as before.

Current electrophysiological analyses demonstrated that OHC size and electromotility was significantly reduced in *Ikzf2*$^{cello/cello}$ mutants. A decrease in OHC electromotility was also reported in heterozygous prestin knock-out (*Slc26a5*$^{+/-}$) mice (Liberman et al., 2002, Wu et al., 2004). However, although both *Slc26a5*$^{+/-}$ and *Ikzf2*$^{cello/cello}$ mice have a similar 50% decrease in *Slc26a5* expression, the peak electromotility of OHCs from *Slc26a5*$^{+/-}$ mice was ~0.5 µm (a 45% reduction compared to *Slc26a5*$^{+/+}$ controls) (Liberman et al., 2002), whilst OHCs from *Ikzf2*$^{cello/cello}$ mice were found to move only 0.138 µm on average (a 75% reduction compared to *Ikzf2*$^{cello/+}$ controls). This difference in electromotility in the presence of similar levels of *Slc26a5* indicates that other factors are contributing to the decreased electromotility, and indeed hearing impairment, in *Ikzf2*$^{cello/cello}$ mice. This could include the reduction in *Ocm* expression, given that previous work has suggested that oncomodulin is involved in the efferent modulation of electromotility (Sakaguchi et al., 1998b, Simmons et al., 2010, Yang et al., 2004). To further investigate this, oncomodulin knock-out mice (*Ocm*$^{tm1e(EUCOMM)Wtsi/tm1e(EUCOMM)Wtsi}$) should be requested from the IMPC and subject to electrophysiological analyses in order to investigate the requirement of oncomodulin for

OHC electromotility. In addition, prestin knock-out mice should be imported into MRC Harwell so that compound mutants could be produced (both *Slc26a5*$^{+/-}$; *Ocm*$^{tm1e(EUCOMM)Wtsi/+}$ mice and *Slc26a5*$^{+/-}$; *Ocm*$^{tm1e(EUCOMM)Wtsi/tm1e(EUCOMM)Wtsi}$ mice, given that *Ocm* expression was decreased by ~0.6-fold in *Ikzf2*$^{cello/cello}$ mice). If the OHC electromotility in these double mutants resembled that of the *Ikzf2*$^{cello/cello}$ mice, then it would confirm that the electromotility phenotype in *Ikzf2*$^{cello/cello}$ animals is primarily due to the dysregulation of *Slc26a5* and *Ocm.* ABR testing of these mice would also determine the contribution that reduced electromotility makes to overall hearing thresholds; if electromotility in double mutants was similar to that of *Ikzf2*$^{cello/cello}$ mice, but auditory thresholds were not as elevated, this would suggest that additional pathways/mechanisms are disrupted in *Ikzf2*$^{cello/cello}$ mice.

Following on from this, another limitation of this work is that only three functional properties of the OHCs – potassium currents, MET function and electromotility – were explored in *Ikzf2*$^{cello/cello}$ mice. Further work should be undertaken to investigate innervation, ion transport and morphology of both the OHCs, IHCs and central auditory system in *Ikzf2*$^{cello/cello}$ mutants to identify any additional pathologies that may be directly contributing to the hearing impairment. This is particularly important, given that a number of GO terms related to neural development and ion transport were enriched within the *Ikzf2*$^{cello/cello}$ RNA-Seq dataset. Furthermore, helios has previously been linked with neuronal differential in the developing brain (Martin-Ibanez et al., 2012) and the OHCs are known to influence neurotransmission and signalling from the IHCs during sound transduction through efferent feedback (Brown and Nuttall, 1984, Dallos and Harris, 1978). Initially, this should involve immunolabelling of cochlear wholemounts using antibodies against known neural and synaptic markers: ribeye, a pre-synaptic hair cell scaffold protein (Engel et al., 2006, Schmitz

et al., 2000); glutamate receptor 2 (GluR2), GluR3 and GluR4, which are subunits of the post-synaptic AMPA-type glutamate receptor on afferent SGNs (Isaac et al., 2007, Huang et al., 2012); and neurofilament, a component of SGNs (Hasko et al., 1990, Berglund and Ryugo, 1991, Despres et al., 1994). Immunolabelling should also be undertaken to study the expression and localisation of ion channels in the hair cells. In addition, transmission electron microscopy should be used to examine the morphology of the ribbon synapse at high resolution. Patch-clamp electrophysiology should also be undertaken to investigate hair cell calcium currents, exocytosis and action potential firing, as in Johnson et al. (2009) and Johnson et al. (2011) and DPOAEs should be performed to assess OHC efferent function, as in Varghese et al. (2005). Finally, immunolabelling of histological brain sections with neural markers and injection of neural tracers should be used to investigate the morphology and neuronal projections of the central auditory system. This should be carried out alongside peak amplitude and interpeak latency ABR measurements, to give an indication of any central processing defects. The ability of *Ikzf2*$^{cello/cello}$ mutants to localise sound signals and adapt to altered spatial cues could also be tested, however, this would have to be undertaken at young ages (~P14) as they exhibit early-onset progressive hearing loss. Together, these analyses will help determine if *Ikzf2*$^{cello/cello}$ mice have any defects in neural development, synaptic morphology, afferent/efferent function, ion transport or central processing that may be contributing to their severely elevated auditory thresholds.

Together with the pegasus IMPC data, the work presented in this thesis provides the first evidence implicating the ikaros family in hearing loss. To further investigate the role of pegasus in the auditory system, the pegasus knock-out IMPC strain (*Ikzf5*$^{tm1(KOMP)Wtsi/tm1(KOMP)Wtsi}$) should be imported into MRC Harwell for full phenotypic and functional characterisation. As with *cello*, this would involve time course studies of protein

localisation, auditory function, ear morphology and hair cell electrophysiology. If hearing impairment is confirmed in pegasus knock-out mice, additional RNA-Seq experiments, utilising RNA extracted from the appropriate cochlear cells, should also be undertaken to assess for transcriptional dysregulation and hence identify potential target genes and pathways of pegasus. As before, this should be followed with chIP experiments, EMSAs and luciferase reporter assays, to fully characterise the relationship of pegasus with any putative target genes.

As mentioned previously, the recent SHIELD hair cell-specific gene expression datasets indicate that *Ikzf5* is expressed in cochlear hair cells and is significantly enriched in the IHCs compared to the OHCs (Figure 7.1 and Figure 7.2) (Liu et al., 2014, Scheffer et al., 2015). If, during the above experiments, expression of pegasus was detected in the OHCs, it would be interesting to determine if helios and pegasus interact and if pegasus is necessary for helios function in the OHCs, especially given that the IKZF proteins are known to heterodimerise with one another (Honma et al., 1999, McCarty et al., 2003, Molnar and Georgopoulos, 1994, Morgan et al., 1997, Perdomo et al., 2000). To this end, genetic interaction studies should be undertaken by crossing *cello* mice with pegasus knock-out mice. As detailed in this thesis, heterozygous *Ikzf2*$^{cello/+}$ mice have normal auditory thresholds. As such, it would be interesting to assess hearing in double heterozygous mice (*Ikzf2*$^{cello/+}$; *Ikzf5*$^{tm1(KOMP)Wtsi/+}$) compared to *cello* single heterozygotes alone (*Ikzf2*$^{cello/+}$) and in *cello* heterozygous : pegasus knock-out homozygous mice (*Ikzf2*$^{cello/+}$; *Ikzf5*$^{tm1(KOMP)Wtsi/tm1(KOMP)Wtsi}$) compared to pegasus knock-out homozygotes alone (*Ikzf5*$^{tm1(KOMP)Wtsi/tm1(KOMP)Wtsi}$) to see if auditory function is worse. Depending on the initial analysis of the pegasus knock-out mice and these crosses, it may also be worth generating double homozygous mice (*Ikzf2*$^{cello/cello}$; *Ikzf5*$^{tm1(KOMP)Wtsi/tm1(KOMP)Wtsi}$) to determine if the phenotypes are additive; that is, does being

additionally homozygous null for pegasus make the *Ikzf2*$^{cello/cello}$ mutant phenotype worse? Are auditory thresholds at P16 more elevated in the double homozygotes than in the *Ikzf2*$^{cello/cello}$ mutants alone? These data would help to determine and elaborate upon any interplay between these two IKZF proteins within the auditory system.

It would also be prudent to investigate the other ikaros family members within the ear; although eos has previously been detected in afferent SGNs (Bao et al., 2004), ikaros and aiolos localisation should be assessed using immunolabelling of wild-type cochlear and vestibular vibratome sections. If auditory expression was found, the appropriate knock-out mice could then be requested through IMPC and imported into MRC Harwell for full phenotypic and functional characterisation.

7.3. Contribution to the Field

The mammalian auditory system detects and processes sound information with extremely high sensitivity and temporal precision thanks to the specialised IHCs and OHCs of the cochlea. Whilst the IHCs are responsible for transmitting sound information to the brain via Type I SGNs (Glowatzki and Fuchs, 2002), the OHCs provide electromechanical amplification to vastly enhance acoustic sensitivity and frequency-selectivity (Dallos and Corey, 1991, Liberman et al., 2002).

Both the IHCs and OHCs arise from common sensory progenitor cells (Morsli et al., 1998), which are driven towards a hair cell fate by the combined expression of the transcription factors ATOH1, GFI1 and POU4F3 (Bermingham et al., 1999, Costa et al., 2015, Wallis et al., 2003, Xiang et al., 1998). The two hair cell subtypes are biophysically indistinguishable

during embryonic development (Housley et al., 2006, Marcotti, 2012) and begin to diverge at birth in the mouse (Kuhn et al., 2011). Following this initial differentiation, immature IHCs and OHCs follow distinct morphological and physiological developmental programmes to acquire their subtype-specific adult-like characteristics prior to the onset of hearing at ~P12 (Ehret, 1976). In the OHCs, this critical period of postnatal development involves the expression of the $I_{K,n}$ membrane current and acquisition of prestin-mediated electromotility, which occur at ~P8 and are crucial for OHC function (Abe et al., 2007, He et al., 1994, Marcotti and Kros, 1999). This postnatal functional maturation is an extremely ordered process, however, the genetic factors that regulate it and underlie the morphological and functional specialisations that are unique to the OHCs are currently largely unknown.

The data presented in my thesis have demonstrated that helios is a novel inner ear transcription factor that begins to be expressed in the OHCs during postnatal development (Figure 7.7). Characterisation of *cello* mice has shown that loss of helios function disrupts the normal acquisition of OHC electromotility, thereby preventing the OHCs from becoming fully functionally mature and suggesting that *Ikzf2*$^{cello/cello}$ mice never acquire normal hearing at ~P12. Whilst more work needs to be done into the transcriptional networks of helios, initial results indicate that it is a putative direct regulator of possibly 40 genes within developing OHCs. Current experimental evidence supports a direct interaction between helios and *Slc26a5* and implicates helios in the transcriptional regulation of *Slc26a5* and, thus, expression of prestin.

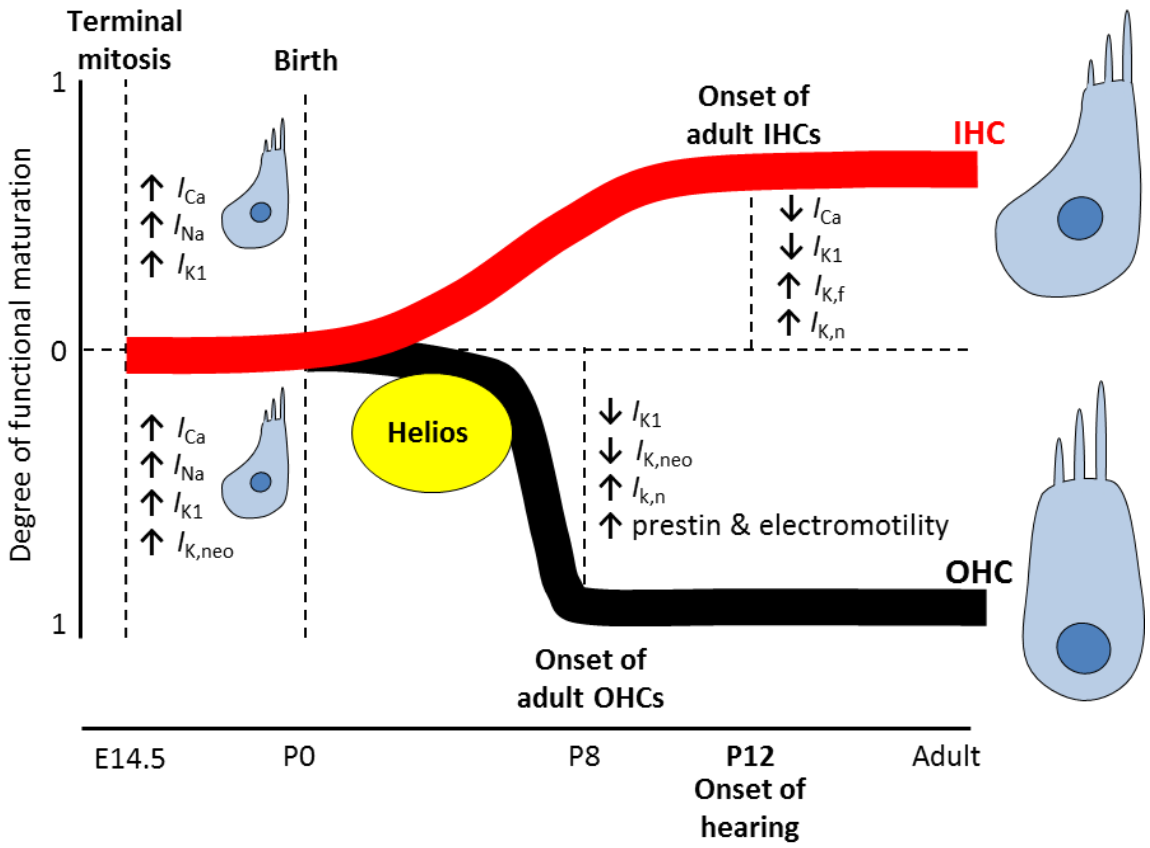

Figure 7.7: Functional maturation of inner hair cells and outer hair cells in the mammalian cochlea.
During embryonic development, immature IHCs and OHCs have a similar repertoire of ion channels and membrane currents, making them electrophysiologically indistinguishable (indicated by '0'). After birth, they begin to diverge in terms of their morphology and physiology in order to become fully differentiated and functionally mature (indicated by '1') prior to the onset of hearing at around postnatal day (P) 12. This involves the downregulation (↓) and expression (↑) of distinct membrane currents in each hair cell subtype, as well as the expression of prestin and the onset of electromotility in OHCs. As a result, IHCs and OHCs acquire adult-like characteristics by ~P12 and ~P8, respectively. Helios begins to be expressed in the OHCs during this critical period of development and is required for the acquisition of their adult-like electromotile properties and proper functional maturation. Adapted from Kuhn et al. (2011). I_{Ca}, inward calcium current; I_{K1}, inward rectifier potassium current; $I_{K,f}$, rapidly-activating large-conductance calcium-activated potassium current; $I_{K,n}$, negatively-activating delayed rectifier potassium current; $I_{K,neo}$, outward potassium current; I_{Na}, inward Na^+ current; E, embryonic day; IHC, inner hair cell; OHC, outer hair cell; P, postnatal day.

Going forward, the translational value of these findings should be investigated by determining whether helios is associated with hearing loss in human populations. The genomic region encoding *Ikzf2* in humans (Chr2q34) has not currently been identified as a candidate locus for either isolated or syndromic hearing loss (Hereditary-Hearing-Loss, 2015). In addition, data from genome wide association studies, including the 1958 British

Birth Cohort study (Power and Elliott, 2006), have not shown any significant associations between *Ikzf2* and auditory dysfunction, to date.

Whilst the importance of helios for human hearing currently remains unknown, the data present in this thesis suggest that helios plays a key role in regulating the transcriptome and functional maturation of developing OHCs in the mouse, thus helping to shed light on the genetic basis underlying their unique physiology and function. This also contributes to knowledge gained from previous transcriptome profiling studies of hair cells in both mice and zebrafish (Hertzano et al., 2011, Liu et al., 2014, McDermott et al., 2007), which sought to identify genes that are differentially expressed between IHCs and OHCs and related to their physiological specialisations. Importantly, these datasets will not only further our understanding of the molecular mechanisms and regulatory networks underlying hair cell development and function, but ultimately may also help with recent efforts to regenerate hair cells through, for example, genetic programming of mouse embryonic stem cells (Almeida-Branco et al., 2014, Costa et al., 2015, Jahan et al., 2015), thus providing a valuable potential therapeutic avenue for sensorineural hearing loss.

7.4. Concluding Remarks

Overall, the data presented in my thesis have strongly implicated *Ikzf2* as a novel hearing loss-causing gene and demonstrated that the helios transcription factor is likely essential for proper OHC maturation and auditory function. As well as establishing a critical role for helios in the mammalian auditory system, this study also reinforces the value of using mouse models in hearing research and for the identification of novel genes and pathways required for auditory function.

Chapter 8 : References

ABE, T., KAKEHATA, S., KITANI, R., MARUYA, S., NAVARATNAM, D., SANTOS-SACCHI, J. & SHINKAWA, H. 2007. Developmental expression of the outer hair cell motor prestin in the mouse. *J Membr Biol,* 215**,** 49-56.

ACEVEDO-AROZENA, A., WELLS, S., POTTER, P., KELLY, M., COX, R. D. & BROWN, S. D. 2008. Enu mutagenesis, a way forward to understand gene function. *Annu Rev Genomics Hum Genet,* 9**,** 49-69.

ACTION-ON-HEARING-LOSS. 2015. *About deafness and hearing loss.* [Online]. Available: http://www.actiononhearingloss.org.uk/your-hearing/about-deafness-and-hearing-loss/statistics.aspx [Accessed 24/09/2015].

ACTON, Q. A. 2013. *Hearing loss: New insights for the healthcare professional,* 2013 ed. Georgia: ScholarlyEditions.

ADZHUBEI, I. A., SCHMIDT, S., PESHKIN, L., RAMENSKY, V. E., GERASIMOVA, A., BORK, P., KONDRASHOV, A. S. & SUNYAEV, S. R. 2010. A method and server for predicting damaging missense mutations. *Nat methods.* United States.

AGOSTON, D. V., SZEMES, M., DOBI, A., PALKOVITS, M., GEORGOPOULOS, K., GYORGY, A. & RING, M. A. 2007. Ikaros is expressed in developing striatal neurons and involved in enkephalinergic differentiation. *J neurochem.* England.

AHMED, Z. M., MORELL, R. J., RIAZUDDIN, S., GROPMAN, A., SHAUKAT, S., AHMAD, M. M., MOHIDDIN, S. A., FANANAPAZIR, L., CARUSO, R. C., HUSNAIN, T., KHAN, S. N., GRIFFITH, A. J., FRIEDMAN, T. B. & WILCOX, E. R. 2003a. Mutations of myo6 are associated with recessive deafness, dfnb37. *Am J Hum Genet,* 72**,** 1315-22.

AHMED, Z. M., RIAZUDDIN, S., AHMAD, J., BERNSTEIN, S. L., GUO, Y., SABAR, M. F., SIEVING, P., GRIFFITH, A. J., FRIEDMAN, T. B., BELYANTSEVA, I. A. & WILCOX, E. R. 2003b. Pcdh15 is expressed in the neurosensory epithelium of the eye and ear and mutant alleles are responsible for both ush1f and dfnb23. *Hum Mol Genet,* 12**,** 3215-23.

AHMED, Z. M., RIAZUDDIN, S., BERNSTEIN, S. L., AHMED, Z., KHAN, S., GRIFFITH, A. J., MORELL, R. J., FRIEDMAN, T. B. & WILCOX, E. R. 2001. Mutations of the protocadherin gene pcdh15 cause usher syndrome type 1f. *Am J Hum Genet,* 69**,** 25-34.

AITKIN, L. M. & PHILLIPS, S. C. 1984. The interconnections of the inferior colliculi through their commissure. *J Comp Neurol,* 228**,** 210-6.

AKIMOVA, T., BEIER, U. H., WANG, L., LEVINE, M. H. & HANCOCK, W. W. 2011. Helios expression is a marker of t cell activation and proliferation. *Plos one.* United States.

ALAGRAMAM, K. N., MURCIA, C. L., KWON, H. Y., PAWLOWSKI, K. S., WRIGHT, C. G. & WOYCHIK, R. P. 2001. The mouse ames waltzer hearing-loss mutant is caused by mutation of pcdh15, a novel protocadherin gene. *Nat Genet,* 27**,** 99-102.

ALBERTS, B., JOHNSON, A., LEWIS, J., RAFF, M., ROBERTS, K. & WALTER, P. 2002. *Molecular biology of the cell,* 2nd ed. New York, Garland Science.

ALLISON, J. P. & RAULET, D. H. 1990. The immunobiology of gamma delta+ t cells. *Semin Immunol,* 2**,** 59-65.

ALLMAN, D., DALOD, M., ASSELIN-PATUREL, C., DELALE, T., ROBBINS, S. H., TRINCHIERI, G., BIRON, C. A., KASTNER, P. & CHAN, S. 2006. Ikaros is required for plasmacytoid dendritic cell differentiation. *Blood.* United States.

ALMEIDA-BRANCO, M. S., CABRERA, S. & LOPEZ-ESCAMEZ, J. A. 2014. Perspectives for the treatment of sensorineural hearing loss by cellular regeneration of the inner ear. *Acta Otorrinolaringol Esp*.

ALSIO, J. M., TARCHINI, B., CAYOUETTE, M. & LIVESEY, F. J. 2013. Ikaros promotes early-born neuronal fates in the cerebral cortex. *Proc Natl Acad Sci U S A,* 110**,** E716-25.

ANDERS, S. & HUBER, W. 2010. Differential expression analysis for sequence count data. *Genome Biol,* 11**,** R106.

ANDERS, S., PYL, P. T. & HUBER, W. 2015. Htseq--a python framework to work with high-throughput sequencing data. *Bioinformatics,* 31**,** 166-9.

ANNIKO, M. 1983. Cytodifferentiation of cochlear hair cells. *Am J Otolaryngol,* 4**,** 375-88.

ANTICA, M., CICIN-SAIN, L., KAPITANOVIC, S., MATULIC, M., DZEBRO, S. & DOMINIS, M. 2008. Aberrant ikaros, aiolos, and helios expression in hodgkin and non-hodgkin lymphoma. *Blood.* United States.

ASANUMA, S., YAMAGISHI, M., KAWANAMI, K., NAKANO, K., SATO-OTSUBO, A., MUTO, S., SANADA, M., YAMOCHI, T., KOBAYASHI, S., UTSUNOMIYA, A., IWANAGA, M., YAMAGUCHI, K., UCHIMARU, K., OGAWA, S. & WATANABE, T. 2013. Adult t-cell leukemia cells are characterized by abnormalities of helios expression that promote t cell growth. *Cancer Sci,* 104**,** 1097-106.

ASHMORE, J. 2008. Cochlear outer hair cell motility. *Physiol Rev,* 88**,** 173-210.

ASHMORE, J. F. 1987. A fast motile response in guinea-pig outer hair cells: The cellular basis of the cochlear amplifier. *J Physiol,* 388**,** 323-47.

ASSAD, J. A., SHEPHERD, G. M. & COREY, D. P. 1991. Tip-link integrity and mechanical transduction in vertebrate hair cells. *Neuron,* 7**,** 985-94.

AVRAHAM, K. B., HASSON, T., STEEL, K. P., KINGSLEY, D. M., RUSSELL, L. B., MOOSEKER, M. S., COPELAND, N. G. & JENKINS, N. A. 1995. The mouse snell's waltzer deafness gene encodes an unconventional myosin required for structural integrity of inner ear hair cells. *Nat Genet,* 11**,** 369-75.

AZAIEZ, H., DECKER, A. R., BOOTH, K. T., SIMPSON, A. C., SHEARER, A. E., HUYGEN, P. L., BU, F., HILDEBRAND, M. S., RANUM, P. T., SHIBATA, S. B., TURNER, A., ZHANG, Y., KIMBERLING, W. J., CORNELL, R. A. & SMITH, R. J. 2015. Homer2, a stereociliary scaffolding protein, is essential for normal hearing in humans and mice. *PLoS Genet,* 11**,** e1005137.

BAINE, I., BASU, S., AMES, R., SELLERS, R. S. & MACIAN, F. 2013. Helios induces epigenetic silencing of il2 gene expression in regulatory t cells. *J Immunol,* 190**,** 1008-16.

BAJO, V. M., NODAL, F. R., MOORE, D. R. & KING, A. J. 2010. The descending corticocollicular pathway mediates learning-induced auditory plasticity. *Nat Neurosci,* 13**,** 253-60.

BAMIOU, D. E., FREE, S. L., SISODIYA, S. M., CHONG, W. K., MUSIEK, F., WILLIAMSON, K. A., VAN HEYNINGEN, V., MOORE, A. T., GADIAN, D. & LUXON, L. M. 2007. Auditory interhemispheric transfer deficits, hearing difficulties, and brain magnetic resonance imaging abnormalities in children with congenital aniridia due to pax6 mutations. *Arch Pediatr Adolesc Med,* 161**,** 463-9.

BANCHEREAU, J. & STEINMAN, R. M. 1998. Dendritic cells and the control of immunity. *Nature,* 392**,** 245-52.

BAO, J., LIN, H., OUYANG, Y., LEI, D., OSMAN, A., KIM, T. W., MEI, L., DAI, P., OHLEMILLER, K. K. & AMBRON, R. T. 2004. Activity-dependent transcription regulation of psd-95 by neuregulin-1 and eos. *Nat Neurosci,* 7**,** 1250-8.

BELYANTSEVA, I. A., ADLER, H. J., CURI, R., FROLENKOV, G. I. & KACHAR, B. 2000. Expression and localization of prestin and the sugar transporter glut-5 during development of electromotility in cochlear outer hair cells. *J Neurosci,* 20**,** Rc116.

BELYANTSEVA, I. A., BOGER, E. T. & FRIEDMAN, T. B. 2003. Myosin xva localizes to the tips of inner ear sensory cell stereocilia and is essential for staircase formation of the hair bundle. *Proc Natl Acad Sci U S A,* 100**,** 13958-63.

BERGLUND, A. M. & RYUGO, D. K. 1991. Neurofilament antibodies and spiral ganglion neurons of the mammalian cochlea. *J Comp Neurol,* 306**,** 393-408.

BERLIN, C. I. 1963. Hearing in mice via gsr audiometry. *J Speech Hear Res,* 6**,** 359-68.

BERMINGHAM-MCDONOGH, O., OESTERLE, E. C., STONE, J. S., HUME, C. R., HUYNH, H. M. & HAYASHI, T. 2006. Expression of prox1 during mouse cochlear development. *J Comp Neurol,* 496**,** 172-86.

BERMINGHAM, N. A., HASSAN, B. A., PRICE, S. D., VOLLRATH, M. A., BEN-ARIE, N., EATOCK, R. A., BELLEN, H. J., LYSAKOWSKI, A. & ZOGHBI, H. Y. 1999. Math1: An essential gene for the generation of inner ear hair cells. *Science,* 284**,** 1837-41.

BESS, F. H., DODD-MURPHY, J. & PARKER, R. A. 1998. Children with minimal sensorineural hearing loss: Prevalence, educational. *Ear Hear,* 19**,** 339-54.

BEURG, M., FETTIPLACE, R., NAM, J. H. & RICCI, A. J. 2009. Localization of inner hair cell mechanotransducer channels using high-speed calcium imaging. *Nat Neurosci,* 12**,** 553-8.

BEURG, M., MICHALSKI, N., SAFIEDDINE, S., BOULEAU, Y., SCHNEGGENBURGER, R., CHAPMAN, E. R., PETIT, C. & DULON, D. 2010. Control of exocytosis by synaptotagmins and otoferlin in auditory hair cells. *J Neurosci,* 30**,** 13281-90.

BEUTNER, D. & MOSER, T. 2001. The presynaptic function of mouse cochlear inner hair cells during development of hearing. *J Neurosci,* 21**,** 4593-9.

BEUTNER, D., VOETS, T., NEHER, E. & MOSER, T. 2001. Calcium dependence of exocytosis and endocytosis at the cochlear inner hair cell afferent synapse. *Neuron.* United States.

BIRKENHAGER, R., OTTO, E., SCHURMANN, M. J., VOLLMER, M., RUF, E. M., MAIER-LUTZ, I., BEEKMANN, F., FEKETE, A., OMRAN, H., FELDMANN, D., MILFORD, D. V., JECK, N., KONRAD, M., LANDAU, D., KNOERS, N. V., ANTIGNAC, C., SUDBRAK, R., KISPERT, A. & HILDEBRANDT, F. 2001. Mutation of bsnd causes bartter syndrome with sensorineural deafness and kidney failure. *Nat Genet,* 29**,** 310-4.

BOETTGER, T., HUBNER, C. A., MAIER, H., RUST, M. B., BECK, F. X. & JENTSCH, T. J. 2002. Deafness and renal tubular acidosis in mice lacking the k-cl co-transporter kcc4. *Nature,* 416**,** 874-8.

BOETTGER, T., RUST, M. B., MAIER, H., SEIDENBECHER, T., SCHWEIZER, M., KEATING, D. J., FAULHABER, J., EHMKE, H., PFEFFER, C., SCHEEL, O., LEMCKE, B., HORST, J., LEUWER, R., PAPE, H. C., VOLKL, H., HUBNER, C. A. & JENTSCH, T. J. 2003. Loss of k-cl co-transporter kcc3 causes deafness, neurodegeneration and reduced seizure threshold. *Embo j,* 22**,** 5422-34.

BOGGS, S. S., TREVISAN, M., PATRENE, K. & GEOGOPOULOS, K. 1998. Lack of natural killer cell precursors in fetal liver of ikaros knockout mutant mice. *Nat Immun,* 16**,** 137-45.

BOLZ, H., VON BREDERLOW, B., RAMIREZ, A., BRYDA, E. C., KUTSCHE, K., NOTHWANG, H. G., SEELIGER, M., CABRERA, M. D. S., VILA, M. C., MOLINA, O. P., GAL, A. & KUBISCH, C. 2001. Mutation of cdh23, encoding a new member of the cadherin gene family, causes usher syndrome type 1d. *Nature Genetics,* 27**,** 108-112.

BORK, J. M., PETERS, L. M., RIAZUDDIN, S., BERNSTEIN, S. L., AHMED, Z. M., NESS, S. L., POLOMENO, R., RAMESH, A., SCHLOSS, M., SRISAILPATHY, C. R. S., WAYNE, S., BELLMAN, S., DESMUKH, D., AHMED, Z., KHAN, S. N., KALOUSTIAN, V. M. D., LI, X. C., LALWANI, A., BITNER-GLINDZICZ, M., NANCE, W. E., LIU, X. Z., WISTOW, G., SMITH, R. J. H., GRIFFITH, A. J., WILCOX, E. R., FRIEDMAN, T. B. & MORELL, R. J. 2001. Usher syndrome 1d and nonsyndromic autosomal recessive deafness dfnb12 are caused by allelic mutations of the novel cadherin-like gene cdh23. *American Journal of Human Genetics,* 68**,** 26-37.

BRAMHALL, N. F., SHI, F., ARNOLD, K., HOCHEDLINGER, K. & EDGE, A. S. 2014. Lgr5-positive supporting cells generate new hair cells in the postnatal cochlea. *Stem Cell Reports,* 2**,** 311-22.

BRANDT, A., STRIESSNIG, J. & MOSER, T. 2003. Cav1.3 channels are essential for development and presynaptic activity of cochlear inner hair cells. *J neurosci.* United States.

BROWN, K. E., BAXTER, J., GRAF, D., MERKENSCHLAGER, M. & FISHER, A. G. 1999. Dynamic repositioning of genes in the nucleus of lymphocytes preparing for cell division. *Mol cell.* United States.

BROWN, K. E., GUEST, S. S., SMALE, S. T., HAHM, K., MERKENSCHLAGER, M. & FISHER, A. G. 1997. Association of transcriptionally silent genes with ikaros complexes at centromeric heterochromatin. *Cell.* United States.

BROWN, M. C. 2014. Single-unit labeling of medial olivocochlear neurons: The cochlear frequency map for efferent axons. *J Neurophysiol,* 111**,** 2177-86.

BROWN, M. C. & NUTTALL, A. L. 1984. Efferent control of cochlear inner hair cell responses in the guinea-pig. *J Physiol,* 354**,** 625-46.

BROWN, R. S., SANDER, C. & ARGOS, P. 1985. The primary structure of transcription factor tfiiia has 12 consecutive repeats. *Febs lett.* Netherlands.

BROWN, S. D., HARDISTY-HUGHES, R. E. & MBURU, P. 2008. Quiet as a mouse: Dissecting the molecular and genetic basis of hearing. *Nat rev genet.* England.

BROWN, S. D. & MOORE, M. W. 2012. The international mouse phenotyping consortium: Past and future perspectives on mouse phenotyping. *Mamm Genome,* 23**,** 632-40.

BROWNELL, W. E., BADER, C. R., BERTRAND, D. & DE RIBAUPIERRE, Y. 1985. Evoked mechanical responses of isolated cochlear outer hair cells. *Science,* 227**,** 194-6.

BURNS, J. C. & CORWIN, J. T. 2014. Responses to cell loss become restricted as the supporting cells in mammalian vestibular organs grow thick junctional actin bands that develop high stability. *J Neurosci,* 34**,** 1998-2011.

CAI, Q., DIERICH, A., OULAD-ABDELGHANI, M., CHAN, S. & KASTNER, P. 2009. Helios deficiency has minimal impact on t cell development and function. *J immunol.* United States.

CAI, T., JEN, H. I., KANG, H., KLISCH, T. J., ZOGHBI, H. Y. & GROVES, A. K. 2015. Characterization of the transcriptome of nascent hair cells and identification of direct targets of the atoh1 transcription factor. *J neurosci.* United States: 2015 the authors 0270-6474/15/355870-14$15.00/0.

CAI, T., SEYMOUR, M. L., ZHANG, H., PEREIRA, F. A. & GROVES, A. K. 2013. Conditional deletion of atoh1 reveals distinct critical periods for survival and function of hair cells in the organ of corti. *J Neurosci,* 33**,** 10110-22.

CARIAPPA, A., TANG, M., PARNG, C., NEBELITSKIY, E., CARROLL, M., GEORGOPOULOS, K. & PILLAI, S. 2001. The follicular versus marginal zone b lymphocyte cell fate decision is regulated by aiolos, btk, and cd21. *Immunity.* United States.

CARNEY, P. R. & SILVER, J. 1983. Studies on cell migration and axon guidance in the developing distal auditory system of the mouse. *J Comp Neurol,* 215**,** 359-69.

CAROLA, R., HARLEY, J. P. & NOBACK, C. R. 1992. *Human anatomy and physiology,* 2nd ed. New York: McGraw-Hill.

CHANG, E. H., VAN CAMP, G. & SMITH, R. J. 2003. The role of connexins in human disease. *Ear Hear,* 24**,** 314-23.

CHEATHAM, M. A., ZHENG, J., HUYNH, K. H., DU, G. G., EDGE, R. M., ANDERSON, C. T., ZUO, J., RYAN, A. F. & DALLOS, P. 2007. Evaluation of an independent prestin mouse model derived from the 129s1 strain. *Audiol Neurootol,* 12**,** 378-90.

CHELLAPPA, R., LI, S., PAULEY, S., JAHAN, I., JIN, K. & XIANG, M. 2008. Barhl1 regulatory sequences required for cell-specific gene expression and autoregulation in the inner ear and central nervous system. *Mol Cell Biol,* 28**,** 1905-14.

CHEN, P., JOHNSON, J. E., ZOGHBI, H. Y. & SEGIL, N. 2002. The role of math1 in inner ear development: Uncoupling the establishment of the sensory primordium from hair cell fate determination. *Development,* 129**,** 2495-505.

CHEN, P. & SEGIL, N. 1999. P27(kip1) links cell proliferation to morphogenesis in the developing organ of corti. *Development,* 126**,** 1581-90.

CHEN, W. C. & DAVIS, R. L. 2006. Voltage-gated and two-pore-domain potassium channels in murine spiral ganglion neurons. *Hear Res,* 222**,** 89-99.

CHO, Y., GONG, T. W., KANICKI, A., ALTSCHULER, R. A. & LOMAX, M. I. 2004. Noise overstimulation induces immediate early genes in the rat cochlea. *Brain Res Mol Brain Res,* 130**,** 134-48.

CHOI, H. S., PARK, K. J., HWANG, S. C., PARK, H. Y., KIM, Y. S. & PARK, K. 2008. The role of peroxiredoxin iii in the ototoxic drug-induced mitochondrial apoptosis of cochlear hair cells. *Acta Otolaryngol,* 128**,** 944-51.

CHOI, Y., SIMS, G. E., MURPHY, S., MILLER, J. R. & CHAN, A. P. 2012. Predicting the functional effect of amino acid substitutions and indels. *PLoS One,* 7**,** e46688.

CHURCH, D. M., GOODSTADT, L., HILLIER, L. W., ZODY, M. C., GOLDSTEIN, S., SHE, X., BULT, C. J., AGARWALA, R., CHERRY, J. L., DICUCCIO, M., HLAVINA, W., KAPUSTIN, Y., MERIC, P., MAGLOTT, D., BIRTLE, Z., MARQUES, A. C., GRAVES, T., ZHOU, S., TEAGUE, B., POTAMOUSIS, K., CHURAS, C., PLACE, M., HERSCHLEB, J., RUNNHEIM, R., FORREST, D., AMOS-LANDGRAF, J., SCHWARTZ, D. C., CHENG, Z., LINDBLAD-TOH, K., EICHLER, E. E. & PONTING, C. P. 2009. Lineage-specific biology revealed by a finished genome assembly of the mouse. *PLoS Biol,* 7**,** e1000112.

COBB, B. S., MORALES-ALCELAY, S., KLEIGER, G., BROWN, K. E., FISHER, A. G. & SMALE, S. T. 2000. Targeting of ikaros to pericentromeric heterochromatin by direct DNA binding. *Genes Dev,* 14**,** 2146-60.

COLVIN, J. S., BOHNE, B. A., HARDING, G. W., MCEWEN, D. G. & ORNITZ, D. M. 1996. Skeletal overgrowth and deafness in mice lacking fibroblast growth factor receptor 3. *Nat Genet,* 12**,** 390-7.

COREY, D. P. 2006. What is the hair cell transduction channel? *J physiol.* England.

CORNS, L. F., JOHNSON, S. L., KROS, C. J. & MARCOTTI, W. 2014. Calcium entry into stereocilia drives adaptation of the mechanoelectrical transducer current of mammalian cochlear hair cells. *Proc natl acad sci u s a.* United States.

CORTES, M. & GEORGOPOULOS, K. 2004. Aiolos is required for the generation of high affinity bone marrow plasma cells responsible for long-term immunity. *J exp med.* United States.

COSTA, A., SANCHEZ-GUARDADO, L., JUNIAT, S., GALE, J. E., DAUDET, N. & HENRIQUE, D. 2015. Generation of sensory hair cells by genetic programming with a combination of transcription factors. *Development,* 142**,** 1948-59.

COTANCHE, D. A. & CORWIN, J. T. 1991. Stereociliary bundles reorient during hair cell development and regeneration in the chick cochlea. *Hear Res,* 52**,** 379-402.

COX, B. C., CHAI, R., LENOIR, A., LIU, Z., ZHANG, L., NGUYEN, D. H., CHALASANI, K., STEIGELMAN, K. A., FANG, J., CHENG, A. G. & ZUO, J. 2014. Spontaneous hair cell regeneration in the neonatal mouse cochlea in vivo. *Development,* 141**,** 816-29.

COX, R. M., ALEXANDER, G. C. & GRAY, G. A. 2005. Who wants a hearing aid? Personality profiles of hearing aid seekers. *Ear Hear,* 26**,** 12-26.

CROUCH, J. J., SAKAGUCHI, N., LYTLE, C. & SCHULTE, B. A. 1997. Immunohistochemical localization of the na-k-cl co-transporter (nkcc1) in the gerbil inner ear. *J Histochem Cytochem,* 45**,** 773-8.

CULBERTSON, J. L. & GILBERT, L. E. 1986. Children with unilateral sensorineural hearing loss: Cognitive, academic, and. *Ear Hear,* 7**,** 38-42.

DABDOUB, A., MONTCOUQUIOL, M. & KELLEY, M. 2005. Planar cell polarity in the vertebrate inner ear. *In:* MLODZIK, M. (ed.) *Advances in developmental biology: Planar cell polarization during development.* California: Elsevier, pp. 107-130.

DABDOUB, A., PULIGILLA, C., JONES, J. M., FRITZSCH, B., CHEAH, K. S., PEVNY, L. H. & KELLEY, M. W. 2008. Sox2 signaling in prosensory domain specification and subsequent hair cell differentiation in the developing cochlea. *Proc Natl Acad Sci U S A,* 105**,** 18396-401.

DAHL, J. A. & COLLAS, P. 2008. A rapid micro chromatin immunoprecipitation assay (microchip). *Nat Protoc,* 3**,** 1032-45.

DAHL, J. A. & COLLAS, P. 2009. Microchip: Chromatin immunoprecipitation for small cell numbers. *Methods Mol Biol,* 567**,** 59-74.

DALLOS, P. 1992. The active cochlea. *J Neurosci,* 12**,** 4575-85.

DALLOS, P. 2008. Cochlear amplification, outer hair cells and prestin. *Curr Opin Neurobiol,* 18**,** 370-6.

DALLOS, P., BILLONE, M. C., DURRANT, J. D., WANG, C. & RAYNOR, S. 1972. Cochlear inner and outer hair cells: Functional differences. *Science,* 177**,** 356-8.

DALLOS, P. & COREY, M. E. 1991. The role of outer hair cell motility in cochlear tuning. *Curr Opin Neurobiol,* 1**,** 215-20.

DALLOS, P. & HARRIS, D. 1978. Properties of auditory nerve responses in absence of outer hair cells. *J Neurophysiol,* 41**,** 365-83.

DALLOS, P., HE, D. Z., LIN, X., SZIKLAI, I., MEHTA, S. & EVANS, B. N. 1997. Acetylcholine, outer hair cell electromotility, and the cochlear amplifier. *J Neurosci,* 17**,** 2212-26.

DALLOS, P., WU, X., CHEATHAM, M. A., GAO, J., ZHENG, J., ANDERSON, C. T., JIA, S., WANG, X., CHENG, W. H., SENGUPTA, S., HE, D. Z. & ZUO, J. 2008. Prestin-based outer hair cell motility is necessary for mammalian cochlear amplification. *Neuron.* United States.

DALLOS, P., ZHENG, J. & CHEATHAM, M. A. 2006. Prestin and the cochlear amplifier. *J Physiol,* 576**,** 37-42.

DALTON, D. S., CRUICKSHANKS, K. J., KLEIN, B. E., KLEIN, R., WILEY, T. L. & NONDAHL, D. M. 2003. The impact of hearing loss on quality of life in older adults. *Gerontologist,* 43**,** 661-8.

DARROW, K. N., MAISON, S. F. & LIBERMAN, M. C. 2007. Selective removal of lateral olivocochlear efferents increases vulnerability to acute acoustic injury. *J Neurophysiol,* 97**,** 1775-85.

DAU, J. & WENTHOLD, R. J. 1989. Immunocytochemical localization of neurofilament subunits in the spiral ganglion of normal and neomycin-treated guinea pigs. *Hear Res,* 42**,** 253-63.

DE JONGHE, P., TIMMERMAN, V., CEUTERICK, C., NELIS, E., DE VRIENDT, E., LOFGREN, A., VERCRUYSSEN, A., VERELLEN, C., VAN MALDERGEM, L., MARTIN, J. J. & VAN BROECKHOVEN, C. 1999. The thr124met mutation in the peripheral myelin protein zero (mpz) gene is associated with a clinically distinct charcot-marie-tooth phenotype. *Brain,* 122 (Pt 2)**,** 281-90.

DEGERMAN, E., RAUCH, U., GORANSSON, O., LINDBERG, S., HULTGARDH, A. & MAGNUSSON, M. 2011. Identification of new signaling components in the sensory epithelium of human saccule. *Front Neurol,* 2**,** 48.

DEJARDIN, J. & KINGSTON, R. E. 2009. Purification of proteins associated with specific genomic loci. *Cell,* 136**,** 175-86.

DELPIRE, E., LU, J., ENGLAND, R., DULL, C. & THORNE, T. 1999. Deafness and imbalance associated with inactivation of the secretory na-k-2cl co-transporter. *Nat Genet,* 22**,** 192-5.

DENG, M., YANG, H., XIE, X., LIANG, G. & GAN, L. 2014. Comparative expression analysis of pou4f1, pou4f2 and isl1 in developing mouse cochleovestibular ganglion neurons. *Gene Expr Patterns,* 15**,** 31-7.

DENMAN-JOHNSON, K. & FORGE, A. 1999. Establishment of hair bundle polarity and orientation in the developing vestibular system of the mouse. *J Neurocytol,* 28**,** 821-35.

DENOYELLE, F., MARLIN, S., WEIL, D., MOATTI, L., CHAUVIN, P., GARABEDIAN, E. N. & PETIT, C. 1999. Clinical features of the prevalent form of childhood deafness, dfnb1, due to a connexin-26 gene defect: Implications for genetic counselling. *Lancet,* 353**,** 1298-303.

DENOYELLE, F., WEIL, D., MAW, M. A., WILCOX, S. A., LENCH, N. J., ALLEN-POWELL, D. R., OSBORN, A. H., DAHL, H. H., MIDDLETON, A., HOUSEMAN, M. J., DODE, C., MARLIN, S., BOULILA-ELGAIED, A., GRATI, M., AYADI, H., BENARAB, S., BITOUN, P., LINA-GRANADE, G., GODET, J., MUSTAPHA, M., LOISELET, J., EL-ZIR, E., AUBOIS, A., JOANNARD, A., LEVILLIERS, J., GARABEDIAN, E. N., MUELLER, R. F., GARDNER, R. J., PETIT, C. & ET AL. 1997. Prelingual deafness: High prevalence of a 30delg mutation in the connexin 26 gene. *Hum Mol Genet,* 6**,** 2173-7.

DESPRES, G., LEGER, G. P., DAHL, D. & ROMAND, R. 1994. Distribution of cytoskeletal proteins (neurofilaments, peripherin and map-tau) in the cochlea of the human fetus. *Acta Otolaryngol,* 114**,** 377-81.

DI PALMA, F., HOLME, R. H., BRYDA, E. C., BELYANTSEVA, I. A., PELLEGRINO, R., KACHAR, B., STEEL, K. P. & NOBEN-TRAUTH, K. 2001. Mutations in cdh23, encoding a new type of cadherin, cause stereocilia disorganization in waltzer, the mouse model for usher syndrome type 1d. *Nature Genetics,* 27**,** 103-107.

DOETZLHOFER, A., BASCH, M. L., OHYAMA, T., GESSLER, M., GROVES, A. K. & SEGIL, N. 2009. Hey2 regulation by fgf provides a notch-independent mechanism for maintaining pillar cell fate in the organ of corti. *Dev Cell,* 16**,** 58-69.

DOVAT, S., MONTECINO-RODRIGUEZ, E., SCHUMAN, V., TEITELL, M. A., DORSHKIND, K. & SMALE, S. T. 2005. Transgenic expression of helios in b lineage cells alters b cell properties and promotes lymphomagenesis. *J immunol.* United States.

DRIVER, E. C. & KELLEY, M. W. 2009. Specification of cell fate in the mammalian cochlea. *Birth Defects Res C Embryo Today,* 87**,** 212-21.

DRIVER, E. C., PRYOR, S. P., HILL, P., TURNER, J., RUTHER, U., BIESECKER, L. G., GRIFFITH, A. J. & KELLEY, M. W. 2008. Hedgehog signaling regulates sensory cell formation and auditory function in mice and humans. *J Neurosci,* 28**,** 7350-8.

DU, D. & LOU, X. 2014. Generation of induced pluripotent stem cells from neonatal mouse cochlear cells. *Differentiation*.

EBERMANN, I., SCHOLL, H. P., CHARBEL ISSA, P., BECIROVIC, E., LAMPRECHT, J., JURKLIES, B., MILLAN, J. M., ALLER, E., MITTER, D. & BOLZ, H. 2007. A novel gene for usher syndrome type 2: Mutations in the long isoform of whirlin are associated with retinitis pigmentosa and sensorineural hearing loss. *Hum Genet,* 121**,** 203-11.

ECHTELER, S. M. 1992. Developmental segregation in the afferent projections to mammalian auditory hair cells. *Proc Natl Acad Sci U S A,* 89**,** 6324-7.

EHRET, G. 1976. Development of absolute auditory thresholds in the house mouse (mus musculus). *J Am Audiol Soc,* 1**,** 179-84.

EHRET, G. & FRANKENREITER, M. 1977. Quantitative analysis of cochlear structures in the house mouse in relation to mechanisms of acoustical information processing. *Journal of Comparative Physiology,* 122**,** 65-85.

ELGOYHEN, A. B., JOHNSON, D. S., BOULTER, J., VETTER, D. E. & HEINEMANN, S. 1994. Alpha 9: An acetylcholine receptor with novel pharmacological properties expressed in rat cochlear hair cells. *Cell.* United States.

ELLIOTT, J., JOLICOEUR, C., RAMAMURTHY, V. & CAYOUETTE, M. 2008. Ikaros confers early temporal competence to mouse retinal progenitor cells. *Neuron.* United States.

EMSLIE-SMITH, D., PATERSON, C. R., SCRATCHERD, T. & READ, N. W. 1988. Textbook of physiology (bds). 11th ed. Edinburgh: Churchill Livingstone.

ENGEL, J., BRAIG, C., RUTTIGER, L., KUHN, S., ZIMMERMANN, U., BLIN, N., SAUSBIER, M., KALBACHER, H., MUNKNER, S., ROHBOCK, K., RUTH, P., WINTER, H. & KNIPPER, M. 2006. Two classes of outer hair cells along the tonotopic axis of the cochlea. *Neuroscience,* 143**,** 837-49.

ERKMAN, L., MCEVILLY, R. J., LUO, L., RYAN, A. K., HOOSHMAND, F., O'CONNELL, S. M., KEITHLEY, E. M., RAPAPORT, D. H., RYAN, A. F. & ROSENFELD, M. G. 1996. Role of transcription factors brn-3.1 and brn-3.2 in auditory and visual system development. *Nature,* 381**,** 603-6.

ESTEVEZ, R., BOETTGER, T., STEIN, V., BIRKENHAGER, R., OTTO, E., HILDEBRANDT, F. & JENTSCH, T. J. 2001. Barttin is a cl- channel beta-subunit crucial for renal cl- reabsorption and inner ear k+ secretion. *Nature,* 414**,** 558-61.

EVANS, M. G. 1996. Acetylcholine activates two currents in guinea-pig outer hair cells. *J Physiol,* 491 (Pt 2)**,** 563-78.

EYBALIN, M. 1993. Neurotransmitters and neuromodulators of the mammalian cochlea. *Physiol Rev,* 73**,** 309-73.

EZZAT, S. & ASA, S. L. 2008. The emerging role of the ikaros stem cell factor in the neuroendocrine system. *J Mol Endocrinol,* 41**,** 45-51.

EZZAT, S., MADER, R., FISCHER, S., YU, S., ACKERLEY, C. & ASA, S. L. 2006. An essential role for the hematopoietic transcription factor ikaros in hypothalamic-pituitary-mediated somatic growth. *Proc Natl Acad Sci U S A,* 103**,** 2214-9.

EZZAT, S., MADER, R., YU, S., NING, T., POUSSIER, P. & ASA, S. L. 2005a. Ikaros integrates endocrine and immune system development. *J Clin Invest,* 115**,** 1021-9.

EZZAT, S., YU, S. & ASA, S. L. 2005b. The zinc finger ikaros transcription factor regulates pituitary growth hormone and prolactin gene expression through distinct effects on chromatin accessibility. *Mol Endocrinol,* 19**,** 1004-11.

FADEN, H., DUFFY, L. & BOEVE, M. 1998. Otitis media: Back to basics. *Pediatr Infect Dis J,* 17**,** 1105-12; quiz 1112-3.

FEKETE, D. M., ROUILLER, E. M., LIBERMAN, M. C. & RYUGO, D. K. 1984. The central projections of intracellularly labeled auditory nerve fibers in cats. *J Comp Neurol,* 229**,** 432-50.

FERREIROS-VIDAL, I., CARROLL, T., TAYLOR, B., TERRY, A., LIANG, Z., BRUNO, L., DHARMALINGAM, G., KHADAYATE, S., COBB, B. S., SMALE, S. T., SPIVAKOV, M., SRIVASTAVA, P., PETRETTO, E., FISHER, A. G. & MERKENSCHLAGER, M. 2013. Genome-wide identification of ikaros targets elucidates its contribution to mouse b-cell lineage specification and pre-b-cell differentiation. *Blood,* 121**,** 1769-82.

FLOCK, A. & CHEUNG, H. C. 1977. Actin filaments in sensory hairs of inner ear receptor cells. *J Cell Biol,* 75**,** 339-43.

FORGE, A., SOUTER, M. & DENMAN-JOHNSON, K. 1997. Structural development of sensory cells in the ear. *Semin Cell Dev Biol,* 8**,** 225-237.

FORGE, A. & WRIGHT, T. 2002. The molecular architecture of the inner ear. *Br Med Bull,* 63**,** 5-24.

FRANCESCHINI, A., SZKLARCZYK, D., FRANKILD, S., KUHN, M., SIMONOVIC, M., ROTH, A., LIN, J., MINGUEZ, P., BORK, P., VON MERING, C. & JENSEN, L. J. 2013. String v9.1: Protein-protein interaction networks, with increased coverage and integration. *Nucleic Acids Res,* 41**,** D808-15.

FRANKEL, A. D., BERG, J. M. & PABO, C. O. 1987. Metal-dependent folding of a single zinc finger from transcription factor iiia. *Proc Natl Acad Sci U S A,* 84**,** 4841-5.

FRIEDLAND, D. R., POPPER, P., EERNISSE, R., RINGGER, B. & CIOFFI, J. A. 2006. Differential expression of cytoskeletal genes in the cochlear nucleus. *Anat Rec A Discov Mol Cell Evol Biol,* 288**,** 447-65.

FRIEDMAN, R. A., VAN LAER, L., HUENTELMAN, M. J., SHETH, S. S., VAN EYKEN, E., CORNEVEAUX, J. J., TEMBE, W. D., HALPERIN, R. F., THORBURN, A. Q., THYS, S., BONNEUX, S., FRANSEN, E., HUYGHE, J., PYYKKO, I., CREMERS, C. W., KREMER, H., DHOOGE, I., STEPHENS, D., ORZAN, E., PFISTER, M., BILLE, M., PARVING, A., SORRI, M., VAN DE HEYNING, P. H., MAKMURA, L., OHMEN, J. D., LINTHICUM, F. H., JR., FAYAD, J. N., PEARSON, J. V., CRAIG, D. W., STEPHAN, D. A. & VAN CAMP, G. 2009. Grm7 variants confer susceptibility to age-related hearing impairment. *Hum Mol Genet,* 18**,** 785-96.

FRITZSCH, B., PIRVOLA, U. & YLIKOSKI, J. 1999. Making and breaking the innervation of the ear: Neurotrophic support during ear development and its clinical implications. *Cell Tissue Res,* 295**,** 369-82.

FROLENKOV, G. I. 2006. Regulation of electromotility in the cochlear outer hair cell. *J physiol.* England.

FROLENKOV, G. I., MAMMANO, F., BELYANTSEVA, I. A., COLING, D. & KACHAR, B. 2000. Two distinct ca(2+)-dependent signaling pathways regulate the motor output of cochlear outer hair cells. *J Neurosci,* 20**,** 5940-8.

FUJII, K., ISHIMARU, F., NAKASE, K., TABAYASHI, T., KOZUKA, T., NAOKI, K., MIYAHARA, M., TOKI, H., KITAJIMA, K., HARADA, M. & TANIMOTO, M. 2003. Over-expression of short isoforms of helios in patients with adult t-cell leukaemia/lymphoma. *Br j haematol.* England.

FURNESS, D. N., RICHARDSON, G. P. & RUSSELL, I. J. 1989. Stereociliary bundle morphology in organotypic cultures of the mouse cochlea. *Hear Res,* 38**,** 95-109.

GALIC, M. & GIEBEL, W. 1989. An electron microscopic study of the function of the root cells in the external spiral sulcus of the cochlea. *Acta Otolaryngol Suppl,* 461**,** 1-15.

GANDHI, R., KUMAR, D., BURNS, E. J., NADEAU, M., DAKE, B., LARONI, A., KOZORIZ, D., WEINER, H. L. & QUINTANA, F. J. 2010. Activation of the aryl hydrocarbon receptor induces human type 1 regulatory t cell-like and foxp3(+) regulatory t cells. *Nat Immunol,* 11**,** 846-53.

GATES, G. A. & MILLS, J. H. 2005. Presbycusis. *Lancet,* 366**,** 1111-20.

GEORGOPOULOS, K., BIGBY, M., WANG, J. H., MOLNAR, A., WU, P., WINANDY, S. & SHARPE, A. 1994. The ikaros gene is required for the development of all lymphoid lineages. *Cell.* United States.

GEORGOPOULOS, K., MOORE, D. D. & DERFLER, B. 1992. Ikaros, an early lymphoid-specific transcription factor and a putative mediator for t cell commitment. *Science,* 258**,** 808-12.

GETNET, D., GROSSO, J. F., GOLDBERG, M. V., HARRIS, T. J., YEN, H. R., BRUNO, T. C., DURHAM, N. M., HIPKISS, E. L., PYLE, K. J., WADA, S., PAN, F., PARDOLL, D. M. & DRAKE, C. G. 2010. A role for the transcription factor helios in human cd4(+)cd25(+) regulatory t cells. *Mol immunol.* England: 2010 Elsevier Ltd.

GETNET, D., MARIS, C. H., HIPKISS, E. L., GROSSO, J. F., HARRIS, T. J., YEN, H. R., BRUNO, T. C., WADA, S., ADLER, A., GEORGANTAS, R. W., JIE, C., GOLDBERG, M. V., PARDOLL, D. M. & DRAKE, C. G. 2009. Tumor recognition and self-recognition induce distinct transcriptional profiles in antigen-specific cd4 t cells. *J immunol.* United States.

GIBSON, F., WALSH, J., MBURU, P., VARELA, A., BROWN, K. A., ANTONIO, M., BEISEL, K. W., STEEL, K. P. & BROWN, S. D. M. 1995. A type vii myosin encoded by the deafness gene shaker-1. *Nature,* 374**,** 62-64.

GILLESPIE, P. G. 1995. Molecular machinery of auditory and vestibular transduction. *Curr Opin Neurobiol,* 5**,** 449-55.

GIROTTO, G., VUCKOVIC, D., BUNIELLO, A., LORENTE-CANOVAS, B., LEWIS, M., GASPARINI, P. & STEEL, K. P. 2014. Expression and replication studies to identify new candidate genes involved in normal hearing function. *PLoS One,* 9**,** e85352.

GLOBAL-ANATOMY. 2015. *Neuroscience resource page* [Online]. Available: http://www.neuroanatomy.wisc.edu/coursebook/audclinical04.pdf [Accessed 04/12/2015].

GLOWATZKI, E. & FUCHS, P. A. 2002. Transmitter release at the hair cell ribbon synapse. *Nat neurosci.* United States.

GLUZMAN, Y. 1981. Sv40-transformed simian cells support the replication of early sv40 mutants. *Cell,* 23**,** 175-82.

GOMEZ-CASATI, M. E., FUCHS, P. A., ELGOYHEN, A. B. & KATZ, E. 2005. Biophysical and pharmacological characterization of nicotinic cholinergic receptors in rat cochlear inner hair cells. *J physiol.* England.

GOODYEAR, R. J., LEGAN, P. K., WRIGHT, M. B., MARCOTTI, W., OGANESIAN, A., COATS, S. A., BOOTH, C. J., KROS, C. J., SEIFERT, R. A., BOWEN-POPE, D. F. & RICHARDSON, G. P. 2003. A receptor-like inositol lipid phosphatase is required for the maturation of developing cochlear hair bundles. *J neurosci.* United States.

GOTTSCHALK, R. A., CORSE, E. & ALLISON, J. P. 2012. Expression of helios in peripherally induced foxp3+ regulatory t cells. *J Immunol,* 188**,** 976-80.

GRAHAM, F. L., SMILEY, J., RUSSELL, W. C. & NAIRN, R. 1977. Characteristics of a human cell line transformed by DNA from human adenovirus type 5. *J Gen Virol,* 36**,** 59-74.

GREVERS, G. 2010. Challenges in reducing the burden of otitis media disease: An ent perspective on improving management and prospects for prevention. *Int J Pediatr Otorhinolaryngol,* 74**,** 572-7.

GRILLET, N., SCHWANDER, M., HILDEBRAND, M. S., SCZANIECKA, A., KOLATKAR, A., VELASCO, J., WEBSTER, J. A., KAHRIZI, K., NAJMABADI, H., KIMBERLING, W. J., STEPHAN, D., BAHLO, M., WILTSHIRE, T., TARANTINO, L. M., KUHN, P., SMITH, R. J. & MULLER, U. 2009. Mutations in loxhd1, an evolutionarily conserved stereociliary protein, disrupt hair cell function in mice and cause progressive hearing loss in humans. *Am J Hum Genet,* 85**,** 328-37.

GROFF, J. A. & LIBERMAN, M. C. 2003. Modulation of cochlear afferent response by the lateral olivocochlear system: Activation via electrical stimulation of the inferior colliculus. *J Neurophysiol,* 90**,** 3178-200.

GROGER, N., FROHLICH, H., MAIER, H., OLBRICH, A., KOSTIN, S., BRAUN, T. & BOETTGER, T. 2010. Slc4a11 prevents osmotic imbalance leading to corneal endothelial dystrophy, deafness, and polyuria. *J Biol Chem,* 285**,** 14467-74.

GROSS, J., ANGERSTEIN, M., FUCHS, J., STUTE, K. & MAZUREK, B. 2011a. Expression analysis of prestin and selected transcription factors in newborn rats. *Cell Mol Neurobiol,* 31**,** 1089-101.

GROSS, J., STUTE, K., FUCHS, J., ANGERSTEIN, M., AMARJARGAL, N. & MAZUREK, B. 2011b. Effects of retinoic acid and butyric acid on the expression of prestin and gata-3 in organotypic cultures of the organ of corti of newborn rats. *Dev Neurobiol,* 71**,** 650-61.

GROVES, A. K., ZHANG, K. D. & FEKETE, D. M. 2013. The genetics of hair cell development and regeneration. *Annu Rev Neurosci,* 36**,** 361-81.

GUETA, R., TAL, E., SILBERBERG, Y. & ROUSSO, I. 2007. The 3d structure of the tectorial membrane determined by second-harmonic imaging microscopy. *J Struct Biol,* 159**,** 103-10.

GUINAN, J. 1996. The physiology of olivocochlear efferents. *In:* DALLOS, P., POPPER, A. & FAY, R. (eds.) *The cochlea.* New York: Springer Verlag.

HACKNEY, C. M., OSEN, K. K., OTTERSEN, O. P., STORM-MATHISEN, J. & MANJALY, G. 1996. Immunocytochemical evidence that glutamate is a neurotransmitter in the cochlear nerve: A quantitative study in the guinea-pig anteroventral cochlear nucleus. *Eur J Neurosci,* 8**,** 79-91.

HAFIDI, A. 1998. Peripherin-like immunoreactivity in type ii spiral ganglion cell body and projections. *Brain Res,* 805**,** 181-90.

HAHM, K., COBB, B. S., MCCARTY, A. S., BROWN, K. E., KLUG, C. A., LEE, R., AKASHI, K., WEISSMAN, I. L., FISHER, A. G. & SMALE, S. T. 1998. Helios, a t cell-restricted ikaros family member that quantitatively associates with ikaros at centromeric heterochromatin. *Genes Dev,* 12**,** 782-96.

HAHM, K., ERNST, P., LO, K., KIM, G. S., TURCK, C. & SMALE, S. T. 1994. The lymphoid transcription factor lyf-1 is encoded by specific, alternatively spliced mrnas derived from the ikaros gene. *Mol Cell Biol,* 14**,** 7111-23.

HALLWORTH, R., MCCOY, M. & POLAN-CURTAIN, J. 2000. Tubulin expression in the developing and adult gerbil organ of corti. *Hear Res,* 139**,** 31-41.

HAMERNIK, R. P., TURRENTINE, G. & WRIGHT, C. G. 1984. Surface morphology of the inner sulcus and related epithelial cells of the cochlea following acoustic trauma. *Hear Res,* 16**,** 143-60.

HANAS, J. S., HAZUDA, D. J., BOGENHAGEN, D. F., WU, F. Y. & WU, C. W. 1983. Xenopus transcription factor a requires zinc for binding to the 5 s rna gene. *J Biol Chem,* 258**,** 14120-5.

HARAKSINGH, R. R., JAHANBANI, F., RODRIGUEZ-PARIS, J., GELERNTER, J., NADEAU, K. C., OGHALAI, J. S., SCHRIJVER, I. & SNYDER, M. P. 2014. Exome sequencing and genome-wide copy number variant mapping reveal novel associations with sensorineural hereditary hearing loss. *BMC Genomics,* 15**,** 1155.

HARDISTY-HUGHES, R. E., PARKER, A. & BROWN, S. D. 2010. A hearing and vestibular phenotyping pipeline to identify mouse mutants with hearing impairment. *Nat Protoc,* 5**,** 177-90.

HARDISTY-HUGHES, R. E., TATEOSSIAN, H., MORSE, S. A., ROMERO, M. R., MIDDLETON, A., TYMOWSKA-LALANNE, Z., HUNTER, A. J., CHEESEMAN, M. & BROWN, S. D. 2006. A mutation in the f-box gene, fbxo11, causes otitis media in the jeff mouse. *Hum Mol Genet,* 15**,** 3273-9.

HARDISTY, R. E., ERVEN, A., LOGAN, K., MORSE, S., GUIONAUD, S., SANCHO-OLIVER, S., HUNTER, A. J., BROWN, S. D. & STEEL, K. P. 2003. The deaf mouse mutant jeff (jf) is a single gene model of otitis media. *J Assoc Res Otolaryngol,* 4**,** 130-8.

HARIBHAI, D., LIN, W., EDWARDS, B., ZIEGELBAUER, J., SALZMAN, N. H., CARLSON, M. R., LI, S. H., SIMPSON, P. M., CHATILA, T. A. & WILLIAMS, C. B. 2009. A central role for induced regulatory t cells in tolerance induction in experimental colitis. *J immunol.* United States.

HARKER, N., NAITO, T., CORTES, M., HOSTERT, A., HIRSCHBERG, S., TOLAINI, M., RODERICK, K., GEORGOPOULOS, K. & KIOUSSIS, D. 2002. The cd8alpha gene locus is regulated by the ikaros family of proteins. *Mol cell.* United States.

HARNISCHFEGER, G., NEUWEILER, G. & SCHLEGEL, P. 1985. Interaural time and intensity coding in superior olivary complex and inferior colliculus of the echolocating bat molossus ater. *J Neurophysiol,* 53**,** 89-109.

HARTMAN, B. H., HAYASHI, T., NELSON, B. R., BERMINGHAM-MCDONOGH, O. & REH, T. A. 2007. Dll3 is expressed in developing hair cells in the mammalian cochlea. *Dev Dyn,* 236**,** 2875-83.

HASKO, J. A., RICHARDSON, G. P., RUSSELL, I. J. & SHAW, G. 1990. Transient expression of neurofilament protein during hair cell development in the mouse cochlea. *Hear Res,* 45**,** 63-73.

HAYASHI, T., KOKUBO, H., HARTMAN, B. H., RAY, C. A., REH, T. A. & BERMINGHAM-MCDONOGH, O. 2008a. Hesr1 and hesr2 may act as early effectors of notch signaling in the developing cochlea. *Dev Biol,* 316**,** 87-99.

HAYASHI, T., RAY, C. A. & BERMINGHAM-MCDONOGH, O. 2008b. Fgf20 is required for sensory epithelial specification in the developing cochlea. *J Neurosci,* 28**,** 5991-9.

HE, D. Z., EVANS, B. N. & DALLOS, P. 1994. First appearance and development of electromotility in neonatal gerbil outer hair cells. *Hear Res,* 78**,** 77-90.

HEFFNER, H. E. & HEFFNER, R. S. 2007. Hearing ranges of laboratory animals. *J Am Assoc Lab Anim Sci,* 46**,** 20-2.

HEFFNER, R. S., KOAY, G. & HEFFNER, H. E. 1996. Sound localization in chinchillas, iii: Effect of pinna removal. *Hear Res,* 99**,** 13-21.

HEINRICH, U. R., BRIEGER, J., SELIVANOVA, O., FELTENS, R., EIMERMACHER, A., SCHAFER, D. & MANN, W. J. 2006. Cox-2 expression in the guinea pig cochlea is partly altered by moderate sound exposure. *Neurosci Lett,* 394**,** 121-6.

HENKART, P. A. 1985. Mechanism of lymphocyte-mediated cytotoxicity. *Annu Rev Immunol,* 3**,** 31-58.

HENRY, K. R. & MCGINN, M. D. 1992. The mouse as a model for human audition. A review of the literature. *Audiology,* 31**,** 181-9.

HEQUEMBOURG, S. & LIBERMAN, M. C. 2001. Spiral ligament pathology: A major aspect of age-related cochlear degeneration in c57bl/6 mice. *J Assoc Res Otolaryngol,* 2**,** 118-29.

HEREDITARY-HEARING-LOSS. 2015. *Hereditary hearing loss homepage* [Online]. Available: http://hereditaryhearingloss.org/ [Accessed 17/06/2015].

HERTZANO, R., DROR, A. A., MONTCOUQUIOL, M., AHMED, Z. M., ELLSWORTH, B., CAMPER, S., FRIEDMAN, T. B., KELLEY, M. W. & AVRAHAM, K. B. 2007. Lhx3, a lim domain transcription factor, is regulated by pou4f3 in the auditory but not in the vestibular system. *Eur J Neurosci,* 25**,** 999-1005.

HERTZANO, R., ELKON, R., KURIMA, K., MORRISSON, A., CHAN, S. L., SALLIN, M., BIEDLINGMAIER, A., DARLING, D. S., GRIFFITH, A. J., EISENMAN, D. J. & STROME, S. E. 2011. Cell type-specific transcriptome analysis reveals a major role for zeb1 and mir-200b in mouse inner ear morphogenesis. *PLoS Genet,* 7**,** e1002309.

HERTZANO, R., MONTCOUQUIOL, M., RASHI-ELKELES, S., ELKON, R., YUCEL, R., FRANKEL, W. N., RECHAVI, G., MOROY, T., FRIEDMAN, T. B., KELLEY, M. W. & AVRAHAM, K. B. 2004. Transcription profiling of inner ears from pou4f3(ddl/ddl) identifies gfi1 as a target of the pou4f3 deafness gene. *Hum Mol Genet,* 13**,** 2143-53.

HESS, A., BLOCH, W., ARNHOLD, S., ANDRESSEN, C., STENNERT, E., ADDICKS, K. & MICHEL, O. 1998. Nitric oxide synthase in the vestibulocochlear system of mice. *Brain Res,* 813**,** 97-102.

HILDEBRAND, M. S., KAHRIZI, K., BROMHEAD, C. J., SHEARER, A. E., WEBSTER, J. A., KHODAEI, H., ABTAHI, R., BAZAZZADEGAN, N., BABANEJAD, M., NIKZAT, N., KIMBERLING, W. J., STEPHAN, D., HUYGEN, P. L., BAHLO, M., SMITH, R. J. & NAJMABADI, H. 2010. Mutations in tmc1 are a common cause of dfnb7/11 hearing loss in the iranian population. *Ann Otol Rhinol Laryngol,* 119**,** 830-5.

HIRSCH, J. G. 1960. Antimicrobial factors in tissues and phagocytic cells. *Bacteriol Rev,* 24**,** 133-40.

HOELTER, S. M., DALKE, C., KALLNIK, M., BECKER, L., HORSCH, M., SCHREWE, A., FAVOR, J., KLOPSTOCK, T., BECKERS, J., IVANDIC, B., GAILUS-DURNER, V., FUCHS, H., HRABE DE

ANGELIS, M., GRAW, J. & WURST, W. 2008. "Sighted c3h" mice--a tool for analysing the influence of vision on mouse behaviour? *Front Biosci,* 13**,** 5810-23.

HOLLEY, M. C. 2005. Keynote review: The auditory system, hearing loss and potential targets for drug development. *Drug Discov Today,* 10**,** 1269-82.

HOLMES, M. L., HUNTINGTON, N. D., THONG, R. P., BRADY, J., HAYAKAWA, Y., ANDONIOU, C. E., FLEMING, P., SHI, W., SMYTH, G. K., DEGLI-ESPOSTI, M. A., BELZ, G. T., KALLIES, A., CAROTTA, S., SMYTH, M. J. & NUTT, S. L. 2014. Peripheral natural killer cell maturation depends on the transcription factor aiolos. *Embo j*.

HONMA, Y., KIYOSAWA, H., MORI, T., OGURI, A., NIKAIDO, T., KANAZAWA, K., TOJO, M., TAKEDA, J., TANNO, Y., YOKOYA, S., KAWABATA, I., IKEDA, H. & WANAKA, A. 1999. Eos: A novel member of the ikaros gene family expressed predominantly in the developing nervous system. *Febs Letters,* 447**,** 76-80.

HOSOKAWA, Y., MAEDA, Y. & SETO, M. 1999. Human helios, an ikaros-related zinc finger DNA binding protein: Cdna cloning and tissue expression pattern. *Immunogenetics.* United States.

HOUSLEY, G. D. & ASHMORE, J. F. 1992. Ionic currents of outer hair cells isolated from the guinea-pig cochlea. *J Physiol,* 448**,** 73-98.

HOUSLEY, G. D., MARCOTTI, W., NAVARATNAM, D. & YAMOAH, E. N. 2006. Hair cells--beyond the transducer. *J Membr Biol,* 209**,** 89-118.

HRYNKOW, S. H., MOREST, D. K., BRUMWELL, C. & RUTISHAUSER, U. 1998. Spatio-temporal diversity in the microenvironments for neural cell adhesion molecule, neural cell adhesion molecule-polysialic acid, and l1-cell adhesion molecule expression by sensory neurons and their targets during cochleo-vestibular innervation. *Neuroscience,* 87**,** 401-22.

HUANG, L. C., BARCLAY, M., LEE, K., PETER, S., HOUSLEY, G. D., THORNE, P. R. & MONTGOMERY, J. M. 2012. Synaptic profiles during neurite extension, refinement and retraction in the developing cochlea. *Neural dev.* England.

HUANG, L. C., GREENWOOD, D., THORNE, P. R. & HOUSLEY, G. D. 2005. Developmental regulation of neuron-specific p2x3 receptor expression in the rat cochlea. *J Comp Neurol,* 484**,** 133-43.

HUDSPETH, A. J. 1989. How the ear's works work. *Nature,* 341**,** 397-404.

HUME, C. R., BRATT, D. L. & OESTERLE, E. C. 2007. Expression of lhx3 and sox2 during mouse inner ear development. *Gene Expr Patterns,* 7**,** 798-807.

ISAAC, J. T., ASHBY, M. C. & MCBAIN, C. J. 2007. The role of the glur2 subunit in ampa receptor function and synaptic plasticity. *Neuron,* 54**,** 859-71.

ISAACSON, J. E. & VORA, N. M. 2003. Differential diagnosis and treatment of hearing loss. *Am Fam Physician,* 68**,** 1125-32.

IVES, D. G., BONINO, P., TRAVEN, N. D. & KULLER, L. H. 1995. Characteristics and comorbidities of rural older adults with hearing impairment. *J Am Geriatr Soc,* 43**,** 803-6.

IWANO, T., YAMAMOTO, A., OMORI, K., AKAYAMA, M., KUMAZAWA, T. & TASHIRO, Y. 1989. Quantitative immunocytochemical localization of na+,k+-atpase alpha-subunit in the lateral wall of rat cochlear duct. *J Histochem Cytochem,* 37**,** 353-63.

IZUMIKAWA, M., MINODA, R., KAWAMOTO, K., ABRASHKIN, K. A., SWIDERSKI, D. L., DOLAN, D. F., BROUGH, D. E. & RAPHAEL, Y. 2005. Auditory hair cell replacement and hearing improvement by atoh1 gene therapy in deaf mammals. *Nat Med,* 11**,** 271-6.

JABOR, M. A. & AMEDEE, R. G. 1997. Cerumen impaction. *J La State Med Soc,* 149**,** 358-62.

JACOBSON, M., KIM, S., ROMNEY, J., ZHU, X. & FRISINA, R. D. 2003. Contralateral suppression of distortion-product otoacoustic emissions declines with age: A comparison of findings in cba mice with human listeners. *Laryngoscope,* 113**,** 1707-13.

JACQUES, B. E., MONTCOUQUIOL, M. E., LAYMAN, E. M., LEWANDOSKI, M. & KELLEY, M. W. 2007. Fgf8 induces pillar cell fate and regulates cellular patterning in the mammalian cochlea. *Development,* 134**,** 3021-9.

JAHAN, I., PAN, N. & FRITZSCH, B. 2015. Opportunities and limits of the one gene approach: The ability of atoh1 to differentiate and maintain hair cells depends on the molecular context. *Front Cell Neurosci,* 9**,** 26.

JAHAN, I., PAN, N., KERSIGO, J., CALISTO, L. E., MORRIS, K. A., KOPECKY, B., DUNCAN, J. S., BEISEL, K. W. & FRITZSCH, B. 2012. Expression of neurog1 instead of atoh1 can partially rescue organ of corti cell survival. *PLoS One,* 7**,** e30853.

JAHAN, I., PAN, N., KERSIGO, J. & FRITZSCH, B. 2010. Neurod1 suppresses hair cell differentiation in ear ganglia and regulates hair cell subtype development in the cochlea. *PLoS One,* 5**,** e11661.

JAHAN, I., PAN, N., KERSIGO, J. & FRITZSCH, B. 2013. Beyond generalized hair cells: Molecular cues for hair cell types. *Hear Res,* 297**,** 30-41.

JAN, T. A., CHAI, R., SAYYID, Z. N., VAN AMERONGEN, R., XIA, A., WANG, T., SINKKONEN, S. T., ZENG, Y. A., LEVIN, J. R., HELLER, S., NUSSE, R. & CHENG, A. G. 2013. Tympanic border cells are wnt-responsive and can act as progenitors for postnatal mouse cochlear cells. *Development,* 140**,** 1196-206.

JANKY, R., VERFAILLIE, A., IMRICHOVA, H., VAN DE SANDE, B., STANDAERT, L., CHRISTIAENS, V., HULSELMANS, G., HERTEN, K., NAVAL SANCHEZ, M., POTIER, D., SVETLICHNYY, D., KALENDER ATAK, Z., FIERS, M., MARINE, J. C. & AERTS, S. 2014. Iregulon: From a gene list to a gene regulatory network using large motif and track collections. *PLoS Comput Biol,* 10**,** e1003731.

JENSEN, L. J., KUHN, M., STARK, M., CHAFFRON, S., CREEVEY, C., MULLER, J., DOERKS, T., JULIEN, P., ROTH, A., SIMONOVIC, M., BORK, P. & VON MERING, C. 2009. String 8--a global view on proteins and their functional interactions in 630 organisms. *Nucleic Acids Res,* 37**,** D412-6.

JERUD, E. S., BRICARD, G. & PORCELLI, S. A. 2006. Cd1d-restricted natural killer t cells: Roles in tumor immunosurveillance and tolerance. *Transfusion Medicine and Hemotherapy,* 33**,** 18-36.

JIN, Z., LIANG, G. H., COOPER, E. C. & JARLEBARK, L. 2009. Expression and localization of k channels kcnq2 and kcnq3 in the mammalian cochlea. *Audiol Neurootol,* 14**,** 98-105.

JINEK, M., CHYLINSKI, K., FONFARA, I., HAUER, M., DOUDNA, J. A. & CHARPENTIER, E. 2012. A programmable dual-rna-guided DNA endonuclease in adaptive bacterial immunity. *Science,* 337**,** 816-21.

JOHN, L. B. & WARD, A. C. 2011. The ikaros gene family: Transcriptional regulators of hematopoiesis and immunity. *Molecular Immunology,* 48**,** 1272-1278.

JOHNSON, K. R., ERWAY, L. C., COOK, S. A., WILLOTT, J. F. & ZHENG, Q. Y. 1997. A major gene affecting age-related hearing loss in c57bl/6j mice. *Hearing Research,* 114**,** 83-92.

JOHNSON, K. R., ZHENG, Q. Y. & ERWAY, L. C. 2000. A major gene affecting age-related hearing loss is common to at least ten inbred strains of mice. *Genomics,* 70**,** 171-180.

JOHNSON, S. L., ECKRICH, T., KUHN, S., ZAMPINI, V., FRANZ, C., RANATUNGA, K. M., ROBERTS, T. P., MASETTO, S., KNIPPER, M., KROS, C. J. & MARCOTTI, W. 2011.

Position-dependent patterning of spontaneous action potentials in immature cochlear inner hair cells. *Nat Neurosci,* 14**,** 711-7.

JOHNSON, S. L., FORGE, A., KNIPPER, M., MUNKNER, S. & MARCOTTI, W. 2008. Tonotopic variation in the calcium dependence of neurotransmitter release and vesicle pool replenishment at mammalian auditory ribbon synapses. *J Neurosci,* 28**,** 7670-8.

JOHNSON, S. L., FRANZ, C., KNIPPER, M. & MARCOTTI, W. 2009. Functional maturation of the exocytotic machinery at gerbil hair cell ribbon synapses. *J Physiol,* 587**,** 1715-26.

JOHNSON, S. L., MARCOTTI, W. & KROS, C. J. 2005. Increase in efficiency and reduction in ca2+ dependence of exocytosis during development of mouse inner hair cells. *J Physiol,* 563**,** 177-91.

JONES, J. M., MONTCOUQUIOL, M., DABDOUB, A., WOODS, C. & KELLEY, M. W. 2006. Inhibitors of differentiation and DNA binding (ids) regulate math1 and hair cell formation during the development of the organ of corti. *J Neurosci,* 26**,** 550-8.

JONULEIT, H., SCHMITT, E., STASSEN, M., TUETTENBERG, A., KNOP, J. & ENK, A. H. 2001. Identification and functional characterization of human cd4(+)cd25(+) t cells with regulatory properties isolated from peripheral blood. *J Exp Med,* 193**,** 1285-94.

JUDICE, T. N., NELSON, N. C., BEISEL, C. L., DELIMONT, D. C., FRITZSCH, B. & BEISEL, K. W. 2002. Cochlear whole mount in situ hybridization: Identification of longitudinal and radial gradients. *Brain Res Brain Res Protoc,* 9**,** 65-76.

JUSTICE, M. J., NOVEROSKE, J. K., WEBER, J. S., ZHENG, B. H. & BRADLEY, A. 1999. Mouse enu mutagenesis. *Human Molecular Genetics,* 8**,** 1955-1963.

KACHAR, B., BROWNELL, W. E., ALTSCHULER, R. & FEX, J. 1986. Electrokinetic shape changes of cochlear outer hair cells. *Nature,* 322**,** 365-8.

KACHAR, B., KURIMA, K., EBRAHIM, S., PAN, B., NAKANISHI, H., MILLIS, B., CUI, R., KAWASHIMA, Y., HOLT, J. & GRIFFITH, A. Tmc1 and tmc2 localize at the site of mechanotransduction in mammalian inner ear hair cell stereocilia. Association for Research in Otolaryngology 38th Annual MidWinter Meeting, 2015 Maryland, USA.

KACHAR, B., PARAKKAL, M., KURC, M., ZHAO, Y. & GILLESPIE, P. G. 2000. High-resolution structure of hair-cell tip links. *Proceedings of the National Academy of Sciences of the United States of America,* 97**,** 13336-13341.

KALLBERG, M., WANG, H., WANG, S., PENG, J., WANG, Z., LU, H. & XU, J. 2012. Template-based protein structure modeling using the raptorx web server. *Nat Protoc,* 7**,** 1511-22.

KALTENBACH, J. A. & FALZARANO, P. R. 1994. Postnatal development of the hamster cochlea. I. Growth of hair cells and the organ of corti. *J Comp Neurol,* 340**,** 87-97.

KAWASHIMA, Y., GELEOC, G. S., KURIMA, K., LABAY, V., LELLI, A., ASAI, Y., MAKISHIMA, T., WU, D. K., DELLA SANTINA, C. C., HOLT, J. R. & GRIFFITH, A. J. 2011. Mechanotransduction in mouse inner ear hair cells requires transmembrane channel-like genes. *J Clin Invest,* 121**,** 4796-809.

KEELE, C. A., NEIL, E. & JOELS, N. 1982. *Samson wright's applied physiology,* 13th ed. Oxford: Oxford University Press.

KELLEY, C. M., IKEDA, T., KOIPALLY, J., AVITAHL, N., WU, L., GEORGOPOULOS, K. & MORGAN, B. A. 1998. Helios, a novel dimerization partner of ikaros expressed in the earliest hematopoietic progenitors. *Curr biol.* England.

KELLEY, M. W. 2007. Cellular commitment and differentiation in the organ of corti. *Int J Dev Biol,* 51**,** 571-83.

KELLEY, M. W., TALREJA, D. R. & CORWIN, J. T. 1995. Replacement of hair cells after laser microbeam irradiation in cultured organs of corti from embryonic and neonatal mice. *J Neurosci,* 15**,** 3013-26.

KEMPERMAN, M. H., HOEFSLOOT, L. H. & CREMERS, C. W. 2002. Hearing loss and connexin 26. *J R Soc Med,* 95**,** 171-7.

KHARKOVETS, T., HARDELIN, J. P., SAFIEDDINE, S., SCHWEIZER, M., EL-AMRAOUI, A., PETIT, C. & JENTSCH, T. J. 2000. Kcnq4, a k+ channel mutated in a form of dominant deafness, is expressed in the inner ear and the central auditory pathway. *Proc Natl Acad Sci U S A,* 97**,** 4333-8.

KIEHL, T. R., FISCHER, S. E., EZZAT, S. & ASA, S. L. 2008. Mice lacking the transcription factor ikaros display behavioral,alterations of an anti-depressive phenotype. *Experimental Neurology,* 211**,** 107-114.

KIERNAN, A. E., AHITUV, N., FUCHS, H., BALLING, R., AVRAHAM, K. B., STEEL, K. P. & HRABE DE ANGELIS, M. 2001. The notch ligand jagged1 is required for inner ear sensory development. *Proc Natl Acad Sci U S A,* 98**,** 3873-8.

KIERNAN, A. E., PELLING, A. L., LEUNG, K. K., TANG, A. S., BELL, D. M., TEASE, C., LOVELL-BADGE, R., STEEL, K. P. & CHEAH, K. S. 2005. Sox2 is required for sensory organ development in the mammalian inner ear. *Nature,* 434**,** 1031-5.

KIESSLING, R., KLEIN, E. & WIGZELL, H. 1975. "Natural" killer cells in the mouse. I. Cytotoxic cells with specificity for mouse moloney leukemia cells. Specificity and distribution according to genotype. *Eur J Immunol,* 5**,** 112-7.

KIKKAWA, Y., MBURU, P., MORSE, S., KOMINAMI, R., TOWNSEND, S. & BROWN, S. D. 2005. Mutant analysis reveals whirlin as a dynamic organizer in the growing hair cell stereocilium. *Hum Mol Genet,* 14**,** 391-400.

KIKKAWA, Y., SHITARA, H., WAKANA, S., KOHARA, Y., TAKADA, T., OKAMOTO, M., TAYA, C., KAMIYA, K., YOSHIKAWA, Y., TOKANO, H., KITAMURA, K., SHIMIZU, K., WAKABAYASHI, Y., SHIROISHI, T., KOMINAMI, R. & YONEKAWA, H. 2003. Mutations in a new scaffold protein sans cause deafness in jackson shaker mice. *Hum Mol Genet,* 12**,** 453-61.

KIKUCHI, T., ADAMS, J. C., MIYABE, Y., SO, E. & KOBAYASHI, T. 2000. Potassium ion recycling pathway via gap junction systems in the mammalian cochlea and its interruption in hereditary nonsyndromic deafness. *Med Electron Microsc,* 33**,** 51-6.

KIKUCHI, T., KIMURA, R. S., PAUL, D. L. & ADAMS, J. C. 1995. Gap junctions in the rat cochlea: Immunohistochemical and ultrastructural analysis. *Anat Embryol (Berl),* 191**,** 101-18.

KIM, J., SIF, S., JONES, B., JACKSON, A., KOIPALLY, J., HELLER, E., WINANDY, S., VIEL, A., SAWYER, A., IKEDA, T., KINGSTON, R. & GEORGOPOULOS, K. 1999. Ikaros DNA-binding proteins direct formation of chromatin remodeling complexes in lymphocytes. *Immunity.* United States.

KIM, S., FRISINA, D. R. & FRISINA, R. D. 2002. Effects of age on contralateral suppression of distortion product otoacoustic emissions in human listeners with normal hearing. *Audiol Neurootol,* 7**,** 348-57.

KIM, S. J., BIEGANSKI, T., SOHN, Y. B., KOZLOWSKI, K., SEMENOV, M., OKAMOTO, N., KIM, C. H., KO, A. R., AHN, G. H., CHOI, Y. L., PARK, S. W., KI, C. S., KIM, O. H., NISHIMURA, G., UNGER, S., SUPERTI-FURGA, A. & JIN, D. K. 2011. Identification of signal peptide domain sost mutations in autosomal dominant craniodiaphyseal dysplasia. *Hum Genet,* 129**,** 497-502.

KIMURA, R. S. 1975. The ultrastructure of the organ of corti. *Int Rev Cytol,* 42**,** 173-222.
KIRJAVAINEN, A., SULG, M., HEYD, F., ALITALO, K., YLA-HERTTUALA, S., MOROY, T., PETROVA, T. V. & PIRVOLA, U. 2008. Prox1 interacts with atoh1 and gfi1, and regulates cellular differentiation in the inner ear sensory epithelia. *Dev Biol,* 322**,** 33-45.
KIRSTETTER, P., THOMAS, M., DIERICH, A., KASTNER, P. & CHAN, S. 2002. Ikaros is critical for b cell differentiation and function. *Eur j immunol.* Germany.
KNIPPER, M., BANDTLOW, C., GESTWA, L., KOPSCHALL, I., ROHBOCK, K., WIECHERS, B., ZENNER, H. P. & ZIMMERMANN, U. 1998. Thyroid hormone affects schwann cell and oligodendrocyte gene expression at the glial transition zone of the viiith nerve prior to cochlea function. *Development,* 125**,** 3709-18.
KOBAYASHI, K., UCHIDA, S., OKAMURA, H. O., MARUMO, F. & SASAKI, S. 2002. Human clc-kb gene promoter drives the egfp expression in the specific distal nephron segments and inner ear. *J Am Soc Nephrol,* 13**,** 1992-8.
KOBAYASHI, T., ZADRAVEC, D. & JACOBSSON, A. 2007. Elovl2 overexpression enhances triacylglycerol synthesis in 3t3-l1 and f442a cells. *FEBS Lett,* 581**,** 3157-63.
KOEHLER, K. R. & HASHINO, E. 2014. 3d mouse embryonic stem cell culture for generating inner ear organoids. *Nat Protoc,* 9**,** 1229-44.
KOO, S. K., HILL, J. K., HWANG, C. H., LIN, Z. S., MILLEN, K. J. & WU, D. K. 2009. Lmx1a maintains proper neurogenic, sensory, and non-sensory domains in the mammalian inner ear. *Dev Biol,* 333**,** 14-25.
KORRAPATI, S., ROUX, I., GLOWATZKI, E. & DOETZLHOFER, A. 2013. Notch signaling limits supporting cell plasticity in the hair cell-damaged early postnatal murine cochlea. *PLoS One,* 8**,** e73276.
KROS, C. J., RUPPERSBERG, J. P. & RUSCH, A. 1998. Expression of a potassium current in inner hair cells during development of hearing in mice. *Nature,* 394**,** 281-4.
KUBBA, H., PEARSON, J. P. & BIRCHALL, J. P. 2000. The aetiology of otitis media with effusion: A review. *Clin Otolaryngol Allied Sci,* 25**,** 181-94.
KUBISCH, C., SCHROEDER, B. C., FRIEDRICH, T., LUTJOHANN, B., EL-AMRAOUI, A., MARLIN, S., PETIT, C. & JENTSCH, T. J. 1999. Kcnq4, a novel potassium channel expressed in sensory outer hair cells, is mutated in dominant deafness. *Cell,* 96**,** 437-46.
KUDO, M. & NIIMI, K. 1978. Ascending projections of the inferior colliculus onto the medial geniculate body in the cat studied by anterograde and retrograde tracing techniques. *Brain Res,* 155**,** 113-7.
KUHN, S., JOHNSON, S. L., FURNESS, D. N., CHEN, J., INGHAM, N., HILTON, J. M., STEFFES, G., LEWIS, M. A., ZAMPINI, V., HACKNEY, C. M., MASETTO, S., HOLLEY, M. C., STEEL, K. P. & MARCOTTI, W. 2011. Mir-96 regulates the progression of differentiation in mammalian cochlear inner and outer hair cells. *Proc Natl Acad Sci U S A,* 108**,** 2355-60.
KUMAR, P., HENIKOFF, S. & NG, P. C. 2009. Predicting the effects of coding non-synonymous variants on protein function using the sift algorithm. *Nat protoc.* England.
KURIMA, K., PETERS, L. M., YANG, Y., RIAZUDDIN, S., AHMED, Z. M., NAZ, S., ARNAUD, D., DRURY, S., MO, J., MAKISHIMA, T., GHOSH, M., MENON, P. S., DESHMUKH, D., ODDOUX, C., OSTRER, H., KHAN, S., DEININGER, P. L., HAMPTON, L. L., SULLIVAN, S. L., BATTEY, J. F., JR., KEATS, B. J., WILCOX, E. R., FRIEDMAN, T. B. & GRIFFITH, A. J. 2002. Dominant and recessive deafness caused by mutations of a novel gene, tmc1, required for cochlear hair-cell function. *Nat Genet,* 30**,** 277-84.

LAINE, H., DOETZLHOFER, A., MANTELA, J., YLIKOSKI, J., LAIHO, M., ROUSSEL, M. F., SEGIL, N. & PIRVOLA, U. 2007. P19(ink4d) and p21(cip1) collaborate to maintain the postmitotic state of auditory hair cells, their codeletion leading to DNA damage and p53-mediated apoptosis. *J Neurosci,* 27**,** 1434-44.

LAINE, H., SULG, M., KIRJAVAINEN, A. & PIRVOLA, U. 2010. Cell cycle regulation in the inner ear sensory epithelia: Role of cyclin d1 and cyclin-dependent kinase inhibitors. *Dev Biol,* 337**,** 134-46.

LALANI, S. R., SAFIULLAH, A. M., MOLINARI, L. M., FERNBACH, S. D., MARTIN, D. M. & BELMONT, J. W. 2004. Sema3e mutation in a patient with charge syndrome. *J Med Genet,* 41**,** e94.

LANE, P. W. 1963. Whirler mice: A recessive behavior mutation in linkage group viii. *J Hered,* 54**,** 263-6.

LANFORD, P. J., LAN, Y., JIANG, R., LINDSELL, C., WEINMASTER, G., GRIDLEY, T. & KELLEY, M. W. 1999. Notch signalling pathway mediates hair cell development in mammalian cochlea. *Nat Genet,* 21**,** 289-92.

LANFORD, P. J., SHAILAM, R., NORTON, C. R., GRIDLEY, T. & KELLEY, M. W. 2000. Expression of math1 and hes5 in the cochleae of wildtype and jag2 mutant mice. *J Assoc Res Otolaryngol,* 1**,** 161-71.

LAUTERMANN, J., TEN CATE, W. J., ALTENHOFF, P., GRUMMER, R., TRAUB, O., FRANK, H., JAHNKE, K. & WINTERHAGER, E. 1998. Expression of the gap-junction connexins 26 and 30 in the rat cochlea. *Cell Tissue Res,* 294**,** 415-20.

LEAKE, P. A., HRADEK, G. T., HETHERINGTON, A. M. & STAKHOVSKAYA, O. 2011. Brain-derived neurotrophic factor promotes cochlear spiral ganglion cell survival and function in deafened, developing cats. *J Comp Neurol,* 519**,** 1526-45.

LELLI, A., ASAI, Y., FORGE, A., HOLT, J. R. & GELEOC, G. S. 2009. Tonotopic gradient in the developmental acquisition of sensory transduction in outer hair cells of the mouse cochlea. *J Neurophysiol,* 101**,** 2961-73.

LEMASURIER, M. & GILLESPIE, P. G. 2005. Hair-cell mechanotransduction and cochlear amplification. *Neuron,* 48**,** 403-15.

LEWIS, J. 1998. Notch signalling and the control of cell fate choices in vertebrates. *Semin Cell Dev Biol,* 9**,** 583-9.

LEWIS, M. A., QUINT, E., GLAZIER, A. M., FUCHS, H., DE ANGELIS, M. H., LANGFORD, C., VAN DONGEN, S., ABREU-GOODGER, C., PIIPARI, M., REDSHAW, N., DALMAY, T., MORENO-PELAYO, M. A., ENRIGHT, A. J. & STEEL, K. P. 2009. An enu-induced mutation of mir-96 associated with progressive hearing loss in mice. *Nat genet.* United States.

LI, H., ROBLIN, G., LIU, H. & HELLER, S. 2003. Generation of hair cells by stepwise differentiation of embryonic stem cells. *Proc Natl Acad Sci U S A,* 100**,** 13495-500.

LI, S., MARK, S., RADDE-GALLWITZ, K., SCHLISNER, R., CHIN, M. T. & CHEN, P. 2008. Hey2 functions in parallel with hes1 and hes5 for mammalian auditory sensory organ development. *BMC Dev Biol,* 8**,** 20.

LI, S., PRICE, S. M., CAHILL, H., RYUGO, D. K., SHEN, M. M. & XIANG, M. 2002. Hearing loss caused by progressive degeneration of cochlear hair cells in mice deficient for the barhl1 homeobox gene. *Development,* 129**,** 3523-32.

LI, W., WU, J., YANG, J., SUN, S., CHAI, R., CHEN, Z. & LI, H. 2014. Notch inhibition induces mitotically generated hair cells in mammalian cochleae via activating the wnt pathway. *Proc Natl Acad Sci U S A*.

LIBERMAN, M. C., GAO, J., HE, D. Z., WU, X., JIA, S. & ZUO, J. 2002. Prestin is required for electromotility of the outer hair cell and for the cochlear amplifier. *Nature.* England.

LIIPPO, J., NERA, K. P., VEISTINEN, E., LAHDESMAKI, A., POSTILA, V., KIMBY, E., RIIKONEN, P., HAMMARSTROM, L., PELKONEN, J. & LASSILA, O. 2001. Both normal and leukemic b lymphocytes express multiple isoforms of the human aiolos gene. *Eur j immunol.* Germany.

LIM, D. J. 1986. Functional structure of the organ of corti: A review. *Hear Res,* 22**,** 117-46.

LIM, D. J. & ANNIKO, M. 1985. Developmental morphology of the mouse inner ear. A scanning electron microscopic observation. *Acta Otolaryngol Suppl,* 422**,** 1-69.

LIN, F. R., METTER, E. J., O'BRIEN, R. J., RESNICK, S. M., ZONDERMAN, A. B. & FERRUCCI, L. 2011a. Hearing loss and incident dementia. *Arch Neurol,* 68**,** 214-20.

LIN, Y. S., CHEN, C. M., SOONG, B. W., WU, Y. R., CHEN, H. M., YEH, W. Y., WU, D. R., LIN, Y. J., POON, P. W., CHENG, M. L., WANG, C. H. & CHERN, Y. 2011b. Dysregulated brain creatine kinase is associated with hearing impairment in mouse models of huntington disease. *J Clin Invest,* 121**,** 1519-23.

LIPPE, W. R., WESTBROOK, E. W. & RYALS, B. M. 1991. Hair cell regeneration in the chicken cochlea following aminoglycoside toxicity. *Hear Res,* 56**,** 203-10.

LIU, H., PECKA, J. L., ZHANG, Q., SOUKUP, G. A., BEISEL, K. W. & HE, D. Z. 2014. Characterization of transcriptomes of cochlear inner and outer hair cells. *J Neurosci,* 34**,** 11085-95.

LIU, M., PEREIRA, F. A., PRICE, S. D., CHU, M. J., SHOPE, C., HIMES, D., EATOCK, R. A., BROWNELL, W. E., LYSAKOWSKI, A. & TSAI, M. J. 2000. Essential role of beta2/neurod1 in development of the vestibular and auditory systems. *Genes Dev,* 14**,** 2839-54.

LIU, W. & DAVIS, R. L. 2014. Calretinin and calbindin distribution patterns specify subpopulations of type i and type ii spiral ganglion neurons in postnatal murine cochlea. *J Comp Neurol,* 522**,** 2299-318.

LIU, X. Z., OUYANG, X. M., XIA, X. J., ZHENG, J., PANDYA, A., LI, F., DU, L. L., WELCH, K. O., PETIT, C., SMITH, R. J., WEBB, B. T., YAN, D., ARNOS, K. S., COREY, D., DALLOS, P., NANCE, W. E. & CHEN, Z. Y. 2003. Prestin, a cochlear motor protein, is defective in non-syndromic hearing loss. *Hum Mol Genet,* 12**,** 1155-62.

LIU, X. Z., WALSH, J., TAMAGAWA, Y., KITAMURA, K., NISHIZAWA, M., STEEL, K. P. & BROWN, S. D. 1997. Autosomal dominant non-syndromic deafness caused by a mutation in the myosin viia gene. *Nat Genet,* 17**,** 268-9.

LIU, Z., DEARMAN, J. A., COX, B. C., WALTERS, B. J., ZHANG, L., AYRAULT, O., ZINDY, F., GAN, L., ROUSSEL, M. F. & ZUO, J. 2012. Age-dependent in vivo conversion of mouse cochlear pillar and deiters' cells to immature hair cells by atoh1 ectopic expression. *J Neurosci,* 32**,** 6600-10.

LONGO-GUESS, C. M., GAGNON, L. H., COOK, S. A., WU, J., ZHENG, Q. Y. & JOHNSON, K. R. 2005. A missense mutation in the previously undescribed gene tmhs underlies deafness in hurry-scurry (hscy) mice. *Proc Natl Acad Sci U S A,* 102**,** 7894-9.

LORENZ, W. W., MCCANN, R. O., LONGIARU, M. & CORMIER, M. J. 1991. Isolation and expression of a cdna encoding renilla reniformis luciferase. *Proc Natl Acad Sci U S A,* 88**,** 4438-42.

LOWENHEIM, H., FURNESS, D. N., KIL, J., ZINN, C., GULTIG, K., FERO, M. L., FROST, D., GUMMER, A. W., ROBERTS, J. M., RUBEL, E. W., HACKNEY, C. M. & ZENNER, H. P.

1999. Gene disruption of p27(kip1) allows cell proliferation in the postnatal and adult organ of corti. *Proc Natl Acad Sci U S A,* 96**,** 4084-8.

LUKASHKIN, A. N., RICHARDSON, G. P. & RUSSELL, I. J. 2010. Multiple roles for the tectorial membrane in the active cochlea. *Hear Res,* 266**,** 26-35.

LUMPKIN, E. A., COLLISSON, T., PARAB, P., OMER-ABDALLA, A., HAEBERLE, H., CHEN, P., DOETZLHOFER, A., WHITE, P., GROVES, A., SEGIL, N. & JOHNSON, J. E. 2003. Math1-driven gfp expression in the developing nervous system of transgenic mice. *Gene Expr Patterns,* 3**,** 389-95.

LV, K., HUANG, H., LU, Y., QIN, C., LI, Z. & FENG, J. Q. 2010. Circling behavior developed in dmp1 null mice is due to bone defects in the vestibular apparatus. *Int J Biol Sci,* 6**,** 537-45.

MADDALO, D., MANCHADO, E., CONCEPCION, C. P., BONETTI, C., VIDIGAL, J. A., HAN, Y. C., OGRODOWSKI, P., CRIPPA, A., REKHTMAN, N., DE STANCHINA, E., LOWE, S. W. & VENTURA, A. 2014. In vivo engineering of oncogenic chromosomal rearrangements with the crispr/cas9 system. *Nature,* 516**,** 423-7.

MAISON, S. F., LUEBKE, A. E., LIBERMAN, M. C. & ZUO, J. 2002. Efferent protection from acoustic injury is mediated via alpha9 nicotinic acetylcholine receptors on outer hair cells. *J Neurosci,* 22**,** 10838-46.

MARAZITA, M. L., PLOUGHMAN, L. M., RAWLINGS, B., REMINGTON, E., ARNOS, K. S. & NANCE, W. E. 1993. Genetic epidemiological studies of early-onset deafness in the u.S. School-age population. *Am J Med Genet,* 46**,** 486-91.

MARCOTTI, W. 2012. Functional assembly of mammalian cochlear hair cells. *Exp Physiol,* 97**,** 438-51.

MARCOTTI, W., GELEOC, G. S., LENNAN, G. W. & KROS, C. J. 1999. Transient expression of an inwardly rectifying potassium conductance in developing inner and outer hair cells along the mouse cochlea. *Pflugers Arch,* 439**,** 113-22.

MARCOTTI, W., JOHNSON, S. L., HOLLEY, M. C. & KROS, C. J. 2003a. Developmental changes in the expression of potassium currents of embryonic, neonatal and mature mouse inner hair cells. *J Physiol,* 548**,** 383-400.

MARCOTTI, W., JOHNSON, S. L. & KROS, C. J. 2004. Effects of intracellular stores and extracellular ca(2+) on ca(2+)-activated k(+) currents in mature mouse inner hair cells. *J Physiol,* 557**,** 613-33.

MARCOTTI, W., JOHNSON, S. L., RUSCH, A. & KROS, C. J. 2003b. Sodium and calcium currents shape action potentials in immature mouse inner hair cells. *J Physiol,* 552**,** 743-61.

MARCOTTI, W. & KROS, C. J. 1999. Developmental expression of the potassium current ik,n contributes to maturation of mouse outer hair cells. *J Physiol,* 520 Pt 3**,** 653-60.

MARTIN-IBANEZ, R., CRESPO, E., ESGLEAS, M., URBAN, N., WANG, B., WACLAW, R., GEORGOPOULOS, K., MARTINEZ, S., CAMPBELL, K., VICARIO-ABEJON, C., ALBERCH, J., CHAN, S., KASTNER, P., RUBENSTEIN, J. L. & CANALS, J. M. 2012. Helios transcription factor expression depends on gsx2 and dlx1&2 function in developing striatal matrix neurons. *Stem Cells Dev,* 21**,** 2239-51.

MARTIN-IBANEZ, R., CRESPO, E., URBAN, N., SERGENT-TANGUY, S., HERRANZ, C., JAUMOT, M., VALIENTE, M., LONG, J. E., PINEDA, J. R., ANDREU, C., RUBENSTEIN, J. L. R., MARIN, O., GEORGOPOULOS, K., MENGOD, G., FARINAS, I., BACHS, O., ALBERCH, J. & CANALS, J. M. 2010. Ikaros-1 couples cell cycle arrest of late striatal precursors with neurogenesis of enkephalinergic neurons. *Journal of Comparative Neurology,* 518**,** 329-351.

MASUDA, M., DULON, D., PAK, K., MULLEN, L. M., LI, Y., ERKMAN, L. & RYAN, A. F. 2011. Regulation of pou4f3 gene expression in hair cells by 5' DNA in mice. *Neuroscience,* 197**,** 48-64.

MASUDA, M., TANAKA, K. F., KANZAKI, S., WAKABAYASHI, K., OISHI, N., SUZUKI, T., IKENAKA, K. & OGAWA, K. 2008. Gfap aggregates in the cochlear nerve increase the noise vulnerability of sensory cells in the organ of corti in the murine model of alexander disease. *Neurosci Res,* 62**,** 15-24.

MATSUBARA, A., LAAKE, J. H., DAVANGER, S., USAMI, S. & OTTERSEN, O. P. 1996. Organization of ampa receptor subunits at a glutamate synapse: A quantitative immunogold analysis of hair cell synapses in the rat organ of corti. *J Neurosci,* 16**,** 4457-67.

MATSUKURA, S., STELLATO, C., PLITT, J. R., BICKEL, C., MIURA, K., GEORAS, S. N., CASOLARO, V. & SCHLEIMER, R. P. 1999. Activation of eotaxin gene transcription by nf-kappa b and stat6 in human airway epithelial cells. *J Immunol,* 163**,** 6876-83.

MATTHEWS, J. C., HORI, K. & CORMIER, M. J. 1977. Purification and properties of renilla reniformis luciferase. *Biochemistry,* 16**,** 85-91.

MBURU, P., KIKKAWA, Y., TOWNSEND, S., ROMERO, R., YONEKAWA, H. & BROWN, S. D. M. 2006. Whirlin complexes with p55 at the stereocilia tip during hair cell development. *Proceedings of the National Academy of Sciences of the United States of America,* 103**,** 10973-10978.

MBURU, P., MUSTAPHA, M., VARELA, A., WEIL, D., EL-AMRAOUI, A., HOLME, R. H., RUMP, A., HARDISTY, R. E., BLANCHARD, S., COIMBRA, R. S., PERFETTINI, I., PARKINSON, N., MALLON, A. M., GLENISTER, P., ROGERS, M. J., PAIGE, A. J., MOIR, L., CLAY, J., ROSENTHAL, A., LIU, X. Z., BLANCO, G., STEEL, K. P., PETIT, C. & BROWN, S. D. 2003. Defects in whirlin, a pdz domain molecule involved in stereocilia elongation, cause deafness in the whirler mouse and families with dfnb31. *Nat Genet,* 34**,** 421-8.

MBURU, P., ROMERO, M. R., HILTON, H., PARKER, A., TOWNSEND, S., KIKKAWA, Y. & BROWN, S. D. M. 2010. Gelsolin plays a role in the actin polymerization complex of hair cell stereocilia. *Plos One,* 5.

MCCARTY, A. S., KLEIGER, G., EISENBERG, D. & SMALE, S. T. 2003. Selective dimerization of a c2h2 zinc finger subfamily. *Mol cell.* United States.

MCCOY, S. L., TUN, P. A., COX, L. C., COLANGELO, M., STEWART, R. A. & WINGFIELD, A. 2005. Hearing loss and perceptual effort: Downstream effects on older adults' memory for speech. *Q J Exp Psychol A,* 58**,** 22-33.

MCDERMOTT, B. M., JR., BAUCOM, J. M. & HUDSPETH, A. J. 2007. Analysis and functional evaluation of the hair-cell transcriptome. *Proc Natl Acad Sci U S A,* 104**,** 11820-5.

MCLEAN, W. J., SMITH, K. A., GLOWATZKI, E. & PYOTT, S. J. 2009. Distribution of the na,k-atpase alpha subunit in the rat spiral ganglion and organ of corti. *J Assoc Res Otolaryngol,* 10**,** 37-49.

MEHTA, A. K. 1985. An in-vitro comparison of the disintegration of human ear wax by five cerumenolytics commonly used in general practice. *Br J Clin Pract,* 39**,** 200-3.

MELCHIONDA, S., AHITUV, N., BISCEGLIA, L., SOBE, T., GLASER, F., RABIONET, R., ARBONES, M. L., NOTARANGELO, A., DI IORIO, E., CARELLA, M., ZELANTE, L., ESTIVILL, X., AVRAHAM, K. B. & GASPARINI, P. 2001. Myo6, the human homologue of the gene responsible for deafness in snell's waltzer mice, is mutated in autosomal dominant nonsyndromic hearing loss. *Am J Hum Genet,* 69**,** 635-40.

MENDOZA, J. 2011. Trapezoid body. *In:* KREUTZER, J., DELUCA, J. & CAPLAN, B. (eds.) *Encyclopedia of clinical neuropsychology.* New York: Springer.

MERCHANT, S. N., RAVICZ, M. E., PURIA, S., VOSS, S. E., WHITTEMORE, K. R., JR., PEAKE, W. T. & ROSOWSKI, J. J. 1997. Analysis of middle ear mechanics and application to diseased and reconstructed ears. *Am J Otol,* 18**,** 139-54.

MERZENICH, M. M., GARID, J. N. & VIVION, M. 1983. Animals. *In:* MOORE, E. J. (ed.) *Bases of auditory brain-stem evoked responses.* New York: Grune and Stratton.

MERZENICH, M. M., KNIGHT, P. L. & ROTH, G. L. 1975. Representation of cochlea within primary auditory cortex in the cat. *J Neurophysiol,* 38**,** 231-49.

MEYER, A. C., FRANK, T., KHIMICH, D., HOCH, G., RIEDEL, D., CHAPOCHNIKOV, N. M., YARIN, Y. M., HARKE, B., HELL, S. W., EGNER, A. & MOSER, T. 2009. Tuning of synapse number, structure and function in the cochlea. *Nat Neurosci,* 12**,** 444-53.

MEYER ZUM GOTTESBERGE, A. M., GROSS, O., BECKER-LENDZIAN, U., MASSING, T. & VOGEL, W. F. 2008. Inner ear defects and hearing loss in mice lacking the collagen receptor ddr1. *Lab Invest,* 88**,** 27-37.

MIC, F. A., MOLOTKOV, A., FAN, X., CUENCA, A. E. & DUESTER, G. 2000. Raldh3, a retinaldehyde dehydrogenase that generates retinoic acid, is expressed in the ventral retina, otic vesicle and olfactory pit during mouse development. *Mech Dev,* 97**,** 227-30.

MICHNA, M., KNIRSCH, M., HODA, J. C., MUENKNER, S., LANGER, P., PLATZER, J., STRIESSNIG, J. & ENGEL, J. 2003. Cav1.3 (alpha1d) ca2+ currents in neonatal outer hair cells of mice. *J Physiol,* 553**,** 747-58.

MILLER, J., MCLACHLAN, A. D. & KLUG, A. 1985. Repetitive zinc-binding domains in the protein transcription factor iiia from xenopus oocytes. *EMBO J,* 4**,** 1609-14.

MINAMI, Y., SHIMADA, S., MIYAHARA, H., MATSUNAGA, T. & TOHYAMA, M. 1998. Selective expression of mercurial-insensitive water channel (aqp-4) gene in hensen and claudius cells in the rat cochlea. *Acta Otolaryngol Suppl,* 533**,** 19-21.

MINOWA, O., IKEDA, K., SUGITANI, Y., OSHIMA, T., NAKAI, S., KATORI, Y., SUZUKI, M., FURUKAWA, M., KAWASE, T., ZHENG, Y., OGURA, M., ASADA, Y., WATANABE, K., YAMANAKA, H., GOTOH, S., NISHI-TAKESHIMA, M., SUGIMOTO, T., KIKUCHI, T., TAKASAKA, T. & NODA, T. 1999. Altered cochlear fibrocytes in a mouse model of dfn3 nonsyndromic deafness. *Science,* 285**,** 1408-11.

MISTRIK, P., DAUDET, N., MORANDELL, K. & ASHMORE, J. F. 2012. Mammalian prestin is a weak cl(-)/hco(3)(-) electrogenic antiporter. *J Physiol,* 590**,** 5597-610.

MIYABE, Y., KIKUCHI, T. & KOBAYASHI, T. 2002. Comparative immunohistochemical localizations of aquaporin-1 and aquaporin-4 in the cochleae of three different species of rodents. *Tohoku J Exp Med,* 196**,** 247-57.

MOLNAR, A. & GEORGOPOULOS, K. 1994. The ikaros gene encodes a family of functionally diverse zinc finger DNA-binding proteins. *Mol Cell Biol,* 14**,** 8292-303.

MONASTA, L., RONFANI, L., MARCHETTI, F., MONTICO, M., VECCHI BRUMATTI, L., BAVCAR, A., GRASSO, D., BARBIERO, C. & TAMBURLINI, G. 2012. Burden of disease caused by otitis media: Systematic review and global estimates. *PLoS One,* 7**,** e36226.

MOODY, S. A. 2014. *Principles of developmental genetics,* 2nd ed. London: Elsevier.

MOORE, J. K. 2000. Organization of the human superior olivary complex. *Microsc Res Tech,* 51**,** 403-12.

MORGAN, B., SUN, L., AVITAHL, N., ANDRIKOPOULOS, K., IKEDA, T., GONZALES, E., WU, P., NEBEN, S. & GEORGOPOULOS, K. 1997. Aiolos, a lymphoid restricted transcription

factor that interacts with ikaros to regulate lymphocyte differentiation. *EMBO J,* 16**,** 2004-13.

MORRISON, A., HODGETTS, C., GOSSLER, A., HRABE DE ANGELIS, M. & LEWIS, J. 1999. Expression of delta1 and serrate1 (jagged1) in the mouse inner ear. *Mech Dev,* 84**,** 169-72.

MORSLI, H., CHOO, D., RYAN, A., JOHNSON, R. & WU, D. K. 1998. Development of the mouse inner ear and origin of its sensory organs. *J Neurosci,* 18**,** 3327-35.

MORTAZAVI, A., WILLIAMS, B. A., MCCUE, K., SCHAEFFER, L. & WOLD, B. 2008. Mapping and quantifying mammalian transcriptomes by rna-seq. *Nat Methods,* 5**,** 621-8.

MOUNT, D. B. & ROMERO, M. F. 2004. The slc26 gene family of multifunctional anion exchangers. *Pflugers Arch,* 447**,** 710-21.

MOUSE GENOME SEQUENCING, C., WATERSTON, R. H., LINDBLAD-TOH, K., BIRNEY, E., ROGERS, J., ABRIL, J. F., AGARWAL, P., AGARWALA, R., AINSCOUGH, R., ALEXANDERSSON, M., AN, P., ANTONARAKIS, S. E., ATTWOOD, J., BAERTSCH, R., BAILEY, J., BARLOW, K., BECK, S., BERRY, E., BIRREN, B., BLOOM, T., BORK, P., BOTCHERBY, M., BRAY, N., BRENT, M. R., BROWN, D. G., BROWN, S. D., BULT, C., BURTON, J., BUTLER, J., CAMPBELL, R. D., CARNINCI, P., CAWLEY, S., CHIAROMONTE, F., CHINWALLA, A. T., CHURCH, D. M., CLAMP, M., CLEE, C., COLLINS, F. S., COOK, L. L., COPLEY, R. R., COULSON, A., COURONNE, O., CUFF, J., CURWEN, V., CUTTS, T., DALY, M., DAVID, R., DAVIES, J., DELEHAUNTY, K. D., DERI, J., DERMITZAKIS, E. T., DEWEY, C., DICKENS, N. J., DIEKHANS, M., DODGE, S., DUBCHAK, I., DUNN, D. M., EDDY, S. R., ELNITSKI, L., EMES, R. D., ESWARA, P., EYRAS, E., FELSENFELD, A., FEWELL, G. A., FLICEK, P., FOLEY, K., FRANKEL, W. N., FULTON, L. A., FULTON, R. S., FUREY, T. S., GAGE, D., GIBBS, R. A., GLUSMAN, G., GNERRE, S., GOLDMAN, N., GOODSTADT, L., GRAFHAM, D., GRAVES, T. A., GREEN, E. D., GREGORY, S., GUIGO, R., GUYER, M., HARDISON, R. C., HAUSSLER, D., HAYASHIZAKI, Y., HILLIER, L. W., HINRICHS, A., HLAVINA, W., HOLZER, T., HSU, F., HUA, A., HUBBARD, T., HUNT, A., JACKSON, I., JAFFE, D. B., JOHNSON, L. S., JONES, M., JONES, T. A., JOY, A., KAMAL, M., et al. 2002. Initial sequencing and comparative analysis of the mouse genome. *Nature,* 420**,** 520-62.

MU, M. Y., CHARDIN, S., AVAN, P. & ROMAND, R. 1997. Ontogenesis of rat cochlea. A quantitative study of the organ of corti. *Brain Res Dev Brain Res,* 99**,** 29-37.

MUALLEM, D. & ASHMORE, J. 2006. An anion antiporter model of prestin, the outer hair cell motor protein. *Biophys J,* 90**,** 4035-45.

MUELLER, K. L., JACQUES, B. E. & KELLEY, M. W. 2002. Fibroblast growth factor signaling regulates pillar cell development in the organ of corti. *J Neurosci,* 22**,** 9368-77.

MUELLER, R. F., NEHAMMER, A., MIDDLETON, A., HOUSEMAN, M., TAYLOR, G. R., BITNER-GLINDZCIZ, M., VAN CAMP, G., PARKER, M., YOUNG, I. D., DAVIS, A., NEWTON, V. E. & LENCH, N. J. 1999. Congenital non-syndromal sensorineural hearing impairment due to connexin 26 gene mutations--molecular and audiological findings. *Int J Pediatr Otorhinolaryngol,* 50**,** 3-13.

MURATA, J., TOKUNAGA, A., OKANO, H. & KUBO, T. 2006. Mapping of notch activation during cochlear development in mice: Implications for determination of prosensory domain and cell fate diversification. *J Comp Neurol,* 497**,** 502-18.

NABATAME, S., OKINAGA, T., IMAI, K., KAMIO, N., KAGITANI-SHIMONO, K., NAGAI, T., KUROSAWA, K. & OZONO, K. 2007. [effect of carbamazepine on epilepsy with 1p36 deletion syndrome]. *No To Hattatsu,* 39**,** 289-94.

NAKASE, K., ISHIMARU, F., AVITAHL, N., DANSAKO, H., MATSUO, K., FUJII, K., SEZAKI, N., NAKAYAMA, H., YANO, T., FUKUDA, S., IMAJOH, K., TAKEUCHI, M., MIYATA, A., HARA, M., YASUKAWA, M., TAKAHASHI, I., TAGUCHI, H., MATSUE, K., NAKAO, S., NIHO, Y., TAKENAKA, K., SHINAGAWA, K., IKEDA, K., NIIYA, K. & HARADA, M. 2000. Dominant negative isoform of the ikaros gene in patients with adult b-cell acute lymphoblastic leukemia. *Cancer Res,* 60**,** 4062-5.

NAKASE, K., ISHIMARU, F., FUJII, K., TABAYASHI, T., KOZUKA, T., SEZAKI, N., MATSUO, Y. & HARADA, M. 2002. Overexpression of novel short isoforms of helios in a patient with t-cell acute lymphoblastic leukemia. *Exp hematol.* Netherlands.

NAKAZAWA, K. 2001. Ultrastructural localization of calmodulin in gerbil cochlea by immunogold electron microscopy. *Hear Res,* 151**,** 133-140.

NATHAN, C. F., MURRAY, H. W. & COHN, Z. A. 1980. The macrophage as an effector cell. *N Engl J Med,* 303**,** 622-6.

NAYAGAM, B. A., MUNIAK, M. A. & RYUGO, D. K. 2011. The spiral ganglion: Connecting the peripheral and central auditory systems. *Hear Res,* 278**,** 2-20.

NAZ, S., GRIFFITH, A. J., RIAZUDDIN, S., HAMPTON, L. L., BATTEY, J. F., JR., KHAN, S. N., WILCOX, E. R. & FRIEDMAN, T. B. 2004. Mutations of espn cause autosomal recessive deafness and vestibular dysfunction. *J Med Genet,* 41**,** 591-5.

NC3RS. 2015. *Guidelines* [Online]. Available: https://www.nc3rs.org.uk/guidelines [Accessed 01/12/2015].

NEYROUD, N., TESSON, F., DENJOY, I., LEIBOVICI, M., DONGER, C., BARHANIN, J., FAURE, S., GARY, F., COUMEL, P., PETIT, C., SCHWARTZ, K. & GUICHENEY, P. 1997. A novel mutation in the potassium channel gene kvlqt1 causes the jervell and lange-nielsen cardioauditory syndrome. *Nat Genet,* 15**,** 186-9.

NICHOGIANNOPOULOU, A., TREVISAN, M., NEBEN, S., FRIEDRICH, C. & GEORGOPOULOS, K. 1999. Defects in hemopoietic stem cell activity in ikaros mutant mice. *J Exp Med,* 190**,** 1201-14.

NICHOLS, D. H., PAULEY, S., JAHAN, I., BEISEL, K. W., MILLEN, K. J. & FRITZSCH, B. 2008. Lmx1a is required for segregation of sensory epithelia and normal ear histogenesis and morphogenesis. *Cell Tissue Res,* 334**,** 339-58.

NIN, F., HIBINO, H., DOI, K., SUZUKI, T., HISA, Y. & KURACHI, Y. 2008. The endocochlear potential depends on two k+ diffusion potentials and an electrical barrier in the stria vascularis of the inner ear. *Proc Natl Acad Sci U S A,* 105**,** 1751-6.

NOBEN-TRAUTH, K., ZHENG, Q. Y. & JOHNSON, K. R. 2003. Association of cadherin 23 with polygenic inheritance and genetic modification of sensorineural hearing loss. *Nature Genetics,* 35**,** 21-23.

NORAMLY, S. & GRAINGER, R. M. 2002. Determination of the embryonic inner ear. *J Neurobiol,* 53**,** 100-28.

OBHOLZER, N., WOLFSON, S., TRAPANI, J. G., MO, W., NECHIPORUK, A., BUSCH-NENTWICH, E., SEILER, C., SIDI, S., SOLLNER, C., DUNCAN, R. N., BOEHLAND, A. & NICOLSON, T. 2008. Vesicular glutamate transporter 3 is required for synaptic transmission in zebrafish hair cells. *J Neurosci,* 28**,** 2110-8.

OFFNER, F. F., DALLOS, P. & CHEATHAM, M. A. 1987. Positive endocochlear potential: Mechanism of production by marginal cells of stria vascularis. *Hear Res,* 29**,** 117-24.

OHLEMILLER, K. K., HUGHES, R. M., LETT, J. M., OGILVIE, J. M., SPECK, J. D., WRIGHT, J. S. & FADDIS, B. T. 1997. Progression of cochlear and retinal degeneration in the tubby (rd5) mouse. *Audiol Neurootol,* 2**,** 175-85.

OLA, R., LEFEBVRE, S., BRAUNEWELL, K. H., SAINIO, K. & SARIOLA, H. 2012. The expression of visinin-like 1 during mouse embryonic development. *Gene Expr Patterns,* 12**,** 53-62.

OLIVER, D., HE, D. Z., KLOCKER, N., LUDWIG, J., SCHULTE, U., WALDEGGER, S., RUPPERSBERG, J. P., DALLOS, P. & FAKLER, B. 2001. Intracellular anions as the voltage sensor of prestin, the outer hair cell motor protein. *Science,* 292**,** 2340-3.

OLIVER, D., PLINKERT, P., ZENNER, H. P. & RUPPERSBERG, J. P. 1997. Sodium current expression during postnatal development of rat outer hair cells. *Pflugers Arch,* 434**,** 772-8.

OLIVER, D. L. 2000. Ascending efferent projections of the superior olivary complex. *Microsc Res Tech,* 51**,** 355-63.

OSHIMA, T., OKABE, S. & HIROKAWA, N. 1992. Immunocytochemical localization of 205 kda microtubule-associated protein (205 kda map) in the guinea pig organ of corti. *Brain Res,* 590**,** 53-65.

PABO, C. O., PEISACH, E. & GRANT, R. A. 2001. Design and selection of novel cys2his2 zinc finger proteins. *Annu Rev Biochem,* 70**,** 313-40.

PAN, B., GELEOC, G. S., ASAI, Y., HORWITZ, G. C., KURIMA, K., ISHIKAWA, K., KAWASHIMA, Y., GRIFFITH, A. J. & HOLT, J. R. 2013. Tmc1 and tmc2 are components of the mechanotransduction channel in hair cells of the mammalian inner ear. *Neuron,* 79**,** 504-15.

PAN, F., YU, H., DANG, E. V., BARBI, J., PAN, X., GROSSO, J. F., JINASENA, D., SHARMA, S. M., MCCADDEN, E. M., GETNET, D., DRAKE, C. G., LIU, J. O., OSTROWSKI, M. C. & PARDOLL, D. M. 2009. Eos mediates foxp3-dependent gene silencing in cd4+ regulatory t cells. *Science,* 325**,** 1142-6.

PAN, N., JAHAN, I., KERSIGO, J., DUNCAN, J. S., KOPECKY, B. & FRITZSCH, B. 2012. A novel atoh1 "self-terminating" mouse model reveals the necessity of proper atoh1 level and duration for hair cell differentiation and viability. *PLoS One,* 7**,** e30358.

PAN, W., JIN, Y., STANGER, B. & KIERNAN, A. E. 2010. Notch signaling is required for the generation of hair cells and supporting cells in the mammalian inner ear. *Proc Natl Acad Sci U S A,* 107**,** 15798-803.

PANZA, F., SOLFRIZZI, V. & LOGROSCINO, G. 2015. Age-related hearing impairment-a risk factor and frailty marker for dementia and ad. *Nat Rev Neurol,* 11**,** 166-75.

PARKINSON, N., HARDISTY-HUGHES, R. E., TATEOSSIAN, H., TSAI, H. T., BROOKER, D., MORSE, S., LALANE, Z., MACKENZIE, F., FRAY, M., GLENISTER, P., WOODWARD, A. M., POLLEY, S., BARBARIC, I., DEAR, N., HOUGH, T. A., HUNTER, A. J., CHEESEMAN, M. T. & BROWN, S. D. 2006. Mutation at the evi1 locus in junbo mice causes susceptibility to otitis media. *PLoS Genet,* 2**,** e149.

PARRAGA, G., HORVATH, S., HOOD, L., YOUNG, E. T. & KLEVIT, R. E. 1990. Spectroscopic studies of wild-type and mutant "zinc finger" peptides: Determinants of domain folding and structure. *Proc Natl Acad Sci U S A,* 87**,** 137-41.

PARRAGA, G., HORVATH, S. J., EISEN, A., TAYLOR, W. E., HOOD, L., YOUNG, E. T. & KLEVIT, R. E. 1988. Zinc-dependent structure of a single-finger domain of yeast adr1. *Science,* 241**,** 1489-92.

PARSONS, C. H., LANYON, R. G., SCHNUPP, J. W. & KING, A. J. 1999. Effects of altering spectral cues in infancy on horizontal and vertical sound localization by adult ferrets. *J Neurophysiol,* 82**,** 2294-309.

PATUZZI, R. B. & THOMPSON, M. L. 1991. Cochlear efferent neurones and protection against acoustic trauma: Protection of outer hair cell receptor current and interanimal variability. *Hear Res,* 54**,** 45-58.

PAUTER, A. M., OLSSON, P., ASADI, A., HERSLOF, B., CSIKASZ, R. I., ZADRAVEC, D. & JACOBSSON, A. 2014. Elovl2 ablation demonstrates that systemic dha is endogenously produced and is essential for lipid homeostasis in mice. *J Lipid Res,* 55**,** 718-28.

PENG, A. W., BELYANTSEVA, I. A., HSU, P. D., FRIEDMAN, T. B. & HELLER, S. 2009. Twinfilin 2 regulates actin filament lengths in cochlear stereocilia. *J neurosci.* United States.

PENNACCHIO, L. A. 2003. Insights from human/mouse genome comparisons. *Mamm Genome,* 14**,** 429-36.

PERDOMO, J., HOLMES, M., CHONG, B. & CROSSLEY, M. 2000. Eos and pegasus, two members of the ikaros family of proteins with distinct DNA binding activities. *J biol chem.* United States.

PEROTTI, E. A., GEORGOPOULOS, K. & YOSHIDA, T. 2015. An ikaros promoter element with dual epigenetic and transcriptional activities. *PLoS One,* 10**,** e0131568.

PETERS, C., OBERG, H. H., KABELITZ, D. & WESCH, D. 2014. Phenotype and regulation of immunosuppressive vdelta2-expressing gammadelta t cells. *Cell Mol Life Sci,* 71**,** 1943-60.

PETIT, C. 2006. From deafness genes to hearing mechanisms: Harmony and counterpoint. *Trends Mol Med,* 12**,** 57-64.

PETIT, C., LEVILLIERS, J. & HARDELIN, J. P. 2001. Molecular genetics of hearing loss. *Annu Rev Genet,* 35**,** 589-646.

PHIPPARD, D., LU, L., LEE, D., SAUNDERS, J. C. & CRENSHAW, E. B., 3RD 1999. Targeted mutagenesis of the pou-domain gene brn4/pou3f4 causes developmental defects in the inner ear. *J Neurosci,* 19**,** 5980-9.

PICKLES, J. O., COMIS, S. D. & OSBORNE, M. P. 1984. Cross-links between stereocilia in the guinea pig organ of corti, and their possible relation to sensory transduction. *Hearing Research,* 15**,** 103-112.

PIRVOLA, U., YLIKOSKI, J., PALGI, J., LEHTONEN, E., ARUMAE, U. & SAARMA, M. 1992. Brain-derived neurotrophic factor and neurotrophin 3 mrnas in the peripheral target fields of developing inner ear ganglia. *Proc Natl Acad Sci U S A,* 89**,** 9915-9.

PIRVOLA, U., YLIKOSKI, J., TROKOVIC, R., HEBERT, J. M., MCCONNELL, S. K. & PARTANEN, J. 2002. Fgfr1 is required for the development of the auditory sensory epithelium. *Neuron,* 35**,** 671-80.

PITTLER, S. J. & BAEHR, W. 1991. Identification of a nonsense mutation in the rod photoreceptor cgmp phosphodiesterase beta-subunit gene of the rd mouse. *Proc Natl Acad Sci U S A,* 88**,** 8322-6.

PLATZER, J., ENGEL, J., SCHROTT-FISCHER, A., STEPHAN, K., BOVA, S., CHEN, H., ZHENG, H. & STRIESSNIG, J. 2000. Congenital deafness and sinoatrial node dysfunction in mice lacking class d l-type ca2+ channels. *Cell,* 102**,** 89-97.

PODOSHIN, L., BEN-DAVID, J. & TESZLER, C. B. 1997. Pediatric and geriatric tinnitus. *Int Tinnitus J,* 3**,** 101-103.

POWER, C. & ELLIOTT, J. 2006. Cohort profile: 1958 british birth cohort (national child development study). *Int J Epidemiol,* 35**,** 34-41.

PROBST, F. J., FRIDELL, R. A., RAPHAEL, Y., SAUNDERS, T. L., WANG, A. H., LIANG, Y., MORELL, R. J., TOUCHMAN, J. W., LYONS, R. H., NOBEN-TRAUTH, K., FRIEDMAN, T. B.

& CAMPER, S. A. 1998. Correction of deafness in shaker-2 mice by an unconventional myosin in a bac transgene. *Science,* 280**,** 1444-1447.

PULIGILLA, C., FENG, F., ISHIKAWA, K., BERTUZZI, S., DABDOUB, A., GRIFFITH, A. J., FRITZSCH, B. & KELLEY, M. W. 2007. Disruption of fibroblast growth factor receptor 3 signaling results in defects in cellular differentiation, neuronal patterning, and hearing impairment. *Dev Dyn,* 236**,** 1905-17.

QUINTANA, F. J., JIN, H., BURNS, E. J., NADEAU, M., YESTE, A., KUMAR, D., RANGACHARI, M., ZHU, C., XIAO, S., SEAVITT, J., GEORGOPOULOS, K. & KUCHROO, V. K. 2012. Aiolos promotes th17 differentiation by directly silencing il2 expression. *Nat Immunol,* 13**,** 770-7.

QUWAILID, M. M., HUGILL, A., DEAR, N., VIZOR, L., WELLS, S., HORNER, E., FULLER, S., WEEDON, J., MCMATH, H., WOODMAN, P., EDWARDS, D., CAMPBELL, D., RODGER, S., CAREY, J., ROBERTS, A., GLENISTER, P., LALANNE, Z., PARKINSON, N., COGHILL, E. L., MCKEONE, R., COX, S., WILLAN, J., GREENFIELD, A., KEAYS, D., BRADY, S., SPURR, N., GRAY, I., HUNTER, J., BROWN, S. D. M. & COX, R. D. 2004. A gene-driven enu-based approach to generating an allelic series in any gene. *Mammalian Genome,* 15**,** 585-591.

RAFF, M. C. 1973. T and b lymphocytes and immune responses. *Nature,* 242**,** 19-23.

RAFFIN, C., PIGNON, P., CELSE, C., DEBIEN, E., VALMORI, D. & AYYOUB, M. 2013. Human memory helios- foxp3+ regulatory t cells (tregs) encompass induced tregs that express aiolos and respond to il-1beta by downregulating their suppressor functions. *J Immunol,* 191**,** 4619-27.

RAFT, S., NOWOTSCHIN, S., LIAO, J. & MORROW, B. E. 2004. Suppression of neural fate and control of inner ear morphogenesis by tbx1. *Development,* 131**,** 1801-12.

RAMAKRISHNAN, N. A., DRESCHER, M. J., KHAN, K. M., HATFIELD, J. S. & DRESCHER, D. G. 2012. Hcn1 and hcn2 proteins are expressed in cochlear hair cells: Hcn1 can form a ternary complex with protocadherin 15 cd3 and f-actin-binding filamin a or can interact with hcn2. *J Biol Chem,* 287**,** 37628-46.

RAPHAEL, Y. & ALTSCHULER, R. A. 2003. Structure and innervation of the cochlea. *Brain res bull.* United States.

REALE, R. A. & IMIG, T. J. 1980. Tonotopic organization in auditory cortex of the cat. *J Comp Neurol,* 192**,** 265-91.

REBOLLO, A. & SCHMITT, C. 2003. Ikaros, aiolos and helios: Transcription regulators and lymphoid malignancies. *Immunol cell biol.* Australia.

REUSS, S. 1998. Nitric oxide synthase in the auditory brain stem. *Neuroreport,* 9**,** 3643-6.

REYNAUD, D., DEMARCO, I. A., REDDY, K. L., SCHJERVEN, H., BERTOLINO, E., CHEN, Z., SMALE, S. T., WINANDY, S. & SINGH, H. 2008. Regulation of b cell fate commitment and immunoglobulin heavy-chain gene rearrangements by ikaros. *Nat immunol.* United States.

RICKHEIT, G., MAIER, H., STRENZKE, N., ANDREESCU, C. E., DE ZEEUW, C. I., MUENSCHER, A., ZDEBIK, A. A. & JENTSCH, T. J. 2008. Endocochlear potential depends on cl- channels: Mechanism underlying deafness in bartter syndrome iv. *Embo j,* 27**,** 2907-17.

ROBERTS, L. E., EGGERMONT, J. J., CASPARY, D. M., SHORE, S. E., MELCHER, J. R. & KALTENBACH, J. A. 2010. Ringing ears: The neuroscience of tinnitus. *J Neurosci,* 30**,** 14972-9.

ROBERTSON, N. G., LU, L., HELLER, S., MERCHANT, S. N., EAVEY, R. D., MCKENNA, M., NADOL, J. B., JR., MIYAMOTO, R. T., LINTHICUM, F. H., JR., LUBIANCA NETO, J. F.,

HUDSPETH, A. J., SEIDMAN, C. E., MORTON, C. C. & SEIDMAN, J. G. 1998. Mutations in a novel cochlear gene cause dfna9, a human nonsyndromic deafness with vestibular dysfunction. *Nat Genet,* 20**,** 299-303.

ROCKE, D., RUAN, L., ZHANG, Y., GOSSETT, J., DURBIN-JOHNSON, B. & AVIRAN, S. 2015. Excess false positive rates in methods for differential gene expression analysis using rna-seq data. *bioRxiv* [Online].

ROSENBLUTH, J. 1962. The fine structure of acoustic ganglia in the rat. *J Cell Biol,* 12**,** 329-59.

ROTH, B. & BRUNS, V. 1992. Postnatal development of the rat organ of corti. Ii. Hair cell receptors and their supporting elements. *Anat Embryol (Berl),* 185**,** 571-81.

ROTH, G. L., AITKIN, L. M., ANDERSEN, R. A. & MERZENICH, M. M. 1978. Some features of the spatial organization of the central nucleus of the inferior colliculus of the cat. *J Comp Neurol,* 182**,** 661-80.

ROUILLER, E. 1997. Functional organisation of the auditory pathways. *In:* EHRET, G. & ROMAND, R. (eds.) *The central auditory system.* Oxford: Oxford University Press.

ROUX, I., SAFIEDDINE, S., NOUVIAN, R., GRATI, M., SIMMLER, M. C., BAHLOUL, A., PERFETTINI, I., LE GALL, M., ROSTAING, P., HAMARD, G., TRILLER, A., AVAN, P., MOSER, T. & PETIT, C. 2006. Otoferlin, defective in a human deafness form, is essential for exocytosis at the auditory ribbon synapse. *Cell,* 127**,** 277-89.

RUBEN, R. J. 1967. Development of the inner ear of the mouse: A radioautographic study of terminal mitoses. *Acta Otolaryngol***,** Suppl 220:1-44.

RUBEN, R. J. 2000. Redefining the survival of the fittest: Communication disorders in the 21st century. *Laryngoscope,* 110**,** 241-5.

RUEL, J., EMERY, S., NOUVIAN, R., BERSOT, T., AMILHON, B., VAN RYBROEK, J. M., REBILLARD, G., LENOIR, M., EYBALIN, M., DELPRAT, B., SIVAKUMARAN, T. A., GIROS, B., EL MESTIKAWY, S., MOSER, T., SMITH, R. J., LESPERANCE, M. M. & PUEL, J. L. 2008. Impairment of slc17a8 encoding vesicular glutamate transporter-3, vglut3, underlies nonsyndromic deafness dfna25 and inner hair cell dysfunction in null mice. *Am J Hum Genet,* 83**,** 278-92.

RYE, M. S., WIERTSEMA, S. P., SCAMAN, E. S., OOMMEN, J., SUN, W., FRANCIS, R. W., ANG, W., PENNELL, C. E., BURGNER, D., RICHMOND, P., VIJAYASEKARAN, S., COATES, H. L., BROWN, S. D., BLACKWELL, J. M. & JAMIESON, S. E. 2011. Fbxo11, a regulator of the tgfbeta pathway, is associated with severe otitis media in western australian children. *Genes Immun,* 12**,** 352-9.

RZADZINSKA, A. K., NEVALAINEN, E. M., PROSSER, H. M., LAPPALAINEN, P. & STEEL, K. P. 2009. Myosinviia interacts with twinfilin-2 at the tips of mechanosensory stereocilia in the inner ear. *PLoS One,* 4**,** e7097.

SABBATTINI, P., LUNDGREN, M., GEORGIOU, A., CHOW, C., WARNES, G. & DILLON, N. 2001. Binding of ikaros to the lambda5 promoter silences transcription through a mechanism that does not require heterochromatin formation. *EMBO J,* 20**,** 2812-22.

SAFIEDDINE, S., EL-AMRAOUI, A. & PETIT, C. 2012. The auditory hair cell ribbon synapse: From assembly to function. *Annu Rev Neurosci,* 35**,** 509-28.

SAFIEDDINE, S. & WENTHOLD, R. J. 1999. Snare complex at the ribbon synapses of cochlear hair cells: Analysis of synaptic vesicle- and synaptic membrane-associated proteins. *Eur J Neurosci,* 11**,** 803-12.

SAKAGUCHI, N., CROUCH, J. J., LYTLE, C. & SCHULTE, B. A. 1998a. Na-k-cl cotransporter expression in the developing and senescent gerbil cochlea. *Hear Res,* 118**,** 114-22.

SAKAGUCHI, N., HENZL, M. T., THALMANN, I., THALMANN, R. & SCHULTE, B. A. 1998b. Oncomodulin is expressed exclusively by outer hair cells in the organ of corti. *J Histochem Cytochem,* 46**,** 29-40.

SAKAGUCHI, S., SAKAGUCHI, N., ASANO, M., ITOH, M. & TODA, M. 1995. Immunologic self-tolerance maintained by activated t cells expressing il-2 receptor alpha-chains (cd25). Breakdown of a single mechanism of self-tolerance causes various autoimmune diseases. *J Immunol,* 155**,** 1151-64.

SANZ, E., EVANOFF, R., QUINTANA, A., EVANS, E., MILLER, J. A., KO, C., AMIEUX, P. S., GRISWOLD, M. D. & MCKNIGHT, G. S. 2013. Ribotag analysis of actively translated mrnas in sertoli and leydig cells in vivo. *PLoS One,* 8**,** e66179.

SANZ, E., YANG, L., SU, T., MORRIS, D. R., MCKNIGHT, G. S. & AMIEUX, P. S. 2009. Cell-type-specific isolation of ribosome-associated mrna from complex tissues. *Proc Natl Acad Sci U S A,* 106**,** 13939-44.

SCHEFFER, D. I., SHEN, J., COREY, D. P. & CHEN, Z. Y. 2015. Gene expression by mouse inner ear hair cells during development. *J Neurosci,* 35**,** 6366-80.

SCHINDELIN, J., ARGANDA-CARRERAS, I., FRISE, E., KAYNIG, V., LONGAIR, M., PIETZSCH, T., PREIBISCH, S., RUEDEN, C., SAALFELD, S., SCHMID, B., TINEVEZ, J. Y., WHITE, D. J., HARTENSTEIN, V., ELICEIRI, K., TOMANCAK, P. & CARDONA, A. 2012. Fiji: An open-source platform for biological-image analysis. *Nat methods.* United States.

SCHLINGMANN, K. P., KONRAD, M., JECK, N., WALDEGGER, P., REINALTER, S. C., HOLDER, M., SEYBERTH, H. W. & WALDEGGER, S. 2004. Salt wasting and deafness resulting from mutations in two chloride channels. *N Engl J Med,* 350**,** 1314-9.

SCHMITZ, F., KONIGSTORFER, A. & SUDHOF, T. C. 2000. Ribeye, a component of synaptic ribbons: A protein's journey through evolution provides insight into synaptic ribbon function. *Neuron,* 28**,** 857-72.

SCHOFIELD, B. R. & CANT, N. B. 1999. Descending auditory pathways: Projections from the inferior colliculus contact superior olivary cells that project bilaterally to the cochlear nuclei. *J Comp Neurol,* 409**,** 210-23.

SCHRADERS, M., OOSTRIK, J., HUYGEN, P. L., STROM, T. M., VAN WIJK, E., KUNST, H. P., HOEFSLOOT, L. H., CREMERS, C. W., ADMIRAAL, R. J. & KREMER, H. 2010. Mutations in ptprq are a cause of autosomal-recessive nonsyndromic hearing impairment dfnb84 and associated with vestibular dysfunction. *Am J Hum Genet,* 86**,** 604-10.

SCHRADERS, M., RUIZ-PALMERO, L., KALAY, E., OOSTRIK, J., DEL CASTILLO, F. J., SEZGIN, O., BEYNON, A. J., STROM, T. M., PENNINGS, R. J., SECO, C. Z., OONK, A. M., KUNST, H. P., DOMINGUEZ-RUIZ, M., GARCIA-ARUMI, A. M., DEL CAMPO, M., VILLAMAR, M., HOEFSLOOT, L. H., MORENO, F., ADMIRAAL, R. J., DEL CASTILLO, I. & KREMER, H. 2012. Mutations of the gene encoding otogelin are a cause of autosomal-recessive nonsyndromic moderate hearing impairment. *Am J Hum Genet,* 91**,** 883-9.

SCHRAFF, S. A. 2008. Contemporary indications for ventilation tube placement. *Curr Opin Otolaryngol Head Neck Surg,* 16**,** 406-11.

SCHRAUWEN, I., EALY, M., HUENTELMAN, M. J., THYS, M., HOMER, N., VANDERSTRAETEN, K., FRANSEN, E., CORNEVEAUX, J. J., CRAIG, D. W., CLAUSTRES, M., CREMERS, C. W., DHOOGE, I., VAN DE HEYNING, P., VINCENT, R., OFFECIERS, E., SMITH, R. J. & VAN CAMP, G. 2009. A genome-wide analysis identifies genetic variants in the reln gene associated with otosclerosis. *Am J Hum Genet,* 84**,** 328-38.

SCHUKNECHT, H. F. & GACEK, M. R. 1993. Cochlear pathology in presbycusis. *Ann Otol Rhinol Laryngol,* 102**,** 1-16.

SCHULTE, B. A. & STEEL, K. P. 1994. Expression of alpha and beta subunit isoforms of na,k-atpase in the mouse inner ear and changes with mutations at the wv or sld loci. *Hear Res,* 78**,** 65-76.

SCHULZE-BAHR, E., WANG, Q., WEDEKIND, H., HAVERKAMP, W., CHEN, Q., SUN, Y., RUBIE, C., HORDT, M., TOWBIN, J. A., BORGGREFE, M., ASSMANN, G., QU, X., SOMBERG, J. C., BREITHARDT, G., OBERTI, C. & FUNKE, H. 1997. Kcne1 mutations cause jervell and lange-nielsen syndrome. *Nat Genet,* 17**,** 267-8.

SEAL, R. P., AKIL, O., YI, E., WEBER, C. M., GRANT, L., YOO, J., CLAUSE, A., KANDLER, K., NOEBELS, J. L., GLOWATZKI, E., LUSTIG, L. R. & EDWARDS, R. H. 2008. Sensorineural deafness and seizures in mice lacking vesicular glutamate transporter 3. *Neuron,* 57**,** 263-75.

SEGADE, F., DALY, K. A., ALLRED, D., HICKS, P. J., COX, M., BROWN, M., HARDISTY-HUGHES, R. E., BROWN, S. D., RICH, S. S. & BOWDEN, D. W. 2006. Association of the fbxo11 gene with chronic otitis media with effusion and recurrent otitis media: The minnesota come/rom family study. *Arch Otolaryngol Head Neck Surg,* 132**,** 729-33.

SELLARS, M., REINA-SAN-MARTIN, B., KASTNER, P. & CHAN, S. 2009. Ikaros controls isotype selection during immunoglobulin class switch recombination. *J exp med.* United States.

SERRE, K., BENEZECH, C., DESANTI, G., BOBAT, S., TOELLNER, K. M., BIRD, R., CHAN, S., KASTNER, P., CUNNINGHAM, A. F., MACLENNAN, I. C. & MOHR, E. 2011. Helios is associated with cd4 t cells differentiating to t helper 2 and follicular helper t cells in vivo independently of foxp3 expression. *Plos one.* United States.

SHABBIR, M. I., AHMED, Z. M., KHAN, S. Y., RIAZUDDIN, S., WARYAH, A. M., KHAN, S. N., CAMPS, R. D., GHOSH, M., KABRA, M., BELYANTSEVA, I. A. & FRIEDMAN, T. B. 2006. Mutations of human tmhs cause recessively inherited non-syndromic hearing loss. *J Med Genet,* 43**,** 634-40.

SHARMA, M. D., HUANG, L., CHOI, J. H., LEE, E. J., WILSON, J. M., LEMOS, H., PAN, F., BLAZAR, B. R., PARDOLL, D. M., MELLOR, A. L., SHI, H. & MUNN, D. H. 2013. An inherently bifunctional subset of foxp3+ t helper cells is controlled by the transcription factor eos. *Immunity,* 38**,** 998-1012.

SHER, A. E. 1971. The embryonic and postnatal development of the inner ear of the mouse. *Acta Otolaryngol Suppl,* 285**,** 1-77.

SHOTWELL, S. L., JACOBS, R. & HUDSPETH, A. J. 1981. Directional sensitivity of individual vertebrate hair cells to controlled deflection of their hair bundles. *Ann N Y Acad Sci,* 374**,** 1-10.

SIMMLER, M. C., COHEN-SALMON, M., EL-AMRAOUI, A., GUILLAUD, L., BENICHOU, J. C., PETIT, C. & PANTHIER, J. J. 2000a. Targeted disruption of otog results in deafness and severe imbalance. *Nat Genet,* 24**,** 139-43.

SIMMLER, M. C., ZWAENEPOEL, I. I., VERPY, E., GUILLAUD, L., ELBAZ, C., PETIT, C. & PANTHIER, J. J. 2000b. Twister mutant mice are defective for otogelin, a component specific to inner ear acellular membranes. *Mamm Genome,* 11**,** 961-966.

SIMMONS, D., HORNAK, A. & LIBERMAN, C. 2015. Targeted deletion of oncomodulin changes sensitivity to high frequencies before causing progressive hearing loss. *Association for Research in Otolaryngology 38th Annual MidWinter Meeting.* Baltimore, USA.

SIMMONS, D. D. 2002. Development of the inner ear efferent system across vertebrate species. *J Neurobiol,* 53**,** 228-50.

SIMMONS, D. D. & LIBERMAN, M. C. 1988. Afferent innervation of outer hair cells in adult cats: I. Light microscopic analysis of fibers labeled with horseradish peroxidase. *J Comp Neurol,* 270**,** 132-44.

SIMMONS, D. D., MANSDORF, N. B. & KIM, J. H. 1996. Olivocochlear innervation of inner and outer hair cells during postnatal maturation: Evidence for a waiting period. *J comp neurol.* United States.

SIMMONS, D. D., TONG, B., SCHRADER, A. D. & HORNAK, A. J. 2010. Oncomodulin identifies different hair cell types in the mammalian inner ear. *J Comp Neurol,* 518**,** 3785-802.

SIMON, E., PERROT, X. & MERTENS, P. 2009. [functional anatomy of the cochlear nerve and the central auditory system]. *Neurochirurgie,* 55**,** 120-6.

SKARNES, W. C., ROSEN, B., WEST, A. P., KOUTSOURAKIS, M., BUSHELL, W., IYER, V., MUJICA, A. O., THOMAS, M., HARROW, J., COX, T., JACKSON, D., SEVERIN, J., BIGGS, P., FU, J., NEFEDOV, M., DE JONG, P. J., STEWART, A. F. & BRADLEY, A. 2011. A conditional knockout resource for the genome-wide study of mouse gene function. *Nature,* 474**,** 337-42.

SLEPECKY, N. 1996. Structure of the mammalian cochlea. *In:* DALLOS, P., POPPER, A. & FAY, R. (eds.) *The cochlea.* New York: Springer.

SMITH, C. A., LOWRY, O. H. & WU, M. L. 1954. The electrolytes of the labyrinthine fluids. *Laryngoscope,* 64**,** 141-53.

SMITH, R. J., BERLIN, C. I., HEJTMANCIK, J. F., KEATS, B. J., KIMBERLING, W. J., LEWIS, R. A., MOLLER, C. G., PELIAS, M. Z. & TRANEBJAERG, L. 1994. Clinical diagnosis of the usher syndromes. Usher syndrome consortium. *Am J Med Genet,* 50**,** 32-8.

SOBIN, A. & ANNIKO, M. 1984. Early development of cochlear hair cell stereociliary surface morphology. *Arch Otorhinolaryngol,* 241**,** 55-64.

SOBKOWICZ, H. M. 1992. The development of innervation in the organ of corti. *In:* ROMAND, R. (ed.) *Development of auditory and vestibular systems 2.* Amsterdam: Elsevier.

SOBKOWICZ, H. M., AUGUST, B. K. & SLAPNICK, S. M. 2002. Influence of neurotrophins on the synaptogenesis of inner hair cells in the deaf bronx waltzer (bv) mouse organ of corti in culture. *Int J Dev Neurosci,* 20**,** 537-54.

SON, E. J., WU, L., YOON, H., KIM, S., CHOI, J. Y. & BOK, J. 2012. Developmental gene expression profiling along the tonotopic axis of the mouse cochlea. *PLoS One,* 7**,** e40735.

SONG, L. & SANTOS-SACCHI, J. 2010. Conformational state-dependent anion binding in prestin: Evidence for allosteric modulation. *Biophys J,* 98**,** 371-6.

SOUTER, M., NEVILL, G. & FORGE, A. 1995. Postnatal development of membrane specialisations of gerbil outer hair cells. *Hear Res,* 91**,** 43-62.

SPICER, S. S. & SCHULTE, B. A. 1998. Evidence for a medial k+ recycling pathway from inner hair cells. *Hear Res,* 118**,** 1-12.

SPIDEN, S. L., BORTOLOZZI, M., DI LEVA, F., DE ANGELIS, M. H., FUCHS, H., LIM, D., ORTOLANO, S., INGHAM, N. J., BRINI, M., CARAFOLI, E., MAMMANO, F. & STEEL, K. P. 2008. The novel mouse mutation oblivion inactivates the pmca2 pump and causes progressive hearing loss. *PLoS Genet,* 4**,** e1000238.

SPOENDLIN, H. 1969. Innervation patterns in the organ of corti of the cat. *Acta Otolaryngol,* 67**,** 239-54.

SPOENDLIN, H. 1972. Innervation densities of the cochlea. *Acta Otolaryngol,* 73**,** 235-48.

SRIDHARAN, R. & SMALE, S. T. 2007. Predominant interaction of both ikaros and helios with the nurd complex in immature thymocytes. *J biol chem.* United States.

STAECKER, H., VAN DE WATER, T. R., LEFEBVRE, P. P., LIU, W., MOGHADASSI, M., GALINOVIC-SCHWARTZ, V., MALGRANGE, B. & MOONEN, G. 1996. Ngf, bdnf and nt-3 play unique roles in the in vitro development and patterning of innervation of the mammalian inner ear. *Brain Res Dev Brain Res,* 92**,** 49-60.

STAMATAKI, S., FRANCIS, H. W., LEHAR, M., MAY, B. J. & RYUGO, D. K. 2006. Synaptic alterations at inner hair cells precede spiral ganglion cell loss in aging c57bl/6j mice. *Hear Res,* 221**,** 104-18.

STEINMAN, R. M. & COHN, Z. A. 2007. Pillars article: Identification of a novel cell type in peripheral lymphoid organs of mice. I. Morphology, quantitation, tissue distribution. J. Exp. Med.1973. 137: 1142-1162. *J immunol.* United States.

STENFELT, S. 2006. Middle ear ossicles motion at hearing thresholds with air conduction and bone conduction stimulation. *J Acoust Soc Am,* 119**,** 2848-58.

STENFELT, S. & GOODE, R. L. 2005. Bone-conducted sound: Physiological and clinical aspects. *Otol Neurotol,* 26**,** 1245-61.

SUBHA, S. T. & RAMAN, R. 2006. Role of impacted cerumen in hearing loss. *Ear Nose Throat J,* 85**,** 650, 652-3.

SUGIMOTO, N., OIDA, T., HIROTA, K., NAKAMURA, K., NOMURA, T., UCHIYAMA, T. & SAKAGUCHI, S. 2006. Foxp3-dependent and -independent molecules specific for cd25+cd4+ natural regulatory t cells revealed by DNA microarray analysis. *Int immunol.* England.

SUGITA, K., HANAKAWA, S., HONDA, T., KONDOH, G., MIYACHI, Y., KABASHIMA, K. & NOMURA, T. 2015. Generation of helios reporter mice and an evaluation of the suppressive capacity of helios regulatory t cells in vitro. *Exp Dermatol*.

SUN, L., HEEREMA, N., CROTTY, L., WU, X., NAVARA, C., VASSILEV, A., SENSEL, M., REAMAN, G. H. & UCKUN, F. M. 1999. Expression of dominant-negative and mutant isoforms of the antileukemic transcription factor ikaros in infant acute lymphoblastic leukemia. *Proc Natl Acad Sci U S A,* 96**,** 680-5.

SUN, L., LIU, A. & GEORGOPOULOS, K. 1996. Zinc finger-mediated protein interactions modulate ikaros activity, a molecular control of lymphocyte development. *EMBO J,* 15**,** 5358-69.

SZARAMA, K. B., GAVARA, N., PETRALIA, R. S., KELLEY, M. W. & CHADWICK, R. S. 2012. Cytoskeletal changes in actin and microtubules underlie the developing surface mechanical properties of sensory and supporting cells in the mouse cochlea. *Development,* 139**,** 2187-97.

SZIKLAI, I., SZONYI, M. & DALLOS, P. 2001. Phosphorylation mediates the influence of acetylcholine upon outer hair cell electromotility. *Acta Otolaryngol,* 121**,** 153-6.

TABAYASHI, T., ISHIMARU, F., TAKATA, M., KATAOKA, I., NAKASE, K., KOZUKA, T. & TANIMOTO, M. 2007. Characterization of the short isoform of helios overexpressed in patients with t-cell malignancies. *Cancer Sci,* 98**,** 182-8.

TADA, T., TAKEMORI, T., OKUMURA, K., NONAKA, M. & TOKUHISA, T. 1978. Two distinct types of helper t cells involved in the secondary antibody response: Independent and synergistic effects of ia- and ia+ helper t cells. *J Exp Med,* 147**,** 446-58.

TAKATORI, H., KAWASHIMA, H., MATSUKI, A., MEGURO, K., TANAKA, S., IWAMOTO, T., SANAYAMA, Y., NISHIKAWA, N., TAMACHI, T., IKEDA, K., SUTO, A., SUZUKI, K.,

KAGAMI, S., HIROSE, K., KUBO, M., HORI, S. & NAKAJIMA, H. 2015. Helios enhances treg cell function in cooperation with foxp3. *Arthritis Rheumatol,* 67**,** 1491-502.

TAKUMI, Y., NAGELHUS, E. A., EIDET, J., MATSUBARA, A., USAMI, S., SHINKAWA, H., NIELSEN, S. & OTTERSEN, O. P. 1998. Select types of supporting cell in the inner ear express aquaporin-4 water channel protein. *Eur J Neurosci,* 10**,** 3584-95.

TARAZONA, S., GARCIA-ALCALDE, F., DOPAZO, J., FERRER, A. & CONESA, A. 2011. Differential expression in rna-seq: A matter of depth. *Genome Res,* 21**,** 2213-23.

TAYLOR, R. R., JAGGER, D. J. & FORGE, A. 2012. Defining the cellular environment in the organ of corti following extensive hair cell loss: A basis for future sensory cell replacement in the cochlea. *PLoS One,* 7**,** e30577.

THORNTON, A. M., KORTY, P. E., TRAN, D. Q., WOHLFERT, E. A., MURRAY, P. E., BELKAID, Y. & SHEVACH, E. M. 2010. Expression of helios, an ikaros transcription factor family member, differentiates thymic-derived from peripherally induced foxp3+ t regulatory cells. *J immunol.* United States.

TILNEY, L. G., DEROSIER, D. J. & MULROY, M. J. 1980. The organization of actin filaments in the stereocilia of cochlear hair cells. *J Cell Biol,* 86**,** 244-59.

TILNEY, L. G., TILNEY, M. S. & DEROSIER, D. J. 1992. Actin filaments, stereocilia, and hair cells: How cells count and measure. *Annu Rev Cell Biol,* 8**,** 257-74.

TOLOMEO, J. A. & HOLLEY, M. C. 1997. Mechanics of microtubule bundles in pillar cells from the inner ear. *Biophys J,* 73**,** 2241-7.

TOMLINSON, S. E., RAJAKULENDRAN, S., TAN, S. V., GRAVES, T. D., BAMIOU, D. E., LABRUM, R. W., BURKE, D., SUE, C. M., GIUNTI, P., SCHORGE, S., KULLMANN, D. M. & HANNA, M. G. 2013. Clinical, genetic, neurophysiological and functional study of new mutations in episodic ataxia type 1. *J Neurol Neurosurg Psychiatry,* 84**,** 1107-12.

TORTORA, G. J. & GRABOWSKI, S. R. 1993. *Principles of anatomy and physiology,* 7th ed. New York: HarperCollins.

TRINH, L. A., FERRINI, R., COBB, B. S., WEINMANN, A. S., HAHM, K., ERNST, P., GARRAWAY, I. P., MERKENSCHLAGER, M. & SMALE, S. T. 2001. Down-regulation of tdt transcription in cd4(+)cd8(+) thymocytes by ikaros proteins in direct competition with an ets activator. *Genes Dev,* 15**,** 1817-32.

TSAKIROPOULOU, E., KONSTANTINIDIS, I., VITAL, I., KONSTANTINIDOU, S. & KOTSANI, A. 2007. Hearing aids: Quality of life and socio-economic aspects. *Hippokratia,* 11**,** 183-6.

TYSON, J., TRANEBJAERG, L., BELLMAN, S., WREN, C., TAYLOR, J. F., BATHEN, J., ASLAKSEN, B., SORLAND, S. J., LUND, O., MALCOLM, S., PEMBREY, M., BHATTACHARYA, S. & BITNER-GLINDZICZ, M. 1997. Isk and kvlqt1: Mutation in either of the two subunits of the slow component of the delayed rectifier potassium channel can cause jervell and lange-nielsen syndrome. *Hum Mol Genet,* 6**,** 2179-85.

UCHIKAWA, M., KAMACHI, Y. & KONDOH, H. 1999. Two distinct subgroups of group b sox genes for transcriptional activators and repressors: Their expression during embryonic organogenesis of the chicken. *Mech Dev,* 84**,** 103-20.

UHLMANN, R. F., LARSON, E. B., REES, T. S., KOEPSELL, T. D. & DUCKERT, L. G. 1989. Relationship of hearing impairment to dementia and cognitive dysfunction in older adults. *Jama,* 261**,** 1916-9.

URBAN, J. A. & WINANDY, S. 2004. Ikaros null mice display defects in t cell selection and cd4 versus cd8 lineage decisions. *J immunol.* United States.

VARGHESE, G. I., ZHU, X. & FRISINA, R. D. 2005. Age-related declines in distortion product otoacoustic emissions utilizing pure tone contralateral stimulation in cba/caj mice. *Hear Res,* 209**,** 60-7.

VATER, M., MENG, J. & FOX, R. 2004. Hearing organ evolution and specialization: Early and later mammals. *In:* MANLEY, G., POPPER, A. & FAY, R. (eds.) *Evolution of the vertebrate auditory system.* New York: Springer-Verlag.

VERHAGEN, J. & WRAITH, D. C. 2010. Comment on "expression of helios, an ikaros transcription factor family member, differentiates thymic-derived from peripherally induced foxp3+ t regulatory cells". *J immunol.* United States.

VERPY, E., LEIBOVICI, M., MICHALSKI, N., GOODYEAR, R. J., HOUDON, C., WEIL, D., RICHARDSON, G. P. & PETIT, C. 2011. Stereocilin connects outer hair cell stereocilia to one another and to the tectorial membrane. *J Comp Neurol,* 519**,** 194-210.

VERPY, E., MASMOUDI, S., ZWAENEPOEL, I., LEIBOVICI, M., HUTCHIN, T. P., DEL CASTILLO, I., NOUAILLE, S., BLANCHARD, S., LAINE, S., POPOT, J. L., MORENO, F., MUELLER, R. F. & PETIT, C. 2001. Mutations in a new gene encoding a protein of the hair bundle cause non-syndromic deafness at the dfnb16 locus. *Nat Genet,* 29**,** 345-9.

VERPY, E., WEIL, D., LEIBOVICI, M., GOODYEAR, R. J., HAMARD, G., HOUDON, C., LEFEVRE, G. M., HARDELIN, J. P., RICHARDSON, G. P., AVAN, P. & PETIT, C. 2008. Stereocilin-deficient mice reveal the origin of cochlear waveform distortions. *Nature,* 456**,** 255-8.

VETTER, D. E., MANN, J. R., WANGEMANN, P., LIU, J., MCLAUGHLIN, K. J., LESAGE, F., MARCUS, D. C., LAZDUNSKI, M., HEINEMANN, S. F. & BARHANIN, J. 1996. Inner ear defects induced by null mutation of the isk gene. *Neuron,* 17**,** 1251-64.

VOLKMAN, A. & GOWANS, J. L. 1965. The production of macrophages in the rat. *Br J Exp Pathol,* 46**,** 50-61.

VON BÉKÉSY, G. 1952. Dc resting potentials inside the cochlear partition. *J Acoust Soc Am,* 24**,** 72-76.

VON BÉKÉSY, G. 1954. Some electro-mechanical properties of the organ of corti. *Ann Otol Rhinol Laryngol,* 63**,** 448-68.

VON BÉKÉSY, G. 1955. Contribution on the question of frequency analysis in the cochlea. *Arch Ohren Nasen Kehlkopfheilkd,* 167**,** 238-55.

VON BÉKÉSY, G. 1960. *Experiments in hearing,* New York: McGraw-Hill.

VON HEHN, C. A., BHATTACHARJEE, A. & KACZMAREK, L. K. 2004. Loss of kv3.1 tonotopicity and alterations in camp response element-binding protein signaling in central auditory neurons of hearing impaired mice. *J Neurosci,* 24**,** 1936-40.

VREUGDE, S., EREVEN, A., KROS, C. J., MARCOTTI, W., FUCHS, H., KURIMA, K., WILCOX, E. R., FRIEDMAN, T. B., GRIFFITH, A. J., BALLING, R., DE ANGELIS, M. H., AVRAHAM, K. B. & STEEL, K. P. 2002. Beethoven, a mouse model for dominant, progressive hearing loss dfna36. *Nature Genetics,* 30**,** 257-258.

WAGUESPACK, J., SALLES, F. T., KACHAR, B. & RICCI, A. J. 2007. Stepwise morphological and functional maturation of mechanotransduction in rat outer hair cells. *J Neurosci,* 27**,** 13890-902.

WALLIS, D., HAMBLEN, M., ZHOU, Y., VENKEN, K. J., SCHUMACHER, A., GRIMES, H. L., ZOGHBI, H. Y., ORKIN, S. H. & BELLEN, H. J. 2003. The zinc finger transcription factor gfi1, implicated in lymphomagenesis, is required for inner ear hair cell differentiation and survival. *Development,* 130**,** 221-32.

WALTERS, B. J., LIU, Z., CRABTREE, M., COAK, E., COX, B. C. & ZUO, J. 2014. Auditory hair cell-specific deletion of p27kip1 in postnatal mice promotes cell-autonomous generation of new hair cells and normal hearing. *J Neurosci,* 34**,** 15751-63.

WALTERS, B. J. & ZUO, J. 2013. Postnatal development, maturation and aging in the mouse cochlea and their effects on hair cell regeneration. *Hear Res,* 297**,** 68-83.

WANG, A., LIANG, Y., FRIDELL, R. A., PROBST, F. J., WILCOX, E. R., TOUCHMAN, J. W., MORTON, C. C., MORELL, R. J., NOBEN-TRAUTH, K., CAMPER, S. A. & FRIEDMAN, T. B. 1998a. Association of unconventional myosin myo15 mutations with human nonsyndromic deafness dfnb3. *Science,* 280**,** 1447-51.

WANG, C., GONG, B., BUSHEL, P. R., THIERRY-MIEG, J., THIERRY-MIEG, D., XU, J., FANG, H., HONG, H., SHEN, J., SU, Z., MEEHAN, J., LI, X., YANG, L., LI, H., LABAJ, P. P., KREIL, D. P., MEGHERBI, D., GAJ, S., CAIMENT, F., VAN DELFT, J., KLEINJANS, J., SCHERER, A., DEVANARAYAN, V., WANG, J., YANG, Y., QIAN, H. R., LANCASHIRE, L. J., BESSARABOVA, M., NIKOLSKY, Y., FURLANELLO, C., CHIERICI, M., ALBANESE, D., JURMAN, G., RICCADONNA, S., FILOSI, M., VISINTAINER, R., ZHANG, K. K., LI, J., HSIEH, J. H., SVOBODA, D. L., FUSCOE, J. C., DENG, Y., SHI, L., PAULES, R. S., AUERBACH, S. S. & TONG, W. 2014. The concordance between rna-seq and microarray data depends on chemical treatment and transcript abundance. *Nat Biotechnol,* 32**,** 926-32.

WANG, J. H., AVITAHL, N., CARIAPPA, A., FRIEDRICH, C., IKEDA, T., RENOLD, A., ANDRIKOPOULOS, K., LIANG, L., PILLAI, S., MORGAN, B. A. & GEORGOPOULOS, K. 1998b. Aiolos regulates b cell activation and maturation to effector state. *Immunity.* United States.

WANG, J. H., NICHOGIANNOPOULOU, A., WU, L., SUN, L., SHARPE, A. H., BIGBY, M. & GEORGOPOULOS, K. 1996. Selective defects in the development of the fetal and adult lymphoid system in mice with an ikaros null mutation. *Immunity.* United States.

WANG, W., KIM, H. J., LV, P., TEMPEL, B. & YAMOAH, E. N. 2013. Association of the kv1 family of k+ channels and their functional blueprint in the properties of auditory neurons as revealed by genetic and functional analyses. *J Neurophysiol,* 110**,** 1751-64.

WANGEMANN, P. 2002. K+ cycling and the endocochlear potential. *Hear Res,* 165**,** 1-9.

WARNER, S. J., HUTSON, M. R., OH, S. H., GERLACH-BANK, L. M., LOMAX, M. I. & BARALD, K. F. 2003. Expression of zic genes in the development of the chick inner ear and nervous system. *Dev Dyn,* 226**,** 702-12.

WEBER, T., CORBETT, M. K., CHOW, L. M., VALENTINE, M. B., BAKER, S. J. & ZUO, J. 2008. Rapid cell-cycle reentry and cell death after acute inactivation of the retinoblastoma gene product in postnatal cochlear hair cells. *Proc Natl Acad Sci U S A,* 105**,** 781-5.

WEIL, D., BLANCHARD, S., KAPLAN, J., GUILFORD, P., GIBSON, F., WALSH, J., MBURU, P., VARELA, A., LEVILLIERS, J., WESTON, M. D. & ET AL. 1995. Defective myosin viia gene responsible for usher syndrome type 1b. *Nature,* 374**,** 60-1.

WEIL, D., EL-AMRAOUI, A., MASMOUDI, S., MUSTAPHA, M., KIKKAWA, Y., LAINE, S., DELMAGHANI, S., ADATO, A., NADIFI, S., ZINA, Z. B., HAMEL, C., GAL, A., AYADI, H., YONEKAWA, H. & PETIT, C. 2003. Usher syndrome type i g (ush1g) is caused by mutations in the gene encoding sans, a protein that associates with the ush1c protein, harmonin. *Hum Mol Genet,* 12**,** 463-71.

WEIL, D., KUSSEL, P., BLANCHARD, S., LEVY, G., LEVI-ACOBAS, F., DRIRA, M., AYADI, H. & PETIT, C. 1997. The autosomal recessive isolated deafness, dfnb2, and the usher 1b syndrome are. *Nat Genet,* 16**,** 191-3.

WHITE, P. M., DOETZLHOFER, A., LEE, Y. S., GROVES, A. K. & SEGIL, N. 2006. Mammalian cochlear supporting cells can divide and trans-differentiate into hair cells. *Nature,* 441**,** 984-7.

WHO. 2015. *Deafness and hearing loss* [Online]. Available: http://www.who.int/mediacentre/factsheets/fs300/en/ [Accessed 24/09/2015].

WILSON, J. L., HENSON, M. M. & HENSON, O. W., JR. 1991. Course and distribution of efferent fibers in the cochlea of the mouse. *Hear res.* Netherlands.

WINANDY, S., WU, P. & GEORGOPOULOS, K. 1995. A dominant mutation in the ikaros gene leads to rapid development of leukemia and lymphoma. *Cell,* 83**,** 289-99.

WOODS, C., MONTCOUQUIOL, M. & KELLEY, M. W. 2004. Math1 regulates development of the sensory epithelium in the mammalian cochlea. *Nat Neurosci,* 7**,** 1310-8.

WU, X., GAO, J., GUO, Y. & ZUO, J. 2004. Hearing threshold elevation precedes hair-cell loss in prestin knockout mice. *Brain res mol brain res.* Netherlands.

XIA, A. P., IKEDA, K., KATORI, Y., OSHIMA, T., KIKUCHI, T. & TAKASAKA, T. 2000. Expression of connexin 31 in the developing mouse cochlea. *Neuroreport,* 11**,** 2449-53.

XIANG, M., GAO, W. Q., HASSON, T. & SHIN, J. J. 1998. Requirement for brn-3c in maturation and survival, but not in fate determination of inner ear hair cells. *Development,* 125**,** 3935-46.

XU, Y. Z., KANAGARATHAM, C., JANCIK, S. & RADZIOCH, D. 2013. Promoter deletion analysis using a dual-luciferase reporter system. *Methods Mol Biol,* 977**,** 79-93.

YANG, D., THALMANN, I., THALMANN, R. & SIMMONS, D. D. 2004. Expression of alpha and beta parvalbumin is differentially regulated in the rat organ of corti during development. *J Neurobiol,* 58**,** 479-92.

YIN, H., XUE, W., CHEN, S., BOGORAD, R. L., BENEDETTI, E., GROMPE, M., KOTELIANSKY, V., SHARP, P. A., JACKS, T. & ANDERSON, D. G. 2014. Genome editing with cas9 in adult mice corrects a disease mutation and phenotype. *Nat Biotechnol,* 32**,** 551-3.

YOSHIDA, T. & GEORGOPOULOS, K. 2014. Ikaros fingers on lymphocyte differentiation. *Int J Hematol*.

YOSHIDA, T., LANDHUIS, E., DOSE, M., HAZAN, I., ZHANG, J., NAITO, T., JACKSON, A. F., WU, J., PEROTTI, E. A., KAUFMANN, C., GOUNARI, F., MORGAN, B. A. & GEORGOPOULOS, K. 2013. Transcriptional regulation of the ikzf1 locus. *Blood,* 122**,** 3149-59.

YU, H. C., ZHAO, H. L., WU, Z. K. & ZHANG, J. W. 2011. Eos negatively regulates human gamma-globin gene transcription during erythroid differentiation. *PLoS One,* 6**,** e22907.

ZABRANSKY, D. J., NIRSCHL, C. J., DURHAM, N. M., PARK, B. V., CECCATO, C. M., BRUNO, T. C., TAM, A. J., GETNET, D. & DRAKE, C. G. 2012. Phenotypic and functional properties of helios+ regulatory t cells. *PLoS One,* 7**,** e34547.

ZAMPINI, V., RUTTIGER, L., JOHNSON, S. L., FRANZ, C., FURNESS, D. N., WALDHAUS, J., XIONG, H., HACKNEY, C. M., HOLLEY, M. C., OFFENHAUSER, N., DI FIORE, P. P., KNIPPER, M., MASETTO, S. & MARCOTTI, W. 2011. Eps8 regulates hair bundle length and functional maturation of mammalian auditory hair cells. *PLoS Biol,* 9**,** e1001048.

ZHANG, L. I. & POO, M. M. 2001. Electrical activity and development of neural circuits. *Nat Neurosci,* 4 Suppl**,** 1207-14.

ZHANG, M., DING, D. & SALVI, R. 2002. Expression of heregulin and erbb/her receptors in adult chinchilla cochlear and vestibular sensory epithelium. *Hear Res,* 169**,** 56-68.

ZHANG, Z., SWINDLE, C. S., BATES, J. T., KO, R., COTTA, C. V. & KLUG, C. A. 2007. Expression of a non-DNA-binding isoform of helios induces t-cell lymphoma in mice. *Blood.* United States.

ZHENG, J., SHEN, W., HE, D. Z., LONG, K. B., MADISON, L. D. & DALLOS, P. 2000a. Prestin is the motor protein of cochlear outer hair cells. *Nature,* 405**,** 149-55.

ZHENG, J. L. & GAO, W. Q. 2000. Overexpression of math1 induces robust production of extra hair cells in postnatal rat inner ears. *Nat Neurosci,* 3**,** 580-6.

ZHENG, J. L., SHOU, J., GUILLEMOT, F., KAGEYAMA, R. & GAO, W. Q. 2000b. Hes1 is a negative regulator of inner ear hair cell differentiation. *Development,* 127**,** 4551-60.

ZHENG, L., SEKERKOVA, G., VRANICH, K., TILNEY, L. G., MUGNAINI, E. & BARTLES, J. R. 2000c. The deaf jerker mouse has a mutation in the gene encoding the espin actin-bundling proteins of hair cell stereocilia and lacks espins. *Cell.* United States.

ZHENG, L., SEKERKOVA, G., VRANICH, K., TILNEY, L. G., MUGNAINI, E. & BARTLES, J. R. 2000d. The deaf jerker mouse has a mutation in the gene encoding the espin actin-bundling proteins of hair cell stereocilia and lacks espins. *Cell,* 102**,** 377-85.

ZHOU, X., JEN, P. H., SEBURN, K. L., FRANKEL, W. N. & ZHENG, Q. Y. 2006. Auditory brainstem responses in 10 inbred strains of mice. *Brain res.* Netherlands.

ZHU, Y. & ZHAO, H. B. 2010. Atp-mediated potassium recycling in the cochlear supporting cells. *Purinergic Signal,* 6**,** 221-9.

ZIEGLER, E. A., BRIEGER, J., HEINRICH, U. R. & MANN, W. J. 2004. Immunohistochemical localization of cyclooxygenase isoforms in the organ of corti and the spiral ganglion cells of guinea pig cochlea. *ORL J Otorhinolaryngol Relat Spec,* 66**,** 297-301.

ZINE, A., AUBERT, A., QIU, J., THERIANOS, S., GUILLEMOT, F., KAGEYAMA, R. & DE RIBAUPIERRE, F. 2001. Hes1 and hes5 activities are required for the normal development of the hair cells in the mammalian inner ear. *J Neurosci,* 21**,** 4712-20.

Chapter 9 : Appendix

Table 9.1: Raw auditory phenotyping data from the *MPC-173* MRC Harwell ENU Ageing Screen G3 cohort.

Mouse ID	3 Month Clickbox	6 Month Clickbox	9 Month Clickbox	9 Month ABR				12 Month Clickbox
				8 kHz	16 kHz	32 kHz	Click	
MPC-173/2.2b	2	2	2	40	35	45	20	2
MPC-173/2.2l	2	2	2	40	30	50	20	2
MPC-173/2.2a	2	2	2	40	30	35	20	2
MPC-173/2.3a	2	2	2	30	30	50	20	2
MPC-173/2.3b	2	2	2	-	-	-	-	2
MPC-173/2.1a	2	0	0	85	85	90	85	0
MPC-173/2.1b	0	0	0	80	80	100	100	0
MPC-173/2.1c	0	0	0	80	100	80	100	0
MPC-173/2.1d	0	0	0	100	90	85	100	0
MPC-173/2.1e	2	0	0	85	85	80	100	0
MPC-173/2.1i	2	2	2	35	25	45	20	2
~~*MPC-173/2.1j*~~	2	2	-	-	-	-	-	-
MPC-173/2.1k	2	2	2	25	30	25	15	2
MPC-173/2.2d	2	2	2	30	25	25	20	2
MPC-173/2.2j	2	0	0	75	90	90	100	0
MPC-173/2.2k	2	2	2	40	35	40	20	2
MPC-173/2.1f	2	2	2	45	35	50	25	2
MPC-173/2.1g	0	0	0	85	85	85	100	0
MPC-173/2.1h	0	0	0	100	80	100	100	0
MPC-173/2.2e	0	0	0	100	100	90	100	0
MPC-173/2.2f	2	2	2	25	25	30	15	2
~~*MPC-173/2.2g*~~	2	-	-	-	-	-	-	-
MPC-173/2.2h	2	2	2	25	20	25	20	2
MPC-173/2.2i	0	0	0	85	100	100	100	0
MPC-173/2.7a	2	0	0	85	100	100	100	0
~~*MPC-173/2.7b*~~	2	0	-	-	-	-	-	-
MPC-173/2.7c	2	2	2	-	-	-	-	2
MPC-173/2.7d	2	2	2	-	-	-	-	2
MPC-173/2.7e	2	2	2	-	-	-	-	2
MPC-173/2.7f	2	2	2	-	-	-	-	2
MPC-173/2.7g	2	2	2	-	-	-	-	2
MPC-173/2.7h	2	2	2	-	-	-	-	2
MPC-173/2.7i	2	2	2	-	-	-	-	2
MPC-173/2.7j	2	2	2	-	-	-	-	2
MPC-173/2.8f	2	2	2	-	-	-	-	2
MPC-173/2.7k	2	2	2	-	-	-	-	2
MPC-173/2.7l	2	2	2	-	-	-	-	2
MPC-173/2.7m	0	0	0	85	90	100	100	0
MPC-173/2.7n	0	0	0	90	100	100	100	0
MPC-173/2.7o	0	0	0	85	85	85	100	0

Mouse ID	3 Month Clickbox	6 Month Clickbox	9 Month Clickbox	9 Month ABR				12 Month Clickbox
				8 kHz	16 kHz	32 kHz	Click	
~~*MPC-173/2.7p*~~	2	2	-	-	-	-	-	-
MPC-173/2.7q	2	2	2	35	30	45	25	2
MPC-173/2.8g	2	2	2	-	-	-	-	2
MPC-173/2.8h	2	2	2	-	-	-	-	2
MPC-173/2.8i	2	2	2	-	-	-	-	2
MPC-173/2.7r	2	2	2	-	-	-	-	2
MPC-173/2.7s	2	1	2	35	30	40	20	2
MPC-173/2.8a	2	2	2	-	-	-	-	2
MPC-173/2.8b	2	2	2	-	-	-	-	2
MPC-173/2.8c	2	0	0	100	75	100	100	0
MPC-173/2.8d	2	2	2	-	-	-	-	2
MPC-173/2.8e	2	2	2	-	-	-	-	2
MPC-173/2.9a	2	0	0	100	90	90	100	0
MPC-173/2.9b	2	1	2	40	30	40	20	2
MPC-173/2.9c	2	2	2	25	25	30	20	2
MPC-173/2.9d	2	2	2	-	-	-	-	2
~~*MPC-173/2.9e*~~	2	0	0	90	90	85	100	-
MPC-173/2.9f	2	2	2	-	-	-	-	2
MPC-173/2.9g	2	2	2	-	-	-	-	2
MPC-173/2.9h	2	2	2	-	-	-	-	2
Total number of affected:	**= 10 / 60 (16.7%)**	**= 18 / 59 (30.5%)**	**= 17 / 56 (30.4%)**	**= 17 / 32 (53.1%)**				**= 16 / 55 (29.1%)**

Affected animals and their corresponding auditory phenotyping data are highlighted in purple. Due to time constraints, ABR analysis was only undertaken for 32 mice of the G3 cohort. Mice which were culled partway through the screen, either due to health concerns or fighting wounds, are marked with a striked line through their ID. ABR, auditory-evoked brainstem response; kHz, kiloHertz; *MPC-173, MUTA-PED-C3PDE-173.*

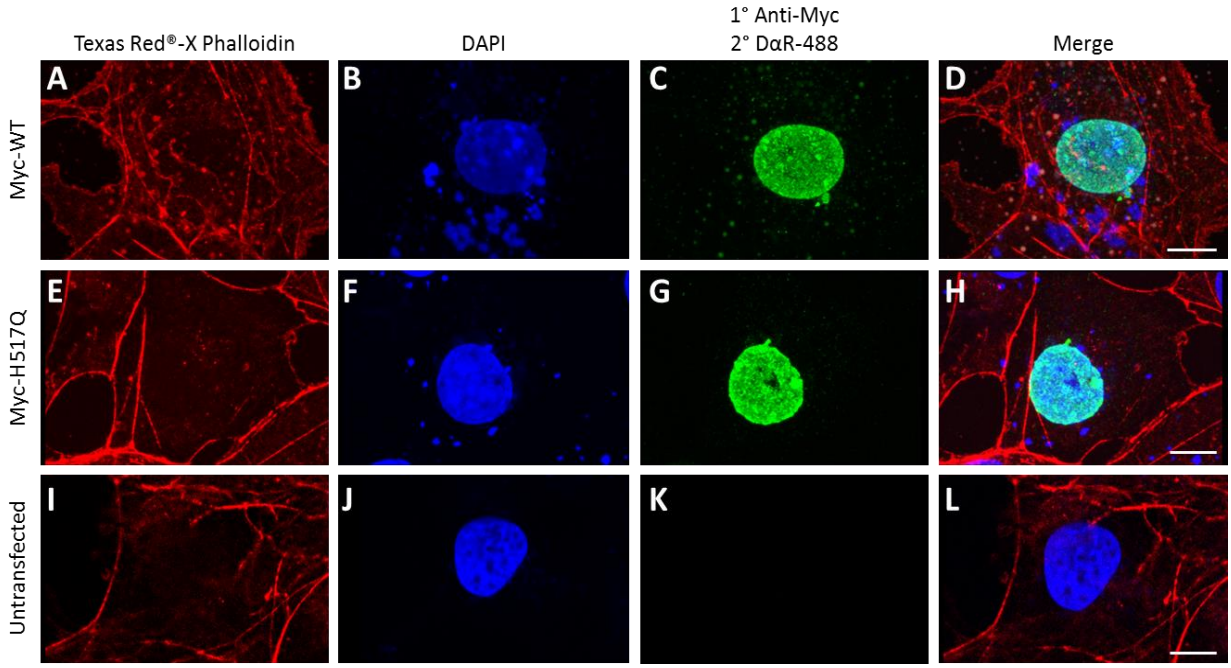

Figure 9.1: *In vitro* subcellular localisation of c-Myc-tagged wild-type and H517Q helios.
Cos-7 cells were transfected with Myc-WT or Myc-H517Q helios then visualised by immunofluorescence. **(A-D)** Myc-WT helios (green) co-localises with DAPI (blue), a nuclear marker, confirming nuclear localisation. **(E-H)** Myc-H517Q helios shows a similar pattern of labelling, indicating that the *cello* mutation does not affect nuclear localisation. **(I-L)** No anti-Myc labelling is observed in the untransfected negative control (x63 magnification, scale bar = 10µm). DαR-488, donkey anti-rabbit Alexa Fluor® 488.

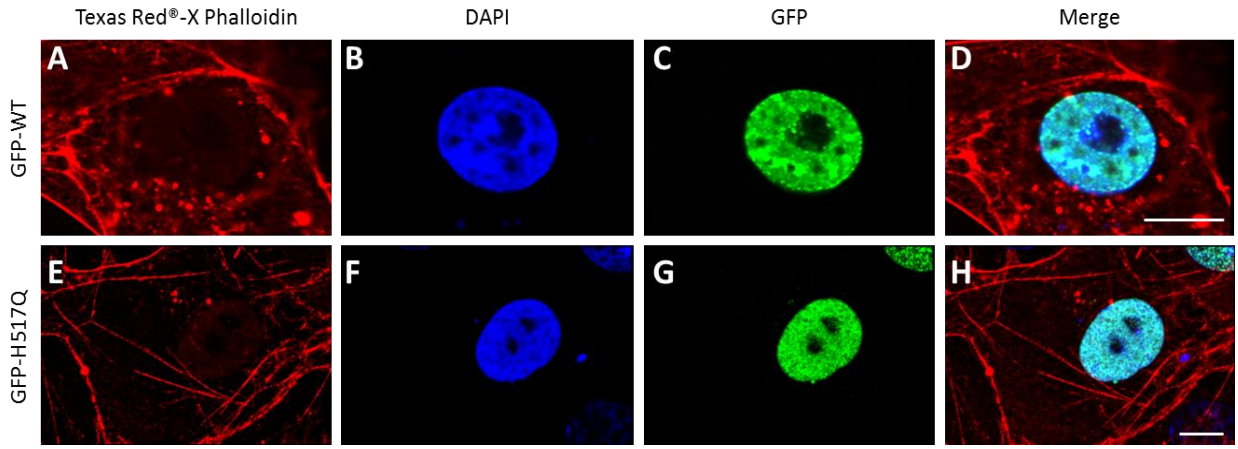

Figure 9.2: *In vitro* subcellular localisation of EGFP-tagged wild-type and H517Q helios.
Cos-7 cells were transfected with GFP-WT or GFP-H517Q helios then visualised by immunofluorescence. **(A-D)** GFP-WT helios (green) co-localises with DAPI (blue), a nuclear marker, confirming nuclear localisation. **(E-H)** GFP-H517Q helios shows a similar pattern of labelling, indicating that the *cello* mutation does not affect nuclear localisation (x63 magnification, scale bar = 10µm). GFP, green fluorescent protein.

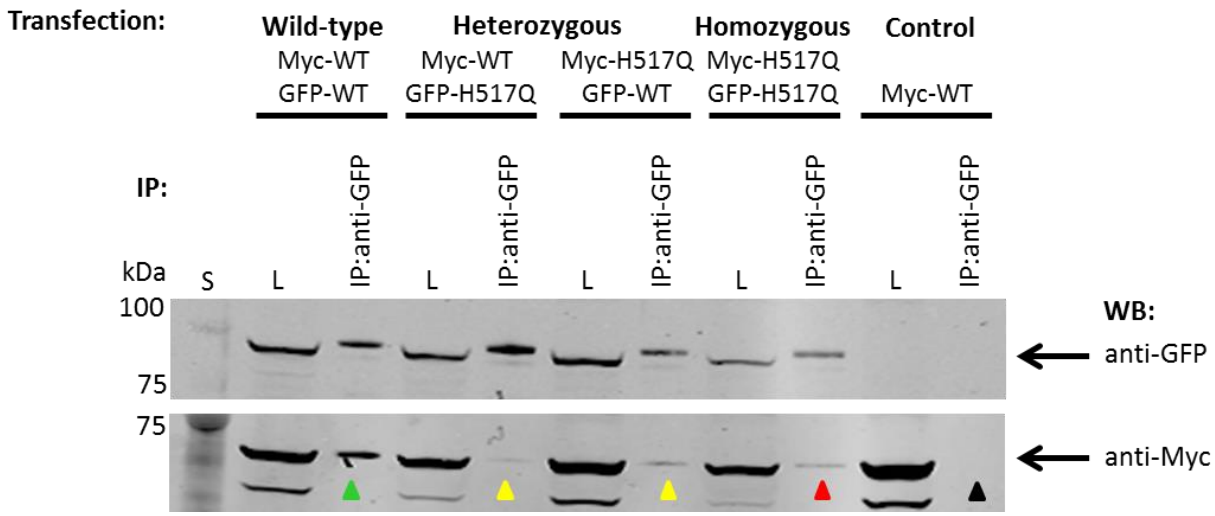

Figure 9.3: Co-immunoprecipitation of c-Myc-tagged and EGFP-tagged helios.
c-Myc-tagged and EGFP-tagged helios fusion proteins were transiently co-transfected into HEK293T cells to mimic a wild-type, heterozygous or homozygous state. IP was carried out with an anti-GFP antibody then IP reactions and their corresponding cell lysate were run on a western blot to investigate helios dimerisation. In each cell lysate, Myc-WT and Myc-H517Q (both ~62kDa) and GFP-WT and GFP-H517Q (both ~88kDa) were expressed at similar levels. In wild-type co-transfections, Myc-WT helios was pulled down with GFP-WT helios, as shown by the Myc co-IP band (green arrowhead), confirming homodimerisation. In the heterozygous co-transfections, GFP-WT helios can pull-down Myc-H517Q helios and GFP-H517Q helios can pull-down Myc-WT helios, but at a reduced efficiency, shown by the weaker co-IP bands (yellow arrowheads). A weak Myc Co-IP band was also observed in the homozygous co-transfections (red arrowhead), indicating that homodimerisation between GFP-H517Q helios and Myc-H517Q helios is severely impaired. In the single transfection negative control, no GFP IP or Myc co-IP band is observed (black arrowhead). GFP-H517Q, EGFP-tagged H517Q helios; GFP-WT, EGFP-tagged WT helios; IP, immunoprecipitation; kDa, kilodaltons; L, lysate; Myc-H517Q, c-Myc-tagged H517Q helios; Myc-WT, c-Myc-tagged wild-type helios; S, protein standard; WB, western blot.

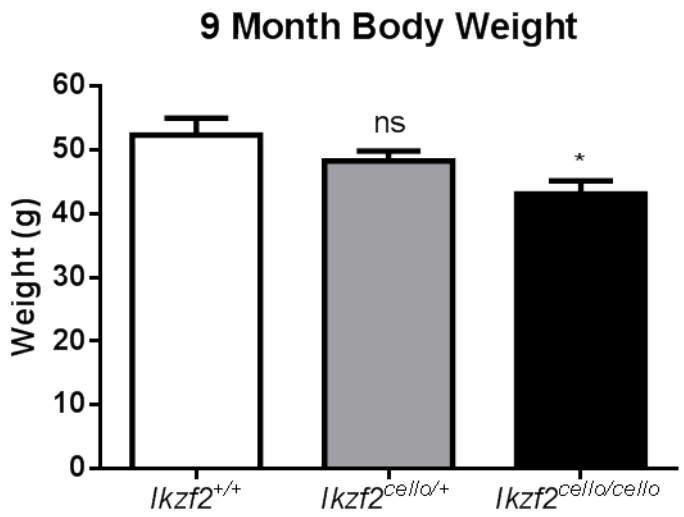

Figure 9.4: Body weight of *Ikzf2*$^{+/+}$, *Ikzf2*$^{cello/+}$ and *Ikzf2*$^{cello/cello}$ male mice at nine months of age.
Within the original *MPC-173* Ageing Screen G3 cohort, the body weight of *Ikzf2*$^{+/+}$ (n = 4), *Ikzf2*$^{cello/+}$ (n = 2) and *Ikzf2*$^{cello/cello}$ (n = 6) male mice was measured at nine months of age. *Ikzf2*$^{+/+}$ and *Ikzf2*$^{cello/+}$ animals were found to be similar in weight, whilst *Ikzf2*$^{cello/cello}$ mutants weighed significantly less than *Ikzf2*$^{+/+}$ controls. Data are shown as mean ± s.e.m. Statistical analysis: one-way ANOVA, * = $p \leq 0.05$. g, grams.

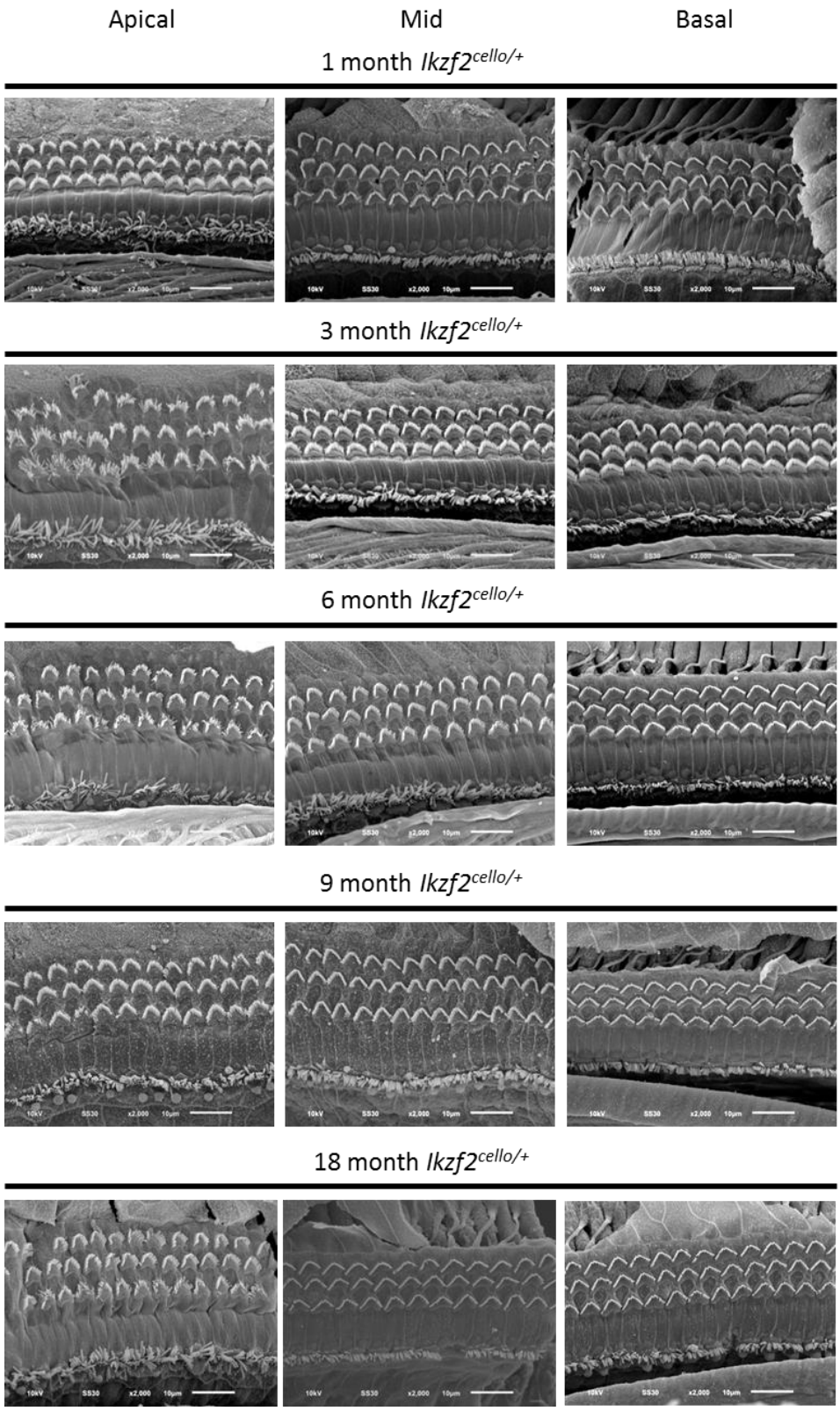

Figure 9.5: Scanning electron micrographs of the organ of Corti of *Ikzf2*$^{cello/+}$ mice at one, three, six, nine and 18 months of age.

Cochleae were collected from *Ikzf2*$^{cello/+}$ mice at one, three, six, nine and 18 months of age, then fine dissected to expose hair cells and processed for scanning electron microscopy. At all of the time points investigated, *Ikzf2*$^{cello/+}$ cochleae display the display the typical organisation of one row of IHCs and three rows of OHCs, with no hair cell dysmorphology or degeneration evident.

Table 9.2: Statistical analysis of outer hair cell counts for *Ikzf2*$^{+/+}$, *Ikzf2*$^{cello/+}$ and *Ikzf2*$^{cello/cello}$ mice at one, three, six, nine and 18 months of age.

	***Ikzf2*$^{+/+}$ OHC Counts at Apex**				***Ikzf2*$^{+/+}$ OHC Counts at Mid**				***Ikzf2*$^{+/+}$ OHC Counts at Base**			
	1 m	**3 m**	**6 m**	**9 m**	**1 m**	**3 m**	**6 m**	**9 m**	**1 m**	**3 m**	**6 m**	**9 m**
1 m	-	-	-	-	-	-	-	-	-	-	-	-
3 m	>0.05	-	-	-	>0.05	-	-	-	>0.05	-	-	-
6 m	>0.05	>0.05	-	-	>0.05	>0.05	-	-	>0.05	>0.05	-	-
9 m	>0.05	>0.05	>0.05	-	>0.05	>0.05	>0.05	-	0.0495	>0.05	>0.05	-
18 m	>0.05	>0.05	>0.05	>0.05	>0.05	>0.05	>0.05	>0.05	>0.05	>0.05	>0.05	0.0249

	***Ikzf2*$^{cello/+}$ OHC Counts at Apex**				***Ikzf2*$^{cello/+}$ OHC Counts at Mid**				***Ikzf2*$^{cello/+}$ OHC Counts at Base**			
	1 m	**3 m**	**6 m**	**9 m**	**1 m**	**3 m**	**6 m**	**9 m**	**1 m**	**3 m**	**6 m**	**9 m**
1 m	-	-	-	-	-	-	-	-	-	-	-	-
3 m	>0.05	-	-	-	0.0348	-	-	-	>0.05	-	-	-
6 m	>0.05	>0.05	-	-	>0.05	>0.05	-	-	>0.05	>0.05	-	-
9 m	>0.05	>0.05	>0.05	-	>0.05	>0.05	>0.05	-	>0.05	>0.05	>0.05	-
18 m	>0.05	>0.05	>0.05	>0.05	>0.05	>0.05	>0.05	>0.05	>0.05	>0.05	>0.05	>0.05

	***Ikzf2*$^{cello/cello}$ OHC Counts at Apex**				***Ikzf2*$^{cello/cello}$ OHC Counts at Mid**				***Ikzf2*$^{cello/cello}$ OHC Counts at Base**			
	1 m	**3 m**	**6 m**	**9 m**	**1 m**	**3 m**	**6 m**	**9 m**	**1 m**	**3 m**	**6 m**	**9 m**
1 m	-	-	-	-	-	-	-	-	-	-	-	-
3 m	0.0021	-	-	-	0.0392	-	-	-	0.0086	-	-	-
6 m	<0.0001	<0.0001	-	-	<0.0001	<0.0001	-	-	<0.0001	0.0005	-	-
9 m	<0.0001	<0.0001	>0.05	-	<0.0001	<0.0001	>0.05	-	<0.0001	0.0003	>0.05	-
18 m	<0.0001	<0.0001	>0.05	>0.05	<0.0001	<0.0001	>0.05	>0.05	<0.0001	0.0004	>0.05	>0.05

Statistical analysis: one-way ANOVA. Statistically significant results are highlighted in purple. m, month; OHC, outer hair cell.

Table 9.3: Statistical analysis of inner hair cell counts for *Ikzf2*$^{+/+}$, *Ikzf2*$^{cello/+}$ and *Ikzf2*$^{cello/cello}$ mice at one, three, six, nine and 18 months of age.

	***Ikzf2*$^{+/+}$ IHC Counts at Apex**				***Ikzf2*$^{+/+}$ IHC Counts at Mid**				***Ikzf2*$^{+/+}$ IHC Counts at Base**			
	1 m	**3 m**	**6 m**	**9 m**	**1 m**	**3 m**	**6 m**	**9 m**	**1 m**	**3 m**	**6 m**	**9 m**
1 m	-	-	-	-	-	-	-	-	-	-	-	-
3 m	>0.05	-	-	-	>0.05	-	-	-	>0.05	-	-	-
6 m	>0.05	>0.05	-	-	>0.05	>0.05	-	-	>0.05	>0.05	-	-
9 m	>0.05	>0.05	>0.05	-	>0.05	>0.05	>0.05	-	>0.05	>0.05	>0.05	-
18 m	>0.05	>0.05	>0.05	>0.05	0.0360	>0.05	>0.05	>0.05	>0.05	>0.05	>0.05	>0.05

	***Ikzf2*$^{cello/+}$ IHC Counts at Apex**				***Ikzf2*$^{cello/+}$ IHC Counts at Mid**				***Ikzf2*$^{cello/+}$ IHC Counts at Base**			
	1 m	**3 m**	**6 m**	**9 m**	**1 m**	**3 m**	**6 m**	**9 m**	**1 m**	**3 m**	**6 m**	**9 m**
1 m	-	-	-	-	-	-	-	-	-	-	-	-
3 m	>0.05	-	-	-	>0.05	-	-	-	>0.05	-	-	-
6 m	>0.05	>0.05	-	-	>0.05	>0.05	-	-	>0.05	>0.05	-	-
9 m	>0.05	>0.05	>0.05	-	>0.05	>0.05	>0.05	-	>0.05	>0.05	>0.05	-
18 m	>0.05	>0.05	>0.05	>0.05	>0.05	>0.05	>0.05	>0.05	>0.05	>0.05	>0.05	>0.05

	***Ikzf2*$^{cello/cello}$ IHC Counts at Apex**				***Ikzf2*$^{cello/cello}$ IHC Counts at Mid**				***Ikzf2*$^{cello/cello}$ IHC Counts at Base**			
	1 m	**3 m**	**6 m**	**9 m**	**1 m**	**3 m**	**6 m**	**9 m**	**1 m**	**3 m**	**6 m**	**9 m**
1 m	-	-	-	-	-	-	-	-	-	-	-	-
3 m	>0.05	-	-	-	>0.05	-	-	-	>0.05	-	-	-
6 m	>0.05	>0.05	-	-	>0.05	>0.05	-	-	0.0306	>0.05	-	-
9 m	>0.05	>0.05	>0.05	-	>0.05	>0.05	>0.05	-	0.0002	0.0021	0.0312	-
18 m	>0.05	>0.05	>0.05	>0.05	0.0426	0.0426	>0.05	>0.05	<0.0001	<0.0001	0.0002	0.0306

Statistical analysis: one-way ANOVA. Statistically significant results are highlighted in purple. IHC, inner hair cell; m, month.

Table 9.4: The 467 genes identified by RNA-Seq to be significantly dysregulated in *Ikzf2*$^{cello/cello}$ cochleae compared to *Ikzf2*$^{+/+}$ at postnatal day 8.

Ensembl ID (ENS)	Read Count *Ikzf2*$^{+/+}$	Read Count *Ikzf2*$^{cello/cello}$	Fold Change	p Value	FDR	Gene Symbol
MUSG00000039714	16.95	0.00	N/A	1.01E-05	1.23E-03	*Cplx3*
MUSG00000073658	12.18	0.00	N/A	1.44E-04	1.13E-02	*Crygb*
MUSG00000034384	11.57	0.00	N/A	1.99E-04	1.45E-02	*Barhl2*
MUSG00000020428	11.12	0.00	N/A	2.72E-04	1.85E-02	*Gabra6*
MUSG00000059632	10.96	0.00	N/A	2.76E-04	1.87E-02	*Krtap8-1*
MUSG00000029595	10.06	0.00	N/A	5.22E-04	3.12E-02	*Lhx5*
MUSG00000029546	9.53	0.00	N/A	7.29E-04	4.04E-02	*Uncx*
MUSG00000031354	466.54	2.10	-221.88	1.67E-49	4.37E-45	*Amelx*
MUSG00000029286	61.89	1.02	-60.76	5.85E-11	2.64E-08	*Enam*
MUSG00000030399	32.15	0.54	-59.30	1.24E-07	2.35E-05	*Ckm*
MUSG00000040046	94.20	2.45	-38.48	5.88E-13	4.27E-10	*Tph1*
MUSG00000024992	16.87	0.48	-35.40	7.45E-05	6.63E-03	*Pde6c*
MUSG00000029288	266.29	7.93	-33.56	5.87E-25	3.07E-21	*Ambn*
MUSG00000037771	14.30	0.48	-30.01	2.84E-04	1.91E-02	*Slc32a1*
MUSG00000038255	44.09	1.56	-28.25	5.09E-08	1.09E-05	*Neurod2*
MUSG00000048015	29.05	1.08	-26.80	2.08E-06	3.00E-04	*Neurod4*
MUSG00000043301	12.47	0.48	-26.17	6.76E-04	3.80E-02	*Kcnj6*
MUSG00000031972	207.60	10.33	-20.09	1.04E-17	3.01E-14	*Acta1*
MUSG00000026468	15.12	1.02	-14.84	6.39E-04	3.65E-02	*Lhx4*
MUSG00000061816	113.70	7.67	-14.82	2.59E-11	1.33E-08	*Myl1*
MUSG00000034701	112.17	7.61	-14.75	7.73E-11	3.37E-08	*Neurod1*
MUSG00000041578	28.60	2.04	-14.04	2.74E-05	2.89E-03	*Crx*
MUSG00000049583	18.74	1.43	-13.11	3.68E-04	2.35E-02	*Grm5*
MUSG00000002100	25.79	1.97	-13.08	6.99E-05	6.35E-03	*Mybpc3*
MUSG00000041534	41.76	3.40	-12.28	6.47E-06	8.37E-04	*Rbp3*
MUSG00000068154	51.95	4.49	-11.58	1.39E-06	2.08E-04	*Insm1*
MUSG00000027168	46.78	4.55	-10.28	5.97E-06	7.85E-04	*Pax6*
MUSG00000025386	39.36	4.07	-9.66	2.18E-05	2.36E-03	*Pde6g*
MUSG00000031097	71.55	8.48	-8.44	8.95E-07	1.50E-04	*Tnni2*
MUSG00000024041	33.33	4.01	-8.31	1.28E-04	1.03E-02	*Cryaa*
MUSG00000055775	85.28	11.42	-7.47	1.35E-06	2.05E-04	*Myh8*
MUSG00000028602	50.75	7.39	-6.86	2.27E-05	2.45E-03	*Tnfrsf8*
MUSG00000086938	29.47	4.62	-6.38	4.03E-04	2.53E-02	*4930481A15Rik*
MUSG00000027073	186.50	30.46	-6.12	2.51E-09	8.01E-07	*Prg2*
MUSG00000023439	64.21	10.60	-6.06	4.49E-05	4.37E-03	*Gnb3*
MUSG00000026535	88.01	15.62	-5.63	5.27E-06	7.13E-04	*Ifi202b*
MUSG00000030672	188.78	35.40	-5.33	4.42E-08	9.63E-06	*Mylpf*
MUSG00000052234	69.56	13.90	-5.01	5.73E-05	5.31E-03	*Epx*
MUSG00000057003	59.37	13.63	-4.35	4.68E-04	2.86E-02	*Myh4*

Ensembl ID (ENS)	Read Count *Ikzf2*$^{+/+}$	Read Count *Ikzf2*$^{cello/cello}$	Fold Change	p Value	FDR	Gene Symbol
MUSG00000036972	72.49	16.69	-4.34	2.09E-04	1.50E-02	*Zic4*
MUSG00000029618	4953.53	1150.91	-4.30	4.43E-37	5.79E-33	*Ocm*
MUSG00000032368	303.21	71.56	-4.24	8.59E-09	2.32E-06	*Zic1*
MUSG00000032517	166.05	40.13	-4.14	2.05E-06	2.98E-04	*Mobp*
MUSG00000049598	150.94	39.36	-3.83	6.50E-06	8.37E-04	*Vsig8*
MUSG00000095526	159.09	45.38	-3.51	1.19E-05	1.43E-03	*Gm10243*
MUSG00000044254	123.79	35.40	-3.50	1.18E-04	9.71E-03	*Pcsk9*
MUSG00000002930	434.32	153.18	-2.84	4.14E-07	7.22E-05	*Ppp1r17*
MUSG00000031654	161.14	57.61	-2.80	3.45E-04	2.25E-02	*Cbln1*
MUSG00000039783	199.70	71.48	-2.79	7.43E-05	6.63E-03	*Kmo*
MUSG00000033498	768.83	325.84	-2.36	1.29E-07	2.43E-05	*Strc*
MUSG00000020932	301.60	128.54	-2.35	3.78E-04	2.40E-02	*Gfap*
MUSG00000027863	312.62	133.62	-2.34	1.58E-04	1.22E-02	*Cd2*
MUSG00000029015	1016.59	440.68	-2.31	1.66E-08	4.13E-06	*Slc26a5*
MUSG00000044086	1270.23	564.31	-2.25	3.83E-09	1.18E-06	*Lmod3*
MUSG00000003411	312.65	139.04	-2.25	2.51E-04	1.75E-02	*Rab3b*
MUSG00000073643	2547.71	1152.72	-2.21	3.55E-11	1.69E-08	*Wdfy1*
MUSG00000031883	571.81	281.63	-2.03	6.06E-05	5.56E-03	*Car7*
MUSG00000064023	825.10	414.35	-1.99	7.71E-06	9.70E-04	*Klk8*
MUSG00000026304	567.01	287.20	-1.97	2.04E-04	1.47E-02	*Rab17*
MUSG00000034472	769.98	402.71	-1.91	6.69E-05	6.09E-03	*Rasd2*
MUSG00000041782	976.62	512.45	-1.91	1.17E-05	1.41E-03	*Lad1*
MUSG00000045410	522.67	276.20	-1.89	2.66E-04	1.84E-02	*Akr1e1*
MUSG00000054134	6961.72	3732.19	-1.87	5.35E-09	1.59E-06	*Umodl1*
MUSG00000067786	1938.25	1054.78	-1.84	1.27E-06	1.98E-04	*Nnat*
MUSG00000038600	1126.15	616.84	-1.83	6.21E-06	8.08E-04	*Atp6v0a4*
MUSG00000024497	1223.18	677.06	-1.81	1.21E-05	1.44E-03	*Pou4f3*
MUSG00000029359	929.47	518.18	-1.79	5.98E-05	5.50E-03	*Tesc*
MUSG00000073774	564.95	316.51	-1.78	8.54E-04	4.59E-02	*Kncn*
MUSG00000036412	852.10	485.00	-1.76	2.30E-04	1.63E-02	*Arsi*
MUSG00000024749	823.79	473.26	-1.74	2.71E-04	1.85E-02	*Tmc1*
MUSG00000059406	21210.22	12223.24	-1.74	8.70E-06	1.08E-03	*Tmprss9*
MUSG00000036095	863.16	510.58	-1.69	4.76E-04	2.90E-02	*Dgkb*
MUSG00000053141	1236.05	734.37	-1.68	1.14E-04	9.49E-03	*Ptprt*
MUSG00000049515	1294.18	776.08	-1.67	1.59E-04	1.22E-02	*Espnl*
MUSG00000090291	1454.58	880.14	-1.65	7.46E-05	6.63E-03	*Lrrc10b*
MUSG00000028865	905.15	556.32	-1.63	8.23E-04	4.46E-02	*Cd164l2*
MUSG00000029503	3275.40	2046.24	-1.60	2.48E-05	2.65E-03	*P2rx2*
MUSG00000035852	1169.17	730.74	-1.60	6.18E-04	3.55E-02	*Misp*
MUSG00000027221	1329.20	842.80	-1.58	4.48E-04	2.76E-02	*Chst1*
MUSG00000032068	2926.99	1864.89	-1.57	1.10E-04	9.20E-03	*1600029D21Rik*

Ensembl ID (ENS)	Read Count *Ikzf2*$^{+/+}$	Read Count *Ikzf2*$^{cello/cello}$	Fold Change	p Value	FDR	Gene Symbol
MUSG00000016942	2378.13	1530.16	-1.55	1.99E-04	1.45E-02	*Tmprss6*
MUSG00000049265	1448.52	934.90	-1.55	4.43E-04	2.74E-02	*Kcnk3*
MUSG00000033453	1562.87	1011.73	-1.54	7.31E-04	4.05E-02	*Adamts15*
MUSG00000039194	3187.99	2072.05	-1.54	1.35E-04	1.07E-02	*Rlbp1*
MUSG00000031838	2684.31	1749.40	-1.53	1.25E-04	1.02E-02	*Ifi30*
MUSG00000059970	1615.06	1053.84	-1.53	6.19E-04	3.55E-02	*Hspa2*
MUSG00000059751	10480.28	6884.23	-1.52	6.81E-04	3.81E-02	*Rps3a3*
MUSG00000026955	1828.20	1217.00	-1.50	6.21E-04	3.55E-02	*Sapcd2*
MUSG00000031400	4947.98	3305.69	-1.50	3.89E-04	2.45E-02	*G6pdx*
MUSG00000033419	1398.73	2097.51	1.50	2.66E-04	1.84E-02	*Snap91*
MUSG00000061353	3912.93	5870.28	1.50	3.43E-04	2.24E-02	*Cxcl12*
MUSG00000031227	1018.31	1529.11	1.50	5.85E-04	3.40E-02	*Magee1*
MUSG00000028364	3212.17	4827.97	1.50	4.77E-04	2.90E-02	*Tnc*
MUSG00000026442	3292.77	4953.11	1.50	2.43E-04	1.72E-02	*Nfasc*
MUSG00000021314	1044.06	1573.05	1.51	4.87E-04	2.94E-02	*Amph*
MUSG00000004110	1594.84	2404.44	1.51	7.99E-04	4.35E-02	*Cacna1e*
MUSG00000039126	1088.24	1641.07	1.51	6.48E-04	3.69E-02	*Prune2*
MUSG00000020262	1366.93	2061.72	1.51	3.23E-04	2.12E-02	*Adarb1*
MUSG00000038418	1817.24	2741.40	1.51	9.25E-04	4.89E-02	*Egr1*
MUSG00000038576	1135.39	1713.21	1.51	5.00E-04	3.00E-02	*Susd4*
MUSG00000022974	2152.65	3257.23	1.51	3.13E-04	2.07E-02	*Paxbp1*
MUSG00000027894	1422.33	2156.07	1.52	1.87E-04	1.39E-02	*Slc6a17*
MUSG00000070524	2371.24	3602.48	1.52	1.28E-04	1.03E-02	*Fcrlb*
MUSG00000037259	966.56	1469.52	1.52	5.58E-04	3.30E-02	*Dzank1*
MUSG00000001986	1751.54	2669.79	1.52	2.46E-04	1.73E-02	*Gria3*
MUSG00000033949	916.00	1398.06	1.53	6.72E-04	3.79E-02	*Trim36*
MUSG00000057969	1894.13	2895.27	1.53	9.62E-05	8.30E-03	*Sema3b*
MUSG00000072553	3537.88	5417.03	1.53	5.85E-04	3.40E-02	*Gm525*
MUSG00000036745	1443.78	2216.64	1.54	1.31E-04	1.05E-02	*Ttll7*
MUSG00000022419	957.32	1476.76	1.54	4.26E-04	2.65E-02	*Deptor*
MUSG00000052889	729.57	1125.66	1.54	6.12E-04	3.53E-02	*Prkcb*
MUSG00000056966	4182.63	6461.34	1.54	3.13E-05	3.21E-03	*Gjc3*
MUSG00000030077	888.31	1376.43	1.55	8.73E-04	4.66E-02	*Chl1*
MUSG00000038486	1056.71	1637.99	1.55	1.41E-04	1.12E-02	*Sv2a*
MUSG00000047766	1072.60	1665.48	1.55	2.55E-04	1.77E-02	*Lrrc49*
MUSG00000041220	1247.53	1942.48	1.56	1.00E-04	8.54E-03	*Elovl6*
MUSG00000001506	11815.95	18490.60	1.56	8.44E-04	4.56E-02	*Col1a1*
MUSG00000032890	725.15	1136.86	1.57	3.12E-04	2.07E-02	*Rims3*
MUSG00000057614	1532.62	2403.69	1.57	1.19E-04	9.78E-03	*Gnai1*
MUSG00000022479	749.29	1176.57	1.57	8.62E-04	4.62E-02	*Vdr*
MUSG00000044533	841.20	1323.63	1.57	5.69E-06	7.56E-04	*Rps2*

Ensembl ID (ENS)	Read Count *Ikzf2*$^{+/+}$	Read Count *Ikzf2*$^{cello/cello}$	Fold Change	p Value	FDR	Gene Symbol
MUSG00000076281	809.02	1275.10	1.58	4.52E-04	2.77E-02	*Gm24270*
MUSG00000025964	1438.42	2272.68	1.58	4.74E-05	4.56E-03	*Adam23*
MUSG00000028111	3982.19	6304.57	1.58	9.41E-05	8.15E-03	*Ctsk*
MUSG00000019997	1622.28	2570.40	1.58	1.16E-04	9.61E-03	*Ctgf*
MUSG00000057457	3323.20	5268.47	1.59	1.09E-04	9.20E-03	*Phex*
MUSG00000025092	3232.58	5132.08	1.59	1.08E-05	1.30E-03	*Hspa12a*
MUSG00000019194	874.23	1388.82	1.59	2.04E-04	1.47E-02	*Scn1b*
MUSG00000004892	1812.79	2888.08	1.59	9.37E-05	8.14E-03	*Bcan*
MUSG00000029608	543.98	868.29	1.60	2.46E-04	1.73E-02	*Rph3a*
MUSG00000052949	916.30	1464.64	1.60	9.08E-05	7.94E-03	*Rnf157*
MUSG00000061080	792.15	1268.03	1.60	1.60E-04	1.22E-02	*Lsamp*
MUSG00000029084	1143.99	1832.43	1.60	1.94E-04	1.43E-02	*Cd38*
MUSG00000062661	716.66	1148.14	1.60	2.01E-04	1.46E-02	*Ncs1*
MUSG00000025855	803.27	1287.02	1.60	1.16E-04	9.62E-03	*Prkar1b*
MUSG00000032179	1663.47	2667.40	1.60	5.72E-05	5.31E-03	*Bmp5*
MUSG00000025321	3767.18	6041.24	1.60	5.46E-06	7.33E-04	*Itgb8*
MUSG00000003279	638.22	1026.62	1.61	4.68E-04	2.86E-02	*Dlgap1*
MUSG00000033192	1219.35	1972.92	1.62	4.00E-05	3.96E-03	*Lpcat2*
MUSG00000076258	1294.94	2095.59	1.62	3.32E-05	3.38E-03	*Gm23935*
MUSG00000020893	1197.27	1937.74	1.62	8.93E-05	7.84E-03	*Per1*
MUSG00000019894	1722.00	2798.51	1.63	9.54E-06	1.18E-03	*Slc6a15*
MUSG00000000276	1153.38	1878.92	1.63	4.23E-05	4.13E-03	*Dgke*
MUSG00000043531	898.37	1465.74	1.63	5.46E-05	5.10E-03	*Sorcs1*
MUSG00000052572	595.82	973.43	1.63	2.84E-04	1.91E-02	*Dlg2*
MUSG00000043004	1408.37	2303.00	1.64	1.33E-05	1.56E-03	*Gng2*
MUSG00000029095	647.58	1061.63	1.64	2.71E-04	1.85E-02	*Ablim2*
MUSG00000032186	1679.54	2753.71	1.64	5.93E-06	7.82E-04	*Tmod2*
MUSG00000046442	647.85	1062.38	1.64	1.77E-04	1.34E-02	*Ppm1e*
MUSG00000068923	1992.10	3268.41	1.64	3.52E-06	4.95E-04	*Syt11*
MUSG00000040537	1352.06	2218.98	1.64	1.58E-05	1.81E-03	*Adam22*
MUSG00000026764	1955.20	3219.71	1.65	2.62E-06	3.74E-04	*Kif5c*
MUSG00000013523	1066.44	1765.01	1.66	1.58E-05	1.81E-03	*Bcas1*
MUSG00000074622	713.14	1180.29	1.66	7.11E-05	6.42E-03	*Mafb*
MUSG00000001348	2014.14	3339.38	1.66	3.49E-05	3.48E-03	*Acp5*
MUSG00000029086	1646.84	2748.86	1.67	1.87E-05	2.09E-03	*Prom1*
MUSG00000025892	632.59	1057.33	1.67	9.90E-05	8.46E-03	*Gria4*
MUSG00000028524	552.40	923.41	1.67	1.70E-04	1.29E-02	*Sgip1*
MUSG00000073557	1707.27	2861.68	1.68	1.47E-05	1.72E-03	*Ppp1r12b*
MUSG00000032878	717.46	1205.84	1.68	5.01E-05	4.78E-03	*Ccdc85a*
MUSG00000018411	734.58	1235.04	1.68	2.11E-05	2.31E-03	*Mapt*
MUSG00000074971	698.68	1182.60	1.69	8.11E-05	7.19E-03	*Fibin*

Ensembl ID (ENS)	Read Count *Ikzf2*$^{+/+}$	Read Count *Ikzf2*$^{cello/cello}$	Fold Change	p Value	FDR	Gene Symbol
MUSG00000073940	870.58	1474.24	1.69	2.07E-05	2.28E-03	*Hbb-bt*
MUSG00000017412	465.40	790.28	1.70	3.71E-04	2.36E-02	*Cacnb4*
MUSG00000039809	330.38	561.37	1.70	8.47E-04	4.56E-02	*Gabbr2*
MUSG00000038608	706.70	1203.60	1.70	5.32E-05	5.02E-03	*Dock10*
MUSG00000030731	377.82	643.90	1.70	7.88E-04	4.31E-02	*Syt3*
MUSG00000046480	615.23	1048.52	1.70	9.77E-05	8.41E-03	*Scn4b*
MUSG00000031385	468.78	801.94	1.71	3.40E-04	2.22E-02	*Plxnb3*
MUSG00000040035	451.06	771.74	1.71	2.02E-04	1.47E-02	*Disp2*
MUSG00000026200	545.39	935.29	1.71	2.92E-04	1.95E-02	*Glb1l*
MUSG00000041762	545.20	935.18	1.72	1.39E-04	1.10E-02	*Gpr155*
MUSG00000026610	943.32	1619.26	1.72	5.17E-06	7.03E-04	*Esrrg*
MUSG00000049721	475.77	818.13	1.72	1.70E-04	1.29E-02	*Gal3st1*
MUSG00000027674	615.83	1061.60	1.72	5.32E-05	5.02E-03	*Pex5l*
MUSG00000022456	621.28	1071.62	1.72	2.17E-05	2.36E-03	*Sept3*
MUSG00000059857	395.74	682.90	1.73	5.27E-04	3.14E-02	*Ntng1*
MUSG00000078190	943.79	1635.99	1.73	4.13E-05	4.06E-03	*Dnm3os*
MUSG00000053192	1065.52	1848.99	1.74	1.51E-06	2.25E-04	*Mllt11*
MUSG00000022454	554.04	962.89	1.74	2.52E-04	1.76E-02	*Nell2*
MUSG00000055407	759.83	1322.29	1.74	1.24E-05	1.48E-03	*Map6*
MUSG00000029135	622.74	1084.02	1.74	1.43E-04	1.12E-02	*Fosl2*
MUSG00000074657	2139.86	3729.40	1.74	1.64E-07	3.01E-05	*Kif5a*
MUSG00000025777	383.71	671.85	1.75	2.26E-04	1.60E-02	*Gdap1*
MUSG00000021719	1175.89	2059.37	1.75	7.10E-06	9.02E-04	*Rgs7bp*
MUSG00000038264	1741.80	3052.54	1.75	7.42E-07	1.26E-04	*Sema7a*
MUSG00000007440	778.88	1367.29	1.76	8.33E-06	1.04E-03	*Pcdha2*
MUSG00000023000	396.51	696.83	1.76	2.04E-04	1.47E-02	*Dhh*
MUSG00000030806	1065.60	1889.26	1.77	9.82E-07	1.59E-04	*Stx1b*
MUSG00000048388	594.21	1057.82	1.78	2.35E-05	2.52E-03	*Fam171b*
MUSG00000050953	1246.62	2223.95	1.78	4.46E-06	6.13E-04	*Gja1*
MUSG00000026797	2185.00	3898.43	1.78	7.19E-08	1.46E-05	*Stxbp1*
MUSG00000010175	549.79	982.22	1.79	2.15E-05	2.35E-03	*Prox1*
MUSG00000023236	1192.57	2132.17	1.79	4.05E-07	7.11E-05	*Scg5*
MUSG00000006782	6349.70	11353.67	1.79	3.71E-08	8.44E-06	*Cnp*
MUSG00000005716	1948.07	3483.58	1.79	4.35E-08	9.57E-06	*Pvalb*
MUSG00000053046	418.57	750.45	1.79	1.02E-04	8.63E-03	*Brsk2*
MUSG00000053025	566.97	1017.21	1.79	1.86E-05	2.09E-03	*Sv2b*
MUSG00000031425	5170.35	9305.11	1.80	2.48E-08	6.00E-06	*Plp1*
MUSG00000046167	1712.06	3082.38	1.80	1.21E-07	2.31E-05	*Gldn*
MUSG00000027848	809.73	1462.60	1.81	9.67E-06	1.19E-03	*Olfml3*
MUSG00000025348	367.70	665.20	1.81	2.68E-04	1.85E-02	*Itga7*
MUSG00000079598	551.82	999.79	1.81	9.91E-06	1.21E-03	*Clec2l*

Ensembl ID (ENS)	Read Count *Ikzf2*$^{+/+}$	Read Count *Ikzf2*$^{cello/cello}$	Fold Change	p Value	FDR	Gene Symbol
MUSG00000026678	9017.28	16477.28	1.83	1.32E-06	2.03E-04	*Rgs5*
MUSG00000027173	280.51	512.59	1.83	5.12E-04	3.06E-02	*Depdc7*
MUSG00000042873	458.16	837.26	1.83	2.78E-05	2.92E-03	*Lhfpl4*
MUSG00000070565	2988.88	5462.64	1.83	2.81E-08	6.74E-06	*Rasal2*
MUSG00000056071	443.65	810.89	1.83	1.82E-04	1.36E-02	*S100a9*
MUSG00000034040	365.52	673.45	1.84	1.53E-04	1.18E-02	*Wbscr17*
MUSG00000023033	624.30	1151.27	1.84	3.77E-06	5.28E-04	*Scn8a*
MUSG00000031775	1045.53	1928.25	1.84	8.29E-08	1.65E-05	*Pllp*
MUSG00000004098	575.38	1061.48	1.84	9.75E-06	1.20E-03	*Col5a3*
MUSG00000026000	1765.00	3263.23	1.85	3.18E-08	7.50E-06	*Lancl1*
MUSG00000057716	306.79	567.45	1.85	1.52E-04	1.18E-02	*Tmem178b*
MUSG00000022658	301.60	557.91	1.85	1.44E-04	1.13E-02	*Tagln3*
MUSG00000004267	2349.28	4355.00	1.85	5.45E-09	1.60E-06	*Eno2*
MUSG00000005125	2577.88	4802.87	1.86	8.50E-09	2.32E-06	*Ndrg1*
MUSG00000021250	324.46	606.45	1.87	4.89E-04	2.95E-02	*Fos*
MUSG00000003410	351.35	656.81	1.87	4.20E-05	4.11E-03	*Elavl3*
MUSG00000063626	432.06	810.15	1.88	1.76E-05	1.98E-03	*Unc5d*
MUSG00000041073	284.59	533.84	1.88	1.88E-04	1.40E-02	*Nacad*
MUSG00000022619	786.28	1477.53	1.88	1.77E-07	3.24E-05	*Mapk8ip2*
MUSG00000024190	481.98	906.38	1.88	4.64E-05	4.50E-03	*Dusp1*
MUSG00000038077	246.41	464.35	1.88	3.48E-04	2.26E-02	*Kcna6*
MUSG00000012428	289.31	545.26	1.88	7.65E-04	4.21E-02	*Steap4*
MUSG00000019906	254.57	480.18	1.89	3.68E-04	2.35E-02	*Lin7a*
MUSG00000071658	357.45	674.74	1.89	3.15E-05	3.21E-03	*Gng3*
MUSG00000031298	400.66	759.28	1.90	2.95E-05	3.06E-03	*Gpr64*
MUSG00000042182	550.74	1045.66	1.90	1.25E-06	1.96E-04	*Bend6*
MUSG00000068373	461.95	877.44	1.90	7.37E-06	9.30E-04	*D430041D05Rik*
MUSG00000029291	929.20	1773.06	1.91	5.05E-08	1.09E-05	*Rufy3*
MUSG00000060780	190.33	364.66	1.92	7.81E-04	4.28E-02	*Lrrtm1*
MUSG00000037843	182.25	352.11	1.93	7.79E-04	4.28E-02	*Vstm2l*
MUSG00000034656	282.90	547.64	1.94	1.22E-04	1.00E-02	*Cacna1a*
MUSG00000046186	312.21	605.17	1.94	2.88E-04	1.93E-02	*Cd109*
MUSG00000039716	363.07	705.56	1.94	2.89E-05	3.01E-03	*Dock3*
MUSG00000042662	1197.03	2326.32	1.94	1.25E-08	3.20E-06	*Dusp15*
MUSG00000041670	250.16	487.71	1.95	1.50E-04	1.17E-02	*Rims1*
MUSG00000031144	789.16	1538.93	1.95	2.26E-08	5.59E-06	*Syp*
MUSG00000035964	181.08	353.27	1.95	7.66E-04	4.21E-02	*Tmem59l*
MUSG00000041020	555.66	1088.57	1.96	9.68E-07	1.59E-04	*Map7d2*
MUSG00000061603	425.85	834.88	1.96	5.49E-06	7.33E-04	*Akap6*
MUSG00000038623	571.95	1122.35	1.96	9.65E-07	1.59E-04	*Tm6sf1*
MUSG00000024403	474.53	935.48	1.97	1.65E-06	2.44E-04	*Atp6v1g2*

Ensembl ID (ENS)	Read Count *Ikzf2*$^{+/+}$	Read Count *Ikzf2*$^{cello/cello}$	Fold Change	p Value	FDR	Gene Symbol
MUSG00000034336	1078.87	2134.58	1.98	1.92E-09	6.44E-07	*Ina*
MUSG00000039601	696.19	1378.85	1.98	5.27E-08	1.12E-05	*Rcan2*
MUSG00000060257	227.80	451.99	1.98	1.13E-04	9.46E-03	*Scrt2*
MUSG00000005045	210.49	419.78	1.99	1.78E-04	1.34E-02	*Chd5*
MUSG00000000120	720.79	1447.21	2.01	8.46E-09	2.32E-06	*Ngfr*
MUSG00000070695	245.74	494.31	2.01	5.37E-05	5.03E-03	*Cntnap5a*
MUSG00000030337	2613.45	5263.62	2.01	1.06E-10	4.55E-08	*Vamp1*
MUSG00000053332	1495.41	3014.77	2.02	1.25E-09	4.37E-07	*Gas5*
MUSG00000008489	327.62	662.82	2.02	6.59E-06	8.44E-04	*Elavl2*
MUSG00000061451	262.44	532.21	2.03	3.37E-05	3.41E-03	*Tmem151a*
MUSG00000030683	203.18	413.05	2.03	1.33E-04	1.06E-02	*Sez6l2*
MUSG00000018865	631.34	1284.36	2.03	2.40E-08	5.87E-06	*Sult4a1*
MUSG00000030500	344.90	702.75	2.04	4.27E-06	5.91E-04	*Slc17a6*
MUSG00000017737	1676.93	3419.29	2.04	3.39E-09	1.06E-06	*Mmp9*
MUSG00000029861	129.02	263.07	2.04	6.64E-04	3.76E-02	*Fam131b*
MUSG00000021194	586.13	1196.31	2.04	3.81E-08	8.58E-06	*Chga*
MUSG00000039057	251.28	512.93	2.04	3.04E-05	3.14E-03	*Myo16*
MUSG00000032564	213.23	435.67	2.04	9.22E-05	8.03E-03	*Cpne4*
MUSG00000039252	257.62	526.69	2.04	4.12E-05	4.06E-03	*Lgi2*
MUSG00000027438	731.95	1497.58	2.05	9.29E-09	2.48E-06	*Napb*
MUSG00000041607	18596.26	38127.81	2.05	1.92E-07	3.46E-05	*Mbp*
MUSG00000011751	195.25	400.78	2.05	1.91E-04	1.41E-02	*Sptbn4*
MUSG00000015467	293.45	602.48	2.05	1.43E-05	1.68E-03	*Egfl8*
MUSG00000025375	3470.91	7127.15	2.05	2.64E-11	1.33E-08	*Aatk*
MUSG00000032011	668.66	1374.73	2.06	7.95E-09	2.24E-06	*Thy1*
MUSG00000035849	233.90	481.14	2.06	5.36E-05	5.03E-03	*Krt222*
MUSG00000039278	194.70	401.19	2.06	9.83E-05	8.43E-03	*Pcsk1n*
MUSG00000027500	1181.72	2441.73	2.07	3.01E-11	1.48E-08	*Stmn2*
MUSG00000019775	218.29	452.03	2.07	6.46E-05	5.90E-03	*Rgs17*
MUSG00000037217	369.37	766.40	2.07	1.16E-06	1.83E-04	*Syn1*
MUSG00000056306	238.78	496.41	2.08	3.68E-05	3.66E-03	*Sertm1*
MUSG00000043924	988.99	2059.82	2.08	5.20E-10	1.92E-07	*Ncmap*
MUSG00000016349	1441.14	3009.00	2.09	1.23E-11	6.87E-09	*Eef1a2*
MUSG00000007021	155.59	325.22	2.09	2.11E-04	1.51E-02	*Syngr3*
MUSG00000029361	445.87	933.23	2.09	3.34E-07	5.89E-05	*Nos1*
MUSG00000042115	198.31	415.17	2.09	8.82E-05	7.76E-03	*Klhdc8a*
MUSG00000032549	1134.89	2377.60	2.10	5.48E-11	2.51E-08	*Rab6b*
MUSG00000097767	1319.94	2766.47	2.10	4.21E-10	1.57E-07	*Miat*
MUSG00000048148	159.58	334.97	2.10	3.66E-04	2.35E-02	*Nwd1*
MUSG00000008658	186.41	392.79	2.11	1.08E-04	9.15E-03	*Rbfox1*
MUSG00000051243	452.33	956.00	2.11	3.69E-08	8.44E-06	*Islr2*

Ensembl ID (ENS)	Read Count *Ikzf2*$^{+/+}$	Read Count *Ikzf2*$^{cello/cello}$	Fold Change	p Value	FDR	Gene Symbol
MUSG00000007944	131.18	278.12	2.12	3.65E-04	2.35E-02	*Ttc9b*
MUSG00000034842	730.74	1551.60	2.12	2.01E-09	6.60E-07	*Art3*
MUSG00000037224	154.25	327.70	2.12	2.49E-04	1.75E-02	*Zfyve28*
MUSG00000034958	219.86	467.32	2.13	2.30E-05	2.48E-03	*Atcay*
MUSG00000026959	217.33	462.87	2.13	3.12E-05	3.21E-03	*Grin1*
MUSG00000002190	148.74	317.68	2.14	2.22E-04	1.58E-02	*Clgn*
MUSG00000056054	244.90	523.33	2.14	7.12E-05	6.42E-03	*S100a8*
MUSG00000031391	346.51	740.70	2.14	7.47E-07	1.26E-04	*L1cam*
MUSG00000068615	155.01	331.52	2.14	1.27E-04	1.03E-02	*Gjd2*
MUSG00000020953	14590.11	31286.40	2.14	1.45E-07	2.69E-05	*Coch*
MUSG00000026204	111.78	240.21	2.15	5.78E-04	3.38E-02	*Ptprn*
MUSG00000043298	109.56	235.92	2.15	8.73E-04	4.66E-02	*Smco3*
MUSG00000049176	305.60	659.00	2.16	2.22E-06	3.19E-04	*Frmpd4*
MUSG00000048385	404.89	875.29	2.16	9.07E-08	1.78E-05	*Scrt1*
MUSG00000031762	201.83	436.38	2.16	5.01E-05	4.78E-03	*Mt2*
MUSG00000065037	278.70	602.59	2.16	1.53E-05	1.77E-03	*Rn7sk*
MUSG00000095139	313.97	678.93	2.16	1.17E-06	1.84E-04	*Pou3f2*
MUSG00000031465	128.64	278.26	2.16	5.02E-04	3.01E-02	*Angpt2*
MUSG00000027071	256.17	555.67	2.17	3.22E-06	4.54E-04	*P2rx3*
MUSG00000027834	688.43	1494.47	2.17	1.42E-10	5.90E-08	*Serpini1*
MUSG00000042453	298.21	647.41	2.17	1.90E-06	2.78E-04	*Reln*
MUSG00000026344	276.36	600.24	2.17	1.67E-05	1.90E-03	*Lypd1*
MUSG00000029307	3235.45	7028.21	2.17	2.65E-11	1.33E-08	*Dmp1*
MUSG00000000792	163.25	355.42	2.18	1.55E-04	1.19E-02	*Slc5a5*
MUSG00000032854	1624.54	3537.96	2.18	5.68E-13	4.24E-10	*Ugt8a*
MUSG00000036634	568.30	1239.04	2.18	2.23E-09	7.21E-07	*Mag*
MUSG00000035226	150.41	328.20	2.18	1.19E-04	9.79E-03	*Rims4*
MUSG00000026424	440.57	962.74	2.19	6.96E-08	1.42E-05	*Gpr37l1*
MUSG00000025154	2352.69	5160.21	2.19	3.02E-13	2.47E-10	*Arhgap19*
MUSG00000036564	3742.38	8209.62	2.19	1.34E-13	1.16E-10	*Ndrg4*
MUSG00000027254	3502.79	7699.18	2.20	1.75E-13	1.48E-10	*Map1a*
MUSG00000032355	169.21	372.24	2.20	4.69E-05	4.53E-03	*Mlip*
MUSG00000024743	644.61	1435.98	2.23	1.96E-10	7.55E-08	*Syt7*
MUSG00000037996	810.54	1805.69	2.23	1.75E-11	9.34E-09	*Slc24a2*
MUSG00000005338	559.80	1252.93	2.24	5.30E-10	1.93E-07	*Cadm3*
MUSG00000043670	300.05	672.09	2.24	5.23E-07	8.99E-05	*Diras1*
MUSG00000034891	451.29	1011.09	2.24	5.96E-09	1.73E-06	*Sncb*
MUSG00000000223	1761.77	3961.03	2.25	9.25E-13	5.90E-10	*Drp2*
MUSG00000026904	643.17	1448.87	2.25	2.78E-09	8.76E-07	*Slc4a10*
MUSG00000056755	93.54	210.83	2.25	8.60E-04	4.62E-02	*Grm7*
MUSG00000021700	349.68	788.49	2.25	1.10E-07	2.14E-05	*Rab3c*

Ensembl ID (ENS)	Read Count *Ikzf2*$^{+/+}$	Read Count *Ikzf2*$^{cello/cello}$	Fold Change	p Value	FDR	Gene Symbol
MUSG00000070570	1061.48	2396.21	2.26	8.68E-13	5.82E-10	*Slc17a7*
MUSG00000050578	426.13	963.20	2.26	8.71E-08	1.72E-05	*Mmp13*
MUSG00000082229	312.50	707.52	2.26	2.64E-07	4.69E-05	*Nap1l2*
MUSG00000031543	629.15	1425.33	2.27	1.54E-10	6.15E-08	*Ank1*
MUSG00000003657	4036.87	9155.44	2.27	2.87E-14	2.88E-11	*Calb2*
MUSG00000028370	381.35	866.03	2.27	4.34E-08	9.57E-06	*Pappa*
MUSG00000018217	16228.21	36859.87	2.27	2.02E-09	6.60E-07	*Pmp22*
MUSG00000062785	725.58	1650.45	2.27	1.11E-10	4.69E-08	*Kcnc3*
MUSG00000040907	4005.25	9115.24	2.28	9.58E-15	1.09E-11	*Atp1a3*
MUSG00000020264	373.37	852.02	2.28	1.91E-07	3.46E-05	*Slc36a2*
MUSG00000060568	213.68	487.75	2.28	2.56E-05	2.72E-03	*Fam78b*
MUSG00000037868	450.85	1029.23	2.28	6.43E-09	1.85E-06	*Egr2*
MUSG00000024042	1193.42	2729.74	2.29	8.10E-12	4.71E-09	*Sik1*
MUSG00000027350	930.30	2132.24	2.29	8.37E-13	5.76E-10	*Chgb*
MUSG00000015134	1220.43	2802.27	2.30	1.11E-13	1.00E-10	*Aldh1a3*
MUSG00000017400	441.24	1015.64	2.30	1.34E-09	4.60E-07	*Stac2*
MUSG00000046709	567.01	1305.34	2.30	1.56E-10	6.15E-08	*Mapk10*
MUSG00000054459	1009.97	2332.24	2.31	4.34E-13	3.44E-10	*Vsnl1*
MUSG00000054423	493.58	1140.14	2.31	3.81E-10	1.44E-07	*Cadps*
MUSG00000039114	330.70	764.73	2.31	6.67E-08	1.37E-05	*Nrn1*
MUSG00000008874	301.58	698.16	2.31	1.09E-06	1.75E-04	*Clec3a*
MUSG00000053519	89.29	206.77	2.32	5.67E-04	3.35E-02	*Kcnip1*
MUSG00000022054	3419.12	7923.86	2.32	1.62E-15	2.23E-12	*Nefm*
MUSG00000033615	3150.91	7332.00	2.33	9.25E-16	1.42E-12	*Cplx1*
MUSG00000046613	98.76	230.16	2.33	3.84E-04	2.43E-02	*Vwa5b2*
MUSG00000049252	117.79	274.83	2.33	1.79E-04	1.34E-02	*Lrp1b*
MUSG00000022055	2741.14	6398.86	2.33	7.32E-16	1.20E-12	*Nefl*
MUSG00000033579	392.45	916.23	2.33	8.19E-09	2.28E-06	*Fa2h*
MUSG00000043557	2828.80	6623.66	2.34	9.80E-16	1.42E-12	*Mdga1*
MUSG00000022449	383.98	899.17	2.34	1.19E-08	3.07E-06	*Adamts20*
MUSG00000027584	73.15	172.47	2.36	8.32E-04	4.51E-02	*Oprl1*
MUSG00000033981	243.52	575.05	2.36	9.79E-07	1.59E-04	*Gria2*
MUSG00000055561	254.53	601.16	2.36	3.05E-06	4.34E-04	*Spink5*
MUSG00000055430	697.53	1649.91	2.37	2.27E-12	1.41E-09	*Nap1l5*
MUSG00000045994	296.78	702.27	2.37	1.19E-07	2.28E-05	*B3gat1*
MUSG00000020396	3447.29	8160.12	2.37	4.72E-16	8.23E-13	*Nefh*
MUSG00000022212	210.11	497.65	2.37	1.33E-06	2.04E-04	*Cpne6*
MUSG00000060240	883.13	2092.43	2.37	1.06E-13	9.86E-11	*Cend1*
MUSG00000039838	89.08	211.31	2.37	2.73E-04	1.85E-02	*Slc45a1*
MUSG00000021730	137.58	327.21	2.38	3.43E-05	3.44E-03	*Hcn1*
MUSG00000053198	5134.22	12230.65	2.38	1.87E-15	2.43E-12	*Prx*

Ensembl ID (ENS)	Read Count *Ikzf2*$^{+/+}$	Read Count *Ikzf2*$^{cello/cello}$	Fold Change	p Value	FDR	Gene Symbol
MUSG00000055567	451.03	1075.00	2.38	1.38E-09	4.69E-07	*Unc80*
MUSG00000023064	318.66	760.75	2.39	1.62E-08	4.07E-06	*Sncg*
MUSG00000075316	70.38	168.47	2.39	5.29E-04	3.14E-02	*Scn9a*
MUSG00000061911	83.25	199.50	2.40	2.72E-04	1.85E-02	*Myt1l*
MUSG00000060212	77.43	187.42	2.42	3.70E-04	2.36E-02	*Pcnxl2*
MUSG00000026452	708.73	1717.65	2.42	5.30E-13	4.07E-10	*Syt2*
MUSG00000021613	440.69	1068.80	2.43	1.52E-10	6.15E-08	*Hapln1*
MUSG00000066058	1457.55	3543.15	2.43	3.87E-16	7.46E-13	*Cldn19*
MUSG00000074802	1381.04	3364.42	2.44	1.95E-15	2.43E-12	*Gas2l3*
MUSG00000027273	2410.71	5895.21	2.45	6.02E-17	1.57E-13	*Snap25*
MUSG00000027833	101.27	247.74	2.45	1.10E-04	9.20E-03	*Shox2*
MUSG00000022523	382.30	937.65	2.45	7.52E-10	2.66E-07	*Fgf12*
MUSG00000032796	215.18	527.85	2.45	5.71E-07	9.76E-05	*Lama1*
MUSG00000040428	944.87	2323.83	2.46	2.73E-14	2.86E-11	*Plekha4*
MUSG00000033316	87.42	215.71	2.47	1.80E-04	1.35E-02	*Galnt9*
MUSG00000028931	706.97	1745.42	2.47	8.17E-13	5.76E-10	*Kcnab2*
MUSG00000060924	101.03	250.29	2.48	8.34E-05	7.36E-03	*Csmd1*
MUSG00000031376	185.22	460.31	2.49	1.29E-06	2.00E-04	*Atp2b3*
MUSG00000021301	232.41	580.48	2.50	1.15E-07	2.23E-05	*Hecw1*
MUSG00000053863	350.53	875.92	2.50	5.63E-08	1.17E-05	*Mepe*
MUSG00000063531	427.98	1074.74	2.51	6.30E-11	2.79E-08	*Sema3e*
MUSG00000086096	57.87	145.36	2.51	9.31E-04	4.91E-02	*Gm12688*
MUSG00000046844	409.96	1031.33	2.52	3.38E-11	1.63E-08	*Vat1l*
MUSG00000038276	400.61	1010.16	2.52	1.58E-10	6.15E-08	*Asic3*
MUSG00000087620	53.06	134.49	2.53	7.53E-04	4.16E-02	*5330434G04Rik*
MUSG00000090125	242.32	614.68	2.54	3.26E-08	7.62E-06	*Pou3f1*
MUSG00000020836	259.18	661.23	2.55	5.63E-08	1.17E-05	*Coro6*
MUSG00000036062	240.57	613.97	2.55	3.33E-08	7.72E-06	*N28178*
MUSG00000097545	122.95	314.53	2.56	1.48E-05	1.72E-03	*A930011O12Rik*
MUSG00000025221	102.41	263.97	2.58	3.38E-05	3.41E-03	*Kcnip2*
MUSG00000042846	107.62	277.70	2.58	1.75E-05	1.98E-03	*Lrrtm3*
MUSG00000052468	234.79	606.33	2.58	4.01E-08	8.97E-06	*Pmp2*
MUSG00000036123	94.75	246.73	2.60	3.44E-05	3.44E-03	*Slc9a3*
MUSG00000033061	142.10	372.15	2.62	1.70E-06	2.50E-04	*Resp18*
MUSG00000058740	126.26	332.24	2.63	5.29E-06	7.13E-04	*Kcnt1*
MUSG00000047746	244.55	646.16	2.64	1.13E-08	2.96E-06	*Fbxo40*
MUSG00000059213	203.05	537.69	2.65	1.31E-07	2.45E-05	*Ddn*
MUSG00000058975	385.07	1021.60	2.65	1.29E-11	7.01E-09	*Kcnc1*
MUSG00000037872	55.26	146.67	2.65	4.09E-04	2.55E-02	*Darc*
MUSG00000028546	729.72	1944.68	2.66	3.99E-16	7.46E-13	*Elavl4*
MUSG00000041828	285.45	764.47	2.68	6.89E-10	2.47E-07	*Abca8a*

Ensembl ID (ENS)	Read Count *Ikzf2*$^{+/+}$	Read Count *Ikzf2*$^{cello/cello}$	Fold Change	p Value	FDR	Gene Symbol
MUSG00000079597	70.79	190.04	2.68	3.10E-04	2.06E-02	*Gm5483*
MUSG00000070866	182.28	491.06	2.69	8.07E-08	1.62E-05	*Zfp804a*
MUSG00000051596	50.54	136.45	2.70	8.92E-04	4.75E-02	*Otop1*
MUSG00000007594	163.08	440.54	2.70	4.66E-07	8.07E-05	*Hapln4*
MUSG00000029544	134.25	368.00	2.74	1.37E-06	2.07E-04	*Cabp1*
MUSG00000040797	520.61	1430.39	2.75	1.11E-14	1.20E-11	*Iqsec3*
MUSG00000038128	655.47	1803.43	2.75	8.93E-17	2.12E-13	*Camk4*
MUSG00000027978	97.12	267.70	2.76	1.28E-05	1.52E-03	*Prss12*
MUSG00000064329	452.18	1254.18	2.77	3.04E-14	2.94E-11	*Scn1a*
MUSG00000091712	94.52	262.69	2.78	1.65E-05	1.88E-03	*Sec14l5*
MUSG00000033849	129.08	361.73	2.80	1.07E-06	1.73E-04	*B3galt2*
MUSG00000031688	52.04	147.66	2.84	1.97E-04	1.45E-02	*Pou4f2*
MUSG00000021268	84.25	239.58	2.84	2.03E-05	2.25E-03	*Meg3*
MUSG00000026826	227.94	648.35	2.84	6.57E-09	1.87E-06	*Nr4a2*
MUSG00000030283	189.64	543.33	2.86	1.31E-08	3.32E-06	*St8sia1*
MUSG00000034683	186.32	539.30	2.89	4.97E-09	1.49E-06	*Ppp1r1c*
MUSG00000028176	33.13	96.46	2.91	6.79E-04	3.81E-02	*Lrrc7*
MUSG00000040724	290.58	846.92	2.91	1.18E-11	6.70E-09	*Kcna2*
MUSG00000056569	30329.58	88599.24	2.92	1.10E-08	2.92E-06	*Mpz*
MUSG00000074796	81.36	239.49	2.94	2.87E-05	3.00E-03	*Slc4a11*
MUSG00000016346	421.88	1242.66	2.95	3.29E-15	3.90E-12	*Kcnq2*
MUSG00000067261	82.85	245.40	2.96	4.08E-06	5.68E-04	*Foxd3*
MUSG00000066258	60.25	179.67	2.98	1.26E-04	1.02E-02	*Trim12a*
MUSG00000022651	48.14	143.68	2.98	3.67E-04	2.35E-02	*Retnlg*
MUSG00000054162	2163.48	6473.00	2.99	1.84E-24	8.03E-21	*Spock3*
MUSG00000025189	40.14	120.37	3.00	3.12E-04	2.07E-02	*Cnnm1*
MUSG00000047976	2403.59	7210.20	3.00	3.98E-24	1.49E-20	*Kcna1*
MUSG00000038756	61.17	188.89	3.09	1.95E-05	2.17E-03	*Ttll6*
MUSG00000039488	55.39	172.65	3.12	2.62E-05	2.78E-03	*Cntn5*
MUSG00000025370	82.41	261.83	3.18	9.59E-07	1.59E-04	*Cdh9*
MUSG00000086844	121.92	399.34	3.28	2.99E-08	7.11E-06	*B230206H07Rik*
MUSG00000063253	341.79	1123.25	3.29	3.55E-16	7.46E-13	*Scoc*
MUSG00000074652	135.35	445.40	3.29	4.32E-09	1.31E-06	*Myh7b*
MUSG00000052861	40.27	132.72	3.30	5.83E-05	5.39E-03	*Dnah6*
MUSG00000042817	32.85	110.99	3.38	1.76E-04	1.33E-02	*Flt3*
MUSG00000044349	1904.66	6926.18	3.64	2.10E-30	1.83E-26	*Snhg11*
MUSG00000023034	505.10	1838.41	3.64	4.37E-22	1.43E-18	*Nr4a1*
MUSG00000068794	165.79	619.26	3.74	8.96E-13	5.85E-10	*Col28a1*
MUSG00000005994	21.97	83.35	3.79	1.30E-04	1.04E-02	*Tyrp1*
MUSG00000027955	133.29	513.50	3.85	4.48E-11	2.09E-08	*Fam198b*
MUSG00000078921	14.84	57.62	3.88	6.75E-04	3.80E-02	*Tgtp2*

Ensembl ID (ENS)	Read Count *Ikzf2*$^{+/+}$	Read Count *Ikzf2*$^{cello/cello}$	Fold Change	p Value	FDR	Gene Symbol
MUSG00000085698	36.07	144.46	4.00	4.81E-06	6.58E-04	*Gm16022*
MUSG00000075014	47.86	206.77	4.32	2.54E-07	4.55E-05	*Gm10800*
MUSG00000001494	117.32	509.24	4.34	7.08E-12	4.21E-09	*Sost*
MUSG00000060441	11.13	49.03	4.41	9.08E-04	4.82E-02	*Trim5*
MUSG00000090222	14.51	73.87	5.09	5.18E-05	4.92E-03	*Gm16340*
MUSG00000097503	6.32	34.78	5.50	4.85E-04	2.94E-02	*3110045C21Rik*
MUSG00000047495	4.81	30.85	6.41	3.09E-04	2.06E-02	*Dlgap2*
MUSG00000073902	5.95	41.18	6.92	7.46E-05	6.63E-03	*Gm1966*
MUSG00000060087	10.07	73.17	7.27	1.62E-06	2.40E-04	*Gm10074*
MUSG00000028081	65.19	648.90	9.95	2.12E-26	1.39E-22	*Rps3a1*
MUSG00000005681	0.53	12.70	23.98	3.29E-04	2.16E-02	*Apoa2*
MUSG00000038257	0.98	24.67	25.22	6.74E-06	8.59E-04	*Glra3*
MUSG00000073491	0.98	27.85	28.46	1.11E-06	1.78E-04	*Pydc4*
MUSG00000098050	0.00	50.95	∞	4.14E-12	2.51E-09	*Gm5345*
MUSG00000074252	0.00	25.87	∞	5.32E-08	1.12E-05	*Gm10654*
MUSG00000085926	0.00	16.36	∞	6.13E-06	8.01E-04	*Gm12299*
MUSG00000076038	0.00	9.53	∞	2.71E-04	1.85E-02	*Gm22774*
MUSG00000093843	0.00	8.82	∞	7.17E-04	3.99E-02	*Gm25939*

FDR, false detection rate; N/A, not applicable.

Table 9.5: Gene ontology enrichment of biological processes within the 57 significantly downregulated genes identified by RNA-Seq analysis of *Ikzf2*$^{cello/cello}$ cochleae at postnatal day 8.

GO ID	GO Term	Number of Genes	Associated Genes
GO:0030182	neuron differentiation	14	*Barhl2, Strc, Pax6, Pcsk9, Insm1, Pde6c,Cbln1, Lhx5, Uncx, Neurod1, Lhx4, Neurod4, Gfap, Neurod*
GO:0048699	generation of neurons	15	*Barhl2, Strc, Pax6, Pcsk9, Insm1, Pde6c,Cbln1, Lhx5, Uncx, Grm5, Neurod1, Lhx4, Neurod4, Gfap, Neurod2*
GO:0003310	pancreatic A cell differentiation	3	*Insm1, Neurod1, Pax6*
GO:0022008	neurogenesis	15	*Barhl2, Strc, Pax6, Pcsk9, Insm1, Pde6c, Cbln1, Lhx5, Uncx, Grm5, Neurod1, Lhx4, Neurod4, Gfap, Neurod2*
GO:0044707	single-multicellular organism process	31	*Mobp, Slc26a5, Ambn, Cbln1, Acta1, Lhx5, Uncx, Grm5, Mylpf, Tph1, Barhl2, Strc, Pax6, Zic1, Insm1, Lmod3, Neurod1, Neurod2, Pcsk9, Tnni2, Myh4, Neurod4, Myh8, Cryaa, Pde6g, Pde6c, Lhx4, Mybpc3, Gfap, Myl1, Crygb*
GO:0009887	organ morphogenesis	12	*Strc, Enam, Ambn, Pax6, Pde6c, Uncx, Amelx, Neurod1, Lhx4, Mybpc3, Crygb, Cryaa*
GO:0048513	organ development	20	*Ambn, Cbln1, Acta1, Lhx5, Uncx, Neurod4, Cryaa, Mylpf, Tph1, Strc, Pax6, Zic1, Insm1, Pde6c, Neurod1, Crx, Lhx4, Mybpc3, Crygb, Neurod2*
GO:0006936	muscle contraction	6	*Lmod3, Myh8, Tnni2, Myl1, Myh4, Mybpc3*
GO:0048731	system development	23	*Mobp, Ambn, Cbln1, Acta1, Lhx5, Uncx, Grm5, Mylpf, Tph1, Barhl2, Strc, Pax6, Zic1, Insm1, Neurod1, Pcsk9, Neurod4, Cryaa, Pde6c, Lhx4, Mybpc3, Gfap, Crygb*
GO:0032501	multicellular organismal process	31	*Mobp, Slc26a5, Ambn, Cbln1, Acta1, Lhx5, Uncx, Grm5, Mylpf, Tph1, Barhl2, Strc, Pax6, Zic1, Insm1, Lmod3, Neurod1, Neurod2, Pcsk9, Tnni2, Myh4, Neurod4, Myh8, Cryaa, Pde6g, Pde6c, Lhx4, Mybpc3, Gfap, Myl1, Crygb*
GO:0009888	tissue development	15	*Strc, Enam, Ambn, Pax6, Insm1, Pde6c, Acta1, Uncx, Neurod1, Crx, Mybpc3, Neurod4, Crygb, Cryaa, Mylpf*
GO:0021510	spinal cord development	5	*Lhx5, Lhx4, Uncx, Zic1, Pax6*
GO:0030154	cell differentiation	21	*Pcsk9, Cbln1, Acta1, Lhx5, Uncx, Grm5, Neurod4, Cryaa, Barhl2, Strc, Pax6, Zic1, Insm1, Pde6c, Lmod3, Neurod1, Crx, Lhx4, Mybpc3, Gfap, Crygb*

GO, gene ontology.

Table 9.6: Gene ontology enrichment of biological processes within the 219 significantly upregulated genes identified by RNA-Seq analysis of *Ikzf2*$^{cello/cello}$ cochleae at postnatal day 8.

GO ID	GO Term	Number of Genes	Associated Genes
GO:0022843	voltage-gated cation channel activity	8	*Kcnt1, Scn1a, Kcna1, Kcna2, Snap25, Scn9a, Kcnip2, Kcnab2*
GO:0005261	cation channel activity	10	*Scn1a, Snap25, Scn9a, Accn3, Kcnt1, Kcna1, Kcna2, Slc4a11, Kcnip2, Kcnab2*
GO:0046873	metal ion transmembrane transporter activity	11	*Slc9a3, Scn1a, Snap25, Scn9a, Kcnt1, Atp2b3, Kcna1, Kcna2, Slc4a11, Kcnip2, Kcnab2*
GO:0015077	monovalent inorganic cation transmembrane transporter activity	10	*Slc9a3, Scn1a, Snap25, Scn9a, Kcnt1, Kcna1, Kcna2, Slc4a11, Kcnip2, Kcnab2*
GO:0005249	voltage-gated potassium channel activity	6	*Kcna1, Kcnt1, Kcna2, Snap25, Kcnip2, Kcnab2*
GO:0022890	inorganic cation transmembrane transporter activity	11	*Slc9a3, Scn1a, Scn9a, Kcnt1, Atp2b3, Kcna1, Slc4a11, Kcnab2, Snap25, Kcna2, Kcnip2*
GO:0008324	cation transmembrane transporter activity	12	*Slc9a3, Scn1a, Scn9a, Kcnt1, Atp2b3, Kcna1, Slc4a11, Kcnab2, Snap25, Accn3, Kcna2, Kcnip2*
GO:0005267	potassium channel activity	6	*Kcna1, Kcnt1, Kcna2, Snap25, Kcnip2, Kcnab2*
GO:0015079	potassium ion transmembrane transporter activity	6	*Kcnt1, Kcna1, Kcna2, Snap25, Kcnip2, Kcnab2*
GO:0005251	delayed rectifier potassium channel activity	4	*Kcna1, Kcna2, Kcnq2, Kcnc1*
GO:0005216	ion channel activity	7	*Scn1a, Snap25, Accn3, Kcnt1, Slc4a11, Kcnip2, Kcnab2*
GO:0005244	voltage-gated ion channel activity	5	*Kcnt1, Scn1a, Snap25, Kcnip2, Kcnab2*
GO:0015267	channel activity	7	*Scn1a, Snap25, Accn3, Kcnt1, Slc4a11, Kcnip2, Kcnab2*
GO:0022836	gated channel activity	6	*Scn1a, Snap25, Accn3, Kcnt1, Kcnip2, Kcnab2*
GO:0005272	sodium channel activity	3	*Scn9a, Slc4a11, Scn1a*

GO, gene ontology.

Table 9.7: The cluster of 96 genes identified from the SHIELD to exhibit a temporal expression pattern in cochlear hair cells highly correlated to that of *Ikzf2*.

Ensembl ID (ENS)	Gene Symbol	Gene Name
MUSG00000078572	*1810043H04Rik*	RIKEN cdna 1810043H04 gene
MUSG00000025783	*4930412O13Rik*	RIKEN cdna 4930412O13 gene
MUSG00000030207	*8430419L09Rik*	RIKEN cdna 8430419L09 gene
MUSG00000043122	*A530016L24Rik*	RIKEN cdna A530016L24 gene
MUSG00000021044	*Adck1*	Aarf domain containing kinase 1
MUSG00000042797	*Aqp11*	Aquaporin 11
MUSG00000044217	*Aqp5*	Aquaporin 5
MUSG00000023017	*Asic1*	Acid-sensing (proton-gated) ion channel 1
MUSG00000020788	*Atp2a3*	Atpase, Ca++ transporting, ubiquitous
MUSG00000034566	*Atp5h*	ATP synthase, H+ transporting, mitochondrial F0 complex, subunit D
MUSG00000050856	*Atp5k*	ATP synthase, H+ transporting, mitochondrial F1F0 complex, subunit E
MUSG00000020566	*Atp6v1c2*	Atpase, H+ transporting, lysosomal V1 subunit C2
MUSG00000029458	*Brap*	BRCA1 associated protein
MUSG00000007122	*Casq1*	Calsequestrin 1
MUSG00000046691	*Chtf8*	CTF8, chromosome transmission fidelity factor 8
MUSG00000030652	*Coq7*	Demethyl-Q 7
MUSG00000041697	*Cox6a1*	Cytochrome c oxidase subunit via polypeptide 1
MUSG00000035885	*Cox8a*	Cytochrome c oxidase subunit viiia
MUSG00000028528	*Dnajc6*	Dnaj (Hsp40) homolog, subfamily C, member 6
MUSG00000039358	*Drd5*	Dopamine receptor D5
MUSG00000037419	*Endod1*	Endonuclease domain containing 1
MUSG00000079157	*Fam155a*	Family with sequence similarity 155, member A
MUSG00000071604	*Fam189a2*	Family with sequence similarity 189, member A2
MUSG00000032977	*Fam207a*	Family with sequence similarity 207, member A
MUSG00000049872	*Fam26e*	Family with sequence similarity 26, member E
MUSG00000037536	*Fbxo34*	F-box protein 34
MUSG00000027865	*Gdap2*	Ganglioside-induced differentiation-associated-protein 2
MUSG00000051335	*Gfod1*	Glucose-fructose oxidoreductase domain containing 1
MUSG00000035900	*Gramd4*	GRAM domain containing 4
MUSG00000018102	*Hist1h2be*	Histone cluster 1, h2be
MUSG00000040820	*Hlcs*	Holocarboxylase synthetase (biotin- [propriony-Coenzyme A-carboxylase (ATP-hydrolysing)] ligase)
MUSG00000025813	*Homer2*	Homer homolog 2
MUSG00000078963	*Hsbp1l1*	Heat shock factor binding protein 1-like 1
MUSG00000021721	*Htr1a*	5-hydroxytryptamine (serotonin) receptor 1A
MUSG00000025997	*Ikzf2*	Ikaros family zinc finger 2
MUSG00000022969	*Il10rb*	Interleukin 10 receptor, beta
MUSG00000063646	*Jakmip1*	Janus kinase and microtubule interacting protein 1
MUSG00000001552	*Jup*	Junction plakoglobin
MUSG00000079436	*Kcnj13*	Potassium inwardly-rectifying channel, subfamily J, member 13

Ensembl ID (ENS)	Gene Symbol	Gene Name
MUSG00000032254	*Kif23*	Kinesin family member 23
MUSG00000078813	*Leng1*	Leukocyte receptor cluster (LRC) member 1
MUSG00000044086	*Lmod3*	Leiomodin 3 (fetal)
MUSG00000059149	*Mfsd4*	Major facilitator superfamily domain containing 4
MUSG00000029022	*Miip*	Migration and invasion inhibitory protein
MUSG00000027612	*Mmp24*	Matrix metallopeptidase 24
MUSG00000052373	*Mpp3*	Membrane protein, palmitoylated 3
MUSG00000023967	*Mrps18a*	Mitochondrial ribosomal protein S18A
MUSG00000016427	*Ndufa1*	NADH dehydrogenase (ubiquinone) 1 alpha subcomplex, 12
MUSG00000022354	*Ndufb9*	NADH dehydrogenase (ubiquinone) 1 beta subcomplex, 9
MUSG00000020889	*Nr1d1*	Nuclear receptor subfamily 1, group D, member 1
MUSG00000075033	*Nxpe3*	Neurexophilin and PC-esterase domain family, member 3
MUSG00000029153	*Ociad2*	OCIA domain containing 2
MUSG00000029618	*Ocm*	Oncomodulin
MUSG00000026833	*Olfm1*	Olfactomedin 1
MUSG00000026239	*Pde6d*	Phosphodiesterase 6D, cgmp-specific, rod, delta
MUSG00000024851	*Pitpnm1*	Phosphatidylinositol transfer protein, membrane-associated 1
MUSG00000035934	*Pknox2*	Pbx/knotted 1 homeobox 2
MUSG00000021209	*Ppp4r4*	Protein phosphatase 4, regulatory subunit 4
MUSG00000021737	*Psmd6*	Proteasome (prosome, macropain) 26S subunit, non-atpase, 6
MUSG00000002372	*Ranbp3*	RAN binding protein 3
MUSG00000035504	*Reep6*	Receptor accessory protein 6
MUSG00000024883	*Rin1*	Ras and Rab interactor 1
MUSG00000022540	*Rogdi*	Rogdi homolog (Drosophila)
MUSG00000036192	*Rorb*	RAR-related orphan receptor beta
MUSG00000032485	*Scap*	SREBF chaperone
MUSG00000037990	*Sh3rf3*	SH3 domain containing ring finger 3
MUSG00000024134	*Six2*	Sine oculis-related homeobox 2
MUSG00000029015	*Slc26a5*	Solute carrier family 26, member 5
MUSG00000026435	*Slc45a3*	Solute carrier family 45, member 3
MUSG00000029650	*Slc46a3*	Solute carrier family 46, member 3
MUSG00000002210	*Smg9*	Smg-9 homolog, nonsense mediated mRNA decay factor (C. Elegans)
MUSG00000078350	*Smim1*	Small integral membrane protein 1
MUSG00000037049	*Smpd1*	Sphingomyelin phosphodiesterase 1, acid lysosomal
MUSG00000040767	*Snrnp25*	Small nuclear ribonucleoprotein 25 (U11/U12)
MUSG00000021594	*Srd5a1*	Steroid 5 alpha-reductase 1
MUSG00000032333	*Stoml1*	Stomatin-like 1
MUSG00000033498	*Strc*	Stereocilin
MUSG00000026470	*Stx6*	Syntaxin 6
MUSG00000023118	*Sympk*	Symplekin
MUSG00000051397	*Tacstd2*	Tumor-associated calcium signal transducer 2
MUSG00000026279	*Thap4*	THAP domain containing 4
MUSG00000024749	*Tmc1*	Transmembrane channel-like gene family 1

Ensembl ID (ENS)	Gene Symbol	Gene Name
MUSG00000031791	*Tmem38a*	Transmembrane protein 38A
MUSG00000033177	*Tmprss7*	Transmembrane serine protease 7
MUSG00000032536	*Trak1*	Trafficking protein, kinesin binding 1
MUSG00000002043	*Trappc6a*	Trafficking protein particle complex 6A
MUSG00000031028	*Tub*	Tubby candidate gene
MUSG00000030137	*Tuba8*	Tubulin, alpha 8
MUSG00000054134	*Umodl1*	Uromodulin-like 1
MUSG00000020163	*Uqcr11*	Ubiquinol-cytochrome c reductase, complex III subunit XI
MUSG00000063882	*Uqcrh*	Ubiquinol-cytochrome c reductase hinge protein
MUSG00000025481	*Urah*	Urate (5-hydroxyiso-) hydrolase
MUSG00000071528	*Usmg5*	Upregulated during skeletal muscle growth 5
MUSG00000024037	*Wdr4*	WD repeat domain 44
MUSG00000029029	*Wrap73*	WD repeat containing, antisense to Trp73
MUSG00000028811	*Yars*	Tyrosyl-tRNA synthetase 2

Table 9.8: RNA-Seq expression data of the 40 putative direct target genes of helios in *Ikzf2*$^{cello/cello}$ cochleae compared to *Ikzf2*$^{+/+}$ at postnatal day 8.

Ensembl ID (ENS)	Read Count *Ikzf2*$^{+/+}$	Read Count *Ikzf2*$^{cello/cello}$	Fold Change	p Value	FDR	Gene Symbol
MUSG00000029015	1016.59	440.68	-2.31	1.66E-08	4.13E-06	*Slc26a5*
MUSG00000054134	6961.72	3732.19	-1.87	5.35E-09	1.59E-06	*Umodl1*
MUSG00000030137	151.38	96.02	-1.58	9.85E-02	1.00	*Tuba8*
MUSG00000033177	257.01	163.59	-1.57	4.36E-02	0.74	*Tmprss7*
MUSG00000036192	962.79	621.01	-1.55	1.84E-03	0.09	*Rorb*
MUSG00000051397	716.10	485.53	-1.47	1.20E-02	0.33	*Tacstd2*
MUSG00000042797	1145.49	836.25	-1.37	1.77E-02	0.42	*Aqp11*
MUSG00000024134	1920.74	1407.67	-1.36	9.65E-03	0.28	*Six2*
MUSG00000026435	274.71	207.35	-1.32	1.53E-01	1.00	*Slc45a3*
MUSG00000026833	1829.79	1415.72	-1.29	4.33E-02	0.74	*Olfm1*
MUSG00000035504	361.76	282.74	-1.28	1.90E-01	1.00	*Reep6*
MUSG00000021044	1486.29	1181.19	-1.26	6.78E-02	0.93	*Adck1*
MUSG00000001552	5491.44	4438.04	-1.24	5.00E-02	0.80	*Jup*
MUSG00000002043	1158.47	951.70	-1.22	1.33E-01	1.00	*Trappc6a*
MUSG00000020889	805.00	678.89	-1.19	2.08E-01	1.00	*Nr1d1*
MUSG00000023967	1151.24	975.91	-1.18	2.11E-01	1.00	*Mrps18a*
MUSG00000025997	943.19	799.77	-1.18	2.01E-01	1.00	*Ikzf2*
MUSG00000037990	576.40	500.77	-1.15	4.02E-01	1.00	*Sh3rf3*
MUSG00000032485	2425.53	2117.28	-1.15	2.47E-01	1.00	*Scap*
MUSG00000035900	2586.17	2266.64	-1.14	2.53E-01	1.00	*Gramd4*
MUSG00000030207	2626.14	2382.33	-1.10	4.08E-01	1.00	*8430419L09Rik*
MUSG00000025813	1452.05	1336.48	-1.09	5.08E-01	1.00	*Homer2*
MUSG00000023118	3647.34	3361.04	-1.09	4.39E-01	1.00	*Sympk*
MUSG00000032536	8375.54	7766.34	-1.08	4.91E-01	1.00	*Trak1*
MUSG00000020788	2656.59	2519.58	-1.05	6.01E-01	1.00	*Atp2a3*
MUSG00000047246	114.83	109.05	-1.05	8.40E-01	1.00	*Hist1h2be*
MUSG00000050856	1477.45	1444.71	-1.02	8.73E-01	1.00	*Atp5k*
MUSG00000029153	1121.50	1101.20	-1.02	8.92E-01	1.00	*Ociad2*
MUSG00000063882	4936.45	4856.08	-1.02	8.97E-01	1.00	*Uqcrh*
MUSG00000035934	970.44	984.27	1.01	9.32E-01	1.00	*Pknox2*
MUSG00000031028	384.13	393.14	1.02	8.28E-01	1.00	*Tub*
MUSG00000043122	115.24	123.58	1.07	7.73E-01	1.00	*A530016L24Rik*
MUSG00000027612	358.94	386.99	1.08	5.98E-01	1.00	*Mmp24*
MUSG00000059149	593.13	645.16	1.09	6.07E-01	1.00	*Mfsd4*
MUSG00000021721	25.19	27.93	1.11	8.10E-01	1.00	*Htr1a*
MUSG00000029022	349.37	392.33	1.12	5.98E-01	1.00	*Miip*
MUSG00000051335	762.15	863.95	1.13	3.51E-01	1.00	*Gfod1*
MUSG00000028528	955.37	1128.86	1.18	1.40E-01	1.00	*Dnajc6*
MUSG00000063646	127.44	249.13	1.95	2.06E-03	0.09	*Jakmip1*
MUSG00000024851	N/A	N/A	N/A	N/A	N/A	*Pitpnm1*

FDR, false detection rate; N/A, not applicable.